Jordan Journal

of

Biological

Sciences

An International Peer-Reviewed Scientific Journal

Financed by the Scientific Research and Innovation Support Fund

This title is indexed in Scopus

refine your research
SCOPUS

Instructions to Authors

Scopes

Study areas include cell biology, genomics, microbiology, immunology, molecular biology, biochemistry, embryology, immunogenetics, cell and tissue culture, molecular ecology, genetic engineering and biological engineering, bioremediation and biodegradation, bioinformatics, biotechnology regulations, gene therapy, organismal biology, microbial and environmental biotechnology, marine sciences. The JJBS welcomes the submission of manuscript that meets the general criteria of significance and academic excellence. All articles published in JJBS are peer-reviewed. Papers will be published approximately one to two months after acceptance.

Type of Papers

The journal publishes high-quality original scientific papers, short communications, correspondence and case studies. Review articles are usually by invitation only. However, Review articles of current interest and high standard will be considered.

Submission of Manuscript

Manuscript, or the essence of their content, must be previously unpublished and should not be under simultaneous consideration by another journal. The authors should also declare if any similar work has been submitted to or published by another journal. They should also declare that it has not been submitted/ published elsewhere in the same form, in English or in any other language, without the written consent of the Publisher. The authors should also declare that the paper is the original work of the author(s) and not copied (in whole or in part) from any other work. All papers will be automatically checked for duplicate publication and plagiarism. If detected, appropriate action will be taken in accordance with International Ethical Guideline. By virtue of the submitted manuscript, the corresponding author acknowledges that all the co-authors have seen and approved the final version of the manuscript. The corresponding author should provide all co-authors with information regarding the manuscript, and obtain their approval before submitting any revisions. Electronic submission of manuscripts is strongly recommended, provided that the text, tables and figures are included in a single Microsoft Word file. Submit manuscript as e-mail attachment to the Editorial Office at: JJBS@hu.edu.jo. After submission, a manuscript number will be communicated to the corresponding author within 48 hours.

Peer-review Process

It is requested to submit, with the manuscript, the names, addresses and e-mail addresses of at least 4 potential reviewers. It is the sole right of the editor to decide whether or not the suggested reviewers to be used. The reviewers' comments will be sent to authors within 6-8 weeks after submission. Manuscripts and figures for review will not be returned to authors whether the editorial decision is to accept, revise, or reject. All Case Reports and Short Communication must include at least one table and/ or one figure.

Preparation of Manuscript

The manuscript should be written in English with simple lay out. The text should be prepared in single column format. Bold face, italics, subscripts, superscripts etc. can be used. Pages should be numbered consecutively, beginning with the title page and continuing through the last page of typewritten material.

The text can be divided into numbered sections with brief headings. Starting from introduction with section 1. Subsections should be numbered (for example 2.1 (then 2.1.1, 2.1.2, 2.2, etc.), up to three levels. Manuscripts in general should be organized in the following manner:

Title Page

The title page should contain a brief title, correct first name, middle initial and family name of each author and name and address of the department(s) and institution(s) from where the research was carried out for each author. The title should be without any abbreviations and it should enlighten the contents of the paper. All affiliations should be provided with a lower-case superscript number just after the author's name and in front of the appropriate address.
The name of the corresponding author should be indicated along with telephone and fax numbers (with country and area code) along with full postal address and e-mail address.

Abstract

The abstract should be concise and informative. It should not exceed **350 words** in length for full manuscript and Review article and **150 words** in case of Case Report and/ or Short Communication. It should briefly describe the purpose of the work, techniques and methods used, major findings with important data and conclusions. No references should be cited in this part. Generally non-standard abbreviations should not be used, if necessary they should be clearly defined in the abstract, at first use.

Keywords

Immediately after the abstract, **about 4-8 keywords** should be given. Use of abbreviations should be avoided, only standard abbreviations, well known in the established area may be used, if appropriate. These keywords will be used for indexing.

Abbreviations

Non-standard abbreviations should be listed and full form of each abbreviation should be given in parentheses at first use in the text.

Introduction

Provide a factual background, clearly defined problem, proposed solution, a brief literature survey and the scope and justification of the work done.

Materials and Methods

Give adequate information to allow the experiment to be reproduced. Already published methods should be mentioned with references. Significant modifications of published methods and new methods should be described in detail. Capitalize trade names and include the manufacturer's name and address. Subheading should be used.

Results

Results should be clearly described in a concise manner. Results for different parameters should be described under subheadings or in separate paragraph. Results should be explained, but largely without referring to the literature. Table or figure numbers should be mentioned in parentheses for better understanding.

Discussion

The discussion should not repeat the results, but provide detailed interpretation of data. This should interpret the significance of the findings of the work. Citations should be given in support of the findings. The results and discussion part can also be described as separate, if appropriate. The Results and Discussion sections can include subheadings, and when appropriate, both sections can be combined

Conclusions

This should briefly state the major findings of the study.

Acknowledgment

A brief acknowledgment section may be given after the conclusion section just before the references. The acknowledgment of people who provided assistance in manuscript preparation, funding for research, etc. should be listed in this section.

Tables and Figures

Tables and figures should be presented as per their appearance in the text. It is suggested that the discussion about the tables and figures should appear in the text before the appearance of the respective tables and figures. No tables or figures should be given without discussion or reference inside the text.

Tables should be explanatory enough to be understandable without any text reference. Double spacing should be maintained throughout the table, including table headings and footnotes. Table headings should be placed above the table. Footnotes should be placed below the table with superscript lowercase letters. Each table should be on a separate page, numbered consecutively in Arabic numerals.

Each figure should have a caption. The caption should be concise and typed separately, not on the figure area. Figures should be self-explanatory. Information presented in the figure should not be repeated in the table. All symbols and abbreviations used in the illustrations should be defined clearly. Figure legends should be given below the figures.

References

References should be listed alphabetically at the end of the manuscript. Every reference referred in the text must be also present in the reference list and vice versa. In the text, a reference identified by means of an author's name should be followed by the year of publication in parentheses (e.g.(Brown,2009)). For two authors, both authors' names followed by the year of publication (e.g.(Nelson and Brown, 2007)). When there are more than two authors, only the first author's name followed by "*et al.*" and the year of publication (e.g (Abu-Elteen *et al.*, 2010)). When two or more works of an author has been published during the same year, the reference should be identified by the letters "a", "b", "c", etc., placed after the year of publication. This should be followed both in the text and reference list. e.g., Hilly, (2002a, 2002b); Hilly, and Nelson, (2004). Articles in preparation or submitted for publication, unpublished observations, personal communications, etc. should not be included in the reference list but should only be mentioned in the article text (e.g., Shtyawy,A., University of Jordan, personal communication). Journal titles should be abbreviated according to the system adopted in Biological Abstract and Index Medicus, if not included in Biological Abstract or Index Medicus journal title should be given in full. The author is responsible for the sccuracy and completeness of the references and for their correct textual citation. Failure to do so may result in the paper being withdraw from the evaluation process. Example of correct reference form is given as follows:-

<u>Reference to a journal publication:</u>

Bloch BK. 2002. Econazole nitrate in the treatment of *Candida vaginitis*. *S Afr Med J.*, **58**:314-323.

Ogunseitan OA and Ndoye IL. 2006. Protein method for investigating mercuric reductase gene expression in aquatic environments. *Appl Environ Microbiol.*, **64**: 695-702.

Hilly MO, Adams MN and Nelson SC. 2009. Potential fly-ash utilization in agriculture. *Progress in Natural Sci.*, **19**: 1173-1186.

<u>Reference to a book:</u>
Brown WY and White SR.1985. **The Elements of Style**, third ed. MacMillan, New York.

<u>Reference to a chapter in an edited book:</u>
Mettam GR and Adams LB. 2010. How to prepare an electronic version of your article. In: Jones BS and Smith RZ (Eds.), **Introduction to the Electronic Age**. Kluwer Academic Publishers, Netherlands, pp. 281–304.

<u>Conferences and Meetings:</u>
Embabi NS. 1990. Environmental aspects of distribution of mangrove in the United Arab Emirates. Proceedings of the First ASWAS Conference. University of the United Arab Emirates. Al-Ain, United Arab Emirates.

<u>Theses and Dissertations:</u>
El-Labadi SN. 2002. Intestinal digenetic trematodes of some marine fishes from the Gulf of Aqaba. MSc dissertation, The Hashemite University, Zarqa, Jordan.

Nomenclature and Units
Internationally accepted rules and the international system of units (SI) should be used. If other units are mentioned, please give their equivalent in SI.

For biological nomenclature, the conventions of the *International Code of Botanical Nomenclature, the International Code of Nomenclature of Bacteria,* and the *International Code of Zoological Nomenclature* should be followed.
Scientific names of all biological creatures (crops, plants, insects, birds, mammals, etc.) should be mentioned in parentheses at first use of their English term.

Chemical nomenclature, as laid down in the *International Union of Pure and Applied Chemistry* and the official recommendations of the *IUPAC-IUB Combined Commission on Biochemical Nomenclature* should be followed. All biocides and other organic compounds must be identified by their Geneva names when first used in the text. Active ingredients of all formulations should be likewise identified.

Math formulae

All equations referred to in the text should be numbered serially at the right-hand side in parentheses. Meaning of all symbols should be given immediately after the equation at first use. Instead of root signs fractional powers should be used. Subscripts and superscripts should be presented clearly. Variables should be presented in italics. Greek letters and non-Roman symbols should be described in the margin at their first use.

To avoid any misunderstanding zero (0) and the letter O, and one (1) and the letter l should be clearly differentiated. For simple fractions use of the solidus (/) instead of a horizontal line is recommended. Levels of statistical significance such as: $^*P < 0.05$, $^{**}P < 0.01$ and $^{***}P < 0.001$ do not require any further explanation.

Copyright

Submission of a manuscript clearly indicates that: the study has not been published before or is not under consideration for publication elsewhere (except as an abstract or as part of a published lecture or academic thesis); its publication is permitted by all authors and after accepted for publication it will not be submitted for publication anywhere else, in English or in any other language, without the written approval of the copyright-holder. The journal may consider manuscripts that are translations of articles originally published in another language. In this case, the consent of the journal in which the article was originally published must be obtained and the fact that the article has already been published must be made clear on submission and stated in the abstract. It is compulsory for the authors to ensure that no material submitted as part of a manuscript infringes existing copyrights, or the rights of a third party.

Ethical Consent

All manuscripts reporting the results of experimental investigation involving human subjects should include a statement confirming that each subject or subject's guardian obtains an informed consent, after the approval of the experimental protocol by a local human ethics committee or IRB. When reporting experiments on animals, authors should indicate whether the institutional and national guide for the care and use of laboratory animals was followed.

Plagiarism

The JJBS hold no responsibility for plagiarism. If a published paper is found later to be extensively plagiarized and is found to be a duplicate or redundant publication, a note of retraction will be published, and copies of the correspondence will be sent to the authors' head of institute.

Galley Proofs

The Editorial Office will send proofs of the manuscript to the corresponding author as an e-mail attachment for final proof reading and it will be the responsibility of the corresponding author to return the galley proof materials appropriately corrected within the stipulated time. Authors will be asked to check any typographical or minor clerical errors in the manuscript at this stage. No other major alteration in the manuscript is allowed. After publication authors can freely access the full text of the article as well as can download and print the PDF file.

Publication Charges

There are no page charges for publication in Jordan Journal of Biological Sciences, except for color illustrations,

Reprints

Ten (10) reprints are provided to corresponding author free of charge within two weeks after the printed journal date. For orders of more reprints, a reprint order form and prices will be sent with article proofs, which should be returned directly to the Editor for processing.

Disclaimer

Articles, communication, or editorials published by JJBS represent the sole opinions of the authors. The publisher shoulders no responsibility or liability what so ever for the use or misuse of the information published by JJBS.

Indexing

JJBS is indexed and abstracted by:

DOAJ (Directory of Open Access Journals)	CABI
Google Scholar	EBSCO
Journal Seek	CAS (Chemical Abstract Service)
HINARI	ETH- Citations
Index Copernicus	Open J-Gat
NDL Japanese Periodicals Index	SCImago
SCIRUS	Clarivate Analytics (Zoological Abstract)
OAJSE	Scopus
ISC (Islamic World Science Citation Center)	AGORA (United Nation's FAO database)
Directory of Research Journal Indexing (DRJI)	SHERPA/RoMEO (UK)
Ulrich's	

The Hashemite University
Deanship of Scientific Research
TRANSFER OF COPYRIGHT AGREEMENT

Journal publishers and authors share a common interest in the protection of copyright: authors principally because they want their creative works to be protected from plagiarism and other unlawful uses, publishers because they need to protect their work and investment in the production, marketing and distribution of the published version of the article. In order to do so effectively, publishers request a formal written transfer of copyright from the author(s) for each article published. Publishers and authors are also concerned that the integrity of the official record of publication of an article (once refereed and published) be maintained, and in order to protect that reference value and validation process, we ask that authors recognize that distribution (including through the Internet/WWW or other on-line means) of the authoritative version of the article as published is best administered by the Publisher.

To avoid any delay in the publication of your article, please read the terms of this agreement, sign in the space provided and return the complete form to us at the address below as quickly as possible.

Article entitled:--

Corresponding author: --

To be published in the journal: Jordan Journal of Biological Sciences (JJBS)

I hereby assign to the Hashemite University the copyright in the manuscript identified above and any supplemental tables, illustrations or other information submitted therewith (the "article") in all forms and media (whether now known or hereafter developed), throughout the world, in all languages, for the full term of copyright and all extensions and renewals thereof, effective when and if the article is accepted for publication. This transfer includes the right to adapt the presentation of the article for use in conjunction with computer systems and programs, including reproduction or publication in machine-readable form and incorporation in electronic retrieval systems.

Authors retain or are hereby granted (without the need to obtain further permission) rights to use the article for traditional scholarship communications, for teaching, and for distribution within their institution.

☐ I am the sole author of the manuscript

☐ I am signing on behalf of all co-authors of the manuscript

☐ The article is a 'work made for hire' and I am signing as an authorized representative of the employing company/institution

Please mark one or more of the above boxes (as appropriate) and then sign and date the document in black ink.

Signed:_____ Name printed: _____
Title and Company (if employer representative) : _____
Date: _____

Data Protection: By submitting this form you are consenting that the personal information provided herein may be used by the Hashemite University and its affiliated institutions worldwide to contact you concerning the publishing of your article.

Please return the completed and signed original of this form by mail or fax, or a scanned copy of the signed original by e-mail, retaining a copy for your files, to:

Hashemite University
Jordan Journal of Biological Sciences
Zarqa 13115 Jordan
Fax: +962 5 3903338
Email: jjbs@hu.edu.jo

Editorial Preface

Jordan Journal of Biological Sciences (JJBS) is a refereed, quarterly international journal financed by the Scientific Research and Innovation Support Fund, Ministry of Higher Education and Scientific Research in cooperation with the Hashemite University, Jordan. JJBS celebrated its 12th commencement this past January, 2020. JJBS was founded in 2008 to create a peer-reviewed journal that publishes high-quality research articles, reviews and short communications on novel and innovative aspects of a wide variety of biological sciences such as cell biology, developmental biology, structural biology, microbiology, entomology, molecular biology, biochemistry, medical biotechnology, biodiversity, ecology, marine biology, plant and animal biology, plant and animal physiology, genomics and bioinformatics.

We have watched the growth and success of JJBS over the years. JJBS has published 14 volumes, 60 issues and 800 articles. JJBS has been indexed by SCOPUS, CABI's Full-Text Repository, EBSCO, Clarivate Analytics- Zoological Record and recently has been included in the UGC India approved journals. JJBS Cite Score has improved from 0.7 in 2019 to 1.4 in 2021 (Last updated on 6 March, 2022) and with Scimago Institution Ranking (SJR) 0.22 (Q3) in 2021.

A group of highly valuable scholars have agreed to serve on the editorial board and this places JJBS in a position of most authoritative on biological sciences. I am honored to have six eminent associate editors from various countries. I am also delighted with our group of international advisory board members coming from 15 countries worldwide for their continuous support of JJBS. With our editorial board's cumulative experience in various fields of biological sciences, this journal brings a substantial representation of biological sciences in different disciplines. Without the service and dedication of our editorial; associate editorial and international advisory board members, JJBS would have never existed.

In the coming year, we hope that JJBS will be indexed in Clarivate Analytics and MEDLINE (the U.S. National Library of Medicine database) and others. As you read throughout this volume of JJBS, I would like to remind you that the success of our journal depends on the number of quality articles submitted for review. Accordingly, I would like to request your participation and colleagues by submitting quality manuscripts for review. One of the great benefits we can provide to our prospective authors, regardless of acceptance of their manuscripts or not, is the feedback of our review process. JJBS provides authors with high quality, helpful reviews to improve their manuscripts.

Finally, JJBS would not have succeeded without the collaboration of authors and referees. Their work is greatly appreciated. Furthermore, my thanks are also extended to The Hashemite University and the Scientific Research and Innovation Support Fund, Ministry of Higher Education and Scientific Research for their continuous financial and administrative support to JJBS.

<div style="text-align: right;">

Professor Wedyan ,Mohammed A.
March, 2024

</div>

CONTENTS

Unraveling the Intricacies of Gut Microbiome, Psychology, and Viral Pandemics: A Holistic Perspective

Ariyo Shahin Jafari [1], Shahram Agah [2], Muhannad I. Massadeh [3], Mojdeh Valizadeh [4], Hakimeh Karami [5], Amir Sasan Mozaffari Nejad [5,6,*]

[1] *Department of Medical Parasitology and Virology, Sechenov University, Malaya Pirogovskaya Str., 20, 119435 Moscow, Russia;*
[2] *Colorectal Research Center, Iran University of Medical Sciences, Tehran, Iran;* [3] *Department of Biology and Biotechnology, Faculty of Science, The Hashemite University, Zarqa, Jordan;* [4] *Department of Psychology, Islamic Azad University, Rasht Branch, Rasht, Iran;* [5] *Universal Scientific Education and Research Network (USERN) JMU Office, Jiroft University of Medical Sciences, Jiroft, Iran;* [6] *Bio Environmental Health Hazards Research Center, Jiroft University of Medical Sciences, Jiroft, Iran*

Amid the relentless onslaught of the COVID-19 pandemic, it has become increasingly clear that comprehending the connection mid the gut microbiome, mental health, and Viral illnesses is essential for developing effective strategies to tackle these global threats (Burchill *et al.,* 2021; Rishi *et al.,* 2021; Bransfield *et al.,* 2023). The human microbiota, a diverse ecosystem rich in various microbial groups such as fungi, viruses, and bacteria, is essential for supporting host health and regulating immune responses (Yoo *et al.,* 2020; Zheng *et al.,* 2020; Maciel-Fiuza *et al.,* 2023). For example, recent research has indicated that specific gut bacteria, such as Bacteroides fragilis, can induce regulatory T cells in the gut, which are crucial for sustaining immune tolerance and avoiding autoimmune disorders (Ramakrishna *et al.,* 2019; Zhang *et al.,* 2022). Additionally, studies have demonstrated the significance of metabolites generated by gut microbiota, including short-chain fatty acids, in influencing immune cell activity and managing inflammation (Kim 2021; Yao *et al.,* 2022). Furthermore, the gut microbiome has been implicated in modulating the efficacy of vaccines (Kumar *et al.,* 2022). For this reason, the several studies demonstrated that the makeup of the gut microbiota influences the generation of vaccine-specific antibodies, thereby affecting vaccine responsiveness (Lynn *et al.,* 2022; Huang *et al.,* 2023). This underscores the significance of taking into account the gut microbiome when designing vaccination strategies, especially in the context of viral pandemics. In parallel, new evince has clarified the reciprocal relationship between the gut microbiome and mental health. Dysbiosis, or an imbalance in the gut microbial ecosystem, has been linked to various psychiatric disorders, including depression and anxiety (Clapp *et al.,* 2017; Halverson and Alagiakrishnan 2020). Therefore, the recent systematic review studies were highlighted that individuals with depression exhibit changes in the makeup of their gut microbiota, indicating a possible connection between gut dysbiosis and mental health disorders (Safadi *et al.,* 2022; Grau-Del Valle *et al.,* 2023). The COVID-19 pandemic has further underscored the intricate interplay between infectious diseases, psychological well-being, and gut health. Reports suggest that people with COVID-19 frequently exhibit gastrointestinal signs, such as diarrhea and vomiting, alongside respiratory symptoms (Shahgolzari *et al.,* 2021; Jin *et al.,* 2022). Moreover, the psychological effects of the pandemic, including heightened stress and anxiety, has been widely documented (Panchal *et al.,* 2020). To address these multifaceted challenges, a comprehensive approach is imperative. Public health measures aimed at curbing viral spread must be complemented by interventions targeting the gut microbiome and psychological resilience. For instance, dietary interventions that promote a healthy gut microbiota, such as consuming fiber-rich foods and probiotics, could bolster immune function and mitigate the risk of viral infections (Sundararaman *et al.,* 2020; Harper *et al.,* 2021). Additionally, mental health support services should be expanded to address the psychological fallout of the pandemic, particularly among vulnerable populations (Reiriz *et al.,* 2023). In conclusion, the convergence of gut microbiome research, psychology, and infectious disease control presents a unique opportunity to enhance our understanding of viral pandemics and develop innovative strategies for prevention and management. By adopting a holistic approach that considers the intricate interplay between host-microbiome interactions, psychological well-being, and immune function, we can better equip ourselves to navigate the challenges posed by current and future pandemics.

References

Bransfield, R. C., C. Mao and R. Greenberg. 2023. Microbes and Mental Illness: Past, Present, and Future. *Healthcare* **12(1)**: 83.

Burchill, E., E. Lymberopoulos, E. Menozzi, S. Budhdeo, J. R. McIlroy, J. Macnaughtan and N. Sharma. 2021. The unique impact of COVID-19 on human gut microbiome research. *Front Med* **8**: 652464.

Clapp, M., N. Aurora, L. Herrera, M. Bhatia, E. Wilen and S. Wakefield. 2017. Gut microbiota's effect on mental health: The gut-brain axis. *Clin Pract* **7(4)**: 987.

Grau-Del Valle, C., J. Fernández, E. Solá, I. Montoya-Castilla, C. Morillas and C. Bañuls. 2023. Association between gut microbiota and psychiatric disorders: a systematic review. *Front Psychol* **14**: 1215674.

Halverson, T. and K. Alagiakrishnan. 2020. Gut microbes in neurocognitive and mental health disorders. *Ann Med* **52(8)**: 423-443.

Harper, A., V. Vijayakumar, A. C. Ouwehand, J. Ter Haar, D. Obis, J. Espadaler, S. Binda, S. Desiraju and R. Day. 2021. Viral

[*] Corresponding author. e-mail: asmozafarinejad@yahoo.in.

Infections, the Microbiome, and Probiotics. *Front Cell Infect Microbiol* **10**: 596166.

Huang, B., J. Wang and L. Li. 2023. Recent five-year progress in the impact of gut microbiota on vaccination and possible mechanisms. *Gut Pathog* **15(1)**: 27.

Jin, S., X. Lu and C. Xu. 2022. COVID-19 induces gastrointestinal symptoms and affects patients' prognosis. *J Int Med Res* **50(10)**: 1-11.

Kim, C. H. 2021. Control of lymphocyte functions by gut microbiota-derived short-chain fatty acids. *Cell Mol Immunol* **18(5)**: 1161-1171.

Kumar, M., M. M. James, M. Kumawat, B. Nabi, P. Sharma, N. Pal, S. Shubham, R. R. Tiwari, D. K. Sarma and R. Nagpal. 2022. Aging and Microbiome in the Modulation of Vaccine Efficacy. *Biomedicines* **10(7)**: 1545.

Lynn, D. J., S. C. Benson, M. A. Lynn and B. Pulendran. 2022. Modulation of immune responses to vaccination by the microbiota: implications and potential mechanisms. *Nat Rev Immunol* **22(1)**: 33-46.

Maciel-Fiuza, M. F., G. C. Muller, D. M. S. Campos, P. do Socorro Silva Costa, J. Peruzzo, R. R. Bonamigo, T. Veit and F. S. L. Vianna. 2023. Role of gut microbiota in infectious and inflammatory diseases. *Front Microbiol* **14**: 1098386.

Panchal, N., R. Kamal, K. Orgera, C. Cox, R. Garfield, L. Hamel and P. Chidambaram. 2020. The implications of COVID-19 for mental health and substance use. *Kaiser Family Foundation* **21**: 1-16.

Ramakrishna, C., M. Kujawski, H. Chu, L. Li, S. K. Mazmanian and E. M. Cantin. 2019. Bacteroides fragilis polysaccharide A induces IL-10 secreting B and T cells that prevent viral encephalitis. *Nat Commun* **10(1)**: 2153.

Reiriz, M., M. Donoso-González, B. Rodríguez-Expósito, S. Uceda and A. I. Beltrán-Velasco. 2023. Impact of COVID-19 confinement on mental health in youth and vulnerable populations: an Extensive Narrative Review. *Sustainability* **15(4)**: 3087.

Rishi, P., A. Kaur and H. Kaur (2021). COVID-19 Pandemic and Mental Illness: Impact of Gut Microbiota. **Delineating Health and Health System: Mechanistic Insights into Covid 19 Complications:** 349-368.

Safadi, J. M., A. M. Quinton, B. R. Lennox, P. W. Burnet and A. Minichino. 2022. Gut dysbiosis in severe mental illness and chronic fatigue: a novel trans-diagnostic construct? A systematic review and meta-analysis. *Mol Psychiatry* **27(1)**: 141-153.

Shahgolzari, M., A. Yavari, Y. Arjeini, S. M. Miri, A. Darabi, A. S. M. Nejad and M. Keshavarz. 2021. Immunopathology and Immunopathogenesis of COVID-19, what we know and what we should learn. *Gene Rep* **25**: 101417.

Sundararaman, A., M. Ray, P. Ravindra and P. M. Halami. 2020. Role of probiotics to combat viral infections with emphasis on COVID-19. *Appl Microbiol Biotechnol* **104**: 8089-8104.

Yao, Y., X. Cai, W. Fei, Y. Ye, M. Zhao and C. Zheng. 2022. The role of short-chain fatty acids in immunity, inflammation and metabolism. *Crit Rev Food Sci Nutr* **62(1)**: 1-12.

Yoo, J. Y., M. Groer, S. V. O. Dutra, A. Sarkar and D. I. McSkimming. 2020. Gut microbiota and immune system interactions. *Microorganisms* **8(10)**: 1587.

Zhang, Y., D. Sun, X. Zhao, Y. Luo, H. Yu, Y. Zhou, Y. Gao, X. Han, Y. Duan and N. Fang. 2022. Bacteroides fragilis prevents aging-related atrial fibrillation in rats via regulatory T cells-mediated regulation of inflammation. *Pharmacol Res* **177**: 106141.

Zheng, D., T. Liwinski and E. Elinav. 2020. Interaction between microbiota and immunity in health and disease. *Cell Res* **30(6)**: 492-506.
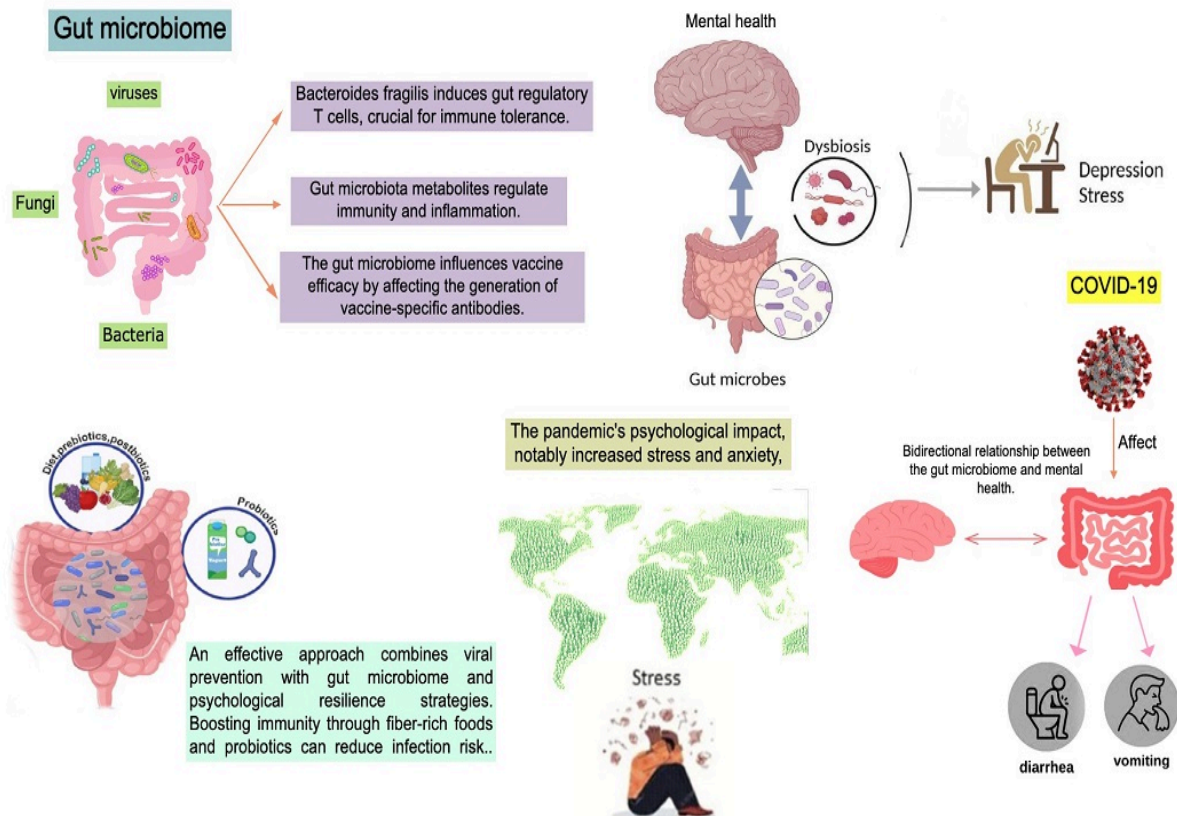
Achene and pollen morphology of the genus *Crepis* L. in Egypt and its systematic significance

Amina. Z. Abo-Elnaga[1], Sami H Rabei[1], Ibrahim A Elgamal[2,*]

[1]Botany and Microbiology Department, Faculty of Science, Damietta University, New Damietta 34517, Egypt; [2] Tilad Environmental Consultation, Riyadh, KSA.

Abstract

In this study, achene, and pollen morphology of *Crepis* L. species in Egypt were investigated by scanning electron microscopy. *Crepis* genus is represented by eight species viz *C. aculeata* (DC.) Boiss., *C. aspera* L., *C.libyca* (Pamp.) Babc. *C. micrantha* Czerep., *C. nigricans* Viv., *C. sancta* (L.) Bormm., *C. senecioide* Del. and *C clausonis* pomel. However, due to occurrence uncertainty regarding *C. clausonis* in Egypt, this study focuses on the remaining seven species. The achenes exhibit morphological diversity, being either homomorphic or dimorphic, with or without a beak, and occasionally winged. Their surface texture varies from smooth to spiculate or scabridulous, with longitudinal ribbing. The pappus is either persistent or deciduous and consists exclusively of setae. Key diagnostic features for differentiating Egyptian *Crepis* species include achene polymorphism, variations in surface sculpturing, shape, beak presence, width, and the minimum and maximum lengths of both peripheral and central achenes, as well as pappus length. The pollen grains of *Crepis* species are characterized as echinolophate and 3-colporate, with apertures located in poral lacunae forming compound structures. The polar area is distinctly defined and covered with echinae. Morphological features such as pollen grain shape and polar area structure hold significant taxonomic value for species delimitation within the genus.This study highlights the importance of achene and pollen traits in distinguishing *Crepis* species in Egypt and provides valuable insights for their taxonomy and classification.

Keywords: Achene characters, *Crepis,* Micro-morphology, pollen characters.

1. Introduction

Crepis genus is a taxonomically problematic, with a lack of perceptive characters (Enke and Gemeinholzer 2008); the genus *Crepis* belongs to subtribe Crepidinae, tribe Lactuceae of the family Asteraceae. Polymorphism is widespread within *Crepis* genus, and many taxonomic features associated with aerial and underground parts vary within a species rather than between closely related species, often leading to unclear species-specific boundaries (Kalmuk, et al 2018). *Crepis* genus comprises about 200 species (Mabberley, 2008), widely distributed in the northern hemisphere and Africa. Eight species were recorded in Egypt *C. micrantha* Czerep, *C. libyca* (Pamp.) Shab., *C. senecioides* Delile, *C. nigricans* Viv., *C. aspera* L., C. *aculeata* (DC.) Boiss and *C. sancta* (L.) Bornm., however, the presence of *C. clausonis* (Pomel) Batt. & Trab. remains uncertain. (Boulos, 2002; 2009).

Both morphology and fruit anatomy provided significant taxonomic information (Karaismailoğlu, 2015). The micromorphological characteristics of the achene viz surface sculpture and the shape of the pappus and its ultrastructure are often used to classify and identify different genera and taxa of the tribe Cichorieae (Pak *et al*., 2001; Zhu *et al*., 2006; Kilian, *et al* 2009; Zhang *et al*., 2013; Karanović *et al*., 2016. However, there are only a

few taxonomic studies on the achenes micromorphs of the genus *Crepis*, and these are limited in range and restricted to a limited representative of the genus (Enke, 2009; Karaismailoğlu, 2015; Inceer *et al*., 2016). Therefore, based on the previously studied, a comprehensive investigation of the micromorphological structure of *Crepis* achenes has not yet been conducted.

Pollen morphology is highly significant for the taxonomist; the taxonomic and evolutionary importance of pollen morphology may be at specific, generic and/or higher levels (Davis and Heywood, 1973).

Wortley *et. al.,* (2012) presented a bibliography of one hundred and seventy-two references which indicates the great level of research activity currently taking place in Asteraceae pollen grains morphology.

Pollen grains of Lactuceae were first examined in detail by Wodehouse (1935). Comprehensive surveys of pollen grains in the tribe Lactuceae were carried out by Tomb (1975), Blackmore, (1976), and Skvarla *et al*. (1977). Pollen morphology of some Egyptian species of Lactuceae was studied by Abou El-Naga (1990) and Abou El-Naga and El- Housseini (1995) and Osman (2006). The most comprehensive pollen studies of Crepidinae are those of Blackmore, and Person (1996) and Wang *et al*. (2009). The objectives of this study are to examine the achene micro morphological as well as pollen grain characteristics

---

* Corresponding author. e-mail: Ibrahim_abdelrafee@yahoo.com.

in 7 species of *Crepis* grown in Egypt, and evaluate its taxonomical significance.

2. Material and methods

2.1 We have studied the achene and pollen morphology of the other 7 species, *C. micrantha* Czer., whi Bormm., *C.libyca* (Pamp.) Shab., *C. senecioides* Delile, *C. nigricans* Viv., C. *aspera* L., *C. aculeata* (DC.) Boiss and *C. sancta* (L.) which considered as a synonym of *Lagoseris sancta* in (Tackholm, 1974; Lack, 2007).

The achenes and pollen grains were taken from herbarium specimens, kept in the Cairo University (CAI), Royal Botanic Gardens (K) and British museum natural history (BM) herbaria. Table (1) lists these specimens with locality, date of collection, name of the collectors and the number. Nomenclature followed (Boulos 2002; 2009); purification of scientific name followed The *Plant List* https://wfoplantlist.org/ and catalogue of life http://www.catalogueoflife.org/col/search/all/key/Crepis+sancta+/fossil/1/match/1

Table 1. Herbarium samples and collectors. s.n. –collecting number is missing. (CAI) = Cairo University herbarium, (K) = Royal Botanic Gardens herbarium and (BM) = The Natural History Museum Herbarium.

Species	Locality	Date of collection	Collector and number	Herbarium
C. micrantha	Mit El Kholi Moumen, Dikirinis, Dakahlia.	21.5.1967	V. Täckholm s.n.	CAI
	Damietta.	1.5.1922	Simpson 1205	K
	Kharga Oasis	17.4,1876	Ascherson 333	K
C. sancta	Wadi El Higaini, N. Galalah	4.4.1924	Simpson 2609	K
	Wady east of (Anthony's) monastery.	23.3.1928	Simpson 5830	K
	Sinai	23.4.1835	W. Schimper 409	K
C. lybica	Daba'a Mariut coast	31.3.1927	Simpson 4650	BM
	Mersa Matruh	1904	Ball 47	K
	Wadi Habs bet. Mersa Matruh and Agiba	24.3.1974	V. Täckholm s.n.	CAI
C. senecioides	Between Matruh and Barrani	11.4.1932	Shabetai 4760	K
	El Khanka,sandy wast ground	26.1.1923	Simpson 1761	K
	Sinai,Wadi Ferieh, Abu Zeitun	24.4.1961	V. Täckholm s.n.	CAI
C. nigricans	Ad Pyramides Egypt	17.2.1834	Wiest 59	BM
	Abou Roash village	27.4.1924	Simpson 2788	K
	Girgeh	23.4.1874	Schweinfurth 49	K
C. aspera	Mariut: Burg El Arab	15.3.1928	G. Täckholm S.n	CAI
	Rafah, near the station	22.3.1928	G. Täckholm s.n.	CAI
	Suez	2.1906	Muschler s.n.	K
C. aculeata	Sinai: Rafah,Bir el Meleha at the coast.	22.3.1928	G. Tackholm s.n.	CAI
	Sinai, in the garden of Deir el Rabba	25.4.1961	V. Tackholm s.n.	CAI
	Catherin, wadi Tih	8.10.1983	El Hadidi s.n.	CAI

2.2 For achenes, five mature achenes as well as the five pappus were mounted on an adhesive surface on the metal holder for SEM; a total of 48 achenes qualitative and quantitative characters were investigated (table 2).

2.3 For pollen grains scanning using electron microscope, a droplet of acetolyzed containing 10 -15 pollen grains in water suspension was pipetted on to photographic film; this film was attached to SEM stub. The specimens were examined and photographed with Scanning electron microscope (Jeol JSM-25S) at 25 KV in the Electron Microscope Unit, King's College London. A total of 15 qualitative and quantitative characters were investigated (table 3). Data were statistically analyzed using Past software; one factor analysis of variance (ANOVA) was used to examine differences in the mean values among taxa overall, using SPSS (version 22)

3. Terminology

The terminology of the achene microstructure follows Barthlott (1981; 1984); the pollen terminology follows Wodehouse (1928; 1935).

4. Result and Discussion

4.1. Achene characters

4.1.1. Achenes are homomorphic or 2 (-3) - morphic, beaked or not, occasionally winged, smooth, spiculate or scabridulous, longitudinally ribbed. The pappus is either persistent or deciduous and consists exclusively of setae. Based on Achene similarity, achenes of studied species (Fig 1) were classified into two major classes:

(1). Homomorphic achenes (represented by two species); are beakless, 1.5-2 mm long, subcylindrical, glabrous, furrows minutely tuberculatus with truncate apex and pappus 3.5-4 mm long in *C. micrantha* but they are

beaked, 8-13 mm long, curved, 10 ribbed Antrosely spinulose on the ribs and pappus 7-8 mm long in *C. Libyca*.

(2) Heteromorphic achenes including three sub-groups (A) first sub-group; includes achenes that are beakless (both the peripheral and the central achenes) this sub-group includes only one species; includes only *C. sancta* where the m peripheral arginal achenes are 3-4 x 0.5-1.5 mm, oblong, sulcate or smooth, while the central achenes are 3-4 x 0.5 mm, whitish fusiform, ribbed scabridulous, furrows.

B) Second sub-group; includes two types of achenes; the peripheral achenes are beakless, but the central achenes are beaked this sub-group includes two species; *C. aspera* and *C. aculeate*. Where the peripheral achenes in *C. aspera* are 5-6 x 0.5 mm, beakless, Pale Straw colour, strongly compressed, winged while its central achenes are 4-7 x 0.4 mm, beaked, brown, with Deciduous pappus.

Moreover, the outer achenes of *C. aculeate* are 7-8 x 1 mm, slightly compressed, pubescent, yellowish or brownish while its central achenes are 3-3.5 x 0.5 mm, fusiform, glabrous in.

C) The third sub-group comprises two species: *C. senecioides* and *C. nigricans*. which is characterized by having beaked peripheral and central achenes. Moreover, both types of achenes (peripheral and central) in *C. senecioides* are fusiform, with scabridulous surface while the two types of achenes are cylindrical in *C. nigricans*. Furthermore, the peripheral achenes in *C. senecioides* are 1-1.8 x 0.5 mm, compressed, beak 3.5-5.5 mm, while central achenes 3-4 mm, beak 3-4 times as long as the achene body. However, the peripheral achenes in *C. nigricans* are 3-3.5 x 0.2 mm, with coarse beak, beak as long as the body, while the central achenes 5-6 x 0.25 mm, with fine beak, beak 1/3-1/2 the body.
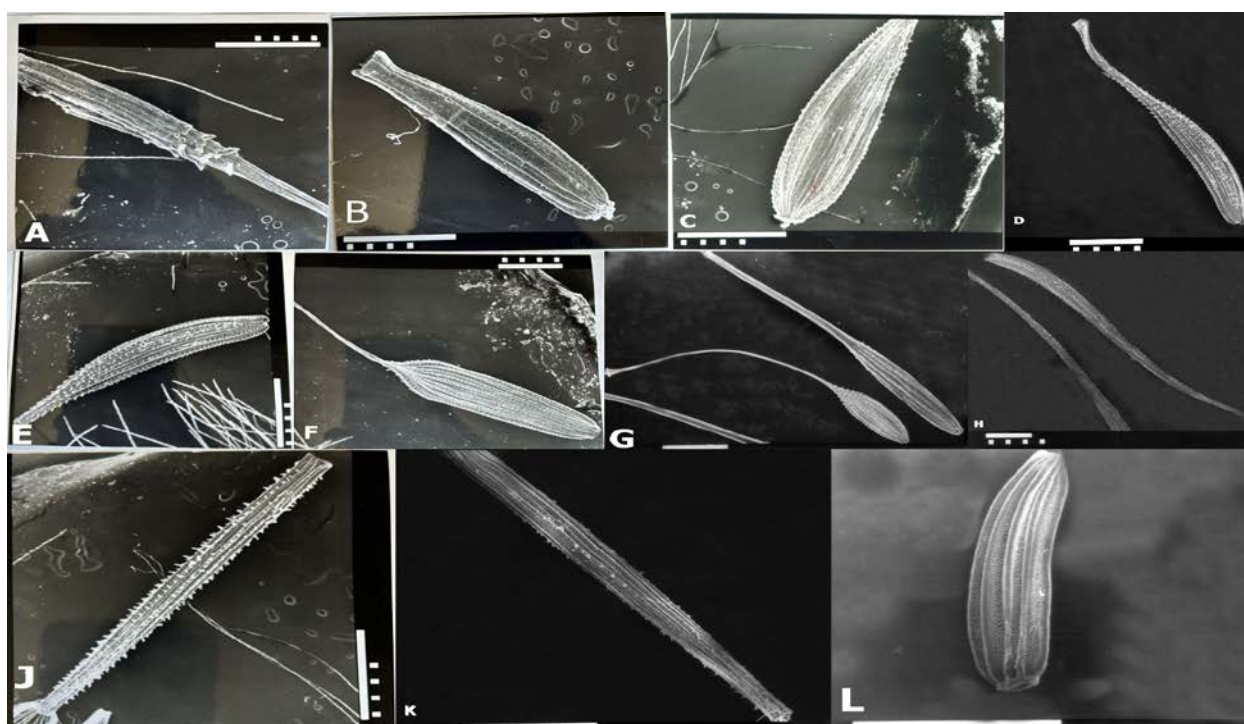
Figure 1. *Crepis* achene; A = *C. aculeata* central achene, B = *C. aculeata* peripheral achene, C= *C. aspera* peripheral achene, D= *C. aspera*, central achene, E = *C. nigricans* central achene, F = *C. nigricans* peripheral achene, G= *C. seneciodes* peripheral achene on top , central achene on down, H = *C. lybica*, J = *C. sancta* central achene , K = *C. sancta* peripheral achene, L= *C. micrantha*, (The scale = 1mm).

3.1.2 A cluster analysis was performed to generate a dendrogram (Fig.2) illustrating the possible relationship between the investigated *Crips* species The analysis was based on Euclidean distance and the paired group method, with achene characteristics and pappus length being the key traits that differentiated the studied species into two main clusters. The first cluster comprised *C. libyca* and was separated from the other species by the maximum length of the peripheral arches. The second cluster included the remaining six species, which were divided into two main subgroups based on peripheral arches dimensions (minimum, maximum length and width): the first group included both *C. micrantha* and *C. sencioides*; the second subgroup included *C. aculeata* in a separate branch and the remaining three species were aggregated in sub-cluster; this agreed with Enke (2008) and Kilian *et al.*

(2009) who found that the pappus is generally an important character for distinguishing groups at all taxonomic levels in the tribe Cichorieae. Achene characteristics such as shape, number of ribs and size as well as pappus shape have been shown to be of significant importance for both phylogeny and the taxonomy genus *Crepis*, and this result is in line with the outcomes cited by Babcock (1947a, 1947b) and Enke (2009).

Statistically, significant differences are found in Marginal and central achene max, minimum length and width, pappus maximum and minimum length (*p<0000)*, Table (2).

Results obtained (Table2 and Fig 2) indicate that there are significant differences in the achene surface sculpturing among *Crepis* target species with an agreement with Nursen *et al.* (2018) who reported that the achene

surface sculpturing shows a high taxonomic significance in distinguishing between the 26 for *Crepis* taxa from Turkey. According to Babcock (1947b), peripheral achenes differed morphologically from the central ones, i.e were dimorphic in some species of *Crepis*. (Fig 1). Among the studied taxa, *C. aculata*, *C. aspera*, *C. sancata*, *C.seneciodes* and *C.nigricans* are annual species and have dimorphic achenes in agreement with Imbert (2002) who observed that both annual and biennial species of *Crepis* have dimorphic achenes . The differences in the micro-sculpture between peripheral and central achenes can affect their dispersal ability.

4.1.2. Taxonomic key based on achene micro-characters.

1. Achenes monomorphic …………………………. 2
1. Achenes dimorphic ………………………………3
2. Achenes short (1.5-2 mm); subcylindrical; ribs glabrous; beakless ……. *C. micrantha*
2. Achenes long (8-13 mm); fusiform ±curved; ribs antrosely spinulose; beaked………………………………….…...*C.lypica*

3. All achenes beakless; achenes Sulcate or smooth ………………….…C. *sancta*
3. All (or at least the central) achenes beaked; ……………………………………….4
4. Peripheral achenes winged; Pale Straw colour, apex not beaked …………….…*C. aspera*
4. Peripheral achenes not winged ……………………………………..……………5
5. Pappus persistent, Peripheral achenes slightly compressed, pubscent, tapering beakless ………………………………………*C.aculeat*
5.Pappus deciduous…………………………………… 6
6.a. Peripheral achenes cylindrical, with rugulose coarse beak surface, beaked as long as the body …………………………………………………….………………... *C. nigricans*
6.b. Peripheral achenes compressed Fusiform, with Scabridulous. 10 ribbed surface and capillary beaks. 3.5-5.5 mm ………………………………… *C. senecioides*

Table 2. showing achenes micro-morphological characters. One-way ANOVA's were performed separately for each of the achene feature to determine the differences among *Crips*. (*p<0.05*)

Species		C. micrantha	C. libyca	Crepis sancta	C. senecioides	C. nigricans	C. aspera	C. aculeata	ANOVA
Achene morphisms		Homomorphic	Homomorphic	Dimorphic	dimorphic	dimorphic	dimorphic	dimorphic	
Peripheral achenes	min length (mm)	1.5	8 including beak	3	1	3.5	5	7	.000
	max length (mm)	2	13 (including beak)	5	1.8	5	6	8	.000
	Width(mm)	0.4	0.8	1	0.5	0.2	0.5	1	.000
	Shape	subcylindrical	fusiform ±curved	Oblong	Fusiform, compressed	cylindrical	Strongly compressed. Winged 10 ribbed	Slightly compressed	
	colour	Tawny brown	brown	whitish	whitish	whitish	Pale Straw colour	Yellowish or brownish	
	Surface	Ribs glabrous, furrows minutely tuberculatus	Antrosely spinulose on the ribs, 10 ribbed	Sulcate or smooth	Scabridulous. 10 ribbed	rugulose coarse beak	Minutely scabridulous	pubescent	
	apex	Truncate beakless	Beaked (4-7 mm)	Truncate, not beaked	Beaked. 3.5-5.5 mm capillary	Beaked as long as the body	Attenuate to a narrow apex not beaked	Tapering beakless	
Central achenes	min length (mm)	-	-	3	3	5	4	3	.000
	max length (mm)	-	-	4	4	6	7	3.5	.000
	Width (mm)	-	-	0.5	NA	0.25	0.4	0.5	.000
	shape	-	-	fusiform	fusiform	cylindrical	Fusiform 10 ribbed	fusiform	
	colour	-	-	brown	Dark brown	brown	brown	brown	
	Surface	-	-	Ribbed, Scabridulous furrows tuberculatus	Scabridulous	Fine beak	Scabridulous	Glabrous striate	
	Apex	-	-	Tapering to truncate not beaked	Beak 3-4 times as long as the achene body	Beak1/3-1/2 the body	Beak 2.5-3 mm	Beak as long as the body	
Carpopodium m	character	-	Well developed	Well, developed	-	Well developed	Well developed	Well developed	
	No. of interruptions	-	4	4	-	4	4	2-4	
pp	duration	persistent	persistent	persistent	deciduous	deciduous	Deciduous	persistent	

Species	C. micrantha	C. libyca	Crepis sancta	C. senecioides	C. nigricans	C. aspera	C. aculeata	ANOVA
Min length (mm)	3.5	7	3.5	1.5	4	3	4	0.002
max length(mm)	4	8	4	5	N. A	4	5	.000
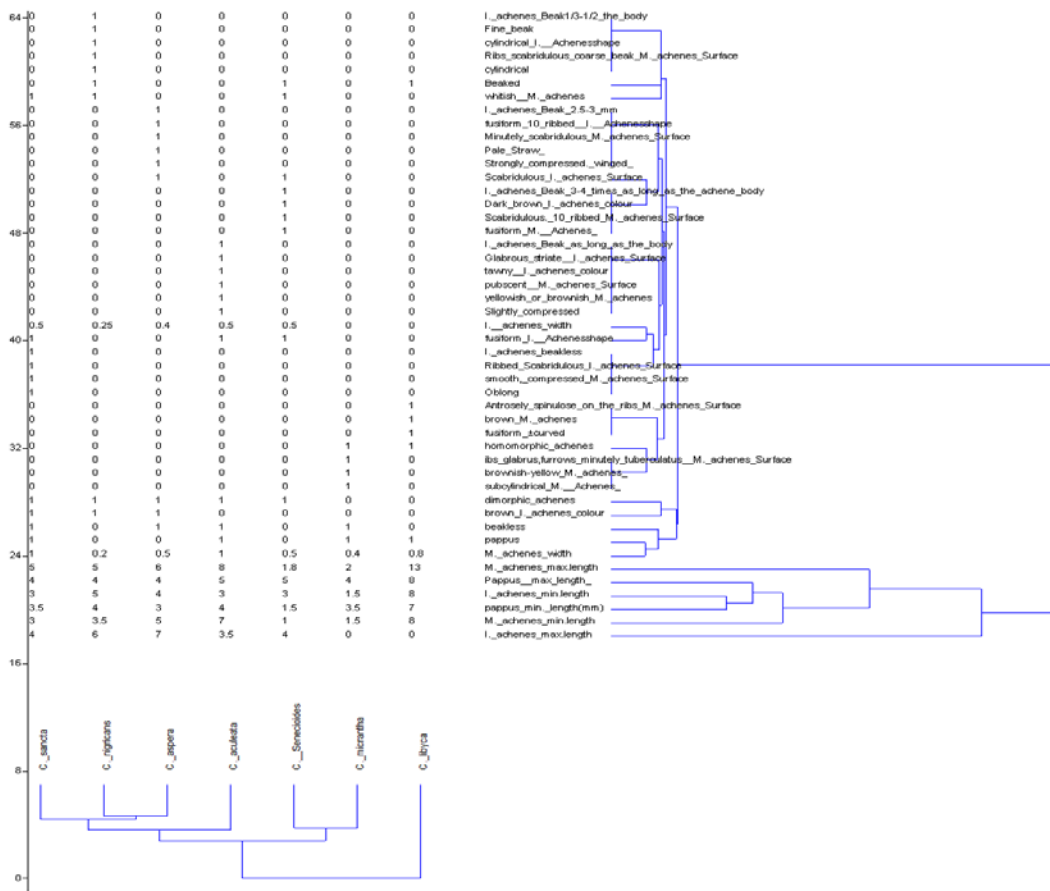
SS

Figure 2. Dendrogram showing the similarity between *Crepis* species using Euclidean distance and the paired group method based on the 48 achene characters

4.2. Pollen grains character

Pollen grains with 15 lacunae (3 poral, 6 paraporal and 6 abporal); 3-colporate, the apertures are situated in poral lacunae flanked in the meridional direction by two abporal lacunae, The poral lacunae are interconnected with the abporal lacunae through interlacunar gaps. The aperture is compound, consisting of:Ectoaperture: A long, broad colpus, divided into three lacunae.

1) Mesoaperture: A slightly elliptical, lolongate porus.
2) Endoaperture: A colpus, lolongate, short, with an acutely tapering end.

The polar area is well-defined and covered with echinae.

4.2.1. ; the polar area is well- defined and provided with echinae. (Table 2; Fig 3)

4.2.2. Based on pollen grain shape, investigated species divided into two main groups:

the first is spheroidal included only *C. sancta*; the second one is oblate-spheroidal that included the rest of studied species. The polar area has small concavities as in *C. Lybica*, while it is solid in the other species; this agrees with the finding mentioned by Osman (2006). It was noticed that the pollen size of the studied taxa ranges from 25 x26 µm (in *C. sancta*) to 41 x 48 µm (in *C. aculeata*). However, the Equatorial diameter ranges between 27 ±0.1 µm (in *C. sancta*) to 34.7 ±1.7 µm (in *C. micrantha.*). Furthermore, the number of echinae in polar area ranged between1- as in *C. aculeata* to 10) as in *C. nigricans.* Moreover, the Exine thickness ranged between 4 µm (in *C. micrantha*) to 7 µm) (in *C. aculeata*). In addition, the long axis of polar area extended between 8µm) as in *C. sancta* to 16 µm as in *C. senecioides.* (Table 3)

Palyno-taxonomical features of pollen grains result shows that *C. sancta* pollen grains are the smallest among the studied species, while C*. aculeata* pollen grains are the largest. Pollen grain shape, as well as the polar area, are useful taxonomic features. A cluster analysis was performed to generate a dendrogram (Fig.4), illustrating the possible relationship between the investigated Crips species using Euclidean distance and the paired group method examined Crips micro-morphological characters. The minimum and maximum Polar axis as well as Equatorial diameter were the most important characters

that separated the studied into two main clusters. The first cluster comprised both C. *aculeata* and *C. senecioides.* The second cluster comprised two subclusters with two sub-groups, one of them included only *C. sancata* and the second subgroup comprised the rest of studied species. Those results are compatible with Akyalçin and Altan (2024), where they concluded that both equatorial and Polar axis dimensions were smaller and significantly different between *Crepis* species growing in Türkiye.

Statistically significant difference was determined among the examined species, regarding all the analyzed quantitative pollen features (p < 0.0005), significant differences were observed in maximum and minimum polar axis, equatorial diameter, and number of echinae in the polar area. However, other features, such as P/E ratio, exine thickness, and exine length, were statistically non-significant (p > 0.0005).

Table 3. Showing pollen grain features (the first value indicates mean value ± standard deviation, while values between bracts indicates minimum and maximum values respectively. One-way ANOVA's were performed separately for each of the pollen grain feature to determine the *Crepis* species. (*p<0.05*)

Species	Polar axis (mm)	Equatorial diameter (mm)	P/E	shape	Exine thickness	Echina length	Echina apart	Long axis of polar area (mm)	Number of echinae on polar area (mm)	polar area
C. micrantha	30.3 ±1.5 (28- 35)	34.7 ±1.7 (30-35)	0.87	OS	4 ±0 (4)	2 ±0 (2)	2 ±0 (2)	12.8 ±1.2 (11-14)	5.7 ±1.4 (3-5)	Solid
C. sancta	27 ±0.2 (25-27)	27 ±0.1 (26-27)	1.0	s	4.5 ±0.5 (4-5)	2 ±0 (2)	2.6 ±0.2 (2.5 3)	9.1 ±0.9 (8-11)	5.2 ±1.5 (3-10)	Solid
C. lybica	32.1 ±2.3 (28- 35)	34.2 ±2.6 (28-35)	0.93	OS	5 ±0.5 (4-6)	2 ±0.5 (1-3)	2.25 ±0.2 (2-2.5)	10.3 ±0.8 (9-11)	7.7 ±1.7 (5-10)	concavities
C. senecioides	32.5±1.5 (30-36)	37.4 ±2 (35-43)	0.86	OS	5.5 ±0.5 (5-6)	2.5 ±0.5 (2-3)	2.5 ±0.5 (2-3)	!4.6 ±0.9 (13-16)	6 ±2 (4-7)	Solid
C. nigricans	31.1 ±1.7 (28-34)	34.5 ±1.4 (32-35)	0.90	OS	5 ±0 (5)	2 ±0 (2)	2.3 ±0.2 (2-2.5)	13.2 ±1.5 (12-16)	9.9 ±1.8 (8-10)	Solid
C. aspera	30.6 ±2.3 (26-34)	34.3 ±2.5 (29-35)	0.89	OS	4.6 ±0.7	2.1 ±0.3 (2-3)	2.2 ±0.3 (2-3)	!0.7 ±1.4 (9-14)	6 ±2.3 (3-10)	Solid
C. aculeata	38.3 ±1.8 (34-41)	43.8 ±2.9 (35-48)	0.87	OS	6.2 ±0.6 (5-7)	3 ±0 (3)	2.6 ±0.3 (2-3)	11.2 ±1.2 (11-13)	3 ±1.5 (1-5)	Solid
ANOVA	0.000	0.000	0.594		0.172	0.835	0.956	0.000	0.000	0.000

Figure 3. pollen grain of studied *Crepis* species. A = *C. sancta*; B = *C. seneciodes;* C= *C. micrantha*, D= *C. lybica*, E = *C. aculeata*; F = *C. nigricans* and G = *C. aspra* (scale line equal 10 microns)
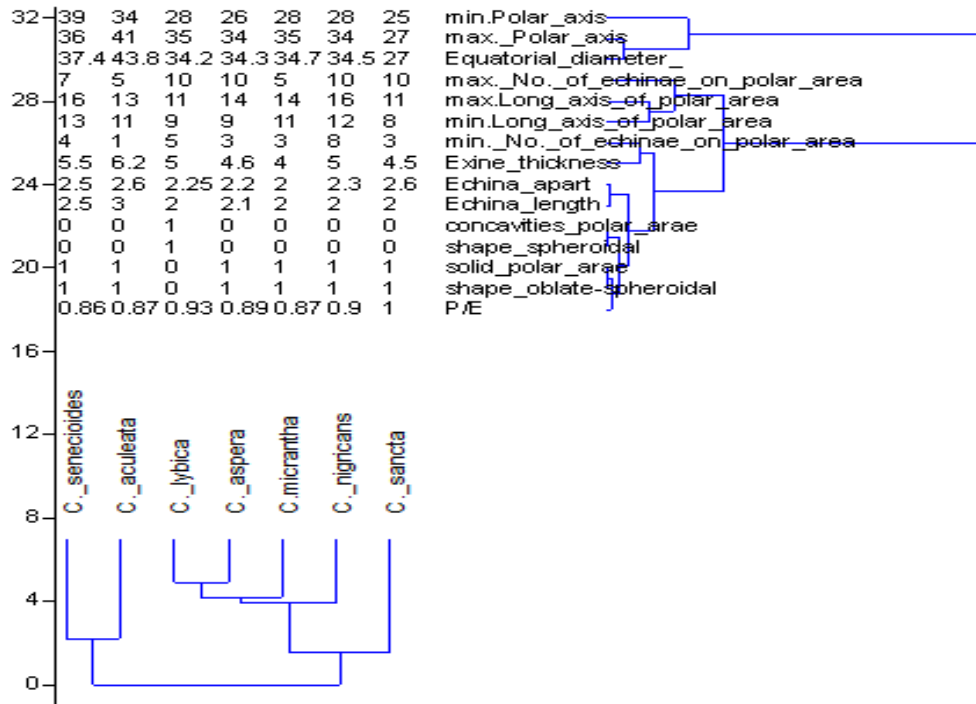
Figure4. Dendrogram showing the similarity between *Crepis* species using Euclidean distance and the paired group method based on 15 pollen characters.

4.2.3. Key to the studied species based on pollen grain.

1 Pollen grains are spheroidal …………………………………………………*C.sancata*

1 Pollen grains non spheroidal ……………………………………………………2

2 The polar area has small concavities………………………………… *C. Lybica*

2 The polar area solid…………………………………………………………3

3 a. Equatorial diameter ranged between (35- 48 µm) …………………........... *C.aculeata*

3 b. long axis of polar area ranges between (11-14 µm); polar axis ranges between (28- 35 µm) ………………………………………....... *C. micrantha*

3 c. long axis of polar area ranges between (12-16 µm); number of echinae on polar area (8-10) .... *C. nigricans*

3 d. Equatorial diameters ranged between (35-43 µm), number of echinae on the polar area 4-7 …………………………………………. *C. senecioides*

3 f. Equatorial diameters ranged between ((29-35µm), Long axis of polar area ranged between (9-14 µm) ……………………………………………….. *C. aspera*

5. Conclusion

Achene and pollen micro-morphology of seven *Crepis* species grown in Egypt were investigated. The present study documented that achenes morphisms as well as the differences in the achene surface sculpturing, achenes, shape, and beaks are valuable for delimitation the Egyptian *Crepis* species. Also, pollen grain shape, as well as the polar area, are useful taxonomic features.

References

Abou El-Naga A. 1990. Taxonomical and Palynological studies of some species of Compositae in Egypt, Ph. D. thesis. Mansoura University.

Abou El-Naga A and El-Husseini N. 1995. Systematic revision of Compositae in Egypt. *Picris* L. Bull. Fac. Sci., Assiut Univ., **24**(1-D), pp. 251-266 (1995).

Akyalçin HM. and Altan S. 2024. Palynology of Taxa of *Crepis* L. Genus Growing in Çanakkale, Türkiye. KSU J. Agric Nat **27** (**1**), 82-91. https://doi.org/10.18016/ksutarimdoga.vi.1288895 K

Barthlott WG. 1981.Epidermal and seed surface characters of plants: systematic applicability and some evolutionary aspects. Nord. J. Bot **1**: 345-355.

Barthlott WG. 1984.Microstructural features of seed surface. In: Heywood VH, Moore DM, eds. **Current concepts in plant taxonomy**. London: Academic Press, 95-105.

Babcock, E. B. 1947a. **The Genus *Crepis*. Part One: The Taxonomy, Phylogeny, Distribution and Evolution of *Crepis***. Berkeley and Los Angeles: University of California Press.

Babcock, E. B. 1947b. **The Genus *Crepis*. Part Two: Systematic Treatment**. Berkeley and Los Angeles: University of California Press

Blackmore S. 1976. Palynology and systematics of tribe Cichorieae, family Compositae. Reading: Unv. Reading. Ph.D. Thesis.

Blackmore S. and Person V. 1996. Palynology and systematics of Crepidinae (Compositae: Lactuceae). Proc. Int. conf. London (pp. 111-122). Kew: R. Bot. Gard.

Boulos L. 2002. **Flora of Egypt**. Verbenaceae – Compositae. Cairo, Egypt: Al Hadara Publishing.

Boulos L. 2009. **Flora of Egypt**, checklist. Al-hadara Publishing.

Davis PH. and Heywood VH. 1973. **Principles of Angiosperm Taxonomy**. Krieger, New York.

Enke N. 2008. **Phylogeny and Character Evolution in the Genus *Crepis* L.** *(Cichorieae, Compositae).* Freien university, Berlin.

Enke N. 2009. Contributions Towards a Revised Infrageneric Classification of *Crepis* (Cichorieae, Compositae)." Willdenowia **39**: 229–245.

Enke N. and Gemeinholzer B. 2008. Babcock Revisited: New Insights into Generic Delimitation and Character Evolution in *Crepis* L. (Compositae: Cichorieae) from ITS and matK Sequence Data." Taxon 57: 756–768.

Imbert E. 2002. Ecological Consequences and Ontogeny of Seed Heteromorphism. PPPEES **5**: 13–36.

Inceer H N., Aksu Kalmuk KV., Imamoglu O., Duman S., Hayirlioglu A, and Arslan G. 2016. Micromorphological, Anatomical and Cytogenetical Studies in Endemic *Crepis macropus* Boiss. & Heldr. (Asteraceae) from Turkey." Acta Bot. Croat. **75**: 173–178.

Jana B. and Mukherjee S K. 2014. Marker characters of cypsela in three taxa of lactuceae (Compositae). ISSN: 0971-2976. J. Botan. Scc. Bengal, **68(1):** 59-64.

Kalmuk N., Inceer H. & Imamoglu K (2018): Achene micromorphology of 26 *Crepis* L. (Asteraceae) taxa from Turkey with notes on its systematic and ecological significance, Bot. Lett., DOI: 10.1080/23818107.2018.1452167

Karanović D., Zorić B., Zlatković P. Boža, and Luković J. 2016. Carpological and Receptacular Morpho- Anatomical Characters of *Inula*, *Dittrichia*, *Limbarda* and *Pulicaria* Species (Compositae, Inuleae): Taxonomic Implications. Flora 219: 48–61.

Karaismailoğlu MC. 2015. Morphological and anatomical features of Cypsela of some *Crepis* taxa (Asteraceae) from Turkey and their taxonomic importance. Pak. J. Bot. **47(4)** 1473-1480.

Kilian N., Gemeinholzer B. and Lack HW. 2009. In Funk, *et al*.(ed) (2009) "*Cichorieae*." In **Systematics, Evolution and Biogeography of Compositae**, 343–383. Vienna: International Association for Plant Taxonomy.

Lack HW. 2007. Tribe Cichorieae Lam. & DC. In J. W. R. Kadereit & C. Jeffrey (Eds), **The families and genera of vascular plants** Vol. 8. Flowering plants. Eudicots. Asterales (pp. 180-198). Berlin: Springer.

Mabberley DJ. 2008. **Mabberley's Plant Book**. Third Edition. Cambridge University Press, UK.

Nursen A., Huseyin I. & Kemal Vehbi Imamoglu .2018.: Achene micromorphology of 26 *Crepis* L. (Asteraceae) taxa from Turkey with notes on its systematic and ecological significance, Bot.Lett., DOI: 10.1080/23818107.2018.1452167

Osman A. 2006. Pollen types of the Egyptian species of tribe Lactuceae (subfamily Cichoroideae-Compositae). Acta Bot. Croat., **65**, 161-180.

Pak J H. Park J. and Whang SS. 2001. Systematic Implications of Fruit Wall Anatomy and Surface Sculpturing of *Microseris* (Asteraceae, Lactuceae) and Relatives. IJPS **162**: 209–220.

Skvarla JJ., Turner BL., Patel VC. and Tomb AS. 1977. Pollen morphology in the Compositae and in morphologically related families. The biology and chemistry of the Compositae. Academic Press, London, New York, NY. pp.141-248.

Tackholm V. 1974. **Student Flora of Egypt** (ed.2), Cairo University.

Tomb RS. 1975. Pollen morphology in tribe Lactuceae (Compositae). Grana, **15**: 79-89.

Wang H., Wortley A H., and Blackmore S. 2009. Pollen morphology of Crepidinae and Lactucinae (Asteraceae: Cichorieae) and its systematic significance. Grana*, **48(3)**, 160– 178. doi:10.1080/00173130902931209

Wodehouse RP. 1928. Phylogenetic value of pollen characters. Ann. Bot. **42**, 891– 934.

Wodehouse RP. 1935. **Pollen grains: Their structure, identification and significance in science and medicine**. New York.

Wortley AH., Blackmore S., Chissoe WF. and Skvarla JJ. 2012. Recent advances in Compositae (Asteraceae) palynology, with Emphasis on unstudied and unplaced taxa. Grana. 51. 10.1080/00173134.2012.668219.

Zhang JW., Boufford DE., and Sun H. 2013. Systematic significance of achene morphology in Soroseris, Syncalathium and Parasyncalathium (Asteraceae: Cichorieae). Bot. J. Linn, **173 (3),** 476–486.

Zhu SX., Qin HN., and Shih C. 2006. Achene wall anatomy and surface sculpturing of Lactuca L. and related genera (Compositae: Lactuceae) with notes on their systematic significance. J. Integr. Plant Biol., **48(4),** 390–399

JJBS

Jordan Journal of Biological Sciences

Effects of Lyophilized Leech Saliva Extract on Cell Migration and Apoptosis in MDA-MB-231 Breast Cancer and HUVEC Cell Lines

Kübranur ÜNAL [1,*], Nihan TIRIK [2], Mehmet Emre EROL [3], Mustafa GÜNGÖRMÜŞ [4], Hüseyin AYHAN [5]

[1] Gazi University, Faculty of Medicine, Department of Medical Biochemistry, Ankara, Turkiye; [2,3] Gazi University, Institute of Health Sciences, Medical Biochemistry, Ankara, Turkiye; [4] Yildirim Beyazit University, Faculty of Dentistry, Basic Sciences, Ankara, Turkiye; [5] Yildirim Beyazit University, Vocational School of Health Services, Department of Medical Services and Techniques, Ankara, Turkiye

Abstract

Breast cancer, a leading global cause of female mortality, necessitates innovative treatment strategies to alleviate the drawbacks associated with conventional therapies. This study explores the potential of Lyophilized Leech Saliva Extract (LLSE) in addressing this need. The impact of LLSE on the MDA-MB-231 breast cancer cells and HUVECs lines was investigated. This research aims to systematically evaluate LLSE's effects on critical cellular processes, including cell migration, apoptosis, necrosis, and viability. Our findings reveal nuanced responses, with LLSE exerting anti-proliferative effects on cancerous MDA-MB-231 cells and a pro-proliferative influence on healthy HUVECs. The study also scrutinises gene expression dynamics, uncovering intricate patterns involving key regulators: EGF (Epidermal Growth Factor), FGF (Fibroblast Growth Factor), and VEGF (Vascular Endothelial Growth Factor). In summary, this research contributes insights into medicinal leech therapy's potential in cancer treatment. With breast cancer treatment's evolving landscape, exploring alternative, less debilitating options becomes crucial. This study addresses this imperative, providing a foundation for future investigations into the rich bioactive compounds in leech saliva.

Keywords: Cell Death, Cell Viability, Cell Proliferation, Leech Saliva Extract, RT-PCR

1. Introduction

Breast cancer arises from the uncontrolled proliferation of epithelial cells originating in the ducts or lobes of the breast. It stands as a significant global health challenge, claiming the lives of approximately 42,000 women each year (Ben-Dror *et al.*, 2022). It is the cancer that causes the most deaths and is the most prevalent among women worldwide (Abdel-Fattah *et al.*, 2006; WHO, 2021). The issue of resistance to conventional chemotherapeutic drugs employed in the treatment of breast cancer remains a significant challenge for scientists. Furthermore, the severe side effects associated with these drugs pose additional concerns. Addressing these challenges is crucial in improving the efficacy and safety of breast cancer treatment strategies. For this reason, scientists today are searching for alternative, more effective treatment methods with fewer side effects (Nedeljković and Damjanović, 2019). When the history of breast cancer treatment is examined, there is evidence that leech therapy has been used for centuries (Karamanou and Androutsos, 2021).

Leeches are members of the Phylum Annelida, also known as the ringed worms. A few species of leeches, mainly in freshwater, also live in terrestrial areas (Elliott and Kutschera, 2011). Although there are more than 600 known leech species, only a few of them (about 15 species) are found in the medical leech category (Baskova *et al.*, 2008; Sig *et al.*, 2017). Medicinal Leech therapy, also known as hirudotherapy, is one of the ancient practices in the history of medicine (Alam *et al.*, 2016). Hirudotherapy has been found in the oldest inscriptions of Egypt, India, Persia, Europe, China, and Anatolia (Gödekmerdan *et al.*, 2011).

At first, it was believed that leech therapy was healing due to the blood-sucking feature of leeches. With the advances in science, biochemical analyses have shown that the therapeutic effects of medicinal leech therapy are actually due to the wide variety of proteins and peptides contained in the saliva of medicinal leeches and secreted into the host's bloodstream during blood sucking (Hildebrandt and Lemke, 2011). According to their specific properties, these molecules show anti-inflammatory, anti-microbial, analgesic, vasodilator, or

---

anaesthetic effects (Sig *et al.*, 2017). The most researched bioactive substances found in medicinal leech saliva are calin and hirudin with anticoagulant properties, bdellins with their anti-inflammatory properties, hyaluronidase with anti-microbial and extracellular matrix degradation activity, acetylcholine and histamine-like substances with their vasodilator effects (Singh, 2010). Previous research has highlighted the potential of leech saliva extract in inhibiting the growth of various tumor types, including gliomas. Studies also show the anti-cancer effects of hirudin, known as an anticoagulant, which is one of the first substances that come to mind regarding leech saliva (Zhao, 2015). Studies have demonstrated the anti-cancer effects of hirudin, an anticoagulant peptide found in leech saliva, which inhibits tumor growth by blocking thrombin and reducing angiogenesis via anti-proliferative properties (Ammar, 2021). Hirudin, along with other bioactive molecules such as eglin and bdellins, contributes to the therapeutic potential of leech saliva by modulating various cellular processes involved in cancer progression (Michalsen *et al.*, 2007; Abdualkader *et al.*, 2013).

Given these promising results of leech therapy in cancer treatment, our study aims to explore the efficacy of lyophilized leech saliva extract (LLSE) on a different cancer type, specifically breast cancer. This experimental study evaluates the effects of different doses of LLSE on cell migration, apoptosis, necrosis, and cell viability of the MDA-MB-231 breast cancer cell line and HUVEC cell line. By examining these parameters, the underlying mechanisms through which LLSE exerts its anti-cancer effects will be understood, and its potential as a novel therapeutic strategy for breast cancer will be explored.

2. Materials and Methods

2.1. Extraction of Leech Saliva

Mediterranean medicinal leech *Hirudo verbana* Carena, 1820 (Clitellata, Hirudinea, Hirudo) is used in this study (Tessler *et al.*, 2018). The leeches were obtained from an approved sterile leech farm in Isparta, Turkiye. The exact origin and species of the leeches were identified using a stereo zoom microscope (Euromex NZ.1903-S, Germany) with a camera to diagnose and examine their morphological characteristics. Morphological criteria were used to confirm the species identification of the leeches (Neubert and Nesemann, 1999; Davies and Govedich, 2001). They were maintained by changing their water regularly every 2-3 days. The leech saliva was obtained without sacrificing the leeches (Abdualkader *et al.*, 2011). All leeches were starved for about three months in case they were fed before. A phagostimulatory solution containing 0.07-M NaCl with 0.0005-M arginine was prepared at 37°C to feed the leeches. After the leeches were satiated, they were kept in a plastic test tube immersed in an ice-filled beaker until they were

temporarily paralyzed and vomited up all the solution they had absorbed. Then, milking was performed by squeezing the leech from the tail to the head to collect the remainder of the leech saliva. Only the colourless (blood-free) salivary fluids vomited by the fed leeches were pooled. Then, this liquid was passed through a membrane filter (Sartorius minisart, Hannover, Germany) to remove unwanted particles. After centrifuging these substances (10 min, 2500 rpm, 4°C), the supernatant was lyophilized (Christ Lyophilizer - Freeze Dryer - Alpha 2-4 LD, Germany) and used in our experiments. The collected samples were kept homogeneous by creating stock, divided into Eppendorf, stored at -20 °C, and protected from light. Freeze drying or lyophilization is the process of sublimation of ice in a frozen material to minimise the amount of liquid in the materials (Smith, 2012).

2.2. Protein Determination of the LLSE

The total protein concentration of lyophilized leech saliva extract (LLSE) was assessed using the Bradford Protein Assay Kit (ABP Biosciences, USA). This assay allows for rapid and specific measurement, minimizing waiting times and potential proteolysis effects (Kielkopf *et al.*, 2020). LLSE doses were adjusted based on protein concentration to the following levels: 800 μg/mL, 400 μg/mL, 200 μg/mL, and 100 μg/mL. The dosage to be used in this study is prepared using serial dilution. To determine the molecular weights of peptides and proteins in LLSE, Sodium dodecyl-sulfate polyacrylamide gel electrophoresis (SDS-PAGE) was employed. A 15% resolving gel using the tris-glycine SDS-PAGE method was utilized, with visualization of protein bands achieved through the Coomassie blue dye method. All experiments were conducted under standard conditions at 25 °C.

2.3. Cell Lines and Cell Cultures

Human Breast Cancer Cell (MDA-MB-231™) and Human Umbilical Vein Endothelial Cell (HUVEC – CRL-1730™) lines obtained from ATCC, USA, were utilized in this study. Cells were transported to our laboratory following manufacturer guidelines under cold chain conditions.

2.4. Cell Viability Test (MTT Assay)

Cell viability and proliferation were assessed utilizing the 3 - (4,5 - dimethylthiazol-2-yl) - 2,5 - diphenyltetrazolium bromide (MTT) assay. The dosage to be used in this study was determined by previously published data (Ünal *et al.*, 2023). Cells were plated and treated with varying concentrations of LLSE (800 μg/mL, 400 μg/mL, 200 μg/mL, and 100 μg/mL), with untreated cells serving as controls. After incubation for 24 or 48 hours, formazan crystals, indicative of viable cells, were dissolved using isopropyl alcohol. Absorbance was measured at 570 nm (BioTek® Synergy HT microplate reader, USA). Cell viability was calculated as follows:

$$\text{Cell viability }(\%) = (\text{Mean absorbance of treated well} / \text{Average absorbance of control well}) \times 100.$$

Control well values were designated as 100% viable cells. Cell viability and cytotoxicity were expressed as percentages relative to control values. Thiazolyl Blue Tetrazolium Bromide (Sigma, USA) was used in the assay. IC50 and EC50 values were determined through serial dilutions of LLSE.

2.5. Cell Migration Assay

Cell migration experiments were done via an xCELLigence, impedance-based real-time cell analyzer (RTCA) device and cell invasion and migration plate (CIM-plate 16) (ACEA Biosciences Inc., California, USA). The CIM plate consists of a top and a bottom

chamber. The top chamber provides wells to hold the cells and is equipped with gold electrodes below a separating membrane to measure the impedance. The bottom chamber contains the cell media, where the LLSE is added. The migration of cells towards the chemoattractant through the membrane is measured by the changes in impedance values on the gold electrodes below the membrane.

100 µL of the DMEM with 10% FBS and penicillin-streptomycin containing the chemoattractants at 200 µg/mL and 800 µg/mL concentrations were added in each well of the bottom well. Media containing no chemoattractant was used as a Control. Then, the top chamber was placed onto the bottom chamber. Medium without the chemoattractant was added to the wells of the top chamber to moisten the membrane. Then, the CIM plate was placed into the DP station for 30 minutes in the cell culture incubator, and a baseline measurement was taken. Then, the MDA-MB-231 cells and HUVECs were seeded into the wells of the top chamber at 4×10^3 cells/well concentration (determined via prior optimization measurements), and the cell index measurements were taken at 30-minute intervals. The cell migration index was calculated as follows:

2.6. Real-Time PCR (RT-PCR)

EGF (Epidermal Growth Factor), FGF (Fibroblast Growth Factor), and VEGF (Vascular Endothelial Growth Factor) expression levels were determined by RT-PCR using EnTurbo™ SYBR Green PCR SuperMix kit (ELK Biotechnology, China). Reactions were performed on the ABI 7500 RT-PCR device (Applied Biosystem, USA). According to the $2^{-\Delta\Delta Ct}$ method, the expression levels of the housekeeping gene were first determined, and then normalisation was determined according to the control. mRNA isolation was performed via Hybrid-R and RiboEx Kit (Gene-All, South Korea), and cDNA synthesis was performed using the EntiLink 1st Strand cDNA Synthesis Kit (ELK Biotechnology, China). The primer sequences are as follows:

(House-keeping gene) GAPDH, 5'-GAAGGTGAAGGTCGGAGTCAAC-3' and 5'-CAGAGTTAAAAGCAGCCCTGGT-3';

FGF, 5′ -AGTGTGTGCTAACCGTTACCT- 3′ and 5′ -ACTGCCCAGTTCGTTTCAGTG- 3′;

VEGFA, 5′ -AGGGCAGAATCATCACGAAGT- 3′ and 5′ -AGGGTCTCGATTGGATGGCA- 3′;

EGF, 5′ -GACAGGCCACCTCGTCG-3′ and 5′ -TGCGTGAGCTTGTTACTCGT- 3′.

2.7. Flow Cytometry

Apoptosis and necrosis in the MDA-MB-231 and HUVEC cell lines were assessed using Annexin V-FITC Apoptosis Detection Kits (BD Pharmingen™, Cat. No: 556570, England). The analysis was performed via flow cytometry using the Accuri™ C6 Plus device (BD Biosciences, UK).

2.8. Statistical Analysis

Data were analyzed using IBM SPSS 21 (IBM SPSS Inc., Chicago, IL) for statistical analyses and GraphPad Prism 5.0 (GraphPad Software, USA) for IC50 and EC50 determinations. Mean ± standard deviation (mean ± sd) was used as descriptive statistics. One-way ANOVA was used to scrutinize mean disparities across multiple groups, while Student's t-test was utilized to compare means

between two distinct groups. Subsequent pairwise comparisons among the groups were conducted using Bonferroni's test at $p < 0.05$ to discern the underlying cause of the observed statistical significance.

IC50 determination and curve fitting were conducted using GraphPad Prism 5.0 software (USA). Each data point represents the average of triplicate samples.

3. Results

3.1. Protein Determination of the LLSE

Analysis of the LLSE using SDS-PAGE revealed the presence of a diverse mixture comprising over 20 proteins/polypeptides, with molecular weights ranging from 13 kDa to 260 kDa (see Figure 1). This indicates a complex protein composition within the LLSE, which may contribute to its bioactive properties.
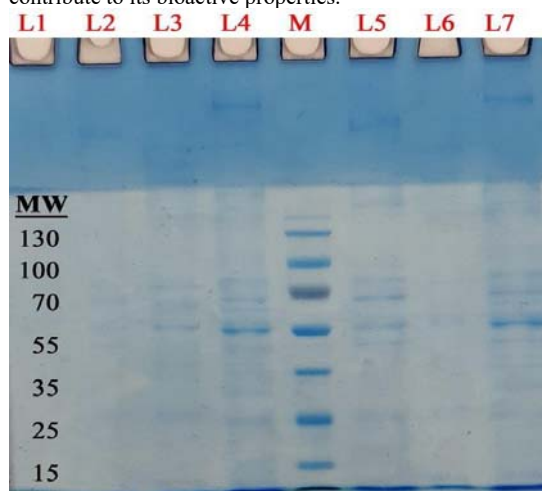
Figure 1. Separation of LLSE peptides and proteins by SDS-PGE method with 15% resolving gel.

M: Molecular Mass Marker (kDa)

Lane 2, 3, 4, 5 ,6 and 7: LLSE

MW: Molecular Weight

3.2. Effect of LLSE on Cell Viability

Following LLSE application for 24 hours or 48 hours in the MDA-MB-231 cell line, IC50 doses were determined to be 470 µg/mL and 467 µg/mL, respectively, indicating a dose-dependent effect of LLSE with consistent efficacy across exposure times (see Figure 2A, and 2B). Conversely, analysis of EC50 results in the HUVEC cell line following LLSE application for 24 hours and 48 hours revealed EC50 doses of 108.4 µg/mL and 150.3 µg/mL, respectively. These findings suggest that a 24-hour LLSE application is preferable, achieving similar outcomes with a lower dose compared to the 48-hour application in terms of proliferation (see Figures 3A and 3B).

The impact of LLSE on proliferation was evaluated in two distinct cell lines: the cancerous MDA-MB-231 cell line and the healthy HUVEC cell line, using the MTT assay. In MDA-MB-231 cells, LLSE doses ranging from 400 to 100 µg/mL showed no significant differences in cell viability compared to the control group at both 24 hours and 48 hours. However, 800 µg/mL resulted in a

considerable decrease in cell viability at both time points ($p < 0.05$) (see Figure 4A and 4B). Conversely, in the HUVEC line, LLSE doses ranging from 800 to 100 µg/mL significantly increased cell viability compared to the control group at both 24 hours and 48 hours ($p < 0.05$) (see Figures 5A and 5B). These results underscore the differential effects of LLSE on cell proliferation between cancerous and healthy cell lines, highlighting its potential as a therapeutic agent with selective cytotoxicity towards cancer cells while promoting viability in healthy cells.
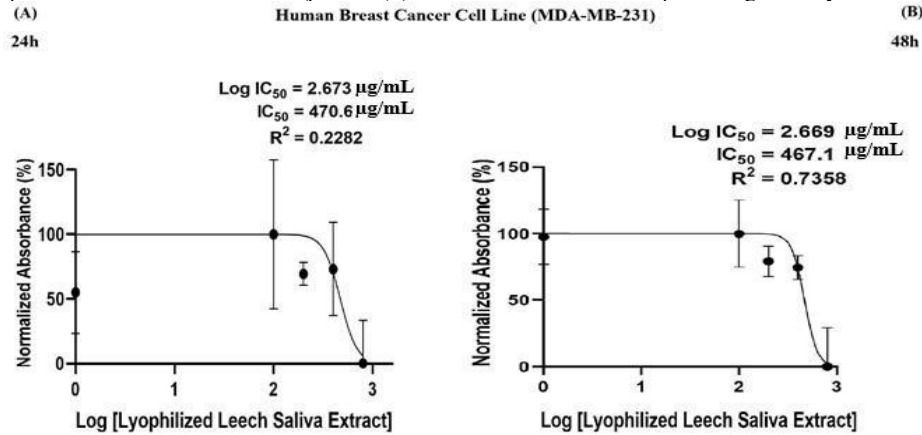
Figure 2: Identification of IC_{50} values in LLSE-exposed **MDA-MB-231** cell line; **(A)** 24h, and **(B)** 48h
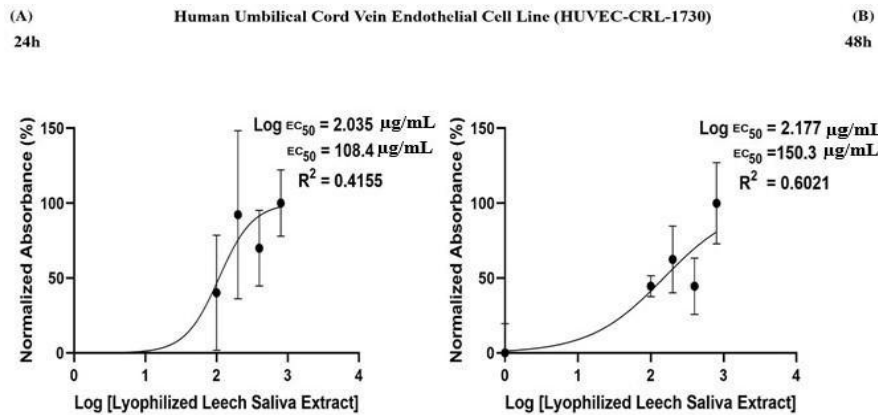
Figure 3: Identification of EC_{50} values in LLSE-exposed **HUVEC** line; **(A)** 24h, and **(B)** 48h
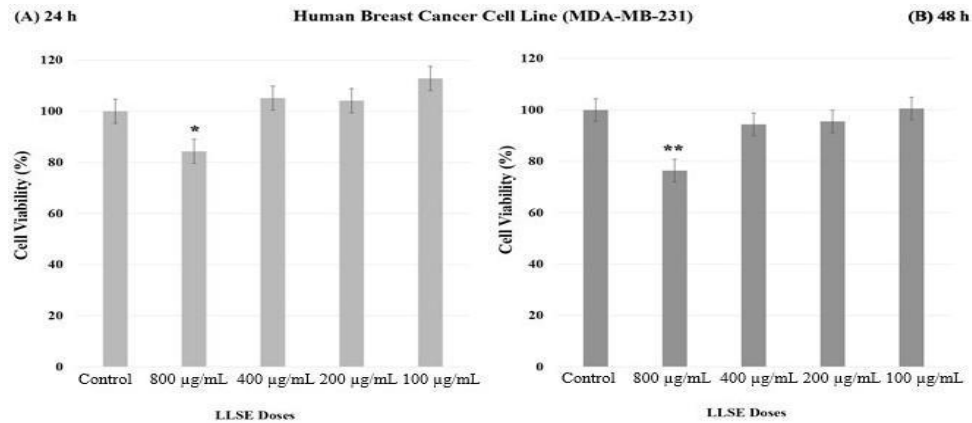
Figure 4: MTT assay for MDA-MB-231 cell line at 24h and 48h

Effects of LSSE on the MDA-MB-231 cell line viability. Data were expressed as mean ± SD of not less than three independent experiments.

All concentrations of LLSE (400–100 µg/mL) did not cause differences, and 800 µg/mL of LLSE decreased the cell viability in **the MDA-MB-231 cell line** compared to the control group at **(A)** 24 h (* $p < 0.05$). **(B)** 48 h)

(A) 24 h

Human Umbilical Cord Vein Endothelial Cell Line (HUVEC-CRL-1730)

(B) 48 h
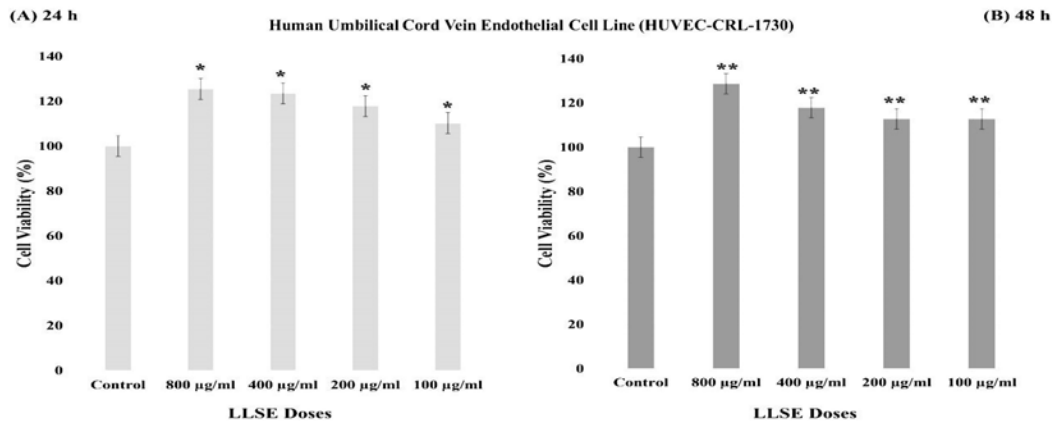
Figure 5. MTT assay for HUVEC line at 24h and 48h

Effects of LSSE on the HUVEC line viability. Data were expressed as mean ± SD of not less than three independent experiments.

All concentrations of LLSE (800–100 µg/mL) significantly increased cell viability in **the HUVEC line** compared to the control group at **(A)** 24 h (* $p < 0.05$). **(B)** 48 h), (** $p < 0.05$).4h and 48 h (** $p < 0.05$).

3.3. Effect of LLSE on Cell Migration

For the MDA-MB-231 cell line, RM analysis showed a statistically significant difference in the cell migration index increase between the dosages ($p < 0.0001$). As shown in Figure 6A, the pairwise comparison indicated that the cell migration index significantly decreased in the 800 µg/mL LLSE compared to the 200 µg/mL LLSE and the control group ($p < 0.0001$).For the HUVEC line, RM analysis showed a statistically significant difference in the cell migration index increase between the dosages ($p < 0.0001$). As shown in Figure 6B, the pairwise comparison indicated that the cell migration index significantly increased in the 200 µg/mL LLSE and the 800 µg/mL LLSE compared to the control group ($p < 0.0001$).

(A)

(B)
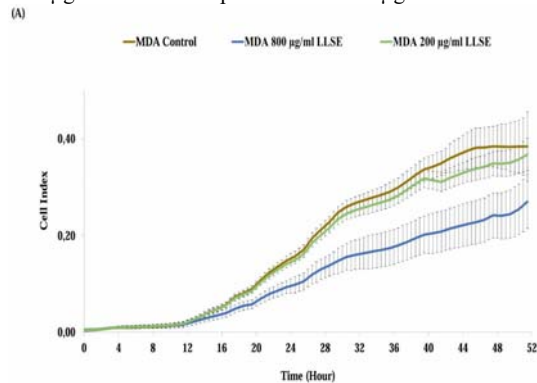
(A) Effects of LLSE on the **MDA-MB-231** cell line.

The graph shows the cell migration index of MDA-MB-231 cells treated with different doses of lyophilized leech saliva extract (LLSE) over a 52-hour period. The groups include the control (no LLSE treatment), 800 µg/mL LLSE, and 200 µg/mL LLSE. The cell migration index was measured every hour for a total of 52 hours. The data points represent the mean ± SD of three independent experiments (n=3).

Error bars indicate standard deviation (SD). A statistically significant difference ($p < 0.0001$) was observed between the groups, with the 800 µg/mL LLSE group showing the most substantial decrease in cell migration index compared to the control and 200 µg/mL LLSE group

(B) Effects of LLSE on **the HUVEC line**.

The graph shows the cell migration index of HUVEC cells treated with different doses of lyophilized leech saliva extract (LLSE) over 52 hours. The groups include the control (no LLSE treatment), 800 µg/mL LLSE, and 200 µg/mL LLSE. The cell migration index was measured every hour for 52 hours. The data points represent the mean ± SD of three independent experiments (n=3). Error bars indicate standard deviation (SD). A statistically significant difference ($p < 0.0001$) was observed between the groups, with the 800 µg/mL LLSE group showing the most substantial increase in cell migration index compared to the control and 200 µg/mL LLSE group.

Figure 6: Migration curves of the MDA-MB-231 cell and HUVEC lines (800 µg/mL LLSE, 200 µg/mL LLSE, and control)

3.4. Effects of LLSE on the mRNA Gene Expressions

In the MDA-MB-231 cell line, FGF mRNA expression significantly decreased in all doses (800, 400, 200, and 100 µg/ mL) compared to the control (* $p < 0.001$). Treatment with 800 µg/mL LLSE notably reduced mRNA expression of EGF, FGF, and VEGF compared to the control group (** $p < 0.001$). Moreover, treatment with 400 µg/mL LLSE significantly increased VEGF and EGF mRNA expression compared to the control and all doses (800, 400, 200, and 100 µg/ mL) (*** $p < 0.001$) (Table 1). Conversely, in the HUVEC line, treatment with 100 µg/mL of LLSE significantly increased mRNA expression of EGF, FGF, and VEGF compared to the control group

and all doses (800, 400, 200, and 100 µg/ mL) (**** $p < 0.001$) (Table 2).

Table 1. mRNA expression levels of EGF, FGF, and VEGFA on the **MDA-MB-231** cell line

Groups	FGF Mean ± SD (n=3)	VEGF Mean ± SD (n=3)	EGF Mean ± SD (n=3)
Control	0,94 ± 0,11	1,15 ± 0,1	1,00 ± 0,10
800 µg/mL	0,35 ± 0,07 *, **	0,85± 0,07 **	0,93 ± 1,17 **
400 µg/mL	0,60 ± 0,06 *	2,57±0,29 ***	2,10 ± 0,39 ***
200 µg/mL	0,37 ± 0, 10 *	1, 58 ± 0,16	1, 56 ± 0,12
100 µg/mL	0,46 ± 0,07 *	1,4 ± 0,24	1,27 ± 0,12
p Value	*$p < 0.001$ **$p < 0.001$	**$p < 0.001$ ***$p < 0.001$	**$p < 0.001$ ***$p < 0.001$

* mRNA expression of FGF was significantly lower in all treated groups compared to the control group, (*p < 0.001).

800 µg/mL of LLSE significantly decreased the mRNA expression of FGF, VEGF, and EGF compared to the control (p < 0.001).

400 µg/mL of LLSE significantly upregulated VEGF and EGF mRNA expression compared to the control and all other groups (p < 0.001).

Table 2. mRNA expression levels of EGF, FGF, and VEGF on the **HUVEC** cell line

Groups	FGF Mean ± SD (n=3)	VEGF Mean ± SD (n=3)	EGF Mean ± SD (n=3)
Control	0,95 ± 0,06	1,15 ± 0,06	0,94 ± 0,17
800 µg/mL	1,80 ± 0,41	0,90 ± 0,20	1,18 ± 1,12
400 µg/mL	1,90 ± 0,70	1,93 ± 0,10	1,91 ± 0,29
200 µg/mL	1,19 ± 0,38	1, 96 ± 0,70	1, 39 ± 0,11
100 µg/mL	3,74 ± 0,46 ****	3,58 ± 0,44 ****	2,48 ± 0,36 ****
p Value	****$p < 0.001$	****$p < 0.001$	****$p < 0.001$

100 µg/mL of LLSE significantly upregulated mRNA expression of FGF, VEGF, and EGF compared to the control and all other groups. (*p < 0.001).

3.5. Effects of LLSE on Apoptosis and Necrosis

While drugs or natural products used in cancer treatment are expected to induce cell death in the cancerous cells, this is the opposite for the healthy cells. Therefore, to observe the effects of LLSE on the cancerous and healthy cell lines, cell lines were analysed by flow cytometry after the cells were exposed to LLSE for 24 hours.

It was determined that all doses (800, 400, 200, and 100 µg/ mL) of LLSE on the MDA-MB-231 cell line caused necrosis; the necrosis percentages were determined as 8.5%, 5.8%, 6.9%, and 6.3%, respectively (see Figure 7A). At the same time, 800 µg/mL LLSE was determined as the dose that caused the most necrosis in the MDA-MB-231 cell line. On the other hand, all doses of LLSE (800, 400, 200, and 100 µg/ mL) did not cause any significant apoptosis or necrosis in the HUVEC line (see Figure 7B).
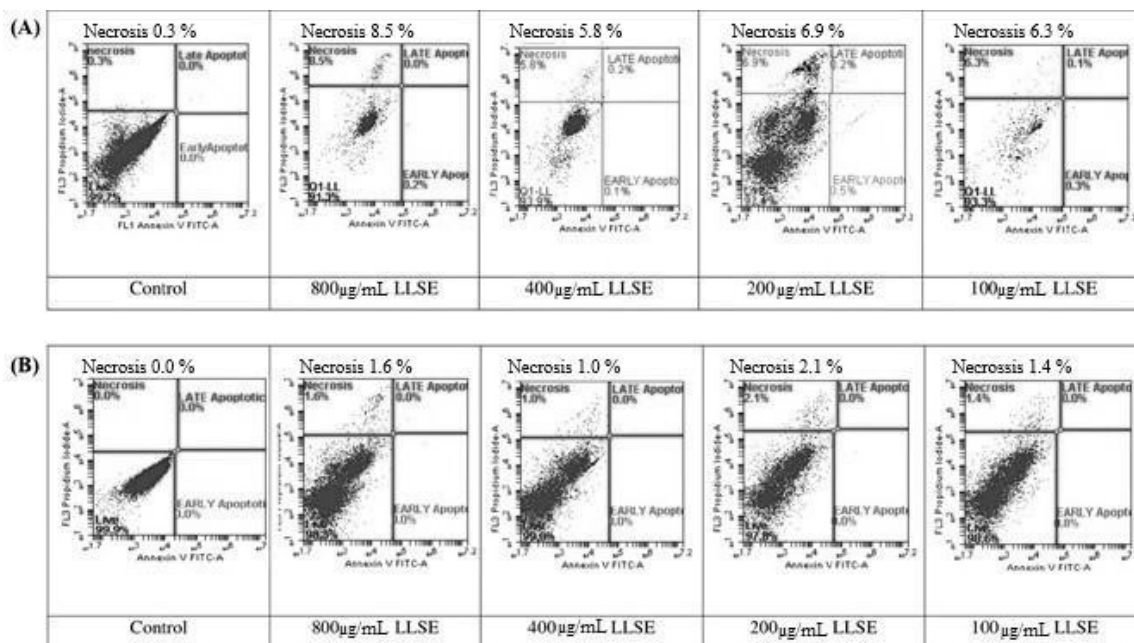
Figure 7: Investigation of apoptotic and necrotic effects of LLSE by flow cytometry analysis, **(A)** the **MDA-MB-231** cell line, **(B)** the **HUVEC** line.

4. Discussion

Imbalances in programmed cell death, a fundamental physiological process, are pivotal in determining cancer cell fate. Cancer initiation arises from DNA alterations, prompting uncontrolled cell division, leading to a disparity between proliferation and apoptosis (Ouyang *et al.,* 2012). Breast cancer, second only to lung cancer in female mortality globally, is linked to lifestyle factors like alcohol consumption and obesity, accounting for approximately 30% of cases (Giaquinto *et al.,* 2022; Öztecik *et al.,* 2023).

While cytotoxic drugs remain crucial in cancer therapy, their severe side effects drive interest in traditional and complementary medicine approaches (Muhamad *et al.,* 2012). Leech saliva extract emerges as a potential candidate for cancer treatment due to its rich composition of over a hundred bioactive compounds influencing cell proliferation and migration in a dose-dependent manner (Shakouri *et al.,* 2022).

Our investigation revealed distinct effects of LLSE at varying doses on cancerous versus healthy cell lines. Specifically, in the MDA-MB-231 cell line, LLSE exhibited dose-dependent reductions in cell proliferation and migration, with the 800 µg/mL dose proving the most efficacious—additionally, LLSE induced apoptosis and necrosis in these cancer cells. Conversely, in the HUVEC line, LLSE promoted cell proliferation and migration *in vitro*, with no significant apoptosis or necrosis observed compared to the control group.

The dose-dependent response of MDA-MB-231 cells to LLSE, leading to decreased cell viability, is particularly noteworthy. Variations in LLSE response were identified based on dosage, duration (24 h and 48 h), and cell line selection using the MTT assay. An IC50 value of 470 µg/mL was calculated, with no discernible difference between 24-hour and 48-hour LLSE administrations in the MDA-MB-231 cell line. Notably, the 800 µg/mL dose of LLSE consistently reduced cell viability in both 24-hour and 48-hour assays. Given that this dose exceeded the IC50 value, it likely accounts for the significant decrease in cell viability. The differential findings between the 800 µg/mL dose and the IC50 value (470 µg/mL) highlight the dose-dependent nature of LLSE's effects. Specifically, while the IC50 value indicates the concentration at which LLSE reduces cell viability by 50%, the 800 µg/mL dose surpasses this threshold and results in a more pronounced reduction in cell viability, which suggests that higher concentrations of LLSE may enhance its cytotoxic effects on MDA-MB-231 cells, potentially leading to more effective inhibition of cancer cell proliferation and survival. Additionally, the consistency of the 800 µg/mL dose's impact across both 24-hour and 48-hour time points underscores its robust efficacy, making it a critical focal point for understanding LLSE's therapeutic potential. Furthermore, a separate study on the breast fibroblast cell line (Hs 578Bst) demonstrated that non-lyophilized leech saliva augmented cell proliferation, migration, and mRNA expression associated with these effects (Ünal *et al.*, 2023). This finding underscores the differential impact of LLSE on cancerous versus healthy cell lines, suggesting its potential as a targeted therapeutic agent.

Cell migration assays revealed an inhibitory effect of LLSE on the migration index of MDA-MB-231 cells, reinforcing its potential role in impeding cancer cell spread. In the literature, migration assay may be used to measure the invasion ability of cancer cell lines (Tan *et al.,* 2023). LLSE demonstrated a stimulating effect on the migration index of HUVEC cells, suggesting potential angiogenic or wound-healing properties in healthy cells. These findings are consistent with prior research indicating the contextual effects of leech saliva, notably highlighting the efficacy of the 800 µg/mL dose above the IC50 in enhancing cell migration.

In a study evaluating LLSE's impact on cell migration, breast cancer cells (MCF-7) and HUVEC lines were investigated. A scratching assay revealed complete coverage of the scratch area by HUVEC cells treated with LLSE after 48 hours, contrasting with the lack of closure observed in MCF-7 cells. This result suggests that LLSE may inhibit the migration of breast cancer cells (Shakouri *et al.,* 2022). Similarly, hirudin, derived from medicinal leech saliva, inhibited cell migration in a glomerular endothelial cell line, particularly in diabetic mice with microangiopathy (Pang *et al.,* 2020).

In vitro studies suggest that LLSE decreases cell migration in cancerous and pathological cell lines; it enhances migration in healthy cell lines (Ünal *et al.,* 2023). Moreover, LLSE's effects on wound healing have been investigated in both *in vitro* and *in vivo* models, with several studies demonstrating positive outcomes (Zakian *et al.,* 2022; Koeppen *et al.,* 2020).

As one of the critical regulators of angiogenesis, VEGF (vascular endothelial growth factor) has crucial roles in endothelial cell proliferation and migration and promotes neovascularization through its binding to the VEGF receptor (VEGFR) (Ferrara, 2004). EGF (epidermal growth factor) is important in embryonic development, development, and wound healing. It binds to the epidermal growth factor receptor (EGFR) and activates signal cascades with many effects, such as cell proliferation, reduced apoptosis, and angiogenesis (Jorissen *et al.*, 2003). Finally, FGF (fibroblast growth factor) is one of the growth factors involved in soft-tissue growth and regeneration, primarily through its interaction with fibroblast growth factor receptors (FGFRs) (Turner and Grose, 2010).

In the MDA-MB-231 cell line, treatment with 800 µg/mL LLSE reduced mRNA expression for EGF, FGF, and VEGF compared to the control group. Additionally, treatment with 400 µg/mL LLSE significantly increased VEGF and EGF mRNA expression compared to the control and all other treatment doses. In contrast, in the HUVEC line, treatment with 100 µg/mL LLSE led to a significant up-regulation of mRNA expression for EGF, FGF, and VEGF compared to all other doses. In a study conducted by Shakouri *et al.* on the effect of *H. medicinalis* saliva on tumour angiogenesis, it was shown that leech saliva application reduced VEGF-A gene expression in the MCF-7 cancer cell line. (Shakouri *et al.*, 2022).

The fact that a substance exhibits different effects at different doses in cell culture studies indicates that the substance in question has a complex interaction with biological mechanisms in the cells. This phenomenon indicates that cells exposed to a particular substance show various responses depending on the substance (Lau *et al.,* 2020). The effects observed on different cell lines may be

due to the diversity of factors such as cell receptors, signalling pathways, gene expression, and metabolism, depending on the interaction of the substance with the cells. This diversity may be based on biological differences between cell types (Bondos *et al.*, 2022).

In our study, all doses of LLSE caused apoptosis and necrosis in the MDA-MB-231 cell line, with the 800 µg/mL dose causing the most necrosis, while in the HUVEC line cell viability was found to be close to 100% in the flow cytometry analysis performed after applying LLSE, and it was determined that the cells neither underwent apoptosis nor necrosis significantly.

When the literature is examined, there are no studies on the effect of direct leech saliva application on apoptosis or necrosis, as in our study. Instead, studies investigate hirudin's effect on apoptosis or necrosis from the medicinal leeches' saliva (Zhu *et al.*, 2019). These results show that hirudin attenuates apoptosis induced by thrombin in the HMVECs (Human Microvascular Endothelial Cells). A healthy endothelial cell line was used in our study as well. In a study, the effects of hirudin found in the salivary secretion of *H. medicinalis* were observed in glioblastoma tumour cell lines (LN-229 and U251). In this context, it was shown that hirudin treatment drove glioma cells to apoptosis and inhibited glioma cell survival (Zhao, 2015). In another study, the effect of hirudin on bladder cancer cell lines (EJ and J82) and their exosomes was investigated.

Flow cytometry analysis performed after hirudin administration showed that apoptosis significantly increased in both bladder cancer cell lines. It is shown that hirudin significantly induces bladder cancer cell apoptosis (Shen *et al.*, 2022). When the effects of leech saliva on cell death were evaluated by flow cytometry, quite different results can be found in the literature. While hirudin obtained from leech saliva increases the apoptosis in cancer cells, it protects healthy cells from apoptosis. Similarly, it was determined that the cells underwent apoptosis and necrosis after LLSE application in the MDA-MB-231 cell line, while the opposite effect was observed in the HUVEC cell line. Cancer cells often exhibit distinct receptor expression, cellular signaling pathways, and tumor microenvironment profiles compared to healthy cells. The differential responses to varying drug doses can be attributed to several interconnected factors, including pharmacokinetics, receptor saturation, and cellular adaptation mechanisms (Hanahan and Weinberg, 2011; Maman and Witz, 2017). As a result, that can lead to differential responses to bioactive compounds found in leech saliva.

The apoptosis and necrosis assessments further contribute to the nuanced understanding of LLSE's effects. MDA-MB-231 cells exhibited apoptosis and necrosis, particularly at higher doses, indicating a potential cytotoxic impact. Conversely, HUVEC cells showed no significant apoptosis or necrosis, supporting that LLSE might spare healthy cells from such detrimental effects.

Medicinal leech saliva, a complex mixture of bioactive substances, prominently features hirudin, a potent and natural thrombin inhibitor with unique anticoagulant properties. Unlike heparin, hirudin operates independently of cofactors, simplifying its application in preventing blood clot formation (Ünal *et al.*, 2023). The saliva also contains destabilase and vasodilator substances like acetylcholine, alongside other notable components including bdellins, satin, and LCI (leech carboxypeptidase inhibitor) (Liu *et al.*, 2019). These substances stand out for their anti-inflammatory effects, adding another dimension to the therapeutic potential of medicinal leech saliva in areas ranging from anticoagulation to wound healing and vascular health.

Among the limiting factors of the study are budget constraints and the insufficient quantity of available LLSE, which have hindered the conduct of comprehensive tests on the biological activity of LLSE. Nevertheless, meaningful data were obtained when dose groups with limited LLSE were compared with the control. However, the findings from the comparisons provided valuable insights into the effects of LLSE. Future studies exploring the molecular mechanisms of LLSE's effects on different doses and cell lines could reveal important information. This detailed investigation may help us understand how LLSE influences specific genes, signalling pathways, and cell metabolic processes. Molecular-level analyses like these can contribute to a more comprehensive understanding of how LLSE acts at the cellular level and may aid in evaluating potential therapeutic applications.

5. Conclusion

In conclusion, this study provides valuable insights into the differential effects of LLSE on breast cancer cells (MDA-MB-231) and healthy endothelial cells (HUVEC). The observed anti-proliferative, anti-migratory, and potential pro-apoptotic effects in the breast cancer cell line suggest that LLSE possesses promising properties for cancer therapy. Conversely, the enhanced cell viability and migration, along with the absence of apoptosis or necrosis in healthy cells, suggest a context-dependent and selective impact.

The nuanced findings underscore the need for further investigations to decipher leech saliva's intricate mechanisms and potential therapeutic applications in cancer treatment and wound healing. The dual nature of LLSE's impact, inhibiting cancer cells while promoting health in endothelial cells, opens avenues for targeted therapeutic development.

Our results have shown that medicinal leech saliva extract is an intelligent biological agent that works in different ways according to the characteristics of the cell line. Different and variable effects of leech saliva on the cell viability, migration, and death of various cell lines may depend on the selected medicinal leech species, the protein dose or content of the leech saliva, and the applied cell line. We hope this data, reported for the first time, will pave the way for further *in vitro* and *in vivo* studies. Further translational research is warranted to validate these *in vitro* findings and explore the clinical relevance of leech saliva in cancer therapy.

Conflict of Interests

There are no conflicts of interests between the authors and family members of the scientific and medical committee members or members of the potential conflicts of interest, counselling, expertise, working conditions, share, holding, and similar situations in any firm.

Ethics approval

Ethics committee approval is not required as commercially available cell lines were used in this study.

Funding

Additional Information

This study was partially presented as an oral presentation at the Association of Biochemists and Molecular Biologists at the B and H Conference on May 18-20, 2023, in Sarajevo, Bosnia and Herzegovina.

References

Ammar, AE. 2021. The anticancer activity of leech saliva extract and the role of protease activated receptor 1 (PAR-1) in prostate cancer. Doctoral dissertation, University of British Columbia, British Columbia, Canada.

Abdel-Fattah MS, Atoum M, Abdel-Rahman S and Alobous, A. 2009. Genetic Polymorphism of Manganese Superoxide Dismutase (MnSOD) Among Breast Cancer and Benign Breast Patients in Jordan: A Preliminary Study. *Jordan J Biol Sci.*, **2 (2)**: 77-82.

Abdualkader AM, Merzouk A, Ghawi AM and Alaama M. 2011. Some biological activities of Malaysian leech saliva extract. *IIUM Engineering Journal.*, **12 (4)**.

Alam SS, Ahmad W and Yunus SS. 2016. Irsal-e-Alaq (Leech Therapy/Hirudo therapy) in Surgical Diseases: A review. *IJARVM.*, **1 (4):** 23-27.

Baskova IP, Kostrjukova ES, Vlasova MA, Kharitonova OV, Levitskiy SA, Zavalova LL and Lazarev VN. 2008. Proteins and peptides of the salivary gland secretion of medicinal leeches *Hirudo verbana*, *H. medicinalis*, and *H. orientalis*. *Biochemistry (Mosc).,* **73 (3)**: 315-320.

Ben-Dror J, Shalamov M. and Sonnenblick A. 2022. The history of early breast cancer treatment. *Genes.,* **13 (6):** 960.

Davies, RW and Govedich FR. 2001. Annelida: euhirudinea and acanthobdellidae. **Ecology and classification of North American freshwater invertebrates.**, 2, pp. 465-504.

Elliott JM and Kutschera U. 2011. Medicinal leeches: historical use, ecology, genetics, and conservation. *Freshwater Reviews.,* **4 (1):** 21-41.

Ferrara, N. 2004. Vascular endothelial growth factor: basic science and clinical progress. *Endocr Rev.*, **25(4),** 581-611.

Giaquinto AN, Sung H, Miller KD, Kramer JL, Newman LA, Minihan A and Siegel RL. 2022. Breast cancer statistics, 2022. *CA Cancer J Clin.*, **72 (6)**, 524-541.

Gödekmerdan A, Arusan S, Bayar B and Saglam N. 2011. Medicinal leeches and hirudotherapy. *Türkiye Parazitoloji Dergisi.*, **35 (4)**: 234.

Hanahan, D and Weinberg RA. 2011. Hallmarks of cancer: the next generation. *Cell J.*, **144(5)**, 646-674.

Hildebrandt JP and Lemke S. 2011. Small bite, large impact–saliva and salivary molecules in the medicinal leech, Hirudo medicinalis. *Naturwissenschaften.*, **98 (12)**, 995-1008.

Jorissen RN, Walker F, Pouliot N, Garrett TP, Ward CW and Burgess AW. 2003. Epidermal growth factor receptor: mechanisms of activation and signalling., **The EGF receptor family**, 33-55.

Karamanou M and Androutsos G. 2021. Louis-Joseph-Marie Robert (1771-1850) and his method for the prevention of breast cancer. *Journal of BU ON.*, **26 (1)**: 284-287.

Kielkopf CL, Bauer W and Urbatsch IL. 2020. Bradford assay for determining protein concentration. *Cold Spring Harb Protoc.*, **2020 (4)**.

Koeppen D, Aurich M, Pasalar M, and Rampp T. 2020. Medicinal leech therapy in venous congestion and various ulcer forms: Perspectives of Western, Persian and Indian medicine. *J Tradit Complement Med.,* **10 (2)**: 104-109.

Lau H, Corrales N, Rodriguez S, Luong C, Mohammadi M, Khosrawipour V and Lakey J. 2020. Dose-dependent effects of necrostatin-1 supplementation to tissue culture media of young porcine islets. *PLoS One.,* **15 (12)**.

Liu Z, Tong X, Su Y, Wang D, Du X and Zhao F. 2019. In-depth profiles of bioactive large molecules in saliva secretions of leeches determined by combining salivary gland proteome and transcriptome data. *J Proteomics.*, **200**: 153-160.

Maman, S., & Witz, I. P. (2018). A history of exploring cancer in context. *Nat Rev Cancer.*, **18(6)**, 359-376.

Michalsen A, Roth M and Dobos GJ. 2011. **Medicinal leech therapy,** First ed. Thieme, Germany.

Bondos Se, Dunker AK and Uversky VN. 2022. Intrinsically disordered proteins play diverse roles in cell signaling. *CCS.,* **20(1)**, 20.

Muhamad M, Merriam S, and Suhami N. 2012. Why breast cancer patients seek traditional healers. *Int J Breast Cancer.,* **2012 (1),** 689168.

Nedeljković M and Damjanović A. 2019. Mechanisms of chemotherapy resistance in triple-negative breast cancer — how we can rise to the challenge. *Cells.,* **8 (9)**: 957.

Nesemann H and Neubert E. 1999. Bd. 6/2: Annelida, Clitellata: Branchiobdellida, Acanthobdellea, Hirudinea. *Spektrum Heidelberg.*, 187.

Ouyang L, Shi Z, Zhao S, Wang FT, Zhou TT, Liu B and Bao JK. 2012. Programmed cell death pathways in cancer: a review of apoptosis, autophagy and programmed necrosis. *Cell Prolif.,* **45 (6)**: 487-498.

Öztecik FE, Baylan M and Yılmaz MB. 2023. Effect of some fatty acids on apoptosis related genes in human breast cancer. *Indian J Exp Biol.,* **61 (02)**: 83-89.

Pang X, Zhang Y, Peng Z, Shi X, Han J and Xing Y. 2020. Hirudin reduces nephropathy microangiopathy in STZ-induced diabetes rats by inhibiting endothelial cell migration and angiogenesis. *Life Sci.*, **255**: 117779.

Shakouri A, Kahroba H, Hamishekar H and Abdolalizadeh J. 2022. Nanoencapsulation of *Hirudo medicinalis* proteins in liposomes as a nanocarrier for inhibiting angiogenesis through targeting VEGFA in the Breast cancer cell line (MCF-7). *BI.,* **12 (2)**: 115.

Shen Y, Ye H, Zhang D, Yang M, Ji Y, Tang L and Yuan, L. 2022. The role of exosomal CDC6 in the hirudin-mediated suppression of the malignant phenotype of bladder cancer cells. *Gene.,* **821**: 146269.

Sig AK, Guney M, Guclu AU and Ozmen E. 2017. Medicinal leech therapy — an overall perspective. *Integr Med Res.,* **6 (4)**: 337-343.

Singh AP. 2010. Medicinal leech therapy (hirudotherapy): a brief overview. *Complement Ther Clin Pract.*, **16 (4)**: 213-215.

Smith D. 2012. Culture collections. **Advances in applied microbiology**, Elsevier. **79:** 73-118.

Tan CG, Teng L, Wang W, Gao W and Zhang Y. 2023. Prognostic significance of microRNA-20a-5p levels which promotes proliferation and invasion by targeting cyclin G2 in small cell lung cancer. *Indian J Exp Bio.l,* **61 (03)**: 159-166.

Tessler M, de Carle D, Voiklis ML, Gresham OA, Neumann JS, Cios S and Siddall ME. 2018. Worms that suck: Phylogenetic analysis of Hirudinea solidifies the position of Acanthobdellida and necessitates the dissolution of Rhynchobdellida. *Mol Phylogenet Evol.*, **127**, 129-134.

Turner N and Grose R. 2010. Fibroblast growth factor signalling: from development to cancer. *Nat Rev Cancer.,* **10(2)**, 116-129.

Ünal K, Erol ME and Ayhan H. 2023. Literature review on the effectiveness of medicinal leech therapy in the wound healing. *Ank Med J.,* **23 (1)**, 151-164.

Ünal K, Tırık N, Erol ME, İbrahimkhanlı L, Elçi PM and Ayhan H. 2023. The Investigation of Effects of Medicinal Leech Saliva Extract on the Breast Fibroblast Cell Line *In Vitro*: An Experimental Study. *J Tradit Complem Med.*, **6 (2)**: 142-151.

World Health Organisation (WHO). 2021. "Breast Cancer." from https://www.who.int/news-room/fact-sheets/detail/breast-cancer.

Zakian A, Ahmadi HA, Keleshteri MH, Madani A, Tehrani-Sharif M, Rezaie A and Pasha MBM. 2022. Study on the effect of medicinal leech therapy (*Hirudo medicinalis*) on full-thickness excisional wound healing in the animal model. *Res J Vet Sci.,* **153**: 153-168.

Zhao L. 2015. Hirudin inhibits cell growth via ERK/MAPK signaling in human glioma. *Int J Clin Exp Med.,* **8 (11)**: 20983.

Zhu J, Pan X, Lin B, Lin G, Pradhan R, Long F and Ying G. 2019. The effect of hirudin on antagonisting thrombin induced apoptosis of human microvascular endothelial cells. *Acta Cir Bras.,* **34 (1)**.

Comparative Studies on Antibacterial Activities of Chitosan, Silver Nanoparticles and Maggot Based chitosan-silver Nanocomposites Against Fish Pathogens.

Joseph A. Olugbojo[1,*], Adeolu A. Akinyemi[2], Samuel O. Obasa[2], and Enock O. Dare[3]

[1]Department of Biological Sciences, Bells University of Technology, Ota, Ogun State, Nigeria; [2]Department of Aquaculture and Fisheries Management, Federal University of Agriculture, Abeokuta, Ogun State, Nigeria; [3]Department of Chemistry, Federal University of Agriculture, Abeokuta, Ogun State, Nigeria

Abstract

The current study explored the *ex- situ* bio-fabrication of maggot-based chitosan-silver nanocomposites (CS-AgNCs), silver nanoparticles (AgNPs) and chitosan (CS). It was conducted in view of an increasing demand to replace antibiotics with nanomaterials due to their eco-friendliness, non-hazardous and biocompatibility. AgNPs were prepared using *Cassia fistula* leaf extract as bio-reductant, CS was prepared from maggot chitin, while *ex-situ* bio-fabrication technique was used to synthesize CS-AgNCs. The integrity of the formed nanoparticles and polymer composites were established through ultra violet-visible (UV-Vis.) spectrophotometry, Fourier transform infrared (FTIR) spectroscopy, X-ray diffraction (XRD), scanning electron microscopy (SEM), and energy dispersive x-ray (EDX) analysis. To evaluate and compare their antibacterial potency, *Aeromonas schubertii, Aeromonas hydrophila, Vibrio parahaemolyticus, Klebsiella aerogene* and *Proteus mirabilis* strains were selected as test organisms. Antibacterial activity tests were carried out using agar well diffusion technique. Data collected were subjected to analysis of variance (ANOVA). The result depicted hexagonal and cuboidal AgNPs and CS respectively, while CS-AgNCs were observed as chitosan matrix embedded with AgNPs. The average particle size of AgNPs, CS and CS-AgNCs were 24.94 nm, 30.95 nm and 65.03 as observed on SEM. The XRD analysis showed that they were all crystalline in nature. *In-vitro* antibacterial activities revealed a marked difference ($P<.0.05$) in the inhibition zones after tested the nanoparticles and the polymer composites on each of the bacteria except CS-AgNC and CS, whose difference are not significant ($P>.0.05$) when tested on *V. parahaemolyticus* (16.00 ± 1.15 and 15.50 ± 1.73) mm and *P. mirabilis* (19.00 ± 2.31 and 19.00 ± 1.15) mm. This outcome clarified that the polymer composites were the most effective against the test bacteria whose zone of inhibition was highest, ranging from 15.00 ± 2.31 mm to 22.50 ± 0.58 mm, followed by chitosan; 12.50 ± 0.58 mm to 19.00 ± 1.15 mm and least in AgNPs; 8.00 ± 1.15 mm to 13.00 ± 1.15 mm. Consequently, maggot-based chitin from which chitosan was produced is rarely used to produce chitosan, thus making CS-AgNP a novel nanocomposite, which can be used for pond water treatment and fish diseases associated with the test pathogens.

Key words: Bio-fabrication, Maggot-based chitin, Nano-antibacterial, Polymer composites, Scanning electron microscopy, Silver nanoparticles, X-ray Diffraction.

1. Introduction:

The problem of pathogenic bacteria has limited effective fish production and availability in global aquaculture industry. Among fish diseases, those caused by bacteria spread widely than those caused by other pathogens, and have brought much distress due to serious economic losses through high mortality (Olugbojo and Ayoola, 2015). Increase in resistance of various bacteria to several antibiotics has also limited a gainful treatment and thus emphasized the need to develop a new antimicrobial (Quesada *et al*., 2013). In addition, available literature has shown that there are limited reports on the use of nanoparticles for prophylactic and therapeutic treatment

in aquaculture, especially on evaluation of antibacterial activity of silver nanoparticles using *Cassia fistula* as bioreductant, Chitosan, and Maggot–based Chitosan silver nanocomposites on pathogenic bacteria isolates such as: A. *schubertii, A. hydrophila, V. parahaemolyticus, K. aerogene* and *P. mirabilis* from *Clarias gariepinus (*African mud catfish) in Nigeria.

From the literature search, there has not been previous work on antibacterial sensitivity of *A. schubertii* using Chitosan, silver nanoparticles, and Chitosan silver nanocomposites as antibacterial agents, apart from some antibiotics which have been used to control *A. schubertii* infections in some fishes. *A. schubertii* is a rare *Aeromonas sp* pathogen in fish, and there is lesser report on its incidence or outbreak in fish farms, the prevalent

* Corresponding author. e-mail: josephgbojo2012@gmail.com.

ones being *A. hydrophila, A. veronii, and A. Caviae.* However, *A. schubertii* was first reported in brackish water wild tilapia (*Oreochromis niloticus*) in China by Zhuling *et al.* (2019). It was noted that the natural infection route was through damage on fish skin and digestive tract. Moreover, antibiotic sensitivity test carried out showed that *A. schubertii* was susceptible to Norflorxacin and Rifampicin but resistant to several other antibiotics. Chen *et al* (2012) also isolated and characterized *A. schubertii* from a diseased snakehead fish (*channel maculate* - Lacepede) suffering high mortality. *In-vitro* antibiotic susceptibility test revealed that it was susceptible to cefoxitin, cefoperazone, and chloramphenicol. Also, Thai *et al* (2023) discovered a prevalence and antibiotic resistant *A. schubertii* causing internal white spot diseases on another snake head fish (*C. striata*) in the Mekong delta, Vietma. The antibiotic susceptibility test also revealed that all the identified isolates of *A. schubertii* were phenotypically multi drug resistant. The multiple antibiotic resistance index ranged from 0.33 to 0.92, being resistant against 11 out of 12 tested antibiotics, showing that *A. schubertii* was responsible for white spot diseases in snake head fish. All report so far has been that *A. schubertii* was highly resistant to varieties of antibiotic drug while being sensitive to some.

For a long time, *K. aerogene* and *P. mirabilis* have been considered as opportunistic pathogens; however, Zhai *et al* (2023) in his research on the outbreak of *A. veronii* and *P. mirabilis* in yellow catfish and channel catfish discovered that *P. mirabilis*, has a high potential with grave possibility of becoming a serious threat to fish. He noted that yellow catfish were more responsive to *A. veronii* than *P. mirabilis*, while *P. mirabilis* weakens and exposes fish to infections with little resistance. The number of *A. veronii* in the *P. mirabilis* immersion challenged group increased and was 15% higher than that in the control group. This is in agreement with *P. mirabilis* making their hosts more prone to disease through the differentiation of swarmer cell with the expression of virulence factors (Zhai *et al.*, 2023). *A. veronii* causes protrusion of the abdomen and ovarian damage while *P. mirabilis* also causes distension of the abdomen and skin redness. However, *P. mirabilis* might render the host responsive to *A. veronii* attack, even though the underlying mechanism is yet to be clarified (Zhai *et al.,* 2023).

 A related research conducted by Adeyemo *et al.,* (2023) validated the fact that obligatory fish pathogens share the same environment with other resident and opportunistic pathogens with the possibility of sharing and transferring genetic materials, thereby affirming the high possibility of such bacterial assuming the same status with obligatory bacteria fish pathogen. This report is in consonant with Adeshina *et al.* (2016) who reported same on pathogenic *Klebsiella* species in cultured African Catfish.

This study focuses on synthesis, characterization and *in-vitro* antibacterial activity of Chitosan, silver nanoparticles, and Chitosan silver nanocomposites against *A. schubertii, A. hydrophila, V. parahaemolyticus, K. aerogene* and *P. mirabilis* isolates from *C. gariepinus*.

Nanotechnology can be defined as the synthesis, characterization, and utilization of nano-sized (1-100nm) materials for the development of science (Nikalje, 2015). It deals with the materials, whose structures exhibit novel and improved physical, chemical, and biological properties, and can find wide applications both in human and veterinary medicine (Fajardo, 2022 and Abass *et al.*, 2022).

Over the centuries, the antimicrobial activities of silver based compounds against different species of micro-organisms has been well-known. The heat and chemical resistance of Silver nanoparticles (AgNPs) is responsible for its wide acceptance and utilization as antibacterial agents. Properties such as size, shape, and increasing surface oxidation which leads to the release of silver ion (Ag+) have earned it unreserved accreditation (Ghotakar *et al*, 2019). AgNP can rapidly oxidize and release silver ion because of its large surface area to volume ratio. Although the exact mode of its antibiotic activity is yet to be fully understood, it has been reported in several literatures that because of the ultra-small size of AgNP, it easily penetrates through the cell walls of pathogens, and causes cell disruptions (Aktar *et al.,* 2017). It was also reported that the generation of reactive oxygen species and free radicals causes cell membrane damage and death when silver nanoparticle is introduced especially at a nano-scaled size (Dayem et al, 2017). Since the effectiveness of any antimicrobial depends largely on the surface area to volume ratio, likewise the antimicrobial activity of any NPs also depends on how small the particle size is. When the particle size become smaller, the surface area to volume ratio also increases.

The use of Nanoparticles and their composites in treating bacteria fish diseases is rarely investigated. Among the few works that have been carried out on antibacterial effect of silver nanoparticles is the study conducted by Islam *et al.* (2021). He worked on green synthesis of AgNP and their antagonistic effect on fish larvae pathogenic bacteria using leave extract of mangrove plants (*Avicennia marina*) as reducing and stabilizing agent. The result showed the formation of nano-sized AgNP which ranges from 15-25nm. A well identified *Vibrio spp* (from fish sample) through cultural, morphological and biochemical characterization was used as test organisms. The result of antibacterial sensitivity test on various *species* of *Vibrio* showed zone of inhibition which varies between 13.00-12.00 mm, indicating efficient impact on these pathogens. Moreover, Silver (Ag) nanoparticles have high therapeutic potential and exhibit good antimicrobial activity above several other nanoparticles. It also exhibits high potency even at a very low concentration (Govindan *et al.,* 2012). In this study, *C. fistula* leaf extract was used to synthesize silver nanoparticles due to its rare use in the syntheses of nanoparticles, despite its excellent constituent phytochemicals.

Chitin is a natural polymer derived from various living organisms, while chitosan is a product of chitin through the process of deacetylation. Apart from cellulose, chitin abounds among organisms such as fungi, microorganisms, and animals whose exoskeleton are made of chitin. It can find application as antibacterial, antitumor, and immune enhancement agent (Kaur *et al*, 2013). Chitosan also possesses properties such as biodegradability, biocompatibility, non-toxicity, renewability, and bioavailability. It is mostly preferred to synthetic polymers due to its low price and high presence in living organisms. Chitosan has already gained much application in various

fields which include Biotechnology, Food Technology, Agriculture and Veterinary medicine (Younes and Rinaudo, 2015).

The utilization of polymer composites such as chitosan-silver nanocomposites in the development of novel antibacterial has attracted much attention in recent years due to their eco-friendliness and biocompatibility. They can easily be broken down by enzymes in animal body, and the degradation products are not toxic. The synergistic incorporation of metal nanoparticles in the polymeric matrix to produce polymer composites has significantly improved the potency of chitosan and its biological action against microorganism (Dayem et al, 2017). In addition, the appealing properties of chitosan-silver nanocomposites such as biocompatibility and biodegradability made it very useful in several biomedical applications including non-inflammatory reaction after application in the host's body (Nowack *et al.*, 2011).

CS–AgNC is a rare nanocomposite that has been used as antibacterial agent especially maggot based type. Chitosan present in the nanocomposite help to prolong the activity of silver on the bacterial cell while protecting the host cells from silver toxicity which is a major advantage of a silver doped chitosan nanocomposites. In this work, Silver nanoparticles were first synthesized using *C. fistula* leaf extract as bio-reductant, chitosan was also synthesized through a simple chemical method of extraction and deacetylation of cultured maggot chitin, while CS-AgNCs were synthesized through synergistic combination at ratio one to four (1:4) of Silver and Chitosan, respectively through *ex-situ* bio-fabrication techniques.

The primary aim of this research is to evaluate and compare the antibacterial activity of Chitosan, AgNPs and Chitosan – Silver nanocomposites (*in vitro*) and make recommendation to the fish farmers, researchers and fish extension workers, based on the most potent one among the three as against the usual toxic antibiotics. It also seeks to contribute significantly to sustainable development goals 1 and 2 (poverty alleviation and food security).

2. Materials and Methods

2.1. Construction of maggot production Unit (Maggotry)

The Maggotry was made of wooden culture unit according to Hezron *et al.,* (2019) with some modifications. Figure 1 shows the longitudinal section while Fig 2 shows the 3 dimensional view of the culture unit. It consists of a large chamber (1200 x 840 x 580 mm), with two lids at the top, an outermost wooden lid of 10 mm thick, and an inner lid of about 10 mm wire mesh net. The inner net lid was designed to allow house flies to enter and lay their eggs on the exposed substrate while keeping away reptiles and rodents from gaining entry. The outermost wooden lid serves as the main door. It is not supposed to be closed completely (one-quarter closed) in order to allow fresh air into the chamber. It is also used to prevent rain, and direct sunlight from reaching into the chamber. The height of the maggotry above the ground is 600 mm.
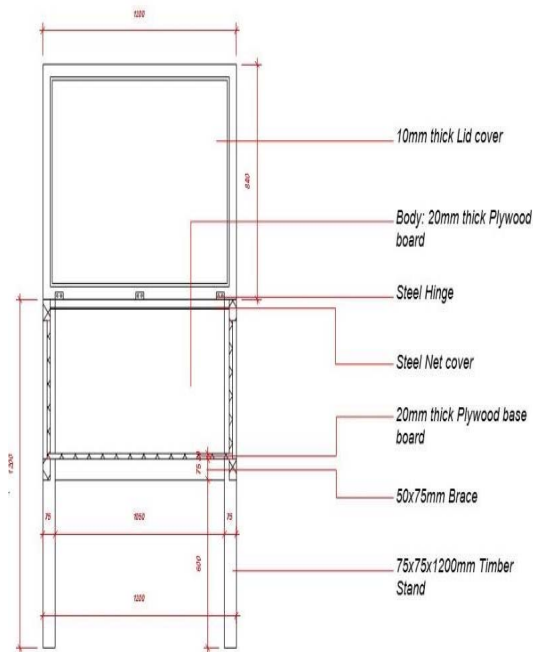
Figure 1. A longitudinal section of Maggot culture unit
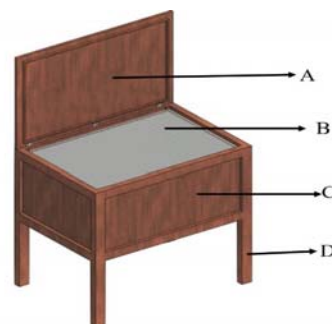
Figure: 2. 3D view of maggot culture unit.

Legend: A- Outer wooded lid. B - Inner net lid. C - Main compartment. D - Stand/Wooden leg

2.2. Culturing of housefly Maggot (Musca domestica)

The maggot of *Musca domestica* was cultured at Bells University Staff estate, Ota, Ogun State. Poultry waste was collected from Onibuku poultry farm and spread in a specially developed maggot culture unit (Figures 1 and 2). Fresh cattle blood and offal were also collected from Arobieye abattoir, Idi-Iroko road, Ota, which serve as attractants to house fly. These were added together and mixed properly to constitute substrate. The maggotry was left open for about 8-10 hrs to allow adult house fly (*M. domestica)* to converge and lay eggs, as the odour from the substrate continue to attract them. After the exposure period, a perforated black polythene sheet was used to cover the substrate so as to provide darkness in order to aid incubation and also allow water to penetrate into the substrate to prevent desiccation. The substrate was kept moisty daily to make it habitable for the prospective larvae. Larvae were harvested on the last day of the larval stage (7th day after oviposition) before they turn to pupa. They were washed, blanched with hot water, and preserved for further use (Akpodiete *et al.*, 1997; Hezron *et al.,* 2019.

2.2.1. Extraction of Chitin from maggot of Musca Domestica and Preparation of Chitosan

Chitin and chitosan were prepared from the maggot (larva stage) of *M. domestica* according to the method described by Kim *et al,* 2016, and Cristiano *et al*, 2019, with modifications as shown in the flow chart (Figure 3). The larval was washed to remove foreign materials and residual muscle particles using warm water. They were then dried at 50^0C in hot air oven overnight. After drying, they were grinded to 1mm particle size using Philip HR-2815 grinder. 50g of dried maggots were weighed into 250 ml conical flask and decalcified for 3 hours in 150 ml of 2M HCL solution at room temperature. It was then rinsed. The sample was soaked again in 200 ml of 1.25M NAOH at 95^0C for 3hours to remove the protein (deproteinization). It was rinsed again thoroughly with water to neutral pH and then dried for 24 hours at 70^0C in hot air oven. This process is known as chitin extraction.

Chitosan was produced from chitin through a process called deacetylation, according to the method described by Kim *et al* (2016).

2.3. Deacetylation of Chitin

Chitin extracted from maggot were boiled in 100ml of 50% NAOH (w/v) solution at 95^0C for 3 hours. The chitosan produced from chitin was washed to a neutral pH with tap water and then dried for 24hrs at 70^0C in hot air oven. It was then grinded into powder and kept in a dried place for further use.
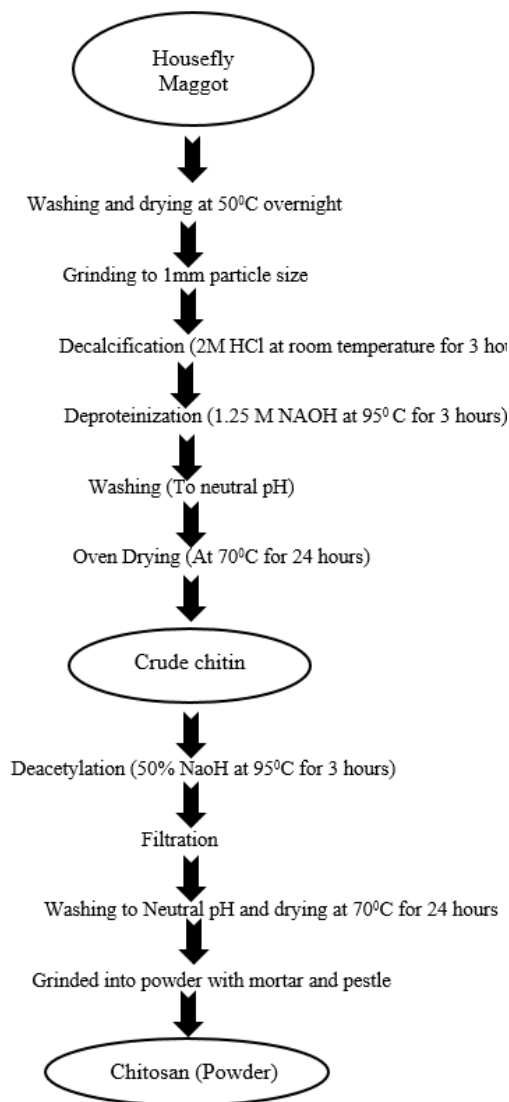
Figure 3. Flow chart of chitin and chitosan preparation

2.4 Preparation of Cassia fistula (Golden shower) leaves extract

Leaves of *Cassia fistula* was obtained from Covenant University, Ota Ogun state, and was authenticated in the Department of Biological Sciences Bells University of Technology, Ota by a botanist. 20g of the leaves was washed with distilled water to remove the dust particles and then air dried for about two weeks. The dried *C. fistula* leaves were cut into small pieces and boiled with 100 ml of distilled water at 70^0C for 1 hour. After boiling, the extract was cooled and separated by filtration to remove impurities, while the clear solution was used for the reduction of silver nitrate ($AgNO_3$) to silver nanoparticles (Irshad *et al.*, 2014)

2.5 Synthesis of silver nanoparticles

Silver nitrate was purchased from Sigma chemical company, U.K. (Product No. R4036/37/38). C. *fistula* (leaves) aqueous extract and 1mM $AgNO_3$ were mixed in the ratio 1:10 and heated on a hot plate with magnetic stirrer at 60^0C for 30 min until colour change (reddish

brown) was observed. The colour change indicate the formation of silver nanoparticles. The simple reaction equation and electron transfer equation leading to the formation of pure silver nanoparticles after donated the valence electron, are shown in equation 1 and 2 below.

Simple equation of reaction

$$AgNO_3 + \text{Plant extract (}C.\ fistula\text{)} \rightarrow AgNPs \qquad (1)$$
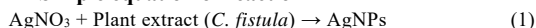
Electron transfer equation (redox reaction)

$$Ag^+ + e^- \rightarrow Ag^0 \qquad (2)$$
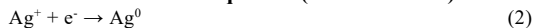
2.4. Preparation of Chitosan-silver nanocomposite (CS-AgNCs)

0.228g of dried Chitosan powder (Plate 2a) was added to 15ml of 1% glacial acetic acid and vigorously stirred for 15 minutes in hot plate with magnetic stirrer at 60^0C to forms homogeneous slurry. The use of glacial acetic acid is to protonate the amine group present in the Chitosan. 0.0456g of Green Synthesized Silver nanoparticles (Plate 1b) was added to the chitosan slurry (in ration 1:4 of AgNP to Chitosan) and continued stirring for about 30 minutes. The mixture (Chitosan and AgNP) turned brown. It was transferred into petri dishes, and dried in a desiccator between 3-5 day at room temperature. It was grinded again into powder (Plate 1c) using mortar and pestle, and sifted to obtain a fine powder using laboratory test sieve (90 micros mesh size, model no- BS410-1-2000, U.K). This reaction is illustrated in equation 3, and plate 1 (a, b and c) in a pictorial form (Govindan *et al* 2012, Olaniyan *et al*, 2016, and Badawy *et al*, 2019).

Simple equation of reaction

$$\text{Chitosan (CS)} + AgNPs \rightarrow \text{CS-AgNCs} \qquad (3)$$
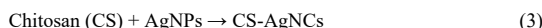
Pictorial equation showing the physical forms of the reactants (CS and AgNP) and the product (CS-AgNP)
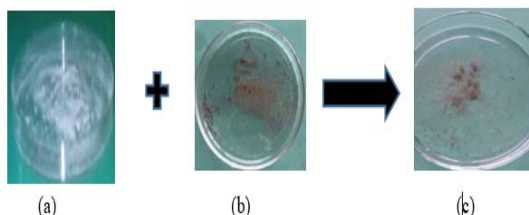
Plate 1: (a) Chitosan film (b) Silver nanoparticles (c) Chitosan-Ag nanocomposite powder

2.5. Characterization Techniques

UV-Vis spectrophotometer (BOSCH 750N) was used to determine the optical characteristics of Chitosan slurry, silver nanoparticles, and the polymer composites. The absorption wavelength was determined by placing each aliquot sample taken at time intervals in quartz cuvette operated at a resolution of 1 nm, and deionized water was used as reference solvent.

The morphology and microstructure were determined using Field Emission Scanning Electron Microscope, GEMINI Ultra 55 (FESEM). The samples were fixed on carbon tape and kept for overnight drying. Then the samples were gold coated (100nm) and viewed under the scanning electron microscope operated at 5kV. The Energy Dispersive X-ray analysis was carried out with the EDX Spectrophotometer attached to FESEM

GEMINI Ultra 55 to analyze the constituent elements in AgNPs, Chitosan, and Chitosan-Silver nanocomposites (CS-AgNCs).

X-Ray Diffraction was done to determine the crystallinity of the nanoparticles and polymer composites using the Rigaku smartLab diffractometer which has nickel filtered Cu Ka radiation, and operated at 40 kV, 40 mA at room temperature.

The chemical composition of the pure and dried samples of the nanomaterials was analyzed using FTIR Spectrophotometer (Perkin-Elmer 100 series) in the diffuse reflectance mode, from 4000 cm^{-1} – 600 cm^{-1} wavenumbers, at a resolution of $6cm^{-1}$ in KBr pellet to determine the various functional group that are present in the samples. (Swarnalathan *et al*, 2012).

The data obtained were analyzed using Origin Pro Software

2.6. Antibacterial activities of Chitosan, Silver nanoparticles and Chitosan-Ag Nanocomposites

Antibacterial activity was screened using agar well diffusion method. Mueller Hinton agar plates were swabbed using sterile L-shaped glass rods with mature broth cultures of *A. schubertii, A. hydrophila, V. parahaemolyticus, K. aerogene* and *P. mirabilis.* Plates were then incubated for 24 hours. Using a sterile cork borer, wells of appropriate dimension were made on each Petri dish. 200mg/ml of each of the NPs and polymer composites in sterile DMSO was used, while 200mg/ml of a conventional antibacterial drug (Ofloxacin) was also used as control. 200mg/ml was chosen after other lesser concentrations did not yield positive results. All plates were simultaneously incubated at 37 °C for 24 hrs. After the incubation period, the diameter of inhibition zones of each well was measured. Each sample was tested in two replicate, and the average values were calculated. Minimum inhibitory concentration (MIC) and Minimum bactericidal concentration (MBC) of each of the nanoparticles and the polymer composites were also determined according to CLSI (2012) guide.

2.7. Statistical analysis

Data were subjected to Analysis of variance (ANOVA) using the SPSS (Statistical Package for the Social Sciences) and 10 Microsoft Excel. Means were separated using Duncan multiple range test (DMRT) ($P<0.05$).

3. Result and Discussion

3.1. UV-Visible Spectra of silver nanoparticles, chitosan and chitosan-silver nanocomposites

The results in Figure 4a, 4b and 4c showed the formation of silver nanoparticles, chitosan and CS-Ag NCs. AgNps were first depicted by the Surface Plasmon Resonance (SPR) band (400 nm) at the visible range (Figure 4a). Silver nanoparticles formed at 400nm were found within the standard wavelength range of silver nanoparticle (400-450 nm) according to Ghafouri *et al*, 2017 and Akintayo *et al,* 2020, showing that AgNps were well prepared and thus confirmed their actual formation. In figure 4b, chitosan was found at 240nm, which is typical of a pure chitosan, whose absorption peak usually falls within UV range, 200-300nm (Olaniyan *et al.*, 2016).

Also, Chitosan-Ag nanocomposites were clearly depicted in Figure 4c by a distinct silver nanoparticles' peak at the visible region (400 nm) and chitosan peak at the UV-region (240 nm) on the spectrum which confirmed that the polymer composites was truly formed and composed of silver nanoparticles and Chitosan. This result corroborates the previous finding (Olaniyan *et al*, 2016; Govinda *et al*, 2012; and Zondi *et al*, 2018).
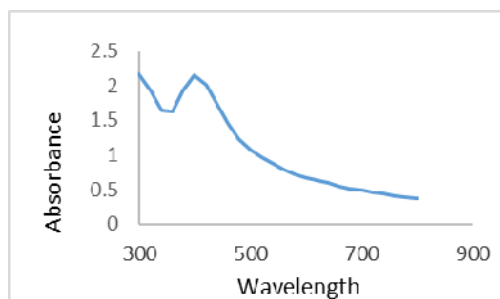
Figure. 4a: UV-Visible specrum of AgNP at 400 nm
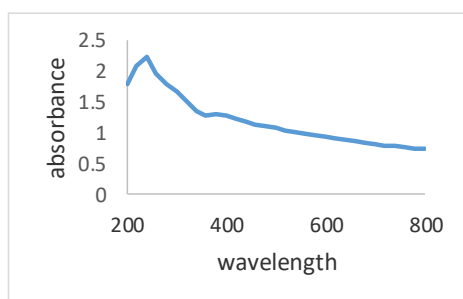
Figure 4b. V-Visible Spectrum showing Chitosan at 240nm
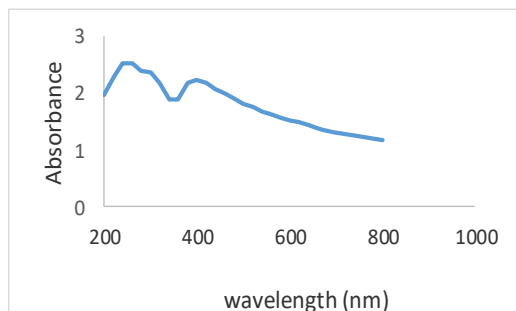
Figure 4c. UV-Visible Spectrum showing Chitosan-silver nanocomposites (CS-AgNCs) at 400nm and 240 nm for AgNP and Chitosan.

3.2. FTIR spectrum of Silver NPs, Chitosan and Chitosan Silver nanocomposites (CS-AgNCs)

The FTIR spectrum shows the bonds which represent functional groups found in AgNPs, CS and CS-AgNC. FTIR absorption peaks were generally found between 4000.00 - 500.00 cm^{-1} range. On silver nanoparticle, the evidence of capping arising by the interaction with the biomolecules present in the plant extract during the reaction are shown by five prominent peaks (Fig 5a) at 3238.89 cm^{-1}, 2924.89 cm^{-1}, 1621.06 cm^{-1}, 1293.76 cm^{-1}, and 1028.65 cm^{-1} which correspond to O-H stretching of

the phenolic compounds, C-H stretching of the fatty acids, C=C stretching of the alkenes, C-O stretching of the 3^0 alcohol group and a C-O-C asymmetric band of ethers respectively. The result depicted the presence of bioactive compounds such as phenols, flavonoids and saponins in the *cassia fistula* leaf extract which participated in AgNPs capping. This result is in tandem with the findings of Mohanta *et al*., 2017 and Danish *et al*., 2022.

The FTIR spectrum of chitosan (Fig. 5b) shows O–H stretching vibration of the phenolic compounds at 3437.63 cm^{-1}, N-H stretching of the amine group at 3258.50 cm^{-1}, C-H stretching of the alkane group (Alkynyl sp3 C-H) at 2921.91 cm^{-1}, O-H bending of the carboxylic acid group at 1659.69cm^{-1}, N-H bending of the amine bond at 1614.70 cm^{-1}, and C-O stretching of the other phenolic compounds at 1375.58 cm^{-1} which matches well with the report by Govinda *et al.*, 2012, Tesfaye *et al.*, 2023 and Zondi *et al.*, 2018.

The FTIR spectrum of CS–Ag nanocomposites was depicted in Fig. 5c. The peaks were found at 3342.15 cm^{-1}, 2916.80 cm^{-1}, 1633.75 cm^{-1}, 1369.36 cm^{-1} and 1027.22 cm^{-1}. These peaks represent functional groups that are found in the polymer composites. The shifting in the CS peaks was also observed in 1750-2000 cm^{-1} range as small irregular bands which may be due to the interaction of Ag with CS in the nanocomposites. These bonds also show that AgNps were bond to chitosan. The absorption peak at 3342.15 cm^{-1} corresponds to O-H stretching of the Phenol group. 2916.80 cm^{-1} correspond to C-H functionality of the alkane group. 1633.75 cm^{-1} corresponds to the C=O stretching of the benzene. 1369.36 cm^{-1} aligns with C-O stretching vibrations of the alcohol group, possibly present in the chitosan matrix while 1027.22 cm^{-1} also align with C-O-C asymmetric band of ethers, which stabilizes the silver nanoparticles in the composites. This result corresponds to the previous finding by Govinda *et al.*, 2012; Gowda and Sriram, 2023.

3.3. XRD pattern of silver nanoparticles, chitosan and Chitosan-Silver Nanocomposites (CS- AgNCs)

The structural properties of the synthesized silver nanoparticles, chitosan and CS–Ag nanocomposites were analyzed using the XRD technique (Fig. 6a, 6b and 6c). This analytical technique is particularly based on diffraction of crystalline material to know the extent of crystallinity. The obtained XRD pattern of silver nanoparticles (Fig. 6a) were observed in the 5 peaks at 2θ angles of 32.37^0, 38.26^0, 44.43^0, 64.08^0, and 77.59^0 which correspond to 101, 111, 200, 220 and 311 reflection planes, respectively. Moreover, the face-centered cubic formation of synthesized AgNPs of various dimensions may be seen in the four intense peaks obtained at 38.26^0 (111), 44.43^0 (200), 64.08^0 (220) and 77.59^0 (311). The peak obtained at 32.37^0 was considered to have been formed due to the crystallization of other organic compounds in the *C. fistula* leaf extract used to synthesize the silver nanoparticles. The results confirmed the crystalline characteristic and face-centered cubic structure of the phytosynthesized AgNPs whose intense bands are in good ascent with reference card (JCPDS Card No. 4-0783) and are in consonance with the reported findings (Bharathi *et al*., 2018; Ahmad, 2023 and Danish *et al.*, 2022).

The obtained XRD pattern for chitosan is shown in Fig 6b. The prominent peaks appeared at 2θ values of 9.40^0,

19.27^0 and 26.28^0 which match well with the literature values (Govinda *et al.*, 2012; Nam and Luong, 2019). They also depicted the crystalline nature of the chitosan. However, the peak at 20.27^0 and other peaks towards the right hand side of the chitosan XRD spectrum are due to chitosan having the cellulose structure which can possess α-type or β-type characteristic peak (Manikadan, 2015). The broadening of 31.80^0, 39.16^0 and 48.19^0 peaks is due to the amorphous nature of the chitosan as a polymorphic biopolymer (Ramon *et al*., 2023). There was no identified impurity peak in the chitosan XRD pattern.

The presence of chitosan and silver peaks as observed from the XRD pattern of CS–Ag nanocomposite is shown in Fig 6c. The graph shows different diffractions at 2θ values of 9.67^0 (020), 20.56^0 (102), 38.34^0 (111), 44.47^0 (200), 64.49^0 (220) and 77.48^0 (311). The prominent CS peaks were observed in the composites graph at 9.67^0 and 20.56^0 while silver nanoparticles were also found at 38.34^0, 44.47^0, 64.49^0 and 77.48^0 on the spectrum showing that both chitosan and silver were involved in the formation of the nanocomposites. These results are similar to the typical Chitosan-silver nanocomposites as described by Selim *et al. (*2020) and Govinda *et al.* (2012).
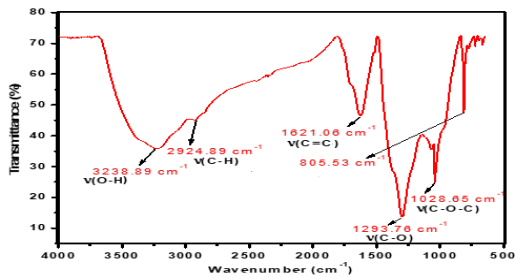
Figure 5a: FTIR Spectrum of Silver nanopartccles
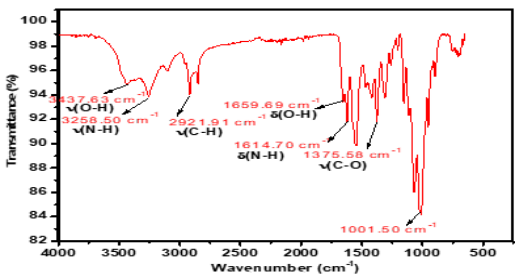
Figure 5b. FTIR Spectrum of chitosan
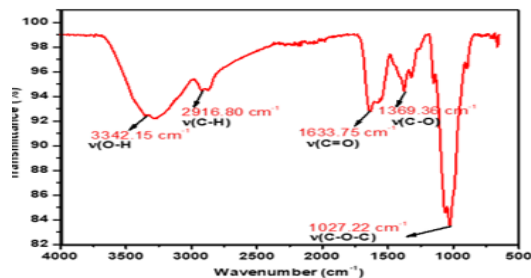
Figure 5c. FTIR spectrum of CS-AgNCs
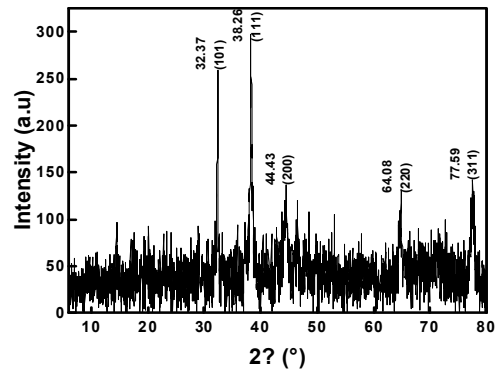
Figure 6a. XRD pattern of Silver nanoparticles (AgNPs)
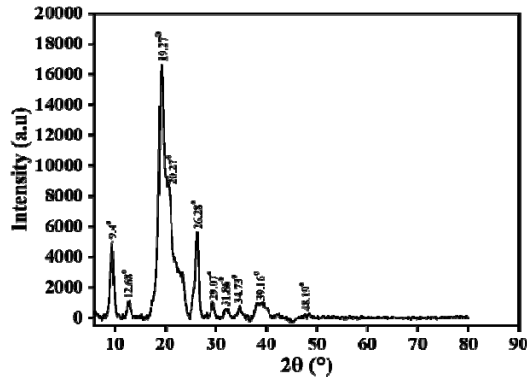
Figure 6b. XRD pattern of chitosan
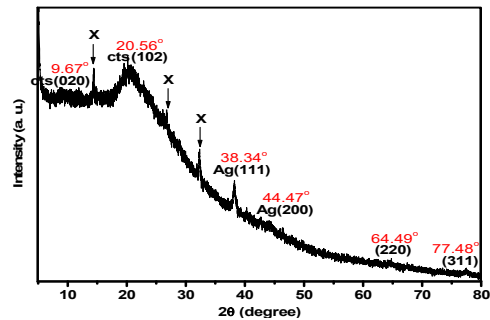
Figure 6c: XRD Pattern of CS-AgNCs

3.4 SEM Image of Silver NPs, Chitosan and Chitosan-silver nanocomposites

The scanning electron microscope was used to determine the morphological characteristics of the silver nanoparticles, chitosan and CS-Ag nanocomposites (CS-AgNCs) (Fig. 7a, 7b and 7c). For AgNP, the micrograph depicted individual AgNP in which some are hexagonal and some spherical with average size of 24.94 at x 100, 000 magnifications with some agglomerations (Fig. 7a). The SEM images revealed the bio-molecule coating of the phytosynthesized AgNPs. This layer also confirms the significance of plant extract metabolites in the synthesis and stabilization of AgNPs. These findings are in tandem with those observed by Danish *et al*., (2022), Oves *et al*., (2018) and Banala et al, 2015

SEM analysis of Chitosan nanoparticles depicted cuboidal shape morphology with no agglomeration, and

average size of 30.95 nm at x 100,000 magnification (Fig. 7b).

SEM image of the polymer composite as observed at the surface was shown in figure 7c. It provided the morphology and size of the chitosan-silver nanocomposite which aggregates into irregular structures. The synthesized polymer composites are in the form of aggregates, with low dispersibility but high stability. SEM image also showed that silver nanoparticles were embedded in the chitosan matrix (Govinda *et al.,* 2012) and the composites formed depicted a nose-shaped morphology with irregular size distribution at the average of 62.45nm (Kamari *et al.*, 2009).

3.5 EDX Spectrum of Silver NPs, Chitosan and Chitosan-Ag Nanocomposites

The Energy Dispersive X-ray (EDX) analysis of silver nanoparticles, chitosan and chitosan-Ag Nanocomposites was done to determine the elemental composition of each of the nanoparticles and composites (Figure 8a, 8b and 8c respectively) using EDX analyzer. The typical EDX spectrum of AgNP showed the presence of silver peak in the range of 2.5-4.0 Kev (Fig. 8a). This showed that the synthesized nanoparticles contain silver. The bands also revealed the presence of carboxyl group (C-O) from the plant chemicals used in the synthesis, with carbon and oxygen found between 0.0-0.1kev and 0.1-0.2Kev ranges respectively. However, silver has the highest percentage atomic weight which is responsible for the highest EDX peak, showing that silver nanoparticle is truly formed. This result is in agreement with the previous findings (Banala *et al.*, 2015).

The EDX analysis of chitosan (CON) was depicted in figure 8b. The observed peak was found between 0.0-0.25 Kev, showing that chitosan was purely formed. There were no impurities or any other compound observed in the EDX spectrum.

The typical EDX spectrum of chitosan embedded silver nanocomposites, synthesized at ratio1:5 of AgNP to chitosan is shown in figure 8c. The observed visible peak of Chitosan (CON) at 0.0-0.5Kev and silver (Ag) between 2.5-3.0 Kev depicts the presence of chitosan and silver. Hence, the samples contain chitosan and silver nanoparticles as a polymer composite (Govinda *et al.,* 2012 and Badawy *et al.*, 2019). However, Chitosan showed higher EDX peak above Silver due to its higher percentage composition.

Successful preparation of chitosan silver nanocomposites was also revealed by their physical appearances (Plates 1: a, b and c). Plate 1a shows the maggot-based chitosan powder (whitish colour), plate 1b shows silver nanoparticles. The reaction of the two substances leads to the synthesis of chitosan-silver nanocomposites (Light brown) which indicates a perfect immobilization of silver into chitosan through the reaction as stated in equation 2, yielding a stable chitosan-silver nanocomposite. However, the reaction was conducted in a wet form, in which chitosan used was in form of slurry.
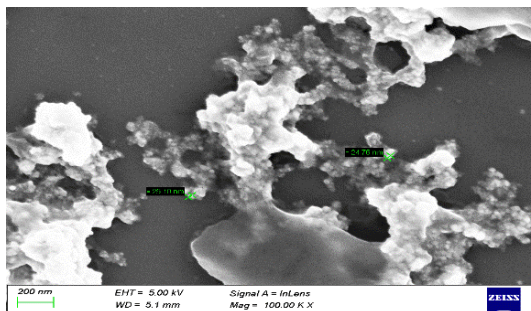
Figure 7a. SEM image of silver nanoparticles
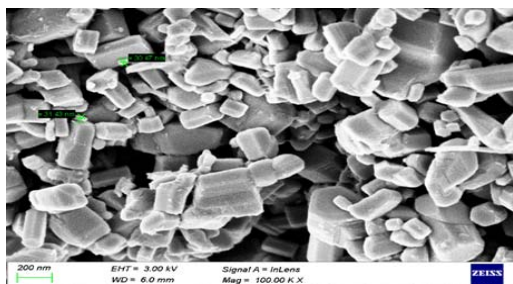
Figure 7b. SEM image of Chitosan
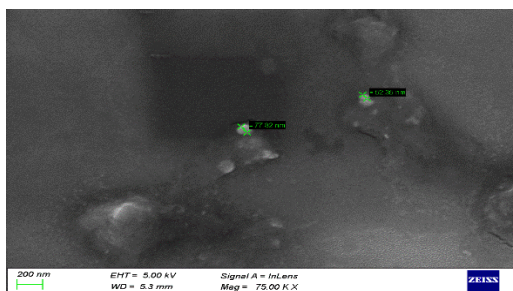
Figure 7c. SEM Image of Chitosan-Ag Nanocompos
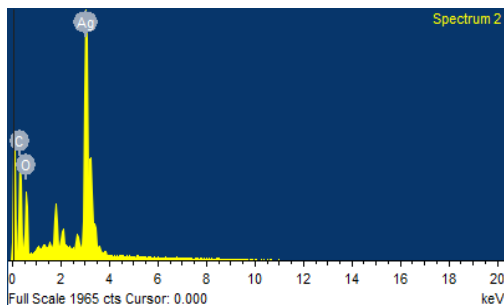
Figure 8a. EDX Spectrum of Silver nanoparticles (AgNP)
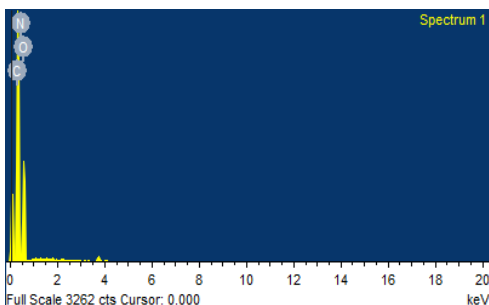
Figure 8b. EDX Spectrum of chitosan (CS)
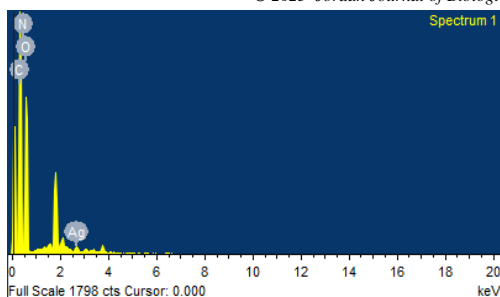
Figure 8c. EDX Spectrum of Chitosan-silver nanocomposites (CS-AgNCs)

3.4. in-vitro Antibacterial activity

The results of antibacterial activities of biosynthesized silver nanoparticles (AgNPs), Chitosan (CS) and Chitosan-Silver nanocomposites (CS-AgNCs) using agar well diffusion procedure are shown in Table 1. The result showed zones of inhibition which are measured in millimeters. The values were statistically analyzed using analysis of variance (ANOVA). From the three nanoparticles tested, *A. schubertii* strain depicted the largest inhibition zones with CS-AgNCs (12.50 mm), followed by Chitosan (12.50 mm) and least inhibition zone with AgNP (8.00 mm) along the column.

There was significant difference (P<0.05) in the values of the inhibition zones exhibited by *A. schubertii* in response to the effect of each of the nanoparticles, with the highest sensitivity to CS-AgNCs. *A. hydrophyla* also showed the largest inhibition zone with CS-AgNCs among the three nanoparticles (17.50 mm), followed by chitosan (13.00 mm) and then AgNP (8.50 mm). The difference in the inhibition zones among the nanomaterials was highly significant (P<0.05). A similar trend was found among *V. parahaemolyticus*, *K. aerogene*, and *P. mirabilis* with high sensitivity to CS-AgNCs (16.00 mm, 22.50 mm, and 19.00 mm respectively) than Chitosan (15.50 mm, 15.25 mm, and 19.00 mm respectively) and AgNPs (12.50 mm, 13.00 mm and 13.00 mm respectively). The difference observed in the zone of inhibition by each bacterium on each of the nanoparticle along the column is highly significant (P<0.05) (Table 1). However, antibiotics (Ofloxacin) control displayed higher antibacterial efficacy on each of the bacteria than all the tested nanoparticles (Table 1), except for its limitation due to high toxicity on water and fish, which is a serious concern in aquaculture industry. Moreover, these results showed that CS-AgNCs has an excellent antibacterial potential than Chitosan and AgNPs.

Table 1. Antibacterial sensitivity test of Chitosan-Silver nanocomposites, silver nanoparticles and Chitosan (Mean±SD in Millimeter)

Nanoparticles	*A. schubertii*	*A. hydrophyla*	*V. parahaemolyticus*	*K. aerogene*	*P. mirabilis*
AgNPs	8.00[d]±1.15	8.50[d]±0.58	12.50[c]±0.58	13.00[d]±1.15	13.00[c]±1.15
CS-AgNCs	15.00[b]±2.31	17.50[b]±1.73	16.00[b]±1.15	22.50[b]±0.58	19.00[b]±2.31
Chitosan	12.50[c]±0.58	13.00[c]±1.15	15.50[b]±1.73	15.25[c]±0.87	19.00[b]±1.15
Ofloxacin (Control)	26.50[a]±0.58	26.50[a]±0.58	27.50[a]±0.58	26.50[a]±0.58	26.50[a]±0.58

Concentration- 200mg/ml, AgNPs – Silver Nanoparticles,
Value = Mean±SD
*Superscript of the same alphabet along the column shows that there was no significant difference (P>0.05)
*Superscript of different alphabet along the column shows that there was significant difference (P<0.05)

The ANOVA results of Minimum inhibitory concentration (MIC) is shown in Table 2. The Table depicted the lowest concentration of the nanoparticles at which the pathogens were rendered inactive or prevented from multiplying. According to Table 1, CS-AgNCs depicted the least minimum inhibitory concentration when tested on each of the bacteria isolates (25.04 ± 0.01 mg/mL, 18.50±7.51 mg/mL, 18.75±7.51 mg/mL, 12.03±0.03 mg/mL, and 6.23±0.03 mg/mL) which means that lesser concentration of CS-AgNCs will be needed to inhibit the growth of each of the test bacteria isolates, followed by chitosan (37.50±14.43 mg/mL, 50.01±0.02mg/mL, 18.75±7.22 mg/mL, 12.03±0.03 mg/mL and 37.50±14.43 mg/mL), and AgNP (100.03 ± 0.03 mg/mL, 100.09±0.10 mg/mL, 25.02±0.02 mg/mL, 12.52±0.01 mg/mL, and 25.02±0.02 mg/mL). This shows that higher concentration of AgNP will be needed to inhibit the growth of each of the bacterial isolates than will be needed for CS-AgNCs and Chitosan. There were significant differences (P<0.05) in the MIC recorded on the three nanoparticles against each of the test bacteria islolates (*A schubertii, A. hydrophyla, V. parahaemolyticus, K. aerogene, and P. mirabilis*) along the column (Table 2). This result showed that CS-AgNCs has the highest potential than AgNP and Chitosan against all tested fish pathogens. Nevertheless, Ofloxacin (Control) gives the least concentration that will be needed to inhibit the growth of each of these bacteria (3.13±0.01 mg/mL, 3.13a±0.01 mg/mL 2.13±1.16 mg/mL, 3.13±0.01 mg/mL and 3.13±0.01 mg/mL) but high toxicity of antibiotics on fish and pond water, and constant resistance to antibiotics makes it undesirable in aquaculture industry.

Table 2. Minimum Inhibitory Concentration (MIC) of Chitosan-Silver nanocomposites, Silver nanoparticles and Chitosan (Mean ± SD in mg/mL)

Nanoparticles	*A. schubertii*	*A. hydrophyla*	*V. parahaemolyticus*	*K. aerogene*	*P. mirabilis*
AgNP	100.03[a]±0.03	100.09[a]±0.10	25.02[a]±0.02	12.52[a]±0.01	25.02[b]±0.02
CS-AgNCs	37.50[b]±14.43	18.50[c]±7.51	18.75[b]±7.22	6.25[c]±0.00	37.50[a]±14.43
Chitosan	25.04[c]±0.01	50.01[b]±0.02	12.23[c]±0.03	12.03[b]±0.03	6.23[c]±0.03
Ofloxacin (Control)	3.13[d]±0.01	3.13[d]±0.01	2.13[d]±1.16	3.13[d]±0.01	3.13[d]±0.01

Concentration - 100 mg/ml, Control - Ofloxacin, AgNP – Silver nanocomposites

Value = Mean±SD

[*]Superscript of the same alphabet along the column shows that there was no significant difference (P>0.05)

[*]Superscript of different alphabet along the column shows that there was significant difference (P<0.05)

The ANOVA results of Minimum Bactericidal Concentrations (MBC) are shown in Table 3. The Table depicted the lowest concentration of the nanoparticles at which the pathogens were completely destroyed. *A schubertii, A. hydrophyla, V. parahaemolyticus, K. aerogene, and P. mirabilis* strains were completely destroyed when tested with 37.50±14.43 mg/mL, 18.50±7.51 mg/mL, 18.75 ±7.22 mg/mL, 9.38±3.61 mg/mL and 37.50± 14.43 mg/ mL of CS-AgNCs respectively. Also, the minimum bactericidal concentrations when testing the above listed bacterial strain with Chitosan were 50.02±0.02 mg/mL, 50.01 ±0.01 mg/mL, 18.75±7.22 mg/mL, 25.52±0.02 mg/mL and 37.50±14.43 mg/mL respectively. For Silver nanoparticle, the MBC on each of the bacterial isolates were 100.01±0.02 mg/mL, 100.03±0.03 mg/mL, 25.03±0.03 mg/mL, 25.03±0.03 mg/mL and 50.00±0.00 mg/mL respectively. The result depicted a significant difference in the MBC of the nanoparticles on each bacterial strain along the column except on *K. aerogenes* and *P. mirabilis*. *K. aerogene* showed no significant difference in its MBC values when tested on AgNP and Chitosan, but with CS-AgNCs, the difference was highly significant. Likewise, *P. mirabilis* depicted no significant difference in the MBC value when tested on Ofloxacin and CS-AgNC, but with Chitosan and AgNP the difference was highly significant (Table 3).

Table 3. Minimum bactericidal Concentration (MBC) of Chitosan-Silver nanocomposites, silver nanoparticles and Chitosan (Mean ± SD in mg/mL)

Nanoparticles	*A. schubertii*	*A. hydrophyla*	*V. parahaemolyticus*	*K. aerogene*	*P. mirabilis*
AgNP	100.01[a]±0.01	100.03[a]±0.03	25.03[a]±0.03	25.03[a]±0.03	50.00[a]±0.00
CS-AgNCs	37.50[c]±14.43	18.50[c]±7.51	18.75[b]±7.22	9.38[b]±0.00	37.50[b]±14.43
Chitosan	50.02[b]±0.02	50.01[b]±0.01	12.53[c]±0.03	25.52[a]±0.02	6.28[c]±0.03
Ofloxacin (Control)	3.13[d]±0.00	3.13[d]±0.00	3.13[d]±0.00	3.13[c]±0.00	3.13[c]±0.00

Concentration- 100 mg/ml, Control- Ofloxacin, AgNP – Silver nanocomposites

Value = Mean±SD

[*]Superscript of the same alphabet along the column shows that there was no significant difference (P>0.05)

[*]Superscript of different alphabet along the column shows that there was significant difference (P<0.05)

Study on antibacterial activities showed that chitosan-silver nanocomposites displayed an excellent antibacterial efficacy against *A. schubertii, A. hydrophila, V. parahaemolyticus, K. aerogene* and *P. mirabilis.* Generally, antibacterial activity of *A. schubertii* among other test pathogens depicted the least sensitivity, although when tested with CS- AgNCs, it was highly sensitive, unlike chitosan and silver nanoparticles. This suggest that while *A. schubertii* can be resistant to varieties of antibiotics, using alternative antibacterial such as CS-AgNCs, chitosan or AgNP can be more effective, including treatment of fish disease caused by *A. schubertii,* and *A. hydrophila,* which are fish pathogens notably responsible for Motile *Aeromonas Septicemia* disease in freshwater fishes, and are capable of causing high motality (Kartikaningsih *et al.*, 2020). Antibacterial sensitivity test depicted higher sensitivity compared to *A. schubertii, and V. parahemolyticus* when tested on CS-AgNCs, although Chitosan was more effective on *V. pahamolyticus* than *A. hydrophila*. This result was supported by Sahar *et al.*, (2018) whose result on biosynthesized AgNP showed that *A. hydrophyla* was very sensitive to AgNP at 37.00±3.08 mm (inhibition zone) and *V. parahaemolyticus* at 10.00±0.77 mm inhibition zones, depicting a high

sensitivity. Truong *et al.,* (2020) also reported that chitosan synergized with silver nanoparticles enhance antibacterial effect on pathogenic *A. hydrophyla* causing cytotoxicity and cell disruption leading to bacteria death. Likewise, Salah *et al.,* (2023) reported that chitosan and AgNp exhibited high inhibitory activities against *A. hydrophyla* and subsp. *Hydrophyla* on *A. niloticus* as a novel alternative to antibiotics. The inhibition zones were 15.00 mm and 25 00 mm.

However, *P. mirabilis* and *K. aerogene* showed high sensitivity to CS-AgNCs followed by Chitosan and AgNP. The issue here is that while these pathogens are seen as opportunistic, there is a high tendency for them to behave as obligatory fish pathogen, thus more research is needed on them especially in an *in-vivo* investigation.

Minimum Inhibitory Concentration and Minimum Bactericidal Concentration also showed that all test pathogens were sensitive to the three nanomaterials in the following order: CS-AgNCs > Chitosan > AgNP. According to table 2, at a lower dose (25.04 mg/mL, 18.50 mg/mL, 12.23 mg/mL, 12.03 mg/mL, and 6.23 mg/mL), CS-AgNCs was able to inhibit the growth of each bacterium. The same trend was also observed in the minimum bactericidal concentration (MBC). At 50.02

mg/mL, 50.01 mg/mL, 12.53 mg/mL, 25.52 mg/mL, and 6.28 mg/mL, CS-AgNCs was able to completely destroy each bacterium, showing that CS-AgNP has a surpassing antibacterial efficacy, follow by Chitosan, and Silver nanoparticles (Tables 2 and 3). This result is in tandem with the report by Salah *et al.* (2023) who also conducted a similar research on chitosan and silver nanoparticles. He reported that they both have *in vitro* and *in vivo* antibacterial inhibitory and bactericidal property which made them effective broad spectrum antimicrobial agent against multidrug resistant aquaculture threatening pathogens than antibiotics. He also described the mechanism of their antibacterial action, stating that polymer source nanoparticles (such as chitosan and its composites) absorb and destabilize bacteria cell wall, alter membrane permeability, inhibit DNA replication, translation and transcription, and cause reactive oxygen species generation, while inorganic nanoparticles such as silver nanoparticles penetrate cell walls and release silver ions which interact with protein and enzymes synthesis leading to ribosomal denaturation. Honorary *et al.* (2011) also made it clear that high molecular weight of chitosan on whose matrix silver was embedded to form a composite (CS-AgNCs) is a more effective stabilizer (with its inherent antimicrobial property) owing to its flexibility, and with its synergistic combination with Silver nanoparticles, it greatly increased its antibacterial efficacy. Also the small sizes of the nanoparticles and composites produced aids easy and effective penetration into the bacterial cells. These reports are also supported in other literatures *(*Truong *et al.,* 2020; Badawy *et al*., 2019; and Tawfik *et al*., 2021).

4. Conclusion

In this study, Chitosan, AgNP and CS-AgNCs were successfully synthesized through eco-friendly techniques which were confirmed by the results obtained from their characterization. The result of antibacterial activity also showed that the nanoparticles and composites (CS-AgNCs, Chitosan and AgNPs) were all effective against the test bacteria pathogens with CS-AgNCs exhibiting the highest antibacterial efficacy.

Consequently, due to their non-toxicity and biocompatibility, these nanomaterials, most especially CS-AgNCs, can serve as effective antimicrobial agents in fish processing, preservation, pond water treatment, inclusion in fish feed for both prophylactic and therapeutic treatments, thereby enhancing fish production in Nigeria and Sub-Sahara Africa, and contribute significantly to sustainable development goals on food security (SDG 2 of the World Health Organization). The use of housefly maggot serves as a mean of converting waste to wealth. It also helps to regulate environmental pollution through low cost and eco-friendly method. The production of chitosan to realize one of the objectives of this research is a potential avenue to reduce poverty and create job opportunity to the teaming population (SGD 1 of the WHO) if employed industrially. Apart from the use of house fly maggots, other examples of arthropods (shrimps, crabs, millipedes), and mollusks could be explored, whose body consists of higher percentage of chitin but are usually treated as wastes and thus disposed. 'These wastes' can be converted to wealth.

Declaration of Interest Statement

The authors declare no conflict of interests on this research article.

References

Abbas G, Jaffery S, Hashmi, AH, Arshad, M, Usmani, SJ, Imran MS, Taweer A, Tariq M, Saleem M, Arshad M, Amin Q, Khan AA, Alvi MA, Shabbir SB, Qureshi RAM, Mustafa A, Iqbal TA, Iqbal A, Hassan M, Abbas S, Zafar R, Abbas W, Abbas H, Mohyyuddin SG, Ismail W, AL-Taey DKA and Shaukat B. 2022. Current prospects of nanotechnology uses in animal production and its future scenario. *Pakistan J of Sci.* 74 (3):203-222. DOI:10.57041/pjs.v74i3.789

Adeshina I, Abdrahman SA and Yusuf AA. 2016. Occurrence of Klebsiella Species in Cultured African Catfish in Oyo State, South-West Nigeria. *Nigeria J of Vet Med*. African Journal on line (AJOL). 37 (1).

Adeyemo OK, Aina OO, Alarape SA, Bodunde O, Hanson L, Wills R, Subasinghe R, Delamare-Deboutteville J, Khor L, Chadag M. 2023. Isolation and characterization of *Klebsiella* and *Pseudomonas* species from farmed African catfish in Nigeria and their implications. *World aqua society*. World conference on Aquaculture, February 23-26, 2023. New Orleans, Louisiana, USA 555 Canal Street New Orleans, LA 70130, United States.

Ahmad A, Mukherjee P and Senapati S. 2003. Extracellular biosynthesis of silver nanoparticles using the fungus *Fusarium oxysporum*. *Colloids & Surfaces B: Biointerf*, 28 (4): 313–318.

Akintayo GO, Lateef A, Azeez MA, Asafa TB, Oladipo IC, Badmus JA, Ojo SA, Elegbede JA, Gueguim-Kana EB, Beukes LS and Yekeen TA. 2020. Synthesis, Bioactivities and cytotoxicity of animal fur-mediated silver nanoparticles. *IOP Conf. series: Mat. Sci. & Eng*. 805:012041. Doi-10.1088/1757-899X/805/1/012041

Akpodiete OJ, Ologhobo AD and Oluyemi JA. 1997. Production and Nutritive Value of Housefly Maggot Meal on Three Substrates of Poultry Faeces. *J. of Appl. Animal Res.*, 12 (1):101-106, DOI: 10.1080/09712119.1997.9706192. https://doi.org/10.1080/09712119.1997.9706192

Akter M, Sikder T, Rahman M, Ullah A, Hossain K, Hosokawa SB, Saito T and Kurasaki M. 2017. A systematic review on silver nanoparticles-induced cytotoxicity: Physicochemical properties and perspectives. *J of Adv Res*. 9:1–16. doi: 10.1016/j.jare.2017.10.008

Badawy MEI, Lotfy TMR and Shawir SMS. 2019. Preparation and antibacterial activity of chitosan-silver nanoparticles for application in preservation of minced meat. *Bulletin of the Nat. Res. Centre*. 43:83 https://doi.org/10.1186/s42269-019-0124-8

Banala RE, Nagati VB, and Karnati PR. 2015. Green synthesis and characterization of Carica papaya leaf extract coated silver nanoparticles through X-ray diffraction, electron microscopy and evaluation of bactericidal properties. *Saudi J. of Bio. Sci*. 22:637-644

Bharathi D, Diviya JM, Vasantharaj S, Bhuvaneshwari V. 2018. Biosynthesis of silver nanoparticles using stem bark extracts of Diospyros Montana and their antioxidant and antibacterial

activities. *J. Nanostructure Chem.* 8:83–92. 10.1007/s40097-018-0256-7

Chen YF, Liang RS, Zhuo XL, Wu XT. 2012. Isolation and characterization of *Aeromonas schubertii* from diseased snakehead, *Channa maculata* (Lacepède). *J of Fish Diseases* 35(6):421-30. DOI:10.1111/j.1365-2761.2012.01362.x

CLSI. 2014. Clinical and Laboratory Standards Institute. **Performance Standard for Antimicrobial Susceptibility Testing**; Twenty-fourth information supplement. CLSI Document M100-S24, Wayne, 34(1).

Cristiano C, Dolores VP, Maria RG, Siyuan D, Roberta C, and Piera Di Martino. 2019. Chitin and Chitosans: Characteristics, Eco-Friendly Processes, and Applications in Cosmetic Science- a review. *Marine Drug.* Vol. 17:(1) 369:1-30. doi:10.3390/md17060369

Danish M, Shahid M, Ahamad L, Raees K, Hatamleh AA, Al-Dosary MA, Mohamed A, Abdulrhman Y, Wasel A, Singh UB and Danish S. 2022. Nano-pesticidal potential of Cassia fistula (L.) leaf synthesized silver nanoparticles (Ag-CfL-NPs): Deciphering the phytopathogenic inhibition and growth augmentation in Solanum lycopersicum (L). *Frontiers in Mic.* 10:1-18

Dayem, A.A; Hossain, M.K.; Lee, S.B.; Kim, K.; Saha, S.K.; Yang, G.-M.; Choi, H.Y.; Cho, S.-G. 2017. The Role of Reactive Oxygen Species (ROS) in the Biological Activities of Metallic Nanoparticles. *Int. J. Mol. Sci*, 18, 120.

Fajardo C, Martinez-Rodriguez G, Blasco J, Mancera JM, Thomas B, De Donato M. 2022. Nanotechnology in aquaculture: Applications, perspectives and regulatory challenges. *Aqua and Fish.* Vol. 7(2):188-200. https//doi.org/10.1016/j.aaf.2021.12.006.

Ghafouri SM, Entezari M, Taghva A and Zahra Tayebi, Z. 2017. Biosynthesis and evaluation of the characteristics of silver nanoparticles using *Cassia fistula* fruit aqueous extract and its antibacterial activity. *Adv. Nat. Sci*.: Nanosci. Nanotechnol. https://doi.org/10.1088/043-6254/aa92bb

Govindan S, Nivethaa EA, Saravanan R, Narayanan V, Stephen A. 2012. Synthesis and characterization of chitosan–silver nanocomposite. *J. Appl Nanosci.* 2:299–303. springerlink.coms

Gowda PS and Sriram S. 2023. Green synthesis of chitosan silver nanocomposites and their antifungal activity against *Colletotrichum truncatum* causing anthracnose in chillies. *Plant nanobio.* Vol. 5. doi. https/doi.org/10.101016/j.plana.

Hezron L, Madalla N and Sebastian W, Chenyambuga SW. 2019. Mass production of maggots for fish feed using naturally occurring adult houseflies (*Musca domestica*). *Livestock Res for Rural Dev.* 31(4)

Honary S, Ghajar K, Khazaeli P and Shalchian P. 2011. Preparation, Characterization and Antibacterial Properties of Silver-Chitosan Nanocomposites Using Different Molecular Weight Grades of Chitosan. *Tropical J of Pharm Res.* 2011. 10 (1): 69-74.

Huang S, Wang L, Liu L, Hou Y, and Lu-Li L. 2015. Nanotechnology in agriculture, livestock, and aquaculture in China. A review. *Agron. Sustain. Dev.* 35:369–400. DOI 10.1007/s13593-014-0274-x

Irshad MD, Zafaryab MD, Man S, and Moshahid M. 2014. Comparative Analysis of the Antioxidant Activity of *Cassia fistula* Extracts, *Int J of Med Chem* Vol.12.

Islam NU, Jalil K and Shahid M. 2021. Green synthesis and biological activities of gold Nanoparticles functionalized with *Salix alba*. *Arab J Chem*. http://doi.org/10.1016/j.arabj

c.2015.06.025

Kamari A, Ngah WS, Chang MY and Cheah ML. 2009. Sorption of acid dyes unto GLA and H_2 SO_4 cross-linked Chitosan beads. *Desalination*. 249:1180-1189

Kartikaningsih H, Yahya F, Rohman Z and Jaziri AA. 2020. Characteristics of *Aeromonas hydrophila*-infected Catfish (*Clarias sp.*). International Conference on Sustainable Aquatic Resources IOP Conf. Series: Earth and Environmental Science. 10:493-500. 012036 *IOP Pub*. doi:10.1088/1755-1315/493/1/012036

Kaur P, Choudhary, A and Thakur RR. 2012. Synthesis of Chitosan-Silver Nanocomposites and their Antibacterial Activity. *Int. J. of Sci and Eng. Res*, Volume 4, Issue 4, ISSN 2229-5518

Kim MW, Han YS, Jo H. 2016. Extraction of chitin and chitosan from housefly, *Musca Domestica,* pupa shells. *Entomol Res*. 46: 324–328.

Manikandan A and Sathiyabama M. 2016. Preparation of Chitosan nanoparticles and its effect on detached rice leaves infected with Pyricularia grisea *Int. J. of Bio. Macro*. 84:58-61. doi: 10.1016/j.ijbiomac.2015.11.083.

Mohanta YK, Panda SK, Jayabalan R, Nanaocha SN, Bastia AK and Mohanta TK. 2017. Antimicrobial, Antioxidant and Cytotoxic Activity of Silver Nanoparticles Synthesized by Leaf Extract of *Erythrina suberosa* (Roxb.). *Frontier in molecular biosci*. 4 (14):1-7. doi: 10.3389/fmolb.2017.00014

Nam NH and Luong NH. 2019. Nanoparticles: synthesis and applications. Materials for biomedical applications. doi: 10.1016/B978-0-08-102814-8.00008-1. 211-240.

Nikalje AP. 2015. Nanotechnology and its Applications in Medicine. *Medicinal chem.* 5 (2): 81-89. http://dx.doi.org/10/4172/2161-0444.1000247.

Nowack B, Krug HF and Height M. 2011. 120 years of Nanosilver History, Implication for Policy Makers. *Environ. Sci. Technol.*, 45: 1177–1183.

Olaniyan OJ, Dare EO, Adetunji OR, Adedeji OO and Ogungbesan, SO. 2016. Synthesis and Characterization of Chitosan-Silver Nanocomposite Film Nano Hybrids and Composites ISSN: 2297-3400, 11:22-29. Doi:10.4028/www.scientific.net/NHC. *Trans Tech Pub*, Switzerland

Olugbojo JA and Ayoola SO. 2015. Comparative studies of bacteria load in fish species of Commercial importance at the aquaculture unit and lagoon front of the University of Lagos, Lagos. *Int J of Fish and Aqua*. 7(4):37-46. www.academicjournals.org/ijfa

Oves M, Rauf MA, Aslam M, Qari HA, Sonbol H, Ahmad I, ZamanGS, and Saeed M. 2021. Green synthesis of silver nanoparticles by *Conocarpus Lancifolius* plant extract and their antimicrobial and anticancer activities. *Saudi J of Bio Sci* 29(1): 460–471. doi: 10.1016/j.sjbs.2021.09.007

Ramon DR, Torres SP, Tenorio AY, Gómez SA, and Valencia AA. 2023. Chitosan: Properties and Its Application in Agriculture in Context of Molecular Weight *Polymers*. *15*(13), 2867; https://doi.org/10.3390/polym15132867

Sahar WM., and Hala H. Abd El-latif. 2018. Characterization and application of biosynthesized AgNP by marine pseudomonas. *J. of Pure and Appl. Micro*. 12 (3):1289-1299. https://doi.org/10.22207/JPAM.12.3.31.

Salah MA, Eissa AE, Abdel-Razek, N and El-Ramlawy, AO. 2023. Chitosan nanoparticles and green synthesized silver nanoparticles as novel alternatives to antibiotics for preventing *A. hydrophila subsp.*

hydrophila infection in Nile tilapia, *Oreochromis niloticus. Int J of Vet Sci & Med.*. 11(1): 38–54. Published online doi: 10.1080/23144599.2023.2205338

Selim YA, Maha A. Azb MA, Islam Ragab I and Abd El-Azim MHM. 2020. Green Synthesis of Zinc Oxide Nanoparticles Using Aqueous Extract of *Deverra tortuosa* and their Cytotoxic Activities. *Sci Reports*. 10:3445 |https://doi.org/10.1038/s41598-020-60541-1 4

Song YS, Seo DJ, Ju WT, Park RD and Jung WJ. 2014. Preparation of chitosan with sodium hydroxide according to condition of temperatures. *J of Chitin and Chitosan* 19: 8–14.

Swarnalathan R, Christina RS and Payas B. 2012. Evaluation of in vitro antidiabetic activity of *Sphaeranthus amaranthoides* silver nanoparticles. *Int J of Nanomat Biostructure*, 2 (3): 25–29.

Tawfik M, Tawfik I, Ahmed MA. El-Masry. 2021. Preparation of Chitosan Nanoparticles and its Utilization as Novel Powerful Enhancer for Both Dyeing Properties and Antimicrobial Activity of Cotton Fabrics. *Biointerface Res in Appl Chem*. 11 (5):13652 – 13666. https://doi.org/10.33263/BRIAC115.1365213666

Tesfaye, M., Gonfa, Y., Tadesse, G., Temesgen,T and Periyasamy, S. 2023. Green synthesis of silver nanoparticles using *Vernonia amygdalina* plant extract and its antimicrobial activities. *Heliyon*. 9(6):11-20. doi: 10.1016/j.heliyon.2023.e17356

Thai HHP, Kim D, Thi C, Quach Van Q. Nguyen, PT Nguyen, TL. 2023. Prevalence and antibiotic resistance of Aeromonas schubertii causing internal white spot disease on snakehead fish, Channa striata, in the Mekong Delta, Vietnam. *J of World Aqua Soc*. 23: 1-17. DOI: 10.1111/jwas.12954

Truong T, Nguyenb D, Hien Quoc Nguyena. 2020. Nanocomposite of silver nanoparticles/diatomite against bacteria pathogens of catfish. *Int J of Vet sci & med*. Hanh Thi Research and Development Center for Radiation Technology, Vietnam Atomic Energy Institute, 202A, Street 11, Linh Xuan Ward, Thu Duc District, Ho Chi Minh City.

Younes I and Rinaudo M. 2015: Review Chitin and Chitosan Preparation from Marine Sources. Structure, Properties and Applications. *Marine drugs*. 13: 1133-1174; doi: 10.3390/md13031133.ISSN:1660-3397 www.mdpi.com/journal/marinedrugs

Zhai W, Wang WQ, Zhu X Jia, X, Chen, L. 2023. Pathogenic infection and microbial composition of yellow catfish (*Pelteobagrus fulvidraco*) challenged by *Aeromonas veronii* and *Proteus mirabilis. Aqua and Fish. 8(2): 166-173*

Zondi N, Moloto MJ, Mubiayi1 PK, Sibiya PN. 2018. Green synthesis of chitosan capped Silver nanoparticles and their antimicrobial activity. *MRS. Adv. Mat. Res. Soc*. DOI: 10.1557/adv.2018.368

Zhuling R, Yan C, Shifeng W, Shubin L., Youfei X, Jiaqing T, Yun S. Weiliang, G,a Yongcan, Z. 2019. First case of Aeromonas schubertii infection in brackish water wild Nile tilapia, *Oreochromis niloticus*, in China. *Aquaculture*. 10.1016/j.aquaculture.2018.11.036.

JJBS

Jordan Journal of Biological Sciences

Association between Sex hormone-binding Globulin Levels and Thyroid Function in Bladder Cancer

Saleem Ali Banihani[1,*], Yasmeen Maher Abu-Gharaibeh[1], Omar M. Halalsheh[2]

[1]Department of Medical Laboratory Sciences, Faculty of Applied Medical Sciences, Jordan university of science and technology, P.O. Box 3030, Irbid 22110, Jordan; [2]Department of General Surgery and Urology, Faculty of Medicine, Jordan University of Science and Technology, P.O. Box 3030, Irbid 22110, Jordan.

Abstract

Previous research has associated thyroid hormones with cancer development and progression, highlighting their role in synthesizing sex hormone-binding globulin (SHBG), which is implicated in cancer growth. However, the specific influence of these hormones and proteins on bladder cancer remains unexplored. This study aims to investigate potential correlations between free triiodothyronine (fT3), free thyroxine (fT4), thyroid-stimulating hormone (TSH), thyroxine-binding globulin (TBG), SHBG, and bladder cancer in Jordanian patients diagnosed with this malignancy. A cohort of 30 bladder cancer patients and 30 matched controls were recruited. Serum levels of fT3, fT4, TSH, TBG, and SHBG were measured using ELISA. Elevated concentrations of fT3 (4.64 ± 0.16 pmol/L), fT4 (14.86 ± 0.37 pmol/L), and SHBG (1227 ± 102.2 nmol/L) were observed in patients compared to healthy individuals ($p = 0.006$, $p = 0.002$, and $p < 0.0001$, respectively). However, TSH (1.47 ± 0.15 mIU/L) and TBG (4.3 ± 0.64 mg/L) levels showed no significant differences ($p = 0.319$, $p = 0.455$, respectively) between the groups. This study confirms a link between higher serum levels of fT3, fT4, and SHBG and the presence of bladder cancer, suggesting these elevated levels may indicate an increased risk. SHBG, in particular, stands out as a potential biomarker for predicting susceptibility to bladder cancer, warranting further investigation.

Keywords: Bladder cancer, thyroxine, thyroid-stimulating hormone, thyroxine-binding globulin, sex hormone binding globulin.

1. Introduction

Bladder cancer, a prevalent malignancy affecting the urinary bladder, poses a significant health burden globally, with various histological subtypes such as transitional cell carcinoma, squamous cell carcinoma, and adenocarcinoma (Babjuk*, et al.*, 2020). Urothelial (transitional cell) carcinoma represents the predominant subtype, comprising approximately 90% of cases (Clark*, et al.*, 2013 Comperat*, et al.*, 2022). Despite advancements in treatment modalities, bladder cancer remains a formidable challenge, ranking as the 10th most common cancer worldwide with an estimated 212,536 deaths and 573,278 new cases in 2020, according to Globocan (Sung*, et al.*, 2021). Bladder cancer is classified into muscle-invasive bladder cancer (MIBC) and non-muscle-invasive bladder cancer (NMIBC) based on the extent of tumor invasion. NMIBC is confined to the urothelium or lamina propria and often recurs but is less likely to progress to a life-threatening stage, whereas MIBC, which invades the detrusor muscle, requires aggressive treatment (Lopez-Beltran*, et al.*, 2024 de Jong*, et al.*, 2023). Smoking remains a well-established risk factor, contributing significantly to the incidence of bladder cancer (Sung*, et al.*, 2021 Zhao*, et al.*, 2022 Jubber*, et al.*, 2023).

Recent work has underscored the significance of sex hormone receptor signaling in the pathogenesis of urothelial cancer (Zhu*, et al.*, 2023). Studies have demonstrated that the activation of androgen and estrogen receptors play a pivotal role in initiating various cellular cascades and pathways linked to urothelial tumorigenesis, including the AKT/ERK pathway (Zheng*, et al.*, 2011).

Thyroxine (T4), a key hormone essential for normal growth, metabolism, and development, has been extensively studied regarding various types of cancer. Studies have revealed the intricate associations between cancer and thyroid hormones (Moeller*, et al.*, 2013). In the last two decades, the understanding of mechanisms by which thyroid hormones exert their effects has notably advanced. Thyroid hormones utilize a non-genomic pathway for their activity, involving a plasma membrane integrin called $\alpha v \beta 3$ as a membrane receptor (Davis*, et al.*, 2016). Importantly, this receptor possesses two distinct hormone binding sites, S1 and S2, each initiating distinct signaling cascades (Freindorf*, et al.*, 2012). The S1 site selectively binds physiological levels of triiodothyronine (T3), activating phosphatidylinositol-3-kinase, subsequently stimulating the transcription factor hypoxia-inducible factor 1 (HIF1) (Moeller*, et al.*, 2013). The expression of HIF1 target genes is closely linked to tumor initiation, progression, invasion, and metastasis (Moeller,

---

* Corresponding author. e-mail: sabanihani@just.edu.jo.

Abbreviations: fT3 Free triiodothyronine; fT4 Free thyroxine; TSH Thyroid-stimulating hormone; TBG Thyroxine-binding globulin; SHBG Sex hormone-binding globulin; HIF1 Hypoxia-inducible factor 1

et al., 2013). In contrast, the second site, S2, exhibits reduced affinity for T4 compared to T3, leading to activation of the ERK1/2 pathway (Lin, *et al.*, 2009).

Thyroid hormones, facilitated by the αvβ3 integrin, promote the proliferation of both blood vessel cells and cancer cells (Davis, *et al.*, 2016). Clinical studies have revealed that hyperthyroidism may be associated with an increased risk of certain solid tumors, while malignancies may progress more slowly or less aggressively in cases of spontaneous hypothyroidism (Hercbergs, *et al.*, 2010). These findings have been reported for various cancers, including lung (Khan, *et al.*, 2016), breast (Tran, *et al.*, 2023), prostate (Chan, *et al.*, 2017), ovary (Ness, *et al.*, 2000), colorectal (Gagliardi, *et al.*, 2023), central nervous system (Mellemgaard, *et al.*, 1998), esophageal (Turkyilmaz, *et al.*, 2010), hematologic cancer (Ghalaut, *et al.*, 2012), and overall solid cancer (Khan, *et al.*, 2016). However, the role of thyroid hormones in bladder cancer remains unexplored.

Emerging research has also delved into the intricate relationship between thyroid hormones and sex hormones, highlighting the significance of thyroid hormone in the synthesis of Sex Hormone-Binding Globulin (SHBG) (Selva, *et al.*, 2009). It is well-established that thyroid hormones facilitate SHBG synthesis (Selva, *et al.*, 2009), regulating the transport and binding of estrogen and androgen hormones to their respective receptors. Moreover, estrogen has been shown to elevate thyroxine-binding globulin (TBG) levels (Robbins, *et al.*, 1978), whereas androgens tend to reduce TBG levels (Tahboub, *et al.*, 2009), with TBG primarily responsible for transporting thyroid hormones to target tissues.

Considering the growing body of evidence linking sex hormones to bladder cancer, coupled with the intricate interplay between sex hormones and thyroid hormones, and the acknowledged role of thyroid hormones in cancer pathogenesis, we aimed to investigate the potential involvement of thyroid hormones in bladder cancer. Our study sought to explore possible associations between thyroid-stimulating hormone (TSH), free thyroxine (fT4), free triiodothyronine (fT3), TBG, SHBG, and bladder cancer among Jordanian individuals diagnosed with this malignancy. We hypothesize that these hormones and proteins may exhibit correlations with an elevated risk and prevalence of bladder cancer. This research endeavor aspires to contribute to the improved management and understanding of bladder cancer.

2. Materials and Methods

2.1. Study Subjects and Sample Collection

This study was a case-control study conducted at the Urology Clinic at Princess Basma Teaching Hospital and the University Hospital of J.U.S.T in Irbid Province, located in the north of Jordan. The study included 30 patients diagnosed with early invasion (stage PT1) bladder cancer. Among these patients, there were 26 males and 4 females, ranging in age from 47 to 83 years. All patients had been diagnosed within 1 year of enrollment, had confirmed histology of bladder cancer, and had not received any prior chemotherapy or radiotherapy

treatments. The study did not impose any age or gender restrictions.

Among the participants, 12 individuals had hypertension and were using angiotensin-converting enzyme inhibitors, four had type I diabetes and were using insulin, and five had type 2 diabetes and were using metformin. Additionally, 30 healthy volunteers of similar age (within 5 years) and gender, with no history of cancer, thyroid disorders, diabetes, high blood pressure, recent surgery, or use of vitamin supplements, were recruited as controls for comparison.

Individuals who had received any form of hormone therapy in the past, as well as those with chronic conditions such as chronic kidney disease, heart disease, uncontrolled diabetes mellitus, cerebrovascular disease history, or a history of any malignancy, were excluded from participating in the study.

It is important to note that this study is designed to investigate the association between specific factors (such as thyroid hormones) and bladder cancer risk in a specific population. The inclusion of controls and the careful consideration of confounding variables, such as age, gender, and medical conditions, helps to ensure reliable and meaningful research findings.

All blood samples were collected during the period from November 2022 to May 2023. Blood Samples were collected from patients and the control group in a plain tube without additives in the early morning without fasting requirements.

2.2. Ethical Approval

In the study, the aims and analysis of the research were transparently and honestly explained to all individuals who were recruited as subjects. Before enrollment, each participant provided written informed consent, signifying their voluntary decision to take part in the study. Additionally, a questionnaire was administered to gather relevant information from the participants. Furthermore, the study protocol and procedures received approval from the Institutional Review Board (IRB) Committee, with the assigned identification number 558-2022, at Jordan University of Science and Technology located in Irbid, Jordan. The IRB's approval signifies that the study design, ethical considerations, and protection of participants' rights were carefully reviewed and deemed acceptable.

2.3. Experimental Design and Sample Preparation

During the study, blood samples were collected from participants in the morning between 9:00 and 11:00 AM. Plain tubes without anticoagulants were used to collect the blood samples. After approximately 20 minutes to allow for clotting, the samples were centrifuged for 5 minutes at a speed of 4000 rpm. This centrifugation process helped to separate the serum from other components of the blood.

Following centrifugation, the serum was carefully separated from each specimen. Each sample was then divided into smaller aliquots and stored at a temperature of -83 °C for future use. We were concerned about the stability of thyroid hormones in frozen samples because we collected them over several months. But based on a recent study, thyroid hormone concentrations are stable even after years when are kept frozen at -25° (Mannisto, *et al.*, 2010). This freezing temperature helped to maintain

the integrity and stability of the samples until they were ready for measurement.

On the day of measurement, the samples were thawed at room temperature and gently mixed by inverting the tubes in a gentle manner. This ensured that the samples were well-mixed and representative of the subsequent measurements and analyses to be conducted. The described process of blood collection, serum separation, and storage followed standard procedures to ensure the quality and consistency of the samples for accurate measurements in the study.

2.4. Biochemical Measurements

Serum concentrations of fT3, fT4, TSH, TBG, and SHBG were determined using enzyme-linked immunosorbent assay (ELISA) kits following the manufacturer's instructions. The TSH, fT4, and fT3 ELISA kits were purchased from Monobind Inc. (Lake Forest, CA 92630, USA), the TBG ELISA kit was purchased from Fine Test (cat no. EH0833; Wuhan Fine Biotech, China), and the SHBG ELISA kit was purchased from Cloud-clone Corp. (cat no. SEA396Hu; USA). To assess SHBG levels, serum samples underwent a 1,000-fold dilution in phosphate-buffered saline supplemented with 0.1% bovine serum albumin (cat no. P3688; Sigma-Aldrich; Merck KGaA, Darmstadt, Germany). Absorbance readings were obtained using an ELx800 microplate reader (Bio Tek Instruments, Inc., Winooski, VT, USA) at a wavelength of 450 nm. Each assay was measured in duplicate, and then the mean was calculated. All these tests were conducted manually in the biochemistry research laboratory at Jordan University of Science and Technology.

2.5. Statistical Analysis

In this investigation, analysis was conducted employing GraphPad Prism version 12 (GraphPad Software Incorporated, San Diego, U.S.A.). To compare samples and controls with normally distributed data, a student's *t*-test was employed. Statistical significance was defined as a "p" value < 0.05. Normality of the data was assessed using the D'Agostino-Pearson and Shapiro-Wilk tests.

3. Results

Table 1 presents the comparison of baseline characteristics between the bladder cancer group (n=30) and the control group (n=30). The parameters analyzed include age, BMI, gender, and medical history. The p-values are above 0.05, suggesting no statistically significant differences between the two groups for these parameters.

Table 1. Baseline characteristics of the study participants.

Parameter	Bladder cancer (n=30)	Control (n=30)	p-value
Age, years $\pm$ SD	64.3 ± 9.8	61 ± 8.7	0.3
BMI, value $\pm$ SD	26.5 ± 3.4	25.9 ± 3.7	0.5
Male, n (%)	26 (86.7)	26 (86.7)	_
Female, n (%)	4 (13.3)	4 (13.3)	_
Medical history, n (%)			
Smoking	25 (83.3)	23 (76.7)	0.5
Hypertension	12 (40)	13 (43.3)	0.8
Diabetes	9 (30)	7 (23.3)	0.6

The fT4 average concentration in the bladder cancer patient group and the control group are illustrated in Figure 1. As demonstrated in the figure, the mean concentration of fT4 was significantly higher (p = 0.002) in the patient group (14.86 ± 0.37) compared to the control group (13.35 ± 0.24).
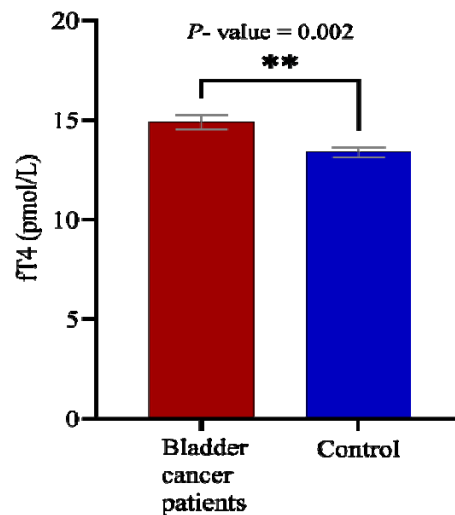
Figure 1. The concentration of free T4 in bladder cancer patients (n = 30) and control (n = 30). The mean concentration of fT4 was significantly higher in the patient group compared to the control group. Data represents the mean value ± S.E.M. (**p < 0.01).

Figure 2 depicts the average concentration of fT3 in the bladder cancer patient group and the control group. As illustrated in the figure, the mean concentration of fT3 was significantly higher (p = 0.006) in the patient group (4.64 ± 0.16) compared to the control group (4.09 ± 0.1).
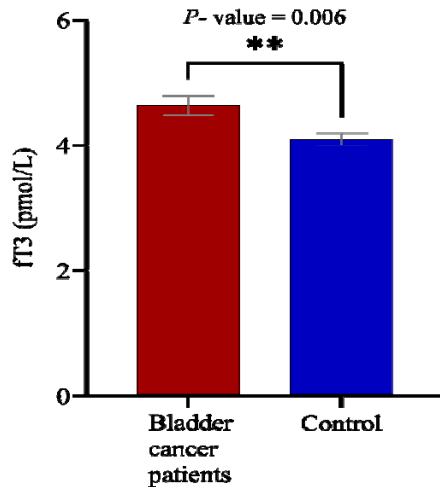
Figure 2. The concentration of free T3 in bladder cancer patients (n=30) and control (n=30). The mean concentration of fT3 was significantly higher in the patient group compared to the control group. Data represents the mean value ± S.E.M. (**p < 0.01).

The average concentration of TSH in the bladder cancer patient group and the control group is represented in Figure 3. As can be seen in the figure, the mean concentration of TSH decreased in the patients group compared to the control, but it did not reach a significant difference (p = 0.319). The mean ± SEM values of TSH in the patient group and control group were (1.47 ± 0.15) and (1.68 ± 0.14), respectively.
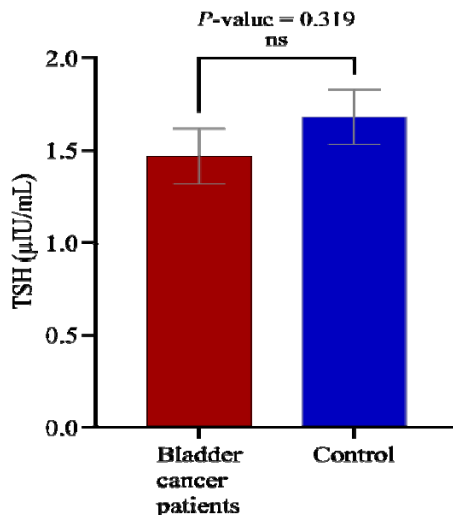
Figure 3. The concentration of free TSH in bladder cancer patients (n=30) and control (n=30). The mean concentration of TSH decreased in the patient group compared to the control group, but the difference was not statistically significant. Data represents the mean value ± S.E.M.

Figure 4 depicts the average concentration of TBG in the bladder cancer patient group and the control group. As illustrated in the figure, the mean concentration of TBG was not significantly different (p = 0.455) between the patient group (4.3 ± 0.64) and the control group (3.8 ± 0.62). The normal range for TBG is $10 - 25$ µg/mL.
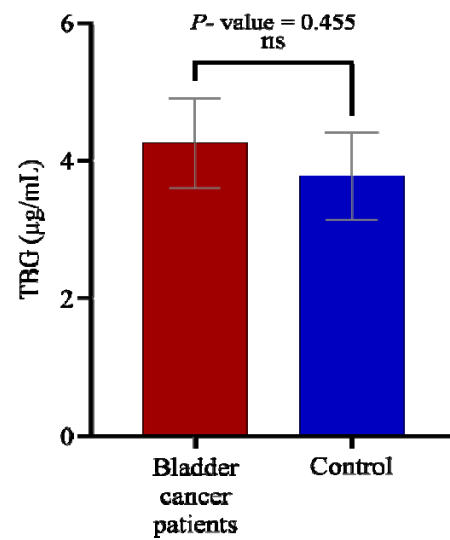
Figure 4. The concentration of TBG in bladder cancer patients (n=30) and control (n=30). The mean concentration of TBG was not significantly different between the patient group and the control group, with a p-value higher than 0.5. Data represents the mean value ± S.E.M.

Figure 5 demonstrates the average concentration of SHBG in the bladder cancer patient group and the control group. As illustrated in the figure, the mean concentration of SHBG was significantly higher (p < 0.0001) in the patient group (1227 ± 102.2) compared to the control group (642.7 ± 69.9).
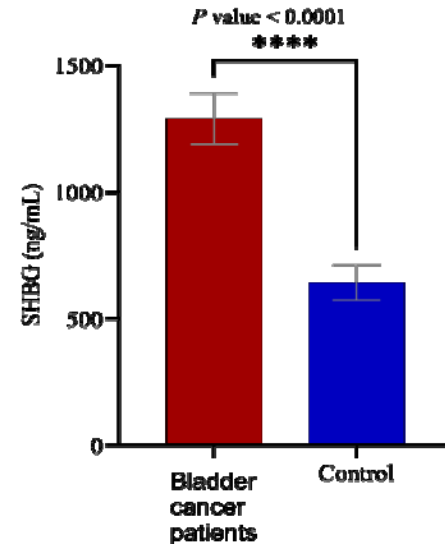
Figure 5. The concentration of SHBG in bladder cancer patients (n=30) and control (n=30). The mean concentration of SHBG was significantly higher in the patient group compared to the control group. Data represents the mean value ± S.E.M. (****p < .0001).

Figure 6 depicts Pearson's correlation between SHBG and thyroid hormones in bladder cancer patients. As illustrated in the figure, there was a strongly positive correlation between SHBG and fT4 concentrations (A: $r^2 = 0.868$, p < 0.0001) and between SHBG and fT3 concentrations (B: $r^2 = 0.893$, p < 0.0001).
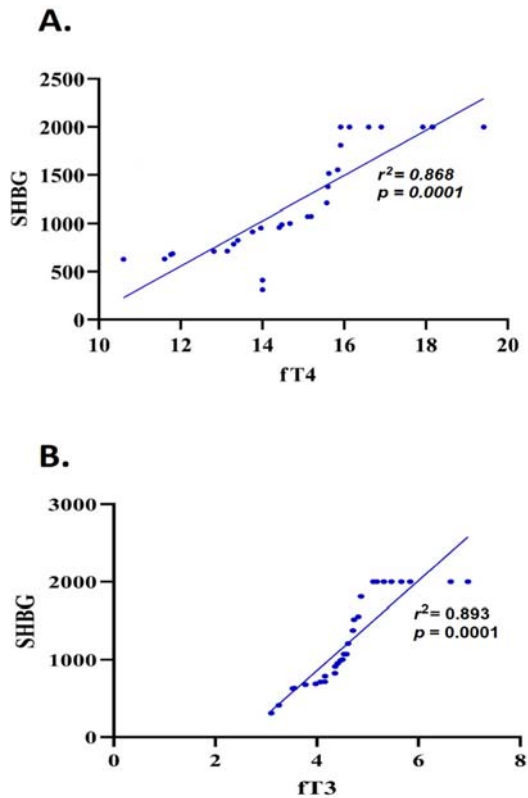
Figure 6: Pearson's correlation scatter plot between SHBG (ng/mL) and fT4 (pmol/L) (**A**), and fT3 (pmol/L) (**B**). There was a strong positive correlation between SHBG and fT4 concentrations and between SHBG and fT3 concentrations.

4. Discussion

Numerous studies have confirmed an association between thyroid hormones and almost all types of cancer, with the exception of bladder cancer (Krashin*, et al.*, 2019 Ma*, et al.*, 2023). Until now, no study has definitively clarified the relationship between thyroid hormones and bladder cancer. Therefore, it was crucial to investigate the connection between thyroid hormones and bladder cancer, which is precisely what we aimed to accomplish in this study.

In this case-control study of untreated early-stage bladder cancer patients, we observed significantly higher levels of fT4 and fT3 in bladder cancer patients compared to healthy controls, while the measurements were still within the known normal range. Conversely, we found that TSH levels decreased in bladder cancer patients when compared to healthy controls; however, this decrease did not reach statistical significance.

We attempted to provide a logical explanation for these findings. Considering that the average age of the study population is 64 years old, it is possible that age-related changes in the hypothalamus-pituitary-thyroid axis could contribute to the observed differences in TSH levels. Previous research has indicated that serum TSH levels tend to increase with age, while fT4 levels remain relatively stable. This discrepancy between TSH and fT4 levels in an elderly population could explain the lack of correlation

observed in our study (Gesing*, et al.*, 2012). Another possible reason is the small sample size that caused the "p" value to not reach the significance level in the TSH test.

To the best of our knowledge, this is the inaugural case-control study that examines the connection between the complete spectrum of thyroid function and bladder cancer, both in Jordan and worldwide. Our research reveals that elevated levels of fT3 and fT4 may be linked to a higher occurrence and risk of bladder cancer. Interestingly, certain aspects of our findings align with the results from Khan et al.'s study, a prospective cohort study encompassing nearly 10,318 participants which demonstrated a significant association between higher levels of FT4 and an increased risk of various types of solid, lung, and breast cancers, while no correlation was observed with TSH levels (Khan*, et al.*, 2016).

In the current study, no difference was observed in TBG concentration between bladder cancer patients and healthy controls. These results validate the accuracy of the thyroid function test outcomes without any interferences. Furthermore, they suggest that individuals with bladder cancer may exhibit elevated levels of total T4 and T3 as well. Additionally, the findings indicate that the observed increases in fT4 and fT3 levels are indeed accurate and meaningful in relation to bladder cancer.

To date, there have been no studies that have definitively established the role of SHBG in bladder cancer. Therefore, in this study, we conducted measurements of SHBG protein concentration in bladder cancer patients for the first time. Our aim was to explore whether these results could provide insights into the potential association between SHBG and the observed differences in incidence rates between males and females.

In this study, SHBG concentration was much higher in bladder cancer patients compared to healthy controls. The increased concentration of SHBG may be attributed to the rise in thyroid hormone levels. Previous studies have shown that high levels of T3 and T4 can stimulate the liver to produce SHBG (Selva*, et al.*, 2009 Rosner*, et al.*, 1984). Consequently, our findings are in line with this relationship. These results could potentially provide an explanation for the high bladder cancer incidence rates in males.

According to Global Cancer Statistics, around 77% of bladder cancer cases occur in men (Sung*, et al.*, 2021). The potential mechanism underlying the impact of SHBG on this disparity in incidence rates can be explained as follows: Numerous studies have demonstrated that SHBG has the ability to stimulate the nongenomic action of androgens. This is attributed to the fact that the binding of androgens by SHBG can activate the cyclic adenosine monophosphate and protein kinase A pathways (Heinlein*, et al.*, 2002). This mechanism may have the potential to influence the transcriptional activation of the nuclear androgen receptor (AR) (Heinlein*, et al.*, 2002).

Moreover, previous studies have revealed that the transcriptional activity of the AR is augmented through protein kinase A stimulation, even in the presence of minimal androgen levels (Sadar, 1999 Nazareth*, et al.*, 1996 Ikonen*, et al.*, 1994). Regarding this mechanism, studies have identified that the proliferation of prostate cells in prostate cancer and the transcriptional activation of AR could be intensified by interactions between

dihydrotestosterone and SHBG through the induction of signal transduction cascades (Nakhla, *et al.*, 1996). Furthermore, weak adrenal androgens or estradiol might contribute to AR transcriptional activity by stimulating SHBG signaling (Nakhla, *et al.*, 1997)cl

In conclusion, this study reveals that there is an association between elevated serum levels of fT4, fT3, and SHBG and bladder cancer. These results suggest that fT4, fT3, and SHBG are positively associated with an increased incidence and risk of bladder cancer. SHBG also emerges as a potential candidate for serving as a valuable biochemical marker to predict susceptibility to bladder cancer. These findings indicate that monitoring and controlling T3, T4, and SHBG levels in bladder cancer patients may have implications for disease management and prognosis.

Nevertheless, it is crucial to emphasize the necessity for validating these findings through larger cohort studies with extended follow-up periods, encompassing a more substantial participant pool, and including gender-based analyses. Moreover, additional research is warranted to clarify the precise involvement of thyroid hormones in bladder cancer patients and delve into their potential impact on cancer progression and onset. Besides, investigating the dynamic interplay between SHBG and other factors contributing to bladder cancer progression could potentially cover the way for the development of targeted diagnostic approaches in the field.

5. Funding

6. Data availability

The data utilized in this study was generated by Department of Medical Laboratory Sciences at Jordan University of Science and Technology. While the data is not currently available online, the authors are willing to provide access to the data upon reasonable request from the editors.

Declarations

Conflict of interest

The authors declare no competing financial or non-financial interests.

Ethical approval

This study received approval from the Jordan University of Science and Technology (IRB 558-2022) and adhered to the ethical principles outlined in the 1964 Helsinki Declaration and its subsequent amendments.

Informed consent

All participants provided written informed consent for the publication of their data.

References

Clark PE, Agarwal N, Biagioli MC, Eisenberger MA, Greenberg RE, Herr HW, Inman BA, Kuban DA, Kuzel TM, Lele SM. 2013. Bladder cancer. *J Natl Compr Cancer Netw.* **11(4)**: 446-75.

Comperat E, Amin MB, Cathomas R, Choudhury A, De Santis M, Kamat A, Stenzl A, Thoeny HC, Witjes JA. 2022. Current best practice for bladder cancer: a narrative review of diagnostics and treatments. *Lancet.* **400(10364)**: 1712-21.

Sung H, Ferlay J, Siegel RL, Laversanne M, Soerjomataram I, Jemal A, Bray F. 2021. Global Cancer Statistics 2020: GLOBOCAN Estimates of Incidence and Mortality Worldwide for 36 Cancers in 185 Countries. *CA Cancer J Clin.* **71(3)**: 209-49.

Lopez-Beltran A, Cookson MS, Guercio BJ, Cheng L. 2024. Advances in diagnosis and treatment of bladder cancer. *BMJ.* **384**: e076743.

de Jong FC, Laajala TD, Hoedemaeker RF, Jordan KR, van der Made ACJ, Boeve ER, van der Schoot DKE, Nieuwkamer B, Janssen EAM, Mahmoudi T, Boormans JL, Theodorescu D, Costello JC, Zuiverloon TCM. 2023. Non-muscle-invasive bladder cancer molecular subtypes predict differential response to intravesical Bacillus Calmette-Guerin. *Sci Transl Med.* **15(697)**: eabn4118.

Zhao X, Wang Y, Liang C. 2022. Cigarette smoking and risk of bladder cancer: a dose-response meta-analysis. *Int Urol Nephrol.* **54(6)**: 1169-85.

Jubber I, Ong S, Bukavina L, Black PC, Comperat E, Kamat AM, Kiemeney L, Lawrentschuk N, Lerner SP, Meeks JJ, Moch H, Necchi A, Panebianco V, Sridhar SS, Znaor A, Catto JWF, Cumberbatch MG. 2023. Epidemiology of Bladder Cancer in 2023: A Systematic Review of Risk Factors. *Eur Urol.* **84(2)**: 176-90.

Zhu S, Zhao H. 2023. Sexual dimorphism in bladder cancer: a review of etiology, biology, diagnosis, and outcomes. *Front Pharmacol.* **14**: 1326627.

Zheng Y, Izumi K, Yao JL, Miyamoto H. 2011. Dihydrotestosterone upregulates the expression of epidermal growth factor receptor and ERBB2 in androgen receptor-positive bladder cancer cells. *Endocr Relat Cancer.* **18(4)**: 451-64.

Moeller LC, Führer D. 2013. Thyroid hormone, thyroid hormone receptors, and cancer: a clinical perspective. *Endocr Relat Cancer.* **20(2)**: R19-R29.

Davis PJ, Goglia F, Leonard JL. 2016. Nongenomic actions of thyroid hormone. *Nat Rev Endocrinol.* **12(2)**: 111-21.

Freindorf M, Furlani TR, Kong J, Cody V, Davis FB, Davis PJ. 2012. Combined QM/MM study of thyroid and steroid hormone analogue interactions with alphavbeta3 integrin. *J Biomed Biotechnol.* **2012**: 959057.

Lin HY, Sun M, Tang HY, Lin C, Luidens MK, Mousa SA, Incerpi S, Drusano GL, Davis FB, Davis PJ. 2009. L-Thyroxine vs. 3,5,3'-triiodo-L-thyronine and cell proliferation: activation of mitogen-activated protein kinase and phosphatidylinositol 3-kinase. *Am J Physiol Cell Physiol.* **296(5)**: C980-91.

Hercbergs AH, Ashur-Fabian O, Garfield D. 2010. Thyroid hormones and cancer: clinical studies of hypothyroidism in oncology. *Curr Opin Endocrinol Diabetes Obes.* **17(5)**: 432-6.

Khan SR, Chaker L, Ruiter R, Aerts JG, Hofman A, Dehghan A, Franco OH, Stricker BH, Peeters RP. 2016. Thyroid Function and Cancer Risk: The Rotterdam Study. *J Clin Endocrinol Metab.* **101(12)**: 5030-36.

Tran TV, Kitahara CM, Leenhardt L, de Vathaire F, Boutron-Ruault MC, Journy N. 2023. The effect of thyroid dysfunction on

breast cancer risk: an updated meta-analysis. *Endocr Relat Cancer*. **30**(**1**): e220155.

Chan YX, Knuiman MW, Divitini ML, Brown SJ, Walsh J, Yeap BB. 2017. Lower TSH and higher free thyroxine predict incidence of prostate but not breast, colorectal or lung cancer. *Eur J Endocrinol*. **177**(**4**): 297-308.

Ness RB, Grisso JA, Cottreau C, Klapper J, Vergona R, Wheeler JE, Morgan M, Schlesselman JJ. 2000. Factors related to inflammation of the ovarian epithelium and risk of ovarian cancer. *Epidemiology*. 111-17.

Gagliardi F, Baldini E, Lori E, Cardarelli S, Pironi D, Lauro A, Tripodi D, Palumbo P, D'Armiento E, Cavallaro G, Polistena A, D'Orazi V, Sibio S, Fallahi P, Antonelli A, D'Andrea V, Ulisse S, Sorrenti S. 2023. Insights on the Association between Thyroid Diseases and Colorectal Cancer. *J Clin Med*. **12**(**6**): 2234.

Mellemgaard A, From G, Jorgensen T, Johansen C, Olsen JH, Perrild H. 1998. Cancer risk in individuals with benign thyroid disorders. *Thyroid*. **8**(**9**): 751-4.

Turkyilmaz A, Eroglu A, Aydin Y, Yilmaz Ö, Karaoglanoglu N. 2010. A new risk factor in oesophageal cancer aetiology: hyperthyroidism. *Acta Chir Belg*. **110**(**5**): 533-36.

Ghalaut VS, Yadav S, Ghalaut P, Yadav A, Sachdeva A, Yadav R, Sharma TK, Shankar V. 2012. Association of insulin like growth factor-1 (IGF-1) and thyroid hormones in patients of acute leukemia. *Clin Lab*. **58**(**3-4**): 227-31.

Khan SR, Chaker L, Ruiter R, Aerts JG, Hofman A, Dehghan A, Franco OH, Stricker BH, Peeters RP. 2016. Thyroid function and cancer risk: the Rotterdam study. *J Clin Endocrinol Metab*. **101**(**12**): 5030-36.

Selva DM, Hammond GL. 2009. Thyroid hormones act indirectly to increase sex hormone-binding globulin production by liver via hepatocyte nuclear factor-4alpha. *J Mol Endocrinol*. **43**(**1**): 19-27.

Robbins J, Cheng SY, Gershengorn MC, Glinoer D, Cahnmann HJ, Edelnoch H. 1978. Thyroxine transport proteins of plasma. Molecular properties and biosynthesis. *Recent Prog Horm Res*. **34**: 477-519.

Tahboub R, Arafah BM. 2009. Sex steroids and the thyroid. *Best Pract Res Clin Endocrinol Metab*. **23**(**6**): 769-80.

Mannisto T, Suvanto E, Surcel HM, Ruokonen A. 2010. Thyroid hormones are stable even during prolonged frozen storage. *Clin Chem Lab Med*. **48**(**11**): 1669-70; author reply 71-2.

Krashin E, Piekielko-Witkowska A, Ellis M, Ashur-Fabian O. 2019. Thyroid Hormones and Cancer: A Comprehensive Review of Preclinical and Clinical Studies. *Front Endocrinol (Lausanne)*. **10**: 59.

Ma Z, Song P, Ji D, Zheng M, Qiu G, Liu Z, Wang B. 2023. Thyroid hormones as biomarkers of lung cancer: a retrospective study. *Ann Med*. **55**(**1**): 2196088.

Gesing A, Lewiński A, Karbownik-Lewińska M. 2012. The thyroid gland and the process of aging; what is new? *Thyroid Res*. **5**(**1**): 1-5.

Rosner W, Aden DP, Khan MS. 1984. Hormonal influences on the secretion of steroid-binding proteins by a human hepatoma-derived cell line. *J Clin Endocrinol Metab*. **59**(**4**): 806-8.

Sung H, Ferlay J, Siegel RL, Laversanne M, Soerjomataram I, Jemal A, Bray F. 2021. Global cancer statistics 2020: GLOBOCAN estimates of incidence and mortality worldwide for 36 cancers in 185 countries. *CA Cancer J Clin*. **71**(**3**): 209-49.

Heinlein CA, Chang C. 2002. The roles of androgen receptors and androgen-binding proteins in nongenomic androgen actions. *Mol Endocrinol*. **16**(**10**): 2181-87.

Sadar MD. 1999. Androgen-independent induction of prostate-specific antigen gene expression via cross-talk between the androgen receptor and protein kinase A signal transduction pathways. *J Biol Chem*. **274**(**12**): 7777-83.

Nazareth LV, Weigel NL. 1996. Activation of the human androgen receptor through a protein kinase A signaling pathway. *J Biol Chem*. **271**(**33**): 19900-7.

Ikonen T, Palvimo JJ, Kallio PJ, Reinikainen P, Janne OA. 1994. Stimulation of androgen-regulated transactivation by modulators of protein phosphorylation. *Endocrinology*. **135**(**4**): 1359-66.

Nakhla AM, Rosner W. 1996. Stimulation of prostate cancer growth by androgens and estrogens through the intermediacy of sex hormone-binding globulin. *Endocrinology*. **137**(**10**): 4126-29.

Nakhla AM, Romas NA, Rosner W. 1997. Estradiol activates the prostate androgen receptor and prostate-specific antigen secretion through the intermediacy of sex hormone-binding globulin. *J Biol Chem*. **272**(**11**): 6838-41.

Viability and Germination Percentage Analysis of *Platanthera bifolia* Seeds at Different Degrees of Maturity

Aleksandra Nabieva[*]

Central Siberian Botanical Garden SB RAS, Department of Biotechnology, Novosibirsk, Zolotodolinskaya str., 101, 630090, Russia, fax: +7 (383) 334-44-33; +79137179824

Abstract

Platanthera bifolia (L.) Rich. (Lesser Butterfly Orchid) is considered difficult to propagate by seeds due to complex environmental requirements, while the number of studies that consider seed age as the experimental variable is insufficient.

The effectiveness of determining the viability of seeds of different ages remains uncertain, as significant discrepancies between staining and germination data are observed for several orchid species.

This study compares three approaches for determining the quality of orchid seeds: asymbiotic germination, vital TTC staining and detection of seeds with embryos.

The aim of the study was: 1) to identify the morphological differences between age-diverse *P. bifolia* seeds; 2) to evaluate the effects of *P. bifolia* seed age and modified nutritious media (1/4 MS and Malmgren) on achieving high germination rates and seedling growth; 3) to determine the relationship between three different assessments of *P. bifolia* seed viability: vital staining using TTC, detection of seeds with embryos, and asymbiotic seed germination.

Assessed by TTC staining, 68.4% of 30 DAA *P. bifolia* seeds were colored, while 41 DAA and 20 DAA seeds exhibited decreased viability – 51.6% and 36.2%, respectively. The percentages of full 30 DAA and 41 DAA seeds with embryos were higher than their viability values in the TTC test, as well as germination frequencies *in vitro*.

The variation in germinability of *P. bifolia* seeds on two different media formulations was marked: 49.1% of 30 DAA *P. bifolia* seeds developed into seedlings on modified Malmgren (mM) medium and 41.3% on 1/4mMS. Moreover, 30 DAA seeds were developed to advanced protocorm stages 3-6 in the mM medium, which was due to the coconut water organic additive. During the same 6-month incubation period, 41 DAA seeds were only able to develop through developmental stages 3 or 4, with no seedlings at the stages 5-6, regardless of the medium used. On the basis of results obtained in the studies of *P. bifolia* seed micromorphology and coat ultrastructure, the most favorable 'harvesting window' for successful *in vitro* seed germination was determined to be the post-anthesis 30 day interval.

Keywords: Orchidaceae, seed viability, germination test, orchid immature seeds

1. Introduction

Platanthera Rich. is one of the most species-rich genera among the orchids of the temperate zone, including 144 accepted species (The World Checklist of Vascular Plants). High morphological plasticity and fast evolution among genus representatives (Gamarra et al., 2008; Efimov, 2011) led to their wide-amplitude ecological characteristics contributing to dispersal in the northern hemisphere, with diversification centers in East Asia and North America. Genus *Platanthera* in the flora of Russia comprises 15 species, several subspecies and varieties (Efimov, 2020). The current trend of decreasing *P. bifolia* populations has led to a shift to a more protected status than 'Least Concerned' owing to habitat degradation (Rankou, 2011). In the Mediterranean countries, the tuber of the species is widely used for salep production (Teoh, 2016), while the leaves are known as a remedy against rheumatism and as an antineuralgic agent in non-traditional medicine (Calevo et al., 2020) owing to the high content of phenolic compounds and flavonoids, such as quercetin and kaempferol in the leaves of individuals from both the disturbed habitats and from natural sites, as detected by Maleva et al. (2021).

Two leaves of oval shape appear at inflorescence base, which is spike-like. There are from 10 to 25 white flowers in the inflorescence, opening not simultaneously but from the base to the top. One flower is open within a few days during the flowering period (Boberg et al., 2014), which occurs between May and July, both in Northern Europe (Esposito et al., 2018) and in central Russia (Vachrameeva et al., 2014), while in Siberia it usually starts 1-2 weeks later. The fruit of *P. bifolia* is a capsule that opens with six long slits, yielding a mean of 4251 seeds, as recorded by Kirillova and Kirillov (2017) from *P. bifolia* capsules gathered in Komi Republic, Russia. Tiny dusty seeds become mature after 2 months of development, and in nature, they may germinate following capsule dehiscence in autumn, but further development of the protocorms occurs after 1-2 winters (Vachrameeva et al., 2014).

---

[*] Corresponding author. e-mail: sibflower05@gmail.com.

In vitro culture, which provides vast opportunities for studying the growth and development of orchid seeds, and for obtaining viable seedlings, is intended to be used to reduce overharvesting of orchids from natural populations (Jolman et al., 2022).

In the wild, most *Platanthera* species are considered mycorrhizal generalists (Betechtina et al., 2013; Vogt-Schilb et al., 2020). For this reason, the symbiotic protocols were utilized for the *in vitro* germination of rare *Platanthera* native to North America, including *Platanthera praeclara* Sheviak and M.L. Bowles (Sharma et al., 2003*), P. leucophaea* (Nutt.) Lindl (Poff et al., 2016).

Low seed germination of *Platanthera* species and slow growth of seedlings in asymbiotic culture reported by Nadarajan et al. (2011) appear to be partly due to the lack of specific nutrients in the medium, required to replace mycorrhizal associations (Rasmussen, 1995). Developing *in vitro* germination strategies is becoming increasingly attractive for horticultural practice, involving autochthonous genetic resources of terrestrial orchid species (Zale et al., 2022).

It is known that immature seeds, if inoculated before dormancy occurs, germinate faster and in more significant proportion than seeds from mature fruits (Kendon et al., 2017). The success of growing seeds from green pods is thoroughly explained by the increased metabolic activity of the seed that reaches the phase of physiological maturity (Dalziell and Tomlinson, 2017). However, incomplete information on seed quality and optimal timing of *in vitro* seed sowing often resulted in inconsistent *in vitro* developing data protocols for *P. bifolia*: it was shown in the study of Tonecki and Dobrzynski (2008) that immature *P. bifolia* seeds germinated better than mature ones, while other authors indicated similar germination ability in both mature and immature seeds of the species (Kulikov and Phillipov, 1998).

Thus, it is important to determine the specific stage of seed development before inoculation, especially when green pod culture is a choice for the micropropagation of terrestrial orchid species. Understanding the factors influencing seed viability can facilitate the interpretation of seed germination results for producing the most appropriate germination protocol for *P. bifolia.*

Testing the viability of seeds by TTC is considered to be a simple but not quite reliable method for determining the optimal seed age inoculation for successful germination *in vitro* (Pradhan et al., 2022). The correlation between seed germination and viability assessed by TTC staining often varied among species (Dowling and Jusaitis, 2012; Metsare et al., 2015) and even within a species (Lemay et al., 2015).

The viability assessed by utilizing the tetrazolium test should be modified for mature seeds because hard-coated seeds require different testa pretreatment for better stain penetration. Scarification with hypochlorite solutions prior to vital staining was reported to increase TTC test effectiveness (Kauth et al., 2008; Custidio et al., 2016), in cases when impermeability is due to the presence of suberin, a waxy substance found on the testa of orchid seeds (Barsberg et al., 2013). However, long-term treatments by NaOCl significantly constrain the viability of the embryos of experimental seeds, damaged by bleaching during a surge in the permeability of the seed coat, which was confirmed by Van Waes and Deberg (1986).

In order to find the appropriate physiological age of seeds for sowing and successful TTC test, a comparison of the ultrastructure of age-diverse seeds may be useful to understand the mechanisms of seed dormancy.

The aims of this study were: (1) to provide morphometric data on *P. bifolia* seed and embryo characteristics along with the seed coat microstructure alterations during maturation; (2) to evaluate germination of age-diverse *P. bifolia* seeds on two different media; (3) to determine the relationship between three different assessments of *P. bifolia* seed viability: vital staining using TTC, detection of seeds with embryos, and asymbiotic seed germination.

2. Material and methods

2.1. Seed source

The studied population is located in the Novosibirsk Region, Russia, and includes approximately 45 individuals, which were found in scattered groups or single plants spread out in the birch forest surrounded by agricultural landscape. The taxonomic identity of the species was confirmed at the I.M. Krasnoborov Herbarium of the Central Siberian Botanical Garden, where a voucher specimen has been placed (NS0049018).

The time of *P. bifolia* pod development was scored when 10 generative specimens were marked during anthesis to recognize them when fruiting. The open-pollinated seeds were harvested in July 2020 from the capsules of the middle parts of inflorescences of the same plants 3 times at the selected intervals: 20 d, 30 d and 41 d after anthesis (DAA), determining their age by taking the date of flower anthesis as a starting point. The seeds were stored for no more than 1 day in the dark at 4 °C prior to inoculation.

After surface sterilization, the seeds from each capsule of definite age were divided into three samples consisting of at least 150 seeds, and three replicates were made to determine three characteristics of seed viability: 1. Number of seeds with embryos; 2. The mean embryo stainability; 3. Germination in the *in vitro* culture.

2.2. Seed-quality testing: embryo presence and biochemical viability

For counting *P. bifolia* seeds with embryos under a stereomicroscope, no additional treatments were required since the cell wall of all tested seeds was quite transparent, and the embryo was clearly visible. The mean percentage of seeds containing well-developed embryos was counted by dividing the number of seeds with embryos by the total number of seeds analyzed × 100 for 10 capsules. Seeds from the same capsule were then used to assess biochemical viability provided by the implementation of the protocols developed by Van Waes and Deberg (1986) and Custidio et al. (2016), ordinarily used to detect the activity of dehydrogenase enzymes as the characteristic of living tissues. The application of this method was carried out by staining *P. bifolia* seeds with 2, 3, 5-triphenyltetrazolium chloride (TTC). For staining, 20 DAA and 30 DAA seeds incubated in 0.5% (w/v) TTC (Sigma, T8877) solution at 30 °C in the dark for 24 hours were then treated twice with distilled water to remove the excess

stain. The viability of 41 DAA *P. bifolia* seeds was assessed using the modified version of the TTC test proposed by Custidio et al. (2016): the seeds were first soaked in 1% (w/v) $Ca(OCl)_2$ for 2 min, then washed three times thoroughly with distilled water and incubated in 0.5% TTC solution for 24 h at 30 °C in the dark. After discarding the TTC solution with distilled water, the seeds were examined under the stereomicroscope Stereo Discovery V 12, Carl Zeiss, Germany. As a result, the embryos appearing to stain different red were scored as viable, while the seeds with pale or unstained embryos were considered unviable. The number of embryos stained by TTC was analyzed for 10 capsules of definite age from three replicates and counted as the mean percentage of viable seeds by dividing the number of stained embryos by the total number of seeds × 100.

2.3. In vitro culture

Intact capsules were surface disinfected under laminar flow, and the seeds were sown on two culture media with different compositions: 1) modified quarter-reduced Murashige and Skoog (1962) medium (1/4 mMS) and Malmgren (1996) medium (mM). The media were solidified with 0.6% Bacto® agar (PanReac®, Barcelona, Spain) and modified similarly by the addition of 1.2% sucrose and 0.1% activated charcoal. Additionally, Malmgren medium was supplemented by an organic additive – 100 ml l^{-1}, coconut water (CW), extracted from green coconut. Before autoclaving at 121 °C and 101 kPa for 20 minutes, the pH of the culture media was adjusted to 5.6.

At least, 150 seeds of definite age were placed on the surface of 200-ml jars and incubated on mM or 1/4 mMS media under continuous darkness for 3 months at 23±2 °C. Then, all germinated cultures were exposed to a photosynthetic photon flux density of 40 µmol $m^{-1}s^{-1}$, provided by cool white fluorescent lamps (Phillips, Poland) under the same temperature, 23±2 °C, during the next 3 months. After inoculation, seed germination, protocorm formation and seedling development were monitored and scored after 3 and 6 months.

2.4. Seed morphometric assay, definition of embryo developmental stages and germination scoring

Morphological measurements of seeds isolated from *P. bifolia* capsules of different ages were performed using the following two equations according to Arditti et al. (1979): seed volume, $SV = 2 [(W/2)^2 × L/2 × π/3]$, where W is seed width; L is seed length; embryo volume, $EV = 4/3π × EL/2 × (EW/2)^2$, where EL is the length of the embryo and EW is the width of the embryo. The percentage of air space in the seed was determined using the formula: $(SV – EV)/SV × 100$.

The evaluations of embryo developmental stages were provided at 3 and 6 months after sowing as follows: observed under stereomicroscopy, germinating seeds were scored on a modified scale of 0 – 7 according to growth stage values reported for *in vitro* studies of other terrestrial orchids (Stewart and Zettler, 2002).

The seeds were considered germinated when the embryo emerging from the testa approximately doubled in size (Stage 2), when imbibed dead seeds became well distinguished from viable seeds. When counting the germination percentages, seeds without an embryo or with an undeveloped embryo were excluded. The initial (G_1)

percentage of germination was assessed as the sum of the percentages of seeds, which developed to the advanced stages recorded after 3 months in relation to the initial percentage of seeds with embryos × 100. Germination (G_2) was scored after 6 months from sowing as the total percentage of germinated seeds and developing protocorms in relation to the initial percentage of seeds with embryos × 100. Final germination was determined as the mean germination percentages scored between the two media after 6 months of seed culture.

2.5. Statistical analysis and data representation

To compare viability assessed by TTC staining and by counting the mean proportion of seeds containing an embryo, seeds were selected from the same capsules of three different ages in three replicates; at least 150 *P. bifolia* seeds were used in each treatment. The mean percentage of seeds without an embryo was measured as a ratio of empty/sowed seeds (×100). Seed viability estimation was made by dividing the number of stained embryos by the total number of embryos counted for seed lots belonging to different age (×100). The result of the *in vitro* germination test was presented as a percentage of the number of germinated seeds to the total number of seeds with an embryo (×100). The percentage of protocorms at a certain developmental stage was scored by dividing the number of seeds that had developed to that stage by the total number of seeds with an embryo (×100).

Germination percentage was recorded as the total percentage of embryo development at Stages 2–6 after 3 and 6 months. The data on the frequency (%) of the developmental protocorm stages, along with all quantitative data, were submitted to the Shapiro-Wilk normality test, and an analysis of variance (ANOVA) in STATISTICA 8 software (StatSoft Inc., Tulsa, OK) was made. Student's t-test was used to determine the statistical difference between the mean morphometric values obtained for the three seed lots, while germination and viability data were transformed to normalize the distribution, but untransformed means were presented as the mean ± standard error (SE). A factorial experiment with a completely randomized design was performed to investigate the effect on germination percentage of two groups of variables and their interaction in a 3 × 2 factorial scheme (three seed ages and two culture media). The differences between means were evaluated with post hoc comparisons using Duncan's Multiple Range Test (DMRT) at a significance level of p<0.05. The Pearson's correlation was used to determine the relationship between the three indicators of seed viability.

3. Results

3.1. Embryo development and morphological changes during seed maturation. TTC staining

The morphological features of *P. bifolia* seeds of different ages along with the ultrastructure of seed coat were investigated. During the development of *P. bifolia* seeds, changes in the size of the capsules and morphological parameters of seeds and embryos have been established. Capsules representing three stages of seed development were predominantly green, but the seed color varied: immature seeds isolated from 20 and 30 DAA

capsules were white, while the color of 41 DAA seeds tended to be creamy white (Fig.1).
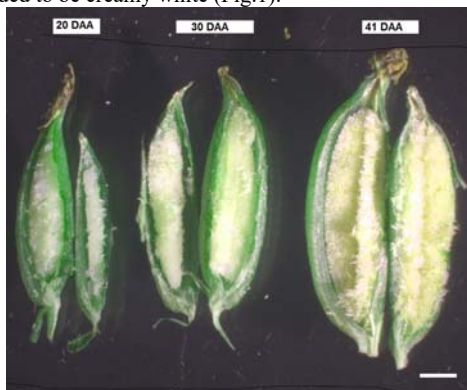
Figure 1. The appearance of immature seeds in longitudinally cut *Platanthera bifolia* capsules of different ages (20 DAA, 30 DAA and 41 DAA), scale bar represents 0.2 cm.

Depending on the degree of maturity, differences in the length and width of capsules of *P. bifolia* were observed (Table 1).

Table 1. Characteristics of *Platanthera bifolia* capsules of different age

The age of maturity	Length of seed capsule, mm	Width of seed capsule, mm
20 DAA	10.5±1.18	3.1±0.33
30 DAA	13.8±2.04	3.8±0.41
41 DAA	15.1±1.89	4.0±0.56

Data represent mean ± standard errors. The length and width of capsules are shown as the average of 10 capsules.

The development of the capsules continued until 41 DAA, but then from 30 to 41 days it slowed down.

The study provides evidence of significant variability between *P. bifolia* seeds of different degrees of maturity at the micro-morphometric level (Table 2), especially between 20 DAA seeds and more mature seeds, while between 30 DAA and 41 DAA slight numerical differences in seed and embryo size were recorded (Table 2).

Table 2. The morphometric characteristics of *Platanthera bifolia* seeds

Seed lots according to their age	Seed dimensions, mm			Embryo dimensions, mm			Air space, %
	Length	Width	Seed volume	Length	Width	Embryo volume	
	M±SE		Volume of seed, $\times 10^{-3}$ mm^3	M±SE		Volume of embryo, $\times 10^{-3}$ mm^3	AS= $\dfrac{SV-EV}{SV} \times 100$
1) 20 days after anthesis	0.56 ± 0.05 b	0.13 ± 0.01 b	2.47 b	0.12 ± 0.01 b	0.09 ± 0.01 b	0.50 c	79.64 a
2) 30 days after anthesis	0.71 ± 0.03 a	0.15 ± 0.01 a	4.19 a	0.14 ± 0.01 a	0.11 ± 0.01 a	0.88 a	78.79 ab
3) 41 days after anthesis	0.75 ± 0.07 a	0.14 ±0.01 b	3.85 ab	0.15 ± 0.03 a	0.12 ± 0.01 a	1.13 b	70.59 b

Note: AS – indicates what part of the empty air space in the seed is occupied, SV and EV – represent volumes of the seed and embryo, respectively. Experimental values represent mean ± standard error (SE); the values in each column followed by the same letter are not significantly different, as determined by Duncan's post hoc test (P< 0.05)

The embryo occupies only a minor proportion of the volume of 20 DAA seeds (20.4%), but its volume substantially increases during maturation. Hence, the size of the embryos of 41 DAA seeds was the largest and occupied 29.4% of the seed volume, and the embryo of 30 DAA seeds – 21.2% of the seed volume, while the values of the air space differed significantly between 20 DAA and 41 DAA seeds (Table 2).

Within 20 DAA capsules, many differentiating ovules associated with placental tissue have been observed (Fig. 2A). Single seeds, free of placental tissue, differed from more mature seeds in the shape of their apical region, which was more rounded than truncated (Fig. 2 B). Most of the 20 DAA seeds have an embryo at a pre-globular stage and a suspensor extending beyond the seed, which is eliminated at the later stages of *P. bifolia* embryo development. It is well distinguished that the testa cells of 20 and 30 DAA seeds are more translucent than in 41 DAA seeds (Fig. 2 A, E, C).
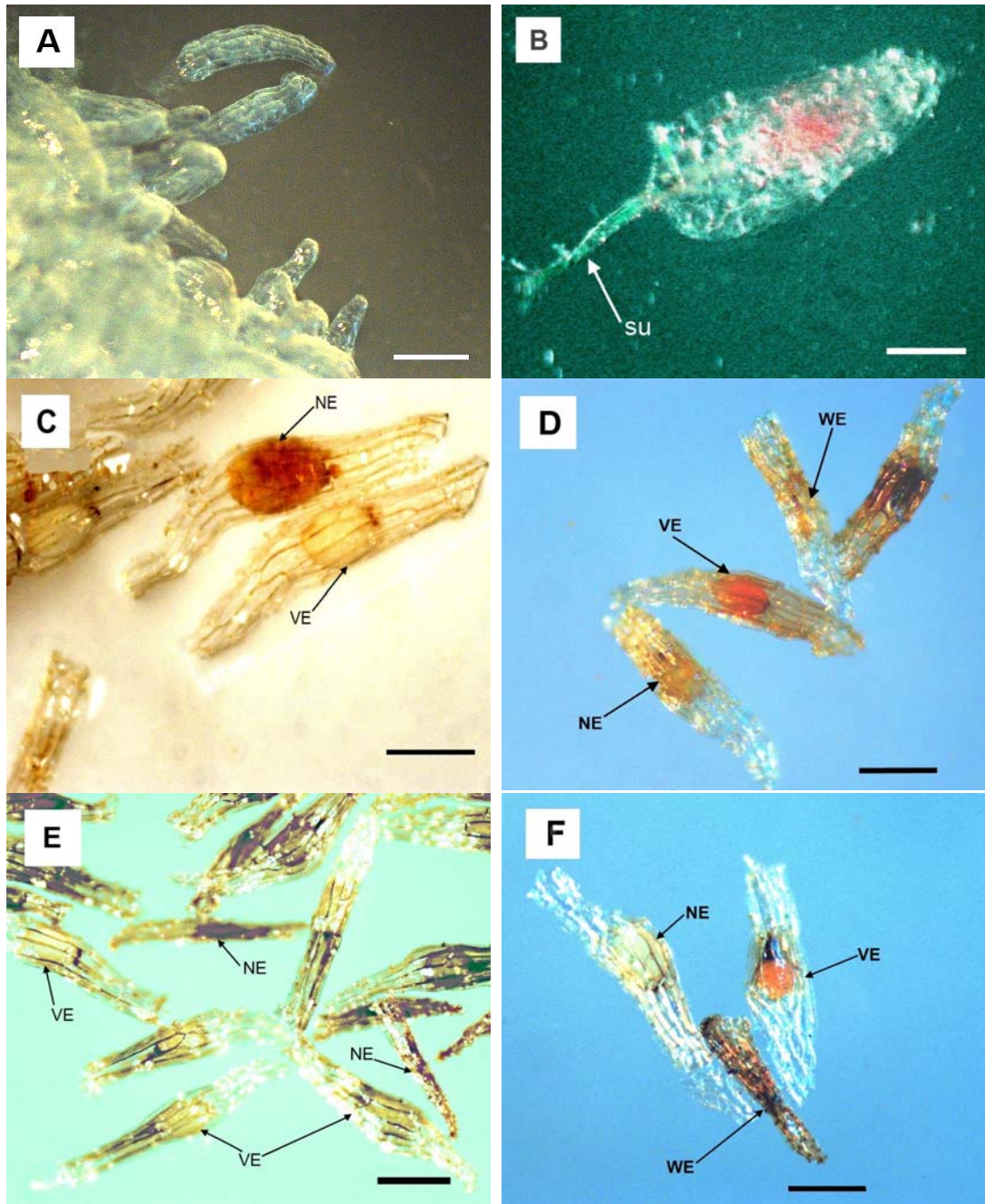
Figure 2. The morphological variability of *Platanthera bifolia* seeds of different ages (A – 20 DAA intact seeds; B – 20 DAA seed after TTC staining, su – suspensor; C – 30 DAA intact seeds; D – 30 DAA seeds after TTC staining; E – 41 DAA intact seeds; F – 41 DAA seeds bleached by 2-minutes treatment with 1% Ca(OCl)$_2$ before TTC staining. Seeds without embryos are marked as WE, viable embryos are identified as VE, and non-viable as NE, respectively. Bar = 250 µm (A), 125 µm (B), 150 µm (C), 200 µm (E, D, F).

As a result of TTC staining, the majority of 30 DAA *P. bifolia* seeds examined microscopically turned out to be viable (68.4%), while the viability of 20 DAA seeds was lower – 36.2%. For seeds collected 41 days after flowering, staining of the embryos was difficult due to the dense inner covering surrounding the embryo (Fig. 2 E). For this reason, the viability of more mature *P. bifolia* seeds was determined after they were bleached for 2 min with 1% Ca(OCl)$_2$ before testing (Fig. 2 F)**,** and as a result, 51.6% of 41 DAA seeds were assessed as viable.

3.2. Embryo presence assessment

P. bifolia embryos are generally ellipsoidal and located at the center of the seed (Fig. 2 A, C). Since an embryo is quite visible through the testa of *P. bifolia* immature seeds under light microscopy, the proportion of seeds with full embryos was easily estimated for the seeds of different ages. The mean proportion of seeds containing an embryo increased from $31.0 \pm 2.4\%$ among 20 DAA seeds to $71.8 \pm 3.6\%$ among 30 DAA seeds and $75.5 \pm 5.4\%$ among 41 DAA seeds. Between 20 DAA seeds and the more mature seeds, the means differed significantly (ANOVA: $F_{(2.33)}$ =

160.4, p = 0.00). Thus, during normal *P. bifolia* seed development, only a small proportion of empty seeds appears to occur among 41 DAA seeds near the maturation age.

3.3. Testa cells ornamentation during maturation

Seed ornamentation was determined by means of scanning electron microscopy (SEM) with a Hitachi TM-1000 microscope (Japan). As seeds matured, cell wall thickening occurred: spindle-shaped 41 DAA seeds have oblique parallel thickenings of the testa anticlinal walls.
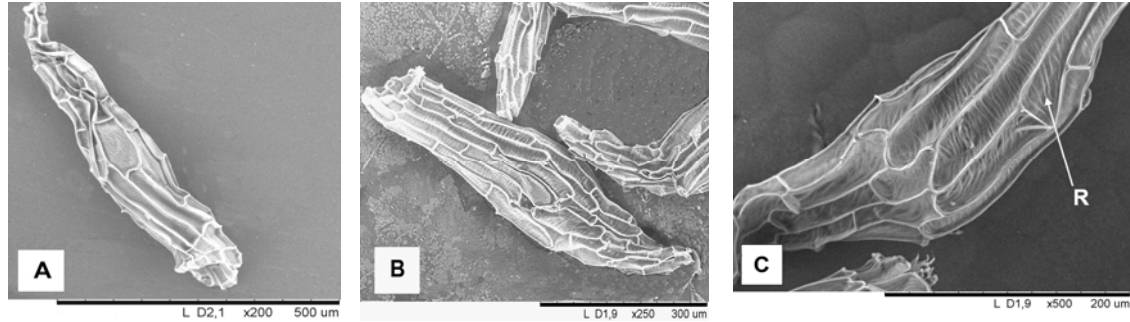
Figure 3. Scanning electron micrographs of A.) 30-day-old seeds. Bar=500 µM; B.) 41-day-old seeds. Bar=300 µM; C.) Elongated testa cells with thickened anticlinal walls and transversal ridges (indicated as R and by arrow) on the periclinal walls of 41-day-old seed are observed. Bar=200 µM.

Outermost layer of the seed coat thickened and compressed into a thin layer covering the embryo and transversal ridges, were revealed on the testa periclinal walls of 41 DAA seeds (Fig.3 C).

3.4. Germination in vitro. The effects of seed age and culture medium

Combinations of two basal media and three ages of capsule maturity were evaluated in the study to assess their effect on asymbiotic germination and subsequent protocorm development in *P. bifolia*. Our observations showed that germination percentage varied depending on seed maturity. Specifically, only a few 20 DAA seeds germinated (developed to Stage 2) both in the mM (3.7%) and 1/4 mMS (4.5%) media after three months, and no survivors were found after six months. Meanwhile, the highest frequency of germination (48.5%) was obtained after 3 months on 1/4 mMS medium with seeds harvested 30 d after anthesis, and a significantly lower percentage (26.9%) was recorded on mM medium (Fig. 4 A). The percentage of 41 DAA seeds, which developed to the embryo advanced stages, did not exceed 24.3% on 1/4 mMS and 25.8% on mM medium (Fig. 4 A).

By the end of the 6 month period, the number of germinated seeds and formed protocorms originating from of 30 DAA capsules was 49.1% on mM medium and 41.3% on 1/4 mMS medium, while during the same period, the recruitment from 41 DAA capsules was approximately the same as 3 months after sowing and included 25.9% germinated seeds and developed protocorms on mM and 21.6% on 1/4 mMS media. Moreover, 30 DAA seeds yielded the greatest percentage of seedlings at stages 5-6 (12.9% on mM and 12.1% on 1/4 mMS media), while 41 DAA seeds were capable of evolving only through 3-4 development stages, but no seedlings reaching stages 5-6 could be found. New germinates were not observed after incubation extended for 6 months, regardless of culture medium or seed age.
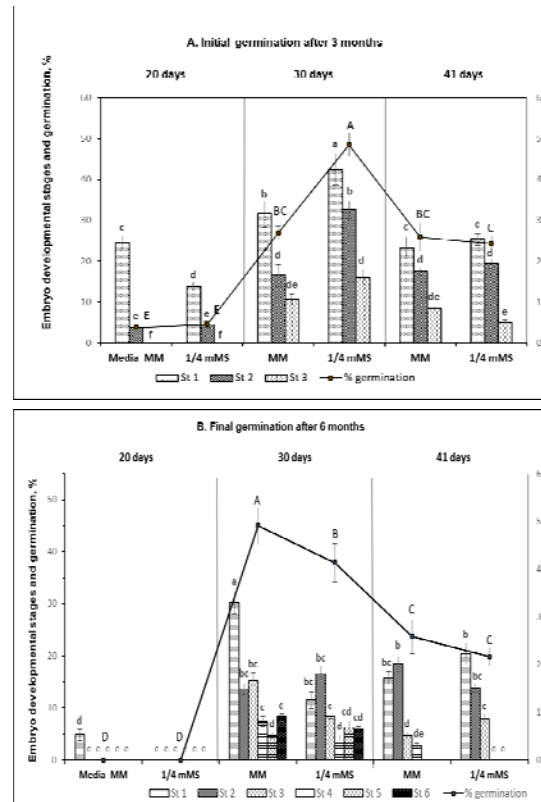
Figure 4 (A, B). Effects of culture medium and age (20-, 30- and 41 DAA) of *Platanthera bifolia* seeds on frequencies of embryo developmental stages and germination assessed after 3 (A) and 6 (B) months. The broken line in the graphs represents the final germination percentages, recorded as the total percentage of Stages 2–6 of embryo development. Vertical bars represent mean ± S.E. Different letters indicate significant differences identified by post hoc comparisons using Duncan's test (P< 0.05).

Germination results obtained after 6 months were significantly different (p< 0.001) between 30 DAA and 41 DAA seeds, regardless of the culture medium used. Although 30 DAA seedling growth was poorer in mM medium evaluated for the first 3 months, this medium composition was more favorable for subsequent seedling development than 1/4 mM medium (Fig. 4 A, B). A statistically significant interaction (p < 0.05) was found between medium composition and seed age, as confirmed by the percentage of germinated seeds and protocorm development after 3 and 6 months (Tables 3, 4).

Table 3. The results of two-way ANOVA showing the F and P values for the effects of seed age and nutritious medium and their interaction on *Platanthera bifolia* seed germination after 3 months of seed culture

Source of variation	Dependent variable	d.f	Mean square	F Value	P Value
Seed age	Seed germination	2	6903.28	389.14	0.00
Medium	Seed germination	1	874.32	49.28	0.00
Seed age* Medium	Seed germination	2	972.27	54.80	0.00

Table 4. The results of two-way ANOVA showing the F and P values for the effects of seed age and nutritious medium and their interaction on *Platanthera bifolia* seed germination after 6 months of seed culture

Source of variation	Dependent variable	d.f	Mean square	F Value	P Value
Seed age	Seed germination	2	11747.93	492.790	0.000000
Medium	Seed germination	1	396.68	16.640	0.000124
Seed age* Medium	Seed germination	2	143.18	6.006	0.004014

Thus, the maximum germination outcome was obtained after 6 months from 30 DAA seeds inoculated onto mM medium, which also contributed to the highest yield of seedlings at advanced stages.

3.5. The relationship determination between three different assessments of P. bifolia seed viability

Minimal percentages were recorded in three viability assessments with 20 DAA P. bifolia seeds, suggesting that these immature seeds were insufficiently developed to germinate. The percentages of 30 DAA and 41 DAA full seeds were higher than their viability estimated by the degree of TTC staining in the tetrazolium test, as well as germination frequencies *in vitro* (Table 5).

Table 5. Three indicators of *Platanthera bifolia* immature seed viability: data from TTC test, assessments of seeds with embryo and *in vitro* germination test.

Experimental values are mean ± standard errors (SE)

Seed lots according to the age	Percentage of seeds with embryos, %	Viability (TTC test), %	Germination after 3 months*, %	Final germination after 6 months*, %
1. 20 days after anthesis	31.0 ± 2.4 b B	36.2 ± 0.9 c A	4.1±0.6 c C	0.0±0.0 c C
2. 30 days after anthesis	71.8 ± 3.6 a A	68.4 ± 4.2 a AB	37.7±2.8 a C	45.2±3.5 a B
3. 41 days after anthesis	75.5 ± 5.4 a A	51.6 ± 3.4 b B	25.0±1.7 b C	23.7±3.3 b C

* In order to estimate the total amount of seeds germinated *in vitro*, the average frequency between the two media was determined between 3 and 6 months of culture. According to Duncan's test, mean values followed by the same lowcase letters in the columns and by the capital letters in the rows do not differ statistically at p < 0.05.

For all ages of *P. bifolia* seeds tested, two methods of viability determination yielded much higher values than the germination test did. Significant differences were recorded: 1) between final *in vitro* germination values and the full seeds percentage: $F_{(2,33)} = 160.34$, p = 0.000; 2) between final *in vitro* germination values and the viability percentages, assessed by TTC test: $F_{(2,33)} = 74.8$, p = 0.000.

When establishing the relationship between the three indicators of seed viability, using Pearson's correlation, the only positive correlation was recorded between 30 DAA seed germination and embryo presence, r = 0. 662 (Table 6), thus suggesting that the full seeds assessment could potentially predict the results of germination test *in vitro* for *P. bifolia* immature seeds the age of which was 30 DAA.

Table 6. Pearson's correlation coefficients and their statistical significance between seed quality measures in *Platanthera bifolia* for seeds with different degrees of maturity (20, 30, 41 days after anthesis)

Indicators/ Seed age (days)	Full (20)	TTC (20)	C G6 (20)	Full (30)	TTC (30)	C G6 (30)	Full (41)	TTC (41)	C G6 (41)
Full* (20)	1.000	0.345	0.090	0.170	0.061	-0.284	-0.146	0.101	-0.115
TTC* (20)	-0.345	1.000	0.081	0.212	-0.047	-0.343	0.368	0.083	0.274
C G6* (20)	0.090	0.081	1.000	-0.093	0.329	-0.455	-0.117	-0.147	-0.068
Full (30)	0.170	-0.212	-0.093	1.000	0.360	0.662	-0.385	-0.683	0.148
TTC (30)	0.061	-0.047	0.329	0.360	1.000	0.106	0.081	-0.441	-0.423
C G6 (30)	-0.284	-0.343	-0.454	0.662	0.106	1.000	-0.427	-0.423	0.125
Full (41)	0.146	0.368	-0.117	0.385	0.081	-0.427	1.000	0.310	-0.263
TTC (41)	0.368	0.083	-0.147	-0.683	-0.441	-0.418	0.311	1.000	-0.495
C G6 (41)	-0.116	0.274	-0.068	0.148	-0.423	0.125	-0.263	-0.495	1.000

* Full – embryo presence; TTC – embryo stainability; C G6 – mean seed germination measured after 6 months between 2 media treatments; seed age is indicated in brackets; quality measures marked in red are statistically significant between each other, $p < 0.05$)

Thus, 41 DAA seeds of *P. bifolia* are characterized by the beginning of maturation, at which the embryo slightly increased in size, while the volume of the seed, along with the proportion of empty air space, decreased. The seeds of this age were characterized by the additional formations, which may lead to their seed coat hardening (Fig. 2 C, E; Fig. 3 C).

The relationship between the three different assessments of the seed viability was not consistent for 20 DAA and 41 DAA *P. bifolia* seeds, while for 30 DAA seeds the relation between the germination test results and the full seeds assessment was approved.

4. Discussion

It is a generally accepted fact that the germination of seeds of representatives of the tropical orchid flora, which have relatively large embryos, does not require a complex of interacting environmental factors for effective germination, while species of orchids of the temperate zone, which have a smaller embryo volume as a rule, exhibited low germination rates both *in situ* and *in vitro* (Prasongsom et al., 2022). The morphological changes identified during *P. bifolia* seed development are in good agreement with the assumption that the seed morphology is linked to dormancy, germination and seed structures' establishment (Alfaro Pinto et al., 2023).

Comparing the morphological characteristics of *P. bifolia* pods (size and color) and seeds (size and volume of seeds/embryos together with the air volume), it seems clear that we are dealing with seeds that have not entered the final stage of embryo development – full maturation stage. At this time, the embryo reaches its maximum size, the levels of auxin, cytokinin and gibberellin decrease, while the level of ABA reaches its maximum, which leads to a slowdown in mitotic activity and the beginning of storage products deposition (Yan et al., 2017).

The mean volume of free airspace detected in this study was from 70.59 to 79.64%, which appears to be the average between the values: 65.7%, obtained at the northern boundary of the species' distribution in Russia (Kirillova and Kirillov, 2017), and 88%, reported by Arditti and Gani (2000), when studying the European populations of this species.

Although the embryo occupied most of the 41 DAA seeds volumes, as compared to more immature seeds

tested, the development of 41 DAA embryos is not yet complete, as evidenced by their continued elongation (Table 2). However, it can be assumed from the fact that the size of the seed is beginning to decrease that the first phase of maturity has already started. Decreased 41 DDA seed germination rate, along with the low stainability of these seeds in the TTC test, also confirm this assumption. Prior to vital staining, scarification with hypochlorite solution was reported to be necessary for mature seeds possessing hard coats to improve the effectiveness of the test (Van Waes and Debergh, 1986; Sawma and Moller, 2002). Intact embryos of *Cephalantera falcate* mature seeds, which were harvested 140 d after pollination, also were not stained by TTC solution, as reported by Yamazaki and Miyoshi (2006).

When testing the viability of immature seeds using the TTC test, it is possible to assess both the viability of the embryo and the viability of various seed tissues by their different stain ability during maturation. Thus, the higher intensity of TTC staining in embryos and testa cells of 20 and 30 DAA seeds was detected due to the pronounced dehydrogenase activity (Fig. 2 B, Table 3). Such an increased staining intensity of immature seeds was often noted in other orchid species of warm, e.g., *Dendrobium* species (Prasongsom et al., 2022), *Acianthera johannensis* (Duarte et al., 2019) and temperate climate, e.g., *Calypso bulbosa* (Yeung and Law, 1992).

Among *P. bifolia* 20 DAA seeds, 31% of seeds with embryos were recorded; however, the full seeds were characterized by an undifferentiated embryo showing strong autofluorescence and by the suspensor, which could be observed outside the micropillar end of the seed (Fig. 2 B). Autofluorescence indicates the non-completed development of the cuticular layer and the lack of phenolic compounds in the seed wall (Yeung, 2022).

The functions of the suspensor appear to be associated with obtaining nutrients from the cells of the inner layer of the outer integument, which is supposed to be an "endosperm substitute" (Donaldson, 2020; Yeung, 2022). The suspensor is eliminated at later stages of *P. bifolia* embryo development since it was not found in 30 and 41 DAA seeds. It seems that in 20 DAA seeds that are still so immature, the embryo is not developed adequately, and thus only minimal germination was observed after 3 months: 3.7% in mM and 4.5% in 1/4 mMS media, while no survivors were found after *in vitro* culturing for 6

months (Fig. 4B). Thereby, the development of the embryo aged 20 DAA was not autonomous in terms of the experiment.

The differences in seed characteristics involved rearrangement in the seed testa, which had completed the periclinal divisions. The physiological state of the embryo, which changes during seed maturation, can also affect the staining test. The influence of seed maturity on the ornamentation of the seed surface was revealed when the smooth periclinal walls of 30 DAA *P. bifolia* seeds changed to a reticulate structure in 41 DAA seeds. Thus, the reason why 41 DAA seeds exhibited viability values in the TTC test below the corresponding values of 30 DAA seeds may be related to the hardening of the seed coat structure during maturation, proved also by electron microscopy. These findings partially contradict both the results of Gamarra et al. (2008), who reported reticulate walls of *P. bifolia* seeds, and Efimov (2011), who characterized *P. bifolia* seeds as having smooth periclinal walls. It is very probable that the authors studied the seeds of different ages.

It is well known that the reason for the lack of seed germination may be the non-optimal composition of the culture medium (Fast, 1982). In modified Malmgren and MS media with the decreased content of macro- and microelements, initiation of seed germination and protocorm formation enhanced in *P. bifolia*. Earlier, Tonecki and Dobrzynski (2008) studied the effect of 1/3 MS on *P. bifolia* seedlings' development, while Vejsadova (2009) used an improved culture medium for this species' seed germination. However, the authors did not emphasize that the response of the orchid to the medium composition depended on the age of seeds used for sowing.

Six months after sowing, protocorm development of both 30 DAA and 41 DAA seeds slowed down on 1/4 mMS medium containing only inorganic nitrogen sources. The lower germination percentages of *P. bifolia* seeds on 1/4 mMS medium could be attributed to high ammonium content in comparison with Malmgren medium, which is enriched in organic additives such as a mixture of amino acids and CW, providing additional sources of organic nitrogen and carbohydrate, which seem to be more efficient than inorganic nitrate and ammonium salts involved in MS (Dulic et al., 2019; Mose et al., 2020). Being added in Malmgren medium, CW supported the advanced *P. bifolia* seedling development but did not promote a high germination rate during the first 3 months, as compared with 1/4 mMS, which did not include the additive.

According to the previous reports, organic nitrogen sources, as opposed to inorganic forms, have a positive effect on seed germination in *Gymnadenia conopsea* (Ostojic et al., 2022), while CW as carbohydrate additive increased the germination of *Cypripedium macrantos* immature seeds (Huh et al., 2016).

The assumption about specific requirements during the formation of *P. bifolia* protocorms is in line with the results obtained by Ponert et al. (2013), who observed that even extremely low nitrate concentrations prevented the development of *Pseudorchis albida* seed outcomes.

Obviously, 41 DAA seeds had morphological or physiological dormancy since 30 DAA *P. bifolia* seeds yielded significantly higher germination percentages owing to the permeability of the seed testa. In fact, the highest germination rate was obtained with 30 DAA seeds, and after maintaining the seedlings on mM medium, they were characterized by a long lifespan *in vitro*, while 41 DAA seeds exhibited reduced seed germination after 6 months of culture, with the same percentages of seeds remaining at Stages 2, 3 and 4 as recorded by 3 months, regardless of which medium was used to prompt germination. Similar results were obtained for immature seeds of *Dendrobium nobile*, when an efficient nutrient uptake for the species germination was observed due to the incomplete cuticle formation (Vasudevan and van Staden, 2010).

The percentages of 30 DAA seeds with embryos and their embryos stainability approved by TTC test are consistent with their germination frequencies *in vitro*, while for the 20 DAA and 41 DAA seeds these data are not consistent.

This is partly in line with Hirano et al. (2005), who reported that the viability test based on TTC staining was not an accurate predictor of germination for immature seeds of terrestrial orchid *Bletilla striata*. The lack of correlation between seed viability and percentages of germinated seeds and formed protocorms is also in line with the results reported by Rasmussen (1995) for *Epipactis helleborine* or by Vujanovic et al. (2000) for *Cypripedium* species, who concluded that special requirements must be met to achieve germination rates close to those expected from seed viability tests. Lee and Yeung (2023) and Soch et al. (2023) showed that when seeds are sown close to their maturation age, their pretreatment by bleaching can improve the hydrophilicity of the seed coat and ensure the permeability of the staining agent. Their findings were confirmed in the present study. In assessing the viability of temperate orchid seeds using the TTC test, the age of the seeds correlating with the degree of seed testa permeability was to be taken into account for better interpretation of germination studies.

5. Conclusion

Morphometric analysis indicates that the color and morphology of both *P. bifolia* fruits and seeds, as well as their dimensions and the presence of ornamentation on the seed coat, are valuable characteristics for understanding the mechanisms of seed dormancy during maturation and predicting the success of seed germination *in vitro*.

The TTC test has not been successful with 20 DAA and 41 DAA *P. bifolia* seeds: 20 DAA seeds exhibited mostly extra stained ability due to the undeveloped embryo structures, while the penetration of tetrazolium into 41 DAA seeds was likely hampered by the thickened testa, resulting in lower results especially for *in vitro* germination test, compared to the same test for 30 DAA seeds.

The differences between stain-determined viability and the percentage of seeds with full embryos were non-significant for 30 DAA seeds, suggesting that both viability assessments could potentially predict the recruitment outcomes of *P. bifolia* immature seeds of this age.

Since the germination rate of *P. bifolia* seeds has been proven to depend on their age, it is important to record the maturity of orchid seeds by the time they are harvested after the anthesis and to study the embryo development

and seed coat ornamentation, which can be the key to improving the success of orchid seed germination *in vitro*.

Acknowledgments

6. References

Alfaro Pinto A, McGill C, Nadarajan J, Archila Morales F and Clavijo McCormick A. 2023. Seed morphology of three neotropical orchid species of the Lycaste genus. *Seeds*, **2:** 331-339.

Arditti J and Ghani AKA. 2000. Numerical and physical properties of orchid seeds and their biological implications. *New Phytol.,* **145**: 367-421.

Arditti J, Michaud JD and Healey PL. 1979. Morphometry of orchid seeds. I. *Paphiopedilum* and native California and related species of *Cypripedium*. *Am J Bot*., **66(10)**: 1128-1137.

Barsberg S, Rasmussen HN and Kodahl N. 2013. Composition of *Cypripedium calceolus* (Orchidaceae) seeds analyzed by attenuated total reflectance IR spectroscopy: in search of understanding longevity in the ground. *Am J Bot*., **100**: 2066-2073.

Betechtina AA, Gajsina DF and Veselkin DV. 2013. Features of the roots structure and mycorrhiza formation of *Platanthera bifolia* and *Dactylorhiza hebridensis* in different age stages. *Orenburg State Univ Vest*., **10(159)**: 172-175.

Boberg E, Alexandersson R, Jonsson M, Maad J, Agren J and Nilsson LA. 2014. Pollinator shifts and the evolution of spur length in the moth-pollinated orchid *Platanthera bifolia*. *Ann Bot*., **113 (2)**: 267-275.

Calevo J, Copetta A, Marchioni I, Bazzicalupo M, Pianta M, Shirmohammadi N, Cornara L. and Giovannini A. 2020. The use of a new culture medium and organic supplement to improve in vitro early stage development of five orchid species. *Plant Biosyst*., 1-9. DOI: https://doi.org/10.1080/11263504.2020.1840454

Custódio C, Marks T, Pritchard H, Hosomi S and Machado-Neto N. 2016. Improved tetrazolium viability testing in orchid seeds with a thick carapace (*Dactylorhiza fuchsii*) or dark seed coat (*Vanda curvifolia*). *Seed Sci Technol*., **44**: 177-188.

Dalziell EL and Tomlinson S. 2017. Reduced metabolic rate indicates declining viability in seed collections: an experimental proof-of-concept. *Conserv Physiol*., **5(1)**, **cox058**.

Donaldson L. 2020. Autofluorescence in Plants. *Molecules*, **25(10)**: **2393**.

Dowling N. and Jusaitis M. 2012. Asymbiotic in vitro germination and seed quality assessment of Australian terrestrial orchids. *Aust J Bot.,* **60**: 592-60.

Duarte MO, Oliveira DMT and Borba EL. 2019. Ontogenesis of ovary and fruit of *Acianthera johannensis* (Pleurothallidinae, Orchidaceae) reveals a particular female embryology. *Flora*, **259**: **151462**.

Dulić J, Ljubojević M, Ognjanov V, Barać G and Dulić T. 2019. *In vitro* germination and seedling development of two European orchid species, *Himantoglossum jankae* Somlyay, Kreutz & Óvári and *Spiranthes spiralis* (L.) Chevall. *In Vitro Cell Dev Biol.-Plant*, **55**: 380-391.

Efimov PG. 2011. An intriguing morphological variability of *Platanthera* s.l. *Eur J Environ Sci.,* **1**: 125-136.

Efimov PG. 2020. Orchids of Russia: annotated checklist and geographic distribution. *Nat Conserv Res.*, **5(1)**: 1-18.

Esposito F, Vereecken NJ, Gammella M, Rinaldi R, Laurent P and Tyteca D. 2018. Characterization of sympatric *Platanthera bifolia* and *Platanthera chlorantha* (Orchidaceae) populations with intermediate plants. *PeerJ*, **6. 10.7717/peerj.4256**.

Fast G. 1982. European terrestrial orchids. Symbiotic and asymbiotic methods. In: Arditti J (Eds.), **Orchid biology reviews and perspectives II**. Comstock Publishing Associates, Ithaca, US, pp. 326–329.

Gamarra R, Galán P, Herrera I and Ortúñez E. 2008. Seed micromorphology supports the splitting of Limnorchis from Platanthera (Orchidaceae). *Nordic J Bot.,* **26**: 61-65.

Hirano T, Godo T, Mii M and Ishikawa K. 2005. Cryopreservation of immature seeds of *Bletilla striata* by vitrification. *Plant Cell Rep*., **23(8)**: 534-539.

Huh YS, Lee JK, Nam SY, Paek KY and Suh GU. 2016. Improvement of asymbiotic seed germination and seedling development of *Cypripedium macranthos* sw. with organic additives. *Plant Biotechnol J*., **43**: 138-145.

Jolman D, Batalla MI, Hungerford A, Norwood P, Tait N and Wallace LE. 2022. The challenges of growing orchids from seeds for conservation: An assessment of asymbiotic techniques. *Appl Plant Sci*., **10(5)**: **e11496**

Kauth PJ, Dutra D, Johnson TR, Stewart SL, Kane ME and Vendrame W. 2008. Techniques and applications of in vitro orchid seed germination. In: Teixeira da Silva JA (Eds.), **Floriculture, ornamental and plant biotechnology: advances and topical issues**. **V.** Global Science Books, Ltd., Isleworth, pp. 375–391.

Kendon JP, Rajaovelona L, Sandford H, Fang R, Bell J and Sarasan V. 2017. Collecting near mature and immature orchid seeds for ex situ conservation: 'in vitro collecting' as a case study. *Bot Stud*., **58(1)**: 1-14.

Kirillova IA and Kirillov DV. 2017. Reproductive biology of *Platanthera bifolia* (L.) Rich. (Orchidaceae) on its northern distribution border (The Komi Republic). *Tomsk State Univ J*., **38**: 68-88.

Kulikov PV and Phillipov EG. 1998. On propagation of temperate zone orchids by tissue culture methods. *Byull Glavn Bot Sada,* **176**: 125-131.

Lee Y-I and Yeung EC. 2023. The orchid seed coat: a developmental and functional perspective. *Bot Stud*., **64**: 27.

Lemay M-A, de Vriendt L, Pellerin S and Poulin M. 2015. *Ex situ* germination as a method for seed viability assessment in a peatland orchid, *Platanthera blephariglottis*. *Am J Bot*., **102**: 390-395.

Maleva MG, Borisova GG, Chukina NV, Novikov PE, Filimonova EI, Lukina NV and Glazyrina MA. 2021. Foliar content of phenolic compounds in P*latanthera bifolia* from natural and transformed ecosystems at different stages of orchid development. *J Sib Fed Univ Biol*., **14**: 274-286.

Malmgren S. 1996. Orchid propagation: theory and practice. In: Proceedings of North American Native Terrestrial Orchid Conference, Maryland, pp. 63–71.

Metsare M, Ilves A, Haldna M, Kull T and Tali K. 2015. Four seed-quality measures in orchids with different pollination systems. *Acta Bot Gallica*, **162(4)**: 263-269.

Mose W, Daryono BS, Indrianto A, Purwantoro A and Semiarti E. Direct somatic embryogenesis and regeneration of an Indonesian orchid Phalaenopsis amabilis (L.) Blume under a variety of plant growth regulators, light regime, and organic substances. *Jordan J. Biol*., 2020. **13(4)**: 509-518.

Murashige T and Skoog FA. 1962. Revised medium for rapid growth and bio assays with tobacco tissue cultures. *Physiol Plant*, **15**: 473-497.

Nadarajan J, Wood S, Marks TR, Seaton PT and Pritchard HW. 2011. Nutritional requirements for in vitro seed germination of 12 terrestrial, lithophytic and epiphytic orchids. *J Trop For Sci*., **23**: 204-212.

Ostojic J, Ljubojevic M, Narandzic T and Pusic M. 2022. *In vitro* culture conditions for asymbiotic germination and seedling development of *Anacamptis pyramidalis* (L.) Rich. and *Gymnadenia conopsea* (L.) R. Br. *S Afr J Bot*., **150**: 829-839.

Poff K, Sharma J and Richards M. 2016. Cold-moist stratification improves germination in a temperate terrestrial orchid. *Castanea*, **81**: 292-301.

Ponert J, Vosolsobe S, Kmecova K and Lipavska H. 2011. European orchid cultivation – from seed to mature plant. *Eur J Environ Sci*., **1**: 95-107.

Pradhan N, Fan X, Martini F, Chen H, Liu H, Gao J and Goodale UM. 2022. Seed viability testing for research and conservation of epiphytic and terrestrial orchids. *Bot Stud*., **63(1)**: 3.

Prasongsom S, Thammasiri K and Pritchard H. 2022. Seed dormancy concepts in orchids*: Dendrobium cruentum* as a model species. *Seed Sci Res*., **32(3)**: 175-186.

Rankou H. 2011. *Platanthera bifolia*. The IUCN Red List of Threatened Species e.T176018A7172664. Available online: https://www.iucnredlist.org/ Accessed on 08 February 2024.

Rasmussen HN. 1995. **Terrestrial orchids: From seed to mycoheterotrophic plant.** Cambridge Univ. Press, Cambridge.

Sawma JT and Mohler CL. 2002. Evaluating seed viability by an unimbibed seed crush test in comparison with the tetrazolium test. *Weed Technol*., **16**: 781-786.

Sharma J, Zettler LW, van Sambeek JW, Ellersieck MR and Starbuck CJ. 2003. Symbiotic seed germination and mycobionts of federally threatened *Platanthera praeclara* (Orchidaceae). *Am Midl Nat*., **149(1)**: 104-120.

Šoch J, Šonka J and Ponert J. 2023. Acid scarification as a potent treatment for an in vitro germination of mature endozoochorous *Vanilla planifolia* seeds. *Bot Stud*., **64**: 9.

Stewart SL and Zettler LW. 2002. Symbiotic germination of three semi-aquatic rein orchids (*Habenaria repens*, *H. quinquiseta, H. macroceratitis*) from Florida. *Aquat Bot*., **72**: 25-35.

Teoh ES. 2016. **Medicinal Orchids of Asia**. Springer International Publishing, Cham, Switzerland.

Tonecki J and Dobrzyński P. 2008. Rozmnażanie storczyka europejskiego *Platanthera bifolia* (L.) L. C. Rich. w warunkach in vitro. *Zesz Probl Postęp Nauk Rol.*, **525**: 419-425.

Vakhrameeva MG, Varlygina TI and Tatarenko IV. 2014. **Orchids of Russia (biology, ecology and protection)**. KMK Scientific Press Ltd., Moscow.

Van Waes JM and Debergh PC. 1986. Adaptation of the tetrazolium method for testing the seed viability, and scanning electron microscopy study of some Western European orchids. *Physiol. Plant*., **66**: 435-442.

Vasudevan R and van Staden J. 2010. In vitro asymbiotic seed germination and seedling growth of *Ansellia africana* Lindl. *Sci. Hortic*., **123 (4)**: 496-504.

Vejsadová H. 2009. *Ex situ* kultivace ohrožené ́odruhu *Platanthera bifolia* (L.). *Acta Pruhoniciana*, **93**: 31-35.

Vogt-Schilb H, Těšitelová T, Kotilínek M, Sucháček P, Kohout P and Jersáková J. 2020. Altered rhizoctonia assemblages in grasslands on exarable land support germination of mycorrhizal generalist, not specialist orchids. *New Phytol*., **227**: 1200-1212.

Vujanovic V, St-Arnaud M, Barabé D and Thibeault G. 2000. Viability testing of orchid seed and the promotion of colouration and germination. *Ann Bot*., **86**: 79-86.

World Checklist of Monocotyledons. 2011. The board of trustees of the Royal Botanical Gardens, Kew. Published online at: http://www.kew.org/wcsp/monocots/.

Yamazaki J and Miyoshi K. 2006. In vitro asymbiotic germination of immature seed and formation of protocorm by *Cephalanthera falcata* (Orchidaceae). *Ann Bot*., **98**: 1197-1206.

Yan X, Tian M, Liu F, Wang C and Zhang Y. 2017. Hormonal and morphological changes during seed development of *Cypripedium japonicum*. *Protoplasma*, **254**: 2315-2322.

Yeung EC. 2022. The orchid embryo - "an embryonic protocorm". *Botany*, **100**: 691-706.

Yeung EC and Law SK. 1992. Embryology of *Calypso bulbosa*. II Embryo Development. *Can J Bot*., **70**: 461-468.

Zale P and Whigham D. 2022. Choosing a favorable substrate to cultivate native orchids symbiotically: examples using *Goodyera tesselata* and *Platanthera blephariglottis*. *HortScience*, **57(2)**: 634-642.

JJBS

Jordan Journal of Biological Sciences

Evaluation of Gene Polymorphisms in Patients with Urinary Oxalate Stones: Cross-sectional Study

Usha Adiga[1,*], Neha Honnalli[2] , Rajeev TP[3]

[1]*Professor, Dept of Biochemistry, Apollo Institute of Medical Sciences & Research Chittoor, India;* [2]*Research Associate, YRC, Mangalore, India;* [3]*Professor, Dept of Urology, KSHEMA , Karnataka*

Abstract

Fetuin-A, a plasma glycoprotein known for its capacity to inhibit calcification, has not been extensively studied regarding its genetic variability, particularly in relation to kidney stone disease. This study aimed to investigate the association between Fetuin-A gene polymorphisms and renal stone disease and to compare serum Fetuin-A levels between individuals with and without kidney stones.

A cross-sectional study was conducted involving 100 kidney stone patients and 100 controls. Two Single Nucleotide Polymorphisms (SNPs) of the fetuin-A gene, c.fet742 C>T (rs4917) and c.fet766 C>G (rs4918), were genotyped using Polymerase Chain Reaction-Restriction Fragment Length Polymorphism (PCR-RFLP). Serum Fetuin-A levels were measured using ELISA. Statistical analysis, including Hardy-Weinberg equilibrium, chi-square tests, linkage disequilibrium, haplotype analysis, and ROC curve analysis, was performed using SPSS version 21, SNP Statonline, and Shesisplus.

No significant association was found between the genotypes of the two SNPs and kidney stone disease (χ^2=0.0833, p=0.772 and χ^2=0.339, p=0.560). Additionally, there was no significant correlation between these SNPs and serum Fetuin-A expression (χ^2=0.254, p=0.613 and χ^2=2.207, p=0.137). However, serum Fetuin-A levels were significantly lower in kidney stone patients compared to controls (p=0.018). Haplotype analysis revealed no significant differences in the distribution frequencies of the (CC, TG, CG) haplotypes of the fetuin-A SNPs between cases and controls. Strong linkage disequilibrium was observed between the two SNPs (D'=0.93, R²=0.77), indicating a strong co-inheritance of the alleles.

To conclude, the study did not find a significant association between Fetuin-A gene polymorphisms and renal stone disease, although serum Fetuin-A levels were lower in individuals with kidney stones.

Keywords: alleles, fetuin A, linkage disequilibrium, polymorphism, renal stone.

1. Introduction

The process of kidney stone formation is intricate and involves multiple sequential steps (Wang et al.,2021). It is a prevalent condition that affects people of various ages, genders, and ethnicities, with a higher occurrence observed between the second and fourth decades of life. Globally, the prevalence of kidney stones is increasing, with a lifetime cumulative incidence ranging from 5 to 10 percent (Rodrigues et al., 2022). This condition carries significant implications for both individuals and society, particularly in regions characterized by hot and arid climates (Wang et al.,2021). The development of calculi containing calcium is a consequence of an imbalance between factors that encourage and inhibit crystallization (Singh et al.,2022). Factors such as hypercalciuria, hyperoxaluria, hypocitraturia, and hypomagnesuria influence the formation of calcium oxalate stones. Urinary pH also plays a pivotal role, as a pH level of 5-6.5 promotes the formation of calcium oxalate stones, while a pH greater than 7.5 favors the development of calcium phosphate stones (Kishore et al 2013; Kumar 2012). Risk factors for calcium oxalate stone formation include low fluid intake, a diet rich in oxalates, and a family history of kidney stones. Kidney stone disease is influenced by a combination of genetic, dietary, and environmental factors (Singh et al.,2022). The increasing prevalence of obesity and hypertension has also been linked to the production of kidney stones (Sayer et al.,2008). Studies have demonstrated that individuals with a family history of nephrolithiasis have a 60% higher risk of developing kidney stones compared to the general population (Ramello et al., 2000).

An underexplored area in kidney stone research is fetuin-A, a glycoprotein that plays a crucial role in the formation and stabilization of calciprotein particles (CPP). These high molecular weight colloidal protein mineral complexes are responsible for transporting and eliminating mineral nanocrystals from the bloodstream. CPPs are essential regulators of calcium extracellular matrix mineralization and serve as systemic inhibitors of soft tissue and vascular calcification (Stenvinkel et al 2005; Rudloff et al., 2022). Low levels of serum fetuin-A have been associated with imbalances in mineralization and increased mortality in individuals with end-stage renal disease (Bouafi et al.,2019; Wang et al.,2018; Kumar et al.,2009; Al-Shuhaib et al.,2019). However, there is a

---

* Corresponding author. e-mail: ushachidu@yahoo.com.

paucity of studies investigating the role of fetuin-A gene polymorphisms in nephrolithiasis. Fetuin-A holds promise as a potential biomarker for predicting the development of calcium oxalate stones.

2. Objectives

This study encompasses a comprehensive investigation into various aspects of Fetuin A and its potential role in urinary kidney stone disease. It commences with the application of bioinformatics methods to pinpoint specific SNPs within the Fetuin A gene that might be associated with urinary kidney stone disease. Subsequently, it delves into the exploration of the connection between these gene polymorphisms and the presence or absence of urinary oxalate stones, along with a comparative analysis of serum Fetuin A levels in individuals afflicted by these stones. The research also scrutinizes the relationship between Fetuin A gene variations and the serum levels of Fetuin A in patients dealing with urinary oxalate stones. In addition, it assesses the correlation between the genetic variations and the metabolic profile of urinary stone disease. Lastly, the study delves into the examination of Linkage Disequilibrium patterns of specific SNPs in the Fetuin A gene, specifically c.742C>T and c.766C>G, in patients both with and without urinary kidney stone disease. This multifaceted approach aims to shed light on the complex interplay between genetic factors, biochemical markers, and urinary stone disease, providing valuable insights into potential diagnostic and therapeutic avenues.

3. Materials and Methods

This cross-sectional study was designed to investigate the relationship between Fetuin-A gene polymorphisms and kidney stone disease. The research was conducted at the Central Research Laboratory of KSHEMA in collaboration with the Department of Urology at Justice K S Hegde Charitable Hospital, Mangalore, Karnataka, India.

3.1. Selection of SNPs by Bioinformatics

In-silico analysis was utilized to identify Single Nucleotide Polymorphisms (SNPs) in the Fetuin-A gene that might be associated with kidney stone disease. Four bioinformatics tools—Sorting Intolerant from Tolerant (SIFT), PolyPhen2, PROVEAN, and I-Mutant 3.0—were employed to evaluate the structural impact, potential detrimental effects, and stability changes of the identified non-synonymous SNPs (nsSNPs).

3.2. Genotyping and Metabolic Parameters Assessment

Inclusion Criteria:

- Cases: Individuals aged 18-65 years with a confirmed diagnosis of kidney stones via ultrasonography and a normal glomerular filtration rate (GFR).
- Controls: Individuals aged 18-65 years without a history of kidney stones, confirmed to have a normal GFR.

Exclusion Criteria:

- Cases: Patients with specific types of stones (e.g., uric acid stones), primary hyperparathyroidism, or any condition that might affect serum calcium and phosphorus levels.

- Controls: Individuals with a family history of urinary stones or gout, and those with abnormal metabolic profiles that could predispose them to kidney stones.

Recruitment Process and Sample Size Calculation:

Patients were recruited from the outpatient department of Urology at Justice K S Hegde Charitable Hospital. The sample size was calculated based on a pilot study, aiming for a power of 80% and a significance level of 0.05, which determined the need for 100 cases and 100 controls. The study was conducted over 36 months, from January 2020 to December 2023.

Ethics Approval and Informed Consent: The study received approval from the Institutional Ethics Committee (Approval No. CEC/NDU/IEC/2020). Written informed consent was obtained from all participants before enrollment, ensuring compliance with ethical standards.

3.3. Laboratory Investigations

A blood sample of three ml was drawn into EDTA vacutainers to analyze gene polymorphisms.

DNA Isolation

DNA was extracted from the blood collected in the EDTA tube using a modified protocol based on Miller et al.'s method. The isolated DNA was quantified using a Nano-drop spectrophotometer at 260nm. The purity of the DNA sample was determined by calculating the ratio of OD260 to OD280. The quantified DNA was then carefully sealed and stored at -20°C until further analysis**.**

Amplification and Genotyping of the gene polymorphism

Genotyping of the genes was confirmed by PCR-RFLP.

Fetuin-A Genotyping:

PCR-RFLP analysis was employed to assess the fetuin-A c.742C>T and c.766C>G single nucleotide polymorphisms.

A forward and reverse oligonucleotide primers were used to amplify the fetuin-A 742C>T polymorphism 5'-CCTCCCACAAGCAGAAAC-3' & 5'-TGATGATTCCGCATACCC-3' designed respectively using Primer 3Plus.The PCR product was digested overnight at 37°C with NlaIII restriction enzyme then visualized using gel electrophoresis with the Gel DocTM EZ imager (Bio-Rad).

For Analysis of fetuin-A 766C>G polymorphism was performed with the oligonucleotide primers forward 5'-GTCACCCCTCCTTGTAAC-3' and reverse 5'-CCCCAATGAGACC ACA-3' for PCR .The PCR product was digested overnight at 37°C with SacI restriction enzyme and digested products were separated on 3% agarose gel.

Biochemical parameters, including serum calcium, phosphorus, uric acid, creatinine, albumin, and Fetuin-A levels, were measured using standardized laboratory techniques.

3.4. Analysis of Linkage Disequilibrium of SNPs and Haplotypes

Linkage disequilibrium (LD) analysis between the SNPs and haplotype analysis was carried out using ShesisPlus and SNPstatonline. This analysis provided

insights into the genetic relationships and co-inheritance patterns of the selected SNPs.

3.5. Statistical Analysis

Statistical analysis was conducted using SPSS version 23. The χ^2 test was used to assess the association between genetic polymorphisms and nephrolithiasis. Metabolic parameters were compared between cases and controls using the Mann-Whitney U test. Additionally, chi-square analysis was applied to evaluate the relationship between gene polymorphisms and metabolic parameters.

4. 3. Results

In the NCBI Reference Protein isoform 2 Sequence (NP_001613.2) of the FETUIN A gene, SIFT analysis was performed, identifying a total of 274 coding variants, encompassing the entire spectrum of variations. Among these, approximately 97% (268 coding variants) were subject to prediction, with 61% (165 variants) classified as "tolerated" and 39% (103 variants) as "harmful." Specifically, the dataset comprised 97% non-synonymous variations (268) and 3% synonymous variations (6). Notably, the analysis identified 97% (256 variants) as novel coding variants. For comprehensive details, please refer to Table 1.

Out of the 274 missense mutations, two specific Single Nucleotide Polymorphisms (SNPs), namely rs4918 (S256N) and rs4917 (M248T), were selected. These SNPs, while having a SIFT score of 0.58 classifying them as "tolerated," were of particular interest due to their association with kidney stone diseases. It is worth mentioning that rs4918 (S256N) is a novel variation. In addition to SIFT, the analysis of these two SNPs was further assessed through Polyphen 2, Provean, and I-Mutant analyses, with the results detailed in Table 1.

Table 1 . Analysis of Fetuin A c.742C>T & c.766C>G Polymorphisms

SNP	Amino Acid Change	SIFT Prediction	SIFT Score	PolyPhen 2 Score	PROVEAN	PROVEAN Score	I-Mutant 3.0 Stability
rs4918 (novel)	S256N	Tolerated	0.58	0.833	Deleterious	-4.994	-0.03 Kcal/mol
rs4917	M248T	Tolerated	1.00	0.00	Neutral	-0.670	-0.70 Kcal/mol

In the study comparing cases (n=100) and controls (n=100), the median age for cases was 46 years with an interquartile range (IQR) of 37-55, whereas the median age for controls was 37 years with an IQR of 26-48. The difference in age between the two groups was statistically significant with a p-value of 0.0011, indicating that cases were significantly older than controls. In terms of sex distribution, 62% of cases were male and 38% were female, while the controls had a higher percentage of males at 78% and a lower percentage of females at 22%.

The study found no statistically significant association between the polymorphism of fetuin-A c.742C>T and individuals prone to developing kidney stones. This is evident from the chi-square value of 0.0833 and the corresponding p-value of 0.772 (Odds Ratio (OR)=1.087, 95% Confidence Interval (CI)=1.914-0.617, as presented in Table 2). Furthermore, there were no noteworthy distinctions observed in the ratio of wild-type and mutant allele variants between the group of individuals with kidney stones and the control group.

Table 2.Association of Fetuin-A Gene Polymorphisms (c.742C>T and c.766C>G) with Renal Stone Disease

Fetuin-A SNP	Genotype	Cases (n=100)	Controls (n=100)	Chi-square Value	p-value	OR (95% CI)
c.742C>T	Wild Type (CC)	59	61	0.0833	0.772	1.087 (0.617-1.914)
	Mutant (CT+TT)	41	39			
c.766C>G	Wild Type (CC)	60	64	0.3396	0.560	0.843 (0.476-1.495)
	Mutant (CG+GG)	40	36			

Similarly, the study did not reveal a significant association between the presence of the Fetuin-A c.766C>G polymorphism and the formation of kidney stones. The chi-square value of 0.3396 and the corresponding p-value of 0.560, along with an Odds Ratio (OR) of 0.843 and a 95% Confidence Interval (CI) ranging from 1.495 to 0.476 (as provided in the results displayed in Table 2), all indicate that there is no significant connection between this polymorphism and kidney stone formation.

Furthermore, among the control group, a higher percentage of individuals (64%) possessed the wild-type allele (CC) compared to the cases (60%). Conversely, cases had a higher percentage (40%) of the mutant allele (CG+GG) compared to the controls (36%), as outlined in Table 2.

To assess the diagnostic capability of fetuin-A in predicting the presence of renal stone disease, a Receiver Operating Characteristic (ROC) curve was constructed. Ultrasound-based stone detection was employed as the gold standard for this evaluation.

Figure 1. ROC for serum fetuin A as a diagnostic marker for kidney stone disease

The ROC curve on the plot was positioned to the left of the diagonal line (Figure 1), yet it did not reach either the upper or the left border. The ROC analysis suggests that Fetuin-A might not be an ideal marker for the diagnosis of renal stone disease, as indicated by an Area Under the Curve (AUC) value of 0.598. The sensitivity was calculated at 61.6%, and the specificity at 54.5%, using a cut-off value of 75.3.

Tables 3 presents the results of an investigation into the potential associations between specific genetic variations (Fetuin A c.742C>T and Fetuin A c.766C>G) and the serum levels of Fetuin A in individuals with urinary oxalate stones. The data is categorized into two groups based on serum levels, with a cutoff point of 75.339 as the dividing criterion. For the Fetuin A c.742C>T variation, the findings show no significant correlation with either serum group, as indicated by the chi-square values, degrees of freedom, and p-values. The odds ratios with their respective 95% confidence intervals reinforce the lack of substantial association. Similarly, the analysis for the Fetuin A c.766C>G variation yielded no significant relationships within either serum subgroup, as demonstrated by the corresponding statistical values. These results suggest that these specific genetic variations may not be significant contributors to variations in serum levels of Fetuin A among individuals with urinary oxalate stones. The findings underscore the complex and multifaceted nature of the interplay between genetic factors and serum biomarkers in this context.

Table 3. Association of Fetuin-A Gene Polymorphisms (c.742C>T and c.766C>G) with Serum Levels of Fetuin-A in Patients with Urinary Oxalate Stones

Fetuin-A SNP	Genotype	Serum Fetuin-A Levels	Chi-square Value, df	p-value	OR (95% CI)
c.742C>T	Wild Type (CC)	<75.339: 24	X^2=0.254, df=1	0.613	1.238 (0.539-2.84)
		>75.339: 36			
	Mutant (CT+TT)	<75.339: 14			
		>75.339: 26			
c.766C>G	Wild Type (CC)	<75.339: 24	X^2=2.207, df=1	0.137	1.894 (0.891-4.42)
		>75.339: 36			
	Mutant (CG+GG)	<75.339: 14			
		>75.339: 26			

The association between different allele models (co-dominant, dominant, recessive, and over dominant) of c.766C>G with kidney stone disease (KSD) did not demonstrate statistical significance (p=0.68, p=0.66, p=0.4, and p=0.88, respectively) (Table 8). In the co-dominant model (adjusted, the "G/G" genotype), there was a 2.10-fold increase in the risk of kidney stone disease, but this association was not statistically significant. Table 4 presents a comprehensive analysis of different models assessing the association between the Fetuin A c.766C>G polymorphism and a specific condition, possibly kidney stones. These models explore various genetic variations and their impact on the risk of the condition, with comparisons between control and case groups. Additionally, they provide odds ratios (OR) and 95% confidence intervals (CI), p-values, and information criteria (AIC and BIC) to evaluate the fit of each model.

The Codominant model scrutinizes the C/C and C/G genotypes individually, revealing no significant differences between cases and controls for these genotypes. The Dominant model groups C/G and G/G genotypes, yielding similar results. The Recessive model also indicates no substantial distinctions between groups, with the G/G genotype not significantly associated with the condition. The Overdominant model pairs C/C and G/G genotypes but does not show significant associations. Finally, the Log-Additive model, assuming a log-additive relationship between genotypes, also fails to establish a significant connection between the genetic variation and the condition.

Collectively, these models suggest that the Fetuin A c.766C>G polymorphism may not be significantly linked to the condition under investigation, as none of the models reveal a statistically significant relationship. The AIC and BIC values further support the notion that these models may not provide a strong fit to the data, emphasizing the complexity of genetic factors in the context of the condition being studied.

Similarly, the association between different allele models (co-dominant, dominant, recessive, and over dominant) of c.742C>T with kidney stone disease (KSD) also showed no significant results (p=0.22, p=0.77, p=0.09, and p=0.56, respectively) (Table 4).

Table 4. Different Models of Fetuin-A c.766C>G and c.742C>T Polymorphisms

Model	Genotype	Control	Case	OR (95% CI)	P-value
Codominant	c.766C>G				0.68
	C/C	63 (63%)	60 (60%)	1.00	
	C/G	35 (35%)	36 (36%)	1.08 (0.60-1.94)	
	G/G	2 (2%)	4 (4%)	2.10 (0.37-11.89)	
Dominant	c.766C>G				0.66
	C/C	63 (63%)	60 (60%)	1.00	
	C/G-G/G	37 (37%)	40 (40%)	1.14 (0.64-2.01)	
Recessive	c.766C>G				0.4
	C/C-C/G	98 (98%)	96 (96%)	1.00	
	G/G	2 (2%)	4 (4%)	2.04 (0.37-11.41)	
Overdominant	c.766C>G				0.88
	C/C-G/G	65 (65%)	64 (64%)	1.00	
	C/G	35 (35%)	36 (36%)	1.04 (0.59-1.86)	
Log-additive	c.766C>G	---	---	1.18 (0.71-1.96)	0.52
Codominant	c.742C>T				0.22
	C/C	59 (59%)	61 (61%)	1.00	
	C/T	41 (41%)	37 (37%)	0.87 (0.49-1.54)	
	T/T	0 (0%)	2 (2%)	NA (0.00-NA)	
Dominant	c.742C>T				0.77
	C/C	59 (59%)	61 (61%)	1.00	
	C/T-T/T	41 (41%)	39 (39%)	0.92 (0.52-1.62)	
Recessive	c.742C>T				0.095
	C/C-C/T	100 (100%)	98 (98%)	1.00	
	T/T	0 (0%)	2 (2%)	NA (0.00-NA)	
Overdominant	c.742C>T				0.56
	C/C-T/T	59 (59%)	63 (63%)	1.00	
	C/T	41 (41%)	37 (37%)	0.85 (0.48-1.49)	
Log-additive	c.742C>T	---	---	1.00 (0.58-1.72)	1.00

Table 4 provides a comprehensive overview of different models used to investigate the relationship between the Fetuin A c.742C>T polymorphisms and a specific condition, potentially kidney stones. These models offer a detailed analysis of the genetic variations and their potential impact on the risk of the condition. Each model presents odds ratios (OR) with their respective 95% confidence intervals (CI), p-values, and information criteria (AIC and BIC) to assess the adequacy of the model fit.

The Codominant model scrutinizes the C/C, C/T, and T/T genotypes individually, indicating no significant differences between cases and controls for these genotypes. The Dominant model groups C/T and T/T genotypes together, yielding similar results. The Recessive model presents no significant distinctions between the two groups, with the T/T genotype not significantly associated with the condition. The Overdominant model pairs C/C and T/T genotypes together but does not establish significant associations. The Log-Additive model, assuming a log-additive relationship between genotypes, also fails to indicate a substantial connection between the genetic variation and the condition.

Collectively, these models suggest that the Fetuin A c.742C>T polymorphism may not be significantly linked to the condition under investigation, as none of the models reveal a statistically significant relationship. The AIC and BIC values further support the notion that these models may not provide a strong fit to the data, underscoring the complexity of genetic factors in the context of the condition being studied.

The current study employed haplotype analysis to estimate haplotype frequencies in a random sample set and resolve ambiguous haplotypes. The analysis platform can

automatically generate results for both individual haplotypes and the entire dataset, independently estimating haplotype frequencies in control and case groups. In case-control studies, low-frequency haplotypes may be combined to yield a single outcome (SHI 2005).

The haplotyping results for the two SNPs are presented in the table. The presence of haplotypes fetuin-A c.742C>T, Fetuin-A c.766C>G (GT), fetuin-A c.742C>T, Fetuin-A c.766C>G (GC), and Haplotypes CC were compared, revealing that the haplotypes fetuin-A c.742C>T, Fetuin-A c.766C>G (GT), and fetuin-A c.742C>T, Fetuin-A c.766C>G (GC) increase the risk of kidney stone disease by 1.14, 1.00, and 0.98, respectively (Table 10).

Table 5 presents the results of haplotype analysis for the Fetuin A gene, specifically considering the combinations of the Fetuin-A c.766C>G and Fetuin-A c.742C>T alleles. The table displays the frequency of each haplotype, along with the odds ratio (OR) and 95% confidence interval (CI) for their potential association with a specific condition, likely kidney stone disease (KSD). Additionally, it reports the global haplotype association p-value.

The analysis reveals that none of the identified haplotypes, including CC, TG, CG, and CT, show a statistically significant association with KSD. The most prevalent haplotype, CC (0.7639 frequency), serves as the reference, with an OR of 1.00. The remaining haplotypes, TG, CG, and CT, do not exhibit significant associations with KSD, as indicated by their respective ORs and p-values. The global haplotype association p-value is 0.44, further underscoring the lack of a significant relationship between these haplotypes and the condition.

Table 5. Haplotype Analysis of Fetuin-A Gene

Haplotype	Case (freq)	Control (freq)	Chi²	Fisher's p	Pearson's p	OR (95% CI)	Frequency	Global haplotype association p-value
CC	149 (0.745)	154 (0.77)	0.34	0.64	0.559	0.872 (0.552-1.37)	0.7639	0.44
TG	43 (0.215)	32 (0.16)	1.985	0.199	0.158	1.437 (0.866-2.386)	0.1764	
CG	6 (0.03)	6 (0.03)	0	1	1	1.00 (0.316-3.15)	0.0311	
CT	---	---	---	---	---	0.37 (0.09-1.47)	0.0286	

Table 5 further examines the association between these haplotypes in case and control groups. It provides the frequency of each haplotype in both groups, along with chi-square, Fisher's p, Pearson's p, and OR values. The analysis confirms that none of the haplotypes, including CC, TG, and CG, display a significant association with KSD when assessed between the case and control groups.

In summary, the haplotype analysis for Fetuin A gene variations does not reveal any significant associations with kidney stone disease. The data suggests that these specific haplotypes, including CC, TG, and CG, do not play a significant role in influencing the risk of developing KSD. The global haplotype association p-value reinforces the absence of a substantial association between these genetic combinations and the condition.

Linkage disequilibrium (LD) was assessed by calculating Lewontin's D' (|D'|) and R2 for each pair of genetic markers. These metrics are commonly utilized in LD analysis, block detection, and SNP tagging studies. They range from 0 to 1, with D' indicating complete LD or correlation between alleles and R2 being more frequently used as it considers allele frequency. D', on the other hand, is independent of allele frequency and only signifies whether alleles are inherited together (Perrera 2022).

In the present study, the calculated D' value was 0.84, indicating that when the rare allele is present, it tends to be inherited on the same haplotype as the common allele (Fig. 2). Meanwhile, the R2 value was 0.7, which suggests that one allele is rare, and the other allele is common (Fig. 3).

Figure 2. Depicting D' of LD

Figure 3. Depicting R^2 of LD

Table 6 displays the demographic characteristics of both cases and controls. In comparison to the controls, the median levels of calcium were significantly higher in cases, with values of 10 (8.95-11.35) versus 9.97 (8.83-12.39). Similarly, the median levels of creatinine were also significantly higher in cases, with values of 1 (0.83-1.27) versus 0.8 (0.56-0.96).

On the other hand, the serum levels of phosphorous, uric acid, and Fetuin-A were significantly lower in patients compared to the controls. The median levels of phosphorous were 5.35 (4.7-6.2) in cases versus 6.11 (4.8-

7.3) in controls. The median levels of uric acid were 4.23 (2.15-5.77) in cases versus 5.13 (4.3-6.14) in controls. Lastly, the median levels of Fetuin-A were 74.09 (59-83) in cases versus 77.83 (70-86) in controls.

Table 6. Biochemical parameters in calcium oxalate stone disease

	Case (n=100)	Controls (n=100)	P value
	Median(interquartile range)	Median(interquartile range)	
Blood Biochemistry			
Uric acid(mg/dL)	4.23(2.15-5.77)	5.13(4.3-6.14)	<0.0001***
Creatinine(mg/dL)	1(0.83-1.27)	0.8(0.56-0.96)	<0.0001***
eGFR(mg/dL)			
Phosphorous(mg/dL)	5.35(4.7-6.2)	6.11(4.8-7.3)	0.0071**
Calcium(mg/dL)	10(8.95-11.35)	9.97(8.83-12.39)	0.739
Albumin(g/dL)	4.31(2.76-4.9)	4.02(3.13-4.64)	0.226
Fetuin-A(ng/ml)	74.09(59-83)	77.83(70-86)	0.018*

Table 7 present a comparison of biochemical parameters between dominant and recessive alleles of fetuin-A c.742C>T and fetuin-A c.766C>G genotypes within both case and control groups.

In the case of the CT+TT genotype for fetuin-A c.742C>T, the analysis revealed that serum uric acid levels were significantly lower in cases (3.9 mg/dL with a range of 2.3-5.7) compared to controls (5.3 mg/dL with a range of 4.2-6.2), with a statistically significant p-value of 0.0017. This suggests that individuals with the CT+TT genotype may exhibit reduced uric acid levels in cases of the condition, likely kidney stone disease. Additionally, the serum calcium levels in patients with the CT+TT genotype were significantly higher than those in the control group.

These findings indicate a potential link between the CT+TT genotype of fetuin-A c.742C>T and altered uric acid and calcium levels, which may have implications in the context of kidney stone disease. Further investigation is needed to understand the underlying mechanisms and clinical relevance of these observed differences in biochemical parameters.

Patients with the CG+GG genotype exhibited some notable differences in biochemical parameters when compared to the control group. Specifically, individuals with the CG+GG genotype had significantly lower levels of uric acid (4 mg/dL with a range of 2.3-5.2) compared to the control group (5.3 mg/dL with a range of 4.3-6), with a p-value of 0.0013. Furthermore, they displayed lower phosphorous levels (5.1 mg/dL with a range of 4.4-6.2) compared to the control group (6 mg/dL with a range of 5.4-7.6). Additionally, patients with the CG+GG genotype had lower serum Fetuin-A levels (70.2 mg/dL with a range of 54.8-81) compared to the control group (77.9 mg/dL with a range of 68.6-86), with a p-value of 0.009. In contrast, they exhibited higher creatinine levels (1 mg/dL with a range of 0.89-1.44) compared to the control group (0.7 mg/dL with a range of 0.5-0.95), with a p-value of less than 0.0001. These findings suggest that the CG+GG genotype may be associated with alterations in these biochemical parameters, potentially related to kidney stone disease.

Table 7. Comparison of biochemical parameters based on fetuin-A genotypes

Biochemical Parameter	Genotype	Case Median (IQR)	Control Median (IQR)	p-value
Fetuin-A c.742C>T				
Age (years)	CC	46 (34-55)	37 (25-50)	0.0322*
	CT+TT	47 (37-57)	38 (26-47)	0.0061**
Uric Acid (mg/dL)	CC	4.2 (1.8-5.8)	4.9 (4.3-6.1)	0.0036**
	CT+TT	3.9 (2.3-5.7)	5.3 (4.2-6.2)	0.0017**
Creatinine (mg/dL)	CC	0.8 (0.6-1.2)	0.8 (0.6-0.9)	0.0014**
	CT+TT	1.0 (0.8-1.4)	0.7 (0.5-0.9)	<0.0001***
Phosphorous (mg/dL)	CC	5.4 (4.8-6.19)	6.3 (4.8-7.5)	0.029
	CT+TT	5.1 (4.4-6.2)	5.7 (4.9-6.8)	0.12
Calcium (mg/dL)	CC	10.7 (9-13)	10 (9-11.4)	0.12
	CT+TT	9.7 (8.6-10.9)	9.3 (8.4-10.4)	0.39
Albumin (g/dL)	CC	4.2 (2.9-4.9)	3.9 (3.1-4.6)	0.33
	CT+TT	4.4 (2.2-4.8)	4.0 (2.9-4.6)	0.4
Fetuin-A (ng/ml)	CC	77.55 (55.3-81.6)	77.86 (70.11-87.8)	0.5
	CT+TT	74.4 (66.8-86.2)	77.69 (70-83)	0.66
Fetuin-A c.766C>G				
Age (years)	CC	36 (26-47)	46 (33-55)	0.005**
	CG+GG	44 (37-54)	39 (26-52)	0.12
Uric Acid (mg/dL)	CC	4.9 (4.3-6.2)	4.2 (1.9-5.8)	0.003**
	CG+GG	4.0 (2.3-5.2)	5.3 (4.3-6.0)	0.0013**
Creatinine (mg/dL)	CC	0.81 (0.6-0.98)	0.96 (0.8-1.2)	0.0007***
	CG+GG	1.0 (0.89-1.44)	0.7 (0.5-0.95)	<0.0001***
Phosphorous (mg/dL)	CC	5.5 (4.7-6.2)	6.2 (4.7-7.3)	0.159
	CG+GG	5.1 (4.4-6.2)	6.0 (5.4-7.6)	0.0045**
Calcium (mg/dL)	CC	10 (8.9-11.3)	10.7 (9-13)	0.086
	CG+GG	9.7 (8.5-10.5)	9.9 (8.9-11)	0.26
Albumin (g/dL)	CC	4.3 (3-4.9)	3.9 (3.2-4.6)	0.099
	CG+GG	2.1 (4.1-4.8)	4.0 (3-4.6)	0.99
Fetuin-A (ng/ml)	CC	77.3 (69.1-87)	78.1 (72.4-83.1)	0.727
	CG+GG	70.2 (54.8-81)	77.9 (68.6-86)	0.009**

For patients with the CT+TT genotype of fetuin-A c.742C>T, they had significantly lower calcium levels compared to those with the CC genotype. However, for patients with the CG+GG genotype of fetuin-A c.766C>G, no significant differences were observed between cases and controls in terms of calcium levels. These differences in calcium levels might be indicative of specific effects associated with these genotypes, highlighting their potential significance in the context of kidney stone disease.

5. Discussion

Fetuin-A, a protein primarily synthesized in the liver, serves as a valuable biomarker in the context of kidney stone disease. It plays a significant role in forming calciprotein particles in collaboration with phosphate and calcium, a process that increases the solubility of these particles and disrupts hydroxyapatite formation, ultimately inhibiting calcification. However, high calcium deposition can gradually deplete fetuin-A levels in the serum, which may lead to mineral precipitation and, consequently, the formation of kidney stones in the renal system (Al-Shuhaib et al.,2019; Roy et al., 2010).

To explore the potential genetic factors involved in kidney stone disease, the current study employed a selection of Single Nucleotide Polymorphisms (SNPs) using bioinformatics tools like SIFT Analysis, Polyphen2, Provean, and I mutant3.0. These tools are instrumental in evaluating the consequences of amino acid substitutions on protein structure, function, and stability. The selected SNPs were assessed based on specific scoring criteria to

determine their impact on protein function and stability (Choi et al., 2012; Kono et al., 2018).

Several prior studies have highlighted the association between the fetuin-A c.766C>G polymorphism and serum fetuin-A levels. In certain populations, G carriers were found to have lower serum fetuin-A concentrations than non-G carriers, and this was observed in diabetic patients and those with coronary artery calcification (Temesszentandrási et al.,2016, Bellia et al.,2012). Additionally, the mutant GG genotype of fetuin-A c.766C>G was linked to lower circulatory fetuin-A levels in patients with type 2 diabetes, particularly in the context of diabetic nephropathy(Umapathy et al.,2022). Furthermore, alleles T and G in the fetuin-A gene were associated with lower serum fetuin-A levels, higher occurrence of coronary artery calcification, and increased mortality rates in individuals with renal transplantation and chronic kidney disease (Jovičić-Pavlović et al.,2022). Patients carrying the FETUIN A 256Ser allele exhibited lower serum fetuin-A levels and higher all-cause and cardiovascular mortality rates if they were inflamed (Stenvinkel et al.,2005).

A significant finding in this study was the dominance of the GG polymorphism of fetuin-A c.766C>G in patients with kidney stone disease, signifying a potential genetic predisposition. It is important to note that the role of fetuin-A gene polymorphisms in kidney stone disease has been a subject of limited exploration, and this study contributes valuable insights(Schafer et al.,2003).

The potential interplay between fetuin-A and kidney stone disease involves complex mechanisms. Fetuin-A appears to regulate calcium burden and deposition, with higher calcium burden potentially leading to reduced fetuin-A protein levels. Conversely, low fetuin-A levels may promote crystal deposition, induce cell injury, and trigger oxidative stress, which can, in turn, lead to crystal adherence, aggregation, and deposition in the kidneys. Fetuin-A is also involved in inhibiting inflammation and oxidative stress, and its levels are negatively correlated with inflammatory markers in various inflammatory diseases (Noori et al.,2020).

To investigate the genetic factors further, gene-based association studies were conducted using the "SHEsis" tool, which allowed for haplotype inference, linkage disequilibrium analysis, and single locus association tests. The strong linkage observed between the two SNPs (rs4917, rs4918) in the FETUIN A gene provides a basis for future research into their co-inheritance and potential implications in kidney stone disease(Aksoy et al.,2010).

In addition to genetic analysis, structural impact assessments of the most damaging nsSNPs were performed using protein modeling tools such as HOPE and I-TASSER. These tools offer insights into how amino acid substitutions can affect protein structure. The structural analysis revealed the specific changes in amino acids and their potential structural consequences, providing valuable information about the genetic variants' effects on fetuin-A(Aksoy et al.,2010).

In summary, this study sheds light on the genetic and structural aspects of fetuin-A in the context of kidney stone disease, offering insights into potential genetic predispositions and the structural consequences of specific genetic variants. The findings emphasize the complex interplay between fetuin-A, genetics, and kidney stone

formation, providing a foundation for further research in this area(Aksoy et al.,2010).

Figure 4. HOPE modelling of c.766C>T

Amino acids exhibit distinctive characteristics, including size, charge, and hydrophobicity. Mutations often involve replacing the original wild-type amino acid with a mutant amino acid that differs in size and hydrophobicity. Typically, the mutant amino acid is larger and less hydrophobic than the wild-type amino acid. These variations in size and hydrophobicity can lead to the disruption of hydrogen bonds within the protein's core, thereby affecting its proper folding process.

For example, in the case of a mutation where Methionine is replaced by Threonine at position 248 (as shown in Figure 5), the HOPE analysis identified a change in charge between the wild-type and mutant amino acids, which stemmed from the hydrophobicity differences between them. This alteration in hydrophobic interactions, whether occurring within the protein's core or on its surface, can hinder the protein's folding. Furthermore, the mutant amino acid's smaller size may pose challenges, particularly if the wild-type amino acid was originally situated deep within the protein's core, as the mutant's larger size might not fit appropriately. This discrepancy in size, charge, and hydrophobicity underscores the potential structural consequences of amino acid mutations in proteins.
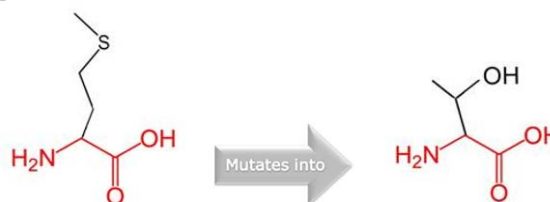
Figure 5. HOPE modelling of c.742C>T

The mutated residue is in close proximity to a residue involved in forming a cysteine bond. Although the cysteine bond itself remains unchanged, the nearby mutation could potentially impact its function. This mutation takes place within a domain known as Cystatin fetuin-A-type 2, and the introduction of an amino acid with differing properties may disrupt the function of this specific domain.

It is worth noting that the wild-type residue at this position is not conserved, meaning that it is not consistently preserved across related protein sequences. Conversely, the mutant residue is more frequently observed in other homologous sequences, suggesting that it is a common variant in proteins similar to the one under study. This indicates that the mutation may not have a detrimental effect on the protein's function. Additionally, the mutant residue is positioned near a highly conserved site, indicating potential stability within the protein structure.

In the I-TASSER analysis, the confidence score (C-score) is employed to predict each protein structure model. A C-score greater than -1.5 indicates a correctly folded structure. Moreover, the Tm score serves as a measure of structural similarity, and a Tm score above 0.5 indicates similarity to other proteins within the same structural classification in the protein database family.

6. Conclusion

In summary, based on the analysis, there is no evidence supporting an association between FETUIN A2 gene polymorphisms and reduced levels of Fetuin-A. The structural changes in the amino acid sequence of fetuin A do not appear to have a significant impact on its function.

Acknowledgements

Funding

Conflicts of interest:

None

References

Aksoy H, Aksoy Y, Ozturk N, Aydin HR, Yildirim AK, Akçay F. 2010. Fetuin-A gene polymorphism in patients with calcium oxalate stone disease. Urology. 75(4): 928-932. doi: 10.1016/j.urology.2009.08.058.

Al-Shuhaib MBS. 2019. D76V, L161R, and C117S are the most pathogenic amino acid substitutions with several dangerous consequences on leptin structure, function, and stability. Egyptian J. Med. Hum. Genet. 20: 32. https://doi.org/10.1186/s43042-019-0033-2.

Bellia C, Tomaiuolo R, Caruso A, Lo Sasso B, Zarrilli F, Carru C, ... Ciaccio M. 2012. Fetuin-A serum levels are not correlated to kidney function in long-lived subjects. Clin. Biochem. 45(9): 637-640.

Bouafi H, Bencheikh S, Mehdi Krami AL, Morjane I, Charoute H, Rouba H, ... Barakat A. 2019. Prediction and structural comparison of deleterious coding nonsynonymous single nucleotide polymorphisms (nsSNPs) in human LEP gene associated with obesity. Biomed. Res. Int. 2019: 1832084. doi: 10.1155/2019/1832084.

Choi Y, Sims GE, Murphy S, Miller JR, Chan AP. 2012. Predicting the functional effect of amino acid substitutions and indels. PLoS One. 7(10): e46688. doi: 10.1371/journal.pone.0046688.

Jovičić-Pavlović S, Simić-Ogrizović S, Bukumirić Z, Erić M, Pavlović N, Kotlica B, Novaković I. 2022. Impact of the fetuin gene polymorphisms in coronary artery calcification and mortality of patients with chronic kidney disease and renal transplant. Genetika. 54(1): 457-472.

Kishore DV, Moosavi F, Varma RK. 2013. Effect of ethanolic extract of *Portulaca oleracea* linn. on ethylene glycol and ammonium chloride induced urolithiasis. Int. J. Pharm. Pharm. Sci. 5(2): 134-140.

Kono TJY, Lei L, Shih CH, Hoffman PJ, Morrell PL, Fay JC. 2018. Comparative genomics approaches accurately predict deleterious variants in plants. G3 (Bethesda). 8(10): 3321-3329. doi: 10.1534/g3.118.200563.

Kumar P, Henikoff S, Ng PC. 2009. Predicting the effects of coding non-synonymous variants on protein function using the SIFT algorithm. Nat. Protoc. 4(7): 1073-1081. https://doi.org/10.1038/nprot.2009.86.

Mohammadi-Noori E, Salehi N, Mozafari H, Elieh Ali Komi D, Saidi M, Bahrehmand F, Kiani A. 2020. Association of FETUIN A gene polymorphisms with serum fetuin-A levels in individuals with cardiovascular calcification in west of Iran. Mol. Biol. Rep. 47(3): 1809-1820. doi: 10.1007/s11033-020-05275-z.

Ramello A, Vitale C, Marangella M. 2000. Epidemiology of nephrolithiasis. J. Nephrol. 13(3): S45-S50.

Rodrigues FG, Neves RFC A, Ormanji MS, Esper PLG, Gaspar M, Pereira RMR, ... Heilberg IP. 2022. Vascular calcification is associated with fetuin-A and cortical bone porosity in stone formers. J. Pers. Med. 12(7): 1120. doi: 10.3390/jpm12071120.

Roy A, Kucukural A, Zhang Y. 2010. I-TASSER: a unified platform for automated protein structure and function prediction. Nat. Protoc. 5(4): 725-738. doi: 10.1038/nprot.2010.5.

Rudloff S, Jahnen-Dechent W, Huynh-Do U. 2022. Tissue chaperoning—the expanded functions of fetuin-A beyond inhibition of systemic calcification. Pflugers Arch. Eur. J. Physiol. 474: 949–962. https://doi.org/10.1007/s00424-022-02688-6.

Sayer JA. 2008. The genetics of nephrolithiasis. Nephron Exp. Nephrol. 110(2): e37-e43. https://doi.org/10.1159/000151730.

Schafer C, Heiss A, Schwarz A, Westenfeld R, Ketteler M, Floege J, ... Jahnen-Dechent W. 2003. The serum protein alpha 2-Heremans-Schmid glycoprotein/fetuin-A is a systemically acting inhibitor of ectopic calcification. J. Clin. Invest. 112(3): 357-366. doi: 10.1172/JCI17202.

Singh P, Harris PC, Sas DJ, Lieske JC. 2022. The genetics of kidney stone disease and nephrocalcinosis. Nat. Rev. Nephrol. 18(4): 224-240. doi: 10.1038/s41581-021-00513-4.

Stenvinkel P, Wang K, Qureshi AR, Axelsson J, Pecoits-Filho R, Gao P, ... Nordfors L. 2005. Low fetuin-A levels are associated with cardiovascular death: Impact of variations in the gene encoding fetuin. Kidney Int. 67(6): 2383-2392. doi: 10.1111/j.1523-1755.2005.00345.x.

Temesszentandrási G, Vörös K, Márkus B, Böröcz Z, Kaszás E, Prohászka Z, ... Kalabay L. 2016. Human fetuin-A Rs4918 polymorphism and its association with obesity in healthy persons and in patients with myocardial infarction in two Hungarian cohorts. Med. Sci. Monit. 22: 2742-2750. doi: 10.12659/msm.896232.

Umapathy D, Subramanyam PV, Krishnamoorthy E, Viswanathan V, Ramkumar KM. 2022. Association of fetuin-A with Thr256Ser exon polymorphism of α2-Heremans Schmid glycoprotein (FETUIN A) gene in type 2 diabetic patients with overt nephropathy. J. Diabetes Complications. 36(1): 108074. doi: 10.1016/j.jdiacomp.2021.108074.

Wang T, Bu CH, Hildebrand S, Jia G, Siggs OM, Lyon S, Beutler B. 2018. Probability of phenotypically detectable protein damage by ENU-induced mutations in the Mutagenetix database. Nat. Commun. 9(1): 441. https://doi.org/10.1038/s41467-017-02806-4.

Wang Z, Zhang Y, Zhang J, Deng Q, Liang H. 2021. Recent advances on the mechanisms of kidney stone formation (Review). Int. J. Mol. Med. 48: 149. https://doi.org/10.3892/ijmm.2021.4982.

Effect of Sucrose Excess and Deprivation on the Physiological Responses and Phytochemical Compound Profiles of Kaffir Lime Calli

Adelia Komalasari, Angellia Melliana Pramesthi, Wulan Usfi Mafiroh, Aries Bagus Sasongko and Woro Anindito Sri Tunjung[*]

Faculty of Biology, Universitas Gadjah Mada, Jl. Teknika Selatan, Sekip Utara, Yogyakarta 55281, Indonesia

Abstract

Background. Kaffir lime (*Citrus hystrix* DC.) calli contain compounds with potential uses in biological activities. The synthesis of these compounds can be enhanced by increasing or decreasing the amount of nutrients. Sucrose provides carbon and energy, which are crucial for the proliferation and development of callus tissue. Sucrose excess or deprivation can generate osmotic potential, which affects the synthesis of bioactive compounds. This study aims to analyze the physiological responses and phytochemical compound profiles of kaffir lime calli due to variations in sucrose concentrations.

Methods. Calli were induced from seed explants using sucrose concentrations of 30 (S1) and 40 (S3) g/L. At the subculture stage, the callus was transferred to a medium with a regular sucrose concentration of 30 g/L (S1), deprivation sucrose concentration of 20 g/L (S2), and excess sucrose concentration of 40 g/L (S3). Observed parameters included biomass, morphology (color and texture), and bioactive compound profiles.

Results. Growth curves indicated that although the groups had the same growth phase patterns, the biomass of G1 calli under the S3–S3 treatment was significantly higher than in other treatments. In addition, the S3–S3 treatment produced the greatest number of compounds, followed by the S1–S2 treatments. This includes the total number of compounds detected by GC-MS and the number of compounds possessing biomedical activities including anticancer, antitumor, antioxidant, anti-inflammatory, antimicrobial, antibacterial, antiviral, and antifungal properties.

Conclusion. Excess and deprivation of sucrose concentration both have effects on kaffir lime calli. Treatment with excessive sucrose (S3 to S3) results in a rise in G1 callus biomass. Meanwhile, treatment with S3 to S3 and S1 to S2 (regular to deprivation) enhances the synthesis of compounds with biomedical activities. This occurs because sucrose stimulates the synthesis of bioactive compounds by serving osmotic stressor and energy source.

Keywords: kaffir lime, callus, sucrose, bioactive compounds, physiological

1. Introduction

Our previous study succeeded in inducing friable and genetically stable calli from kaffir lime (*Citrus hystrix* DC.) seeds (Tunjung *et al*., 2021). These calli contained various bioactive compounds, such as α-pinene and 1,8-cineole, which serve as therapeutic agent (Tunjung *et al*., 2020). The potential in biological activities of kaffir lime calli needs to be developed by increasing their bioactive compound production and maintaining their good growth. One strategy for producing bioactive compounds is the use of plant tissue culture techniques. Through plant tissue culture, the production of bioactive compounds can be enhanced using various strategies such as adding nutrients and growth hormones to the culture medium, adjusting the medium, adding biotic and abiotic elicitors, and introducing precursors. The culture media can be supplemented with macronutrients and micronutrients to provide essential nutrition for the callus, thereby promoting callus growth. Adding specific amounts of nutrients, whether in deficiency or excess, can induce stress, which in turn enhances the synthesis of bioactive compounds (Selwal *et al*., 2023). Incorporating elicitors into the culture medium induces stress conditions that promote the synthesis of bioactive compounds (Laezza *et al*., 2024). The addition of precursors can activate enzymes responsible for the production of bioactive compounds, thus increasing their synthesis rate (Aksenova et al., 2023). For instance, the addition of of glutathione precursors to the culture medium has been shown to enhance cell suspension biomass and organosulfur compound accumulation in *Allium sativum* L. (Setiowati *et al*., 2022). Hence, the addition of precursor, elicitor or nutrient into culture media warrant further investigation.

Sucrose is the predominant carbon source utilized in plant tissue culture. In vitro conditions, added sucrose may play multiple roles as a carbon, energy sources and an osmotic agent that may impose osmotic stress (Dantas *et al*., 2021). The presence of sucrose in culture media

---

[*] Corresponding author. e-mail: wanindito@ugm.ac.id.

facilitates cell division, which is essential for the physiology and biomass of calli (Khan *et al.*, 2018). Moreover, sucrose participates in terpenoid biosynthesis through the glycolysis cycle, producing precursors in the form of acetyl-CoA, which is shunted to the mevalonate process in cytosolic organelles (Stein and Granot, 2019). In the cytosolic pathway, the mevalonate (MVA) cycle can synthesize monoterpenes in plastid organelles (Yu *et al.*, 2015). According to Tholl (2015), 3-hydroxy-3-methylglutaryl-CoA reductase, the primary enzyme in terpenoid biosynthesis, is regulated by the activity of protein kinase SnRK1, which is in turn modulated by glucose as a signal.

At optimal concentrations, sucrose can maintain cell turgor pressure, which is critical in the formation of callus cell structures. Javed, and Ikram, (2008) stated that in the induction of wheat (*Triricum aestivum* L.) calli, a sucrose concentration of as high as 40 g/L in media can impose osmotic pressure and water potential to produce a high biomass weight of 80 mg, while sucrose is 30 g/L produced a biomass weight of 50 mg. At high concentrations, sucrose can act as an abiotic stressor capable of increasing the production of secondary metabolite compounds. A previous study demonstrated that the stem calli of *Wedelia biflora* (L.) D.C exposed to 40 g/L sucrose produced 88 mg of stigmasterol compounds, whereas that exposed to 30 g/L sucrose produced 58.3 mg of stigmasterol compounds (Idris *et al.*, 2018). These data emphasize the importance of optimizing sucrose concentration.

In the current study, we investigated the effect of sucrose excess and deprivation on callus growth. At generation 0 (G0), we used two sucrose concentrations: regular and excessive. At the subculture stage (G1), the calli were subjected to deprivation, regular, and excessive sucrose concentrations. This study aimed to analyze the impact of excess and deprivation of sucrose on the physiological responses and phytochemical profiles of kaffir lime calli.

2. Materials and methods

2.1. Sampling

Kaffir lime fruit was collected from Pekutan, Bayan, Purworejo, Central Java, Indonesia. The temperatures at the sample location were 31°C in the air, 30°C in the soil, 676 Cd for light intensity, and 33% for air humidity. The site was located 232 meters above sea level. The citrus fruits used were three months old. Fruit was selected if it had a diameter of 5–6 cm and fresh green color and was not moldy and excessively wrinkled. The seed explant used was 1–2 cm in diameter.

2.2. Induction of kaffir lime calli

Seed sterilization, callus induction, and subculture were performed by using a method from our previous study (Tunjung *et al.*, 2021). The media used in this study was Murashige and Skoog medium containing macronutrients ($CaCl_2 \cdot 2H_2O$, KNO_3, KH_2PO_4, NH_4NO_3, and $MgSO_4 \cdot 7H_2O$), iron ($FeSO_4 \cdot 7H_2O$ and Na_2–EDTA), micronutrients ($MnSO_4 \cdot H_2O$ of 22.3 mg/L, $ZnSO_4 \cdot 4H_2O$ of 8.6 mg/L, H_3BO_3 of 6.2 mg/L, $CuSO_4 \cdot 5H_2O$ of 0.025 mg/L, $CoCl_2 \cdot 6H_2O$ of 0.025 mg/L, KI of 0.83 mg/L, $NaMoO_4 \cdot 2H_2O$ of 0.25 mg/L), vitamins, and myo-inositol.

The concentration of sucrose varied as follows: 30 g/L (S1) representing the regular concentration, 20 g/L (S2) as the deprivation concentration, and 40 g/L (S3) as the excess concentration. Media were added with a plant growth regulator in the form of 2,4-D:BAP at a ratio of 1:0.5 ppm. Kaffir lime seeds were sterilized with 5.25% NaOCl. The sterile kaffir lime seeds were cut and placed in an incubation room in the dark.

2.3. Subculture of kaffir lime

G0 calli were induced on a medium with sucrose concentrations of 30 g/L and 40 g/L. The calli were weighed every five days to determine their growth phase. Additionally, the texture and color of the calli were analyzed. Subcultures (G1) were initiated when the calli reached the exponential phase, approximately 25–30 days after induction. The calli were then cut into two pieces, each measuring 0.5 cm, and exposed to varying sucrose concentrations in the new medium: 30 g/L (S1), 20 g/L (S2), and 40 g/L (S3). Morphology and growth phase measurements were performed every five days until day 50.

Table 1. Sucrose concentration

Treatment	Sucrose concentration (g/L)	
Group	Generation 0	Generation 1
S1–S1	30	30
S1–S2	30	20
S1–S3	30	40
S3–S1	40	30
S3–S2	40	20
S3–S3	40	40

Notes: S1-S1: regular sucrose concentration to regular sucrose concentration (30 g/L to 30 g/L)

S1-S2: regular sucrose concentration to deprivation sucrose concentration (30 g/L to 20 g/L)

S1-S3: regular sucrose concentration to excess sucrose concentration (30 g/L to 40 g/L)

S3-S1: excess sucrose concentration to regular sucrose concentration (40 g/L to 30 g/L)

S3-S2: excess sucrose concentration to deprivation sucrose concentration (40 g/L to 20 g/L)

S3-S3: excess sucrose concentration to excess sucrose concentration (40 g/L to 40 g/L)

2.4. Physiological and growth parameters of kaffir lime calli

G1 Calli were weighed every 5 days over a 50-day period to construct growth curves. A total of 9 calli were measured at each interval. The wet and dry weights of the calli were recorded, with the dry weight obtained after drying the calli in an oven at 33°C for 7 days. The growth curves were used to identify the lag, exponential, and stationary phases of growth. The lag phase is characterized by minimal changes in callus biomass at the onset of induction. The exponential phase is marked by a substantial increase in callus biomass. The stationary phase is characterized by relatively stable callus biomass. The morphological indices for measurement and observation included callus texture and color. The texture of the observed calli was determined as friable or compact. Calli texture is classified as follows: callus initiation with compact texture (+), callus beginning to spread with

compact texture (++), callus starting to dominate the explant with friable texture (+++), and callus fully dominating with friable texture (++++). The color of calli was determined on the basis of the Royal Horticultural Society color chart.

2.5. Extraction

Calli were harvested at stationary phase and dried until they reached a constant weight. A total of 1 gram dry callus powder was macerated in ethyl acetate for 24 h and remacerated three times. Extracts were analyzed using gas chromatography-mass spectrometry (GC-MS) on an Agilent 7890A system equipped with an Agilent 5977B GC/MS detector (Agilent Technologies, Palo Alto, CA, USA). The MS column used was DB-5MS (5% [phenyl]-

methylpolysiloxane). The NIST 16 library database was employed for compound identification.

2.6. Statistical analysis

One-way ANOVA was performed using SPSS software to examine both wet and dry weights of G1 callus at t 30 days, which is the maximum biomass. In order to find significant variations in the treatment medium, Duncan's Multiple Range Test (DMRT) was then run at a 5% significance level.

3. Result

3.1. Callus growth

The G1 growth curves of the kaffir lime calli over 50 days are shown in Figure 1.
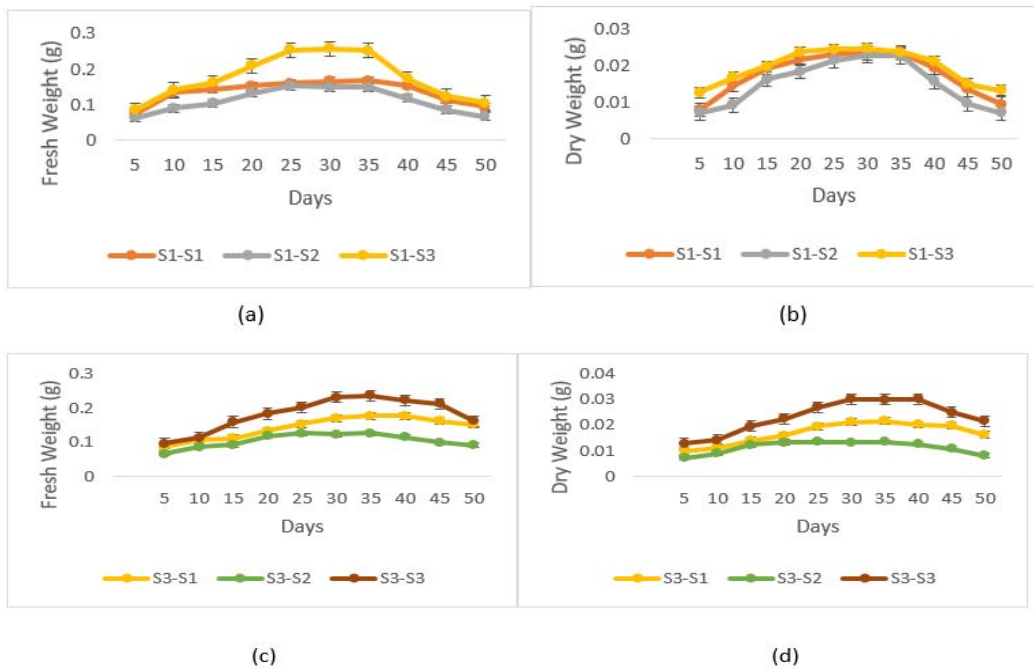
Figure 1. Growth curves of kaffir lime calli. Under deprivation sucrose (a Fresh Weight b. Dry Weight) and excessive sucrose concentration treatment (c. Fresh Weight d. Dry Weight).

The callus growth curve indicated that the biomass of calli under the S1 treatment did not differ significantly, as S1 represents the standard sucrose dose used in Murashige and Skoog medium. In contrast, calli under the S3 treatment showed different biomass weights. The S3–S3

(excess–excess) treatment showed the significant highest biomass, while the lowest was found under the S3–S2 (excess–deprivation) treatment (Figure 2). The striking difference in sucrose concentration between G0 and G1 may have caused the reduction in callus biomass.
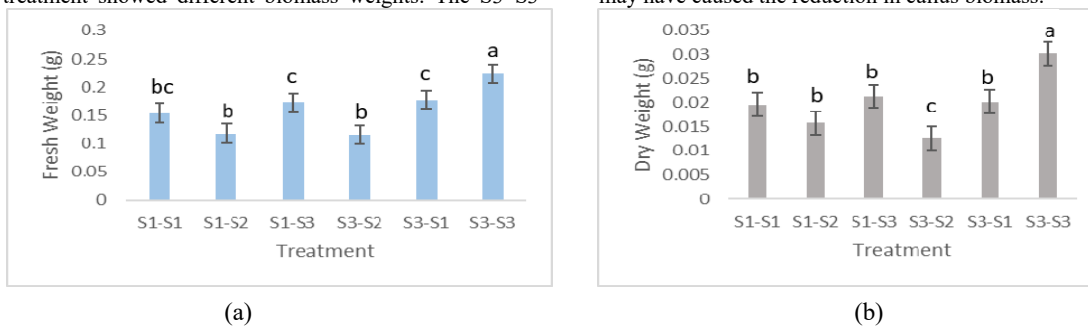
Figure 2. Statistical analysis of G1 Kaffir lime calli. Fresh weight (a) and dry weight (b). Significant different are shown by different letters, according to an ANOVA with a significance level of $\alpha < 0.05$.
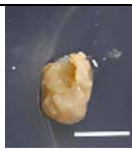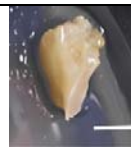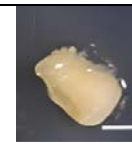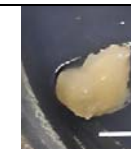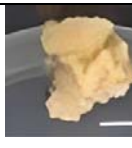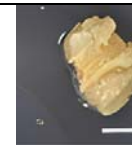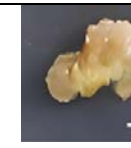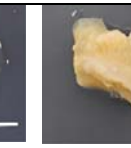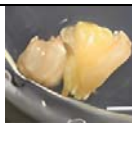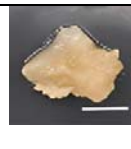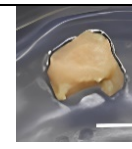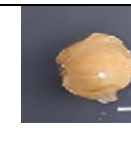
Table 2 presented the growth phases of G1 calli based on their growth curves.

Table 2. Growth phase of G1 kaffir lime calli under various sucrose treatments

Treatment	Growth phase (day)		
	Lag phase	Exponential phase	Stationary phase
S1–S1	5–10	10–30	30–40
S1–S2	5–10	10–30	30–40
S1–S3	5–10	10–30	30–40
S3–S2	5–10	10–30	30–40
S3–S1	5–10	10–30	30–40
S3–S3	5–10	10–30	30–40

Furthermore, no differences were found in the growth phase of each group. Days 5-10 were the lag phase, days 10-30 were the exponential phase, and days 30-40 were the stationary phase. However, callus biomass significantly differed among the treatment groups. Given its dual roles as an osmotic regulator and as a nutrient, which is vital for the embryoid and callus formation, sucrose has the potential to impact callus biomass. Calli must be grown in a controlled media with 30 g/L sucrose (Thaneshwari, 2018). Therefore, excess or deprivation of sucrose will affect callus biomass but not the growth phase of the callus in each sucrose treatment group.

3.2. Physiological responses of kaffir lime calli

The morphological characteristics of kaffir lime calli, including color and texture, are illustrated in Table 3.

Table 3. Color and texture of G1 kaffir lime calli exposed to various sucrose concentrations

Days	S1–S1	S1–S2	S1–S3	S3–S2	S3–S1	S3–S3
Day 10 (Lag phase)						
	Pale yellow: 161C	*Pale greenish yellow*: 160C	*Pale yellow*: 160D	*Pale yellow*: 161C	*Pale yellow*: 161C	*Pale yellow*: 160D
	+++	+++	++++	++++	++++	++++
Day 30 (Exponential phase)						
	Light yellow: 162 C	*Moderately yellow*: 161A	*Moderately yellow*: 161A	*Moderately yellow*: 161A	*Moderately yellow*: 161A	*Moderately yellow*: 161A
	++++	++++	++++	++++	++++	++++
Day 40 (Stationary phase)						
	Moderately yellow: 161A	*Moderately yellow*: 161A	*Moderately yellow*: 161A	*Moderately yellow*: 161A	*Moderately yellow*: 161A	*Moderately yellow*: 161A
	++++	++++	++++	++++	++++	++++

Notes:

S1: 30 g/L, S2: 20 g/L, S3: 40 g/L   ++: The callus has begun to spread throughout the explant and has a compact texture

(−) : Callus has not yet appeared   +++: The callus has begun to dominate the explant and has a friable texture

(+): Callus initiation   ++++ : The callus has dominated the whole section and has a friable texture.

The scale bar represents a size of 1 cm

In this study, varying sucrose concentrations did not cause differences in callus color and texture. This result proves that sucrose excess and deprivation lacked an effect on callus color or texture.

3.3. Compound profiles of kaffir lime calli

Kaffir lime calli exposed to various sucrose concentrations can be used to biosynthesize bioactive compounds. The percentage of peak area, and names of bioactive compounds are shown in Table 4. The percentage of peak area (%) reflects the relative proportion of each detected compound within a sample, highlighting the abundance of each compound in comparison to the total mixture.

Table 4. Bioactive Compounds in Calli Possess Biomedical Activity

No.	Compound	The percentage of peak area in the sucrose treatment (%)						Group	Biomedical activity
		S1–S1	S1–S2	S1–S3	S3–S2	S3–S1	S3–S3		
1	2-Hexanone, 3-methyl-4-methylene	0.42	ND	ND	ND	0.86	ND	Acetic acid hexyl ester	AO, AM (Karthik et al., 2023)
2	*sec*-Butyl nitrite	0.36	ND	ND	1.43	ND	0.07	Heptadecane	AO (Ghasemi et al., 2023)
3	1-Hexyn-3-ol	0.39	ND	ND	ND	1.46	0.29	Alcohol-ketone	AB (Charles et al., 2018)
4	2,4-Nonadienal	0.16	0.21	ND	0.28	ND	0.22	Aldehyde	AF, AO (Bourhia et al., 2021)
5	Heptane, 2,4-dimethyl-	0.1	ND	ND	0.13	ND	ND	Acyclic short-chain alkane	AF, AB (Al-Rahbi et al., 2023)
6	1-Decene, 2,4-dimethyl-	0.56	ND	0.41	ND	ND	ND	Alkene	AC, AO (Al-Mansoub et al., 2021)
7	Naphtalene	5.22	5.5	5.78	4.13	3.77	5.94	Sesquiterpene	AO (Ozen et al., 2018)
8	3-Hexanone, 2,5-dimethyl-	0.16	0.22	ND	0.45	ND	ND	Isobutyl ketone	AM (Karthik et al., 2023)
9	1-Octanol, 2-butyl-	0.2	3.49	ND	3.71	ND	1.47	Aliphatic alcohol	AM, AC (Muzahid et al., 2023)
10	Dodecane, 4,6-dimethyl-	1.17	7.6	ND	1.24	1.44	ND	Alkane	AO and AM (Wiraswati et al., 2023)
11	2-Decenal	0.47	ND	ND	0.89	ND	ND	Unsaturated aldehyde	AM (Wiraswati et al., 2023)
12	Oxalic acid and allyl pentadecyl ester	0.53	0.74	ND	ND	0.28	0.35	Ester	AF, AM (Doughari and Abraham, 2021)
13	1-Undecene, 7-methyl-	3.44	4.11	1.71	4.45	ND	ND	Volatile oil	AO, AI, AB, and AF (Muzahid et al., 2023)
14	Octan-2-one, 3,6-dimethyl-	0.78	0.32	0.33	ND	ND	ND	Branched ketone	AM (Wang et al., 2022)
15	Heptadecane, 2,6,10,14-tetramethyl-	0.31	0.41	ND	ND	ND	ND	Hydrocarbon-alkane	AC (Zare et al., 2023)
16	Decane, 2,3,5,8-tetramethyl-	0.49	1.56	0.73	1.88	ND	2.55	Aliphatic hydrocarbon	AO, AC (Avidlyandi et al., 2021)
17	Diethyl phthalate	0.89	1.01	0.75	2.78	1.37	2.37	Phthalate ester	AO (Amara et al., 2020)
18	2-Piperidinone, *N*-[4-bromo-*n*-butyl]-	0.09	1.07	0.28	0.97	0.29	0.96	Alkaloid	AM (Al-Salman 2019)
19	2,5-Pentadecadien-1-ol	0.24	ND	ND	0.3	ND	0.47	Unsaturated alcoholic compound	AB, AI, AO (Chrząszcz et al., 2023)
20	1,4-Bis(trimethylsilyl)benzene	0.27	0.45	ND	1.99	0.25	0.9	Trimethylsilyl	AO (Wiraswati et al., 2023)
21	1,2-Bis(trimethylsilyl)benzene	0.28	0.64	ND	0.28	0.5	0.91	Trimethylsilyl	AM (El-Zawawy and Mona 2021)
22	1-Undecene, 4-methyl	0.5	0.64	ND	ND	ND	ND	Hydrocarbon	AM (Tleubayeva et al., 2021)
23	2-Heptenal,	ND	0.64	0.28	ND	ND	ND	Unsaturated fatty acids	AT, AV, AI (Gu, et al., 2019)
24	2-Decene	ND	1.09	0.55	ND	ND	ND	Unsaturated aldehyde	AM (Lee et al., 2022)
25	2,4-Decadienal	ND	0.8	0.22	ND	ND	ND	Unsaturated aldehyde-aliphatic aldehyde	AB (Zhang et al., 2020)
26	d-Glycero-d-ido-heptose	ND	0.42	ND	ND	ND	0.9	Sugar	AB (Guo et al., 2021)
27	Cyclotrisiloxane, hexamethyl-	ND	1.31	1.31	11.97	1.47	17.02	Fatty acid-phenolic compound	AM and AO (Gheda and Ismail 2020)
28	Palmitic acid	ND	0.61	20.43	ND	0.79	ND	Saturated fatty acids	AC, AI (Zhu et al., 2021)
29	1-Octyn-3-ol	ND	ND	ND	0.32	ND	0.08	Octynol-alkyne	AM (Xiong et al., 2017)

No.	Compound	The percentage of peak area in the sucrose treatment (%)						Group	Biomedical activity
		S1–S1	S1–S2	S1–S3	S3–S2	S3–S1	S3–S3		
30	Cyclohexane, 1,1,2-trimethyl	ND	ND	ND	0.34	ND	0.53	Fatty acyls-hydrocarbon	AO (Onanuga et al., 2022)
31	Oxirane, 2-butyl-3-methyl-	ND	ND	ND	0.22	ND	0.24	Epoxide heptane	AM (Njoroge et al., 2019)
32	4-Tridecene	ND	0.17	ND	ND	0.17	ND	Fatty acyls-hydrocarbon	AM (Lammers et al., 2021)
33	E-10-Dodecen-1-ol propionate	ND	ND	ND	0.26	ND	0.63	Lipid	AO, AC, AM (Paudel et al., 2020)
34	4-Ethyl-1-hexyn-3-ol	ND	ND	ND	ND	1.46	0.29	Alcohol-ketone	AB (Charles et al., 2018)
35	Tridecane	ND	ND	ND	ND	1.33	3.03	Alkane	AC (Singh and Luqman 2014)
36	Tetradecane, 1-fluoro	ND	ND	ND	ND	0.22	0.92	Tetradecyl fluoride	AB, AM (Nasr et al., 2022)
37	Decane, 2,4,6-trimethyl	ND	ND	ND	ND	0.45	1.1	Alkane hydrocarbon	AO, AM (Wiraswati et al., 2023)
38	Citronellol epoxide	ND	0.52	ND	ND	ND	ND	Derivative terpene epoxide	AC (Ho et al., 2020)
39	9-12, Octadecanoic acid	ND	ND	0.41	ND	ND	ND	Linoleic acid ester	AC, AI (Gheda and Ismail 2020)
40	1-Iodo-2-methylnonane	ND	ND	ND	ND	ND	0.1	Iodine compound	AO (Khan et al., 2021)
41	Dodecanoic acid, 3-hydroxy	ND	ND	ND	ND	ND	1.12	Ethyl ester fatty acid	AC (Ukwubile et al., 2019)

■ Bioactive compounds related to anticancer effects

■ Bioactive compounds related to anticancer and antimicroorganism effects

□ Bioactive compounds related to antimicroorganism effects

Notes: The percentage of peak area (%) reflects the relative proportion of each detected compound within a sample, highlighting the abundance of each compound in comparison to the total mixture. ND = not detected, AC = anticancer, AI = anti-inflammatory, AO = antioxidant, AT = antitumor, AM = antimicrobial, AB = antibacterial, AF = antifungal, AV = antivirus.

The secondary metabolite profiles of calli differed in terms of the types of compounds produced under each treatment. Common compounds produced under almost all treatments included alkanes, such as butane, 1-chloro-3-methyl, and dodecane,4,6-dimethyl-; alkaloids, such as 2-periperidinone and *N*-[4-bromo-*n*-butyl]; fatty acids, namely, 9-octadecenoic acid (*Z*)-, phenylmethyl ester; and terpenoid compounds, specifically, the sesquiterpene naphthalene. The percentage of the peak area of naphthalene compounds, which have anticancer activity, decreased in calli that experienced sucrose excess during G0 and were subcultured on deprivation or regular medium during G1.

Calli grown on regular medium during G0 produced several types of compounds, including aldehydes, such as 2-decenal and 2,4-decadienal; ketones, namely, octan-2-one and 3,6-dimethyl-; fatty alcohols, such as 11-methyldodecanol; fatty acids, including palmitic acid; and monoterpenoids, namely, citronellol epoxide. These compounds were not found in calli grown under sucrose excess during G0. Sucrose excess during G0 resulted in the production of high amounts of compounds. These compounds included alkanes, such as decane, 2,4,6-trimethyl, tridecane, and hexadecane; fatty alcohols, including 1,2:4,5:9,10-triepoxydecane; fatty acids, such as dodecanoic acid and 3-hydroxy; and flavonoids, namely, 7,9-di-tert-butyl-1-oxaspiro(4,5)deca-6,9-diene-2,8-dione.

Table 5. Summary of Bioactive Compounds Detected in Kaffir Lime Calli

Sucrose concentration	Number of compounds					
	S1–S1	S1–S2	S1–S3	S3–S2	S3–S1	S3–S3
Total peak detected in GCMS	45	44	29	44	39	52
Total compounds Possess Biomedical Activity	22	23	13	20	16	24
Bioactive compounds related to anticancer effects (AC, AT, AO &AI)	13	13	9	13	9	15
Bioactive compounds related to antimicroorganism effects (AM,AB,AF &AV)	15	16	6	14	11	15

Notes: AC = anticancer, AI = anti-inflammatory, AO = antioxidant, AT = antitumor, AM = antimicrobial, AB = antibacterial, AF = antifungal, AV = antivirus

According to GCMS data, a total of 29 compounds with low peaks were detected under the S1–S3 treatment, whereas 52 compounds with high peaks were found under the S3–S3 treatment. The number of peaks indicates the variety of compounds detected in the callus. Among these detected compounds, we investigated which bioactive substances exhibit biomedical activity and hold potential for development as traditional medicines. The S3–S3 sucrose treatment produces the highest number of compounds with biomedical activity, followed by the S1–S2 treatment. These results may be due to the effect of sucrose concentrations on osmotic potential; both high and low concentrations can reduce osmotic potential, leading to stress in the calli and the subsequent synthesis of secondary metabolites (De Paiva and Otoni, 2003). Additionally, the S3 treatment was applied during G0 (callus induction), causing the calli to experience stress from the beginning of the experiment.

4. Discussion

In this study, sucrose was added at various concentrations (regular, deprivation, and excess) to kaffir lime calli. Carbohydrates are essential for plants to survive. They serve as a substrate for respiration, function in the synthesis of numerous chemicals, and constitute macromolecule building blocks (Wahyuni *et al*., 2020). Furthermore, carbohydrates may regulate several cellular developmental processes (Dantas *et al*., 2021). Sumaryono et al. (2012) reported that sucrose is the most often utilized carbohydrate source in plant tissue culture because disaccharides are widely used as transporter molecules likely due to their high water solubility. The majority of in vitro studies have shown that sucrose supports growth and can enhance cell biomass (Al-Zubaidy *et al*., 2020). The development of somatic embryos in culture medium is influenced by the amount of sugar concentration (Lema-Ruminska *et al*., 2013).

In this current study, the highest dry and fresh weights of G1 calli were observed in the S1-S3 and S3-S3 (excessive) treatments. The S3-S3 treatment produced significantly higher biomass, whereas the biomass in the S1-S3 treatment was not significantly different from that in the S1-S1 and S1-S2 treatments. The lowest biomass was observed in the S3-S2 (deprivation) treatment. Therefore, among the treatments, exposure to excessive sucrose during G0 or G1 is the best for increasing callus biomass. This result is related to the role of sucrose sucrose as an energy-providing carbon substrate for plant growth in vitro (Homsuwan *et al*., 2021). Sucrose is an essential component of medium for in vitro plant development because it supplies organic nutrients and controls osmotic pressure (Liang *et al*., 2018). The breakdown of sucrose into fructose and glucose increases the osmolality of media. Sucrose concentration can impose osmotic potential on the enlargement of callus cells (Sumaryono *et al*., 2012). It can impose osmotic stress on calli and result in proline accumulation, which is useful for overcoming the effects of osmotic stress due to the total loss of water and carbohydrates (Gerdakaneh *et al*., 2010; Hayat *et al*., 2012). Therefore, the presence of osmotic stress can cause the fresh weight of calli to increase. This situation indicates that calli contain water and carbohydrates (Sari *et al*., 2018).

In cellular metabolism, glucose and fructose, as constituents of sucrose, enter the glycolysis pathway and Krebs cycle to form ATP, which is needed for callus growth. Gerdakaneh et al. (2010) reported that differences in dissolved sucrose concentrations cause variations in turgor and osmotic pressure. In tissue culture, turgor pressure affects the elongation of callus cells. In addition, each cell exhibits different growth responses to changes in turgor pressure due to the addition of sucrose. Moreover, because sucrose promotes cell respiration, which increases callus biomass, its addition accelerates callus growth. Meanwhile, low callus biomass can occur under deprivation treatment because of the response of callus cells to the lack of sucrose as the main energy source for callus growth. Therefore, callus growth is not optimal. The rate of respiration and absorption of nitrogen reduce under low sucrose concentrations. Protein synthesis is therefore may be inhibited as a result of the decrease in available energy (Thaneshwari, 2018).

Morphological characteristics in terms of color or texture showed almost no differences between calli exposed to sucrose deprivation or excess. All G1 calli had a yellowish color and tended to be pale with a friable texture. Callus color is influenced by the color of the explant, namely, the seed. The absence of differences in callus color and texture among treatments indicates that the addition of sucrose does not affect callus morphology.

High (excess) and low (deprivation) concentrations of sucrose affect the amount and type of bioactive compounds produced. Phenylalanine ammonia-lyase (PAL), which can provide precursors for the total biosynthesis of phenolics and flavonoids, may become more active when sucrose is added (Jaafar *et al*., 2012). In the phenylpropanoid pathway, PAL is the main enzyme. It catalyzes the transformation of *trans*-cinnamic acid from L-phenylalanine, which is generated via the shikimate pathway. The phenylpropanoid pathway can convert *trans*-cinnamic acid into intermediate molecules (sinapic and coumaric acids) that can be further transformed into coumarin and chlorogenic acid, which can then be further transformed into secondary metabolites (Sharma *et al*., 2019). These compounds have biological activities including antioxidant, anti-inflammatory, and anticancer activities. Another study revealed that sucrose stimulates anthocyanin biosynthesis in *Arabidopsis thaliana* by upregulating both structural genes and positive transcription factors associated with the flavonoid biosynthesis pathway. Additionally, sucrose may facilitate this process by simultaneously downregulating the negative transcription factor MYBL2 (Kyoko *et al*., 2008). These findings support the study results, which show that the S3–S3 treatment produced the highest total peak and the greatest number of compounds possesses biomedical activity among all treatments. Most of these compounds exhibit anticancer, anti-inflammatory, antioxidant, antitumor, antimicrobial, antibacterial, antifungal, and antiviral activities. This result suggests that high concentrations of sucrose (excessive) are suitable for the production of compounds with biomedical activity.

The S1–S2 deprivation treatment can also potentially stimulate the synthesis of various biomedical compounds, including antibacterial, antimicrobial, and antifungal agents because it causes calli to become stressed due to nutritional deficiencies. It can trigger calli to produce

bioactive compounds because carbohydrates accumulate as signals and provide energy for the synthesis of various chemicals (Lee and Huang, 2014).

Several bioactive compounds were observed under all treatments. They included napththalene, a sesquiterpene; diethyl phthalate, a phthalate ester, and 2-piperidinone, an alkaloid. In addition, two types of terpenoid compounds were detected in calli: naphthalene and citronellol epoxide. Naphthalene compounds had the highest peak area of 5.94% under the S3–S3 treatment, whereas citronellol epoxide was found under the S1–S2 treatment with a peak area of 0.52%. Citronellol epoxide is a citronellol compound resulting from the epoxidation process thus changing the structure of the compound. Peel and leaf of *Citrus* species including *Citrus maxima*, *Citrus limonia*, *Citrus limon*, and *Citrus reticulata* are typical sources of the chemical citronellol (Das *et al.*, 2024), and we could find this compound in kaffir lime's calli

Meanwhile, the first to third highest percentage peak areas in all the detected compound profiles were shown by palmitic acid (S1–S3), cyclotrisiloxane (S3–S3), and dodecane,4-6dimethyl (S1–S2) with peak percentages of 20.43%, 17.02%, and 7.6%, respectively. The highest peak of most of the mentioned compounds occurred under the S3 treatment during G0 and G1 because exposure to high sucrose concentrations before subculture provided calli with sufficient nutrients during G0. Some compounds showed the highest peak or appeared only under the S2 (deprivation) treatment. Sucrose deprivation can induce nutritional stress in calli such that they synthesize bioactive compounds. Liang et al. (2018) provide evidence for this assumption by describing how 20 g/L sucrose may be utilized to ensure that Chinese Kale "Cutiaoyusun" hypocotyls promote an excellent proliferation rate (213.5%) of calli.

Treatment with excess sucrose (S3–S3) also increased the peak areas of several types of compounds with biomedical activity. These compounds included naphthalene; decane, 2,3,5,8-tetramethyl-; cyclotrisiloxane, hexamethyl-; cyclohexane, 1,1,2-trimethyl; E-10-dodecen-1-ol propionate; tridecan; tetradecane, 1-fluoro; and decane, 2,4,6-trimethyl. 1-Iodo-2-methylnonane and dodecanoic acid, 3-hydroxy with anticancer and antioxidant activities were found only under the S3–S3 treatment. These compounds have various roles in the medical field. For example, naphthalene compounds have anticancer activity. A novel family of chalcone derivatives with IC_{50} values of 1.13 ± 0.08, 0.82 ± 0.11 μM, and 0.65 ± 0.06 respectively, showed high cytotoxic action against HCT116, MCF-7, and HepG2 cells in earlier investigations. These compounds included indole and naphthalene groups. Their anticancer method is predicated on blocking the advancement of the cell cycle and tubulin polymerization (Wang *et al.*, 2019). In addition, another study revealed that the compound cyclotrisiloxane, hexamethyl- was present in *Acacia karoo* leaf extract obtained with ethyl acetate solvent. The extract had a large inhibition zone of 33 ± 1.53 mm against *Staphylococcus aureus* (Priyanka *et al.*, 2014).

Accordingly, the S1–S2 and S3–S3 treatments were found to be effective in enhancing biomass, physiological responses, and phytochemical compound synthesis in calli. This is likely because sucrose fulfills the nutritional requirements of calli. Existing nutrients can impose osmotic pressure, which can increase water adsorption and carbohydrates. Adequate nutrition can also support cell division in calli such that calli under different treatments were heavier than those under the S1 and S3 treatments.

Therefore, different treatments must be selected to increase the growth of calli and amount of bioactive compounds. For callus growth, sucrose must be added for energy. For bioactive compound synthesis, sucrose excess (S3–S3) or deprivation (S1–S2) must be imposed to meet nutritional needs and induce nutritional stress.

5. Conclusion

Treatment with various sucrose concentrations affects callus growth and morphology. Among the treatments, S3–S3 during the G1 phase resulted in the highest fresh and dry callus biomass. Treatments with excessive sucrose concentrations (S3–S3) and deprivation sucrose concentrations (S1–S2) are effective in enhancing the production of compounds with biomedical activity. This is because sucrose supplies energy and induces osmotic stress on the callus, which stimulates the synthesis of these compounds.

Acknowledgement

References

Aksenova MA, Nechaeva TL, Zubova MY, Goncharuk EA, Kazantseva VV, Kantanskaya VM, Lapshin PV and Zagoskina NV. 2023. Influence of different precursors on content of polyphenols in *Camellia sinensis* in vitro callus culture. *Plants.*, **12(4)**: 796.

Al-Mansoub MA, Asif M, Revadigar V, Hammad MA, Chear NJ, Hamdan MR, Majid AM, Asmawi MZ and Murugaiyah V. 2021. Chemical composition, antiproliferative and antioxidant attributes of ethanolic extract of resinous sediment from *Etlingera elatior* (Jack.) inflorescence. *Braz J Pharm Sci.*, **57(1)**.

Al-Rahbi BAA, Al-Sadi AM, Al-Harrasi MMA, Al-Sabahi JN, Al-Mahmooli IH, Blackburn D and Velazhahan R. 2023. Effectiveness of endophytic and rhizospheric bacteria from *Moringa* spp. in controlling *Pythium aphanidermatum* damping-off of cabbage. *Plants.*, **12**: 668.

Al-Salman HN. 2019. Antimicrobial activity of the compound 2-Piperidinone, N-[4-Bromo-n-butyl]- extracted from pomegranate peels. *Asian J Pharm.*, **13(01)**.

Al-Zubaidy NA, Ibrahim MM and Musstta MA. 2020. The effect of growth regulators and different concentrations of sucrose in callus induction of sugar leaf plant *Stevia rebaudiana* and its content of stevoiside. *Plant Arch.*, **20(2)**: 4492-4496.

Amara I, Timoumi R, Annabi E, Salem IB and Abid-Essefi S. 2020. Di(2-ethylhexyl) phthalate inhibits glutathione regeneration and dehydrogenases of the pentose phosphate pathway on human colon carcinoma cells. *Cell Stress Chaperones.*, **25(1)**: 151-162.

Avidlyandi A, Adfa M and Yudha SS. 2021. Antitermite activity of methanol extract of lichen *Teloschistes flavicans* (Sw) norman against *Coptotermes curvignathus*. *J Phys Conf Ser.*, **1731**.

Bourhia M, Bouothmany K, Bakrim H, Hadrach, Salamatullah AM, Alzahrani A, Khalil Alyahya H, Albadr NA, Gmouh S and Laglaoui A et al. 2021. Chemical profiling, antioxidant, antiproliferative, and antibacterial potentials of chemically characterized extract of *Citrullus colocynthis* L. *Seeds. Separations.*, **8**: 114.

Charles JI, Iyeopu and Siminialayi, M. 2018. Evaluation of the antibacterial activity of *Chromolaena odorata* in wistar rats and its chemical characterization. *ASRJETS-Journal*., **42(1)**: 111-129.

Chrząszcz M, Miazga-Karska M, Klimek K, Dybowski MP, Typek R, Tchórzewska D and Dos Santos Szewczyk K. 2023. The anti-acne potential and chemical composition of *Knautia drymeia* Heuff. and *Knautia macedonica* Griseb extracts. *Int J Mol Sci*., **24**: 9188.

Dantas LA, Faria PPSA, Dario BMM, Arantes ALM, Silva FG, Avila RG, Pereira PS and Neto AR. 2021. The impact of carbon source on cell growth and the production of bioactive compounds in cell suspensions of *Hancornia speciosa* Gomes. *Sci Rep*., **11(24315)**.

Das S, Saha R, Biswas M, Mondal S and Mahapatra G. 2024. Comparative profiling of volatile compositions of fresh and dehydrated rinds and leaves of different Indian *Citrus* spesies. *Jordan J Biol Sci*., **17(1)**: 9-19.

Doughari JH and Abraham M. 2021. Antifungal activity of *Jatropha curcas* Linn on *Candida albicans* and *Candida tropicalis* associated with neonatal and infantile infections in Yola, Nigeria. *Am J Agric Biol Sci*., **16**: 19-32.

De Paiva Neto VB and Otoni WC. 2003. Carbon sources and their osmotic potential in plant tissue culture: does it matter? *Sci Hortic*., **97(3–4)**, 193–202.

El-Zawawy NA and Mona MM. 2021. Antimicrobial efficacy of Egyptian *Eremina desertorum* and *Helix aspersa* snail mucus with a novel approach to their anti-inflammatory and wound healing potencies. *Sci Rep*., **11(1)**: 24317.

Gerdakaneh M, Mozafari AA, Khalighi A and Sioseh-Mardah A. 2010. The effects of exogenous proline and osmotic stress on morpho-biochemical parameters of strawberry callus. *Afr J Biotechnol*., **9(25)**: 3775-3779.

Ghasemi A, Gheibi S, Kashfi K and Jeddi S. 2023. Anti-oxidant effect of nitrite in the pancreatic islets of type 2 diabetic male rats. *Iran J Basic Med Sci*., **26(4)**: 420-428.

Gheda SF and Ismail G. 2020. Natural products from some soil cyanobacterial extracts with potent antimicrobial, antioxidant and cytotoxic activities. *An Acad Bras Cienc*., **92(2).**

Gu S, Li L, Huang H, Wang B and Zhang T. 2019. Antitumor, antiviral, and anti-inflammatory efficacy of essential oils from *Atractylodes macrocephala* Koidz. produced with different processing methods. *Molecules*., **24(16)**: 2956.

Guo Z. 2021. Heptose-containing bacterial natural products: structures, bioactives, and biosynthesis. *Nat Prod Rep*., **38(10).**

Hayat S, Hayat Q, Alyemeni MN, Wani AS, Pichtel J and Ahmad A. 2012. Role of proline under changing environments: a review. *Plant Signal Behav*., **7(11)**:1456-66.

Ho Y, Suphrom N, Daowtak K, Potup P, Thongsri Y and Usuwanthim K. 2020. Anticancer effect of *Citrus hystrix* DC. leaf extract and its bioactive constituents citronellol and citronellal on the triple negative breast cancer MDA-MB-231 Cell Line. *Pharmaceuticals*., **13**: 476.

Homsuwan N, Kajorn M and Budsaraporn, N. 2021. Effect of sucrose on microtuber induction and inulin accumulation in Jerusalem Artichoke (*Helianthus tuberosus* L.). *CMUJ Nat Sci*., **20(3).**

Idris SN, Ahmed ABA and Taha RM. 2018. Sucrose enhanced stigmasterol production in callus cultures of *Wedelia biflora* (L.) D.C. *Philipp Agric Sci*., **101(3)**: 251–260.

Jaafar HZE, Ibrahim MH and Fakri NFM. 2012. Impact of soil field water capacity on secondary metabolites, phenylalanine ammonia-lyase (PAL), maliondialdehyde (MDA) and photosynthetic responses of Malaysian Kacip Fatimah (*Labisia pumila* Benth). *Molecules*., **17(6)**: 7305–7322.

Javed F and Ikram S. 2008. Effect of sucrose induced osmotic stress on callus growth and biochemical aspects of two wheat genotypes. *Pak J Bot*., **40(4)**: 1487–1495.

Karthik Y, Ishwara KM, Krishnappa S, Devappa R, Anjali GC, Ramakrishna K, Wani MA, Alkafafy M, Hussen AM, Alswat AS, Sayed SM and Mushtaq M. 2023. Antiproliferative activity of antimicrobial peptides and bioactive compounds from the mangrove *Glutamicibacter mysorens*. *Front Microbiol*., **14**: 1096826.

Khan SU, Ullah F, Mehmood S, Fahad S, Ahmad RA, Althobaiti F, Dessoky ES, Saud S, Danish S and Datta R. 2021. Antimicrobial, antioxidant and cytotoxic properties of *Chenopodium glaucum* L. *PLoS* One., **16(10)**: e0255502.

Khan T, Abbasi BH, Zeb A and Ali GS. 2018. Carbohydrate-induced biomass accumulation and elicitation of secondary metabolites in callus cultures of *Fagonia indica*. *Ind Crops Prod*., **126**: 168-176.

Kyoko M, Yoshimi U and Masaru OT. 2008. AtMYBL2, a protein with a single MYB domain, acts as a negative regulator of anthocyanin biosynthesis in Arabidopsis. *Plant J*., **55(6)**: 954–67.

Laezza C, Imbimbo P, D'Amelia V, Marzocchi A, Monti DM, Loria AD, Monti SM, Novellino E, Tenore GC and Rigano MM. 2024. Use of yeast extract to elicit a pulp-derived callus cultures from *Annurca apple* and potentiate its biological activity. *J Funct Foods*., **112**: 105988.

Lammers A, Zweers H, Sandfeld T, Bilde T, Garbeva P, Schramm A and Lalk M. 2021. Antimicrobial Compounds in the Volatilome of Social Spider Communities. *Front Microbiol*., **12**: 700693.

Lee ST and Huang WL. 2014. Osmotic stress stimulates shoot organogenesis in callus of rice (*Oryza sativa* L.) via auxin signaling and carbohydrate metabolism regulation. *Plant Growth Regul*., **73(2)**: 193–204.

Lee SY, Shetye GS, Son SR, Lee H, Klein LL, Yoshihara JK, Ma R, Franzblau SG, Cho S and Jang DS. 2022. Anti-microbial activity of aliphatic alcohols from Chinese Black Cardamom (*Amomum tsao-ko*) against *Mycobacterium tuberculosis* H37Rv. *Plants*., **12(1)**: 34.

Lema-Ruminska J, Goncerzewicz K and Gabriel M. 2013. Influence of absisic acid and sucrose on somatic embryogenesis in cactus *Copiapoa tenuissima* Ritt. Forma *mostruosa*. *ScientificWorldJournal*., **2013**: 513985.

Liang S, He Y, Zheng H, Yuan Q, Zhang F and Sun, B. 2018. Effects of sucrose and browning inhibitors on callus proliferation and anti-browning of chinese kale. *IOP Conf Ser Earth Environ Sci*., **252(2)**: 0–6.

Muzahid AA, Sharmin S, Hossain MS, Ahamed KU, Ahmed N, Yeasmin MS, Ahmed NU, Saha BK, Rana GMM, Maitra B and Bhuiyan MNH. 2023. Analysis of bioactive compounds present in different crude extracts of *Benincasa hispida* and *Cucurbita moschata* seeds by gas chromatography-mass spectrometry. *Heliyon*., **9(1)**.

Nasr Z, El-shershaby H, Sallam K, Abed N, Abd- El ghany I and Sidkey N. 2022. Evaluation of antimicrobial potential of tetradecane extracted from *Pediococcus acidilactici* DSM: 20284 - CM Isolated from Curd Milk. *Egypt J Chem*., **65(3)**, 705-713.

Njoroge S, Mwangi C, Nyerere K, Odhiambo F, Trimba J and Revathi G. 2019. Antimicrobial activity of *Aloe secundiflora* against clinical isolates of *Heliobacter pylori*. *East Afr Med J.,* **1(4)**.

Onanuga AO and Ejike OO. 2022. Chemical compositions and antioxidant activity of volatile oils from *Morinda citrifolia* and *Beta vulgaris* leaves from Nigeria. *Biol Med Natural Prod Chem*., **11(2)**.

Ozen T, Macit M and Toka M. 2018. Screening and evaluation of antioxidant activities of selected naphthalene compounds. *Malaysian Journal of Health Sciences*., **16(1)**, 45-55.

Paudel MR, Joshi PR, Chand K, Sah AK, Acharya S, Pant B and Pant, B. 2020. Antioxidant, anticancer, and antimicrobial effects of *in vitro* developed protocorms of *Dendrobium longicornu. Biotechnol Rep (Amst)*., **28(1)**.

Priyanka C, Kumar P, Shivakumar PB and Karthik L. 2014. In vitro antibacterial activity and gas chromatography-mass spectroscopy analysis of *Acacia karoo* and *Ziziphus mauritiana* Extracts. *J Taibah Univ Sci*., **9**: 1, 13-19.

Sari YP, Kusumawati,E, Saleh C, Kustiawan W and Sukartiningsih S. 2018. Effect of sucrose and plant growth regulators on callogenesis and preliminary secondary metabolic of different explant *Myrmecodia tuberosa. Nusant Biosci*., **10(3)**, 183-192.

Sharma A, Shahzad B, Rehman A, Bhardwaj R, Landi M and Zheng B. 2019. Response of phenylpropanoid pathway and the role of polyphenols in plants under abiotic stress. *Molecules.*, **24(13)**: 2452.

Selwal N, Rahayu F, Herwati A, Latifah E, Supriyono, Suhara C, Suastika IBK, Mahayu WM and Wani AK. 2023. Enhancing secondary metabolite production in plants: Exploring traditional and modern strategies. *J Agric Food Res*., **14**: 100702.

Setiowati FK, Widoretno W, Prasetyawan S and Lukiati B. 2022. Enhanced production of organosulfur bioactive compound in cell suspension culture of single garlic (*Allium sativum* L.) using precusor feeding. *Jordan J Biol Sci*., **15(2)**: 183-191.

Singh D and Luqman S. 2014. A perspective on anticancer potential of Mehndi/Henna. *Biomed Res Ther* 1., **18**.

Stein O and Granot D. 2019. An Overview of Sucrose Synthases in Plants. *Front Plant Sci*., **10**:95. doi: 10.3389/fpls.2019.00095.

Sumaryono, Muslihatin W and Ratnadewi D. 2012. Effect of carbohydrate source on growth and performance of In vitro sago palm (*Metroxylon sagu* Rottb.) plantlets. *HAYATI J Biosci*.,**19(2)**: 88-92.

Thaneshwari CA. 2018. Effect of plant growth regulators and sucrose concentration on callus induction and shoot differentiation from ovary culture of marigold *(Tagetes* spp.). *Int J Chem Stud*., **6(1)**: 618-623.

Tholl D. 2015. Biosynthesis and biological functions of terpenoids in plants. *Adv Biochem Eng Biotechnol*., **148**: 63–106.

Tleubayeva MI, Datkhayev UM, Alimzhanova M, Ishmuratova MY, Korotetskaya NV, Abdullabekova RM, Flisyuk EV and Gemejiyeva NG. 2021. Component composition and antimicrobial activity of CO2 extract of *Portulaca oleracea,* growing in the territory of Kazakhstan. *ScientificWorldJournal*., **2021**: 5434525.

Tunjung WAS, Vita F, Ghea PC, Sugeng T, Lisna H, Dwi P, Yekti AP, Aries BS, Hennisa Nur F and Ari I. 2020. Effect of growth factor in callus induction and bioactive compounds in seed explant of kaffir lime (*Citrus hystrix* DC.). *Indonesian J Pharm*., **31(2)**: 61-68.

Tunjung WAS, Widyasari AF, Iskandar A, Nurulita AJ, Sasongko AB, Indrianto A, Semiarti E and Maryani. 2021. Effect of 2,4-D and BAP on morphological characters and genetic stability of kaffir lime (*Citrus hystrix* DC.) callus cultures among generations. *CMUJ Nat Sci*., **20(3)**: e2021067

Ukwubile CA, Ahmed A, Katsayal UA, Ya'u J and Mejida S. 2019. GC-MS analysis of bioactive compounds from *Melastomastrum capitatum* (Vahl) Fern. Leaf methanol extract: an anticancer plant. *Sci Afr*., **3(1).**

Wahyuni DK, Huda A, Faizah S, Purnobasuki H and Wardojo BPE. 2020. Effect of light, sucrose concentration and repetitive on callus growth and medically important production in *Justicia gendarussa* Burm.f. *Biotechnol Rep (Amst)*., **27(2)**: 1-33.

Wang G, Zhiyun P and Yongjun, L. 2019. Synthesis, anticancer activity and molecular modeling of novel chalcone derivatives containing indole and naphthalene moieties as tubulin polymerization inhibitors. *Chem Pharm Bull*., **67(7)**: 725-728.

Wang NAJ, Zhang Z, Liu Y, Fang J and Yang Z. 2022. The antimicrobial activity and characterization of bioactive compounds in *Peganum harmala* L. based on HPLC and HS-SPME-GC-MS. *Front Microbiol*., **13**: 916371.

Wiraswati HL, Fauziah N, Pradini GW, Kurnia D, Kodir RA, Berbudi A, Arimdayu AR, Laelalugina A and Supandi MIF. 2023. Breynia cernua: chemical profiling of volatile compounds in the stem extract and its antioxidant, antibacterial, antiplasmodial and anticancer activity in vitro and in silico. *Metabolites*., **13(2)**: 281.

Xiong C, Li Q, Li S, Chen C, Chen Z and Huang W. 2017. In vitro antimicrobial activities and mechanism of 1-Octen-3-ol against food-related bacteria and pathogenic fungi. *J Oleo Sci*., **66(9)**: 1041-1049.

Yu Q, Plotto A, Baldwin EA, Bai J, Huang M, Yu Y, Dhaliwal HS and Gmitter FG. 2015. Proteomic and metabolomic analyses provide insight into production of volatile and non-volatile flavor components in mandarin hybrid fruit. *BMC Plant Biol*., **15(1)**.

Zare A, Afshar A, Khoradmehr A, Baghban N, Mohebbi G, Barmak A, Daneshi A, Bargahi A, Nabipour I, Almasi-Turk S, Arandian A, Zibaii MI, Latifi H and Tamadon, A. 2023. Chemical compositions and experimental and computational modeling of the anticancer effects of *Cnidocyte Venoms* of jellyfish *Cassiopea andromeda* and *Catostylus mosaicus* on human adenocarcinoma A549 Cells. *Mar Drugs*., **21(3)**: 168.

Zhang L, Mi S, Liu R, Sang Y and Wang X. 2020. Evaluation of volatile compounds in milks fermented using traditional starter cultures and probiotics based on odor activity value and chemometric techniques. *Molecules*., **25**: 1129.

Zhu S, Jiao W, Xu Y, Hou L, Li H, Shao J, Zhang X, Wang R and Kong D. 2021. Palmitic acid inhibits prostate cancer cell proliferation and metastasis by suppressing the PI3K/Akt pathway. *Life Sci*., **2861**: 120046.

Immunomodulatory Activities of *Cnidoscolus aconitifolius* Leaves Extract via Modulation of TLR4 Expression and Neutrophil Cell Infiltration in Infected Mice

Sholihatil Hidayati[1,*], Dhina Ayu Susanti[1], Rian Anggia Destiawan[2], Istiqomah[3], Lulut Sasmito[4], Rizki Fitrianingtyas[5], Krisa Prawira Firmansyah Putra[1]

[1]Pharmacy Study Program, Faculty of Health Sciences, University dr. Soebandi, Jember, East Java, Indonesia, [2]Medical Laboratory Technology Study Program, Faculty of Health Sciences, University dr. Soebandi, Jember, East Java, Indonesia,, [3]Pharmacy Study Program, Harapan Bangsa School of Health, Jember, East Java, Indonesia,, [4]Health Polytechnic of Ministry of Health, Malang, East Java, Indonesia, [5]Midwifery Education Study Program, Faculty of Health Sciences, University dr. Soebandi, Jember, East Java, Indonesia

Abstract

Toll Like Receptor (TLR) plays a pivotal role in activating innate and adaptive immune responses Modulating TLR4 activation and signaling is crucial in the discovery of immunomodulatory drugs. *Cnidoscolus aconitifolius* leaf extract (CAE) exhibits potent antioxidant properties, suggesting its potential as an immunomodulatory agent. This study aimed to explore the immunomodulatory potential of CAE by assessing neutrophil infiltration and TLR4 expression in Babl/C mice infected with *Salmonella typhimurium*. Thirty *Babl/C* mice were used as experimental animals and divided into 6 groups (n=5). Five days post *Salmonella typhimurium* induction, infected mice were orally treated once daily for 7 days. Evaluation included assessment of neutrophil infiltration in small intestine tissue and TLR4 expression using flow cytometric analysis of lymphoid organs. Results demonstrated that administration of CAE at a dose of 400 mg/kgbw significantly increased neutrophil count (10.00 ± 0.84) compared to the infection-only group (5.00 ± 0.32), with no significant difference compared to the positive control group (10.60 ± 1.36). Evaluation of TLR4 expression revealed that CAE at a dose of 200 mg/kgbw significantly upregulated TLR4 expression (8419.80 ± 276.745) compared to the negative control group (7237.20 ± 162.17), and was comparable to the positive control group (8037.00 ± 206.40). All data showed statistical significance ($p<0.05$). CAE demonstrated the ability to modulate TLR4 expression and enhance neutrophil activity, thereby potentially serving as an immunomodulatory agent.

Keywords: *Cnidoscolus aconitifolius*, immunomodulators; leaves extract; neutrophil; TLR4

1. Introduction

Infectious diseases rank second globally in terms of mortality rates, following cardiovascular disease. Typhoid fever is notably prevalent in several Asian countries (Fitrya et al., 2020). This acute illness is primarily caused by Salmonella enterica, particularly its variant *Salmonella typhimurium* (Cordero-Alba et al., 2016). Salmonella infection poses a public health challenge worldwide and imposes a substantial economic burden on health systems. It ranks as the second most frequently reported gastrointestinal infection and is the primary cause of foodborne outbreaks in Europe cause of foodborne outbreaks in Europe. In 2020, there were 53,169 laboratory-confirmed cases of salmonellosis, resulting in 61 fatalities. According to WHO data, Indonesia has a relatively high incidence of typhoid fever, affecting 81,000 out of 100,000 people (Rahmasari & Lestari, 2018). Individuals with compromised immune systems are particularly vulnerable to typhoid fever (Kalia et al., 2016). The innate immune system, comprising phagocytic cells, plays a critical role in defending against microorganisms and cancerous cells (Venkatalakshmi & Brindha, 2016). Activation of the immune system is essential for aiding the body in combating antigenic substances, which can be facilitated through the use of immunomodulators.

Toll Like Receptor (TLR) is a receptor that plays a role in activating the innate immune response and adaptive immunity. TLRs consists of TLR 1, TLR 2, TLR 4, TLR 5, TLR 6 which are present in the extracellular part of the immune cell and respond to extracellular microorganisms. On the other hand, TLR3, TLR7, TLR8, and TLR9 are located in the endosomal part of immune cells and respond to intracellular viral and bacterial infections (Firmal et al., 2020). TLR4 is an innate immune receptor found on the surface of cells that recognizes patterns of pathogen-associated molecules (PAMPs), including viral proteins. It triggers the production of type I interferons and proinflammatory cytokines to combat infections (Aboudounya & Heads, 2021). TLR4 is expressed not only on the surface of immune cells such as macrophages and dendritic cells, which regulate acute inflammation, but also

---

* Corresponding author. e-mail: sholihatilhidayati@yahoo.co.id.

in various tissue cells for defense against infection and regulation of fibrotic phenotype during tissue damage (Rosadini & Kagan, 2017). TLR4 plays a crucial role in inducing host immune responses against infectious diseases such as bacterial, fungal, viral infections, malaria (Mukherjee et al., 2016). It is present on the plasma membranes of neutrophils, macrophages, dendritic cells, and endothelial cells. Modulating TLR4 activation and signaling is vital in regulating the immune system and developing immunomodulators (Romerio & Peri, 2020). Activation of the immune system is essential to help the body eliminate antigenic substances, which can be stimulated with immunomodulators.

The development of immunomodulators focuses on natural products, which are considered safer and more effective. Plant extracts are widely regarded as potential immunomodulatory agents due to their minimal side effects (Alamgir & Uddin, 2010). Plant-based immunomodulatory activity involves enhancing the function and efficiency of macrophages, granulocytes, complement, natural killer cells, and the production of effector molecules (Jayathirtha & Mishra, 2004). Plant metabolites such as sterols, polysaccharides, alkaloids, flavonoids, lectins, and glycoproteins exhibit immunomodulatory agents (Harun et al., 2015).

Cnidoscolus aconitifolius belongs to the family Euphorbiaceae, which also includes plants like *Phyllanthus niruri* developed as immunomodulatory drugs. Studies on *Cnidoscolus aconitifolius* leaves have identified various activities, such as antibacterial, hepatoprotective, anti-inflammatory (Pérez-González et al., 2018), antidiabetic and anti-hypertension effects (Somade et al., 2021). The 70% ethanol extract of *Cnidoscolus aconitifolius* leaves contains a total flavonoid content of 418.46 ± 3.28 mg QE/g extract. Furthermore, antioxidant activity tests indicate that the extract shows potent antioxidant potential with an IC50 value of 34.3149 μg/ml (Hidayati et al., 2023).

Building upon this background, this study aims to investigate the immunomodulatory activity of *Cnidoscolus aconitifolius*. Specifically, it evaluates the impact of administering *Cnidoscolus aconitifolius* leaf extract on neutrophil cell infiltration and TLR4 expression in Babl/C mice induced by *Salmonella typhimurium* bacteria.

2. Materials and Methods

2.1. Materials

Salmonella typhimurium bacteria were obtained from Brawijaya University, Malang. *Cnidoscolus aconitifolius* leaves were sourced from the Patrang area, Jember, Indonesia. The materials used included ethanol (Merck), TLR4 antibodies (BioLegend, USA), hematoxylin-eosin staining kit (Sigma-Aldrich, USA) and aquadest (Brataco, Indonesia). Tools utilized included a mouse sonde, surgical instruments, a flow cytometric instrument (BD FACS-Calibur, USA).

2.2. Preparation of Cnidoscolus aconitifolius Leaf Extract

A certificate of determination was obtained from the Biology Laboratory, Faculty of Applied Science and Technology, Ahmad Dahlan University with number 489/Lab. Bio/B/XII/2022. The collected leaves were wet

sorted to select only those with a green color, then cleaned and washed using aquadest. Subsequently, they were dried in an oven until completely dry and powdered using a blender. The extraction process began by sorting the *Cnidoscolus aconitifolius* leaves, followed by airing for 3 days and oven-drying at 40°C until dry simplisia formed, which was then ground into powder. Approximately, 500 g of powder was obtained, and the extraction was carried out using the maceration method with 70% ethanol for 1 hour, totaling 600 ml. Remaceration was performed for 2 cycles with 200 ml each. The resulting liquid extract was concentrated using a rotary evaporator (Hidayati et al., 2023).

2.3. Animal Preparation

Thirty male Babl/C mice weighing 20-30 g were acclimatized for 14 days in the experimental animal laboratory of the Faculty of Health Sciences, Universitas dr. Soebandi. Ethical clearance was obtained from the Health Research Ethics Committee of Universitas dr. Soebandi with number 096/KEPK/UDS/III/2023. The mice were divided into 6 groups: a negative control group of healthy mice without infection, a negative control group of mice infected with *Salmonella typhimurium* bacteria and administered a placebo of CMC-Na solution, a positive control group of mice infected with *Salmonella typhimurium* bacteria and treated with the standard immunomodulator Stimuno containing standardized *Phyllanthus niruri L.* extract (Dexa Medica, Indonesia), and treatment groups 1, 2, and 3 consisting of mice infected with *Salmonella typhimurium* bacteria and administered *Cnidoscolus aconitifolius* leaf extract (CAE) at doses of 100 mg/kg bw, 200 mg/kg bw, and 400 mg/kg bw, respectively. Infection induction was performed orally using *Salmonella typhimurium* bacteria at a concentration of 1×10^8 cfu (Destiawan et al., 2023). After 5 days post-induction, mice were evaluated for fecal texture, and tail blood smears were examined with Giemsa staining to detect. The treatment was administered orally once daily for 7 days.

2.4. TLR4 Analysis using Flow cytometer

The TLR4 analysis involved lymphoid organs. The organs were washed and homogenized in 5 ml of phosphate buffer solution. Homogenization was continued until complete organ disruption using the base of a 3 ml syringe plunger, followed by filtration through a mesh and transfer into a 15 ml propylene tube with a 1:3 ratio. The sample was then centrifuged at 2500 rpm for 5 minutes at 10°C, and the supernatant was discarded. The pellet was resuspended in 1 ml of phosphate buffer solution.

Fifty microliters of the suspension were transferred to a 1.5 ml microtube, centrifuged at 2500 rpm for 5 minutes at 10°C, and the supernatant was discarded. Fifty microliters of TLR4 antibody solution were added and incubated for 20 minutes at 4°C in a dark room. Four hundred microliters of PBS were added, and the mixture was transferred to a cuvette for flow cytometry analysis (Djati et al., 2017).

2.5. Histological analysis

Following the post-treatment period, all mice were euthanized, and their intestinal organs were collected and fixed in 4% formalin solution in phosphate buffer for 24 hours. Tissues were subsequently embedded in paraffin,

sectioned at a thickness of 4 μm, deparaffinized in xylene, dehydrated in graded alcohol concentrations, and stained with Hematoxylin-Eosin to assess neutrophil infiltration. Evaluation was performed using a light microscope with a 40X objective and 10X field of view, and the observed areas were selected randomly. The number of neutrophil cells within each tissue area in the images was counted and compared as a percentage relative to the control.

2.6. 2.6 Analysis of Results

The neutrophil count data and TLR4 expression analysis were analyzed using a one-way ANOVA test with a significance level set at $p < 0.05$, using the SPSS software for Windows. Post-hoc comparisons were conducted using the LSD test to determine differences between groups.

3. Results

3.1. Neutrophil cell infiltration effect of Cnidoscolus aconitifolius leaves extract

Neutrophils were visualized using histopathological methods with hematoxylin-eosin staining (figure 1). Neutrophils constitute the initial innate immune defense against invasive infections caused by pathogens (Desai & Lionakis, 2018). Administration of CAE at doses of 100 mg/kgbw, 200 mg/kgbw, and 400 mg/kgbw resulted in increased neutrophil infiltration into the infected tissue.
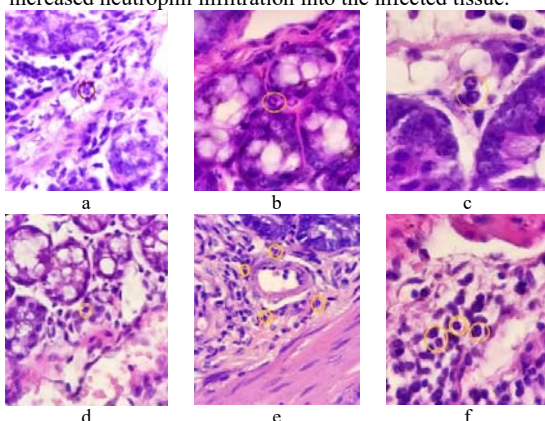
Figure 1. Neutrophil Description in Histological Preparations with Hematoxylin-Eosin Staining. (a) Normal groups, (b) Negative control, (c) Positive control, (d) CAE dose 100 mg/kgbw, (e) CAE dose 200 mg/kgbw, (f) CAE dose 400 mg/kgbw.

In this study, an evaluation of the number of neutrophils was carried out which showed that in the infection group the number of neutrophils in the tissue increased (Figure 2), which was shown by an increase in the number of neutrophil infiltration in the normal group of 0.60 ± 0.40 significantly different from the negative control group 5.00 ± 0.32 ($p < 0.05$). Neutrophils recognize viruses and cells infected with the virus and infiltrate the site of infection. At the beginning of viral infection, neutrophils are rapidly recruited from the blood at the site of infection and mobilized to differentiate and migrate out of the bone marrow (Rawat et al., 2021).

Treatment of CAE dose administration of 400 mg/kgbw was able to increase the number of neutrophils significantly (10.00 ± 0.84) compared to the untreated infection group (5.00 ± 0.32), and this increase was not

significantly different when compared to the positive control group (10.60 ± 1.36) ($p < 0.05$). Bioactive compounds are secondary metabolites found in plants and provide many health benefits if consumed over a long period of time in certain amounts. *Cnidoscolus aconitifolius* contains many bioactive compounds such as phenolic acids, alkaloids, saponins, flavonoids and terpenoids with a unique structure (Panghal et al., 2021a). Flavonoids have been declared therapeutic agents to avoid such damage, since these compounds exhibit anti-inflammatory activity, that is, through modulating the oxidative explosion of neutrophils. The catechol group on the B ring, together with the presence of 3-OH on the C ring and the double bond between C2–C3, is a determinant of activity (Ribeiro et al., 2018).
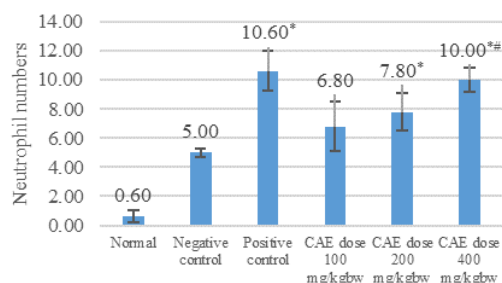
*Significant difference with negative control group ($p < 0.05$)

#No significant different with positive control group ($p < 0.05$)

Figure 2. Profile of the number of neutrophils in mice with *Salmonella thypimurium* faction with administration of CAE

3.2. TLR4 expressions in mice infected with Salmonella thpymurium bacteria

In this study, it was found that TLR4 expression from lymph organs in mice infected with *Salmonella thpymurium* bacteria decreased significantly after acute infection in post treatment from 8766.80 ± 172.73 to 7237.20 ± 162.17 (Figure 3). Research using pigs with lipopolysaccharide administration showed that TLR4 expression in lymph on day 7 decreased significantly (Ghosh et al., 2016; Qin et al., 2020).
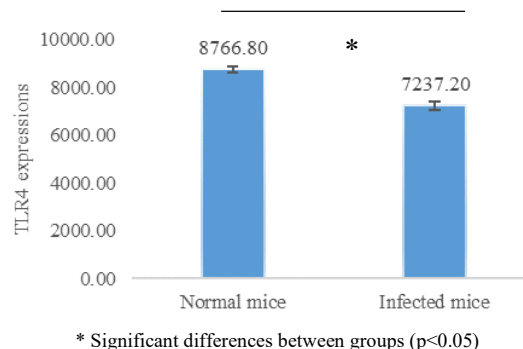
* Significant differences between groups ($p < 0.05$)

Figure 3. TLR4 expression profile in normal mice and mice infected with *Salmonella thypimurium* as shown at the the decreased TLR4 expression after induction

3.3. TLR4 expressions of Cnidoscolus aconitifolius leaves extract

In figure 4 and 5, we can see that after treatment for 7 days orally, CAE dose administration of 200 mg/kgbw showed a significant increase in TLR4 expression

(8419.80± 276.745) compared to the negative control group (7237.20± 162.17) and did not differ significantly from the positive control group (8037.00± 206.40). TLR4 activation is associated with infection repair. TLR4 overexpression can counteract the invasion of Salmonella typhimurium as well as fight gut inflammation in sheep by regulating gut microbiota composition and increasing anti-inflammatory metabolites (Xu et al., 2023).
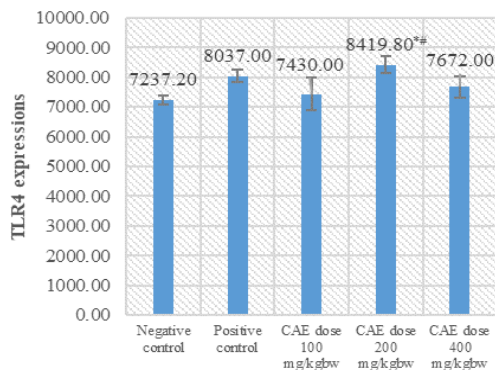
*Significant difference with negative control group (p<0.05)

#No significant different with positive control group (p<0.05)

Figure 4. Effect *Cnidoscolus aconitifolius* leaves extract to TLR4 expressions in mice infected with *Salmonella thypimurium*.
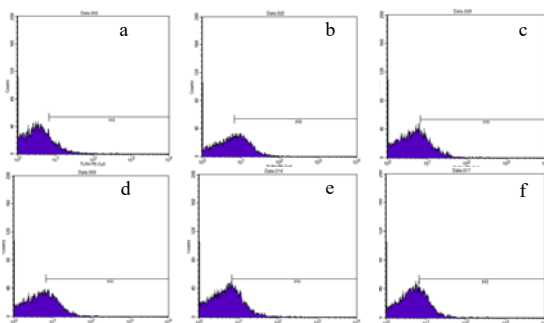
Figure 5. Results of flow cytometric analysis of TLR4 expression in mice infected with *Salmonella thypimurium*. (a) Normal groups, (b) Negative control, (c) Positive control, (d) CAE dose 100 mg/kgbw, (e) CAE dose 200 mg/kgbw, (f) CAE dose 400 mg/kgbw.

4. Discussion

The immune system encompasses a complex network of cells, chemicals, and processes aimed at protecting various body sites from foreign antigens such as microbes (e.g. bacteria, fungi, parasites), viruses, and cancer cells (Marshall et al., 2018). Apart from physical and chemical barriers, the immune system operates through two main defense mechanisms: innate immunity and adaptive immunity. While innate immunity acts as the initial defense against invading pathogens, it works in conjunction with adaptive immunity to provide comprehensive protection against disease (Prabhu, 2023).

Neutrophils, also known as polymorphonuclear leukocytes, develop from blast cells and mature into terminally differentiated cells in the bone marrow before being released into peripheral blood. Under physiological conditions, the number of neutrophil production is 10^{11} per day, which is influenced by cell death and production rate. Neutrophils are relatively short-lived. It is estimated that neutrophils have an age of 8-12 hours in peripheral blood (Ma et al., 2021). During acute infections, neutrophils migrate from the blood into infected tissues, where they execute vital functions including binding, phagocytosis, and the oxidative and non-oxidative killing of intracellular microorganisms. They also release inflammatory mediators extracellularly (Desai & Lionakis, 2018).

In this study, it was determined that CAE at a dose of 200 mg/kgbw and 400 mg/kgbw significantly increased neutrophil infiltration compared to the negative control group (p<0.05). Specifically, only the CAE at 400 mg/kgbw achieved neutrophil levels comparable to the positive control group (10.60±1.36) without significant difference (p>0.05). Neutrophils play a crucial role as the body's primary defense mechanism against bacterial and fungal pathogens, operating swiftly before the adaptive immune responses come into play (Kubes, 2018). The ability of CAE to enhance neutrophils numbers underscores its potential importance in bolstering initial defenses post-infection.

Cnidoscolus aconitifolius leaves are rich in phytochemical compounds, including 9-Octadecenoic (Z) acid and its esters, n-Hexadecanoic acid, n-Octadecanoic acid, n-Octacosane, 1,2,3-Propanetriol derivatives, and l-(+)-Ascorbic acid-2,6-dihexadecanoate, which offer diverse therapeutic benefits (Abayomi et al., 2014).

Flavonoids isolated from *Cnidoscolus aconitifolius* include procyanidin B1, procyanidin B2, catechin, rutin, gallocatechin gallate, epigallocatechin gallate, epicatechin-3-O-gallate, quercetin-3-O-galactoside, quercetin-3-O-glycoside, quercetin-3-O-rhamnoside, trans-reverseratol, quercetin and Kaemferol (Panghal et al., 2021b). Another study reported Japanese papaya leaves had ten carotenoids detected consisting mainly of carotene (43.7-46.1%), lutein (20.8-22.5%) and neo-xanthin (10.92-12.99%). Beta-amyrin (52.2–66.3%), alpha-amyrin (18.5–31.6%) and lupeol (14.8–15.9%) were the most abundant detected phytosterols. These results show that *Cnidoscolus aconitifolius* leaves are a good source of nutrients and bioactive phytochemicals that can support human health and nutrition (Mercy et al., 2019). Plant extracts containing active phytochemicals and various bioactive ingredients such as flavonoids, alkaloids, saponins, quinones, triterpenoids, tannins and phenolics have been claimed to have benefits in various treatments (Nugroho et al., 2020).

The Toll like receptor (TLR) family serves as vital pattern recognition receptors (PRRs) capable of identifying various bacteria and viruses, triggering the secretion of inflammatory cytokines and chemokines. TLR4, predominantly expressed on macrophages, dendritic cells, and neutrophils, plays a critical role in inflammation, autophagy, and oxidative stress during pathogenic infections (Zhang et al., 2021). TLR4 predominantly expressed on macrophages, dendritic cells, and neutrophils plays a critical role in inflammation, autophagy, and oxidative stress during pathogenic infections (Deng et al., 2020). Specifically, TLR4 recognizes lipopolysaccharide endotoxins (LPS), a major component of Gram-negative bacteria, stimulating immune cells to produce proinflammatory cytokines like interleukins (IL)-8, IL-6,

IL-1β, IL-12, and tumor necrosis factor α (TNFα) to combat invading pathogens (Ciesielska et al., 2021).

Research indicates that TLR4 and its downstream genes are expressed across gut and immune tissues at various developmental stages, with tissue-specific variations possibly reflecting differential functional responses to pathogenic stimuli. Notably, TLR4 expression is more pronounced in the spleen, the body's largest immune organ comprising 25% of lymphoid tissue, central to both cellular and humoral immunity (Qin et al., 2020).

5. Conclusion

From this study, it can be concluded that the administration of CAE at a dose of 200 mg/kgbw effectively modulates TLR4 expression and enhances neutrophil activity. This modulation contributes to the activation of the immune response, suggesting that CAE holds promise as a candidate immunomodulatory agent.

Acknowledgment

References

Abayomi O, Olorunfemi EO and Mikailu S. 2014. Phytochemical Analysis of *Cnidoscolus aconitifolius* (Euphorbiaceae) leaf with Spectrometric Techniques. *Niger J Pharm Appl Sci Res*., **3(31)**: 38–49.

Aboudounya MM, & Heads RJ. 2021. COVID-19 and Toll-Like Receptor 4 (TLR4): SARS-CoV-2 May Bind and Activate TLR4 to Increase ACE2 Expression, Facilitating Entry and Causing Hyperinflammation. *Mediators Inflamm.,* **2021(8874339):** 1-18

Alamgir M and Uddin SJ. 2010. **Recent advances on the ethnomedicinal plants as immunomodulatory agents**. Research Signpost, pp. 227-244.

Ciesielska A, Matyje M and Kwiatkowska K. 2021. TLR4 and CD14 trafficking and its influence on LPS-induced pro-inflammatory signaling. *Cell Mol Life Sci.,* **78(4)**: 1233–1261.

Cordero-Alba M, García-Gómez JJ, Aguilera-Herce J and Ramos-Morales F. 2016. Proteomic insight into the effects of the Salmonella ubiquitin ligase SlrP on host cells. *Biochem Biophy Res Comm.*, **472(3)**: 539–544.

Deng JS, Jiang WP, Chen CC, Lee LY, Li PY, Huang WC, Liao JC, Chen HY, Huang SS and Huang GJ. 2020. Cordyceps cicadae mycelia ameliorate cisplatin-induced acute kidney injury by suppressing the TLR4/NF-κB/MAPK and activating the HO-1/Nrf2 and Sirt-1/AMPK pathways in mice. *Oxid Med Cell Longev.*, **2020(7912763):** 1-17

Desai JV and Lionakis MS. 2018. The Role of Neutrophils in Host Defense Against Invasive Fungal Infections. *Curr Clin Microbiol Rep.,* **5(3)**: 181–189.

Destiawan RA, Rahmawati SE, Wijaya AF, Muflihah AI, Nurjanah MH, Hidayati S, and Sari NKY. 2023. Effect Of Black Grape Extract On Cd4+ And Cd8+ Expression In Mice Infected With *Salmonella typhimurium*. *Jurnal Biosains Pascasarjana.*, **24(1SP)**: 54–63.

Djati MS, Habibu H, Jatiatmaja NA and Rifa'I M. 2017. *Elephantopus scaber* L extract-induced CD4+ and CD8+ differentiation from hematopoietic stem cells and progenitor cell proliferation in mice (Mus musculus L). *AIP Conference Proceedings*., **1908(2)**: 2–8.

Firmal P, Shah VK and Chattopadhyay S. 2020. Insight Into TLR4-Mediated Immunomodulation in Normal Pregnancy and Related Disorders. *Front Immunol*., **11(5)**: 1–16.

Fitrya F, Amriani A, Novita RP, Elfita and Setiorini D. 2020. Immunomodulatory effect of Parkia speciosa Hassk. pods extract on rat induced by Salmonella typhimurium. *J Pharm Pharmacog Res.*, **8(5):** 457–465.

Ghosh D, Wikenheiser DJ, Kennedy B, McGovern KE, Stuart JD, Wilson EH and Stumhofer JS. 2016. An Atypical Splenic B Cell Progenitor Population Supports Antibody Production during Plasmodium Infection in Mice. *J Immunol*., **197(5)**: 1788–1800.

Harun NH, Septama AW and Jantan I. 2015. Immunomodulatory effects of selected Malaysian plants on the CD18/11a expression and phagocytosis activities of leukocytes. *Asian Pac J Trop Biomed*., **5(1)**: 48–53.

Hidayati S, Susanti DA, Faizah N and Purwanti A. 2023. *Optimization of Solvent Concentration on Flavonoid Levels of Cnidoscolus aconitifolius Leaf Extract*. Katalisator., **8(2):** 324–333.

Jayathirtha MG and Mishra SH. 2004. Preliminary immunomodulatory activities of methanol extracts of Eclipta alba and *Centella asiatica*. *Phytomedicine*. **11(4):** 361–365.

Kalia P, Kumar NR and Harjai K. 2016. Effect of propolis extract on hematotoxicity and histological changes induced by Salmonella enterica serovar Typhimurium in balb/C mice. *Archiv Biol Sci*., **68(2):** 385–391.

Kubes, P. 2018. The enigmatic neutrophil: what we do not know. *Cell Tiss Res*., **371**: 399–406.

Ma Y, Zhang Y and Zhu L. 2021. Role of neutrophils in acute viral infection. *Immun, Inflamm Dis*., **9(4):** 1186–1196).

Mercy, OI., Catherine, CI and Jude, CI. 2019. Nutrient and bioactive phytochemical compositions of *Cnidoscolus aconitifolius*. *Malay J Biochem Mol Biol*., **22(2):a** 26–36.

Mukherjee S, Karmakar S and Babu SPS. 2016. TLR2 and TLR4 mediated host immune responses in major infectious diseases: a review. *Brazilian J Infec Dis*., **20**: 193–204.

Nugroho RA, Sari YP and Hardi EH. 2020. Inclusion of Myrmecodia pendens bulb Extract in the Diet Stimulates Immune Response in Clarias gariepinus against Aeromonas hydrophila. Jordan J Biol Sci., **13(4)**: 463-468

Panghal A, Shaji AO, Nain K, Garg MK and Chhikara N. 2021. *Cnidoscolus aconitifolius*: Nutritional, phytochemical composition and health benefits – A review. *Bioact Compound Health Dis*., **4(11):** 260–286.

Pérez-González MZ, Siordia-Reyes AG, Damián-Nava P, Hernández-Ortega S, Macías-Rubalcava ML and Jiménez-Arellanes MA. 2018. Hepatoprotective and Anti-Inflammatory Activities of the *Cnidoscolus chayamansa* (Mc Vaugh) Leaf Extract in Chronic Models. *Evid Based Complement Alternat Med.,* **2018(3896517):**1-12.

Prabhu SR. 2023. **An Introduction to Immunology and Immunopathology**. In *Textbook of General Pathology for Dental Students*. Springer. pp. 73–80.

Qin W, Gao Z, Cao Y, Wu Z, Bao W and Wu S. 2020. Developmental expression patterns and correlation analysis of TLR4 and its downstream genes in the intestinal and immune tissues of Meishan pigs. *R. Bras. Zootec.,* **49(e20180296):** 1-12.

Rahmasari V & Lestari K. 2018. Article Review: *Management of Typhoid Fever Therapy: A Study of Pharmacological and Non-Pharmacological Therapies*. Farmaka. **16(1):** 184–195.

Rawat S, Vrati S and Banerjee A. 2021. Neutrophils at the crossroads of acute viral infections and severity. *Mol Aspects Med.,* **81(100996):**1-16

Ribeiro D, Fernandes E and Freitas M. 2018. **Flavonoids as modulators of neutrophils' oxidative burst: Structure-activity relationship**. In *Polyphenols: Mechanisms of Action in Human Health and Disease,* Elsevier. pp. 261–276.

Romerio A and Peri F. 2020. Increasing the chemical variety of small-molecule-based TLR4 modulators: An overview. *Front Immunol*, **11:** 1210.

Rosadini CV and Kagan JC. 2017. Early innate immune responses to bacterial LPS. *Curr Opinion Immunol.*, **44:** 14–19.

Somade OT, Ugbaja RN, Idowu MA and Akinloye OA. 2021. *Cnidoscolus aconitifolius* leaf extract and ascorbate confer amelioration and protection against dimethyl nitrosamine-induced renal toxicity and testicular abnormalities in rats. *Toxicol Rep.*, **8:** 1098–1108.

Venkatalakshmi P and Brindha P. 2016. Antimicrobial activity of aqueous extracts of different parts of Terminalia catappa L. *Int J Curr Microbiol Appl Sci.*, **5(12):** 493–498.

Xu XL, Zhao Y, Chen MM, Li Y, Li Y, Wu SJ, Zhang JL, Zhang XS, Yu K and Lian ZX. 2023. Shifts in intestinal microbiota and improvement of sheep immune response to resist Salmonella infection using Toll-like receptor 4 (TLR4) overexpression. *Front Microbiol.*, **14(2023):**1-15.

Zhang K, Huang Q, Deng S, Yang Y, Li J and Wang S. 2021. Mechanisms of TLR4-Mediated Autophagy and Nitroxidative Stress. *Front Cell Infect Microbiol.*, **11(766590):**1-11.

JJBS

Jordan Journal of Biological Sciences

Ohmic Heating Pretreatment of Mung Bean Seeds: Effects of Voltage Gradient on Seed Germination and Growth of Mung Bean Sprouts

Diang Sagita[1,2,*], Rusdi Hasan[3], Risya Al Zahra[3]

[1]Research Center for Appropriate Technology, National Research and Innovation Agency, Subang, Indonesia; [2]Department of Agricultural and Biosystems Engineering, Faculty of Agricultural Technology, IPB University, Bogor, Indonesia; [3]Department of Biology, Faculty of Mathematics and Natural Sciences, Padjajaran University, Bandung, Indonesia

Abstract

Mung bean (*Vigna radiata* L.) sprouts are agricultural products with many health benefits and are typically harvested within four–five days. In this study, a new pretreatment technique using ohmic heating (OH) technology was applied for the first time prior to seed germination. This study aimed to investigate the effects of OH-based soaking treatment on mung bean germination and growth. The treatments consisted of three OH treatments at a temperature of 35 °C, non-OH at 35 °C, and two control treatments, i.e. at normal temperature (26°C) and no soaking treatment. In OH treatments, three voltage gradients (VG) were used, i.e. 6 V/cm, 10 V/cm, and 14 V/cm. Parameters examined included moisture content (M_c), seed hardness (S_h), seed mass (M_s), surface morphology, percentage of germination (P_{oG}), germination index (G_i), vigor index (V_i), hypocotyl diameter (D_h), sprout length (L_s), and mass of sprouts (M_{os}), and percentage of sprout with leaf (P_{sl}). Results revealed that OH pretreatment positively affected almost all parameters. In addition, VG also impacted on the observed parameters. The OH treatment increased the absorption of water by the seeds, especially OH at VG 14 V/cm, which produced the highest M_c and M_s, and the lowest S_h. OH at VG 14 V/cm exhibited the highest P_{oG}, the highest of G_i and V_i, and P_{sl}; consistently promoted greater seedling growth and biomass accumulation. Principal component analysis found strong positive correlation among M_s, M_c, P_{oG}, G_i, V_i, M_{os}, and P_{sl}. These findings are expected to be used to increase and speed up the production of bean sprouts in industrial applications.

1. Introduction

Mung bean (*Vigna radiata* L.) is a legume plant belonging to the Fabaceae family that is widely cultivated and used in various types of cuisine in Asia and parts of South America, North America, and Australia (Peñas *et al.*, 2010; Dahiya *et al.*, 2015). Mung beans are rich in nutrients such as protein and iron (Zhou *et al.*, 2019). Mung beans can be consumed in the form of sprouts due to having many nutritional contents such as minerals, antioxidants, and various vitamins. In addition, these sprouts contain high phenolics, flavonoids, organic acids, amino acids, and total antioxidant activity compared to the seeds (Wei *et al.*, 2019). Mung bean and its sprouts can be processed into food ingredients by frying, boiling, sautéing, and others (Salvador and Bucu, 2021).

In recent years, there has been a growing interest in enhancing the germination and growth of mung bean sprouts to meet the increasing global demand for nutritious and sustainable food sources. Seed germination is usually defined as the period when a plant grows from a seed (Vrancheva *et al.*, 2020). Germination is the initial process of plant seed embryo growth and development, which becomes active after the process of imbibition or

absorption of water by the seed. Usually, mung bean sprouts can grow for about four to five days after imbibition or even faster (Salvador and Bucu, 2021). The germination rate of seeds depends on the moisture available during the germination stage.

Seed germination is influenced by several external and internal factors. External factors such as light, water, salinity, temperature, pH, and growth hormones (Muttaqin *et al.*, 2019; Saberali and Moradi, 2019; Núñez-Gastélum *et al.*, 2023). High temperature is another external factor that reduces seed dormancy. Internal factors include seed health and genetic factors (Muttaqin *et al.*, 2019).

Traditional seed soaking methods have been widely employed to promote germination, but advancements in agricultural technologies have led to the exploration of alternative techniques to further improve seedling establishment. In the last decade, several intervention strategies have been implemented to stimulate seeds germination such as gamma irradiation (Majeed *et al.*, 2018), ultrasound (Porto *et al.*, 2018), X-irradiation (Al-Enezi *et al.*, 2012), atmospheric-pressure plasma (Zhou *et al.*, 2019), pulse electric fields (Dymek *et al.*, 2012), magnetic field (Harb *et al.*, 2021), and pesticides (Shakir *et al.*, 2016). However, these technologies have several major drawbacks, including expensive costs, lengthy

---

* Corresponding author. e-mail: dian063@brin.go.id.

development times, environmental contamination from chemical residues, and heightened ecological concerns (Fan *et al.*, 2020). Therefore, it is still necessary to develop cost-efficient and environment-friendly technologies to improve the production of sprouts.

Ohmic heating (OH) is a modern and innovative technology that has gained significant attention in various food and agricultural applications due to its ability to generate rapid and uniform heating within biological materials (Patel and Singh, 2018; Sagita *et al.*, 2023). OH works based on the passage of an electrical current through the material, converting electrical energy into heat energy directly. This unique approach offers numerous advantages, including precise temperature control (Sagita *et al.*, 2022), reduced processing time (Sakr and Liu, 2014), high energy efficiency (Sagita *et al.*, 2020), and preserved nutritional attributes (Kaur *et al.*, 2016), which make it an attractive candidate for seed pretreatment. The OH system is highly dependent on the electrical conductivity (EC) of the material. Thus, it is important to determine the EC of each ingredient used. EC refers to the extent to which a substance can conduct electric current (Sakr and Liu, 2014; Patel and Singh, 2018). Some literature recommends that the EC value of materials should be above 0.05 siemens per meter (S/m) (Sagita et al., 2022). For particulate or grain materials that will be heated with OH, a medium with a sufficient EC value is needed, one of which is mineral water (Sagita *et al.*, 2021). Pretreatment with OH-based seed soaking with mineral water as a medium is expected to increase seed germination, where the imbibition process is expected to occur more quickly due to the movement of water at the molecular and even ionic levels (Kaur and Singh, 2016). To the best of our knowledge, no research has been conducted on the application of OH as a pretreatment in the germination process. Therefore, in this study, seed pretreatment was performed by soaking the seeds using OH technology for the first time. This study aimed to determine the effects of soaking OH-based mung bean seed on the germination and growth of mung bean sprouts.

2. Materials and Methods

2.1. Mung bean sample

In this study, Mung bean seeds (*Vigna radiate* L.) was obtained from a local market at Subang, West Java, Indonesia. Prior to experiments, mung bean seed samples were stored in the vacuum plastic chamber at 20-25°C. The initial moisture content of mung bean was 12.3 ± 0.2 % wet basis.

2.2. Ohmic heating apparatus

In this research, an OH apparatus developed by Sagita *et al.* (2024) was used to control the temperature of water for soaking the seed (Figure 1). The heating chamber was a cylindrical OH chamber with a maximum capacity of 1000 cm³, featuring an outer diameter of 100 mm and a wall thickness of 5 mm. The distance between the electrodes was 17 cm. The OH system was equipped with a data recording system using a microcontroller Arduino Mega 2560 (Shenzhen, Guangdong, China). Some of the parameters that can be recorded by the OH system are temperature, voltage, amperage, and time. Temperature was measured using a DS18b20 sensor (Maxim Integrated Products, Inc., California, US), which has an accuracy of ±0.5°C and a precision of ±0.1°C. For monitoring electrical current, an ACS712 sensor (Allegro Microsystems Inc., Manchester, US) was used, with an accuracy and precision of ±0.01 A. The system used AC power at a frequency of 50 Hz and a single phase. Data capture and storage were managed by a real-time clock (RTC) module and an SD card shield. Additionally, a variable transformer (0-250 V) (Focus Technology Co., Ltd., China) was included for voltage regulation. The schematic of the OH device is presented in Figure 2.

Figure 1. Ohmic heating apparatus used for experiment
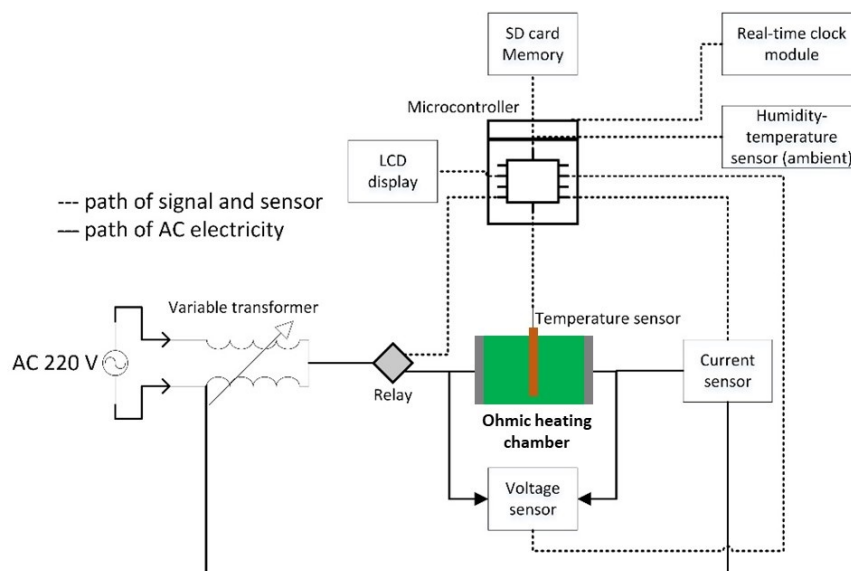
Figure 2. Schematic diagram of ohmic heating system integrated with control system

2.3. Experimental procedures

This study used a completely randomized design (CRD) method with one factor (soaking treatment) with a total of 6 treatments consisting of P1 = OH 6V/cm at 35°C; P2 = OH 10V/cm at 35°C; P3 = OH 14V/cm at 35°C; P4 = non-OH at 35°C; C1 = non-OH at ambient temperature (26°C) (Control 1); C2 = no soaking treatment (Control 2). This study focused on the investigation of voltage gradient effect; thus, all treatments were performed in the same temperature and time, except control 1 and 2.

In the first stage, 500 mL of water was prepared for each of the 5 treatments (P1-P4 and C1). For OH treatment (P1-P3), water was heated using OH based on voltage treatment (6, 10 and 14 V/cm) until it reached a temperature of 35°C. The temperature of 35°C was chosen following Chen *et al.* (2012) which produced the best seed vigor. Conversa and Elia (2009) reported that secondary dormancy in seeds can be alleviated by soaking them at 35°C for several hours. After the temperature reached 35°C, 50 grams of mung bean seeds was put into each OH chamber and the temperature was maintained at 35°C. For P4, water was heated to 35°C using an electric water heater (Q2, Jaya Utama Santikah Ltd., Indonesia) before adding the mung beans. For C1 treatment, water with a temperature of 26°C was directly used for soaking. This water temperature is the temperature in equilibrium with the environmental temperature at Subang Regency, Indonesia. The water used has an initial electrical conductivity of 26.2 mS/m. Soaking treatment was performed for 2 hours. For the C2 treatment, the seed was not given any soaking treatment. Each treatment was carried out with 4 replications.

2.4. Seed monitoring and observation

After soaking stage, the seeds (25 seeds per treatment) were placed in petri dishes which contain 2 pieces of tissue as the planting medium. Observations were carried out for 7 days. To keep the medium still in the moist condition, 5 mL of water was added daily to all samples including C2 which did not undergo soaking treatment. The parameters observed were divided into three stages, viz. after soaking, during germination, and at the end of the germination process. For the post-soaking stage, the following parameters measured were moisture content (M_c), seed hardness (S_h), seed mass (M_s), and surface morphology. During the germination process, the parameters observed included percentage of germination (P_{oG}), percentage of sprout with leaf (P_{sl}), germination index (G_i), and vigor index (V_i) (Zhou *et al.*, 2019). For the 7th DAP, the parameters measured were hypocotyl diameter (D_h), sprout length (L_s), and mass of sprouts (M_{os}).

2.5. Determination of moisture content

The moisture content measurement followed the method of AOAC (1995). Initially, a 2-gram sample (W) was weighed and placed into a ceramic cup. This cup with the sample (W_1) was then heated in an oven at 105°C for 3 hours. After heating, the sample was transferred to a desiccator for 15 minutes and weighed repeatedly until a constant weight (W_2) was achieved. The moisture content was determined using Equation 1. Sample measurements were carried out in 4 repetitions.

$$M_c = \frac{W_1 - W_2}{W} \times 100\%$$

Where M_c is moisture content (%wb), W_1 is mass of cup containing the sample before drying (g), W_2 is mass of cup and sample after drying (g), and W is initial mass of sample (g).

2.6. Determination of seed hardness and mass of single seed

Single seed mass was measured using a digital balance (MH-200, Shenzhen Zime Technology Co., Ltd, China) with an accuracy of 0.01 g. Meanwhile, the seed hardness measurement was performed by using a texture analyzer model TA-XT2 (Stable Microsystems Ltd. Surrey, UK). Measurements were carried out by using 10 seeds per treatment.

2.7. Evaluation of the internal morphology of the seed

The internal morphology of the seeds was observed by using a digital microscope model VHX-7000 (KEYENCE Corp., USA). The magnification used was 50x. Prior to analysis, the top and bottom part of the seed were cut, so that the seed could stand in the sample holder. Observations were randomly carried out on a single seed from each treatment.

2.8. Measurement of growth characteristics of mung bean seeds

Measurement of mung bean growth was carried out from day 1 to day 7 after the seeds were placed in the growing medium, i.e. a Petri dish containing 2 pieces of tissue paper made from 100% of natural fiber (virgin plantation pulp). Parameters measured included percentage of germination (PoG), percentage of sprout with leaf (P_{sl}), hypocotyl diameter (D_h), sprout length (L_s), and mass of sprouts (M_{os}). P_{oG} was observed every day, while P_{sl} was calculated on the third day. D_h measurements were carried out using a caliper with a precision of 0.01 mm for 3 seed samples in each treatment. Measurements of L_s were carried out using a ruler with a precision of 1 mm for 3 samples in each treatment. To measure the mass of sprouts, an analytical balance (MH-200, Shenzhen Zime Technology Co., Ltd, China) with a precision of 0.01 g was used.

2.9. Determination of germination index and vigor index

Several parameters utilized to describe the statistical characteristics of seeds including percentage of germination (P_{oG}), germination index (G_i) and vigor index (V_i) were calculated using Equation 2-4 (Song *et al.*, 2022; Zhou *et al.*, 2019).

$$P_{oG} = \frac{N_t}{N_{TS}} \times 100 \qquad (2)$$

$$G_t = \sum \frac{N_{Dn}}{D_n} = \frac{N_{D1}}{D_1} + \frac{N_{D2}}{D_2} \dots \frac{N_{Dn}}{D_n} \qquad (3)$$

$$V_t = G_t \times L_s \qquad (4)$$

Where N_t is number of germinated seeds, N_{TS} is total number of seeds, N_{Dn} is percentage of seeds grown on day n (%), D_n is day at the time of measurement, and L_s is length of sprouts on the day 7 (cm).

2.10. Data analysis

Experimental tests were replicated for four times at each treatment, and averages were reported with standard deviation. All data for each parameter were analyzed statistically using ANOVA and Duncan post-hoc test at a significance level of 95% using SPSS ver. 21 (IBM Corp., USA). Furthermore, in this study, multivariate analysis was employed viz. principal component analysis (PCA) and hierarchical clustering analysis (HCA). Both were used to evaluate the treatment group and the correlation between dependent variables observed from all treatments. PCA analysis was performed by using FactoMineR package (Lê *et al.*, 2008) in open-source platform (R 4.2.2 statistical software). Prior to PCA and HCA, the data was pre-processed using normalization with the range between 0 and 1.

3. Results

3.1. Moisture content, mass and hardness of mung bean seed

The moisture content of the seeds demonstrated significant variability among the treatments (Table 1). Treatments P1, P2, P3, and P4 displayed higher moisture content compared to the control groups (C1 and C2). Moisture content is closely related to the mass of the seed, where treatments P1, P2, P3, and P4 also resulted in significantly higher seed masses compared to the control groups (C1 and C2) (Table 1). Seed hardness was also found significantly different among the treatments. Notably, treatments P1, P2, P3 exhibited lower seed hardness values compared to the control groups (C1 and C2) and P4 (non-ohmic at 35°C). Control 2 (C2), which received no soaking treatment, displayed the highest seed hardness.

Table 1: Analysis result of mass, moisture content and hardness of seed

Treatment	Single seed mass (g)	Seed hardness (kgf)	Moisture content (%)
P1	0.75 ± 0.04^b	16.79 ± 4.79^a	23.20 ± 0.54^c
P2	0.79 ± 0.03^{bc}	15.87 ± 2.32^a	24.61 ± 0.26^d
P3	0.80 ± 0.05^c	12.90 ± 3.79^a	25.62 ± 0.17^e
P4	$0.77 \pm 0.04b^c$	28.85 ± 6.47^b	22.83 ± 0.39^c
C1	0.70 ± 0.06^a	36.20 ± 3.19^c	16.61 ± 0.07^b
C2	0.67 ± 0.03^a	38.39 ± 5.48^c	12.31 ± 0.15^a

Note: Values are expressed as mean ± standard deviation. Means with different letters were significantly different at p < 0.05 by Duncan Multiple Range Test. P1 = OH 6V/cm at 35°C; P2 = OH 10V/cm at 35°C; P3 = OH 14V/cm at 35°C; P4 = non-OH at 35°C; C1 = non-OH at ambient temperature (Control 1); C2 = No soaking treatment (Control 2)

3.2. Internal morphology of mung bean seeds after pretreatment

Based on the results obtained from a digital microscope with a magnification of 50×, the results of the observations are presented in Figure 3. Visually, the P1, P2, and P3 treatments showed a darker color appearance (from surface to core) which is indicated by the presence of more water absorbed by the seeds.

Figure 3. Visual appearance of cross-sectional area of mung bean seed

3.3. Effect of pretreatment on seed germination of mung bean

The results of the seed germination for 7 days are shown in Figure 4. The results showed a significant difference in P_{oG} occurring on day 1 (24 hours after seeding). The highest P_{oG} were found in treatments P3 and P2 and followed by P1, P4, C1 and C2, respectively. This shows that soaking treatment (P1-P4 and C1) generally increases the percentage of seed germination compared to C2 (without soaking treatment). Treatment C2 showed the lowest P_{oG}, while treatments C1 (soaked in water at room temperature) and P4 (non-OH at 35°C) showed higher P_{oG} than C2. An interesting fact from these results is that the OH treatment (P1-P3) showed higher values than C1, C2, and P4, which was most likely caused by faster water absorption by the seeds due to the presence of an electric current in the water. On the next days, all seeds began to grow with no significant change on the germination percentage among treatments, and the seeds were germinated at a percentage of 96 to 100%.
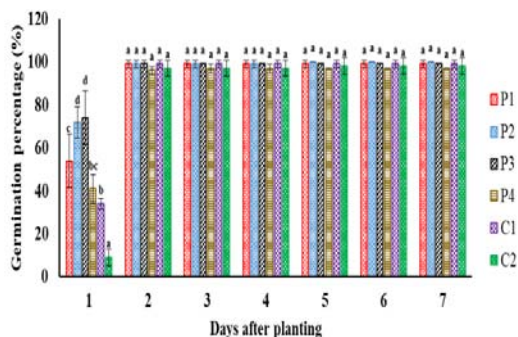
Figure 4. Seed germination percentage of mung bean under different treatment: Bar with different letters in the same day were significantly different at p < :05 by Duncan Multiple Range Test: P1 = OH 6V/cm at 35°C; P2 = OH 10V/cm at 35°C; P3 = OH 14V/cm at 35°C; P4 = non-OH at 35°C; C1 = non-OH at ambient temperature (Control 1); C2 = No soaking treatment (Control 2).

3.4. Germination index and vigor index

The results of the calculation of G_i and V_i parameters are presented in Table 2. It was found that the treatment of mung bean seeds involving OH had a significant positive effect on G_i and V_i compared to the control treatment and without OH. The G_i represents the relative speed and uniformity of seed germination. Treatments P2 and P3 exhibited significantly higher G_i compared to the control groups (C1 and C2). The vigor index is a measure of seedling strength and robustness, reflecting the overall health and vitality of the seedlings. Treatments P2 and P3 demonstrated significantly higher V_i compared to the control groups (C1 and C2).

Table 2. Germination index and vigor index of mung bean sprouts under different pretreatment

Treatment	Germination index	Vigor index
P1	52.92 ± 3.88[c]	651.65 ± 92.66[ab]
P2	57.55 ± 2.25[d]	892.39 ± 190.47[d]
P3	58.20 ± 2.87[d]	865.78 ± 161.44[cd]
P4	48.75 ± 2.53[b]	751.69 ± 26.06[bcd]
C1	47.92 ± 0.66[b]	677.13 ± 146.15[abc]
C2	41.00 ± 1.58[a]	539.50 ± 13.23[a]

Note: Values are expressed as mean ± standard deviation. Means with different letters were significantly different at p < .05 by Duncan Multiple Range Test. P1 = OH 6V/cm at 35°C; P2 = OH 10V/cm at 35°C; P3 = OH 14V/cm at 35°C; P4 = non-OH at 35°C; C1 = non-OH at ambient temperature (Control 1); C2 = No soaking treatment (Control 2)

3.5. Effect of soaking pretreatment on seedling growth of mung bean

Table 3 presents the results of experiments examining the effects of different treatments on the hypocotyl diameter, length of sprout, mass of total sprout, and percentage of sprouts with leaves of mung bean plants.

These parameters are critical indicators of seedling growth and overall plant development.

Table 3. Analysis result of hypocotyl diameter, length of sprout, mass of total sprout, and percentage of sprout with leaf

Treatments	Hypocotyl diameter (mm)	Length of sprout(cm)	Mass of total sprout (g)	Percentage of sprout with leaf at 3rd day (%)
P1	1.1 ± 0.2^b	12.4 ± 2.0^a	5.67 ± 0.59^a	44.0 ± 13.5^{bc}
P2	0.5 ± 0.2^a	15.5 ± 3.1^a	5.88 ± 0.78^a	43.0 ± 5.0^{bc}
P3	1.2 ± 0.0^b	15.0 ± 3.4^a	6.17 ± 0.57^a	56.0 ± 5.7^c
P4	1.0 ± 0.1^b	15.5 ± 1.3^a	5.91 ± 0.22^a	47.0 ± 13.2^{bc}
C1	0.9 ± 0.2^b	14.1 ± 3.0^a	5.60 ± 0.49^a	39.0 ± 11.9^b
C2	0.9 ± 0.2^b	13.2 ± 0.4^a	5.86 ± 1.02^a	23.0 ± 3.8^a

Note: Values are expressed as mean ± standard deviation. Means with different letters were significantly different at $p < .05$ by Duncan Multiple Range Test. P1 = OH 6V/cm at 35°C; P2 = OH 10V/cm at 35°C; P3 = OH 14V/cm at 35°C; P4 = non-OH at 35°C; C1 = non-OH at ambient temperature (Control 1); C2 = No soaking treatment (Control 2).

The hypocotyl diameter represents the width of the seedling stem just above the roots. Treatments P1, P3, and P4 demonstrated larger hypocotyl diameters (average) compared to the control groups (C1 and C2), although the values were not significantly different while treatment P2 produced the lowest value even compared to the control treatments.

The length of the sprouts showed insignificant results at the p-value level <0.05. However, treatments P2, P3 and P4 gave average results above 15 cm, while P1 produced the lowest value even compared to the control treatments. Based on these findings, there is a trade-off phenomenon between P1 and P2 where P1 gives a larger diameter but lower sprout length than P2. This indicates that there is an effect of voltage intensity on germination, where P3 (voltage intensity 14 V/cm) was found to provide optimal hypocotyl diameter and length of sprouts.

The mass of the total sprout represents the weight of the entire seedling. Overall, the total mass was not significantly different at 95% confidence interval. However, the average value showed that the highest value was obtained in the P3 treatment.

The percentage of sprouts with leaves on the third day indicates the rate of early leaf development. Treatment P3 significantly displayed the highest percentage of sprouts with leaves at the third day, followed closely by treatments P1, P2, and P4.

3.6. Multivariate analysis result

The results of PCA are presented in Figure 5, which displays the loadings plot and score plot of each treatment and response variable on the principal components analysis diagram. The loading plot of principal component 1 (PC1) and principal component 2 (PC2) provides a comprehensive representation of the relationships observed among the dependent variables. Together, PC1 and PC2 account for a substantial portion of the total variance, explaining 84.12% of the dataset. PC1 contributes significantly, explaining 69.55% of the variance, while PC2 contributes 14.57%.
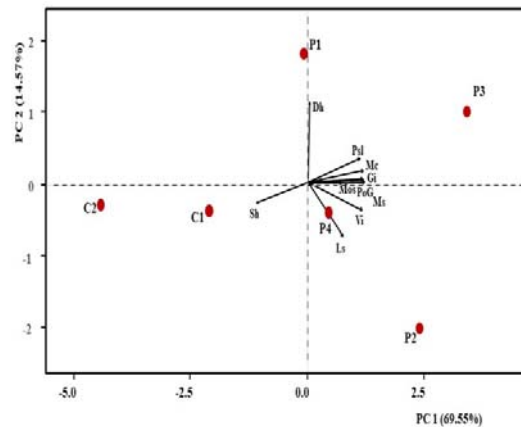
Figure 5. Biplot obtained from PCA of variables comprising mung bean sprout characteristics

Furthermore, in the biplot diagram, the observed samples were scattered in each quadrant. Thus, for better understanding about the treatment group, HCA was performed which is shown in Figure 6. It was found that the treatments with OH and non-OH at 35°C (P1-P4) were in the same cluster and the other cluster was the control group (C1 and C2). P2, P3 and P4 were found to have identical characteristics, indicated by the same cluster and the same colour pattern.
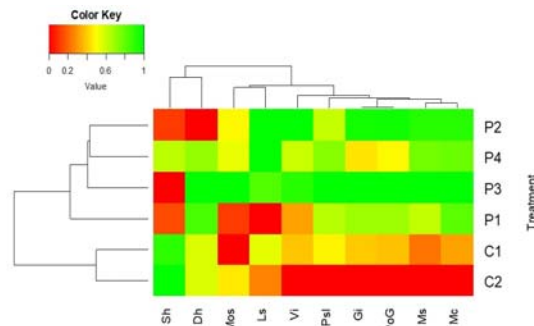
Figure 6. The relationship between treatments and response variables including their cluster; the color of the heat map represents the trend of the treatment impact from the lowest (red) to the highest (green).

4. Discussion

The application of OH pretreatment on mung bean seeds has shown significant and promising results on the germination and growth of mung bean sprouts, as demonstrated in this study where several key findings shed light on the potential benefits of OH pretreatment on speeding up seed germination and sprout growth.

OH pretreatment, particularly at VG 14 V/cm (P3) positively influenced seed development by enhancing water imbibition, resulting in heavier seeds. This shows that OH at a certain VG (14 V/cm) enhanced the ability of seeds to uptake water. In contrast, the seeds subjected to Control 1 (C1), soaked at ambient temperature, exhibited lower mass, possibly due to limited water uptake during soaking. Moreover, the C2 treatment produced the lowest seed mass because it was not given any soaking treatment so there was no water absorption. Other evidence was found on seed hardness, where OH reduced seed hardness, making the seeds more conducive to germination. This finding indicated that the application of OH can potentially alter seed structure and soften the seed coat. Another study reported that OH clearly damaged (weakened) the cell wall network and tissue structure due to the heat and electroporation effects (Allali et al., 2010). This OH effect is similar to the soaking technique with Ammonium gluconate, which can accelerate water uptake in seeds (Chen et al., 2022).

More evidence through moisture content analysis shows the superiority of OH at VG 14/cm, with the highest water content value. This shows that electric current in water with a certain intensity (in this case 14 V/cm) during immersion had a positive influence in terms of faster water absorption. This is in line with the result of Allali et al. (2010), where OH weakens cell walls and tissue structures more quickly due to the combined effects of heat and electroporation. Thus, the same soaking temperature (35 °C) as treatment P3 and P4 gives different water contents where P3 (OH at 14 V/cm) shows a higher value than P4 (without OH). Furthermore, both treatments (P3 and P4) provided higher moisture content than the control (C1) because C1 used a lower water temperature (26 °C). This finding was in line with the research conducted by Coffigniez et al. (2019), where higher water uptake occurs at higher temperatures because cell wall weakening occurs more quickly at higher temperatures, allowing water to enter the cells more quickly. Another study reported that moisture content of soaked seed increased with the increase in temperature and time (Chen et al., 2012), but it should be noted that a higher temperature was not always effective at enhancing germination. According to Chen et al. (2012), the optimum temperature for stimulating seed germination and vigor (e.g. switchgrass seeds) was in the range 35-45°C.

Based on the overall result presented in Table 1, in the P3 treatment, characterized by the application of the highest voltage (14V/cm), the seed exhibited the highest value of mass and moisture content, and the lowest of seed hardness. This could be attributed to the increased collision of electron charges, resulting in higher molecular kinetic energy production so that water molecules can more quickly enter the seed. Another study reported that an electric field may change physiology and improve water absorption due to dipole-dipole interactions (Rifna et al., 2019).

Regarding the visual appearance of the seed cross-sectional area, the P4 treatment showed that many dry crystal grains (indicated by white color) were still present, similar to the control treatments (C1 and C2). This was due to minimal or even no water absorption. These results are consistent with the data in Table 1 where the moisture content of the seeds with the OH treatment at VG 14 V/cm (P3) was the highest compared to other treatments. According to Dymek et al. (2012), electric field treatment such as high pulse electric field resulted in the opening of the cavities within the plasma membrane, which increased the level of inward and outward movement of polar molecules. Numerous studies have demonstrated that the application of a low-intensity, low-frequency electric field can alter the behavior of biosystems (organisms, tissue and cell cultures), including effects on the processes of proliferation, growth, and differentiation (Berg, 1993).

OH pretreatment can increase the germination rate. In addition, it was also revealed that the applied voltage also had an effect, in which the higher the voltage significantly increased the germination rate, where the highest value was the P3 treatment (OH 14 V/cm). This finding was consistent with data on the moisture content of the seeds after soaking, where P3 was the treatment that produced the highest water absorption. Previous study which used pulse electric field also found the same phenomenon, where application of pulse electric field about 12 V/cm increased seed germination percentage (Khotimah et al., 2016). Furthermore, compared to previous studies using the PAW treatment, results of this study were slightly higher. The PAW treatment of seeds that had been soaked 6 hours previously resulted in a range of germination percentages of 60-70% after 24 hours (Fan et al., 2020), while OH treatment at a certain voltage can produce an average germination rate of 74%.

According to Choudhury & Karmakar (2020), germination goes through three phases, viz. the seed imbibition phase, the activation phase, and the germination phase. In the seed imbibition phase, a process of water absorption occurs which involves the apoplast space through the force pushed by the seed. In the activation phase, plant metabolic activity occurs where protein synthesis is in this phase. Then it enters the germination phase, where cell elongation occurs and the appearance of the radicle where the sprouts will grow and develop under suitable conditions. With the intervention of OH treatment, the imbibition and the activation phases might occur faster than without OH treatment.

The implication is that the acceleration of seed emergence and faster seedling growth means that bean sprouts can be harvested more quickly. Specific voltages (P2 and P3) positively influenced the germination process, leading to faster and more synchronized seedling emergence. Conversely, Control 2 (C2) displayed the lowest germination index, suggesting that without any treatment, seed germination might be slower and less consistent.

Regarding vigor index, OH treatments at specific voltages (P2 and P3) contributed to the development of more vigorous and robust seedlings. The enhanced molecular activity due to OH might have promoted seedling growth and vigor. On the other hand, Control 2

(C2) which was soaked in lower temperature showed the lowest vigor index, indicating that untreated seeds might produce weaker and less vigorous seedlings. The G_i and V_i are closely related to the germination rate observed for 7 days, where G_i and V_i increased with the increase of germination speed as presented in Figure 4.

Results of this study when compared with previous studies by Zhou *et al.* (2019) which used plasma treated water (PTW) showed the same pattern, where the V_i of the control treatment was below 400, while the vigor index of the PTW treatment depended on the gas used. N_2-PTW, He-PTW and O_2-PTW provided V_i values ranging from 477.84 – 719.28 which were lower than the optimal results in this study, but not higher than the air-PTW treatment in Zhou *et al.* (2019). This opens opportunities for further research in terms of optimizing the temperature and soaking time of OH-based seeds in order to obtain better results.

Furthermore, this study was in line with previous study which found that germination rate index increased with the increase in temperature (Chen *et al.*, 2012; Goussous *et al.*, 2010). However, it should be noted that there is an upper limit temperature as higher temperatures can damage cell membranes. The optimal temperature for switchgrass seed germination was found to be about 38°C and a higher temperature was may not effective (Chen *et al.*, 2012). In the present study, soaking at 35°C produced higher G_i and V_i compared to the control, which adds to the evidence that this range of temperature values was effective for pretreatment.

OH treatments (VG 14 V/cm) also promoted the early growth and development of the seedling stems, resulting in larger hypocotyls. On the other hand, C1 and C2 displayed the smallest hypocotyl diameter, indicating this treatment might have slower initial stem growth due to lateness in water absorption. Additionally, a high electric field may cause the seed coat to crack, which can enhance its ability to absorb water and nutrients. This improvement could lead to a higher germination rate of mung beans and support the growth of both the hypocotyl and radicle (Zhou *et al.*, 2019). Several relevant previous studies have been conducted by Khotimah *et al.* (2016) and Kiatgamjorn *et al.* (2003), but the mechanism of electric current was different, where they used a static electric field that uses DC current without a heating effect. The results of their study showed that the bean sprouts grown from the treated seeds had heavier in fresh weight, longer roots, stems and leaves in comparison to the control.

The length of the sprout is a key indicator of early seedling growth. Treatments P2, P3, and P4 exhibited significantly longer sprouts compared to the control groups (C1 and C2) and P1. This implies that OH at specific voltages positively influenced the elongation of the seedling shoots, leading to enhanced early growth. Also, it was revealed that OH at 14 V/cm consistently promoted greater seedling growth and biomass accumulation. C2 exhibited the lowest total sprout mass, indicating that untreated seeds might produce weaker and less substantial seedlings. Regarding leaves development, OH treatments, particularly P3, significantly accelerated early leaf development, leading to more advanced and healthier seedlings. Control 2 (C2) exhibited the lowest percentage of sprouts with leaves, indicating that untreated seeds might have delayed leaf emergence.

As comprehensive information, PCA shows robustness in capturing underlying patterns and interdependencies among measured variables, thus providing valuable insight into the factors that influence bean sprout characteristics. PC 1 shows strong positive loadings for seed mass, moisture content, percentage of germination, germination index, vigor index, mass of sprouts, and percentage of sprouts with leaves. It suggests that these variables are highly correlated and contribute most significantly to the variance explained by PC 1. Thus, PC 1 could be interpreted as an overall indicator of seed and sprout quality and vigor. PC 2 has only one strong positive loading which is hypocotyl diameter. The study's findings could be instrumental in optimizing mung bean sprout cultivation practices. By understanding the key variables that influence seed germination, seedling growth, and overall sprout quality, farmers and researchers can focus on specific factors to enhance crop productivity and ensure better-quality sprouts.

5. Conclusion

The experimental results reveal the promising potential of OH as a highly effective seed pretreatment for mung bean sprout production. The application of specific voltages (i.e., 14 V/cm) consistently resulted in accelerated seedling growth, larger hypocotyl diameter, longer sprout length, increased total sprout mass, and advanced early leaf development. P3 treatment (OH at VG 14V/cm) gave a significant effect and produced almost all the optimal values for the parameters measured such as water absorption, total mass of sprouts, seed moisture content, germination rate, germination index, vigor index, and percentage of sprouts with leaves. These findings hold significant implications for industrial practices seeking to optimize mung bean sprout production. Apart from that, these findings also reveal the potential for using OH as a pre-sowing treatment, so that farmers can increase the speed of seedling establishment and foster healthier and more vigorous plants.

References

Al-Enezi N, Al-Bahrany A and Al-Khayri J. 2012. Effect of X-irradiation on date palm seed germination and seedling growth. *Emirates J. Food Agric.*, **24(5)**: 415–424.

Allali H, Marchal L and Vorobiev E. 2010. Effects of vacuum impregnation and ohmic heating with citric acid on the behaviour of osmotic dehydration and structural changes of apple fruit. *Biosys. Eng.*, **106(1)**: 6–13.

AOAC. 1995. Official methods of analysis of AOAC International. , 16th ed Association of Official Analytical Chemist International, Arlington.

Berg H. 1993. Electrostimulation of cell metabolism by low frequency electric and electromagnetic fields. *Bioelectroc. Bioen.*, **31(1)**: 1–25.

Chen B, Jin X, Meng W, Ding F and Li P. 2022. Ammonium gluconate, an innovative seed-soaking agent from waste potatoes. *Sci. Hortic.*, **293**: 110676.

Chen G, Wang Q, Liu Y, Li Y, Cui J, Liu Y, Liu H and Zhang Y. 2012. Modelling analysis for enhancing seed vigour of switchgrass (*Panicum virgatum* L.) using an ultrasonic technique. *Biom. and Bioen.*, **47**: 426–435.

Choudhury A and Karmakar S. 2020. Germination: The way of entering into a new life. *AgriCos e-Newsletter*, **1(6)**: 1–4.

Coffigniez F, Briffaz A, Mestres C, Akissoé L, Bohuon P and El Maâtaoui M. 2019. Impact of soaking process on the microstructure of cowpea seeds in relation to solid losses and water absorption. *Food Res. Inter.*, **119**: 268–275.

Conversa G and Elia A. 2009. Effect of seed age, stratification, and soaking on germination of wild asparagus (Asparagus acutifolius L.). *Sci. Hortic.*, **119(3)**: 241–245.

Dahiya P, Linnemann A, Van Boekel M, Khetarpaul N, Grewal R and Nout M. 2015. Mung bean: Technological and nutritional potential. *Crit. Rev. Food Sci. Nutri.*, **55(5)**: 670–688.

Dymek K, Dejmek P, Panarese V, Vicente AA, Wadsö L, Finnie C and Galindo FG. 2012. Effect of pulsed electric field on the germination of barley seeds. *LWT-Food Sci. Technol.*, **47(1)**: 161–166.

Fan L, Liu X, Ma Y and Xiang Q. 2020. Effects of plasma-activated water treatment on seed germination and growth of mung bean sprouts. *J. Taibah Univ. Sci.*, **14(1)**: 823–830.

Goussous S, Samarah N, Alqudah A and Othman M. 2010. Enhancing seed germination of four crop species using an ultrasonic technique. *Experiment. Agricul.*, **46(2)**: 231–242.

Harb AM, Alnawateer BM and Abu-Aljarayesh I. 2021. Influence of static magnetic field seed treatments on the morphological and the biochemical changes in lentil seedlings (*Lens Culinaris* Medik). *Jordan J. Biol. Sci.*, **14(1)**: 179–186.

Kaur N and Singh AK. 2016. Ohmic heating: concept and applications—a review. *Crit. Rev. Food Sci. Nutri.*, **56(14)**: 2338–2351.

Kaur R, Gul K and Singh AK. 2016. Nutritional impact of ohmic heating on fruits and vegetables — A review. *Cogent Food Agric.*, **66(1)**: 1–15.

Khotimah SN, Romadhon DR and Viridi S. 2016. The effects of static electric field on germination and growth of mungbean seeds (*Vigna radiata* L) in vegetative phase. *ARPN J. Eng. Appl. Sci*, **11**: 13740–13743.

Kiatgamjorn P, Khan-ngern W and Nitta S. 2003. The comparison of electric field intensity effects to the bean sprouts growing.The comparison of electric field intensity effects to the bean sprouts growing, *in Asia-Pacific Conference on Environmental Electromagnetics, 2003. CEEM 2003. Proceedings.*

Lê S, Josse J and Husson F. 2008. FactoMineR: a package for multivariate analysis. *J. Stat. Softw.*, **25(1)**: 1–18.

Majeed A, Muhammad Z, Ullah R and Ali H. 2018. Gamma irradiation i: effect on germination and general growth characteristics of plants–a review. *Pakistan J. Bota.*, **50(6)**: 2449–2453.

Muttaqin M, Putri RI, Putri DA and Matra DD. 2019. The Effectiveness of Germination Pre-Treatment on Mung Beans, Peanuts, and Tomatoes. *IOP Conf. Ser. Earth Environ. Sci.*, **299(1)**: 1–6.

Núñez-Gastélum JA, Arguijo-Sustaita AA, López-Díaz JA, Díaz-Sánchez ÁG, Hernández-Peña CC and Cota-Ruiz K. 2023. Seed germination and sprouts production of Moringa oleifera: A potential functional food? *J. Saudi Soc. Agric. Sci.*, **22(4)**: 223–230.

Patel A and Singh M. 2018. Ohmic heating for food products- a review. *Curr. Appl. Sci. Technol.*, **27(3)**: 1–7.

Peñas E, Gómez R, Frías J and Vidal-Valverde C. 2010. Effects of combined treatments of high pressure, temperature and antimicrobial products on germination of mung bean seeds and microbial quality of sprouts. *Food control*, **21(1)**: 82–88.

Porto CL, Ziuzina D, Los A, Boehm D, Palumbo F, Favia P, Tiwari B, Bourke P and Cullen PJ. 2018. Plasma activated water and airborne ultrasound treatments for enhanced germination and growth of soybean. *Innov. Food Sci. Emerg. Technol.*, **49**: 13–19.

Rifna EJ, Ratish Ramanan K and Mahendran R. 2019. Emerging technology applications for improving seed germination. *Trends in Food Sci. Technol.*, **86**: 95–108.

Saberali SF and Moradi M. 2019. Effect of salinity on germination and seedling growth of Trigonella foenum-graecum, Dracocephalum moldavica, Satureja hortensis and Anethum graveolens. *J. Saudi Soc. Agric. Sci.*, **18(3)**: 316–323.

Sagita D, Darmajana DA and Hidayat DD. 2021. Recent studies and prospective application of ohmic heating for fermentation process: a mini-review. *E3S Web Conf.*, **306**: 04006.

Sagita D, Darmajana DA, Hidayat DD, Novrinaldi and Sitorus A. 2020. Design and performance of ohmic-based fermentor model for controlling fermentation process. *IOP Conf. Ser. Earth Environ. Sci.*, **542(1)**: 012033.

Sagita D, Hidayat DD, Darmajana AD, Rahayuningtyas A and Hariadi H. 2024. Fabrication and performance test of a multipurpose ohmic heating apparatus with a real-time data logging system based on low-cost sensors. *Res. Agric. Eng.*, **70(1)**: 23–34.

Sagita D, Kristanti D, Setiaboma W, Kumalasari R, Ekafitri R, Yulianti LE, Putri DP, Ardiansyah RCE, Desnilasari D and Hariadi H. 2023. Application of ohmic heating for green coffee bean fermentation: effect of voltage gradient on the heating performance, energy, EC, pH, and fermentation index. *J. Biosyst. Eng.*, **48**: 364–373.

Sagita D, Setiaboma W, Kristanti D, Kurniawan YR, Hidayat DD, Darmajana DA, Sudaryanto A and Nugroho P. 2022. Experimental investigation of heating pattern, energy requirement and electrical conductivity in a batch ohmic heating system for coffee fermentation. *Innov. Food Sci. Emerg. Technol.*, **76**: 102946.

Sakr M and Liu S. 2014. A comprehensive review on applications of ohmic heating (OH). *Renew. Sustain. Energy Rev.*, **39(2014)**: 262–269.

Salvador AA and Bucu GC. 2021. Experimental analysis on determination of significant factors in growing mung bean sprouts (length) in a home-based set-up (non-soil germination), in *Proceedings of the International Conference on Industrial Engineering and Operations Management.*

Shakir SK, Kanwal M, Murad W, ur Rehman Z, ur Rehman S, Daud M and Azizullah A. 2016. Effect of some commonly used pesticides on seed germination, biomass production and photosynthetic pigments in tomato (*Lycopersicon esculentum*). *Ecotoxicology*, **25**: 329–341.

Song P, Yue X, Gu Y and Yang T. 2022. Assessment of maize seed vigor under saline-alkali and drought stress based on low field nuclear magnetic resonance. *Biosys. Eng.*, **220**: 135–145.

Vrancheva R, Popova A, Mihaylova D and Krastanov A. 2020. Phytochemical analysis, in vitro antioxidant activity and germination capability of selected grains and seeds. *Jordan J. Biol. Sci.*, **13(3)**: 337–343.

Wei Y, Wang X, Shao X, Xu F and Wang H. 2019. Sucrose treatment of mung bean seeds results in increased vitamin c, total phenolics, and antioxidant activity in mung bean sprouts. *Food Sci. Nutr.*, **7(12)**: 4037–4044.

Zhou R, Li J, Zhou R, Zhang X and Yang S. 2019. Atmospheric-pressure plasma treated water for seed germination and seedling growth of mung bean and its sterilization effect on mung bean sprouts. *Innov. Food Sci. Emerg. Technol.*, **53**: 36–44.

JJBS

Jordan Journal of Biological Sciences

Physicochemical and Microbiological Characteristics of Robusta Coffee Processed Using Wet Fermentation Method with and Without *S. Cerevisiae* Starter Culture

Woro Setiaboma[1,2,*], Dita Kristanti[1,2], Diang Sagita[2], Annisa Dwi Yunniar[2], Lia Ratnawati[2], Yose Rizal Kurniawan[2], Diki Nanang Surahman[2] , Evana Evana[3]

[1] *Research Center of Food Technology and Processing, National Research and Innovation Agency, BRIN, Jl. Raya Jogja-Wonosari Km 31.5, Playen, Yogyakarta, 55861, Indonesia;* [2] *Research Center for Appropriate Technology, National Research and Innovation Agency, BRIN, Jl K.S. Tubun 5, West Java, Subang, 41213, Indonesia;* [3] *Research Center of Pharmaceutical Ingredients and Traditional Medicine, National Research and Innovation Agency, BRIN, Jl. Raya Jakarta, Pakansari, Cibinong, Bogor, West Java ,16912Indonesia*

Abstract

Fermentation is utilized in washed coffee to expedite the degradation of mucilage, thereby altering the coffee's quality. The study investigated the fermentation process of de-pulped Robusta coffee beans with and without *Saccharomyces cerevisiae*. This research purpose was to investigate the effects of fermentation on the physicochemical (moisture, ash, color, total phenolic content, DPPH radical scavenging, and caffeine content) and microbiological (total plate count (TPC), total yeast (TY)) characteristics of de-pulped Robusta coffee produced, using two fermentation conditions (with and without *S. cerevisiae* starter culture) and varying the duration of fermentation (24, 48, and 72 h). The data was analyzed using ANOVA and Duncan' post hoc test, while the relationship between dependent variables and treatments was quantified using principal component analysis (PCA) and hierarchical clustering analysis (HCA). Results showed that the moisture, pH caffein, and total phenolic content of the coffee fermented with and without *S. cerevisiae* starter culture were 1.02-1.32 %; 4.12 to 4.23; 4.03-9.50 ppm; and 350.89-444.08 (GAE mg/100 mL), respectively. The TPC and TY gradually increased with fermentation time, while both parameters were higher in fermentation without *S. cerevisiae*. The PCA revealed that moisture positively correlated with phenolics and caffeine, while negatively correlated with DPPH. The HCA revealed that coffee fermented with and without *S. cerevisiae* starter culture varied significantly.

Keywords : Antioxidant; robusta coffee; spontaneous fermentation; wet process; yeast fermentation

1. Introduction

Coffee has become one of the most common alcohol-free beverages consumed around the globe. The global production of coffee in 2019/2020 was 168.84 million bags. This condition is also supported by a significant transformation of world coffee market as a result of the increasing popularity of "specialty coffee", i.e. coffee with organoleptic characteristics of a particular region (Sunarharum *et al.*, 2014). Coffee grows in many regions in the world such as Africa, South America and Asia. Coffee had a long history in Indonesia and a considerable impact on the country's economic development, with Indonesia ranking as the world's fourth-largest coffee producer in 2019 (Jamil, 2019). It has three dominant species, i.e. *Coffee arabica* (Arabica), *Coffee canephora* (Robusta), and Liberica, where Arabica and Robusta are commonly cultivated in Indonesia.

Both the pre-harvest (genotype, geographical area, climate, and agronomic techniques) and post-harvest (primary processing, drying process, roasting process, and storage conditions) variables influenced the coffee

beverage quality (Elhalis *et al.*, 2021). According to Karim *et al.*(2019), cultivation and post-harvest processing contribute 70% of coffee quality. There are three common techniques for converting coffee cherries into beans, called as wet, dry, and semi-dry (Karim *et al.*, 2019; Pereira *et al.*, 2015). The dry process, known as natural process, is a process where cherry coffee is directly dried without de-pulping process. The semi-dry process involves a pulping process, then the coffee is dried in the form of coffee beans with mucilage. The wet process is conducted by pulping the cherry coffee to obtain the coffee beans with mucilage which is ready for fermentation. The wet method, also known as "washed," requires a significant amount of water during fermentation. If done properly, this kind of treatment preserves the interior properties of coffee beans better and results in a more homogenous green coffee, which yields fewer faulty beans (Pereira *et al.*, 2015; Elhalis *et al.*, 2021; Elhalis *et al.*, 2020; Silva, 2014). As a result, wet processed coffee is thought to be of greater quality and is, therefore, sold at a higher price. Wulandari *et al.* (2021) studied the effect of the processing technique on the sensory and chemical characteristic of coffee produces, where the moisture and the caffeine content of

---

the wet process was lower than dry process, and from the sensory evaluation, both methods were accepted by the panellists. It was reported that the wet process developed the formation of the coffee aroma (Lee *et al.*, 2015) as affected by metabolite activity during fermentation the process.

Fermentation promotes the breakdown of complex organic compounds into simpler ones through the activity of microbes (Sharma *et al.*, 2020). The fermentation process in the wet process of coffee has the purpose to accelerate the degradation of the mucilage (polysaccharides particularly pectin) attached to the coffee beans. The fermentation can be done spontaneously or by adding particular microbes such as yeast, lactic acid bacteria or a combination of both. Elhalis *et al.* (2020) found that the yeast plays a significant part in wet coffee fermentation, producing coffee with higher flavor, fragrance, and overall sensory attribute. The iron and antioxidant levels of Arabica coffee pulp from Mengani, Indonesia, were similar to those found in commercial Brazilian products, as shown by similarity based on multivariate data (Setyobudi *et al.*, 2022)**.** Study on Arabica coffee cherry fermentation using yeast addition revealed that *P. kluyveri* and *S. cerevisiae* were able to create aromatic volatile substances that led to aroma enhancement in roasted coffee (Jimenez *et al.*, 2023; Pereira *et al.*, 2015; Saerens & Swiegers, 2016). Also, Wang *et al.* (2020) performed fermentation on Arabica green coffee beans. They reported that *P. kluyveri* and *S. cerevisiae* were great starter cultures for coffee flavor biological transformation since both improved the fruity component of roasted coffees. Because of its increased sensory quality, high viability, and pectinolytic activity which breaks down mucilage during fermentation and produces volatile compounds *S. cerevisiae* is used as a culture (Elhalis *et al.*, 2023). The quality of the coffee produced will be enhanced by the proper duration of fermentation, not over or under fermentation.

However, study on the fermentation of de-pulped Robusta coffee beans is still limited, especially in the wet processing technique which combine with the *S. cerevisiae* addition and with several fermentation time. Therefore, the goal of the research was to explore the influence of fermentation with and without *S. cerevisiae* addition in the wet processing technique on the chemical characteristic of Robusta coffee produced.

2. Methodology

2.1. Materials

The coffee cherry from the Robusta species was collected from Subang, West Java, Indonesia (-6.728272°S, 107.617418°E). The good (fresh, not rotten and non-empty fruit) and red coffee cherries were sorted and used for experiments. Cherries that were submerged were selected and cherries that floated were discarded. The starter culture used was instant commercial *S. cerevisiae* (Merk "Fermipan", Societe Industrielle Lesaffre (SIL), France) purchased from the local market.

2.2. Fermentation of coffee beans

The red coffee cherries were peeled using a pulper machine to remove the cherry skin, then the coffee beans that still have mucilage were produced and ready for fermentation. The coffee beans were put in plastic jars. In *S. cerevisiae* fermentation, 5 mL of *S. cerevisiae* culture stock was added to the jar with a concentration of 9.32 log colony forming unit (CFU)/mL, while in spontaneous fermentation, the distilled water (5 mL) was added. Stock culture was prepared by adding 0.55 g of "Fermipan" (according to the instructions on the package) into 50 mL of BWP then incubated at 37°C for 24 h. Both *S. cerevisiae* and spontaneous fermentation were fermented for 24, 48, and 72 h (at ambient temperature, 28-30°C). After fermentation, the coffee beans were washed several times with running water before being dried in a cabinet dryer at 50°C for 18 h to produce green coffee beans, consist 12% of moisture content. From this experiment, 6 treatments were generated, i.e. A1 = fermented by *S. cerevisiae* for 24 h, A2 = fermented by *S. cerevisiae* for 48 h, A3 = fermented by *S. cerevisiae* for 72 h, B1= fermented by spontaneous for 24 h, B2= fermented by spontaneous for 48 h, B3= fermented by spontaneous for 72 h.

2.3. Coffee roasting, grinding, and brewing

The dried green bean was roasted to a medium-roasted level using a drum-type coffee roaster developed by Hidayat *et al.* (2020). The initial feeding temperature was 160°C, and the roasting duration was 7 min. After a week, the roasted coffee bean was ground using grinder (Philips HR73010, China). Brewing of ground coffee was conducted by SCAA (2015). A coffee powder (8.25 g) was placed in ceramic glass and added 150 mL hot water. A filter paper was used to remove the spent coffee ground; thus, the liquid coffee extract was obtained. The liquid coffee extract was then used for analysis which consisted of color, pH, phenolic compounds, total tannins, antioxidant activity, and caffeine. The coffee powder was also used and analysed for moisture content and color.

2.4. Total plate counts and total yeast

Total plate count (TPC) and Total Yeast (TY) were determined according to the SNI.19-2897-92 (BSN, 1992). A 10 mL of the liquid fermentation medium was dissolved in 90 mL of Buffered Peptone Water (BPW, Merck, Germany) then homogenized and diluted until 10^{-6}. Then, 1 mL was taken from dilution and placed in a petri dish. A Plate Count Agar media was poured for Total Plate Count analysis, while Potato Dextrose Agar (PDA, Merck, Germany) was poured for total yeast analysis. Incubation was carried out for 24-48 h at 37°C using incubator (BD400, Binder, Germany).

2.5. Moisture content and pH

Gravimetry method was used to determine the moisture content of the roasted coffee powder (AOAC, 2000) in triplicate on all samples. A pH meter (Lab 865, SI Analytics, Germany) was used to determine the pH of the liquid coffee extract.

2.6. Color parameters

The color of the coffee powder and the brewing coffee were measured according to Bicho et al.(2012) using CIE method (Chromameter, NH310, 3NH, China). The color was described according to L (lightness), a*(redness, red-green), and b* (yellowness, yellow-blue).

2.7. Analysis of total phenolic content, antioxidant activity, and caffeine

2.7.1. Total phenolic content

The total phenolic content of coffee extract was determined using Folin-Ciocalteu's method (Haile & Kang, 2020). About 100 µL of sample was diluted with distilled water in a vial. The diluted coffee sample was put in a dark vial, mixed with Folin-Ciocalteu's (Merck, Germany) phenol reagent (100 µL), and incubated for 8 min. After adding 300 µL of 20% Na2CO3 (Merck, Germany), the mixture was incubated for 2 h. Spectrophotometer (UV-Vis 1900, Shimadzu, Japan) was used to detect the absorbance at 765 nm. A plotting curved ($Y=0.077X-0.031$, $R^2= 0.996$) was created using gallic acid (Sigma Aldrich, USA) solutions with serial concentrations of 0, 10, 20, 30, 40, and 50 mg/L. The result was performed as mg Gallic Acid Equivalent per gram of sample (GAE)/ 100 mL.

2.7.2. Antioxidant activity DPPH radical scavenging

The antioxidant activity (DPPH radical scavenging) in the liquid coffee extract was determined according to Haile and Kang (2020). The sample (2 mL) was diluted to distilled water (10 mL). A sample of 800 µL was mixed with 3.2 mL of a 0.1 mM methanol (Merck, Germany)-DPPH (Sigma Aldrich, USA) solution. The mixture was kept in a dark area at room temperature for 30 mins. The sample's absorbance was measured at 515 nm with a spectrophotometer (UV-Vis 1900, Shimadzu, Japan). Ascorbic acid (Merck, Germany) solutions were utilized as the standard curve ($y=1.1341x-1.0471$, $R^2 = 0.999$). The antioxidant activity was quantified in mg/100 mL as Ascorbic acid (AAE).

2.7.3. Caffeine content

The caffeine content analysis was conducted according to Hainil *et al.* (2019). Amount of 2 g of coffee grounds and 150 mL of hot water were put into Erlenmeyer (250 mL) and stirred. Then, the hot coffee was filtrated with filter paper to obtain a liquid coffee extract and was added with 1.5 g of calcium carbonate (CaCO3, Merck, Germany) which was inserted into the separated funnel. The mixture was extracted using 25mL of chloroform (Merck, Germany) by three times, then the chloroform phase was evaporated to obtain the extract caffeine. The sample was added with 1 mL of distilled water and was measured using spectrophotometer UV-Vis 1900 (Shimadzu, Japan) at 200-400 nm. The plotting curve for the caffeine (Sigma Aldrich, USA) solution ($y=0.0502x+0.0014$, $R^2=0.99$) was used, with result expressed in ppm.

2.8. Data analysis

Analysis of Variance (ANOVA) and Duncan's Means Test (IBM SPSS Statistics 26) at a 95% confidence level were used to analyze the data. The PCA was employed to evaluate the relationship between dependent parameters derived in all treatments. The PCA analysis were performed in R-statistical software. Furthermore, interrelationships pattern between variable, and cluster of treatments were described by hierarchical clustering analysis (HCA) using R-statistical. The dependent variable data were standardized (range 0 to 1).

3. Result and discussion

3.1. Microorganisms of wet coffee fermentation

Figure 1 show the total microbes and total yeast during *S. cerevisiae* and spontaneous fermentation. The initial TPC and TY were about 5.86 log CFU/mL, which increased in 48 h to reach 7.87 and 7.96 log CFU/mL, and then dropped to 7.65 and 7.53 log CFU/mL, respectively, at the end of *S. cerevisiae* fermentation. Meanwhile, in spontaneous fermentation, the total microbes reached to 8.28 log CFU/mL at the end of fermentation. The population of yeast was similar to that of *S. cerevisiae* fermentation at the beginning, which reached to 8.24 log CFU/mL in 24 h, but subsequently declined significantly for the rest of the period of fermentation. In this study, the results were slightly different from previous studies which stated that the highest yeast population during spontaneous wet fermentation was 36 and 40 h *(*Elhalis *et al.,* 2020*;* Pereira *et al*., 2014). This might be due to differences in coffee varieties and also fermentation conditions such as temperature and pH.

Total microbes and total yeast in spontaneous fermentation was higher than *S. cerevisiae* fermentation. This occurs due to in spontaneous fermentation, microbial growth occurs naturally and uncontrollably according to the indigenous microorganisms present in coffee beans. Velmourougane (2013) stated that in the freshly pulped Robusta beans, the population of yeast is dominant followed by bacteria and fungi. Meanwhile, in *S. cerevisiae* fermentation, the addition of *S. cerevisiae* inoculum may inhibit the growth of bacteria, other types of yeast and fungi due to substrate competition.
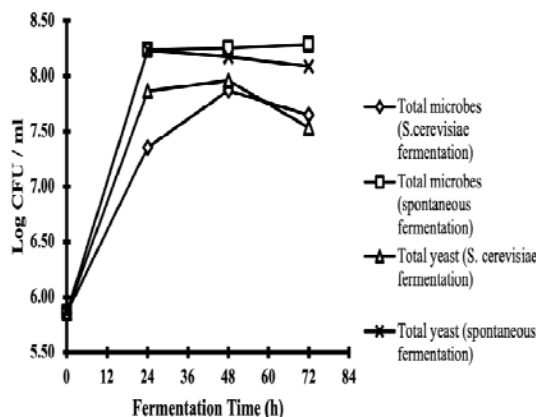
Figure 1. The growth of yeast during *S. cerevisiae* and spontaneous fermentation of the coffee fermented.

Table 1. Total plate counts, total yeast, and final pH of the coffee fermented for Subang.

Sample	TPC (log CFU/mL)	TY (log CFU/mL)	pH
A1	7.35±0.02[c]	7.86±0.07[c]	4.18±0.008[b]
A2	7.87±0.22[b]	7.96±0.22[bc]	4.17±0.07[b]
A3	7.64±0.04[b]	7.53±0.05[d]	4.17±0.08[b]
B1	8.24±0.16[a]	8.24±0.06[a]	4.12±0.02[b]
B2	8.25±0.06[a]	8.17±0.12[a]	4.23±0.01[b]
B3	8.28±0.21[a]	8.09±0.06[ab]	4.43±0.1[a]

The results are presented as mean ± standard deviation. Means in columns with different subscript showed significant differences (p < 0.05). A1-fermented by *S. cerevisiae* (24 h), A2-fermented by *S. cerevisiae* (48 h), A3-fermented by *S. cerevisiae* (72 h), B1-fermented by spontaneous (24 h), B2-fermented by spontaneous (48 h), B3-fermented by spontaneous (72 h).

The final pH of the coffee ranged from 4.12 to 4.23 (Table 1). The pH was decreased during the fermentation, where the initial value was 5.22. A similar observation by Velmourougane (2013) had been reported that the final pH of Robusta coffee was 4.05. A decline in pH occurred due to microbial activity which degraded complex organic compound like polysaccharide in mucilage into simpler sugar and acid components, promoting the growth of microorganisms that produce acids and enhancing coffee flavour. Vaz *et al.*(2022) stated that a long time of fermentation gave a pH decrease, and a combination of appropriate time and temperature of fermentation provided a higher pH decrease. The treatments using *S. cerevisiae* present a major pH reduction (compared to the initial pH), which was proven by the increase of total microbes and total yeast. Thus, the coffee flavour's richness enhances with the increasing diversity of microorganisms during fermentation, as indicated by the gradual decrease in pH values over time (Velmourougane, 2013; Wamuyu *et al.*, 2017).

A larger consortiums microorganism accelerates drying of layer the surface of coffee beans, causing rapid sugar leaching that affects coffee aroma, taste, and color. The fermentation produces acetic and lactic acid, which increase the acidity value in coffee. Additionally, the fermentation process produces alcohol and secondary metabolite like volatile compounds like isoamyl alcohol, phenylethyl alcohol, and aldehydes, which give sweet flavour and fruity aromas. These secondary metabolite are more abundant in combination fermentation compared to single fermentations (Elhalis *et al.*, 2021; Mahingsapun *et al.*, 2022; Zafar *et al.*, 2021).

3.2. Chemical properties of coffee fermentation

The moisture content of coffee was not significantly different in all treatments (ranging from 1.02 to 1.32%), as shown in Table 2. Fermentation has been reported not to affect the moisture content change in coffee bean (Kwak *et al.*, 2012), green coffee bean (Haile & Kang, 2019b), fermented coffee (Kwak *et al.*, 2018) and cascara (Kristanti *et al.*, 2022). This finding is consistent with an investigation performed by (Kristanti and Ratnawati, 2022) which stated that fermentation in the different type of microorganism was not caused the different in moisture content. This occurred due to the drying process performed after fermentation. The moisture content of coffee powder was 1.29-1.80 % (w/w) (Pittia *et al.*, 2007).

The color of the wet coffee powder is shown in Table 3. The lightness of the coffee powder ranged from 29.26-33.16 while the redness value ranged from 1.19-1.96. The duration of fermentation affected the color, where the longer duration produced lower color value both *S. cerevisiae* and spontaneous. This result is in line with (Haile and Kang, 2020) which stated that color properties such as L, a*, and b* values of fermented coffee was lower than non-fermented coffee. This evidence also happened in coffee fermented with different types of *Saccharomyces* in the study by Kwak *et al.* (2018). The color changed during fermentation due to hydrolysis of phenolic compounds (Afoakwa *et al.*, 2008).

Table 2. Moisture content and color profile of wet coffee powder of fermentation *S. cerevisiae* and spontaneous.

Samples	Moisture content(%)	L	a*	b*
A1	1.32±[a]	33.16±0.13[a]	1.96±0.16[a]	3.92±0.22[a]
A2	1.13±[a]	32.86±0.30[ab]	1.49±0.06[b]	3.66±0.06[ab]
A3	1.02±[a]	32.71±0.34[b]	1.33±0.22[b]	3.52±0.04[ab]
B1	1.29±[a]	29.26±0.21[d]	1.30±0.24[b]	3.39±0.32[b]
B2	1.15±[a]	31.92±0.05[c]	1.19±0.36[b]	3.37±0.37[b]
B3	1.15±[a]	31.93±0.28[c]	1.22±0.09[b]	3.34±0.26[b]

The results are presented as mean ± standard deviation. Means in columns with different subscript showed significant differences (p < 0.05). A1-fermented by *S. cerevisiae* (24 h), A2-fermented by *S. cerevisiae* (48 h), A3-fermented by *S. cerevisiae* (72 h), B1-fermented by spontaneous (24 h), B2-fermented by spontaneous (48 h), B3-fermented by spontaneous (72 h).

Table 3 presents the pH and color of brewed coffee, where the pH and color parameters show significantly different results. In both types of fermentation, the pH of brewed coffee showed a decrease in value (significantly different) as the fermentation time increased. Fermentation reduced pH because fermentation converts complex sugars into simple sugars and acidic components. The Millard reaction takes place during roasting when sugar interacts with amino acid in the absence of an enzyme. However, sugar plays a crucial role in the formation of aliphatic acid, which include formic, acetic, glycolic, and lactic acid (Wei and Tanokura, 2015). Research by Bressani *et al.* (2021) showed that fermentation with *S. cerevisiae* produces pyrazine, lactone, furan, and furanone compounds through the Maillard reaction. Fermented natural coffee and pulped natural fermented coffee have acidity, medium to high sweetness, with malic acid dominating in natural coffee and citric acid in pulped coffee. This supports the finding that fermentation has an impact on acid in coffee brew

The lightness value (L*) of brewed coffee produced by spontaneous fermentation was significantly higher than fermented by *S. cerevisiae* (Table 3). The increase in fermentation period caused the decline of lightness values of brewing coffee fermented by both spontaneous and *S. cerevisiae*. These results indicated that the brewed coffee fermented by spontaneously color was brighter than fermented by *S. cerevisiae*. Moreover, the longer fermentation time caused the darker brewed coffee in both fermentation types. The redness (a*) and yellowness (b*) values of coffee fermented by *S. cerevisiae* were significantly higher than those fermented spontaneously.

This indicated that the *S. cerevisiae* fermentation treatment produced a redder and yellower color of coffee. A similar study conducted by (Kwak *et al.*, 2012) and (Kristanti *et al.*, 2022) found that the yeast fermentation had a higher redness and yellowness values than spontaneous fermentation. The redness and yellowness values of coffee powder fermented by spontaneously from 48 to 72 h was increased. This phenomenon indicates that the fermentation time caused the redder and yellowness. According to Kristanti *et al.* (2022), the increasing of fermentation time affected the increase of lightness, redness, and yellowness values in Robusta cascara. The fermentation affected the increase of yellowness value in green coffee bean with medium roasted treatment (Haile and Kang, 2020).

Table 3. The pH value and color profile of brewed coffee fermented by *S. cerevisiae* and spontaneously.

Sample	pH	L	a*	b*
A1	5.66±0.09 [ab]	15.13±0.03[c]	2.40±0.12[a]	4.94±0.02[a]
A2	5.58±0.02 [b]	14.09±0.01[d]	1.79±0.11[c]	4.92±0.02[a]
A3	5.58±0.05 [b]	14.08±0.05[d]	1.64±0.07[d]	4.89±0.03[a]
B1	5.75±0.07 [a]	25.60±0.01[a]	1.37±0.02[e]	3.24±0.02[c]
B2	5.59±0.003 [b]	25.60±0.008[a]	1.35±0.05[e]	3.26±0.03[c]
B3	5.64±0.03[b]	22.65±0.02[b]	2.15±0.01[b]	3.81±0.08[b]

The results are presented as mean ± standard deviation. Means in columns with different subscript showed significant differences (p < 0.05). A1-fermented by *S. cerevisiae* (24 h), A2-fermented by *S. cerevisiae* (48 h), A3-fermented by *S. cerevisiae* (72 h), B1-fermented by spontaneous (24 h), B2-fermented by spontaneous (48 h), B3-fermented by spontaneous (72 h).

3.3. The total phenolic content, DPPH radical scavenging, and caffeine content

In general, total phenolic content (TPC) was significantly different (p<0.05), and the highest TPC value was achieved through spontaneous fermentation, but both 48-h fermentation treatments (A2 and B2) resulted in TPC valued exceeding 390 GAE mg/100mL. Duration of fermentation, both spontaneous and *S. cerevisiae* fermentation, showed an increase in phenolic content, consistent with Tan et al. (2023) research that phenolic compounds are released and form chlorogenic acid, primary phenolic component in roasted coffee beans. Polyphenol are bound to polysaccharide or protein complexes through glycosidic or peptide bonds, respectively. During fermentation, microorganisms break these bond, breaking down phenolic components into smaller compounds, releasing phenolics from the food complex and increasing free phenolic (Wamuyu *et al.*, 2017; Yang *et al.*, 2023). Coffee contains phenolic compounds that are primarily chlorogenic acids with 5-O-caffeoyl-quinic acid, such as caffein, ferulic, p-coumaric, caffeoylquinic acid, 3-feruloylquinic acid, di-caffeoyl-quinic acid, and proanthocyanidin (Parras *et al.*, 2007). However, duration of fermentation lead to a decrease in phenolic content (B3). This finding was consistent with earlier investigations on green coffee bean (Haile and Kang, 2019a), and Robusta cascara (Kristanti *et al.*, 2022). It was reported that the phenolic content decreased as yeast fermentation time increased. The phenolic compounds may degrade into other component due to the fermentation process.

The DPPH values in Table 4 showed significant differences (p<0.05). The DPPH inhibition of coffee increased in *S. cerevisiae* and spontaneous fermentation treatments for 48 h but decreased after 72 h of fermentation. Generally, the DPPH values for spontaneous fermentation were higher than those for *S. cerevisiae* fermentation. This revealed that 48 h of fermentation was the optimal time to the increase antioxidant activity of coffee processed under wet processing method. This study found was in accordance with Haile and Kang (2020), where the DPPH inhibitor of medium roasted coffee was increased after fermentation for 24 h. According to Zofia *et al.* (2020), increasing the fermentation period has an influence on the increasing of DPPH inhibitor green coffee kombucha fermented.

Table 4. Total phenolic content, DPPH radical scavenging, and caffeine content of fermented coffee.

Sample	Total phenolic content (GAE mg/100 mL)	DPPH radical scavenging (AAE mg/100 mL)	Caffeine content(ppm)
A1	360.25±9.47[bc]	2241.80±19.49[d]	9.50±0.05[a]
A2	394.29±16.26[b]	2341.78±35.75[b]	6.00±0.02[d]
A3	365.40±25.67[bc]	2295.39±6.38[c]	4.03±0.18[e]
B1	350.89±1.28[c]	2295.71±11.37[c]	7.89±0.08[b]
B2	463.32±5.51[a]	2480.41±10.14[a]	6.30±0.11[c]
B3	444.08±26.91[a]	2291.49±9.36[c]	6.10±0.05[bc]

The results are presented as mean ± standard deviation. Means in columns with different subscript showed significant differences (p < 0.05). A1-fermented by *S. cerevisiae* (24 h), A2-fermented by *S. cerevisiae* (48 h), A3-fermented by *S. cerevisiae* (72 h), B1-fermented by spontaneous (24 h), B2-fermented by spontaneous (48 h), B3-fermented by spontaneous (72 h).

The caffeine content of the extract fermented coffee is shown in Table 4, and the caffeine ranged from 4.03-9.50 ppm. The highest value was A1 while the lowest was A3. Furthermore, A1 and B1 (fermented for 24 h) produced the highest caffeine compared to the others. The treatments showed that the caffeine content significantly decreased with the increase in fermentation period, where the lowest was obtained in A3 treatment (with *S. cerevisiae* for 72h). Caffeine, as the fermentation time increases, can be degraded by fungi, bacteria, or yeast into uric acid, 7-methylxanthine, and xanthine or dimethyl xanthine (Lakshmi *et al.*, 2013; Mardhatilah *et al.*, 2023; Oktavianawati *et al.*, 2020). This result in this study is in line with a previous study conducted by Mardhatilah *et al.* (2023) which reported that fermentation of Arabica coffee during 30 h using yeast starter reduced caffein content. Due to its weak mannosidic base, caffeine readily breaks down in acidic environments, where it will produce unstable salts. Caffeine content, according to the Food Drug Administration (FDA), should not be more than 0.1% by weight (Health, 2003). The caffeine of Robusta green bean was 1.7-4 %, which is higher than the caffeine of Arabica green bean (0.8-1.4%) (Belitz *et al.*, 2009).

3.4. Principal component analyses and hierarchical clustering analyses

The PCA of the physicochemical of fermented coffee can be seen in Figure 2. Relationship of dependent variables was visualized by either PC1 and PC2 that had

total of 82.48 % in which PCA 1 and PCA2 were 44.14 % and 38.34 %, respectively. The a* value, moisture, total phenolic content, and caffeine content were negatively correlated with TPC and DPPH radical scavenging. Furthermore, the total yeast (TY), lightness (L value), and pH had no correlation with other parameters except the b* value, where the b* value negatively correlated with those parameters.
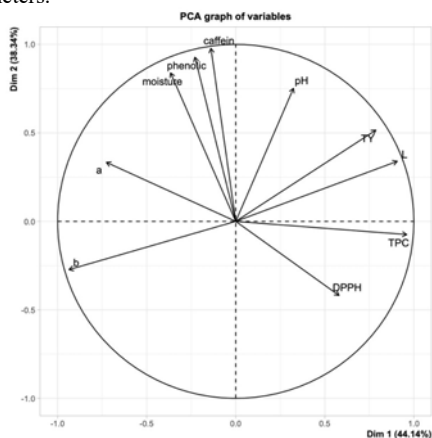
Figure 2. PCA biplot of dependent variables of coffee wet process fermented.

The hierarchical cluster analysis (HCA) was visualised in Figure 3. The HCA found that the fermented coffee was clearly clustered by the type of fermentation (*S. cerevisiae* and spontaneous). The first group was B1 and B2 even thought B3 was solo clustered. The TPC, TY, and L of B1 and B2 was scored of 1 while phenol and moisture were identified score of 0.4 ≥ or ≥ 0.5. In the second group, the samples were clustered with A2 and A3, but A1 was clustered alone due to its the total phenolic, moisture, caffeine, and a* value were higher (score :1). In this case, the HCA interpreted the result of dependent variables that was similar with PCA result. Cluster I contained TPC, TY, L, and DPPH, while Cluster II contained total phenolic, moisture, caffeine, a* value, and pH; and Cluster III was b* value.
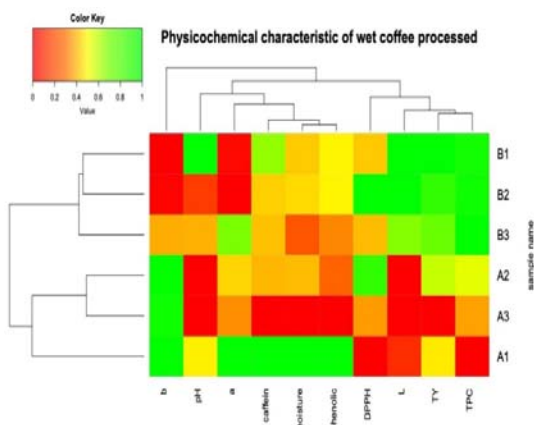
Figure 3. Hierarchical cluster analysis (HCA) of physicochemical of fermented coffee. The color of the tile indicated the strength of the correlations. The green color indicated major while the red indicated minor.

4. Conclusion

Robusta coffee which was fermented using *S. cerevisiae* and spontaneously in the wet processing method had a moisture content of 1.02-1.32%. Total microbes and total yeast in spontaneous fermentation were greater than *S. cerevisiae* fermentation. The caffeine content of the coffee dropped during the fermentation, and the fermentation treatment using *S. cerevisiae* for 42 h produced the lowest caffeine (ppm). The phenolic content during fermentation of coffee declined though the DPPH increased. Although the fermentation treatments reduced bioactive compounds (total phenolic content, DPPH radical scavenging, and caffeine content), the bioactive compounds of spontaneous fermentation were not remarkably as declined as fermented by *S. cerevisiae*. In addition, the fermentation time increased the total microbes and total yeast, while the color of the product became yellowish. Based on the PCA and HCA, the coffee fermented by *S. cerevisiae* and spontaneous was disparate to total plate count, total yeast, b* value, lightness, total phenolic content, and caffeine content.

Conflict of Interests

The authors declare that they have no conflicting interests.

Highlights:

- The fermentation of de-pulped Robusta coffee beans using with and without *S. cerevisiae* change of coffee quality.
- The fermentation treatments reduced bioactive compounds (total phenolic content, DPPH radical scavenging, and caffeine content).
- The antioxidants of spontaneous treatments were not remarkably as decline as the fermented *S. cerevisiae* treatment had.
- Based on the PCA, the coffee wet process fermented by *S. cerevisiae* and spontaneous were disparate to total plate count, total yeast, b* value, lightness, total phenolic content, and caffeine content.

References

Afoakwa EO, Paterson A, Fowler M, and Ryan A. 2008. Flavor formation and character in cocoa and chocolate: A critical review. *Crit Rev Food Sci Nutr*, **48**(9), 840–857. https://doi.org/10.1080/10408390701719272

AOAC. 2000. **Official Methods of Analysis. Method 930.15**. AOAC International Gaithersburg, MD.

Belitz HD, Grosch W, and Schieberle P. 2009. **Food Chemistry**. In *springer*. https://doi.org/10.1201/b18894-16, Berlin.

Bicho NC, Leitão AE, Ramalho JC, and Lidon FC. 2012. Use of colour parameters for roasted coffee assessment. *Ciencia Tecnol Alime*, *32*(**3**), 436–442. https://doi.org/10.1590/S0101-20612012005000068

Bressani APP, Martinez SJ, Sarmento ABI, Borém FM, and Schwan RF. 2021. Influence of yeast inoculation on the quality of fermented coffee (Coffea arabica var. Mundo Novo) processed by natural and pulped natural processes. *Int J Food Microbiol*, *343*(January). https://doi.org/10.1016/j.ijfoodmicro.2021.109107

BSN. 1992. **SNI 19-2897-1992 Cara Uji Cemaran Mikroba**, Jakarta

Elhalis H, Chin XH, and Chow Y. 2023. Soybean fermentation: Microbial ecology and starter culture technology. *Crit Rev Food Sci Nutr*, *0*(**0**), 1–23. https://doi.org/10.1080/10408398.2023.2188951

Elhalis H, Cox J, Frank D, and Zhao J. 2020. The crucial role of yeasts in the wet fermentation of coffee beans and quality. *Int J Food Microbiol*, *333*(May), 108796. https://doi.org/10.1016/j.ijfoodmicro.2020.108796

Elhalis H, Cox J, Frank D, and Zhao J. 2021. Microbiological and Chemical Characteristics of Wet Coffee Fermentation Inoculated With Hansinaspora uvarum and Pichia kudriavzevii and Their Impact on Coffee Sensory Quality. *Front Microbiol*, *12*(August), 1–13. https://doi.org/10.3389/fmicb.2021.713969

Elhalis H, Cox J, and Zhao J. 2020. Ecological diversity, evolution and metabolism of microbial communities in the wet fermentation of Australian coffee beans. *Int J Food Microbiol*, *321*(November 2019), 108544. https://doi.org/10.1016/j.ijfoodmicro.2020.108544

Haile M and Kang WH. 2019a. Antioxidant activity, total polyphenol, flavonoid and tannin contents of fermented green coffee beans with selected yeasts. *Ferment*, *5*(**1**). https://doi.org/10.3390/fermentation5010029

Haile M and Kang WH. 2019b. The Role of Microbes in Coffee Fermentation and Their Impact on Coffee Quality. *J Food Qual*, *2019*. https://doi.org/10.1155/2019/4836709

Haile M and Kang WH. 2020. Antioxidant Properties of Fermented Green Coffee Beans with Wickerhamomyces anomalus (Strain KNU18Y3). *Ferment*, *6*(**1**), 1–16. https://doi.org/10.3390/fermentation6010018

Hainil S, Suhaera S, and Lirtri L. 2019. Quantitative Analysis of Caffeine Levels in Local Coffee (Coffea sp) Powder on Dabo Island with UV-Vis Spectrophotometry. *Borneo J Pharm*, *2*(**2**), 82–86. https://doi.org/10.33084/bjop.v2i2.897

Health MofP. 2003. **Coffee** *FDA* (Vol. 2541, Issue **182**).

Hidayat DD, Sudaryanto A, Kurniawan YR, Indriati A, and Sagita D. 2020. Development and evaluation of drum coffee roasting machine for small-scale enterprises. *INMATEH - Agri Eng*, *60*(**1**), 79–88. https://doi.org/10.35633/INMATEH-60-09

Jamil AS. 2019. Daya Saing Ekspor Kopi di Pasar Global. *Agrisocionomics J Agri Soc Econ Policy*, *8*(**1**), 26–35.

Jimenez EJM, Martins PMM, Vilela ALdeO, Batista NN, Rosa S DVFda, Dias DR, and Schwan RF. 2023. Influence of anaerobic fermentation and yeast inoculation on the viability, chemical composition, and quality of coffee. *Food Biosci*, *51*(November 2022). https://doi.org/10.1016/j.fbio.2022.102218

Karim MA, Wijayanti F, and Sudaryanto A. 2019. Comparative studies of coffee processing methods for decision making in

appropriate technology implementation. *AIP Conf*, *2114*(June 2019). https://doi.org/10.1063/1.5112399

Kristanti D and Ratnawati L. 2022. Physicochemical and Functional Properties of Fermented Adlay (Coix lacryma jobi-L) Flour. *IOP Conf Ser Earth Environ Sci*, *1024*(**1**). https://doi.org/10.1088/1755-1315/1024/1/012026

Kristanti D, Setiaboma W, Ratnawati L, and Sagita D. 2022. Robusta coffee cherry fermentation: Physicochemical and sensory evaluation of fermented cascara tea. *J Food Process Preserv*, *August*, 1–9. https://doi.org/10.1111/jfpp.17054

Kwak HS, Jeong Y, and Kim M. 2018. Effect of Yeast Fermentation of Green Coffee Beans on Antioxidant Activity and Consumer Acceptability. *J Food Qual*, *2018*. https://doi.org/10.1155/2018/5967130

Kwak JH, Paik JK, Kim HI, Kim OY, Shin DY, Kim HJ, Lee J H, and Lee JH. 2012. Dietary treatment with rice containing resistant starch improves markers of endothelial function with reduction of postprandial blood glucose and oxidative stress in patients with prediabetes or newly diagnosed type 2 diabetes. *Atheroscler*, *224*(**2**), 457–464. https://doi.org/10.1016/j.atherosclerosis.2012.08.003

Lakshmi V, Das D, and Das N. 2013. Biodegradation of caffeine by the yeast Trichosporon asahii immobilized in single and hybrid matrices. *Indian J Chem Technol*, *20*(**3**), 195–201.

Lee LW, Cheong MW, Curran P, Yu B, and Liu SQ. 2015. Coffee fermentation and flavor - An intricate and delicate relationship. *Food Chem*, *185*, 182–191. https://doi.org/10.1016/j.foodchem.2015.03.124

Mahingsapun R, Tantayotai P, Panyachanakul T, Samosorn S, Dolsophon K, Jiamjariyatam R, Lorliam W, Srisuk N, and Krajangsang S. 2022. Enhancement of Arabica coffee quality with selected potential microbial starter culture under controlled fermentation in wet process. *Food Biosci*, *48*(May), 101819. https://doi.org/10.1016/j.fbio.2022.101819

Mardhatilah D, Padama F, and Ngatirah. 2023. Development of sustainable arabica coffee fermentation using yeast starter. *IOP Conf Ser Earth Environ Sci*, *1241*(**1**). https://doi.org/10.1088/1755-1315/1241/1/012078

Oktavianawati I, Arimurti S, and Suharjono S. 2020. The Impacts of Traditional Fermentation Method on the Chemical Characteristics of Arabica Coffee Beans from Bondowoso District, East Java. *J Pure Appl Chem Res*, *9*(**2**), 133–141. https://doi.org/10.21776/ub.jpacr.2020.009.02.526

Parras P, Martínez-Tomé M, Jiménez AM, and Murcia MA. 2007. Antioxidant capacity of coffees of several origins brewed following three different procedures. *Food Chem*, *102*(**3**), 582–592. https://doi.org/10.1016/j.foodchem.2006.05.037

Pereira GVdeM, Neto E, Soccol VT, Medeiros ABP, Woiciechowski AL, and Soccol CR. 2015. Conducting starter culture-controlled fermentations of coffee beans during on-farm wet processing: Growth, metabolic analyses and sensorial effects. *Food Res Int*, *75*, 348–356. https://doi.org/10.1016/j.foodres.2015.06.027

Pereira GVdeM, Soccol VT, Pandey A, Medeiros ABP, Andrade Lara JMR, Gollo AL, and Soccol CR. 2014. Isolation, selection and evaluation of yeasts for use in fermentation of coffee beans by the wet process. *Int J Food Microbiol*, *188*(July), 60–66. https://doi.org/10.1016/j.ijfoodmicro.2014.07.008

Pittia P, Nicoli MC, and Sacchetti G. 2007. Effect of moisture and water activity on textural properties of raw and roasted coffee beans. *J Texture Stud*, *38*(**1**), 116–134. https://doi.org/10.1111/j.1745-4603.2007.00089.x

Saerens S and Swiegers J. 2016. Enhancement of coffee quality and flavor by using pichia kluyveri yeast starter culture for coffee fermentation. *U S patent*, *US20160058028A1*.

SCAA. 2015. **SCAA Protocols Cupping Specialty Coffee**. Specialty Coffee Association of America, 1–10. http://www.scaa.org/?page=resources&d=coffee-protocols

Setyobudi RH, Atoum MFM, Damat D, Yandri E, Nugroho YA, Susanti MS, Wahono SK, Widodo W, Zalizar L, Wahyudi A, Saati EA, Maftuchah M, Hussain Z, Yono D, Harsono SS, Mahaswa RK, Susanto H, Adinurani PG, Ekawati I, and Mindarti S. 2022. Evaluation of Coffee Pulp Waste from Coffee Cultivation Areas in Indonesia as Iron Booster. *Jordan J Biol Sci*, *15*(**3**), 475–488. https://doi.org/10.54319/jjbs/150318

Sharma R, Garg P, Kumar P, Bhatia SK, and Kulshrestha S. 2020. Microbial fermentation and its role in quality improvement of fermented foods. *Ferment*, *6*(**4**), 1–20. https://doi.org/10.3390/fermentation6040106

Silva CF. 2014. Microbial activity during coffee fermentation. **Cocoa and Coffee Fermentations**, CFC Pres, UK, 368–423.

Sunarharum WB, Williams DJ, and Smyth HE. 2014. Complexity of coffee flavor: A compositional and sensory perspective. *Food Res Int*, *62*, 315–325. https://doi.org/10.1016/j.foodres.2014.02.030

Tan Y, Wu H, Shi L, Barrow C, Dunshea FR, and Suleria HAR. 2023. Impacts of Fermentation on the Phenolic Composition, Antioxidant Potential, and Volatile Compounds Profile of Commercially Roasted Coffee Beans. *Ferment*, *9*(**10**). https://doi.org/10.3390/fermentation9100918

Vaz CJT, Menezes LS, Santana RC, Sentanín MA, Zotarelli MF, and Guidini CZ. 2022. Effect of Fermentation of Arabica Coffee on Physicochemical Characteristics and Sensory Analysis. *3 Biotech*. **1–14**. https://doi.org/10.21203/rs.3.rs-1555586/v1

Velmourougane K. 2013. Impact of natural fermentation on physicochemical, microbiological and cup quality characteristics of Arabica and Robusta coffee. *Proc Nati Acad Sci India Sec B - Biol Sci*, *83*(**2**), 233–239. https://doi.org/10.1007/s40011-012-0130-1

Wamuyu, K. A., Richard, K., Beatrice, M., & Cecilia, K. (2017). Effect of Different Fermentation Methods on Physicochemical Composition and Sensory Quality of Coffee (Coffea arabica). *IOSR J Environ Sci Toxicol Food Technol*, *11*(**06**), 31–36. https://doi.org/10.9790/2402-1106023136

Wang C, Sun J, Lassabliere B, Yu B, and Liu SQ. 2020. Coffee flavour modification through controlled fermentations of green coffee beans by Saccharomyces cerevisiae and Pichia kluyveri: Part I. Effects from individual yeasts. *Food Res Int*, *136*(July). https://doi.org/10.1016/j.foodres.2020.109588

Wei F and Tanokura M. 2015. Chemical Changes in the Components of Coffee Beans during Roasting. **Coffee in Health and Disease Prevention**, December 2015, 83–91. https://doi.org/10.1016/B978-0-12-409517-5.00010-3

Wulandari S, Ainuri M, and Sukartiko AC. 2021. Biochemical content of Robusta coffees under fully-wash, honey, and natural processing methods. *IOP Conf Ser Earth Environ Sci*, *819*(**1**). https://doi.org/10.1088/1755-1315/819/1/012067

Yang F, Chen C, Ni D, Yang Y, Tian J, Li Y, Chen S, Ye X, and Wang L. 2023. Effects of Fermentation on Bioactivity and the Composition of Polyphenols Contained in Polyphenol-Rich Foods: A Review. *Foods*, *12*(**17**). https://doi.org/10.3390/foods12173315

Zafar M, Bano HS, and Anwar Z. 2021. Orange Peels Valorization For Citric Acid Production Through Single And Co-Culture Fermentation. *Jordan J Biol Sci*, *14*(**2**), 261–266. https://doi.org/10.54319/jjbs/140209

Zofia Nł, Aleksandra Z, Tomasz B, Martyna Z, and Tomasz W. 2020. Effect of Fermentation Time on Antioxidant and Anti-Ageing Properties of Green Coffee. *Molecules*, *25*.

One-Tube Preparation of Magnetic Nanoparticles Specifically Binding to Antibodies for Efficient Foodborne Pathogen Detection

Danh Thi Nguyen[1,2,3,4], Kien-Quang Huynh[1,2,3,4], Tan Tai Nguyen[5], Hieu Tran-Van[1,2,3,4,*]

[1]Laboratory of Biosensors, Faculty of Biology and Biotechnology, University of Science, Ho Chi Minh, Vietnam; [2]Department of Molecular and Environmental Biotechnology, Faculty of Biology and Biotechnology, University of Science, Ho Chi Minh, Vietnam; [3]Laboratory of Molecular Biotechnology, University of Science, Ho Chi Minh, Vietnam; [4]Vietnam National University, Ho Chi Minh, Vietnam; [5]Department of Materials Science, School of Applied Chemistry, Tra Vinh University, Tra Vinh Province, Vietnam

Abstract

In food processing and production, microbiological control is essential. However, complex food matrices and low microorganisms levels require effective sample pretreatment prior to a detection method. Although conventional immunomagnetic bead preparation is time-consuming and environmentally hazardous, immunomagnetic separation is a potential pretreatment technique. This study introduced a streamlined, eco-friendly one-tube 'Mix-and-Match' pretreatment using ProAx1-Fe3O4, a recombinant adapter protein that facilitates regioselective antibody attachment to magnetic nanoparticles. Western Blot and SDS-PAGE were used to confirm the expression of the protein. The nanoparticles coated with ProAx1-Fe3O4 exhibited enhanced stability and antibody binding. They successfully captured *Salmonella* when used with PCR for confirmation, providing a powerful pretreatment approach for identifying foodborne bacteria.

Keywords: Antibody, antibody functionalized magnetic nanoparticles, immobilized antibodies, immunomagnetic separation, magnetic nanoparticles, one-tube preparation.

1. Introduction

Foodborne poisoning, a major public health concern, has a global impact similar to that of HIV/AIDS, malaria, and tuberculosis (Havelaar *et al.*, 2015). The primary causes of food poisoning are pathogenic microorganisms or their toxins (Soto Varela *et al.*, 2016) (Bintsis and Thomas, 2017) (Marrez *et al.*, 2019). Rapid and sensitive detection methods are essential for the detection of these pathogens. Traditionally, cultivating microorganisms has been the most common method (Hassoun *et al.*, 2023), but it is time-consuming (taking five to six days) and requires strict safety protocols (Rodríguez *et al.*, 2018). To overcome these limitations, polymerase chain reaction (PCR) techniques, including standard PCR and Real-time PCR, have been developed to reduce detection time to 12-24 hours and offer high specificity (Hyeon and Deng, 2017) (Zueter and Harun, 2018). However, PCR requires sample enrichment to avoid false positives, which complicates the detection process due to the complexity of food matrices and the low density of pathogenic bacteria.

Immunomagnetic separation (IMS) has emerged as a simple pretreatment method for target bacteria separation and enrichment, providing good quality samples for PCR with high specificity (Hsu *et al.*, 2014). IMS involves capturing target microorganisms with antibody-coated magnetic nanoparticles (MPs) and separating them from the food matrix using magnetism. However, conventional methods for immobilizing antibodies onto MPs often result in protein denaturation or degradation, which reduces their effectiveness. Randomly immobilized antibodies are less effective at binding antigens than orientationally immobilized antibodies (Lu *et al.*, 1996). Therefore, orienting target molecules on the surface of nanoparticles is a key strategy for improving the performance of magnetic particles (Quinn *et al.*, 1999) (Lee *et al.*, 2013) (Gan *et al.*, 2023).

This study developed a novel recombinant adapter protein, ProAx1-Fe3O4 to facilitate antibody conjugation onto MP surfaces. ProAx1-Fe3O4 is a dual-binding protein with one domain specifically binds to ferromagnetic nanoparticles and another recognizes the fragment crystallizable (Fc) region of most immunoglobulins (IgGs). This approach allows the fragment antigen-binding (Fab) regions of IgGs to remain on the MPs surface, improving the effectiveness of antibody binding compared to random immobilization. By fusing the magnetite-binding peptide with protein A, this one-tube preparation method for antibody-specific magnetic nanoparticles offers a rapid, efficient, and straightforward 'Mix-and-Match' pretreatment for immunomagnetic particles (Fig. 1).

---

* Corresponding author. e-mail: tvhieu@hcmus.edu.vn.
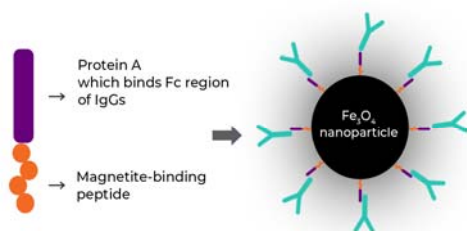
Figure 1. Schematic of 'Mix-and-Match' pretreatment immunomagnetic particles immobilizing antibodies using ProAx1-Fe3O4 binding protein.

2. Materials and Method

2.1. Construction of recombinant pET-proAx1-Fe₃O₄ binding

A DNA fragment encoding for the domain A of protein A was amplified from pET22b-proA plasmid (Tran-Nguyen *et al.*, 2021) by the overlap extension PCR method with specific primers including F-*Nde*I, R1, R2, and R-*Hind*III to generate the ProAx1-Fe₃O₄ binding encoding gene (Table 1). The overlapped reverse primers containing Fe₃O₄ binding peptide encoding gene in which the two Fe₃O₄ binding peptides (HYIDFRW and TVNFKLY) (You *et al.*, 2016) were linked by a GGSG linker. PCR product and plasmid pET22b were digested with the same enzymes *Nde*I and *Hind*III (Thermo Scientific) and ligated by T4 ligase. After that, the recombinant plasmid was chemically transformed into competent *E. coli* DH5α cells and screened with Luria-Bertani (LB-Amp) containing Ampicillin agar plate. The cloning results were experimentally confirmed by PCR colony method using T7 promoter and R-*Hind*III. Plasmid from positive colonies was extracted and sequenced by (PhuSa Biochem Ltd., Vietnam)

Table 1 List of primers used in this study

Primer's name	Primer sequence (5'-3')	Primer pair	Amplicon (bp)
F-*Nde*I	catatggacaacaaattcaacaaagaac		
R1	ccagcgaaaatcaatataatggtcgacggagctcg	F-*Nde*I + R1	261
R2	ttcacggtgccgctgccgcccccagcgaaaatcaat	F-*Nde*I + R2	281
R-*Hind*III	aagcttatacagtttaaagttcacggtgccgct	F-*Nde*I + R-*Hind*III	300
T7 promoter	cgaaattaatacgactcactatagg	T7 promoter + R-*Hind*III	391

Restriction enzymes indicate by underlined letters.

2.2. Expression and confirmation of recombinant ProAx1-Fe₃O₄ binding protein

The pET-proAx1-Fe₃O₄ binding plasmid was transformed into *E. coli* BL21(DE3) chemically competent cells and performed expression with optimum conditions, i.e. the concentration of 1 mM isopropyl β-d-1-thiogalactopyranoside (IPTG), shaking cultured at 25°C, speed of 250 revolutions per minute for 6 hours. The cell pellets were collected and disrupted by sonication on ice to collect proteins in total, supernatant, and pellet fractions, respectively. The protein fractions were analyzed by sodium dodecyl-sulfate polyacrylamide gel electrophoresis (SDS-PAGE) and confirmed by Western Blot and probed with 6xHis antibody (Santa Cruz) and goat anti-mouse IgG-HRP antibody (Proteintech).

2.3. Evaluation the MPs binding ability of ProAx1-Fe₃O₄ binding protein

The synthesis and properties of magnetic nanoparticles were described in (Thanh *et al.*, 2019). Briefly, superparamagnetic nanoparticles were synthesized in the size range of 10-30 nm and were characterized using Transmission Electron Microscope (TEM) and X-Ray diffraction (XRD) to assert their structure and properties. The ProAx1- Fe₃O₄ binding in the total protein fraction was mixed with 25 µL of magnetic particles at 4 °C in 45 minutes for testing binding capability. The particles were collected by the magnetic bar and were washed with phosphate-buffered saline (PBS) solution thrice. Then, the particles were re-washed in 100 µL of PBS and well-vortexed for 20 minutes to test durability. Finally, the solution after incubation with nanoparticles, wash solution, and nanoparticles after washing were collected, treated with loading buffer 6X, and heated at 100 °C for 10 minutes. The binding ability was tested by SDS-PAGE with silver-stained. Non-purified ProAx1- Fe₃O₄ binding and magnetic beads were loaded onto the gel as controls.

2.4. Antibody capturing

The ProAx1-Fe₃O₄ binding-coated magnetic beads (volume of 100 µL) obtained from the previous experiment were mixed with the antibodies that match with the pathogen of interest at 4 °C and for the binding time of 45 minutes to evaluate antibody binding ability. In this study, the *Salmonella* O antiserum Poly A (OMA) (BD Difco) was used. The nanoparticles were magnetically collected and washed twice with PBS. A protein uncoated nanoparticles sample was also performed as a control. After that, all samples were prepared and analyzed by SDS-PAGE with silver staining.

2.5. Testing the ability to detect Salmonella enterica ser. Enteritidis on culture samples

The *Salmonella enterica* ser. Enteritidis (*Salmonella* Enteritidis) used for detection ability testing of MPs in this study was kindly provided by National Agro-Forestry-Fisheries Quality Assurance Department Branch (NAFIQAD) 4. In brief, the *Salmonella* Enteritidis suspension cultured overnight in 37 °C was centrifuged and discarded supernatant. The pellet then was washed thrice and resuspended in 1 mL PBS. After that, the suspension was divided into two samples: (1) was mixed with the MPs conjugated with the polyvalent anti-OMA antibodies, and (2) was mixed with the MPs. Both of them were incubated in room temperature, 30 minutes. Subsequently, the MPs were collected using a magnetic bar and then washed three times with PBS. The MPs were resuspended in 50 µL double-distilled water (ddH₂O) and then heated in 95 °C, 10 minutes to release the microorganisms. Supernatant was separated by using a magnetic bar and used as samples to perform PCR method to detect *Salmonella* Enteritidis with the specific primers for the *inv*A gene.

3. Results and Discussion

3.1. Characterization of magnetic nanoparticles

Figure 2A represented the XRD pattern of the synthesized magnetic nanoparticles based on co-

precipitation method. As shown in Figure 2A, the crystalline nature of synthesized magnetic nanoparticles showed six recognizably different peaks at (220), (311), (400), (511), and (440), which are consistent with the expected composition of Fe_3O_4. The relative intensity and position of diffraction peaks for the pattern mentioned was matched with the database in JCPDS file (No. 01-075-1373) for bulk Fe_3O_4. To examine the size of the nanoparticles, we also performed TEM images of Fe_3O_4 nanoparticles. Figure 2B shows TEM images of the synthesized magnetic nanoparticles, which have an average size of 30 nm. Notably, the Fe3O4 nanoparticles are cubic or octahedral in shape and are monodisperse, which enhances their potential for biomedical applications.
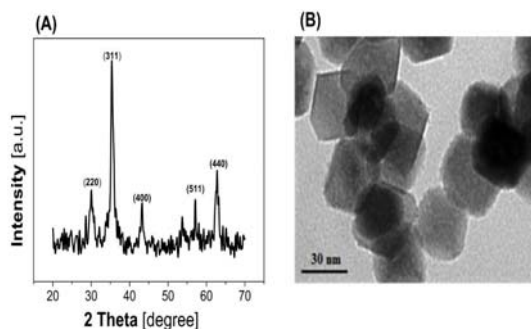
Figure 2. Characterization of synthesized magnetic nanoparticles. (A) XRD patterns and (B) TEM image of the nanoparticles.

3.2. Cloning and expression of ProAx1-Fe₃O₄ binding

Amplicons at 353 bp were obtained by PCR reaction using T7pro and R-*Hind*III primer. Negative control did not have any band, which indicated that there was no contamination in the PCR reaction. Results from sequenced data confirmed the amplified product was identical with published sequences from GenBank and the proAx1-Fe₃O₄ binding gene was cloned in the frame (data not shown). This experimental result showed that the recombinant plasmid was successfully constructed.

The recombinant protein ProAx1-Fe₃O₄ binding was induced from *E. coli* BL21(DE3)/pETT22b-proAx1-Fe₃O₄ binding for expression with a molecular weight of approximately 14.4 kilo Dalton (kDa) that was confirmed by SDS-PAGE analysis. Figure 4 shows an overexpressed protein band at approximately 14.4 kDa in the total protein fraction (Fig. 4A, lane 3). No band was observed in the negative control (Fig. 3A, lanes 1-2), confirming that the protein band in lane 3 corresponds to ProAx1-Fe3O4 binding. Additionally, an overexpressed protein band was present in the supernatant fraction (Fig. 4A, lane 4) but not in the pellet fraction (Fig. 3A, lane 5), indicating that the target protein was solubly expressed. This was further confirmed by Western Blot analysis, which detected the protein in the total and supernatant fractions using an anti-His antibody (Fig. 3B, lanes 3-4). Therefore, the ProAx1-Fe3O4 binding protein with a 6xHis tag was successfully expressed.
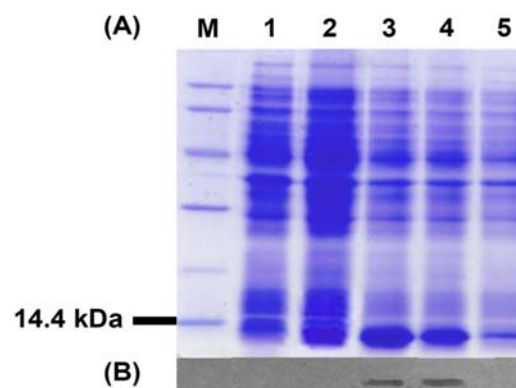
Figure 3. Coomassie blue staining of ProAx1-Fe₃O₄ binding protein expression analyzed by SDS-PAGE on 12.5% gel (A) and confirmed by Western blot probed with 6xHis (B). M, Low range weight protein marker, 97–14.4 kDa; 1, *E. coli* BL21(DE3)/pET22b (+ITPG); 2, *E. coli* BL21(DE3)/pET22b proAx1-Fe₃O₄ binding (-IPTG); 3-5, *E. coli* BL21(DE3)/pET22b proAx1-Fe₃O₄ binding (+IPTG); 3, total protein fraction; 4, supernatant protein fraction; 5, pellet protein fraction.

3.3. Evaluation the binding ability to magnetic nanoparticles

Practically, MPs size is bigger than the pore size of 15% polyacrylamide gel, so the MPs cannot migrate into SDS-PAGE gel. As shown in Figure 4, a single protein band (lane 9) at approximately 14.4 kDa presented in the particle sample after washing and vortexing, equal to the molecular weight of ProAx1-Fe₃O₄ binding (Fig. 4, lane 2), whereas no band was detected in lane 1. After mixing, it can be seen that the majority of proteins were bound to particles, and a minor residual ones remained in the supernatant after removing the particles (Fig. 4, lane 3-8). This demonstrated that ProAx1-Fe₃O₄ binding protein was able to bind to MPs strongly and their conjugate was stable under normal and harsh washing conditions (vortex for 20 minutes). Only one single band of ProAx1-Fe₃O₄ binding protein in lane 9 revealed this protein bound specifically to MPs with ease, which suggested that this protein can be used directly after expression without many steps of purification process in large scale.
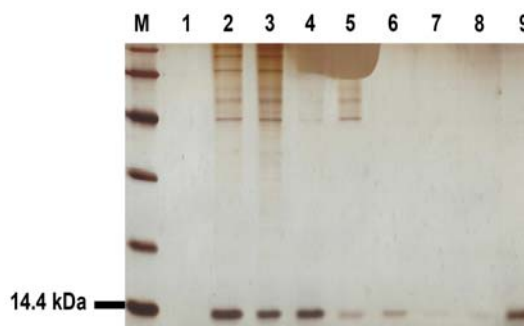
Figure 4. The binding ability to magnetic nanoparticles of ProAx1-Fe₃O₄ binding. M, Low range weight protein marker 97–14.4 kDa; 1, uncoated particles; 2, ProAx1-Fe₃O₄ binding in the total protein fraction after expression; 3, protein and particles before mixing; 4, particles after mixing; 5, supernatant fraction after mixing and removing particles; 6-7, wash fractions; 8, wash and vortex fraction; 9, particles after washing and vortexing.

3.4. Antibody capturing assessment

After testing the binding ability to MPs, the recombinant protein was continued to assess the antibody capturing ability. MPs were subjected to the gel but not shown any protein band (Fig. 5A, lane 1 and Fig. 5B, lane 1). The molecular weight of antibody fragments is approximately 25 kDa and 50 kDa (Fig. 5A, lane 2, and Fig. 5B, lane 3). They formed distinct bands compared to the molecular weight of ProAx1-Fe$_3$O$_4$ binding on the gel (Fig. 5B, lane 4 and 6). In the SDS-PAGE gel, there were a ProAx1-Fe$_3$O$_4$ binding band and two antibody fragment bands in particles after the washing step (Fig. 5B, lane 9), while there was no visible band in wash fractions (Fig. 5B, lane 7-8). This indicated the antibodies were successfully captured. Figure 5A also showed that after mixing with antibodies without the support of ProAx1-Fe$_3$O$_4$ binding protein, the particles were unable to capture antibodies. Consequently, all the amount of antibodies remained in the supernatant (Fig. 5A, lanes 3-5). It can be seen that a negligible amount of antibody appeared after the first washing step (Fig. 5A, lane 6), but it was totally removed after the second step (Fig. 5A, lane 7), which is explained as unspecific bonds between particles and antibodies. After two washing steps, there was no visible band in lane 8; hence, the uncoated particles cannot bind to antibodies (Fig 4A, lane 1, and lane 8). It could also be inferred that the ProAx1-Fe$_3$O$_4$ binding protein was not only able to capture antibodies but also retained the ability to strongly bind to particles under harsh washing conditions.

(A)

(B)
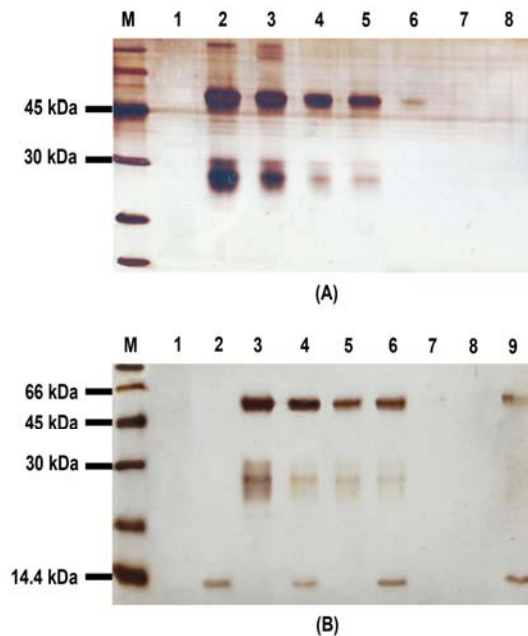
Figure 5. Antibody capturing assessment of uncoated MPs (A) and of ProAx1-Fe$_3$O$_4$ binding coated MPs (B). M, Low range weight protein marker, 97–14.4 kDa; A: 1, uncoated particles; 2, anti-OMA; 3, anti-OMA+particle before mixing; 4, particles after mixing; 5, supernatant after mixing; 6-7, wash fractions; 8, particles after wash; B: 1, uncoated particles; 2, coated particles; 3, anti-OMA; 4, anti-OMA+coated particle before mixing; 5, supernatant after mixing; 6, particles after mixing; 7-8, wash fractions; 9, particles after wash.

Previously, to attach specific antibodies to magnetic nanoparticles, chemical functional groups such as -NH$_2$, -Carbonyldiimidazole were widely used to immobilize protein A on the surface of MPs (Huynh *et al.*, 2020) (Ta *et al.*, 2016). The binding process of these groups is under investigation; the -Carbonyldiimidazole functional group can only react in organic solvents and is easily hydrolyzed in water (Ta *et al.*, 2016). The process of binding these functional groups is also time-consuming. In contrast, the interaction between Fe$_3$O$_4$ binding peptide and MPs (Fe$_3$O$_4$) was mainly formed via electrostatic interaction between iron ions with hydroxyl and carbonyl radicals (Li *et al.*, 2019). Therefore, under strong denaturing agents and harsh conditions such as SDS and high temperature (100 °C), the bound was easily broken. This is convenient for the control and regeneration of MPs. Moreover, protein A is a protein encoded by the *spa* gene with five IgG binding domains (Jansson *et al.*, 1998), which capture Fc region of IgG thereby leaving the Fab regions of IgG flexible when conjugate onto MPs surface. By selecting the strongest A domain, the ProAx1-Fe$_3$O$_4$ binding-coated MPs is possible to bind most antibodies from mammalian species, and notably IgGs, thus leading to act as a model 'Mix-and-Match' immune-magnetic, used for a variety of microorganisms.

3.5. Detection of Salmonella from culture media by PCR-coupled immune-magnetic beads

The results of PCR product electrophoresis on agarose gel in Figure 6 showed that the amplified product from magnetic conjugated anti-OMA antibody (Fig. 6, lane 2) appeared in a band between 200 bp and 400 bp, corresponding to the expected fragment of 285 bp for *Salmonella* gene (Fig. 6, lane 1). Negative control did not have any band (Fig. 6, lane 3). These results indicated that the immune-magnetic separation could be well fit for most polymerase chain reactions for *Salmonella* detection from the culture sample, creating a platform for the application of microorganisms testing in food samples.
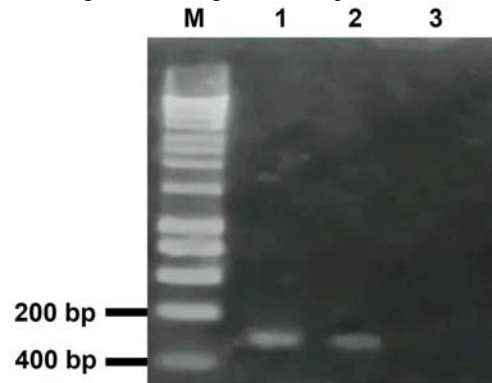
Figure 6. Detection of Salmonella from culture broth by PCR-coupled immune-magnetic beads. M, DNA ladder 1 kilobase; 1, invA gene (positive control); 2, MPs conjugated with anti-Salmonella OMA; 3, MPs.

Furthermore, IMS is an effective method for purifying sample systems from food matrices without easily being clogged by large particles (Ersahin *et al.*, 2012) or limited compatibility with large sample volumes (Garrido-Maestu *et al.*, 2018). Based on IMS technology, Merck's real-time PCR Assurance Genetic Detection System captures only intact bacteria in the pre-enrichment fluid. As a result, unlike other real-time PCR procedures (total DNA extraction from pre-enrichment fluid), the Assurance Genetic Detection System procedure has a false-positive

rate of almost 0% in comparison with traditional methods (Feldsine *et al.*, 2010). Our laboratory-made 'Mix-and-Match' ProAx1-Fe$_3$O$_4$ binding-coated MPs exhibited a broad forthcoming in the field of foodborne bacteria detection. To our best knowledge, this was the first of its kind of 'Mix-and-Match' MPs being prepared. In further experiments, the MPs can be tested for their ability to capture and detect any poisoning microorganisms in food samples.

4. Conclusion

The PCR method is an efficient way to detect pathogens in food by corporating with IMS technology as a pretreatment step in the whole process. In this study, we demonstrated a proof-of-concept for 'Mix-and-Match' MPs by designing, cloning, and expressing the recombinant protein ProAx1-Fe$_3$O$_4$ binding, and performed a specific antibody capturing experiment of ProAx1-Fe$_3$O$_4$ binding-coated magnetic beads. Here, we represented a bi-functional protein (ProAx1-Fe$_3$O$_4$ binding) that could bind to MPs with high affinity and capture antibodies to generate protein-coated MPs for specific detection of microorganisms in the food matrix. These beads underwent a couple of stability tests, antibody binding capability, and microorganism isolation. Our ProAx1-Fe$_3$O$_4$ binding-coated MPs may find potential applications for bacterial detection and disease diagnosis with high efficiency and accuracy.

Declaration of Competing Interest

The authors declare that they have no conflict of interests.

References

Bintsis and Thomas. 2017. Foodborne pathogens. *AIMS Microbiol.*, **3(3)**: 529-563.

Ersahin ME, Ozgun H, Dereli RK, Ozturk I, Roest K and van Lier JB. 2012. A review on dynamic membrane filtration: materials, applications and future perspectives. *Bioresour Technol.*, **122**: 196-206.

Feldsine PT, Jucker MT, Kaur M, Lienau AH and Kerr DE. 2010. Evaluation of the Assurance GDS® for *Salmonella* Method in Foods and Environmental Surfaces: Multilaboratory Collaborative Study. *J AOAC Int.*, **93(1)**: 150-162.

Gan SY, Tye GJ AL, Chew, Ng WK and Lai NS. 2023. Linker-mediated oriented antibody immobilisation strategies for a more efficient immunosensor and diagnostic applications: A review. *Biosens Bioelectron X*, **14**: 100379.

Garrido-Maestu A, Azinheiro S, Carvalho J and Prado M. 2018. Rapid and sensitive detection of viable Listeria monocytogenes in food products by a filtration-based protocol and qPCR. *Food microbiol.*, **73**: 254-263.

Hassoun A, Jagtap S, Garcia-Garcia G, Trollman H, Pateiro M, Lorenzo JM, Trif M and Rusu AV. 2023. Food quality 4.0: From traditional approaches to digitalized automated analysis. J *Food Eng.*, **337**: 111216.

Havelaar AH, Kirk MD, Torgerson PR, Gibb HJ, Hald T, Lake RJ, et al. 2015. World Health Organization Global Estimates and Regional Comparisons of the Burden of Foodborne Disease in 2010. *PLoS Med.*, **12(12)**: e1001923.

Hsu CY, Hsu BM, Chang TY, Hsu TK, Shen SM, Chiu YC, Wang HJ, Ji WT, Fan CW and Chen JL. 2014. Evaluation of immunomagnetic separation for the detection of *Salmonella* in surface waters by polymerase chain reaction. *Int J Environ Res Public Health*, **11(9)**: 9811-9821.

Huynh KQ, Duong DTS, Van Tran T, Nguyen BTT, Tran-Nguyen TS, Tran TL, Phan BT, Ta TKH and Tran-Van H. 2020. Cleavable, Covalently Linked, Affinity Coupling Immune Magnetic Nanoparticles for Specifically Depleting T Cells. *J Electron Mater.*, **49**: 6510-6518.

Hyeon JY and Deng X. 2017. Rapid detection of Salmonella in raw chicken breast using real-time PCR combined with immunomagnetic separation and whole genome amplification. *Food Microbiol.*, **63**: 111-116.

Jansson B, Uhlén M and Nygren PÅ. 1998. All individual domains of staphylococcal protein A show Fab binding. *FEMS Immunol Med Microbiol.*, **20(1)**: 69-78.

Lee JE, Seo JH, Kim CS, Kwon Y, Ha JH, Choi SS and Cha HJ. 2013. A comparative study on antibody immobilization strategies onto solid surface. *Korean J Chem Eng.*, **30**: 1934-1938.

Li Y, Yin G, Pu X, Chen X, Liao X and Huang X. 2019. Novel Bi-Functional 14-mer Peptides with Both Ovarian Carcinoma Cells Targeting and Magnetic Fe3O4 Nanoparticles Affinity. *Materials (Basel)*, **12(5)**: 755.

Lu B, Smyth MR and O'Kennedy R. 1996. Tutorial review. Oriented immobilization of antibodies and its applications in immunoassays and immunosensors. *Analyst*, **121(3)**: 29R-32R.

Marrez DA, Abdel-Rahman GN and Salem Marrez SH. 2019. Evaluation of Pseudomonas fluorescens Extracts as Biocontrol Agents Against some Foodborne Microorganisms. *Jordan J Biol Sci.*, **12(5)**.

Quinn J, Patel P, Fitzpatrick B, Manning B, Dillon P, Daly S, O'Kennedy R, Alcocer M, Lee H, Morgan M and Lang K. 1999. The use of regenerable, affinity ligand-based surfaces for immunosensor applications. *Biosens Bioelectron.*, **14(6)**: 587-595.

Rodríguez FI, Procura F and Bueno DJ. 2018. Comparison of 7 culture methods for *Salmonella* serovar Enteritidis and *Salmonella* serovar Typhimurium isolation in poultry feces. *Poult Sci.*, **97(11)**: 3826-3836.

Soto Varela Z, Pérez Lavalle L and Estrada Alvarado D. 2016. Bacteria causing of foodborne diseases: an overview at Colombia. *Rev. Salud Uninorte*, **32(1)**: 105-122.

Ta TKH, Trinh MT, Long NV, Nguyen TTM, Nguyen TLT, Thuoc TL, Phan BT, Mott D, Maenosono S, Tran-Van H and Le VH. 2016. Synthesis and surface functionalization of Fe3O4-SiO2 core-shell nanoparticles with 3-glycidoxypropyltrimethoxysilane and 1, 1′-carbonyldiimidazole for bio-applications. *Colloids Surf A Physicochem Eng Asp.*, **504**: 376-383.

Thanh BT, Van-Sau N, Ju H, Bashir MJK, Jun HK, Phan TB, Ngo QM, Tran NQ, Hai TH, Van PH and Tan-Tai N. 2019. Immobilization of protein a on monodisperse magnetic nanoparticles for biomedical applications. *J Nanomater.*, **2019 (1)**: 2182471.

Tran-Nguyen TS, Ngo-Luong DT, Nguyen-Phuoc KH, Tran TL and Tran-Van H. 2021. Simultaneously targeting nitrocellulose and antibody by a dual-headed protein. *Protein Expr Purif.*, **177**: 105764.

You F, Yin G, Pu X, Li Y, Hu Y, Huang Z, Liao X, Yao Y and Chen X. 2016. Biopanning and characterization of peptides with Fe3O4 nanoparticles-binding capability via phage display random peptide library technique. *Colloids Surf B Biointerfaces*, **141**: 537-545.

Zueter ARM and Harun AB. 2018. Development and Validation of Conventional PCR for the Detection of the sctQ Gene. *Jordan J Biol Sci.*, **11(4)**: 435 - 439.

JJBS

Jordan Journal of Biological Sciences

Kinetics Profile of Hybridoma Clones SB4 and RD8 Producing Monoclonal Antibodies Against The Spike Protein Of SARS-Cov-2 In Low-Serum Medium

Indri FEBRIANI[1,2], Febby Nurdiya NINGSIH[1,*], Sri Rahayu LESTARI[2], Jodi SURYANGGONO[1], Erba Vidya CIKTA[3], Tika WIDAYANTI[1], Asri SULFIANTI[1], R. Tedjo SASMONO[4], Sabar PAMBUDI[1]

[1]*Research Center for Vaccine and Drugs, National Research and Innovation Agency, South Tangerang, Banten, Indonesia;* [2]*Department of Biology, Faculty of Mathematics and Natural Sciences, Universitas Negeri Malang, Malang, East Java, Indonesia;* [3]*Center of Pharmaceutical and Medical Technology, Agency for the Assessment and Application of Technology (BPPT), Serpong, South Tangerang, Indonesia;* [4]*Eijkman Research Center for Molecular Biology, National Research and Innovation Agency, Cibinong Science Center, Cibinong, West Java, Indonesia*

Abstract

Background. Monoclonal antibodies, the main component of antigen-based rapid diagnostic tests, are produced in vitro through hybridoma cell cultivation supplemented with animal-derived serum, such as fetal bovine serum. The supplementation of FBS in culture medium causes controversy due to the variation of components included in FBS per production, potentially reducing the quality of mAbs. Moreover, the cost of using FBS is high. This study aimed to evaluate the growth capacity of hybridoma clones after being adapted to low serum conditions.

Methods. The clones SB4 and RD8 producing mAb against spike protein of SARS-CoV-2 were used in this study. Cell kinetics were observed and measured for seven days with 10% and 3% FBS supplementation. Then, the mAbs production was measured semi-quantitatively by indirect enzyme-linked immunosorbent assay. In addition, the cell cycle was also evaluated through flow cytometry analysis at 24 h, 48 h, and 72 h of treatment. This study was conducted with a true-experiment method (n=3), and all quantitative results were statistically analyzed.

Results. The results show that supplementation of 3% FBS in these two hybridoma clones gave a different response regarding cell proliferation and productivity. The clone RD8 was excellent in growth kinetics and maintained the mAbs production on low-serum media, while SB4 showed a different pattern.

Conclusion. Accordingly, supplementation of 3% FBS may support hybridoma productivity as a fulfilment of mAbs production while considering the characteristics of each hybridoma clone.

Keywords: monoclonal antibody, rapid diagnostic test, hybridoma cells, fetal bovine serum

1. Introduction

Monoclonal Antibodies (mAbs) are widely commercially used for research, diagnosis, and therapeutics. Therapeutically, mouse-mAbs can be modified into human-mouse chimeric forms for cancer, autoimmune, and degenerative disease treatments (Fesseha, 2020; Sánchez-Robles *et al*., 2021). In COVID-19 Rapid Diagnostic Tests (RDTs), the antigen-antibody reaction, particularly for detecting the spike protein of SARS-CoV-2, relies on mAbs as essential raw materials (Salcedo *et al*., 2022). Therefore, efficient mAbs production is critical. Produced by hybridoma cells from the fusion of splenocytes and myeloma cells, mAbs can be generated either in vitro (bioreactors) or in vivo (ascites). Due to considerations of scale, cost, ethics, and the 3R (Replace, Reduce, Refine) principle, the in vitro method is preferred (Khan, 2023; Verderio *et al*., 2023).

Monoclonal antibodies produced by hybridoma are influenced by the supplementation of growth factors that affect metabolic rates (Sissolak et al., 2019). This process typically uses media supplemented with Fetal Bovine Serum (FBS) in bioreactors or spinner flasks. FBS is a source of vital cell nutrients, such as growth factors, hormones, and amino acids. Thus, its role remains essential and intricate, but its use is controversial due to ethical concerns, contamination risks (Versteegen *et al*., 2021), quality variability, and purification challenges (Groothuis *et al*., 2015; Baker, 2016; Urzì *et al*., 2022). These issues have encouraged researchers to avoid serum usage in hybridoma culture medium.

Although a study by Hashmi *et al*. (2014) showed low mAbs production after cultivation in a medium supplemented with 0.5% FBS, the kinetic profile of the cells was not well evaluated. Thus, we assume that 0.5% FBS supplementation is insufficient to support hybridoma in producing mAbs. Additionally, there is a possibility that

---

* Corresponding author. e-mail: febb001@brin.go.id.

each clone may respond differently to nutritional changes. Therefore, this study compares the growth capacity of two generated hybridomas, clones SB4 and RD8, in response to supplementation with 3% FBS versus 10% FBS. Assessing the cell kinetics after sequential adaptation to low-serum supplementation is required to estimate mAbs production and the optimum period needed. Through this study, we expect to explain the growth profile of clones SB4 and RD8 in culture media with low FBS content. Thus, this study will form the basis for establishing the hybridoma clone with a high capacity of mAbs production.

2. Materials and methods

2.1. Design of experiment

This study is a true experiment and was conducted in at least three independent experiments. Both control and treatment groups were done with three replications, respectively (n = 3).

2.2. Hybridoma cell lines and cell cultivation

Hybridoma cell clones SB4 and RD8 were developed at the Research Center for Vaccine and Drugs, Indonesia. Both clones are confirmed to produce the mouse monoclonal antibody against the Spike Recombinant Protein of SARS-CoV-2 (unpublished data). Hybridomas were adapted in RPMI-1640 growth medium (Gibco^{TM}, USA) with FBS supplementation starting at 10% then gradually reduced to 8%, 5%, and finally, 3% (Sigma®, St. Louis, MO, USA), along with 100 U/mL penicillin-streptomycin (Gibco^{TM}, USA). Each clone was cultivated in a 25 cm² T-flask and then incubated at 37°C with 5% CO_2 following a similar procedure (Parveen and Varalakshmi, 2022; Loniakan *et al.*, 2023). Medium replacement was performed every 2–3 days, while subculture into a large-sized flask was accomplished when cell confluence reached ~70–80%.

2.3. Measurement of growth kinetics of hybridoma cells

The protocol is based on the studies by Bruce *et al.* (2002) and Silva *et al.* (2018), with adjustments and slight modifications of methods. Adapted hybridoma cell clones SB4 and RD8, in RPMI medium supplemented with 3% FBS, were subcultured into Durant bottles equipped with magnetic stirrers. The initial cell density cultivated was 1 x 10⁵ cells/mL, using a batch culture system with a working volume of 70 mL. As a comparator, clones established in a medium containing 10% FBS were cultivated and measured in parallel. Culture samples from days 1 to 7 were collected, with 1 mL for microscopic observation and 500 μL (n = 3) for cell count calculation according to Khalil (2009). Based on the cell numbers determined by culture sampling on days 1 to 7, population doubling time (PDT) and growth rate were calculated using an equation or measured via the OMNI calculator website (https://www.omnicalculator.com/biology/cell-doubling-time).

$$PDT = \frac{\Delta t}{log2\left(\frac{\Delta N}{N0}\right)+1}$$ (Korzyńska & Zychowicz, 2008)

PDT = Population doubling time
Δt = Time taken for 80% confluency
ΔN = Difference in cell number or concentration
N0 = Total cell number seeded or concentration

$$Growth\,rate = \frac{ln\left(\frac{N2}{N1}\right)}{t2-t1}$$ (Singer & McDaniel, 1986)

N or W = Cell number or concentration
N2 = Final cell number or concentration
N1 = Initial cell number or concentration
t = Time

The samples collected from days 1 to 7 were centrifuged, with the supernatant stored at 4°C as a daily mAbs production sample, while the cell pellets were fixed using 70% ethanol (proceed to sub-section 2.5). After day 7, all cultures were harvested by centrifugation to separate the supernatant from the cells. The supernatants containing mAbs were concentrated with Amicon® Ultra Centrifugal Filters 100 kDa MWCO (Merck, Germany) and then stored at -20 °C (Proceed to sub-section 2.6).

2.4. Measurement of monoclonal antibody production by indirect ELISA

The mAbs absorbance measurement protocol refers to the study by Ningsih *et al.* (2023), with adjustments and modifications of methods. A CoronaVac antigen 50 ng/well (Biofarma, Indonesia) and non-structural SARS-CoV-2 proteins (50 ng/well, n=3) produced by the Research Center for Vaccine and Drug, Indonesia, were used as negative controls. These were coated on the Nunc MaxiSorp™ 96-well high-binding microplate (Thermo Scientific, USA) and incubated overnight at 4°C. Samples were then washed with 100 μL/well of phosphate-buffered saline containing 0.1% Tween-20 (PBS-T 0.1%) six times (placed on a shaker for five minutes). Next, samples were incubated for four hours with a blocking buffer containing 5% BSA (Sigma, USA) and then rinsed three times with PBS-T 0.1% in the same manner as previously.

A supernatant sample was used as the tested primary antibody (150 μL/well), a RPMI medium containing FBS was used as a negative control, and a monoclonal antibody against SARS-Cov-2 Spike protein S1 (Cat MA5-36250, Invitrogen, USA) was used as a positive control. After overnight incubation at 4°C, samples were washed with PBS-T 0.1% eight times before being incubated for an hour with a secondary antibody against mouse-conjugated stabilized peroxidase (Cat. 626520, Invitrogen, USA) for the supernatant sample and negative control, and HRP-conjugated goat anti-rabbit (Cat. GTX213110-01, Invitrogen, USA) for the positive control. Next, the samples were washed using PBS-T 0.1% eight times before being incubated for 15 minutes with a 50 μL/well of 1-Step^{TM} Ultra TMB-ELISA (Thermo Scientific, USA). Then, 50 μL/well of H_2SO_4 0.5 N was added to all samples to stop the reaction. Lastly, the optical density at 450 nm was measured using a Synergy HTX Multi-Mode Reader (Agilent Technologies, USA).

2.5. Analysis of cycle cell by flow cytometry

The fixed cells at 24 h, 48 h, and 72 h (n = 3) were centrifugated and washed with sterile PBS 1X. Then, the cells were stained with propidium iodide (PI) solution (Invitrogen, USA) containing RNase A (Sigma, USA) and incubated for 15 minutes (dark condition). Finally, cell

cycle analysis on each sample from both clones was performed using BD AccuriTM C6 Plus flow cytometry (BD Biosciences, USA). A PI solution without a sample is used as a blank. The setting limitations included 10,000 events, medium fluidics velocity, and a threshold of 80,000 on FSC-H.

2.6. Qualitative total protein profiling

The total protein in both mAbs concentrate and flowthrough samples obtained from the previous step (Sub-section 2.3) was quantified using Pierce™ BCA Protein Assay Kits (Thermo Scientific, USA) compared to albumin as the standard. The absorbance was measured at a wavelength of 562 nm.

Then, the protein profile of each sample was analyzed by sodium dodecyl sulphate-polyacrylamide gel electrophoresis (SDS-PAGE) using a 10% polyacrylamide resolving gel. All samples were diluted with 5X loading dye and adjusted to 1 mg total protein in a final volume of 20 μL, then run with Electophoresis WSE-1150 PageRun Ace (Atto, Japan) for at least 90 minutes. A PageRuler™ Plus prestained protein ladder was used as the size indicator (Thermo Scientific, USA). The bands were visualized with Coomassie Brilliant Blue R-250 staining solution (Bio-Rad, USA) followed by a destaining solution (Bio-Rad, USA).

2.7. Statistical analysis

The reported data represent three independent experiments with similar findings and are presented as geometric means ± standard deviations (SD). The normality of all data was tested using Shapiro-Wilk and Levene homogeneity tests. A Mann-Whitney non-parametric test was conducted to compare the differences between 10% and 3% FBS supplementation on all parameters tested for both clones. This test is used in in vitro research by Saleh *et al.* (2021). A *p*-value of less than 0.05 was considered statistically significant. The statistical analysis software used was SPSS version 25, while the graphs were created using Microsoft Excel.

3. Results

3.1. Kinetics of growth and production of monoclonal antibodies (mAbs) by hybridoma clones SB4 and RD8 after adaptation to low-serum medium

This study uses the spike protein of SARS-CoV-2 at the ELISA coating plate stage to test cross-reactivity with commercial mAbs (as a positive control system) and mAbs in the supernatant sample. The ELISA system has been optimized and well-verified.

Figure 1A shows the growth kinetics of hybridoma clone SB4. In media supplemented with 3% FBS, clone SB4 reached the highest density on day 3, approximately $483,970 \pm 76,610$ cells/mL. This value is less than the total viable cells cultivated in media with 10% FBS, yet statistically not significantly different ($p > 0.05$). The PDT and growth rate calculation also support this result. Clone SB4 supplemented with 3% FBS showed a longer PDT than 10% FBS, resulting in a slower growth rate.
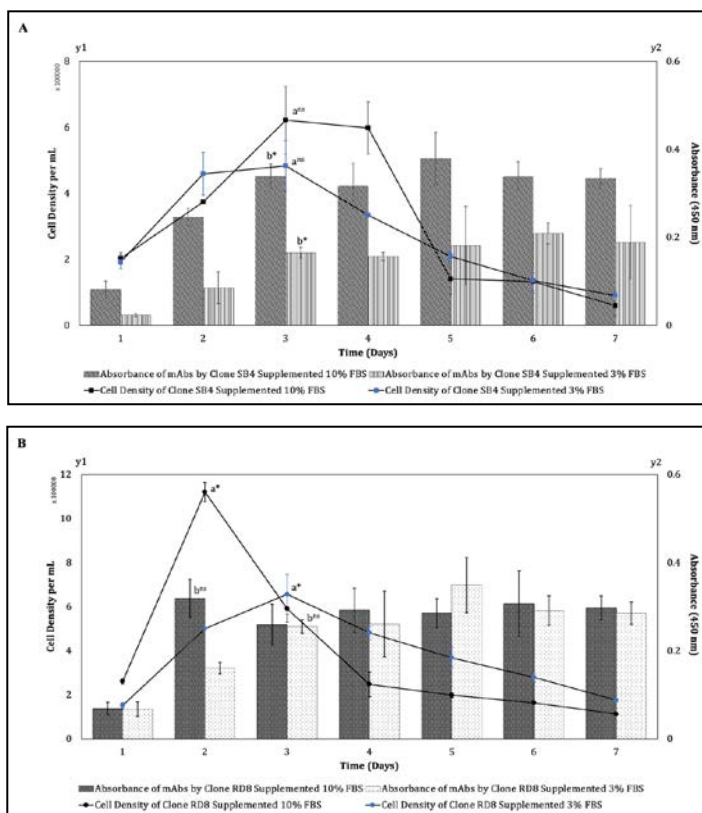
Figure 1. Kinetics of cell growth and mAbs production by hybridoma cells for seven days. (A) Hybridoma clone SB4. (B) Hybridoma clone RD8. The values are presented as geometric mean ± Standard Deviation (SD, n = 3), compared to negative and positive control. The value of the bar considered as the peak for [a])Viable cell density and [b])mAbs production, were analyzed using the Mann-Whitney test and presented as [ns])not significantly different ($p > 0.05$); [*])significantly different (p < 0.05).

The density reduction in media supplemented with 3% FBS also occurred in clone RD8. Figure 1B shows RD8 reached the highest density in 3% FBS on day 3, approximately 656,764 ± 91,320 cells/mL. This value decreased significantly by half compared to the sample cultivated in 10% FBS, which was 1,120,582 ± 43,989 cells/mL on day 2. Additionally, the highest density of clone RD8 with supplementation of 10% FBS also grew faster than in 3% FBS. Meanwhile, the decrease in viable cell number of clone SB4 with 3% FBS was supported by a longer PDT and slower growth rate (see Table 1) but was statistically insignificant. The density and morphological condition of both clones during supplementation with 3% FBS at the end of the log phase are visualized by microscopic observations in Figure 2. The cell density in media supplemented with 3% FBS was less than the cells cultivated with 10% FBS.
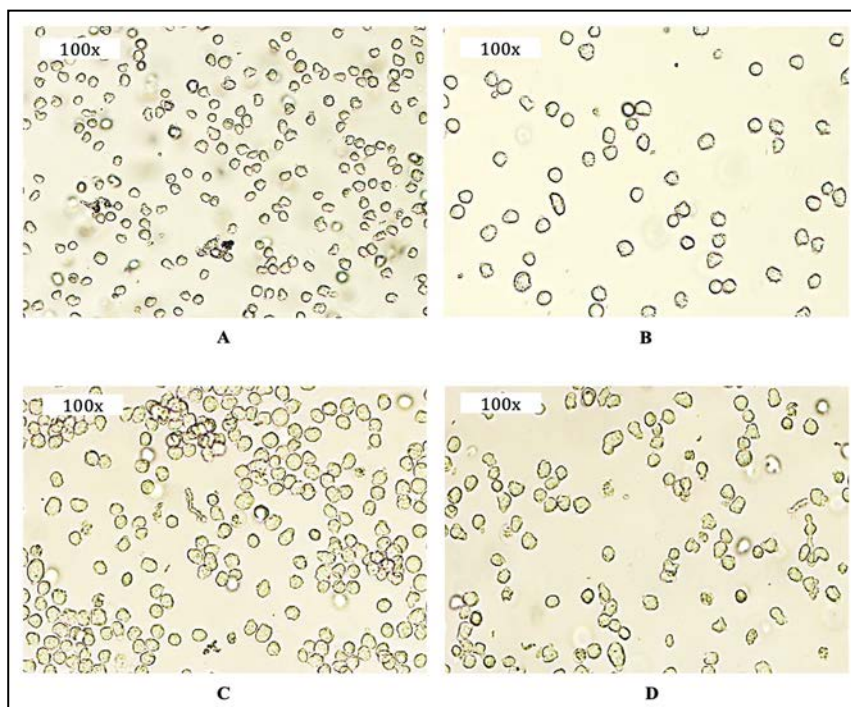
Figure 2. Microscopic observation of hybridoma clones SB4 and RD8 on peak cell density days (100× magnification). One millilitre sample from each culture was collected and placed on the dish. Cell observation of clone SB4 supplemented with (A) 10% FBS on day 3; (B) 3% FBS on day 3. Clone RD8 supplemented with (C) 10% FBS on day 2; (D) 3% FBS on day 3. The figures shown are representative of experiments that showed similar results.

In Figure 1A, based on the relative absorbance level of mAbs, the highest peak of mAbs production by SB4 cells with 3% FBS on day 3 was approximately 0.165 ± 0.011. These values decreased by half compared to supplementation with 10% FBS, which was 0.340 ± 0.027 (significant decrease). The peak absorbance of these clone SB4 mAbs occurs on the day of the peak cell density. Similarly, in the graph of mAbs production by clone RD8 (Figure 1B), the peak of mAbs production also occurred on the peak day of cell density, which is day 3 for RD8 with 3% FBS, at 0.256 ± 0.016. These values are still less than the mAbs production with 10% FBS, which was 0.318 ± 0.04 on day 2 (insignificant decrease).

3.2. Comparison of competence of clones SB4 and RD8 on low-serum medium

In Table 1, the peak growth density of clone RD8 with 3% FBS is still less than that of clone SB4 (difference not significant). However, clone RD8 supplemented with 3% FBS showed a more significant peak of mAbs production than clone SB4, which were 0.256 ± 0.016 and 0.165 ± 0.011, respectively (statistically significant difference).

Table 1. Summary table of growth kinetics and production of mAbs by clones SB4 and RD8 supplemented with 10% and 3% FBS.

Parameters	Clone SB4		Clone RD8	
	10% FBS	3% FBS	10% FBS	3% FBS
Highest density	On day 3 (622,269 ± 103,175 cells/mL)	On day 3 (483,970 ± 76,610 cells/mL)	On day 2 (1,120,582 ± 43,989 cells/mL)	On day 3 (656,764 ± 91,320 cells/mL)
Highest mAbs production	On day 3 (0.340 ± 0.027)	On day 3 (0.165 ± 0.011)	On day 2 (0.318 ± 0.043)	On day 3 (0.256 ± 0.016)
PDT in lag phase–exponential phase	On day 1–3 (29 hours 46 minutes)	On day 1–3 (36 hours 12 minutes)	On day 0–2 (13 hours 46 minutes)	On day 1–3 (22 hours 48 minutes)
Growth rate	On day 1–3 (0.023)	On day 1–3 (0.019)	On day 0–2 (0.050)	On day 1–3 (0.030)

3.3. Decreased FBS levels in the growth medium affect the cell cycle of clones SB4 and RD8

As shown in Figure 3, the percentage of the SB4 cell population in the sub-G1 phase in both FBS contents gradually increased from 24 h to 72 h. Clone SB4 supplemented with 3% FBS tended to have a smaller proportion of dead cells (sub-G1 phase) than cells cultivated with 10% FBS, approximately 9.81 ± 1.40 % and 14.15 ± 0.79 %, respectively (insignificant, $p > 0.05$).

In the S phase, the proportion of SB4 cells supplemented with 3% and 10% FBS from 24 h to 72 h tended to decrease gradually. At 24 h, the relative number of proliferating cells (G2/M) observed in 3% FBS was lower than in 10% FBS. Interestingly, at 72 h, the proportion of G2/M phase cells observed in 3% FBS was approximately four times higher than that in 10% FBS ($p > 0.05$). After 72 h, SB4 cells in medium with 3% FBS had a smaller population proportion of sub-G1 (dead cells) and a higher proportion of G2/M phase (proliferating cells) than those in 10% FBS.
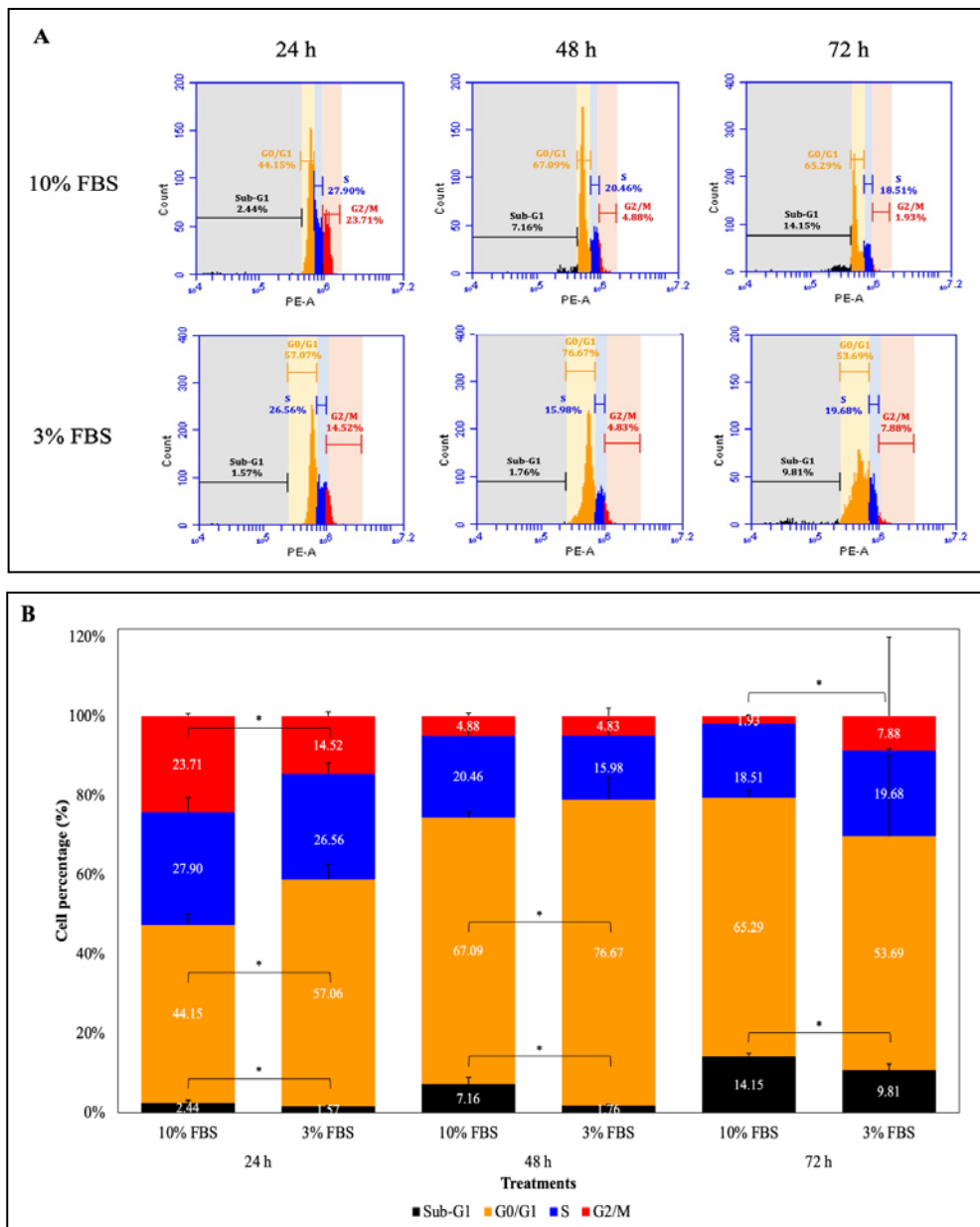
Figure 3. The cell cycle of clone SB4 supplemented with 10% and 3% FBS (n = 3). A. Flow cytometry-based cell cycle spectrum at 24 h, 48 h, and 72 h treatment. B. Cell percentage bar chart per phase at 24 h, 48 h, and 72 h of treatment. The percentage value is the geometric mean, and the system control value already subtracts the relative percentage of cells. The cell cycle spectrum of hybridoma is divided into Sub-G1, G0/G1, S, and G2/M phases with different colour representatives. Cell cycle data were also statistically analyzed using the Mann-Whitney test. *(p ≤ 0.05).
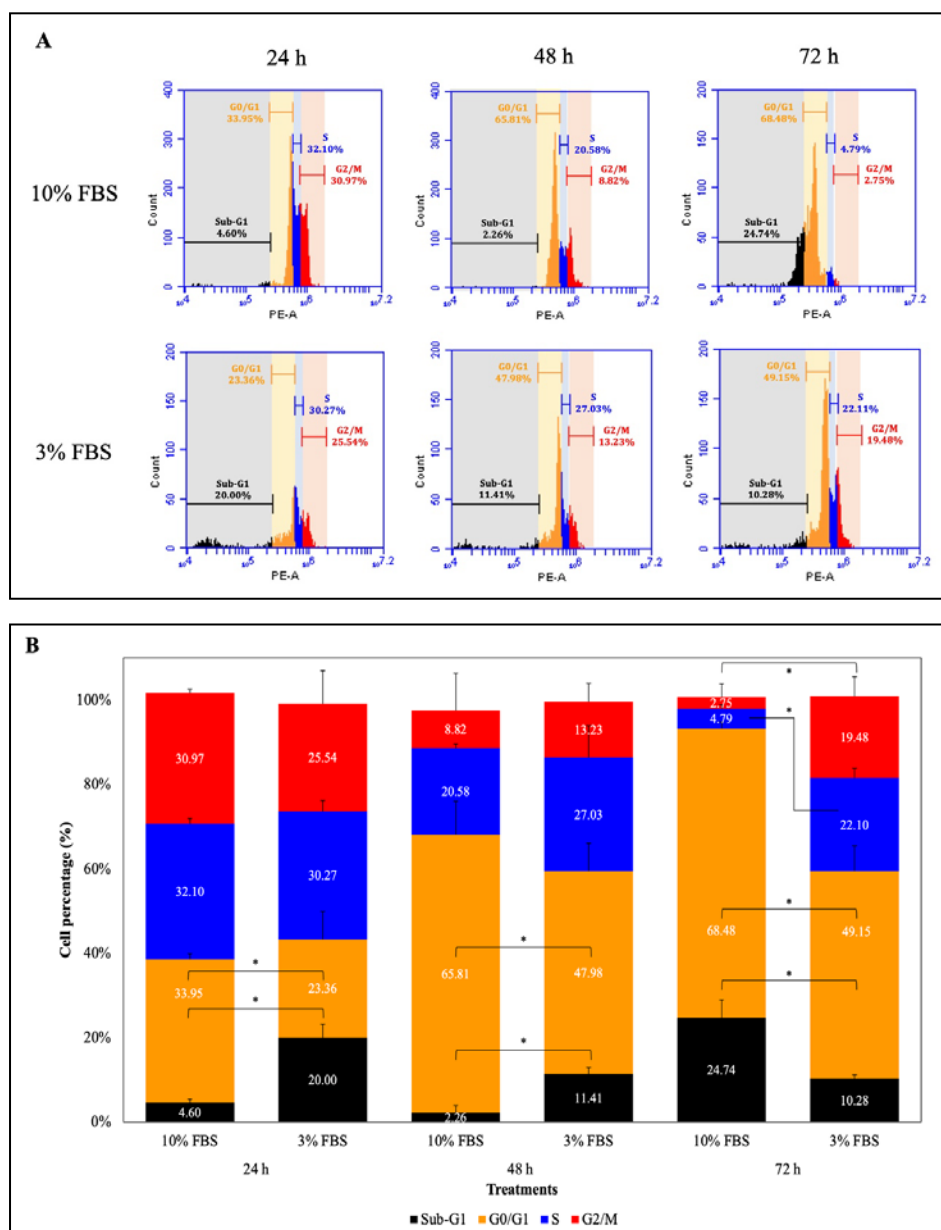
Figure 4. The cell cycle of clone RD8 supplemented with 10% and 3% FBS (n = 3). A. Flow cytometry-based cell cycle spectrum at 24 h, 48 h, and 72 h treatment. B. Cell percentage bar chart per cell cycle phase at 24 h, 48 h, and 72 h treatment. The percentage value is the geometric mean, and the system control value subtracts the relative percentage of cells. The cell cycle spectrum of hybridoma is divided into Sub-G1, G0/G1, S, and G2/M phases with different colour representatives. Cell cycle data were also statistically analyzed using the Mann-Whitney test. *($p \leq 0.05$).

In contrast to clone SB4, the cell cycle of clone RD8 supplemented with 10% FBS resulted in a lower population percentage of dead cells (sub-G1 phase) than in 3% FBS, especially at 24 h and 48 h (see Figure 4). The G0/G1 phase of both FBS percentages increased from 24 h to 72 h. Similarly, there was a gradual decrease in the percentage of cells in the S phase from 24 h to 72 h in both FBS percentages. However, a similar trend, as shown in SB4 cells (Figure 3), was also found in RD8 cells at 72 h. RD8 cells supplemented with 3% FBS showed a lower population of dead cells and a higher population of proliferating cells than those cultured with 10% FBS.

3.4. SDS-PAGE profile of mAbs

Figure 5 shows the presence of IgG heavy chains between 55–70 kDa and IgG light chains at ~25 kDa across

the sample. The heavy and light chains on mAbs from both clones with 3% FBS supplementation were clearly illustrated and thinner than those with 10% FBS. In addition, bands of 25 and ~70 kDa were detected in the flowthrough column. This indicates that the FBS supplementation also introduces proteins with sizes of 25 and ~70 kDa, similar to the light and heavy chains of mAbs. On the other hand, when mAbs concentrate is carried out using Amicon® Ultra-15 centrifugal filters 100 kDa MWCO (Merck Millipore Ltd, Germany), there are mAbs proteins carried over and detected in the flowthrough column and impurity proteins on the mAbs column. The impurity protein profile in 3% FBS supplementation is smaller than in 10% FBS.
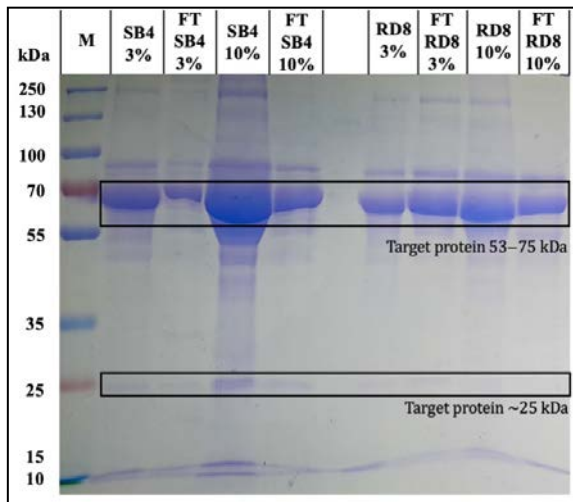
Figure 5. The SDS-PAGE result shows the protein profile of mAbs concentrate from clones SB4 and RD8 and the flowthrough sample collected after centrifugal separation (FT). Equal amounts of protein were loaded into wells of 10% resolving gel for separation (1 mg/well). The shape of the square indicates the target proteins, respectively. M: Marker; FT: Flow Through.

4. Discussion and Conclusion

Our results regarding the viable cell number of RD8 cultivated with 3% FBS are lower than those in a medium with 10% FBS. The decrease in cell proliferation in mammalian cells may occur due to a restricted glucose supply, as the FBS content is also reduced (Silva *et al.*, 2018; Pilgrim *et al.*, 2022). However, insignificant differences in growth kinetics between SB4 cells supplemented with 10% and 3% FBS indicate an adaptation process.

The calculation of the kinetics of SB4 cells in 3% FBS showed that PDT takes almost 7 hours longer than the cells cultivated with 10% FBS (Lindström and Friedman, 2020). This suggests that cells in 3% FBS have a slower growth rate than cells in 10% FBS since the growth rate is inversely correlated to the PDT (Shahrezaei and Marguerat, 2015). A long PDT and slow growth rate are also observed in RD8 cells cultivated in 3% FBS. The growth rate value represents the cell adaptability process (Lindström and Friedman, 2020) and the speed at which the cell population size changes over time.

The low serum content in the medium also results in a lower accumulation of metabolic waste products, as cell proliferation slows down (Konakovsky *et al.*, 2016; Jang *et al.*, 2022). This can be observed in microscopic observations (Figure 2) and supported by cell cycle analysis (Figures 3 and 4). The peak density of hybridoma supplemented with 10% FBS on day 3 indicates population dominance of mortality, thereby increasing apoptosis (sub-G1 phase) and low proliferating cells phase (G2/M phase) (Schellenberg *et al.*, 2022). In contrast, both SB4 and RD8 cells cultivated in 3% FBS showed a small proportion of sub-G1 phase cells and a more significant population of proliferating cells.

Cell growth shown in the results of cell kinetics is supported by cell cycle profile testing, which also describes the period of cell growth and multiplication (Eastman *et al.*, 2020). In the first 24 h, the cell density of

SB4 and RD8 clones in 3% FBS media decreased compared to 10% FBS. This was also shown in the decrease in the percentage of the S phase in both clones at 24h due to the inhibition of cell proliferation by inducing G1 cycle arrest. Thus, cells were inhibited from entering the S or G2/M phase. This inhibition is probably caused by the interaction of CycE and CDK2 in the restriction G0 / G1, which is inhibited (Finn *et al.*, 2016; Fisher and Krasinska, 2022) due to growth factor deficiency and DNA damage, thus promoting cell cycle arrest to allow DNA repair to prevent the propagation of cells with severe DNA damage (Junqueira, 2003; Ozaki and Nakagawara, 2011; Yam *et al.*, 2022).

In contrast to proliferation capacity, reducing FBS supplementation significantly reduces the mAbs produced by SB4 cells. The peak of mAbs production occurs on the day when cell density reaches the highest number because the cell has been in the stationary phase and reached the maximum capacity of mAbs production (Lee and Palsson, 1994; Carvalho *et al.*, 2017), so mAbs production on the day of measurement after that is relatively constant. Meanwhile, the mAbs produced by RD8 cells grown with 3% FBS are not significantly different from those cultivated with 10% FBS. Thus, a low-serum medium may also facilitate mAbs production by RD8 cells. If a comparison is made to determine the productivity of each clone in a low-serum medium (according to Table 1), clone RD8 appears to be excellent in aspects of mAbs production. It is also supported by shorter PDT and has a faster growth rate than clone SB4.

The difference in mAbs production between these two clones is statistically significant. Each SB4 and RD8 clone is developed from B lymphocytes isolated from different mice. Thus, differences in physiological conditions and immunization outcomes may affect the cell's characteristics (Leenaars and Hendriksen, 2005). The various types of antigens in the isolation procedure of B lymphocytes of the two clones also affect the number of specific antibodies produced (Leenaars, 1994; Pedrioli and Oxenius, 2021). Furthermore, protocol aspects and fusion outcomes affect the monoclonality of hybridoma cells, potentially resulting in differences in the capacity to produce antibodies (Holzlohner and Hanack, 2017).

The pattern of the cell cycle may be associated with a non-constant rate of mAbs production, reaching a maximum in the S phase and decreasing gradually from the late S phase to the G2 phase until it reaches a minimum in the M phase (Grilo and Mantalaris, 2019). In addition, RD8 cells with 3% FBS showed a large percentage in the S phase, possibly due to the excellent adaptation process. Moreover, these adaptation processes also induce shorter G1 arrest cycles at 3% FBS, resulting in a relatively more significant number of cells in the G2/M (4n) phase than cells grown with 10% FBS. The S and G2/M phase cell percentage at 3% supplementation was better in clone RD8 than in clone SB4.

The mitotic phase in a 3% FBS low-serum medium is favourable compared to 10% FBS, particularly at the 72-hour observation point. This is attributed to the lower FBS concentration, where a longer duration of cell or serum starvation can increase the proportion of cells arrested in the G0/G1 phase (Huang *et al.*, 2018; Wang and Saponaro, 2021), although some studies have reported a non-significant increase (Baghdadchi, 2013). The increase in

the proportion of cells in the G0/G1 phase in the low-serum medium may lead to an improvement in cell quality during the mitotic phase through mTOR activation for adaptation and cellular repair (Bhowmick *et al.*, 2024) and DNA repair (Chae *et al.*, 2021). However, this could also be influenced by the characteristics of the hybridoma clone.

The result of SDS-PAGE analysis also showed the pattern of IgG profile produced by both clones. The antibodies, mainly IgG, are large molecules with a total weight of approximately 150 kDa, consisting of four polypeptide chains with two identical heavy chains of 53−75 kDa and two light chains of ~25 kDa (Rižner, 2014; Saied *et al.*, 2022). The visualization of impurity proteins included in mAbs production in 3% FBS shows less impurity compared to 10% FBS. Thus, this may facilitate mAbs purification (Pilgrim *et al.*, 2022). Meanwhile, the presence of protein bands in the flowthrough is likely to come from impurity proteins carried over from the FBS and from the mAbs sample triggered by the less-than-optimal effectiveness of Amicon concentration, so that the target protein is carried over to the flowthrough. Implementing Amicon 100k RC aims for reduced particle recovery. However, there is a possibility that the loss of particles was drastic and carried over to the flowthrough (Vergauwen *et al.*, 2017; Tang *et al.*, 2024).

Overall, the productivity of clones SB4 and RD8 in low-serum did not show a significant decrease compared to 10% FBS, which may still be sufficient to support mAbs production. Lastly, hybridoma clone RD8 has excellent adaptation to low-serum medium. However, the metabolic traits of each clone remain unclear. The limitation of this research regarding measuring the growth kinetics of hybridomas is that each repeat was carried out at different times, which may give rise to variations in data. This limitation can be optimized in future research to make it more reproducible.

Acknowledgement

References

Baghdadchi N. 2013. The Effects of Serum Starvation on Cell Cycle Synchronization. *OSR Journal of Student Research.*, **1**(4).

Baker M. 2016. Reproducibility: Respect your cells! *Nature.*, **537**(7620): 433–435.

Bhowmick T, Biswas S and Mukherjee A. 2024. Cellular response during cellular starvation: A battle for cellular survivability. *Cell Biochem Funct.*, **42**(5): 1–11.

Bruce MP, Boyd V, Duch C and White JR. 2002. Dialysis-based bioreactor systems for the production of monoclonal antibodies - Alternatives to ascites production in mice. *J Immunol Methods.*, **264**(1–2): 59–68.

Carvalho LS, da Silva OB, de Almeida GC, de Oliveira JD, Parachin NS and Carmo TS. 2017. Production Processes for Monoclonal Antibodies. **Fermentation Processes.** IntechOpen Publisher, London.

Chae SY, Nam D, Hyeon DY, Hong A, Lee TD, Kim S, Im D, Hong J, Kang C, Lee JW, Hwang D, Lee SW and Kim HI. 2021. DNA repair and cholesterol-mediated drug efflux induce dose-dependent chemoresistance in nutrient-deprived neuroblastoma cells. *iScience.*, **24**(4): 102325.

Eastman AE, Chen X, Hu X, Hartman AA, Morales, AMP, Yang C, Lu J, Kueh HY and Guo S. 2020. Resolving Cell Cycle Speed in One Snapshot with a Live-Cell Fluorescent Reporter. *Cell Reports.*, **31**(12): 107804.

Finn RS, Aleshin A and Slamon DJ. 2016. Targeting the cyclin-dependent kinases (CDK) 4/6 in estrogen receptor-positive breast cancers. *Breast Cancer Res.*, **18**(1): 1–11.

Fisher D and Krasinska L. 2022. Explaining Redundancy in CDK-Mediated Control of the Cell Cycle: Unifying the Continuum and Quantitative Models. *Cells.*, **11**(13).

Grilo AL and Mantalaris A. 2019. A Predictive Mathematical Model of Cell Cycle, Metabolism, and Apoptosis of Monoclonal Antibody-Producing GS–NS0 Cells. *Biotechnol J.*, **14**(11).

Groothuis FA, Heringa MB, Nicol B, Hermens JLM, Blaauboer BJ and Kramer NI. 2015. Dose metric considerations in in vitro assays to improve quantitative in vitro-in vivo dose extrapolations. *Toxicology*, **332**: 30–40.

Hashmi FK, Cail R, Islam M, Saleem Z, Amin U, Hussain K and Saeed H. 2014. Adaptation of WM-68 hybridoma cell-line in minimal serum and serum free culture conditions. *Pakistan J. Zool.*, **46**(2): 355–362.

Holzlohner. 2017. Generation by murine monoclonal antibodies by hybridoma technology. *J Vis Exp*, **119.**

Huang Y, Fu Z, Dong W, Zhang Z, Mu J and Zhang J. 2018. Serum starvation-induces down-regulation of Bcl-2/Bax confers apoptosis in tongue coating-related cells in vitro. *Mol Med Rep.*, **17**(4): 5057–5064.

Jang M, Pete ES and Bruheim P. 2022. The impact of serum-free culture on HEK293 cells: From the establishment of suspension and adherent serum-free adaptation cultures to the investigation of growth and metabolic profiles. *Front Bioeng Biotechnol.*, **10**(September): 1–16.

Junqueira. 2003. **Basic histology.** Mc Graw Hill Publisher, New York.

Khalil A. 2009. Inhibition of the in vitro growth of human mammary carcinoma cell line (MCF-7) by selenium and vitamin E. *Jordan J Biol Sci.*, **2**(1): 37–46.

Khan NT. 2023. Basics of Hybridoma Technology for the generation of monoclonal antibodies. *Anatomy Physiol Biochem Int J.*, **6**(3): 1–4.

Konakovsky V, Clemens C, Müller MM, Bechmann J, Berger M, Schlatter S and Herwig C. 2016. Metabolic control in mammalian fed-batch cell cultures for reduced lactic acid accumulation and improved process robustness. *Bioengineering (Basel).*, **3**(1).

Korzyńska A and Zychowicz M. 2008. A method of estimation of the cell doubling time on basis of the cell culture monitoring data. *Biocybernetics and Biomedical Engineering.*, **28**(4): 75–82.

Lee GM and Palsson BO. 1994. Monoclonal antibody production using free-suspended and entrapped hybridoma cells. *Biotechnol Genet Eng Rev.*, **12**(1): 509–533.

Leenaars M and Hendriksen CFM. 2005. Critical steps in the production of polyclonal and monoclonal antibodies: evaluation and recommendations. *ILAR J.*, **46**(3): 269–279.

Leenaars. 1994. **Adjuvants in laboratory animals.** Ponsen & Looijen publisher.

Lindström HJG and Friedman R. 2020. Inferring time-dependent population growth rates in cell cultures undergoing adaptation. *BMC Bioinformatics.*, **21**(1): 1–14.

Loniakan S, Rafiee A and Monadi A. 2023. Bacteroides Fragilis induce apoptosis and sub G1/G1 arrest via caspase and Nrf2 signaling pathways in HT-29 cell line. *Jordan J Biol Sci.*, **16**(2): 363–369.

Ningsih FN, Widayanti T, Sahlan M, Pramono AP and Pambudi S. 2023. The Effect of Indonesian Royal Jelly Supplementation on the Growth of Hybridoma and Its Monoclonal Antibody Production. *Proceedings of the 1st International Conference for Health Research – BRIN (ICHR 2022).*, **1**: 210–219.

Ozaki T and Nakagawara A. 2011. Role of p53 in cell death and human cancers. *Cancers.*, **3**(1): 994–1013.

Parveen S and Varalakshmi KN. 2022. BAX and P53 Over-Expression Mediated by the Marine Alga Sargassum Myriocystum leads to MCF-7, Hepg2 and Hela Cancer Cells Apoptosis and Induces In-Ovo Anti-Angiogenesis Effects. *Jordan J Biol Sci.*, **15**(2): 275–287.

Pedrioli A and Oxenius A. 2021. Single B cell technologies for monoclonal antibody discovery. *Trends Immunoly.*, **42**(12): 1143–1158.

Pilgrim CR, McCahill KA, Rops JG, Dufour JM, Russell KA and Koch TG. 2022. A Review of Fetal Bovine Serum in the Culture of Mesenchymal Stromal Cells and Potential Alternatives for Veterinary Medicine. *Front Vet Sci.*, **9**(May): 1–11.

Rižner TL. 2014. Teaching the structure of immunoglobulins by molecular visualization and SDS-PAGE analysis. *Biochem Mol Biol Educ.*, **42**(2): 152–159.

Saied ARA, Metwally AA, Alobo M, Shah J, Sharun K and Dhama K. 2022. Bovine-derived antibodies and camelid-derived nanobodies as biotherapeutic weapons against SARS-CoV-2 and its variants: A review article. *Int J Surg.*, **98**(January): 106233.

Salcedo N, Reddy A, Gomez AR, Bosch I and Herrera BB. 2022. Monoclonal antibody pairs against SARS-CoV- 2 for rapid antigen test development. *PLoS Negl Trop Dis.*, **16**(3): 1–19.

Saleh M, Ezz -din D and Al-Masri A. 2021. In vitro genotoxicity study of the lambda-cyhalothrin insecticide on Sf9 insect cells line using Comet assay. *Jordan J Biol Sci.*, **14**(2): 213–217.

Sánchez-Robles EM, Girón R, Paniagua N, Rodríguez-Rivera C, Pascual D and Goicoechea C. (2021). Monoclonal antibodies for chronic pain treatment: Present and future. *Int J Mol Sci.*, **22**(19): 1–26.

Schellenberg J, Nagraik T, Wohlenberg OJ, Ruhl S, Bahnemann J, Scheper T and Solle D. 2022. Stress-induced increase of monoclonal antibody production in CHO cells. *Eng Life Sci.*, **22**(5): 427–436.

Shahrezaei V and Marguerat S. 2015. Connecting growth with gene expression: Of noise and numbers. *Curr Opin Microbiol.*, **25**: 127–135.

Silva BG, da Silva Cunha Tamashiro WM, Ferreira RR, Deffune E and Suazo CAT. 2018. Assessment of kinetic and metabolic features of two hybridomas in suspension culture for production of two monoclonal antibodies for blood typing. *Braz J Chem Eng.*, **35**(2): 497–507.

Singer SR and McDaniel CN. 1986. Analyzing growth in cell cultures..I Calculating growth rates. *Can J Bot.*, **64**(1): 238–241.

Sissolak B, Lingg N, Sommeregger W, Striedner G and Vorauer-Uhl K. 2019. Impact of mammalian cell culture conditions on monoclonal antibody charge heterogeneity: an accessory monitoring tool for process development. *J Ind Microbiol Biotechnol.*, **46**(8): 1167–1178.

Tang S, Tao J and Li Y. 2024. Challenges and solutions for the downstream purification of therapeutic proteins. *Antib Ther.*, **7**(1): 1–12.

Urzì O, Bagge RO and Crescitelli R. 2022. The dark side of foetal bovine serum in extracellular vesicle studies. *J Extracell Vesicles.*, **11**(10).

Verderio P, Lecchi M, Ciniselli CM, Shishmani B, Apolone G and Manenti G. 2023. 3Rs principle and legislative decrees to achieve high standard of animal research. *Animals (Basel).*, **13**(2): 277.

Vergauwen G, Dhondt B, van Deun J, de Smedt E, Berx G, Timmerman E, Gevaert K, Miinalainen I, Cocquyt V, Braems G, van Den Broecke R, Denys H, de Wever O and Hendrix A. 2017. Confounding factors of ultrafiltration and protein analysis in extracellular vesicle research. *Sci Rep.*, **7**(1): 1–12.

Versteegen. 2021. Animal welfare and ethics on the collection of fetal bovine blood for the production of fetal bovine serum. *ALTEX.*, **38**(2).

Wang J and Saponaro M. 2021. Protocol for analysis of G2/M DNA synthesis in human cells. *STAR Protoc.*, **2**(2): 100570.

Yam CQX, Lim HH and Surana U. 2022. DNA damage checkpoint execution and the rules of its disengagement. *Front Cell Dev Biol.*, **10**(October): 1–15.

Human Papillomavirus 16 (HPV16) in the Middle East and North Africa: Molecular, Epidemiology and Clinical Characterization

Rabaa Y Athamneh[1,*], Lo'ai Alanagreh[1,2], Esam Y. Qnais[3] Hamed Alzoubi[4], Abdelrahim Alqudah[5] Rania Algroom[6,1], Maisa M. A. AL-QUDAH[7], Tareq Nayef AlRamadneh[1], Rawan Abudalo[5]

[1] Department of Medical Laboratory Sciences, Faculty of Allied Medical Sciences, Zarqa University, Zarqa 13110, Jordan; [2]Department of Medical Laboratory Sciences, Faculty of Applied Medical Sciences, The Hashemite University, 13133, Zarqa, Jordan; [3]Department of Biology and Biotechnology, Faculty of Science, The Hashemite University, Zarqa 13133, Jordan; [4]Department of Pathology and Microbiology, King Abdullah University Hospital, Faculty of Medicine, Jordan University of Science and Technology, P.O. Box 3030, Irbid 22110, Jordan; [5] Department of Clinical Pharmacy and Pharmacy Practice, Faculty of Pharmaceutical Sciences, The Hashemite University, Zarqa 13133, Jordan; [6]Department of Allied Medical Sciences, Zarqa University College, Al-Balqa Applied University, Jordan; [7]Department of Medical Laboratory Sciences, Faculty of Science, AL-Balqa Applied University, AL-Salt 19117, Jordan.

Abstract

Human papillomavirus (HPV) is the main cause of sexually transmitted infections, globally. Clinical characterization and Phylogenetic analysis of HPV can be useful in improving the preventive and management measures in the Middle East and North Africa (MENA). The objectives of our study were to estimate the prevalence of HPV16 and its associated human cancers and to evaluate phylogenetic clustering proportions as a measure of viral domestic transmission in the MENA region. Gen-Bank was the source of all HPV16 sequences that had been collected in the MENA region; also, the sequence metadata (if obtainable) was retrieved. The probable phylogenetic clusters were identified using Neighbour Joining phylogenetic analysis. The total number of available HPV16 sequences was 997 (which presented just a total of 9 MENA Countries) dispersed as follows: Iran had the highest number of HPV16 sequences (n = 664, 66%), followed by Morocco (n = 176, 17.6%), and Turkey (n= 64, 6.42%)

The findings demonstrated that the MENA have high incidence of HPV 16 infection in females as well as high frequencies of the HPV 16 genotypes (sequences linked to the E6 gene) associated with cervical cancer in the MENA. On the other hand, it was noted that the number of HPV16 available sequences in the MENA region has increased over time. Analysis of the HPV16 clusters revealed that transmission of HPV 16 was between the countries of the MENA region, such as (Morocco and Algeria), (Morocco and Iran) and (Iran, Morocco, and Algeria).

Keyword: Human Papillomavirus; Middle East and North Africa; Epidemiology, phylogenetic; E6 gene; L1gene, HPV16

1. Introduction

Human papillomavirus (HPV) is a small, double-stranded DNA virus responsible for causing both skin-related and sexually transmitted diseases. It belongs to the Papillomaviridae family. (Tommasino, 2014) .HPV is notably one of the most common causes of sexually transmitted infections globally, with both men and women facing a 50% chance of acquiring the virus at least once in their lifetime. (Handler et al., 2015). In addition, HPV has the ability to infect both cutaneous and mucosal epithelial tissues, including those of the skin, upper respiratory tract, and anogenital region.(Tommasino,2014)

The homologous nucleotide sequence of the L1 protein has been used to identify over 200 genotypes of HPV. A phylogenetic tree was constructed, classifying HPV types into five genera: α, β, γ, μ, and v. (Bernard et al., 2010 and de Villiers, 2013). The α genus (mucosal)includes about 30 HPV types linked to the infection of the mucosal

epithelial tissues of the oral and anogenital tracts, as well as benign cutaneous HPV types that cause skin warts. Mucosal HPV types are categorized as low-risk (LR) or High-risk (HR) based on their oncogenic abilities. Infections caused by LR-HPVs (HPV 6 and HPV11) comprise recurrent respiratory papillomatosis, skin warts, and benign gynecological papillomas (Ouda et al., 2021 and Lacey, Lowndes, and Shah 2006).

Furthermore, HR-HPVs (types -16, -18, -31, -33, -35, -39, -45, -51, -52, -55, -56, -58, -59, -68, -73, -82, and -83) have oncogenic ability and are associated to develop the human cancer (Bernard et al., 2010). HR-HPVs are subsequently demonstrated to be linked to a subset of further genital cancers in addition to colorectal, breast, head, and neck, cancers (Brianti, De Flammineis, and Mercuri, n.d.; Delgado-García et al., 2017). Specifically, in cervical cancer, HPV 16 and HPV 18 are often prevalent, with over 96% of these cancers testing positive for both virus types(Smith et al., 2007and Muñoz et al., 2003)

* Corresponding author. e-mail: ralathamnah@zu.edu.jo.

On the other hand, multiple studies (in vitro and in vivo) revealed the β HPV genus to have oncogenic properties (Gabet et al., 2008 and Michel et al., 2006). Nevertheless, the μ, γ, and ν genera are implicated in skin tropism but have no identified roles in oncogenesis (Tommasino, 2014).

The HPV genome measures around 8 kb and has 8 or 9 open-reading frames (ORFs) on the same DNA strand (13). The HPV genome is split into three distinct regions: an early part, which includes the early genes (E1, E2, E4, E5, E6, and E7); a late part, which includes the late genes (L1 and L2); and a non-coding region, known as the long control region (LCR) found between ORFs L1 and E6. (13). The L1 ORF encodes the Main capsid protein L1, which has 55 KDa (Buck, Day, and Trus 2013 and Akhatova et al., 2022). Additionally, the L1 OR is the most conserved genomic sequence. As a result, it is utilized for the phylogenetic categorization of viral types or subtypes (de Villiers ,2013 and de Villiers et al., 2004).

Interestingly, the two major HPV oncoproteins are E6 and E7, and the variants of the E6 and E7 genes in HPV-16 are linked to ongoing HPV infection and cancer development (Cornet et al., 2012). Despite HPV-16 being the most common cancer-causing genotype globally, the type-specific prevalence of medically significant HR-HPVs differs by geographic area (Burk, Harari, and Chen 2013 and Guan et al., 2012). The three most prevalent HPV types found in 74.5% of cervical cancer in Sub-Saharan Africa are HPV-45, HPV-18and HPV-16 (in ascending order of prevalence, whilst the HPV subtypes associated with cancer are generally similar across countries (Cornet et al., 2012 and Cornet et al., 2013).

Numerous studies conducted that, globally revealed the prevalence of HPV infection subtypes in human cancers varied. , demonstrating an association between HPV prevalence and geographical location(Smith et al., 2007 and Fernandes et al., 2020). Thus, studying viral transmission in a region such as the MENA region which shares similar cultural, demographic, and economic characteristics as a whole could be helpful in the epidemiological exploration of virus distribution(Athamneh et al.,2023).

There is a limited data about HPV16 prevalence or HPV16 infection and human cancers as well as the HPV16 transmission in the MENA. Hence, the objectives of our study were to estimate the prevalence of HPV16 and its associated human cancers and to evaluate phylogenetic clustering proportions as a measure of viral domestic transmission in the MENA region.

2. Methodology

2.1. Source of data

A search was performed using the GenBank search tool, part of the National Institutes of Health (NIH) genetic sequence database (www.ncbi.nlm.nih.gov/genbank) to retrieve all available HPV16 sequences collected from the following MENA region countries: Qatar, Egypt, Iraq, Iran, Kuwait, Saudi Arabia (KSA), Somalia, Jordan, Algeria, Bahrain, Oman, Turkey, Morocco, Palestine, Mauritania, Tunisia, Lebanon, Syria, Libya, UAE, Sudan, and Yemen. The search concluded on April 7, 2023, when available metadata for the sequences were also obtained,

including information such as the individual's sex, the country and year of sequence collection, sample data, and the viral gene analyzed. The algorithm used to retrieve the HPV16 sequences, along with the demographic and clinical characterization, is presented in. (Figure 1)
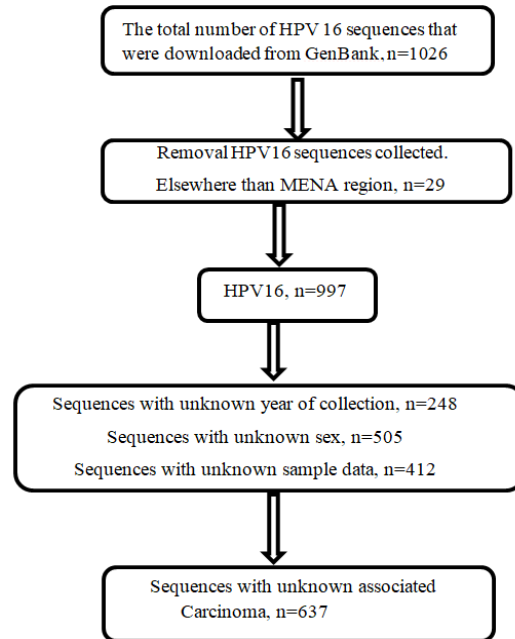
Figure1: The MENA HPV16 sequence selection algorithm served as the foundation for clinical and demographic characterization. MENA: Middle East and North Africa; HPV: Human Papilloma Virus

2.2. Analysis of the MENA Region's Domestic HPV16 Transmission

Phylogenetic tree based on Neighbour Joining (NJ) method analysis of 444 bp sequence of the E6 gene. Root sequence (GenBank NC_001526 accession). The E6 gene is crucial in HPV-related cancer development

The BLAST tool was used to find similar HPV16 GenBank sequences. The most ten similar sequences were found and added to the final NJ analysis along with the MENA region's sequences.   (24). Excluded from the analysis were sequences having stop codons and those with the same accession number.

2.3. Statistical analysis

Analysis was performed with IBM SPSS Statistics. The associations between qualitative variables were appraised through the use of the chi-square ($\chi2$).

3. Results

3.1. The MENA HPV16 Molecular Dataset's characteristics

The sequences were collected between 2004 and 2022, with the total number of HPV16 sequences being 997 sequences (that represented just a total of 9 MENA Countries) were dispersed as follows: Iran had the highest number of HPV16 sequences. (n = 664, 66.6%), followed by Morocco (n = 176, 17.65%), and Turkey (n= 64, 6.42%) as shown in (Figure 2).
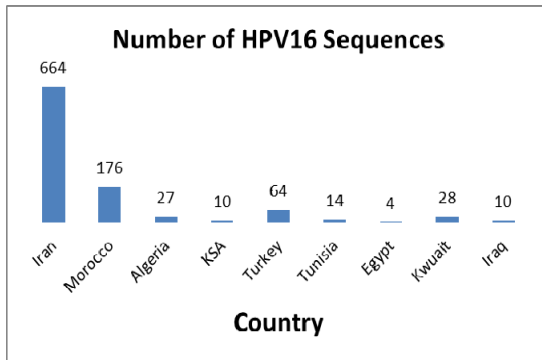
Figure 2: The total number of HPV16 MENA sequences stratified per country. HPV16: Human Papilloma Virus16; MENA: Middle East and North Africa; KSA: Kingdom of Saudi Arabia.

3.2. HPV16 sequences prevalence in the MENA region by sex

There were 492 HPV 16 sequences in total with known sex in the MENA region. Females had a high percentage of the available HPV 16 sequences (n=481,98%), as seen in (Figure 3)
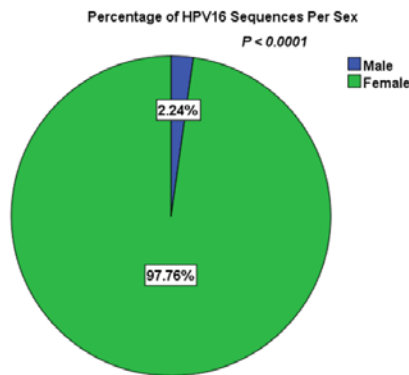
Figure3: percentage of whole HPV16 sequences per sex in the MENA region; HPV16: Human papillomavirus 16; MENA: Middle East and North Africa

3.3. percentage of the HPV16 genes that were analyzed in the MENA region.

The whole number of available HPV16 sequences with known analyzed genes in the MENA region was 988; the L1 gene had the largest percentage of these genes (41.72%), followed by the E6 gene (38%) However, the E5 gene had the lowest proportion (10%). as shown in (Table1).

Table1. The percentage of HPV16 analyzed genes in the MENA region; N: Number of the HPV16 analyzed genes; %: the percentage of analyzed genes; HPV16: Human Papillomavirus 16; MENA: Middle East and North Africa

HPV16 gene	N	%
L1	408	41.29%
L2	6	0.61%
E1	5	0.50%
E5	1	0.10%
E6	379	38.36%
E7	62	6.30%
LCR	127	12.85%

3.4. prevalence of carcinoma-related HPV16 in the MENA region

The total number of available HPV16 sequences that related to the cancer was 360, the most common carcinoma in the MENA region was cervical carcinoma (293:82%), followed by Oropharyngeal squamous cell carcinomas (26:7.28%) as shown in (Table 2). Compared to other cancers, cervical carcinoma had a significantly high percentage in the MENA region (Figure 4).

Table 2: percentage of the HPV16 sequences that related to the carcinoma in the MENA region; HPV16: Human Papillomavirus16; MENA: Middle East and North Africa; N: Number of HPV16 sequences related to carcinoma cases; %: percentage of HPV16 sequences related to carcinoma cases

carcinoma group	N	%
Cervical carcinoma	293	81.2%
prostatic cancer	7	2%
Oropharyngeal squamous cell carcinomas	26	7.2%
Esophageal cancer	20	5.60%
Lung cancer	2	0.56%
Breast cancer	12	3.3%
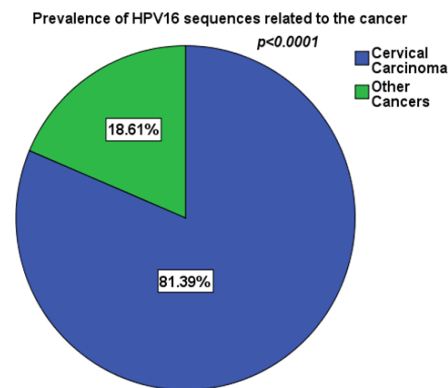
Figure 4: percentage of the HPV16 sequences that related to the cervical cancer and other cancers in the MENA region; HPV16: Human Papillomavirus16; MENA: Middle East and North Africa; other cancers: prostatic cancer Oropharyngeal squamous cell carcinomas, Esophageal cancer, Lung cancer, Breast cancer.

3.5. Prevalence of HPV16 sequences per sample data in the MENA region

The available HPV16 sequences with known sample data were divided into samples per anatomic region (Table 3) and samples from the patient group (Table 4). Regarding the samples per anatomic region, there were about 248 samples. Scientifically, the samples taken from the cervical region had a higher percentage compared to those taken from other regions as presented in (Figure 5). On the other hand, the total number of samples per patient group was about 337 samples (as documented at NCBI the samples were taken from patients with cancer or benign tumors in general without any details). A higher prevalence was noted in samples from patients with cervical cancer (293.87%), followed by those from patients with esophageal cancer (20.59%), as presented in (Table 4).

Table 3. prevalence of samples per anatomic region in the MENA region; MENA: Middle East and North Africa. Cervical region: cervix tissue, cervical scrape, cervical swab, pap smear, cervical smear; N: Number of HPV16 sequences identified in samples across various anatomic regions.; %: percentage of HPV16 sequences identified in samples across various anatomic regions.

samples per anatomic region	N	%
Cervical region	148	59.7%
oral cavity	14	5.64%
Larynx	36	14.50%
Tonsil	2	0.80%
Pharynx	5	2.00%
Saliva	6	2.40%
multiple region	36	14.50%
Genital	1	.0400%
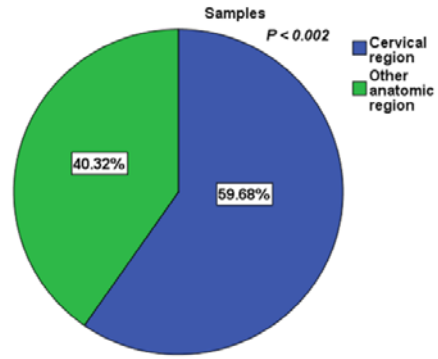
Figure5. Prevalence of samples that were taken from cervical region and other anatomic region in the MENA; MENA: Middle East and North Africa; other anatomic region: oral cavity, larynx, tonsil, pharynx, salivary gland, multiple regions, genital.

Table 4. prevalence of samples per patients' group in the MENA region; MENA: Middle East and North Africa; n: number of the sequences of sample per patients' group; %: percentage of the sequences

sample per patients' group	N	%
patient with cervical carcinoma	293	87.00%
patient with prostatic cancer	7	2.07%
patient with benign prostatic hyperplasia	3	0.89%
patient with Breast cancer	12	3.60%
Esophageal cancer	20	5.93%
lung cancer	2	0.60%

3.6. Prevalence of HPV16 genes that are associated with cancer in the MENA region.

The total number of HPV16 sequences that span apart of E6, L1or L2 genes that were associated with cancers in the MENA region was about 360 sequences. The E6 gene was linked with the highest percentage of cervical carcinoma (224,62.2%), followed by the L1gene (64,17.8%) and L2 gene (5,1.38%). The L1gene was associated with other cancers such as lung cancer (2,0.5%), prostatic cancer (7,1.94%), oropharyngeal squamous cell carcinomas (26,7.2%), esophageal cancer (20,5.5%) and breast cancer (12,3.33%) as presented in (Table 5) A significantly higher prevalence of sequences associated with the E6 gene related to cervical carcinoma was observed compared to other gene sequences, p <0.0001, as illustrated in (Figure 6)

Table 5. Percentage of HPV16 sequences that related to (E6,L1and L2genes) and associated with cancers in the MENA region; HPV16: Human papilloma virus 16 ; MENA :Middle East and North Africa; n:number of the HPV16 sequences; %:percentage of the HPV16 sequences

HPV gene	cervical carcinoma (n, %)	Lung cancer (n, %)	Prostatic cancer (n, %)	Oropharyngeal squamous cell carcinomas (n, %)	Esophageal cancer (n, %)	Breast cancer (n, %)
E6	224,62.2%	0	0	0	0	0
L1	64,17.8%	2,0.05%	7,1.94%	26,7.2%	20,5.5%	12,3.33%
L2	5,1.38%	0	0	0	0	0
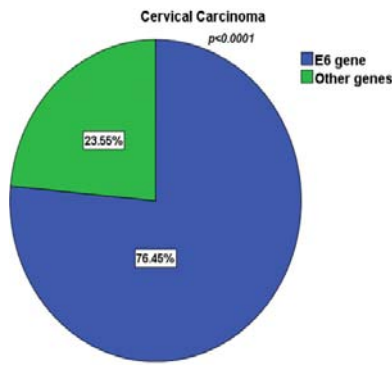
Figure 6. Prevalence of HPV16 sequences related to E6 gene and other genes that were associated with cervical carcinoma in the MENA region; HPV16: Human papilloma virus 16; MENA: Middle East and North Africa; other genes: L1 and L2.

3.7. Variations over time in the number of MENA region HPV16 sequences that are available.

The total number of HPV16 sequences with a known year of collection was 749. We excluded 248 HPV 16 sequences that did not have the dates of collection; there was a significant temporal change in the number of HPV16 MENA sequences that were available. Nonetheless, there was an increase in the number of sequences, particularly between 2012 and 2022, as shown in Figure7.
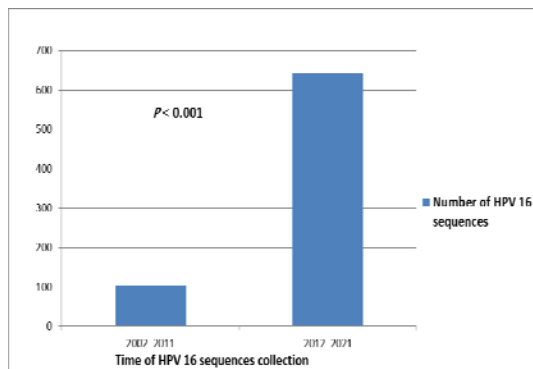
Figure7. HPV16 sequence number in the MENA region over time. HPV16: Human papillomavirus16; MENA: Middle East and North Africa.

3.8. Potential domestic transmission of HPV16 in the MENA

Neighbour Joining analysis was performed to assess the proportion of HPV16 sequences that are probably linked in transmission clusters suggesting domestic transmission, which found the proportion of phylogenetic clustering. According to the size of the cluster, each cluster was classed as a dyad (2 sequences), a small network (3-14 sequences), or a large network (at least fifteen sequences). For the E6 gene, the overall number of sequences contained within domestic phylogenetic clusters was 15/332 (4.52%). Clusters included dyads (n=1, 6.6%), small networks (n=11,73%), and large networks (n=3,20%). Some of the clusters are limited only to one country of the MENA region; for instance, the dyad (Iran (1)), 2 out of 11 of the small networks (Morocco (3), and Iran(3)),1 out of the 3 of the large networks (Morocco

(22)) . On the other hand, some of the small and large networks included the United States and one or more of MENA countries.

Small network[1] :(Guatemala (1), Morocco (1), USA (4) and Iran (8)), small network[2]: (Morocco (1), Guatemala (1), USA (1), and Iran (4)), small network[3]:(Iran (3), Guatemala (1), Morocco (1), and USA (2),

Small network[4]: (Iran(5), Guatemala(1), and USA(2)) ,small network[5] : (Iran(3), Morocco(1), USA(2), and Algeria(1)), small network[6]: (Iran(3), Guatemala(1), Morocco(1),Japan(1) and USA(1)), small network[7]: (Iran(4),USA(2),Morocco(1)),small network[8]: (Algeria(2),Morocco(2)),small network[9] :(Morocco(3),Algeria(1),Iran(10))

Large network[1]: (Morocco (19), and USA (1)), large network [2]: Morocco (10), Iran (19)

A portion of the transmission clusters that originated in the MENA region were collected in two or more countries.: Iran and Morocco (small and large network), Iran, Morocco, and Algeria (small network), Algeria and Morocco (small network). The JN tree, which was utilized to determine the probable transmission clusters in the MENA area was supplied in (Supplementary Materials).

4. Discussion

There is limited data about the phylogenetic examination of HPV transmission in the MENA region, previous studies only covered one country or a region of one country. Investigating the HPV prevalence and phylogenetic of HPV transmission in the MENA region may show trends that might direct preventative measures (Fernandes et al., 2022). Nevertheless, in most MENA countries, there is no HPV infection testing because of stigmatization based on religious or traditional norms, potentially resulting in limited sample sizes alongside low incidence rates of HPV infection, and miscalculating the actual number of cases (Obeid et al., 2020).

The study's main finding was the observation of a high percentage of HPV16 sequences in females as well as a high prevalence of HPV16 sequences that related to cervical cancer in the MENA region, which led to an increase in the prevalence of samples that had been taken from the cervical region. This result seems plausible, considering the prior evidence showed that the prevalence of cervical cancer associated with HPV16 had increased in the MENA region (Obeid et al., 2020).

Significantly, a high prevalence of HPV16 sequences related to the E6 gene that were associated with cervical cancer in the MENA region. This result is consistent with the previous evidence which demonstrated that the two primary HPV oncoproteins are E6 and E7, and variants in the E6 and E7 genes in HPV-16 are linked to ongoing HPV infection and the development of cancer(Cornet et al., 2012 and Mirabello et al., 2017).There are several sequence variants (known as single nucleotide polymorphisms, or SNPs) within the E6/E7 gene region in cervical pre-cancers/cancers as compared to controls(Mirabello et al., 2016).

Another intriguing observation was the high prevalence of gene (L1) analysis in the MENA region. However, it is well known that L1 ORF is the most conserved region out of the eight ORFs in the HPV genome. Hence, it is utilized to detect the new HPV types (29).

Regarding the rising number of HPV16 MENA sequences over time , this may indicate a rise in interest in understanding the molecular epidemiology of HPV associated with human cancers (such as head and neck, or cervical cancer) in the region (Obeid et al., 2020 and McLaughlin, Bultas, and Shorey 2012), which has resulted in generating more sequences that were becoming available for study. This heightened attention is a result of observations of an increase in the prevalence of human cancers associated with HPV in the MENA region (Fernandes et al., 2022 and Obeid et al., 2020).

On the other hand, Asiri et al. reported that in a systematic review and Meta–analysis, the prevalence of HPV had the lowest rate between 2015 and 2019; Asiri and her colleagues detected the prevalence of different genotypes of HPV that were associated with Head and Neck cancer and depend on extracting their data on the published studies published on PubMed, and Google Scholar databases between 1998 and 2019(31), but in our study we depend on extracting our data on HPV 16 sequences downloaded in the NCBI which are associated with different types of cancer. However, other studies are advised to approve this result.

Phylogenetic clusters analyses showed that some of these clusters are limited to one country of the MENA countries. Strong evidence suggesting that HPV genomes are largely static and that sequence changes caused by mutation or recombination are uncommon occurrences. Also, the frequency of Mutational changes apparently is similar to that of the infected host organism's DNA genomes (de Villiers et al., 2004). Furthermore, there is a portion of the transmission clusters collected in Iran and Morocco (small and large network) as well as Iran, Morocco, and Algeria (small network), Algeria and Morocco (small network). This finding is in line with other research results reporting the inter-country transmission of various viruses in the MENA region (such as Hepatitis B virus, Hepatitis C virus and human immunodeficiency virus type 1). Most of the MENA countries share a sociocultural perspective that might inadvertently affect people's behaviour. In addition to some of the MENA countries neighboring each other, such as Morocco, and Algeria, this leads to an increase in the likelihood of viruses transmission in the MENA region(Athamneh et al., 2021, Sallam et al., 2017 and Athamneh et al., 2023).

Notably, most of the small and large networks connected the USA to one or more MENA countries (such as Iran, Algeria, and Morocco). Additionally, four countries (Iran, Guatemala, Morocco, and USA) repeated four times as small networks with different sizes (between 7 to 14 sequences). Additionally, another cluster comprises samples from (Iran, Guatemala, Morocco, Japan, and the USA). Interestingly, Iran is the 18th world's largest country, which is located in the Middle East, with more than 77 million citizens; it has land borders with Turkey, Turkmenistan, Pakistan, Afghanistan, Armenia, Iraq, and Azerbaijan, as well as marine borders with the UAE, Saudi Arabia, Kazakhstan, Russia, and Kuwait. Each one of these countries has endemic infectious illnesses that pose a risk for their neighboring countries, like Iran (34). The geographic position of Iran places it at the crossroads of several regions, making it susceptible to the transboundary spread of infectious diseases endemic to its neighboring countries. Each of these countries faces public health challenges due to endemic infectious diseases, which can easily spread across borders. However, these findings demonstrate the possibility that HPV16 is transmitted across these countries, due to the lack of HPV16 sequences available in many MENA countries and the variation in the number of HPV16 sequences among MENA countries; it is difficult to draw definitive conclusions about possible HPV16 transmission between these countries. Thus, an additional study is suggested to validate these results.

Despite the findings mentioned above, there were some limitations of the current study: First, many MENA countries lacked HPV16 sequences in GenBank (Lebanon, Syria, Bahrain, Palestine, Djibouti, Jordan, Yemen, Qatar, and Oman), in addition to the uneven distribution of HPV16 sequences among countries. Secondly, a portion of the sequences lacked essential metadata, including information on associated cancer, sample data, gender, and collection date. These limitations may have impacted the generalizability of the study results.

5. Conclusion

The clinical characterization of HPV16 in the MENA region has revealed several important findings. There is a notably high prevalence of HPV16 sequences that are strongly linked to cervical cancer in this region. Additionally, a significant number of HPV16 sequences related to the E6 gene, which plays a critical role in the development of cervical cancer, have been identified, further underscoring the virus's impact in the MENA region. This high prevalence has been associated with an overall increase in the number of HPV16 sequences observed in recent years. Moreover, phylogenetic analysis through the transmission cluster has highlighted the occurrence of inter-country transmission of HPV16 across different countries in the MENA region, suggesting that the virus spreads across borders, complicating control efforts. This inter-country transmission points to the need for coordinated regional efforts to manage HPV16 transmission effectively. Looking forward, future epidemiological research focusing on domestic transmission pathways of HPV16 within MENA countries is crucial. Identifying specific risk factors for the spread of HPV16 and evaluating the coverage and effectiveness of HPV vaccination programs in this region will provide valuable insights. Such research is essential to strengthen preventive measures and improve the overall management of HPV16-related diseases, particularly cervical cancer, in the MENA region.

Acknowledgments

References

Tommasino M. The human papillomavirus family and its role in carcinogenesis. Semin Cancer Biol. 2014 Jun 1;26:13–21.

Handler MZ, Handler NS, Majewski S, Schwartz RA. Human papillomavirus vaccine trials and tribulations: Clinical perspectives. J Am Acad Dermatol [Internet]. 2015 Nov 1 [cited 2023 Sep 16];73(5):743–56. Available from: http://www.jaad.org/article/S019096221501748X/fulltext

Bernard HU, Burk RD, Chen Z, van Doorslaer K, Hausen H zur, de Villiers EM. Classification of Papillomaviruses (PVs) Based on 189 PV Types and Proposal of Taxonomic Amendments. Virology [Internet]. 2010 May 5 [cited 2023 Sep 16];401(1):70. Available from: /pmc/articles/PMC3400342/

de Villiers EM. Cross-roads in the classification of papillomaviruses. Virology. 2013 Oct 1;445(1–2):2–10.

Ouda AM, Elsabagh AA, Elmakaty IM, Gupta I, Vranic S, Al-Thawadi H, et al. HPV and Recurrent Respiratory Papillomatosis: A Brief Review. Life [Internet]. 2021 Nov 1 [cited 2023 Sep 16];11(11). Available from: /pmc/articles/PMC8618609/

Lacey CJN, Lowndes CM, Shah K V. Chapter 4: Burden and management of non-cancerous HPV-related conditions: HPV-6/11 disease. Vaccine. 2006 Aug 21;24(SUPPL. 3):S35–41.

Brianti P, De Flammineis E, Mercuri SR. Review of HPV-related diseases and cancers.

Delgado-García S, Martínez-Escoriza JC, Alba A, Martín-Bayón TA, Ballester-Galiana H, Peiró G, et al. Presence of human papillomavirus DNA in breast cancer: A Spanish case-control study. BMC Cancer. 2017;17(1):1–11.

Smith JS, Lindsay L, Hoots B, Keys J, Franceschi S, Winer R, et al. Human papillomavirus type distribution in invasive cervical cancer and high-grade cervical lesions: A meta-analysis update. Int J Cancer [Internet]. 2007 Aug 1 [cited 2023 Sep 17];121(3):621–32. Available from: https://onlinelibrary.wiley.com/doi/full/10.1002/ijc.22527

Muñoz N, Bosch FX, de Sanjosé S, Herrero R, Castellsagué X, Shah K V., et al. Epidemiologic Classification of Human Papillomavirus Types Associated with Cervical Cancer. N Engl J Med. 2003 Feb 6;348(6):518–27.

Gabet AS, Accardi R, Bellopede A, Popp S, Boukamp P, Sylla BS, et al. Impairment of the telomere/telomerase system and genomic instability are associated with keratinocyte immortalization induced by the skin human papillomavirus type 38. FASEB J. 2008 Feb;22(2):622–32.

Michel A, Kopp-Schneider A, Zentgraf H, Gruber AD, de Villiers EM. E6/E7 Expression of Human Papillomavirus Type 20 (HPV-20) and HPV-27 Influences Proliferation and Differentiation of the Skin in UV-Irradiated SKH-hr1 Transgenic Mice. J Virol. 2006;80(22):11153–64.

Bernard HU, Calleja-Macias IE, Dunn ST. Genome variation of human papillomavirus types: Phylogenetic and medical implications. Int J Cancer. 2006;118(5):1071–6.

Buck CB, Day PM, Trus BL. The papillomavirus major capsid protein L1. Virology [Internet]. 2013;445(1–2):169–74. Available from: http://dx.doi.org/10.1016/j.virol.2013.05.038

Akhatova A, Azizan A, Atageldiyeva K, Ashimkhanova A, Marat A, Iztleuov Y, et al. Prophylactic Human Papillomavirus Vaccination: From the Origin to the Current State. Vaccines. 2022;10(11):1–21.

De Villiers EM, Fauquet C, Broker TR, Bernard HU, Zur Hausen H. Classification of papillomaviruses. Virology. 2004 Jun 20;324(1):17–27.

Cornet I, Gheit T, Franceschi S, Vignat J, Burk RD, Sylla BS, et al. Human Papillomavirus Type 16 Genetic Variants: Phylogeny and Classification Based on E6 and LCR. J Virol. 2012;86(12):6855–61.

Burk RD, Harari A, Chen Z. Human papillomavirus genome variants. Virology. 2013;445(1–2):232–43.

Guan P, Howell-Jones R, Li N, Bruni L, De Sanjosé S, Franceschi S, et al. Human papillomavirus types in 115,789 HPV-positive women: A meta-analysis from cervical infection to cancer. Int J Cancer. 2012;131(10):2349–59.

Cornet I, Gheit T, Iannacone MR, Vignat J, Sylla BS, Del Mistro A, et al. HPV16 genetic variation and the development of cervical cancer worldwide. Br J Cancer [Internet]. 2013;108(1):240–4. Available from: http://dx.doi.org/10.1038/bjc.2012.508

Fernandes Q, Gupta I, Vranic S, Al Moustafa AE. Human papillomaviruses and epstein–barr virus interactions in colorectal cancer: A brief review. Pathogens. 2020;9(4):1–20.

Athamneh RY, Arıkan A, Sayan M, Mahafzah A, Sallam M. Variable Proportions of Phylogenetic Clustering and Low Levels of Antiviral Drug Resistance among the Major HBV Sub-Genotypes in the Middle East and North Africa. Pathog (Basel, Switzerland) [Internet]. 2021 Oct 1 [cited 2022 May 15];10(10). Available from: https://pubmed.ncbi.nlm.nih.gov/34684283/

Athamneh RY, Abudalo R, Sallam M, Alqudah A, Alquran H, Amawi KF, et al. Sub-genotypes of hepatitis C virus in the Middle East and North Africa: Patterns of distribution and temporal changes. Infect Genet Evol [Internet]. 2023;109 (February):105412. Available from:
https://doi.org/10.1016/j.meegid.2023.105412

Saitou N, Nei M. The neighbor-joining method: a new method for reconstructing phylogenetic trees. Mol Biol Evol. 1987;4(4):406–25.

Fernandes Q, Allouch S, Gupta I, Elmakaty I, Elzawawi KE, Amarah A, et al. Human Papillomaviruses-Related Cancers: An Update on the Presence and Prevention Strategies in the Middle East and North African Regions. Pathogens. 2022;11(11).

Obeid DA, Almatrrouk SA, Alfageeh MB, Al-Ahdal MNA, Alhamlan FS. Human papillomavirus epidemiology in populations with normal or abnormal cervical cytology or cervical cancer in the Middle East and North Africa: A systematic review and meta-analysis. J Infect Public Health [Internet]. 2020;13(9):1304–13. Available from: https://doi.org/10.1016/j.jiph.2020.06.012

Mirabello L, Yeager M, Yu K, Clifford GM, Xiao Y, Zhu B, et al. HPV16 E7 Genetic Conservation Is Critical to Carcinogenesis. Cell. 2017;170(6):1164-1174.e6.

Mirabello L, Yeager M, Cullen M, Boland JF, Chen Z, Wentzensen N, et al. HPV16 Sublineage Associations with Histology-Specific Cancer Risk Using HPV Whole-Genome Sequences in 3200 Women. J Natl Cancer Inst. 2016;108(9):1–9.

Burk RD, Chen Z, Van Doorslaer K. Human papillomaviruses: Genetic basis of carcinogenicity. Public Health Genomics. 2009;12(5–6):281–90.

McLaughlin L, Bultas M, Shorey S. Human papillomavirus and head and neck cancer. J Nurse Pract. 2012;8(8):663–4.

Asiri SS, Obeid DA, Alhamlan FS. Human papillomavirus associated with head and neck cancer in the middle east and north africa: A systematic review and meta-analysis. J Nat Sci Med [Internet]. 2020 Jul 1 [cited 2024 Sep 9];3(3):170–81. Available from:
https://journals.lww.com/jnsm/fulltext/2020/03030/human_papillomavirus_associated_with_head_and_neck.6.aspx

Athamneh RY, Arıkan A, Sayan M, Mahafzah A, Sallam M. Variable Proportions of Phylogenetic Clustering and Low Levels of Antiviral Drug Resistance among the Major HBV Sub-Genotypes in the Middle East and North Africa. Pathog (Basel, Switzerland) [Internet]. 2021 Oct 15 [cited 2022 Jul 29];10(10). Available from: http://www.ncbi.nlm.nih.gov/pubmed/34684283

Sallam M, Şahin GÖ, Ingman M, Widell A, Esbjörnsson J, Medstrand P. Genetic characterization of human immunodeficiency virus type 1 transmission in the Middle East and North Africa. Heliyon [Internet]. 2017 Jul 1 [cited 2022 Jul 29];3(7):e00352. Available from: /pmc/articles/PMC5506879/

Parhizgari N, Gouya MM, Mostafavi E. Emerging and re-emerging infectious diseases in Iran. Iran J Microbiol. 2017;9(3):122–42.

Genetic Relationship Analysis to Evaluate the Performance of Several Pure Strains and their Individual Hybrids between the RAPD-PCR Indicators in the Yield Traits of Yellow Corn (*Zea mays L.)*

Yasser Hamad Humada[1] (PhD) , Raeed Mejbel Abdullah [2] (PhD),   Farhan Khaleel Hussein[3,*] (MSc)

[1]Department of Biology University of Kirkuk, College of science, Iraq; [2] Northern Technical University, College of Health and Medical Techniques Kirkuk, Kirkuk, Iraq; [3] Department of Biology, College of Education for Pure Sciences, University of Kirkuk, Iraq.

Abstract

In this study, ten genotypes (Gimbson, Saganto, DK 6050, Agr-183, ZM47W, CML494, IK58, ZP505, ZP670, and ZP197) of the yellow corn crop were used. They were introduced into half-diallel crosses. The parents and hybrid were planted in one of the farmers' fields in Kirkuk Governorate using a randomized complete block design (RCBD) with three replications. Data were recorded for the following characteristics: number of ears/plant, ears length, ear diameter, number of rows/ear, number of grains/row, number of grains/ear, weight of 300 grains, and yield of individual plant. The genotypes (parents), (hybrid), and (parents and hybrid) were significant at the level of probability (1%) for all the studied traits; and they were superior in terms of the number of ears/plant, ear diameter (cm), number of grains/row, and grain yield per plant (g). Moreover, the hybrid (2×8) surpassed concerning the characteristic of ear length (cm); and the hybrid (6×8) outperformed in the characteristic of several rows/ear and the number of grains/ear. Furthermore, the hybrid (3×8) achieved superiority regarding the trait weighing 300 grains (gm). In addition, the values of additive genetic variation were more significant than the dominance genetic variation in all traits. However, the values of environmental variation were less than those of additive and dominance variation for all the studied traits. Additionally, regarding variation and genetics, the value of all traits increased in comparison to the values of environmental variance. On the other hand, the values of phenotypic variance increased in all traits in comparison to genetic and environmental variances. In the present study, 15 primers were used; some of them showed complementary sequences on the DNA genotypes. The used primers contained specialized (distinctive) bands for some genotypes included in the study, such as strains ZP-301, ZP-707, UN44052, SH, and hybrids (ZP-301X IK8), (OH40 X IK8), (SH X IK8), (UN44052 X ZP-301), and (OH40 X ZP-707). The hybrid showed the parental bundles as well as the new non-parental bundles. Thus, the RAPD technique has proven its efficiency in studying the purity of hybrids, being an easy and fast technology.

Keywords: *Zea mays L.*, molecular genetics , RAPD technique , DNA genotypes, performance, variability,

1. Introduction

Yellow corn (*Zea mays L.*) is one of the important cereal crops cultivated worldwide, including in Iraq. It has become the third crop after wheat and rice in terms of area and construction because its kernels contain 81% carbohydrates; thus, they are used to feed humans and animals (Ramadan, 2015). Moreover, it easily adjusts to various environmental and climatic conditions; and it can grow in tropical and temperate regions (Olufemi-Salami *et al.*, 2019).

Protein materials (10.6%), oil (4.6%), and kernels are used in manufacturing flour and starch; moreover, whole kernels are used in food appetizers and the green parts are given as fodder for animals; this is in accumulation to their high manufacture ability and their adaptation to different ecological conditions and the probability of growing them in more than one season (Nazer *et al.*, 2013).

The world's corn production during the season (2019) was one billion and 77 thousand tons. America is the top producer of corn in the world, with a total of 370 million and 96 thousand tons, followed by China with a total of 259 million and 7 thousand tons, Brazil with a total production of 82 million tons, the European Union with a total production of 62 million and 10 thousand tons, Argentina with a production of 32 million tons, and Ukraine with a total production of 24 million and 12 thousand tons (Arab Organization for Agricultural Development, 2019). In 2022/2023, the U.S. produced 350 million tons, while Mexico produced 28 million metric tons (Devadoss and Luckstead, 2024). The cultivated area in Iraq in 2020, during the spring and autumn seasons, was about 405.4 thousand dunums, with a

---

* Corresponding author. e-mail: farhankhaleel@uokirkuk.edu.iq.

production of 419.3 thousand tons (Central Statistical Organization, 2020).

Iraq continues to produce yellow maize at a relatively low rate per unit area. Due to inadequate crop service operations and a lack of genotypes with the genetic potential to yield high yields and adapt to the Iraqi environment, this crop is produced per unit area in Iraq less than it should (Al-Issawi and Abood, 2024). Therefore, researchers studying this crop must adopt all available scientific methods, including breeding and improving individual hybrids that stand out for producing superior grain yields by creating strains to produce pure hybrids, cross-crossing them with one of the breeding methods, and genetically evaluating them to determine which hybrid is the best one to use (Al-Zuhairi, 2014).

Genetic variations are the primary source plant breeders consider to improve quantitative traits controlling productivity and quality. Specialists are interested in studying the components of genetic and phenotypic variations of quantitative traits such as grain yield and its components because they are essential in assessing the coefficients of phenotypic and genetic variation, the percentage of heritability, and the expected genetic improvement. The selection programs mainly depend on the existence of genetic variation, understanding of gene behavior, and the correlations between these traits. In addition, identifying the most influential characteristics as a criterion for selection can be determined via the amount of correlation between these traits and the outcome (Al-Jubouri et al., 2011).

In fact, reliance on morphological characteristics is one of the first methods to predict hybrid performance; and it has achieved tangible results. However, it is exaggerated by the surrounding environment (Van Inghelandt et al., 2010). Therefore, new techniques that depend on studying the genotype itself without influencing the environment, known as indicators, have been introduced. Genetic indicators are called (DNA indicators). They rely on DNA as a base material; and they are defined as stable genetic material that is not exaggerated by the environment. Furthermore, these indicators are characterized by stability, unlike genetic indicators that depend on morphological characteristics that interfere with the environment. In addition, DNA is present in all their organism cells at any age and can be extracted from any part of the plant; and these indicators are inherited according to the known laws of Mendel so that they can be followed up in subsequent generations and from the early stages of growth (Shikha et al., 2021; Singh et al., 2023).

Random Amplification Polymorphic DNA (RAPD) is one of the first indicators that depend on the amplification of the DNA Polymerase Chain Reaction (PCR). It is based on single random primers consisting of ten nitrogenous bases. It was developed in 1990 and took a large part in the application of genetics, where they were associated with their complements on the genome by the presence of the DNA polymerase enzyme to show a discrepancy between the genetic structures through the presence or absence of this region on the genome or the number and length of its copies. It is detected by product migration on an agarose gel (Williams et al., 1990). The valuation of genetic diversity is essential for crop improvement, effective administration, and resource conservation (Tahir and Karim, 2011). DNA markers have proved valuable in crop breeding, specifically regarding genetic diversity, and in gene mapping studies. The commonly used PCR-based DNA marker system is RAPD (Tahir and Karim, 2011). Moreover, the RAPD technique is one of the most commonly used molecular markers (Al-Rawashdeh, 2011; Tahir et al., 2018). It is valuable because it requires less sophisticated apparatus and has shown less expense and efficiency in developing many DNA markers quickly (Bardakci, 2001). In addition, RAPD identification techniques can be used at any stage of plant growth and are not exaggerated by environmental features (Lisek et al., 2006). Thus, the main objectives of this study are summarized as follows:

First, the study examines ten pure strains of corn and the resulting single hybrid. Second, it aims to detect DNA genetic variation for the studied models (pure strains and individual hybrid). Third, we focus on determining the genetic relationship between the studied models, particularly between the pure strains as parents of individual hybrids. This is done through utilizing the Random Amplification Polymorphic DNA (RAPD) indices, which is a key tool in understanding the genetic dimension and their groups.

2. Materials and methods

2.1. Plant Materials and Experimental Locations

In this study, ten pure strains of yellow corn were used (Table 1). The strains were entered into a half-diallel cross program according to the second Griffing method (1956) during the fall season in 2020; and (45) individual crosses were obtained. The investigation was carried out in the autumn and spring seasons on one of the farmers' fields in Kirkuk Governorate. First, two parallel ploughs prepared the ground. Then, the field was divided into sections based on need. Next, it was smoothed and amended using mulches. The same practices were implemented every agricultural season, and super fertilizer was used to fertilize the experimental area. After that, triple phosphate P_2O_5, which is a source of phosphorus at a rate of 200 kg/ha, was added in one batch with tillage; and nitrogen fertilizer was added at a rate of 400 kg N/ha. Subsequently, the urea fertilizer (effective nitrogen ratio 46%) was used in two batches: the first was at planting; and the second was after 30 days of planting (Al-Hamdani, 2012). All agricultural operations of irrigation and weeding were carried out with precision, according to the needs of the crop. In addition, the corn stalk borer insect (Sesamia cretica) was controlled during the seasons by using diazinon granular at a concentration of 10% topically, with two applications during each season. The first application was done after 20-25 days of planting; and the second was conducted after two weeks.

Table 1. Strains used in the study and their source.

No. of strain	Strain name	Source	Source to obtain it
1	Gimbson	Italian	College of Agriculture - University of Mosul(UOM)
2	Saganto	Turkish	College of Agriculture - University of Duhok (UOD)
3	DK 6050	Turkish	College of Agriculture - University of Duhok (UOD)
4	Agr-183	Locally	College of Agriculture - University of Duhok (UOD)
5	ZM47W	American	College of Agriculture - University of Mosul(UOM)
6	CML494	Mexican	College of Agriculture - University of Mosul(UOM)
7	IK58	Hungarian	College of Agriculture - University of Duhok (UOD)
8	ZP505	Yugoslavia	College of Agriculture - University of Duhok (UOD)
9	ZP670	Yugoslavia	College of Agriculture - University of Duhok (UOD)
10	ZP197	Yugoslavia	College of Agriculture - University of Duhok (UOD)

The experiment was watered according to the needs of the crops; and the weeds were controlled manually in all seasons. Furthermore, the method of implementing the crossbreeding and comparison program was applied as follows:

Autumn season (2020): The kernels of the ten pure strains were sown in the land where the experiment was carried out. All soil service operations were conducted on three dates; and the period between each date was (7) days, starting from the beginning of July to ensure the compatibility of flowering and the continuation of obtaining pollen grains with high vitality during the period. Next, cultivation was done on two rows for each strain. The length of the rows was (4) m; and the distance between the rows was (0.75) m and between the plants was (0.25) m. Two kernels were put in each jar, then thinned to one plant. All half-crosses were conducted

$$n = \frac{p(p-1)}{2}$$

at the flowering stage of the strains to obtain (45) single hybrids according to the second Griffing method (1956). The pollination was controlled by sampling the male and female inflorescences, as indicated by Ali (1988). Additionally, self-pollination of the pure strains was carried out to ensure the preservation of the genetic purity of the strains and the multiplication of their kernels. At the end of the season and at full maturity, the hybrid and self-pollinating parental corn were harvested for each strain in isolation. The corn was hulled, and then its grains were sprouted and dried for cultivation in the second season.

Spring season (2021): The kernels of the parents and individual hybrids (10 strains + 45 individual hybrids) were sown on three dates: the first date was on the fifteenth of March, the second was one week later, and the third was one week after the second date; this is to ensure consistent flowering and continued obtaining of kernels. High pollen viability was detected during the period of hybridity. Corn was sown for each genotype (strain + single hybrid). The length of the rows was (4) m; and the distance between the rows was (0.75) m and between the plants was (0.25) m. Besides, kernels were placed in one hole, and then reduced to one plant. Moreover, all soil and crop service operations were carried out.

2.2. Genetic statistical analysis

Statistical analysis for all the studied characters was conducted according to the Random Complete Block Design (R.C.B.D.) with three replications to find out the differences between the genotypes, as explained by Hoshmand (2018). The data taken from the ten pure strains and their mutualistic hybrids, except for the half-diallel cross, were analyzed using the second method, the random model proposed by Griffing (1956), in which the number of genotypes subject to investigation $n = \frac{n(n-1)}{2}$ is equal to (55). Additionally, the additive, dominance, and environmental components and the genetic variation were estimated as $\sigma^2 G$; and the phenotypic variation was estimated as $\sigma^2 p$ (Al-Zubaidi and Al-Jubouri, 2016).

2.3. Preparation of the maize samples

Plastic pots were filled with kernels (55 genotypes), including the ten pure strains and their reciprocal hybridization. After the plants grew to about (40) cm, they were moved to the molecular biology lab, where laboratory tests were carried out to extract the genetic material (DNA).

2.4. Genomic DNA isolation

The DNA was extracted from the immature maize leaves using CTAB, the protocol described by Weigand *et al*. (1993), and the principles established by Sahgai-Maroof *et al*. (1984).

2.5. Solutions used for DNA isolation:

The solutions were used to isolate DNA, based on Maniatis *et al*. (2001).

2.6. Method of isolating DNA from maize leaves:

After removing the young leaves from each of the fifty-five genotype samples, they were dried and cleaned with distilled water (DW). Next, they were diced, weighed (0.5 gm), and put into a ceramic mortar filled with liquid nitrogen. Subsequently, the material underwent further processing until a powdery white color emerged. Afterwards, the powder with (5) ml of the CTAB extraction solution were contained in glass tubes. Then, the tubes were submerged in a water bath set at 65 degrees Celsius and shook constantly for 90 minutes throughout the incubation period. After being removed from the water bath, the glass tubes were allowed to reach an average temperature. Then, (4) ml of chloroform ($CHCl_3$), isoamyl alcohol (1:24) solution, was added to every tube and rapidly shaken for 15 minutes. Through using rotors operating at (5,000) rpm or less and at four °C, the mixture

was disposed of after 15 minutes of being housed in tubes within a cooled centrifuge.

Once the discarding time ended, the top aqueous layer was removed using a micropipette and placed into a separate tube. After that, (4) ml of chloroform (CH Cl $_3$), isoamyl alcohol solution, was added, and the mixture was centrifuged for 15 minutes at (5000) rpm or less at four °C. After adding an equivalent amount of cooled ethanol, the mixture was mixed slowly until a white substance that resembled DNA strands appeared.

The DNA strands were extracted using a glass rod with a curved end and then put in a tube with (2) ml of washing solution. Next, the tube was left for 20 minutes. After that, the rod was hoisted into sterile tubes holding (100–200uL) of the dissolving solution. Finally, the DNA samples were stored at -20 °C for subsequent use and periodically mixed until the DNA entirely dissolved.

2.7. Determining of the concentration and pureness of the extracted DNA:

Ultimate purity and concentration of the DNA were obtained by dividing the reading of 260 nanometers by 280 nanometers using the Nano Drop device. This instrument offers simple and rapid results for determining the attention and purity of DNA on the linked computer. At 260 and 280 nanometers, the gadget reads DNA after downloading just one microliter of the material.

2.8. Estimating of DNA molecular sizes:

Electrophoresis was performed on an agarose gel using a DNA size guide (a 100 bp DNA ladder) with known molecular weight to estimate DNA molecular sizes.

2.9. Solutions used in migration:

The solutions used in migration were adopted according to Maniatis et al. (2001). Loading buffer with a power of 10X: Bromophenol blue dye (0.25 g) was dissolved in 50% glycerol to create this solution. Next, 60 mM (PH = 8) of the EDTA solution was added, and the volume was increased to (100 ml) through distilled water (d.w). Finally, it was saved at 4 °C until it was used later.

Ethidium bromide dye: It was prepared by dissolving (100 mg) of colorant powder in 10 ml of distilled water at a concentration of 10 mg/ml. Then, it was stored at 4°C in a sterile bottle until needed to be used. Moreover, 40 uL were taken from it and combined with (1L) of distilled water to make the staining solution for agarose gel.

2.10. Agarose gel preparation process and DNA electrophoresis .

The agarose gel method and DNA electrophoresis were applied according to Maniatis et al. (2001). A 1.5% agarose gel with a volume marker was previously prepared.

2.11. Estimation of molecular weights

In the attendance of typical size indicators (Markers), the molecular weights of the DNA bundles were determined by considering the inverse relationship between their molecular weights and the distance travelled in the gel. The volumetric guide DNA bundles' molecular weights on the "y-axis" and the space travelled by every bundle in the gel on the "x-axis" were shown graphically to create a curve. This curve determines the estimated molecular weight of every bundle.

2.12. Method (RAPD technique):

All solutions were stored at low temperatures, and the process was conducted under sterile conditions. The finishing concentration for RAPD reactions was around (50) micrograms/microliter for every sample. It was reached by diluting the concentrations of the investigated DNA samples using sterile distilled water. The reaction components were combined in a sterile 0.2 ml Premix tube to create the master reaction mixture.

Table 2. represents the main interaction components of the RAPD indicator

Components	Concentration	Volume of each sample
Sterile distilled water	-	16.5 µl
PCR Premix	-	2 µl
Primer	10 picomoles	0.5 µl
DNA sample	(50) ng / microliter	1 µl
Total volume		20 µl

Subsequently, it was placed in the thermo-cycler where there were forty replication cycles; each cycle consisted of thirty seconds at ninety-two degrees Celsius for the denaturation of the double strand DNA, forty-five seconds at thirty-six degrees Celsius for the attachment of the primer to the template DNA, forty-five seconds at eighty-two degrees Celsius for the primer elongation, and finally seventy minutes at eighty-two degrees Celsius for the completion of the elongation phase. After the reaction time, the tubes were removed from the thermo- cycler, and five microliters were withdrawn. The tubes were loaded with previously prepared 1.5% agarose gel, with the Marker loaded on one side. Next, the samples were moved using the electrophoresis apparatus for ninety minutes. The power supply was programmed to the desired voltage (3V/cm between electrodes). Later, the gel was subjected to UV light on a UV ray after being stained by ethidium bromide (EtBr), dyed for 30 minutes, and agitated by a shaker.

2.13. RAPD reactions:

RAPD reactions were implemented, based on Williams et al. (1990), on the DNA samples (55 genotypes) including the ten pure strains and 45 individual crosses.

2.14. Materials and solutions needed to carry out the reaction.

The premix buffer solution was acquired from Bioneer.

Table 3. Shows the components of Premix.

Taq DNA Polymerase	1 U
dATP,dCTP,dGTP,dTTP)(dNTP	250 µM
Tris-HCl (PH 9.0)	10 mM
KCl	30 mM
MgCl2	1.5mM

2.15. Random Primers:

As shown in Table (4), 15 primers were utilized. They were prepared using Operon Technologies, USA.

Table 4. Randomized primers (RAPD) used in this study with their nucleotide sequences.

Primer	Sequence
OPA-07	$^{5'}$GAAACGGGTG$^{3'}$
OPA-09	$^{5'}$GGGTAACGCC$^{3'}$
OPA-11	$^{5'}$CAATCGCCGT$^{3'}$
OPA-13	$^{5'}$CAGCACCCAC$^{3'}$
OPA-18	$^{5'}$AGGTGACCGT$^{3'}$
OPA-19	$^{5'}$CAAACGTCGG$^{3'}$
OPC-01	$^{5'}$TTCGAGCCAG$^{3'}$
OPC-02	$^{5'}$GTGAGGCGTC$^{3'}$
OPC-07	$^{5'}$GTCCCGACGA$^{3'}$
OPC-08	$^{5'}$TGGACCGGTG$^{3'}$
OPC-15	$^{5'}$GACGGATCAG$^{3'}$
OPD-03	$^{5'}$GTCGCCGTCA$^{3'}$
OPD-05	$^{5'}$TGAGCGGACA$^{3'}$
OPD-08	$^{5'}$GTGTGCCCCA$^{3'}$
OPD-18	$^{5'}$GAGAGCCAAC$^{3'}$

Results and discussion

Table (5) displays the findings of the analysis for variance of eight traits. It has been noted that for all the traits under investigation, the genetic differences between the parents and their half-crosses were significant at the possibility level (1%). Parents and hybrids had variations in their genomes, proving that the genotypes are genetically distinct. This outcome is considered a reliable predictor of a crucial input for conducting the genetic analysis of these characteristics and determining the constituent parts of genetic variation. This result agrees with those reported by Al-Jumaily and Al-Zubaidy (2018) and Al-Jubouri *et al*. (2024) .

Table 5. Analysis of variance for (parents), (crosses), and (parents and crosses) for the studied traits.

		(Parents) M.S							
S.O.V	d.f	Individual plant yield	Weight 300tablets	Number of grains/maize ear	number grain/grade	number Rows / maize ear	maize ear diameter	maize ear length	maize ear No./ plant
Duplicates	2	17679.10	5334.00	461926.54	758.33	300.62	71.87	261.86	1.03
Parents	9	**608.25	**187.10	**6577.85	**24.83	**7.46	**1.29	**9.90	**0.10
Experimental error	18	136.88	23.20	1530.67	0.94	1.77	0.21	1.53	0.01
		(crosses) M.S							
S.O.V	d.f	Individual plant yield	Weight 300tablets	Number of grains/maize ear	number grain/grade	number Rows / maize ear	maize ear diameter	maize ear length	maize ear No./ plant
Duplicates	2	72582.35	21116.85	2033661.70	3888.59	1075.27	417.28	1147.93	6.44
Parents	44	**574.72	**136.97	**7235.53	**18.24	**6.94	**3.92	**7.18	**0.11
Experimental error	88	181.35	46.80	1127.89	1.33	1.13	0.75	1.48	0.02
		(parents and crosses) M.S							
S.O.V	d.f	Individual plant yield	Weight 300tablets	Number of grains/maize ear	number grain/grade	number Rows / maize ear	maize ear diameter	maize ear length	maize ear No./ plant
Duplicates	2	90050.07	26390.09	2492291.99	4643.53	1372.99	255.116	1409.58	7.46
Parents	54	**590.55	**144.36	**7072.82	**20.01	**6.91	**0.175	**7.79	**0.11
Experimental error	108	174.49	43.13	1235.18	1.31	1.27	0.035	1.47	0.02

In addition, the results presented in tables (6) and (7) indicate the averages of the genotypes and their hybrids for the studied traits, including the number of ears/plant. The Genotype (8) gave the highest number of ears, amounting to (1,292) ears, while the father passed (2). On the other hand, the lowest number of branches reached (0.542) ears, while the hybrid (4×8) excelled and showed the highest rate of ears (1.414). Furthermore, the hybrid (1×2) was the most diminutive in the number of ears and reached (0.599) ears. Obviously, the averages for the parents and hybrids showed that the hybrids excelled and reflected the highest average for maize ear (0.94), while the parents gave the lowest average (0.85). The overall average for the parents and hybrids was 0.92. Moreover, the maize ear originated at the axil of each leaf in most yellow maize plants but in a different way. If the growth factors are available and effective, where the vigour of the hybrid plays a role in achieving this, they stimulate more than one stem formation on the plant (Al-Sahuki, 1990).

Table 6. Averages of parents' performance for the studied characteristics

Parents features	maize ear No./ plant	maize ear length	maize ear diameter	Number Rows / maize ear	number grain/grade	Number of grains/maize ear	Weight 300tablets	Individual plant yield
1	0.966	11.266	3.874	13.133	25.778	413.460	59.084	117.927
2	0.542	9.789	4.014	10.322	19.856	297.328	44.691	99.251
3	0.610	12.744	3.516	13.911	27.789	413.921	57.611	125.435
4	0.848	12.633	3.969	13.222	27.566	434.150	61.296	126.529
5	0.817	12.422	4.002	12.977	28.244	412.003	58.437	120.521
6	0.865	12.433	4.030	13.011	28.367	379.129	59.971	116.242
7	0.839	12.133	4.073	12.644	26.289	387.500	60.798	114.111
8	1.292	16.888	6.021	16.611	31.044	470.593	77.443	155.123
9	0.873	12.177	3.975	12.711	26.711	370.658	59.289	123.620
10	0.894	11.311	3.819	11.955	25.867	362.351	56.336	113.849
Mean	0.85	12.38	4.13	13.05	26.75	394.11	59.50	121.26
L.S.D 0.01	2.1	2.11	2.12	2.28	1.67	67.11	8.26	20.07

Table 7. shows the averages of the first generation hybrids for the studied traits.

Parents features	maize ear No./ plant	maize ear length	maize ear diameter	Number Rows / maize ear	number grain/grade	Number of grains/maize ear	Weight 300tablets	Individual plant yield
2×1	0.599	10.111	4.049	9.466	19.367	294.751	57.158	112.533
3×1	0.964	13.200	3.909	12.900	28.845	412.864	65.424	112.611
4×1	1.033	13.222	4.219	12.644	28.967	400.071	63.344	128.929
5×1	0.826	13.322	4.088	12.955	27.944	392.379	60.391	115.860
6×1	0.839	12.455	4.160	12.622	28.167	370.779	55.878	108.242
7×1	0.799	12.111	3.847	12.255	27.589	368.891	59.638	99.873
8×1	1.381	16.096	6.973	16.244	30.852	505.809	73.762	144.576
9×1	0.861	11.933	3.859	12.044	28.122	402.013	54.527	104.516
10×1	0.940	12.355	3.964	13.000	28.055	418.246	61.889	124.753
3×2	0.739	10.344	4.033	10.577	19.422	300.041	58.229	110.044
4×2	0.988	13.111	4.029	13.144	28.467	377.846	57.303	105.347
5×2	0.837	13.888	4.021	13.444	29.955	389.918	58.569	111.624
6×2	0.839	13.133	4.067	12.911	28.756	391.859	57.089	108.451
7×2	0.810	12.622	4.011	12.444	26.933	385.863	55.105	97.332
8×2	1.392	16.555	6.908	15.944	31.400	494.920	73.618	127.273
9×2	1.055	13.011	4.143	11.844	28.544	380.183	58.158	114.689
10×2	0.815	11.955	4.113	12.155	27.189	404.018	62.740	115.073
4×3	0.772	12.111	4.061	12.133	27.600	367.138	52.918	89.569
5×3	0.810	12.178	4.031	13.678	26.789	394.289	57.256	105.840
6×3	0.815	12.422	4.139	14.244	25.733	401.371	60.862	115.549
7×3	0.966	12.511	3.988	12.777	27.489	386.390	58.263	110.252
8×3	1.347	16.400	6.918	16.222	31.300	473.693	76.767	141.573
9×3	0.905	13.277	3.858	12.366	29.067	392.586	61.102	128.631
10×3	0.832	13.177	3.917	12.400	27.922	389.587	59.212	110.942
5×4	1.010	13.644	4.008	13.278	28.633	407.914	58.752	118.412
6×4	0.892	12.377	4.033	12.711	27.366	421.559	61.286	106.518
7×4	0.817	13.099	4.041	13.222	28.511	416.541	59.036	122.593
8×4	0.794	13.566	4.103	13.066	29.678	428.602	74.371	155.722
9×4	0.910	12.577	3.951	12.767	28.622	391.689	58.062	119.476
10×4	0.826	11.799	3.877	11.933	27.244	369.507	53.298	99.076
6×5	0.794	12.322	3.876	12.689	28.289	387.674	55.556	104.453
7×5	0.843	12.622	3.832	11.622	28.911	364.009	58.052	103.773
8×5	1.336	16.244	6.106	15.311	31.267	480.421	71.539	124.481
9×5	0.870	12.455	3.743	12.455	28.811	392.856	58.887	114.407
10×5	0.794	11.589	4.126	12.533	27.333	396.382	57.364	103.791
7×6	0.865	12.111	3.588	12.844	28.844	408.437	57.824	98.452
8×6	1.314	14.944	6.447	16.488	30.500	507.010	73.094	117.987

9×6		0.870	12.422	3.997	12.955	27.422	380.454	56.433	105.055
10×6		0.817	11.889	3.905	12.433	24.733	334.059	52.154	84.729
8×7		1.236	16.199	6.522	15.688	31.000	471.991	58.462	118.829
9×7		0.865	12.477	4.129	13.444	28.211	418.891	59.949	104.020
10×7		1.414	15.977	7.399	16.200	31.900	483.554	75.695	131.634
9×8		0.965	15.766	6.787	15.177	31.111	499.198	71.591	128.293
10×8		1.070	14.111	6.935	15.066	30.322	486.776	72.442	118.224
10×9		0.843	13.200	3.997	13.311	27.844	392.231	57.900	127.664
	Mean	0.94	13.18	4.55	13.24	28.25	407.45	61.35	114.48
hybrid	L.S.D 0.01	0.24	1.97	1.40	1.73	1.87	54.49	11.10	21.85
	Mean	0.92	13.03	4.47	13.20	27.97	405.02	61.02	115.71
Parent	L.S.D 0.01	1.98	1.96	1.98	1.82	1.85	56.88	10.62	21.37

Regarding the maize ear length (cm) trait, the male parent (8) offered a significant increase with an average of (16.888) cm. However, the genotype (2) showed the lowest length (9.789) cm. Nevertheless, the hybrid (2 x 8) revealed the highest average (16.555) cm, with an insignificant difference in comparison to the hybrids (1×8), (3×8), (5×8), and (7×8) reaching (16.096) cm, (16.400) cm, (16.244) cm, and (16.199) cm, respectively. It is noteworthy that the shortest maize ear length was in the hybrid (1×2) with an average of (10.111) cm. When observing the results of the general average, we noted that the parents had the lowest maize ear length, reaching (12.38) cm, while the averages of the crosses were higher, reaching (13.18) cm. Additionally, the general average for fathers and hybrids is (13.03) cm, and thus, the father will be (8), and the hybrids resulting from it will reveal significant importance by increasing the components of the yield, and consequently positively affecting the finished product.

Regarding the characteristics of maize ear diameter (cm), parent (8) showed the highest significant increase, amounting to (6.021) cm. In contrast, the genotype (3) manifested the lowest diameter (3.516 cm). The hybrid (4×8) expressed the highest average; it reached (7.399) cm, which is significantly different from the other hybrids. The shortest stem length of the hybrid was (5×9), with an average of (3.743) cm. When observing the overall average results, we noticed that the parents had the most minor stem diameter, reaching (4.13) cm.

In comparison, regarding the average of the hybrids, the largest diameter was (4.55) cm, and the overall average of the parents and hybrids was (4.47) cm. Increasing the number of leaves and the surface area of the leaves leads to enhancing the process of photosynthesis; moreover, increasing the nutritional savings stored in the grains will result in larger size and fullness of the grains, and thus increases the diameter of the ear (Muhanna *et al.*, 2015).

Furthermore, regarding the number of rows/ear, it was found that the father (8) had the most significant value for this trait, which amounted to (16,611) rows. On the contrary, the father (2) reflected the smallest value, amounting to (10,322) rows. The differences between the fathers led to a clear difference in the intercross hybrids. Furthermore, as for the hybrids, the hybrid (6×8) exhibited the most significant value for this trait, reaching (16,488) rows. Besides, it did not differ significantly from the hybrids (1×8), (3×8), and (4×8), which have reached (16,244) rows, (16,222) rows, and (16,200) rows, respectively. On the other hand, the lowest hybrid was

(1×2), which had a value of (9,466) rows. It is also observed that the average of the hybrids reached (13.24) rows, which is higher than the average of the parents that was (13.05) rows. The general number for parents and hybrids is (13.20) rows. The superiority in the number of rows in the maize ear is attributed to its moral superiority over the rest of the hybrids in the diameter of the maize ear, as well as the existence of a highly significant positive relationship between the number of rows in the maize ear and the diameter of the maize ear. This is due to the difference in the genetic compositions in terms of genetics. This also indicates that the hybrids respond to increasing their value.

Additionally, regarding the number of grains/row trait, we noticed that the father (8) was significantly superior, amounting to (31,044) grains. In contrast, the father (2) revealed the lowest value for this characteristic, amounting to (19,856) grains. Regarding the hybrids, the (4x8) hybrid produced a higher rate reaching 31,900 grains. It was similar to the hybrids (2x8), (3x8), (5x8), (7x8), and (8x9), which reached (31,400), (31,300), (31,267), (31,000) and (31,111) grains, respectively. The hybrid (1×2) yielded the lowest average, reaching (19,367) grains. When comparing the parents' typical with the hybrids' average, the hybrids were distinguished by a higher rate of (28.25) grains. In contrast, the parents and the overall average were (26.75) grains and (27.97), respectively. The hybrids response to the increase in this trait is due to the reaction of the father (8) involved in it. This exaggerated the rise in the number of grains, which notably increased the finishing yield. Therefore, to obtain high production, it is obligatory to confirm the use of genetic combinations possessing that possesses a genetic ability offering a high rate regarding this trait; it is considered one of the essential constituents of the yield and results in high productivity (Al-Nasiri, 2016).

Concerning the trait of the number of grains/ear, we noticed that the superiority of the father (8) reached (470.593) grains, while the father (2) achieved the lowest rate, amounting to (297.328) grains. As for the hybrids, (6×8) showed dominance and an average of (507.010) grains, while the hybrid (1×2) had the lowest average, amounting to (294.751) grains. When comparing the fathers' average to the hybrids' average, the hybrids were distinguished by a higher value of (407.45) grains. In contrast, the fathers' and overall average were (394.11) grains and (405.02), respectively. The response of the hybrids to the increase in this trait is due to the reaction of the father (8) involved in it, which exaggerated the

increase in the number of the grains. In turn, this has a positive effect on increasing the finishing yield. To obtain high production, it is obligatory to confirm the use of genetic structures that have a genetic ability offering an average which is high in relation to this trait, which is considered one of the essential constituents of the crop that result in its high productivity (Al-Nasiri, 2016). Furthermore, it is one of the important traits associated with the grain yield; and it is exaggerated by the genetic nature of the plant as well as the environmental factor. Thus, this significant difference indicates that these hybrids respond to the increase in this trait. The superiority of these parents, especially parent (8) and its hybrids, resulted from the accumulation of the net rate of photosynthesis and dry matter, which was completely reflected in the trait and the finishing yield.

Moreover, the weight of 300 kernels (g) is of great importance since it is considered a sign of the productivity of the transfer process and assimilation of synthetic materials from the source to the downstream sink in the kernel storage sites. It is one of the essential components of the yield. We noticed that the father (8) was significantly higher and reached (77.443) gm, while it differed from the father (2) and reflected the lowest value for this trait, amounting to (44.691) gm. As for the hybrid (3×8), it showed superiority at an average of (76.767) gm, and it did not differ significantly from the hybrids (1×8), (2×8), (4×8), (5×8), (6×8), (7×10), (8×9) and (8×10) that were (73.762) gm, (73.618) gm, (75.695) gm, (71.539) gm, (73.094) gm, (74.371) gm, (71.591) gm, and (72.442) gm, respectively. On the contrary, the hybrid (6×10) revealed the lowest average and reached (52.154) gm. When comparing the average of the parents to the average of the hybrids, it was found that the hybrids were characterized by a higher value of (61.35) gm, while the value of the parents was (59.50) gm. On the other hand, the average for parents and the hybrids was (61.02) gm. The superiority of the parents (8) and their hybrids might be due to their superiority in leaf area, which led to the transfer and assimilation of manufactured materials from the source to the downstream sink in the storage sites of the kernel. This characteristic was reflected positively on the outcome (Abu Dahi *et al.*, 2001; Abdullah and Hasan, 2020; Hasan and Abdullah, 2021; Hasan and Abdullah, 2020; Hasan *et al.*, 2022; Muhammad *et al.*, 2021; and Younis *et al.*, 2022).

The characteristic of the plant's grain yield (g) is considered a finishing result of most of the phenotypic and physiological traits of the plant. In fact, the increase in this trait and its components is an essential achievement for plant breeders. By evaluating the arithmetic averages of the parents and the hybrids, we noticed that the father (8) reflected the highest average, amounting to (155.123) gm. However, the parent (2) showed the lowest average for this trait, amounting to (99.251) gm; and the hybrid (4×8) showed the highest average, amounting to (155.722) gm, which did not differ significantly from the hybrids (1×8) and (3×8) that amounted to (144.576) gm and (141.573) gm, respectively. However, the hybrid (6×10) had a lower yield of (84.729) gm, when compared to the rest of the other hybrids. The average of the parents was significantly higher than the average of the hybrids, amounting to

(121.26) gm. The overall average reached (114.48) gm and (115.71) gm, respectively. The superiority of these parents and their hybrids in the kernel yield results from their superiority in the yield constituents, which was remarkably revealed in the finishing yield. The dissimilarities between the parents and the hybrids in the grain yield are due to the dissimilarity in the addition of kernel dry matter and to the increased photosynthesis through the male and female flowering phase, which had positive impact on the finishing yield (Elsahookie, 2007).

Based on the above-mentioned, we concluded the following about the fathers: The father (8) outperformed the other fathers with regard to all the characteristics studied.

In addition, concerning the hybrids, the hybrid (4×8) was distinguished from the other hybrids since it was superior in the number of ears/plant, diameter of the ear (cm), number of grains/row, and grain yield per plant (g). However, the hybrid (2×8) surpassed with regard to the characteristic of ear length (cm). The hybrid (6×8) was superior in terms of number of rows/maize ear and number of grains/maize ear. Finally, the hybrid (3×8) was exceptional in terms of weight of 300 grains (g).

Furthermore, when comparing the average of the parents and the average of the individual hybrids, we noticed that the average of the hybrids was higher than that of the parents in all the studied traits, except for the grain yield per plant (gm). It is also inferred from the above-mentioned that there are differences in the performance of the hybrids in all the studied traits, which can be used in breeding and improvement programs to obtain synthetic varieties or profit from hybrids characterized by high and significant hybrid vigour and superior in grain yield and its components. These results agree with those obtained by Al-Bayati, 2013; Al-Zuhairi, 2014; Al-Karkhi, 2015; and Younis *et al.*, 2022.

Additionally, the extra genetic variation values were more significant than the dominant genetic variation regarding all the characteristics. Table (8) displays the estimates of the environmental σ2E, the dominant σ2D, and the additional genetic variation σ2A for all the traits under investigation. Pure line or mass selection is the most appropriate breeding method for traits in which the values of the additional genetic variation are more significant than the values of the dominant variation. This is because the gene action is additive, which plays a more substantial role in controlling the inheritance of these traits. On the other hand, the dominant genetic action substantially influences qualities if the values of the dominant genetic variation are higher than those of the extra genetic variation. Besides, regarding σ2G and genetic variation, all traits showed an increase in genetic variation in comparison to environmental variance values. Moreover, increasing the genetic variance of a trait resulted in a decrease in its ecological variance. Furthermore, all the traits showed an increase in phenotypic variance values in comparison to the environmental and genetic variances. These findings are consistent with those reported by Abdullah and Hasan, 2020; Younis *et al.*, 2022; Hasan and Abdullah, 2020; Hasan *et al.*, 2022; Muhammad *et al.*, 2021; and Younis *et al.*, 2022.

Table 8. Variance values for the studied traits

Features Parents	maize ear No./ plant	maize ear length	maize ear diameter	number Rows / maize ear	number grain/grade	Number of grains/maize ear	Weight 300tablets	Individual plant yield
σ^2_A	0.329	23.517	11.746	21.375	40.528	19085.332	375.255	969.461
σ^2_D	0.014	0.767	0.230	0.630	3.955	920.598	20.220	139.277
σ^2_e	0.009	0.491	0.180	0.425	0.437	411.727	14.378	58.167
σ^2_G	0.343	24.284	11.976	22.005	44.483	20005.930	395.475	1108.737
σ^2_P	0.352	24.775	12.156	22.431	44.920	20417.657	409.853	1166.904

2.16. Results of RAPD interactions

The effects of the (15) RAPD primers used in this study varied; the primers were found to have corresponding sequences on the DNA of the genotypes (ten pure strains + their hybrids) studied. The following is a review of the results of the primers that showed different bands, as clarified in Table (9):

Primer OPA-01: In PCR procedures, this primer was used to double the genotypes' DNA studied. The primer yielded eight bands, ranging from 600 to 1500 bp, with an average molecular size of two to six. Eight bands, or 100%, of divergent packets, were created using this primer. Its efficiency is (5.369%), which is calculated as the ratio of all the bands it formed to all the packages all the primers produced. In addition to the number of unique bands produced by each primer, this primer's discriminating ability was (6.015%); the parent could be identified if a band was absent (6).

Primer OPA-02: This primer formed (3) bands; their molecular size ranged among (500-1000) bp, at an amount of (1-3) bands for the genetic composition. Moreover, the number of different bands formed by this primer reached (3) bands (100%), while the efficiency of this primer was (2,013%), and its discriminatory ability was (2,256%). This primer produced an absent band marked for the father (3) with a molecular size of (1000) bp. It also made a visible band with a molecular size of (500) bp, distinguishing it as a hybrid (1x5).

Primer OPA-03: This primer displayed five bands, with their molecular sizes restricted to (600-1760) bp. Depending on the genetic content, the rate of band formation was (1-3) bands; and four bands were created in total, representing (80%) of the total packet count, and initiator's efficiency that reached 3,356%. On the other hand, its discerning power reached (3,008%). This primer displayed a distinctive hybrid band (1x5) with a molecular size of (600) bp.

Primer OPA-04: This primer's products were represented by (4) bands. Their molecular sizes extended among (630-1340) bp and among (1-4) bands according to the genetic composition. The number of dissimilar beams was (4), i.e. (100%) of the number of beams. Thus, its efficacy was (2.685%), and its discriminatory capacity was (3.008%).

Primer OPC-05: The results of this primer showed the presence of (6) bands whose molecular sizes were limited to (600-1500) bp and ranged from (1-5) bands, based on the genetic composition. The results also showed the presence of several different bands that reached (6) bands.

That is a percentage of (100%). Accordingly, the efficiency of this primer reached (4.027%), while its discriminatory ability reached (4.511%). Additionally, two genetic structures were distinguished: the father (3), which was characterized by an absent band with molecular size reached (600) bp, and the father (4), which was distinguished by its visible bands with a molecular weight of (1500) bp.

Primer OPC-06: This primer formed (3) bands with molecular size extended among (700-1145) bp, and with an average of (1-3) bands for the genotype. The number of different bundles produced by this primer reached (3) problematic bundles, representing (100%) of the number of bundles produced. This primer recorded an efficiency of (2,013%) and a discrimination ability of (2,256%). It also recorded the distinction of the hybrid (1x6) with a visible bundle with a molecular size of (700) bp.

Primer OPC-07: This primer achieved several bands that reached (7), their molecular sizes were limited to (400-1690) bp. The number of bands varied between the genotypes to range between (2-6) bands; and the number of different bands that it formed reached (6) bands, representing (85,714%) of the number of bands. Furthermore, the efficiency of this primer reached (4,698%), while its discriminatory ability reached (4,511%). Besides, the primer (3) was distinguished by an absent band with a molecular size of (800) bp.

Primer OPC-08: The number of bands logged by this primer was (9) bands; their molecular sizes ranged between (400-1500) bp, with an average of (2-7) bands for genetic composition. Moreover, the number of divergent bands in the primer was (9) bands, with a percentage of (100%) of the number of bands. Accordingly, the efficiency of this initiator reached (6.04%), while its discriminatory ability reached (6.767%). This primer was recorded for the parents (3) and (6) with a visible band and a molecular size of (450) bp and (400) bp for the parents, respectively.

Primer OPC-09: The number of bands reached by this primer was (5) ones with molecular sizes ranged among (300-1530) bp. Additionally, the number of bands for genotypes extended among (1-4) bands; and the number of different bands attained was (4) bands, constituting (80%) of the number of bands. The efficiency of this primer was (3,356%), while its discriminatory ability was (3,008%). The father (6) in this primer was characterized by a visible band with a molecular size of (1530) bp.

Primer OPD-10: The number of bands for this primer was (8) bands; and their molecular sizes were limited to (400-1580) bp, at a rate of (1-5) bands, according to the

genetic composition. Moreover, (7) bands showed a variation of (87, 5%) of the number of bands. Accordingly, the efficiency of this primer reached (5.369); and its discriminatory ability reached (5.263%). The primer (3) was distinguished by a visible band with a molecular size of (800) bp.

Primer OPD-11: This primer produced seven bands, with molecular sizes ranging from (280-1200) bp. The primer had six distinct bands, and the genetic content was restricted to three to seven bands. One band achieved (85,714%) of the total number of bands. Its efficiency was (4,698%); and its discriminating power was (4,511%).

Primer OPD-12: This primer indicated the existence of four bands with molecular sizes ranging from (375-1580) bp. Depending on the genetic composition, there were one to four bands; and the number of bands fluctuated forming three bands in the primer (75%). The efficiency of the primer was (2,685%); and its discriminating power was (2,256%). The absence of a separate band could identify the parent (6), which its molecular size was (370) bp.

Primer OPY-13: This primer reached (9) bands, making it one of the primers with the highest number of bands obtained. Their molecular sizes varied from (200-1590)

bp. The number of bands for the genotypes varied from 1 to 8 bands, reaching a total of (77,777%), representing the number of distinct bands attained by (7) bands. As a result, the efficiency of this primer was (6.04%); and its discriminating power was 5.263%. A discernible band identified this primer's hybrid (1x6) with a molecular size of (1590) bp.

Primer OPY-14: This primer yielded eight bands, with an average of one to seven bands for each genotype and a molecular size limit of (480-1500) bp. Every band this primer created was unique and accounted for 100% of the total number of bands formed. The efficiency of this primer was (5.369%); and its discriminating power was (6.015%). A band is lacking in the hybrid (3x5), with a molecular size of (700) bp, allowing differentiation.

Primer OPD-15: This primer generated nine bands, with an average of four to eight bands per each genotype and a molecular size ranging between (375-1200) bp. The initiator exhibited seven distinct bands, signifying (77,777%) of the total bands. As a result, the efficacy of the initiator was (6.04%); and its discerning capacity was (5,263%).

Table 9. shows the products of primers from DNA bands and their efficiency and discriminatory ability.

Primer code	The total number of packets generated	Molecular size range of bp bands	Output packet rate	Number of different bandss	Percentage of dissimilar packets %	Number of identical bandss	Distinctive genetic makeup			Efficiency %	Discriminating ability %
							Premium installation code	Molecular size of the characteristic bands bp	Type of discrimination		
OPA-01	8	1500-600	6-2	8	100	0	2X4	1500	present	5,369	6,015
							6	500	absent		
OPA-02	3	1000-500	3-1	3	100	0	3	1000	Absent	2,013	2,256
							1X5	500	present		
OPA-03	5	1760-600	3-1	4	80	1	1X5	600	Present	3,356	3,008
OPA-04	4	1340-630	4-1	4	100	0	--	--	-	2,685	3,008
OPC-05	6	1500-600	5-1	6	100	0	3	600	present	4,027	4,511
							4	1500	absent		
OPC-06	3	1145-700	3-1	3	100	0	1X6	700	Present	2,013	2,256
OPC-07	7	1690-400	6-2	6	85,714	1	3	800	Absent	4,698	4,511
OPC-08	9	1500-400	7-2	9	100	0	3	450	Present	6,040	6,767
							6	400	Present		
OPC-09	5	1530-300	4-1	4	80	1	6	1530	Present	3,356	3,008
OPD-10	8	1580-400	5-1	7	87,5	1	3	800	Present	5,369	5,263
OPD-11	7	1200-280	7-3	6	85,714	1	--	--	-	4,698	4,511
OPD-12	4	1580-375	4-1	3	75	1	6	370	Absent	2,685	2,256
OPE-13	6	1465-500	6-1	6	100	0	1X4 6X5	660	Absent	4,027	4,511
								1200	Absent		
OPY-14	8	1500-480	7-1	8	100	0	3X5	700	Absent	5,369	6,015
OPD-15	9	1200-375	8-4	7	77,777	2	--	--	-	6,040	5,263

2.17. Inheritance of DNA bands

Individuals of the first generation inherit some bands through the first father and other bands through the second father. Moreover, some bands are inherited through both parents. They are inherited from parents to the first generation according to the Mendelian inheritance of phenotypic characteristics. There is also another type of bunches; they are new bunches that are not found in either parent (Abdel-Mawgood *et al.*, 2006). A study on individual hybrids of Levantine corn indicated that some bunches were present in the parents that were not in the first generation (Abdel-Mawgood *et al.*, 2006). While

there were new bands in the hybrids that are not present in either parent, the appearance of such bands has been explained by the presence of mutations in the places where the primers join the DNA, the formation of an asymmetric hybrid (Davis *et al.*, 1995), or the occurrence of recombination (Scott *et al.*, 1992). It might be also related to gene expression as reported by Scheuring *et al.* (2006) who conducted a molecular analysis of the typical American yellow corn hybrid (B73xMo17) and its parents and found that approximately 800 pairs of genes in the hybrid had increased gene expression. In some of them, it was ten times higher. Hybridization stimulated several

genes from their parents to show or increase their genetic expression. Table (10) shows the results of the inheritance of bands in individual hybrids regarding all the primers. Additionally, the number of bands in each hybrid was divided into bands inherited from the first parent, bands inherited from the second parent, bundles inherited from both parents, and new bundles that do not exist in either parent.

Table 10. Results of inheritance of DNA bands in individual hybrids as a result of all primers.

Hybrid No.	No. total bands	Source bands inheritance							
		First father		Second father		both parents		New band	
		Band No.	%	Band No.	%	Band No.	%	Band No.	%
(2×1)	85	19	22,352	12	14,117	30	35,294	24	28,235
(3×1)	80	5	6,250	15	18,75	52	65	8	10
(4×1)	77	16	20,779	5	6,494	47	61,039	9	11,688
(5×1)	79	14	17,721	19	24,05	40	50,632	6	7,595
(6×1)	85	20	23,529	4	4,706	46	54,118	15	17,647
(7×1)	83	24	28,915	12	14,457	40	48,193	7	8,434
(8×1)	86	20	23,255	9	10,465	50	58,139	7	8,140
(9×1)	74	7	9,459	10	13,513	55	74,324	2	2,703
(10×1)	75	10	13,333	19	25,333	38	50,666	8	10,667
(3×2)	85	19	22,352	12	14,117	30	35,294	24	28,235
(4×2)	80	5	6,250	15	18,75	52	65	8	10
(5×2)	79	12	15,189	6	7,595	53	67,088	8	10,127
(6×2)	89	25	28,089	13	14,606	38	42,697	13	14,607
(7×2)	79	12	15,189	6	7,595	53	67,088	8	10,127
(8×2)	89	25	28,089	13	14,606	38	42,697	13	14,607
(9×2)	91	11	12,087	7	7,692	63	69,230	10	10,989
(10×2)	85	20	23,529	4	4,706	46	54,118	15	17,647
(4×3)	85	13	15,294	8	9,411	48	56,470	16	18,824
(5×3)	86	20	23,255	9	10,465	50	58,139	7	8,140
(6×3)	85	20	23,529	4	4,706	46	54,118	15	17,647
(7×3)	85	20	23,529	4	4,706	46	54,118	15	17,647
(8×3)	74	7	9,459	10	13,513	55	74,324	2	2,703
(9×3)	86	20	23,255	9	10,465	50	58,139	7	8,140
(10×3)	74	7	9,459	10	13,513	55	74,324	2	2,703
(5×4)	75	10	13,333	19	25,333	38	50,666	8	10,667
(6×4)	83	24	28,915	12	14,457	40	48,193	7	8,434
(7×4)	83	24	28,915	12	14,457	40	48,193	7	8,434
(8×4)	86	20	23,255	9	10,465	50	58,139	7	8,140
(9×4)	83	24	28,915	12	14,457	40	48,193	7	8,434
(10×4)	75	10	13,333	19	25,333	38	50,666	8	10,667
(6×5)	74	15	20,270	11	14,864	41	55,405	7	9,459
(7×5)	85	19	22,352	12	14,117	30	35,294	24	28,235
(8×5)	80	5	6,250	15	18,75	52	65	8	10
(9×5)	77	16	20,779	5	6,494	47	61,039	9	11,688
(10×5)	85	13	15,294	8	9,411	48	56,470	16	18,824
(7×5)	74	15	20,270	11	14,864	41	55,405	7	9,459
(8×5)	85	19	22,352	12	14,117	30	35,294	24	28,235
(9×5)	80	5	6,250	15	18,75	52	65	8	10
(10×5)	79	12	15,189	6	7,595	53	67,088	8	10,127
(7×6)	89	25	28,089	13	14,606	38	42,697	13	14,607
(8×6)	96	15	15,625	8	8,333	64	66,666	9	9,375
(9×6)	91	11	12,087	7	7,692	63	69,230	10	10,989
(10×6)	86	20	23,255	9	10,465	50	58,139	7	8,140
(8×7)	85	20	23,529	4	4,706	46	54,118	15	17,647
(9×7)	85	20	23,529	4	4,706	46	54,118	15	17,647
(10×7)	74	7	9,459	10	13,513	55	74,324	2	2,703
(9×8)	86	20	23,255	9	10,465	50	58,139	7	8,140
(10×8)	86	20	23,255	9	10,465	50	58,139	7	8,140
(10×9)	85	20	23,529	4	4,706	46	54,118	15	17,647

3. Conclusions

One main cereal impacted by climate change is maize (*Zea mays L.*). Thus, it is imperative to produce climate-smart maize to sustain a variety of genetic origins. To achieve this, ten maize inbred lines were used to screen for phenotypic yield-associated traits and grain quality parameters, which were introduced into half-diallel crosses. We observed that the average of the hybrids was higher than that of the parents regarding all the studied traits, except for the grain yield per plant (gm). It is also found that there are differences in the performance of the hybrids with regard to all the studied traits. This can be utilized in breeding and in providing improvement programs to obtain synthetic varieties. Moreover, it can be used to benefit from the hybrids which are characterized by high and significant hybrid vigour and which are superior in grain yield and its components. Consequently, this paves the way to find possible lines with the best grain specifications for enhanced agronomic features. In addition, the study has demonstrated that hybrids exhibited the effectiveness of both parental and novel non-parental bundles, revealing an extensive range of genotypes at the genomic level. It can be extended further to increase the genetic diversity of the populations of maize. Thus, the RAPD technique proved efficient in studying the purity of hybrids, being an easy and fast technology.

References

Abdel-Mawgood, A. L., Ahmed, M. M. M., & Ali, B. A. 2006. Application of molecular markers for hybrid maize (*Zea mays L.*) identification. *J. Food Agric Envirno.*, 4(2), 176-168.

Abdullah, R.M., Hasan, S.A. 2020. Estimation of components of genetic variance using Jinks-Hayman method analysis on the crop of faba bean (*Vicia faba L.*) *Int. J. Agricult. Stat.*, 16(1); pp. 1897-1903.

Abu Dahi, Youssef Muhammad, Ahmed Muhammad Lahmoud, and Ghazi Majeed Al-Kawaz. 2001. The effect of foliar nutrition on yellow maize yield and its components, *Iraqi J. Soil Sci.*, 1(1): 122-137. (in Arabic).

Al-Bayati, Hussein Ali Hindi.2013. Inheritance of individual hybrids in different mating systems for pure lines of yellow maize (*Zea mays L.*) (Ph.D dissertation).Field Crops Department. College of Agriculture and Forestry. University of Al Mosul. Iraq. (in Arabic).

Al-Hamdani, Zakaria Badr Fathi. 2012. The nature of gene action in complete reciprocal crosses of yellow maize (*Zea mays L.*) (Ph.D dissertation). College of Agriculture and Forestry. University of Mosul. Iraq. (in Arabic).

Ali, Hamid Globe. 1988. **Foundations of breeding and genetics of field crops**. Ministry of Higher Education and Scientific Research. University of Baghdad. (in Arabic).

Al-Issawi, N. R., & Abood, N. M. 2024. Response Maize Cultivars (*Zea mays L*) to Foliar Application of Kinetin. *Iraqi J.Agricu.Sci.*, 55(1), 494-504.

Al-Jubouri, Jassim Muhammad Aziz, Ahmed Hawas Al-Jubouri, and Imad Khalaf Al-Qaisi. 2011. Correlations and path analysis for quantitative traits in barley (*Hordeum vulgare L*). The Fifth Scientific Conference of the College of Agriculture - Tikrit University. Tikrit-Iraq. (in Arabic).

Al-Jubouri, R. M., Mohammed, M. I., and Al-Mafarji, T. R. T. 2024. Genetic Analysis of Heterosis and some Genetic Parameters of Half Diallel Crosses in Maize (Zea mays L.). Earth Environ.Sci., 1371 (5).

Al-Jumaily, A. R. A., and Al-Zubaidy, K. M. D. 2018. Estimation of Genetic Parameters for Some Quantitative Characters of Maize. *Kirkuk Univ. J. Agric. Sci.*, 9(3), 117-128.

Al-Karkhi, Muhammad Khader Hassan. 2015. Estimating some genetic parameters and hybrid strength in hemicrosses for introduced genotypes of yellow maize (*Zea mays L.*) (MSc dissertation). Field Crops Department, College of Agriculture - Tikrit University. Iraq . (in Arabic).

Al-Nasiri, Atheer Saber Mustafa. 2016. The effect of some spring varieties, fertilization, and moisture levels at harvest on the growth and yield of yellow corn (*Zea mays L.)* (Ph.D dissertation). Field Crops Department, College of Agriculture - Tikrit University, Iraq (in Arabic).

Al-Rawashdeh, I. M. 2011. Molecular taxonomy among Mentha spicata, Mentha longifolia and Ziziphora tenuior populations using the RAPD technique. *Jordan J Biol Sci.*, 4(2), 63-70.

Al-Sahuki, M. M. 1990. **Yellow corn production and improvement**. Ministry of Higher Education and Scientific Research. Iraq. University of Baghdad. (in Arabic).

Al-Zubaidy, K. M., & Al-Juboury, K. K. A. 2016. **Design and analysis of genetic experiments. Al-Wadah Publishing House**, Kingdom of Jordan-Amman, Tigris Library for Printing, Publishing and Distribution, Republic of Iraq-Baghdad.

Al-Zuhairi, Nizar Suleiman Ali. 2014. The nature of the function of genes using single, triple, and double crosses between pure strains of yellow maize (*Zea mays L.*) and predicting the characteristics of even crosses, (Ph.D dissertation). College of Agriculture and Forestry - University of Mosul. (in Arabic).

Arab Organization for Agricultural Development. 2019. **Yearbook of Agricultural Statistics**, Youm7 website in Egypt. (in Arabic).

Bardakci F. 2001. Random amplified polymorphic DNA (RAPD) markers. Turk. J. Biol., 25:185-196.

Central Statistical Organization . 2020. **Ministry of Planning and Development Cooperation** - Iraq. (in Arabic).

Davis, T. M., Yu, H., Haigis, K. M., & McGowan, P. J. 1995. Template mixing: a method of enhancing detection and interpretation of codominant RAPD markers. *Theo. Appl. Genet.*, 91, 582-588.

Devadoss, S., & Luckstead, J. 2024. US–Mexico GM Corn Trade Dispute. Choices, 39(1), 1-8.

Elsahookie, M. M. 2007 . Dimensions of SCC theory in a maize hybrid- inbred comparison. *Iraqi J. Agric. Sci.*,38(1):128-137.

Griffing, B.1956.**Ageneralised treatment of the use of diallel crosses in quantitative inheritance**.Heredity10:31-50.

Hasan, S. A., & Abdullah, R. M. 2020. Estimating the performance and gene action of a number of individual genotypes and hybrids on the crop of faba bean (*Vicia faba L.*). *Plant Arch.*, 20(2), 8981-8988.

Hasan, S. A., & Abdullah, R. M. 2021. Characterization of genetic variability through the use of RAPDS markers of a group of native and commercial genotypes of bean species. International Journal of Agricultural & Statistical Sciences, *Int. J. Agric. Stat. sci.* , 17, pp. 1141–1147.

Hasan, S. A., Abdullah, R. M., & Hanoon, M. B. 2022. Effect of foliar application with proline on growth, yield, and quality of faba bean (*Vicia Faba L.*)(A review). *Eur. J. Agric. Rural Edu.* (EJARE). Vol. 3 No. 3, 2660-5643.

Hoshmand, R. (2018). Design of experiments for agriculture and the natural sciences. Chapman and Hall/CRC.

Lisek A, Korbin M and Rozpara E. 2006. Using simple generation RAPD Markers todistngushing between sweet cherry (Prunus avium L.) cultivars. *J. Fruit Ornam. Plant Res.,* 14: 53-59.

Maniatis, T.; E.F. Fritsch and J. Sambrook .2001.**In Vitro Application of DNA by the Polymerase Chain Reaction, in Molecular Cloning: A Laboratory Manual. 2nd ed**. , Cold Spring Harbor Laboratory Press, New York, USA, p.691.

Muhammad, NI. Humada, YH. Abdullah, RM . 2021 . Using phenotypic and molecular indicators RAPD-PCR to evaluate the performance and genetic dimension of a number of genotypes and their individual hybrids in the chickpea plant Cicer arietinum L. *Nat. Volatiles & Essent. Oils.*, 2021; 8(4): 11786-11810.

Muhanna, Ahmed Ali, Majed Mouloud Suleiman, and Wafaa Suleiman Khadr. 2015. The effect of humic acid and nitrogen fertilization on some characteristics of yellow maize (*Zea mays L.*) crop components and its productivity. *Jordanian J. Agri.l Sci.*, 11(1): 229-242. (in Arabic).

Nazer Aryannia, Mohammad Reza Enayatgholizadeh and Mehran Sharafizadeh . 2013 . Response of Grain Yield and Yield Components of Two Grainy Maize Hybrids to Plant Density and Natural Weeds Population, *Australian J. Basic Appl. Sci.*, 7(2): 590-597, 2013 ISSN 1991-8178.

Olufemi-Salami, F. K., Akinneye, J. O., & Salami, O. S. (2019). Contact and Fumigant Toxicity of Uvaria afzelli (Scott) against Plodia interpunctella (Hubner) Infesting Maize Grains in Nigeria. *Jordan J. Biol. Sci*., 12(1).

Ramadan, Ahmed Shehab Abdullah. 2015. Estimating some genetic parameters for grain yield and its components in yellow maize (*Zea mays L*), *Al-Anbar J. Agric. Sci.*, 31 (2): 189 – 198. (in Arabic).

Saghai- Maroof, M. A.; Soliman, K. M.; Jorgensen, R. A. and R. W. Allard .1984. Ribosomal DNA spacer length polymorphisms in barley: Mendelian inheritance, chromosomal location and population dynamics *Proc. Natl. Acad. Sci.,* USA. 81: 8014-8018.

Scheuring, C.; R. Barthelson; D. Gailbraith; J. Beltran; J. Cothrin; Z. Zing and H. Zhang .2006. Preliminary analysis of differential gene expression between a maize superior hybrid and its parents using the 57K maize gene-specific long-oligonucleotide microarray. In 48th Ann. Maize *Genet. Conf.*, 9-12. California, USA, p.132.

Scott, M. P., Haymes, K. M., & Williams, S. M. 1992. Parentage analysis using RAPD PCR. *Nucleic Acids Res.*, 20(20), 5493.

Shikha, K., Shahi, J. P., Vinayan, M. T., Zaidi, P. H., Singh, A. K., & Sinha, B. 2021. Genome-wide association mapping in maize: status and prospects. *3 Biotech*, 11(5), 244.

Singh, V. K., Pundir, S., Chaturvedi, D., Kaur, A., Pandey, A., Mandal, S., ... & Kaushik, P. 2023. **Enhancing Maize (*Zea mays L.*) Crop through Advanced Techniques: A Comprehensive Approach.** In New Prospects of Maize. Intech Open.

Tahir, N. A. R., & Karim, H. F. H. 2011. Determination of genetic relationship among some varieties of chickpea (*Cicer arietinum L.*) in Sulaimani by RAPD and ISSR markers. *Jordan J. Biol. Sci.*, 4(2), 77-86.

Tahir, N. A., Lateef, D. D., Omer, D. A., Kareem, S. H., Ahmad, D. A., & Khal, L. H. 2018. Genetic diversity and structure analysis of pea grown in Iraq using microsatellite markers. *Jordan J. Biol. Sci.*, 11(2), 201-207.

Van Inghelandt, D., Melchinger, A. E., Lebreton, C., & Stich, B. 2010. Population structure and genetic diversity in a commercial maize breeding program assessed with SSR and SNP markers. *Theor. Appl. Genet.,* 120, 1289-1299.

Weigand, F.; M. Baum and Udupa .1993. **DNA molecular marker Beijing**: 573 Science Press. pp131-150

Williams, J. G.; A. R. Kubelic ; K. J.Livak ; J. A. Rafalski and S. V. Tingey 1990. DNA polymorphisms amplified by aribitary primers are useful as genetic markers . *nucleic acids Res*. 18 : 6531-6535.

Younis, H. S. Abdul Sattar, A. A. and Amer K. Z. Abdullah, R.M. Hassan, A. S. 2022. Effect of biological and cultivar control to Ear- Cockle Nematode disease caused by the nematode (Anguina tritici) on different genotypes of bread wheat (*Triticum aestivum L.*) *Ann. For. Res.*.65(1): 916-930, 2022.

Younis, H. S., Abdullah, R. M., Hasan, S. A., & Abdul-Sattar, A. A. 2022. Systemic resistance indicators study and seed gall nematode disease caused by Anguina tritici affecting of biological and varietal treatments on bread wheat (*Triticum aestivum L.*). *Int. J. Agric. Stat. Sci,* 18(1), 289-296.

JJBS
Jordan Journal of Biological Sciences

The dual inhibitory effect of adipose-derived mesenchymal stem cell secretome on JAK2/STAT3 and PI3k/AKT/mTOR signaling pathways

Golnaz Mirfendereski[1], Ali Bagheri[1], Sepehr Niknami[1], Mahsa Amin[1,2], Faeze Khaghani[1], Maryam Torshabi[3], Elham Mohit[4], Sara Dabirian[1,*]

[1] Department of Pharmaceutical Biotechnology, School of Pharmacy, Guilan University of Medical Sciences, Rasht, Iran; [2] Department of Pharmaceutical Biotechnology, School of Pharmacy, Mashhad University of Medical Sciences, Mashhad, Iran; [3] Department of Dental Biomaterials, School of Dentistry, Shahid Beheshti University of Medical Sciences, Tehran, Iran; [4] Department of Pharmaceutical Biotechnology, School of Pharmacy, Shahid Beheshti University of Medical Sciences, Tehran, Iran

Abstract

Stem cells are considered as promising candidates to effectively hinder the proliferation of different types of cancers including hepatocellular carcinoma, Kaposi's sarcoma, as well as gastric and breast cancers. Mesenchymal stem cells (MSCs) have attracted a lot of attention among the different categories of such cells. Adipose tissue offers unique advantages as a source of MSCs. Based on some studies, the released substances from MSCs which are regarded as secretome can modulate the growth and survival of tumor cells, along with immunity and angiogenesis by affecting different signaling pathways. JAK/STAT and PI3k/AKT/mTOR signaling pathways play the main role in regulating growth, proliferation, apoptosis, and cancer metastasis. This study aims to assess the cytotoxic effect of human adipose-derived MSC (adMSC) secretome on two cancerous cell lines by co-culturing each cancerous cell line with adMSCs and performing MTT assay, as well as evaluating simultaneous inhibitory effect of adMSC secretome on the expression rates of the genes related to JAK2/STAT3 and PI3k/AKT/mTOR signaling pathways by conducting real-time PCR after co-culturing. The results indicated that adMSC secretome did not exert cytotoxic effect against epidermoid carcinoma (A431) cell line, leading to increased cell viability. However, the percentage of viable cancerous cells significantly reduced following co-culturing of gastric adenocarcinoma (AGS) cell line with adMSCs, indicating different cytotoxic potency of adMSC secretome towards these cell lines. adMSC secretome downregulated the expression rates of Jak2, STAT3, PI3k, and mTOR genes in both co-cultured cell lines, despite different effects against A431 and AGS cell lines, indicating the significance of such signaling pathways in the growth and proliferation of each cancerous cell lines. The results provide opportunities for examining *in vitro* and *in vivo* cytotoxic potency of adMSC secretome against other types of cancers and further evaluation of its downstream mechanisms of action through cancer signaling pathways. Thus, they may lead to the use of adMSC secretome as a novel therapeutic agent in different types of cancers.

Keywords: Cancerous cell line, co-culture techniques, cytotoxicity, gene expression, mesenchymal stem cells, signaling pathways, secretome

1. Introduction

The incidence of cancer is increasing worldwide and the American Cancer Society reports that cancer continues to be the second most prevalent reason for mortality, following heart disease. In addition, cancer stands as the primary reason for death among women aged 40-79 and men aged 60-79 years old (Sung *et al.*, 2021). The survival rate may remain low due to a delay in cancer treatment, resulting in increasing advanced cases, despite the advancements in early detection and treatment strategies for various types of cancer over the past few decades (Siegel *et al.*, 2023). Therefore, innovative therapeutic strategies should be adopted to address advanced or metastatic cancers.

Stem cell therapy has become a hopeful strategy for addressing different forms of cancer including hepatocellular carcinoma, Kaposi's sarcoma, as well as gastric and breast cancers (Alzahrani *et al.*, 2018; Khakoo *et al.*, 2006; Li *et al.*, 2013; Liu *et al.*, 2020; Mohamed *et al.*, 2019; Pakravan *et al.*, 2017). Because of different source of origin, differentiation potency and the ability of transplant to variety of people, mesenchymal stem cells (MSCs) have attracted a lot of attention among the different categories of stem cells (Gopalarethinam *et al.*, 2023). They can be isolated from umbilical cord, amniotic membrane, adipose tissue, bone marrow, and other tissues (Bhat *et al.*, 2021; Cho *et al.*, 2019; Hendrijantini and Hartono, 2019; Zhang *et al.*, 2019). Adipose tissue, which offers unique advantages as a source of MSCs, can be easily obtained from the medical waste of bariatric

surgery, resulting in eliminating any ethical concerns. Additionally, MSCs derived from adipose tissue (adMSCs) can be extracted from patients without the risk of immune rejection (Palencar *et al.*, 2019; Wyles *et al.*, 2015).

The MSCs can interact with tumor cells either by direct contact or by releasing certain substances such as chemokines, growth factors, cytokines, microvesicles, and exosomes with immunomodulatory effects (Crivelli *et al.*, 2017; Jayaramayya *et al.*, 2020). Based on some studies, these released substances, which are considered as secretome, inhibit cancer cell proliferation (Aslam *et al.*, 2021; Mirabdollahi *et al.*, 2019; Moeinabadi-Bidgoli *et al.*, 2022; Sousa *et al.*, 2023). The MSCs can affect different signaling pathways through their secretome (Chang *et al.*, 2022; Jantalika *et al.*, 2022; Ko *et al.*, 2023; Rezaei-Tazangi *et al.*, 2020; Sousa *et al.*, 2023; Yuan *et al.*, 2018) and induce cell apoptosis or suppress cell proliferation, migration, and invasion. Janus kinase 2 (JAK2)/signal transducer and activator of transcription 3 (STAT3) and phosphoinositide 3-kinase (PI3k)/protein kinase B (AKT)/mammalian target of rapamycin (mTOR) signaling pathways play the main roles in controlling cell growth and proliferation, apoptosis, and metastasis in different types of cancers (Al-Husein *et al.*, 2020; Fattahi *et al.*, 2020; Liang *et al.*, 2020; Ma *et al.*, 2020; Mengie Ayele *et al.*, 2022; Miricescu *et al.*, 2020; Mohrherr *et al.*, 2020; Rah *et al.*, 2022; Tewari *et al.*, 2022; Wu *et al.*, 2017; Yang *et al.*, 2020). In addition, aberrant activation of PI3k/AKT/mTOR pathway may result in the development of resistance to apoptosis (Fattahi *et al.*, 2020; Tewari *et al.*, 2022). Based on some reports, simultaneous inhibition of JAK2/STAT5 and PI3k/AKT/mTOR signaling pathways was more effective in reducing cancer cell number, growth of tumor and metastasis, as well as increasing survival *in vivo* compared to only PI3k/AKT/mTOR pathway inhibition (Yeh *et al.*, 2013). Only PI3k/AKT/mTOR signaling pathway inhibition led to uncontrolled activation of the JAK/STAT one and occurrence of metastatic and aggressive behaviors in tumor cells.

Based on the results, (Yeh *et al.*, 2013), simultaneous inhibition of STAT3 and JAK2, as key molecules in JAK2/STAT3 signaling pathway, and PI3k and mTOR, as vital molecules in PI3k/AKT/mTOR signaling pathway, can be regarded as prospective therapeutic targets for cancer treatment.

This study seeks to evaluate the cytotoxicity of MSC-secretome on two distinct cancers including gastric adenocarcinoma (AGS, RRID: CVCL_0139) and epidermoid carcinoma cell lines (A431, RRID: CVCL_0037), as well as reviewing MSC-secretome effect on gene expression rates of Jak2, STAT3, PI3k, and mTOR for achieving a deeper comprehension of the molecular mechanisms by which MSCs exert their influence on cancerous cells.

2. Materials and methods

2.1. Cell culture

Gastric adenocarcinoma (AGS, RRID: CVCL_0139) and epidermoid carcinoma (A431, RRID: CVCL_0037) cell lines (purchased from Pasteur Institute of Iran) and mesenchymal stem cells derived from human adipose (adMSCs, IBRC: C11347, purchased from Iranian Biological Resource Center, Iran) were cultured in Dulbecco's Modified Eagle Medium (DMEM) (Bioidea, Iran) by adding 10% fetal bovine serum (FBS) (Bioidea) and incubated at 37°C in a humidified atmosphere, containing 5% CO_2. Every 48-72 h the culture medium was refreshed and passages 3-5 were utilized for further experiments.

2.2. Assessing cytotoxic effect of adMSC-secretome against cancerous cell lines

In order to determine the cytotoxic effect of adMSC-secretome against cancerous cell lines (A431 and AGS), each cancerous cell line was co-cultured with ad-MSCs for 96 h, followed by conducting MTT assay (Mohammadalizadeh *et al.*, 2022). Briefly, cell line (either A431 or AGS) was seeded in the lower compartments of each well in an insert-containing 6-well plate (SPL, China) at 1.5×10^5 cells/well in complete DMEM medium. Then, ad-MSCs were seeded in the upper compartments (the inserts with the pore size of 8μm) at a density of 6×10^4 cells/well and further incubated for 96 h in the same condition after being incubated for 24 h at 37°C in a humidified atmosphere containing 5% CO_2. Cancerous cell line was included as control without being co-cultured with ad-MSCs. In the next step, all of the inserts were taken out and cancerous cells were washed with phosphate buffered saline (PBS) twice. In the next procedure, MTT (Sigma, Germany) solution were instilled into each well and incubated for 3 h in the same condition. Then, 150 μL of dimethyl sulfoxide (DMSO) (Sigma, Germany) was added to each well after the complete removal of the supernatants. The absorbance microplate reader (Epoch, USA) was applied for determining the optical density (OD) of the solution at 570 nm with the wavelength of 630 nm serving as a reference when formazan crystals were completely dissolved. Each procedure was conducted three times. The subsequent equation was used to determine the percentage of viable cells.

$(OD_{test}/OD_{control}) \times 100$

2.3. Evaluating adMSC-secretome effect on JAk2, STAT3, PI3k, and mTOR gene expressions in cancerous cells

For studying the adMSC-secretome effect on expression rates of JAk2, STAT3, PI3k, and mTOR genes in A431 and AGS cell lines, each cancerous cell line was co-cultured with ad-MSCs for 96 h, followed by conducting real-time PCR. Briefly, all of the inserts were removed and cancerous cells were washed twice with PBS after co-culturing of cancerous cell lines with adMSCs for 96 h (as indicated). Then, total RNA from each cancerous cell line was extracted by use of a Total RNA Extraction kit (Parstous, Iran). The quality of extracted RNA (its concentration and purification) was determined by Take3™ spectrophotometer (BioTek, USA) at A260/A280 ratio. Easy cDNA Synthesis kit (Parstous, Iran) was utilized for cDNA synthesis based on manufacturing instructions. In the next step, the expression rates of genes (JAK2, STAT3, PI3k, and mTOR) in cancerous cell lines were determined by quantitative real-time PCR applying RealQ Plus 2x Master Mix Green High ROX™ (Ampliqon, Denmark) based on manufacturing instructions. Table 1 indicates the list of primers. GAPDH

was considered as the reference gene here. The experiment was conducted in triplicate for each sample. The Livak

($2^{-\Delta\Delta C_T}$) method was employed to determine the gene expression levels (Livak and Schmittgen, 2001).

Table 1. Primer set sequences for quantitative real-time PCR

Gene name	NCBI reference sequence	Primer sequence ('5' - '3')	Product size (bp)	Annealing temperature (°C)
JAK2	NM_004972.4	Forward ATCTGGGGAGTATGTTGCAGAA	124	60
		Reverse GTTGGGTGGATACCAGATCCTTT		
STAT3	NM_139276.3	Forward GAATCACGCCTTCTACAGACT	125	60
		Reverse TTCCGGACATCCTGAAGGT		
PI3k	NM_006218.4	Forward CATGGAGGAGAACCCTTATGTGA	114	60
		Reverse AGCACGAGGAAGATCAGGAATG		
mTOR	NM_004958.4	Forward CAACAAGCGATCCCGAACGA	78	60
		Reverse CCAAGTTCCACACCGTCCAA		
GAPDH	NM_002046.7	Forward TGAAGGTCGGAGTCAACGG	148	60
		Reverse TGGGTGGAATCATATTGGAACA		

2.4. Statistical analysis

Results are expressed as mean ± standard deviation (SD). Statistical analyses were conducted by use of GraphPad Prism Version 9 software (GraphPad Software, USA). The difference between test and control groups in each experiment was calculated utilizing an independent Student's t-test and one-way ANOVA (tukey post-test). A *p*-value less than 0.05 was considered to be a statistically significant difference.

3. Results

3.1. adMSC-secretome showed cytotoxic effect against AGS cell line with no cytotoxicity against A431 cell line

For examining the cytotoxicity of adMSC-secretome on cancerous cell lines, an MTT assay was performed after a 96-h co-culturing of each cell line with adMSCs. As shown in Fig. 1a, the percentage of viable cells in the test group of AGS cell line (76.71 ± 3.97%) is significantly reduced as compared to its control group (*p*-value < 0.0001), while cell viability increases in test group of A431 cell line by 30.12 ± 5.97% (in comparison with control, *p*-value < 0.001) (Fig. 1b), indicating cytotoxicity of adMSC-secretome against AGS cell line.
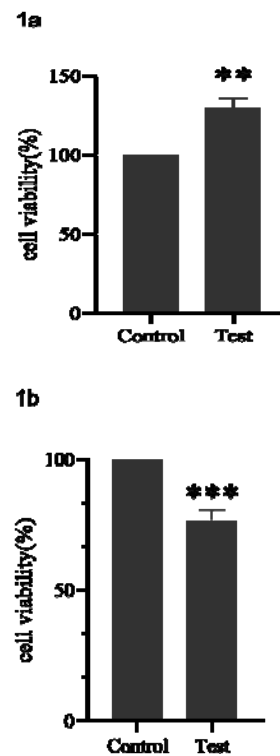

Figure 1. The percentages of viable cells in A431 (1a) and AGS (1b) cell lines after co-culturing with adMSCs; Values are presented as Mean ± SD; ** Significantly different compared to the control group (*p*-value < 0.001); *** Significantly different compared to the control group (*p*-value < 0.0001).

3.2. adMSC-secretome downregulated expression rates of JAk2, STAT3, PI3k, and mTOR genes in both cancerous cell lines

In order to analyze the changes in expression rates of genes related to JAK2/STAT3 and PI3k/AKT/mTOR signaling pathways in each cancerous cell line, real-time PCR was conducted following co-culturing of either A431 or AGS cell lines with adMSCs. As illustrated in Fig. 2, the expression rates of JAk2, STAT3, PI3k, and mTOR genes in both co-cultured cancerous cell lines with adMSCs are significantly reduced compared to control groups (p-value < 0.05 for all of the genes in both cell lines in comparison with control).
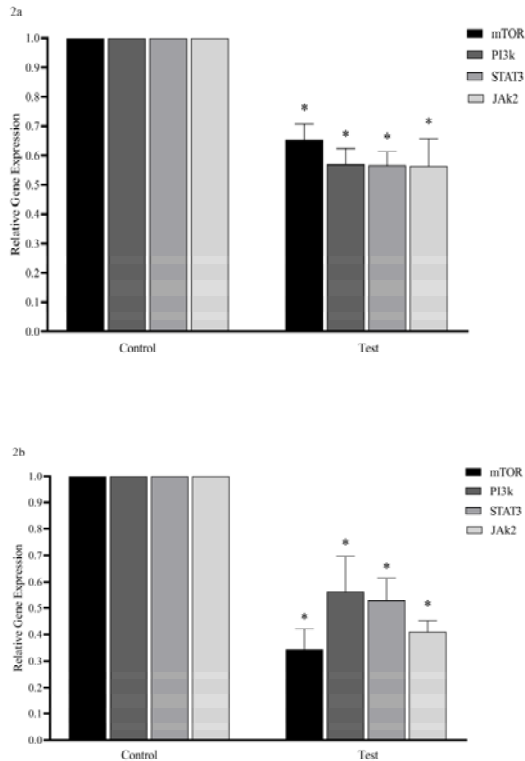

Figure 2. Relative gene expression of mTOR, PI3k, STAT3, JAk2 of in A431 (2a) and AGS (2b) cell lines after co-culturing with adMSCs; Values are presented as Mean ± SD; * Significantly different compared to the control group (p-value < 0.05).

4. Discussion

Stem cells and their secretomes could be regarded as effective cancer therapeutic agents with minimum side effects. Based on the evidence, the MSC and its secretome comprising a diverse range of cytokines and other bioactive molecules can impede the growth of numerous cancer cell types such as cholangiocarcinoma (Jantalika *et al.*, 2022), hepatocellular carcinoma (Hou *et al.*, 2014; Opo *et al.*, 2023; Tang *et al.*, 2016), prostate cancer (Sousa *et al.*, 2023; Takahara *et al.*, 2014), ovarian (Kalamegam *et al.*, 2019), leukemia (Zhu *et al.*, 2009), breast cancer (Pakravan et al,. 2017), and melanoma (Ahn *et al.*, 2015). In addition, some studies revealed that the cancerous behavior in tumor cells is promoted by MSCs (Chen *et al.*, 2019; Halpern *et al.*, 2011; Spaeth *et al.*, 2009; Suzuki et

al., 2011; Xu *et al.*, 2009; Yan *et al.*, 2012; Zhu *et al.*, 2006). Additional investigations are required to thoroughly define the safety and effectiveness of MSC/its secretome and determine its mechanisms of action, considering the opposite effects of MSC or its secretome against cancerous cells. This study aims to evaluate the cytotoxicity of adMSC secretome against gastric adenocarcinoma (AGS) and epidermoid carcinoma (A431) cell lines and determine its inhibitory effect on JAK/STAT and PI3k/AKT/mTOR, as two main cancer signaling pathways.

To this aim, each cancerous cell lines (either AGS or A431) were co-cultured with adMSCs for 96 h, followed by an MTT assay. The results represented that MSC secretome affected AGS and A431cell lines differently, while MSC secretome reduced viable cells in AGS cell line with no cytotoxic effect against A431 cell line. These results are in line with those reported before and confirm the opposite behavior of MSCs towards different cancerous cells. Some researchers (e.g., Goldstein *et al.*, 2010; Sousa *et al.*, 2023) revealed that the proliferative effect of MSCs varied depending on the type of tumor, indicating their different responsiveness toward external stimuli. Besides the type of tumor or cancerous cell line, some other factors may explain such discrepancies in MSC behavior, source of MSCs, co-culturing method, treatment duration, and concertation of MSC conditioned media. The dose- and time-dependent effects of MSCs were shown in different studies (Jantalika *et al.*, 2022; Opo *et al.*, 2023; Sousa *et al.*, 2023).

In addition, this study seeks to determine the effect of adMSC secretome on the expression rates of genes such as JAk2, STAT3, PI3k, and mTOR related to JAK2/STAT3 and PI3k/AKT/mTOR signaling pathways by conducting real-time PCR. Based on the literature review, any alterations in the mRNA level of a gene could be related to the same change in its protein level (Creighton *et al.*, 2010; Deng *et al.*, 2015; Fu *et al.*, 2021; Riquelme *et al.*, 2016). The results represented that adMSC secretome significantly downregulated the expression rates in all of the indicated genes in both cell lines, resulting in inhibiting JAK2/STAT3 and PI3k/AKT/mTOR signaling pathways. Jantalika *et al.* argued that cholangiocarcinoma cell lines underwent apoptosis due to the suppression of JAK2/STAT3 signaling pathways by human chorion-derived mesenchymal stem cells (Jantalika *et al.*, 2022). The findings of this study are consistent with those reported by Sousa *et al.* (2023), indicating that umbilical cord-MSC secretome decreased PI3K/AKT activation in prostate cancer cell lines.

Based on some studies, excessive activation of JAK/STAT and PI3k/AKT/mTOR signaling pathways leads to proliferation, metastasis, and survival in different types of tumor cells (Fattahi *et al.*, 2020; Mengie Ayele *et al.*, 2022; Rah *et al.*, 2022; Tewari *et al.*, 2022). Thus, it is expected that the inhibition of the above-mentioned signaling pathways reduces the cancerous cell viability. The gene downregulation in A431 cell line increased cell viability although downregulation in JAk2, STAT3, PI3k, and mTOR genes might be responsible for the cytotoxic effect of adMSC secretome against AGS cell line. Therefore, it is hypothesized that JAK/STAT and PI3k/AKT/mTOR are not considered as the main proliferative signaling pathways in epidermoid adenocarcinoma and cannot be regarded as candidate

therapeutic targets, while they may be proper targets for therapeutic agents in gastric carcinoma. The aforementioned claim means that activation of some other proliferative signaling pathways in A431 cell line might compensate for the inhibitory effect of MSCs on JAK2/STAT3 and PI3k/AKT/mTOR, leading to increased cell viability in A431 cell line. In addition, Fadhal (2023) reported that the functions of signaling proteins may differ based on the type of cancerous cell.

It is worth to highlight that the simultaneous inhibitory effect of adMSC secretome on both signaling pathways is significant. Further, Yeh *et al.* (2013) asserted that the single inhibitory effect of MSCs on PI3k/AKT/mTOR pathway led to manifestation of metastatic and aggressive tendencies in tumor cells. However, its dual inhibitory effects on both JAK2/STAT5 and PI3k/AKT/mTOR signaling pathways play main role in reducing cancer cell number, growth of tumor and metastasis, as well as increasing survival *in vivo*. Finally, Janku *et al.* (2014) found that combinatorial targeting of two signaling pathways led to an enhanced therapeutic response.

5. Conclusion

This study reported the dual inhibitory effect of adMSC secretome on JAK2/STAT3 and PI3k/AKT/mTOR signaling pathways in epidermoid carcinoma and gastric adenocarcinoma cell lines, confirming the cell line-dependent manner of MSCs with no cytotoxicity against A431 cell line, considering the cytotoxicity of MSCs against such cancerous cell lines. adMSC secretome showed cytotoxic effect against AGS cell line. Furthermore, the downregulation of all of the studied genes related to JAK2/STAT3 and PI3k/AKT/mTOR signaling pathways in both cell lines revealed that the role and significance of each signaling pathway may differ based on tumor type. The aforementioned data confirm the selective cytotoxicity of MSCs against different cancerous cell lines, indicating that determining the precise effects of MSCs on signaling pathways in each type of cancer is needed and can be considered as a guide for utilizing MSC and its secretome in further *in vivo* studies and clinical trials.

Conflict of interest

The authors have no relevant financial or non-financial interests to disclose.

Author contribution

SD performed the study conception and design. Material preparation, experiments, and data collection were performed by GM, AB, SN, MA, FK, and MT. The data were analyzed by MT, EM, and SD. The first draft of the manuscript was written by GM, EM, and SD. All of the authors reviewed the manuscript.

References

Ahn JO, Coh YR, Lee HW, Shin IS, Kang SK and Youn HY. 2015. Human Adipose Tissue-Derived Mesenchymal Stem Cells Inhibit Melanoma Growth *in vitro* and *in vivo*. *Anticancer Res.*, **35(1):** 159–68.

Al-Husein BA, Mhaidat NM and Sweidan RM. 2020. Interaction of Atorvastatin and CX3CR1/Fractalkine in Androgen-Dependent Prostate Cancer Cells: Effect on PI3K Pathway. *Jordan J Biol Sci.*, **13(3):**281–87.

Alzahrani FA, El-Magd MA, Abdelfattah-Hassan A, Saleh AA, Saadeldin IM, El-Shetry ES, Badawy AA and Alkarim S. 2018. Potential Effect of Exosomes Derived from Cancer Stem Cells and MSCs on Progression of DEN-Induced HCC in Rats. *Stem Cells Int.*, **2018:** 8058979.

Aslam N, Abusharieh E, Abuarqoub D, Alhattab D, Jafar H, Alshaer W, Masad RJ and Awidi AS. 2021. An *In vitro* Comparison of Anti-Tumoral Potential of Wharton's Jelly and Bone Marrow Mesenchymal Stem Cells Exhibited by Cell Cycle Arrest in Glioma Cells (U87MG). *Pathol Oncol Res.*, **27:** 584710.

Bhat, Samatha, Pachaiyappan Bhat S, Viswanathan P, Chandanala S, Prasanna SJ and Seetharam RN. 2021. Expansion and Characterization of Bone Marrow Derived Human Mesenchymal Stromal Cells in Serum-Free Conditions. *Sci Rep.*, **11(1):** 3403.

Chang YH, Vuong CK, Ngo NH, Yamashita T, Ye X, Futamura Y, Fukushige M, Obata-Yasuoka M, Hamada H, Osaka M, Hiramatsu Y, Sakurai T and Ohneda O. 2022. Extracellular Vesicles Derived from Wharton's Jelly Mesenchymal Stem Cells Inhibit the Tumor Environment via the MiR-125b/HIF1α Signaling Pathway. *Sci Rep.*, **12(1):** 13550.

Chen J, Ji T, Wu D, Jiang S, Zhao J, Lin H and Cai X. 2019. Human Mesenchymal Stem Cells Promote Tumor Growth via MAPK Pathway and Metastasis by Epithelial Mesenchymal Transition and Integrin A5 in Hepatocellular Carcinoma. *Cell Death Dis.*, **10(6):** 425.

Cho JW, Seo MS, Kang KK and Sung SE. 2019. Effect of Human Thymus Adipose Tissue-Derived Mesenchymal Stem Cells on Myocardial Infarction in Rat Model. *Regen Ther.*, **11:** 192–98.

Creighton CJ, Fu X, Hennessy BT, Casa AJ, Zhang Y, Gonzalez-Angulo AM, Lluch A, Gray JW, Brown PH, Hilsenbeck SG, Osborne CK, Mills GB, Lee AV and Schiff R. 2010. Proteomic and Transcriptomic Profiling Reveals a Link between the PI3K Pathway and Lower Estrogen-Receptor (ER) Levels and Activity in ER+ Breast Cancer. *Breast Cancer Res.*, **12(3):** R40.

Crivelli B, Chlapanidas T, Perteghella S, Lucarelli E, Pascucci L, Brini AT, Ferrero I, Marazzi M, Pessina A, Torre ML and Italian Mesenchymal Stem Cell Group (GISM). 2017. Mesenchymal Stem/Stromal Cell Extracellular Vesicles: From Active Principle to next Generation Drug Delivery System. *J Control Release.*, **262:** 104–17.

Deng X, Zhao Y and Wang B. 2015. MiR-519d-Mediated Downregulation of STAT3 Suppresses Breast Cancer Progression. *Oncol Rep.*, **34(4):** 2188–94.

Fadhal E. 2023. Unraveling the significance of signal transduction pathways: Key players in cancer development and progression. *J Cancer Ther Res.*, **3(1):** 1-9.

Fattahi S, Amjadi-Moheb F, Tabaripour R, Ashrafi GH and Akhavan-Niaki H. 2020. PI3K/AKT/MTOR Signaling in Gastric Cancer: Epigenetics and Beyond. *Life Sci.*, **262:** 118513.

Fu M, Tan L, Lin Z, Lui VCH, Tam PKH, Lamb JR, Zhang Y, Xia H, Zhang R and Chen Y. 2021. Down-Regulation of STAT3 Enhanced Chemokine Expression and Neutrophil Recruitment in Biliary Atresia. *Clin Sci (Lond).,* **135(7):** 865–84.

Goldstein RH, Reagan MR, Anderson K, Kaplan DL and Rosenblatt M. 2010. Human Bone Marrow-Derived MSCs Can Home to Orthotopic Breast Cancer Tumors and Promote Bone Metastasis. *Cancer Res.,* **70(24):** 10044–50.

Gopalarethinam J, Nair AP, Iyer M, Vellingiri B and Subramaniam MD. 2023. Advantages of mesenchymal stem cell over the other stem cells. *Acta Histochem.*, **125(4):** 152041.

Halpern JL, Kilbarger A and Lynch CC. 2011. Mesenchymal Stem Cells Promote Mammary Cancer Cell Migration *in vitro* via the CXCR2 Receptor. *Cancer Lett.,* **308(1):** 91–99.

Hendrijantini N and Hartono P. 2019. Phenotype Characteristics and Osteogenic Differentiation Potential of Human Mesenchymal Stem Cells Derived from Amnion Membrane (HAMSCs) and Umbilical Cord (HUC-MSCs). *Acta Inform Med.*, **27(2):** 72–77.

Hou L, Wang X, Zhou Y, Ma H, Wang Z, He J, Hu H, Guan W and Ma Y. 2014. Inhibitory Effect and Mechanism of Mesenchymal Stem Cells on Liver Cancer Cells. *Tumour Biol.,* **35(2):** 1239–50.

Janku F, Hong DS, Fu S, Piha-Paul SA, Naing A, Falchook GS, Tsimberidou AM, Stepanek VM, Moulder SL, Lee JJ, Luthra R, Zinner RG, Broaddus RR, Wheler JJ and Kurzrock R. 2014. Assessing PIK3CA and PTEN in Early-Phase Trials with PI3K/AKT/MTOR Inhibitors. *Cell Rep.,* **6(2):** 377–87.

Jantalika T, Manochantr S, Kheolamai P, Tantikanlayaporn D, Saijuntha W, Pinlaor S, Chairoungdua A, Paraoan L and Tantrawatpan C. 2022. Human Chorion-Derived Mesenchymal Stem Cells Suppress JAK2/STAT3 Signaling and Induce Apoptosis of Cholangiocarcinoma Cell Lines. *Sci Rep.,* **12(1):** 11341.

Jayaramayya K, Mahalaxmi I, Subramaniam MD, Raj N, Dayem AA, Lim KM, Kim SJ, An JY, Lee Y, Choi Y, Raj A, Cho SG and Vellingiri B. 2020. Immunomodulatory Effect of Mesenchymal Stem Cells and Mesenchymal Stem-Cell-Derived Exosomes for COVID-19 Treatment. *BMB Rep.,* **53(8):** 400–412.

Kalamegam G, Sait KHW, Anfinan N, Kadam R, Ahmed F, Rasool M, Naseer MI, Pushparaj PN and Al-Qahtani M. 2019. Cytokines Secreted by Human Wharton's Jelly Stem Cells Inhibit the Proliferation of Ovarian Cancer (OVCAR3) Cells *in vitro*. *Oncol Lett.,* **17(5):** 4521–31.

Khakoo AY, Pati S, Anderson SA, Reid W, Elshal MF, Rovira II, Nguyen AT, Malide D, Combs CA, Hall G, Zhang J, Raffeld M, Rogers TB, Stetler-Stevenson W, Frank JA, Reitz M and Finkel T. 2006. Human Mesenchymal Stem Cells Exert Potent Antitumorigenic Effects in a Model of Kaposi's Sarcoma. *J Exp Med.,* **203(5):** 1235–47.

Ko E, Yoon T, Lee Y, Kim J and Park YB. 2023. ADSC Secretome Constrains NK Cell Activity by Attenuating IL-2-Mediated JAK-STAT and AKT Signaling Pathway via Upregulation of CIS and DUSP4. *Stem Cell Res Ther.,* **14(1):** 329.

Li Y, Zhao Y, Cheng Z, Zhan J, Sun X, Qian H, Zhu W and Xu W. 2013. Mesenchymal Stem Cell-like Cells from Children Foreskin Inhibit the Growth of SGC-7901 Gastric Cancer Cells. *Exp Mol Pathol.,* **94(3):** 430–37.

Liang R, Chen X, Chen L, Wan F, Chen K, Sun Y and Zhu X. 2020. STAT3 Signaling in Ovarian Cancer: A Potential Therapeutic Target. *J Cancer,* **11(4):** 837–48.

Liu QW, Li JY, Zhang XC, Liu Y, Liu QY, Xiao L, Zhang WJ, Wu HY, Deng KY and Xin HB. 2020. Human Amniotic Mesenchymal Stem Cells Inhibit Hepatocellular Carcinoma in Tumour-Bearing Mice. *J Cell Mol Med.,* **24(18):** 10525–41.

Livak KJ and Schmittgen TD. 2001. Analysis of Relative Gene Expression Data Using Real-Time Quantitative PCR and the $2^{-\Delta\Delta CT}$ Method. *Methods,* **25(4):** 402–8.

Ma JH, Qin L and Li X. 2020. Role of STAT3 Signaling Pathway in Breast Cancer. *Cell Commun Signal.,* **18(1):** 33.

Mengie Ayele T, Tilahun Muche Z, Behaile Teklemariam A, Bogale Kassie A and Chekol Abebe E. 2022. Role of JAK2/STAT3 Signaling Pathway in the Tumorigenesis, Chemotherapy Resistance, and Treatment of Solid Tumors: A Systemic Review. *J Inflamm Res.,* **15:** 1349–64.

Mirabdollahi M, Haghjooyjavanmard S and Sadeghi-Aliabadi H. 2019. An Anticancer Effect of Umbilical Cord-Derived Mesenchymal Stem Cell Secretome on the Breast Cancer Cell Line. *Cell Tissue Bank.,* **20(3):** 423–34.

Miricescu D, Totan A, Stanescu-Spinu II, Badoiu SC, Stefani C and Greabu M. 2020. PI3K/AKT/MTOR Signaling Pathway in Breast Cancer: From Molecular Landscape to Clinical Aspects. *Int J Mol Sci.,* **22(1):** 173.

Moeinabadi-Bidgoli K, Rezaee M, Rismanchi H, Mohammadi MM and Babajani A. 2022. Mesenchymal Stem Cell-Derived Antimicrobial Peptides as Potential Anti-Neoplastic Agents: New Insight into Anticancer Mechanisms of Stem Cells and Exosomes. *Front Cell Dev Biol.,* **10:** 900418.

Mohamed Y, Basyony MA, El-Desouki NI, Abdo WS and El-Magd MA. 2019. The Potential Therapeutic Effect for Melatonin and Mesenchymal Stem Cells on Hepatocellular Carcinoma. *BioMedicine (Taipei),* **9(4):** 24.

Mohammadalizadeh M, Dabirian S, Akrami M and Hesari Z. 2022. SPION Based Magnetic PLGA Nanofibers for Neural Differentiation of Mesenchymal Stem Cells. *Nanotechnology,* **33(37)**.

Mohrherr J, Uras IZ, Moll HP and Casanova E. 2020. STAT3: Versatile Functions in Non-Small Cell Lung Cancer. *Cancers (Basel),* **12(5):** 1107.

Opo FADM, Moulay M, Alrefaei GI, Alsubhi NH, Alkarim S and Rahman MM. 2023. Effect of Co-Culturing Both Placenta-Derived Mesenchymal Stem Cells and Their Condition Medium in the Cancer Cell (HepG2) Migration, Damage through Apoptosis and Cell Cycle Arrest. *Saudi J Biol Sci.,* **30(2):** 103519.

Pakravan K, Babashah S, Sadeghizadeh M, Mowla SJ, Mossahebi-Mohammadi M, Ataei F, Dana N and Javan M. 2017. MicroRNA-100 Shuttled by Mesenchymal Stem Cell-Derived Exosomes Suppresses *In vitro* Angiogenesis through Modulating the MTOR/HIF-1α/VEGF Signaling Axis in Breast Cancer Cells. *Cell Oncol (Dordr).,* **40(5):** 457–70.

Palencar D, Dragunova J, Hulin I and Koller J. 2019. Adipose Derived Mesenchymal Stem Cells Harvesting. *Bratisl Lek Listy.,* **120(9):** 686–89.

Rah B, Rather RA, Bhat GR, Baba AB, Mushtaq I, Farooq M, Yousuf T, Dar SB, Parveen S, Hassan R, Mohammad F, Qassim I, Bhat A, Ali S, Zargar MH and Afroze D. 2022. JAK/STAT Signaling: Molecular Targets, Therapeutic Opportunities, and Limitations of Targeted Inhibitions in Solid Malignancies. *Front Pharmacol.,* **13:** 821344.

Rezaei-Tazangi F, Alidadi H, Samimi A, Karimi S and Kahorsandi L. 2020. Effects of Wharton's Jelly Mesenchymal Stem Cells-Derived Secretome on Colon Carcinoma HT-29 Cells. *Tissue Cell.,* **67:** 101413.

Riquelme I, Tapia O, Espinoza JA, Leal P, Buchegger K, Sandoval A, Bizama C, Araya JC, Peek RM and Roa JC. 2016. The Gene Expression Status of the PI3K/AKT/MTOR Pathway in Gastric Cancer Tissues and Cell Lines. *Pathol Oncol Res.,* **22(4):** 797–805.

Siegel RL, Miller KD, Wagle NS and Jemal A. 2023. Cancer Statistics, 2023. *CA Cancer J Clin.,* **73(1):** 17–48.

Sousa A, Coelho P, Leite F, Teixeira C, Rocha AC, Santos I, Baylina P, Fernandes R, Soares R, Costa R and Gomes A. 2023. Impact of Umbilical Cord Mesenchymal Stromal/Stem Cell Secretome and Cord Blood Serum in Prostate Cancer Progression. *Hum Cell.,* **36(3):** 1160–72.

Spaeth EL, Dembinski JL, Sasser AK, Watson K, Klopp A, Hall B, Andreeff M and Marini F. 2009. Mesenchymal Stem Cell Transition to Tumor-Associated Fibroblasts Contributes to Fibrovascular Network Expansion and Tumor Progression. *PloS One,* **4(4):** e4992.

Sung H, Ferlay J, Siegel RL, Laversanne M, Soerjomataram I, Jemal A and Bray F. 2021. Global Cancer Statistics 2020: GLOBOCAN Estimates of Incidence and Mortality Worldwide for 36 Cancers in 185 Countries. *CA Cancer J Clin.,* **71(3):** 209–49.

Suzuki K, Sun R, Origuchi M, Kanehira M, Takahata T, Itoh J, Umezawa A, Kijima H, Fukuda S and Saijo Y. 2011. Mesenchymal Stromal Cells Promote Tumor Growth through the Enhancement of Neovascularization. *Mol Med.,* **17(7–8):** 579–87.

Takahara K, Ii M, Inamoto T, Komura K, Ibuki N, Minami K, Uehara H, Hirano H, Nomi H, Kiyama S, Asahi M and Azuma H. 2014. Adipose-Derived Stromal Cells Inhibit Prostate Cancer Cell Proliferation Inducing Apoptosis. *Biochem Biophys Res Commun.,* **446(4):** 1102–7.

Tang YM, Bao WM, Yang JH, Ma LK, Yang J, Xu Y, Yang LH, Sha F, Xu ZY, Wu HM, Zhou W, Li Y and Li YH. 2016. Umbilical Cord-Derived Mesenchymal Stem Cells Inhibit Growth and Promote Apoptosis of HepG2 Cells. *Mol Med Rep.,* **14(3):** 2717–24.

Tewari D, Patni P, Bishayee A, Sah AN and Bishayee A. 2022. Natural Products Targeting the PI3K-Akt-MTOR Signaling Pathway in Cancer: A Novel Therapeutic Strategy. *Semin Cancer Biol.,* **80:** 1–17.

Wu X, Tao P, Zhou Q, Li J, Yu Z, Wang X, Li J, Li C, Yan M, Zhu Z, Liu B and Su L. 2017. IL-6 Secreted by Cancer-Associated Fibroblasts Promotes Epithelial-Mesenchymal Transition and Metastasis of Gastric Cancer via JAK2/STAT3 Signaling Pathway. *Oncotarget,* **8(13):** 20741–50.

Wyles CC, Houdek MT, Crespo-Diaz RJ, Norambuena GA, Stalboerger PG, Terzic A, Behfar A and Sierra RJ. 2015. Adipose-Derived Mesenchymal Stem Cells Are Phenotypically Superior for Regeneration in the Setting of Osteonecrosis of the Femoral Head. *Clin Orthop.,* **473(10):** 3080–90.

Xu WT, Bian ZY, Fan QM, Li G and Tang TT. 2009. Human Mesenchymal Stem Cells (HMSCs) Target Osteosarcoma and Promote Its Growth and Pulmonary Metastasis. *Cancer Lett.,* **281(1):** 32–41.

Yan XL, Fu CJ, Chen L, Qin JH, Zeng Q, Yuan HF, Nan X, Chen HX, Zhou JN, Lin YL, Zhang XM, Yu CZ, Yue W and Pei XT. 2012. Mesenchymal Stem Cells from Primary Breast Cancer Tissue Promote Cancer Proliferation and Enhance Mammosphere Formation Partially via EGF/EGFR/Akt Pathway. *Breast Cancer Res Treat.,* **132(1):** 153–64.

Yang L, Shi P, Zhao G, Xu J, Peng W, Zhang J, Zhang G, Wang X, Dong Z, Chen F and Cui H. 2020. Targeting Cancer Stem Cell Pathways for Cancer Therapy. *Signal Transduct Target Ther.,* **5(1):** 8.

Yeh JE, Toniolo PA and Frank DA. 2013. JAK2-STAT5 Signaling: A Novel Mechanism of Resistance to Targeted PI3K/MTOR Inhibition. *JAKSTAT.,* **2(4):** e24635.

Yuan Y, Zhou C, Chen X, Tao C, Cheng H and Lu X. 2018. Suppression of Tumor Cell Proliferation and Migration by Human Umbilical Cord Mesenchymal Stem Cells: A Possible Role for Apoptosis and Wnt Signaling. *Oncol Lett.,* **15(6):** 8536–44.

Zhang J, Zhao J, Mao Q and Xia H. 2019. A Simple, Efficient and Economical Method for Isolating and Culturing Human Umbilical Cord Blood-derived Mesenchymal Stromal Cells. *Mol Med Rep.,* **20(6):** 5257–64.

Zhu W, Xu W, Jiang R, Qian H, Chen M, Hu J, Cao W, Han C and Chen Y. 2006. Mesenchymal Stem Cells Derived from Bone Marrow Favor Tumor Cell Growth *in vivo*. *Exp Mol Pathol.,* **80(3):** 267–74.

Zhu Y, Sun Z, Han Q, Liao L, Wang J, Bian C, Li J, Yan X, Liu Y, Shao C and Zhao RC. 2009. Human Mesenchymal Stem Cells Inhibit Cancer Cell Proliferation by Secreting DKK-1. *Leukemia,* **23(5):** 925–33.

First Report of *Plasmodium* Infectivity and Dynamics of *Anopheles* Mosquito species in Gombe State, Northeastern, Nigeria.

Abdulmalik B.S.[1,*], Abba, E[1]., Ubayo, A[4]., Yoriyo, K.P[1]., Sow, G.J[2]., Chiezey, N.P.[3]., Ndams, I.S.[2,5]

[1] *Department of Zoology, Gombe State University, Gombe, Nigeria;* [2] *Department of Zoology, Ahmadu Bello University Zaria, Kaduna, Nigeria;* [3] *Department of Veterinary Parasitology and Entomology, Ahmadu Bello University Zaria, Kaduna, Nigeria;* [4] *Primary Healthcare Development Agencies, Gombe State Ministry of Health, Gombe, Nigeria;* [5] *Africa Centre of Excellence for Neglected Tropical Diseases, Ahmadu Bello University, Zaria, Nigeria*

Abstract

This study was conducted between January and December 2022 in eight communities in Gombe State, North-East Nigeria. The study aimed at assessing the prevalence of *Plasmodium falciparum* sporozoites in *Anopheles gambiae* s.l. and examining the heterogeneity of *Anopheles* mosquito populations. To collect data, Indoor Pyrethrum Spray Catch (PSC) was employed in three randomly selected houses per community for adult mosquito collection. Additionally, a standard dipper was used to collect immature *Anopheles* stages in a stream, puddles, trailer park and soakaway from thirty (30) breeding sites of eight communities, which were then reared to adulthood in the laboratory. Morphological identification was carried out on all collected mosquitoes, and *An. gambiae* s.l. specimens were further validated using standard PCR protocol to distinguish sibling species. Out of the 3, 837 emerged adults, *An. gambiae* s.l. was the predominant species, constituting 58.33% (2, 238 samples), while *An. rufipes* was the least prevalent at 1.36% (52 samples). Although no significant difference in *Anopheles* composition was observed among the eight study communities ($p > 0.05$, $F = 0.0129$), a significant difference was found between the individual *Anopheles* species ($p < 0.05$, $F = 9.10$). The results indicate that, Adult *An. gambiae* s.l. was distributed across all eight communities, with a Shannon Weiner diversity index of 1.896 and Dominance of 0.1649. Notably, *An. rufipes* exhibited the highest Evenness value of 0.8516 among Anopheline species. Molecular identification of 91 *Anopheles gambiae* s.l. sub-samples revealed that 26.37% were *An. gambiae* s.s, 39.56% were *An. coluzzii*, and 3.30% were *An. arabiensis*. An overall prevalence of 11.00% (2 out of 18 blood-fed female *Anopheles gambiae* s.l.) for *P. falciparum* was established, though limited to one study community. Understanding the diversity, distribution, abundance, and infectivity of *Anopheles* mosquitoes is crucial for effective malaria control and elimination efforts in Gombe State and Nigeria as a whole.

Keywords: Anopheles, communities, composition, diversity, *P. falciparum,* Gombe State.

1. Introduction

Mosquitoes are dipteran flies, similar in appearance with other flies belonging to the family Culicidae. The most important genera of man biting mosquitoes are *Anopheles, Aedes, Culex, Mansoni, Psorphora, Haemagogus* and *Sabethes* (Medeiros-Sousa *et al.,* 2015). *Anopheles* are the most widely distributed mosquito species in Africa, and they are also found in the temperate, tropical and subtropical world except the polar region and altitude above 2000 meter (Ekedo and Ukpai, 2020). They are highly anthropophilic and sometime zoophilic. The genus *Anopheles* contains over 500 species globally, and over 140 described species of the genus have been reported in Africa, out of which eight (8) species are known to be efficient vectors of malaria (Coetzee, 2020; Escobar *et al.*, 2020). Of these Global *Anopheles*

mosquitoes, approximately 60 to70 are vectors of human malaria while 41 are the most dominant malaria vectors (Silva *et al.,* 2014; WHO, 2019). Previous studies have reported thirty (30) *Anopheles* species in Nigeria. However, recent studies from insecticide resistance monitoring and longitudinal surveillance supported by Global Fund and PMI have reported eleven (11) *Anopheles* species across five ecological zones of Nigeria (NMCP, 2020). The Gombe State vector control sentinel site have recorded seven (7) *Anopheles* species (Adeogun *et al.,* 2023) and few of these species have been linked to malaria transmission in Nigeria (Okorie *et al.,* 2011) although, their composition, diversity and vectorial capacity might vary over time.

Anopheles gambiae s.l. complex has nine sibling species that look morphologically similar but genetically and behaviourally may be distinct species that vary in their ability to transmit malaria parasites (Coetzee, 2020). The

---

* Corresponding author. e-mail: abdulmalikabs66@gsu.edu.ng.

sibling species may also vary in terms of feeding habit, distribution, habitat preference, behavior, biting habits as well as vectorial competence(Weeraratne *et al.,* 2017) which makes species identification and distribution vital towards operational control and elimination of malaria (Umar and Ndams, 2022). In addition, *An. gambiae* is known to exist in two distinct species; *An. coluzzii* and *An. gambiae* s.s. representing a distinct species belonging to *Anopheles gambiae* complex (Coetzee, 2020). However, the sibling species are indistinguishable morphologically and their identification is important for effective control intervention (Wahedi *et al.,* 2021).

The female *Anopheles* mosquito transmits pathogens of the genus *Plasmodium; P. vivax, P. malariae, P. ovale, P. falciparum* and *P. knowlesi* which have been documented to cause malaria in humans. Malaria in particular is one of the most severe public health problems worldwide (WHO, 2020) accounting for the death of over 600 thousand people mostly under five aged children and pregnant women every year (WHO, 2023). Nigeria accounted for 31.3% of the global malaria death with an estimated 97 million cases annually (WHO, 2023).

Plasmodium falciparum is the principal malaria agent followed by *P. malariae* in Nigeria and sub-Saharan African (FMoH, 2015). They account for 98% of all malaria cases including severe malaria and parasitization of the placenta in pregnancy leading to pre-mature birth and abortions (FMoH, 2015). Generally, Gombe State accounted for over 1 million malaria cases in 2021

amounting to 2.0% of all malaria cases in Nigeria (WHO, 2022). Although, evidence of malaria vector resistance has been reported in the Gombe State (Oduola *et al.,* 2019; Ahmed-yusuf *et al.,* 2020), there is not enough data to make evidence-based decisions on malaria vector control. This study aimed at providing information on the identity, diversity and *Plasmodium falciparum* infection of *Anopheles gambiae* s.l. in eight communities in Gombe State. This is required to design and implement appropriate malaria vector control and management program in Gombe State.

2. Materials and Methods

2.1. Study Area

Gombe State is situated in the North-Eastern region of Nigeria, spanning latitudes 9°30'00" to 12°30'00" N and longitudes 8°45'00" to 11°45'00" E of the Greenwich Meridian. Covering an area of 18,768 km², it had a projected population of 3,545,032 as per the 2006 census. The State experiences an annual rainfall of 850mm and a temperature of 30 °C, with Sudan Savannah vegetation. It undergoes two distinct seasons: the dry season (November – May) and the rainy season (June – October), with an average rainfall of 850mm. Approximately, 60% of the population is engaged in agriculture, with others involved in business and civil service.
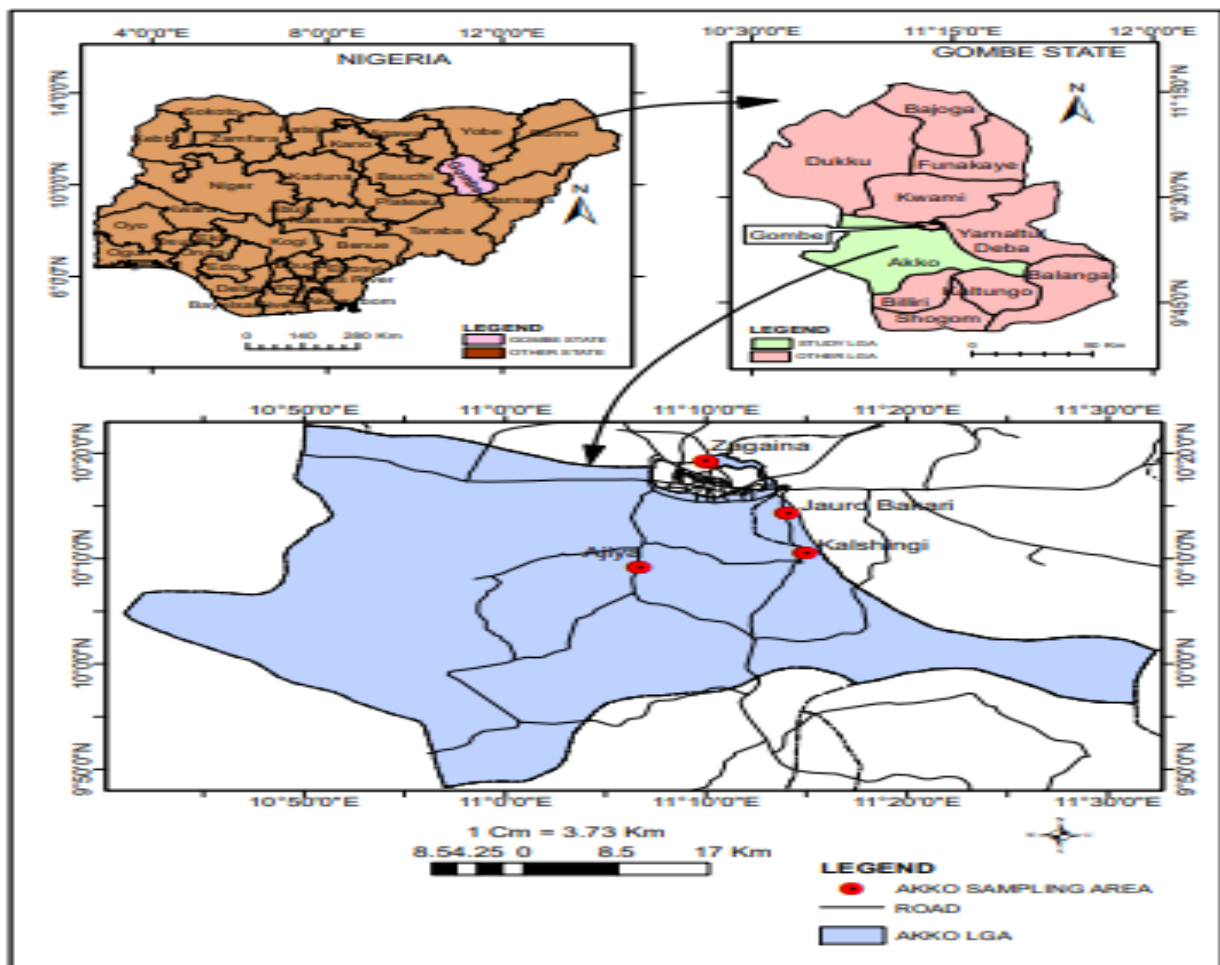

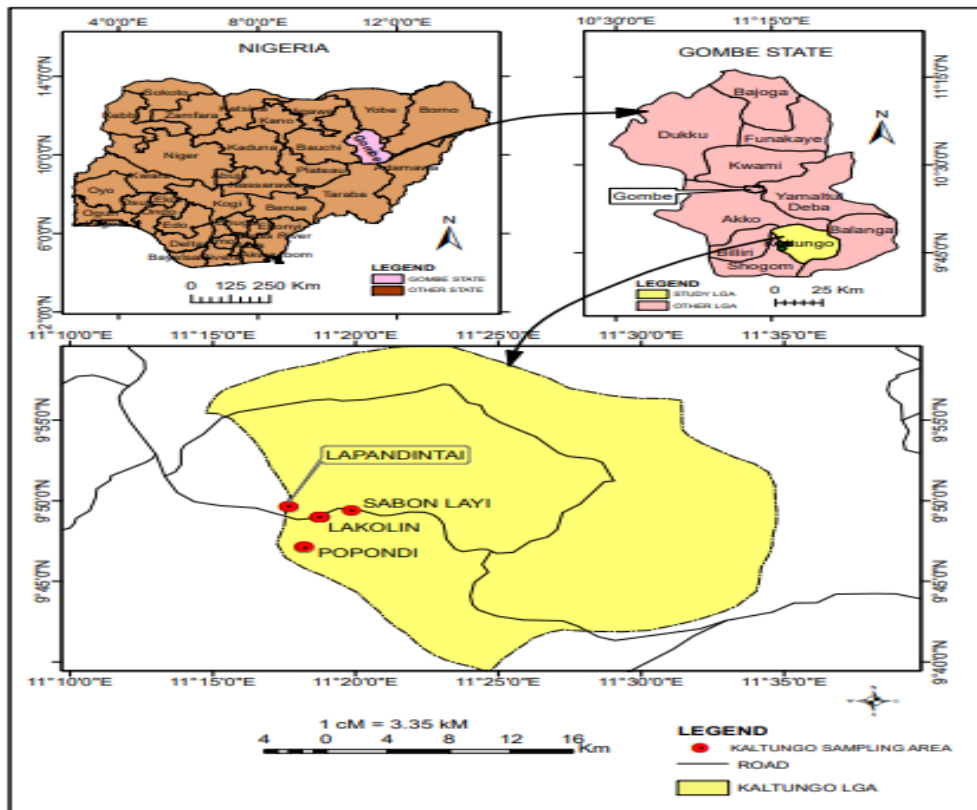**Figure1**. Map of Akko LGA sampling communities (Source: ZASTAL Kashere)

Figure 2. Map of Kaltungo LGA sampling communities (Source: ZASTAL Kashere)

2.2. Ethical Considerations and Consent

No ethical clearance was required for this study. Consent from community leaders was obtained before larval collection through advocacy visits. Additionally, household consent was secured before indoor mosquito collection using pyrethrum spray techniques. All procedures adhered to the 1964 Declarations of Helsinki during the World Medical Assembly (WMA) Finland.

2.3. Study Design

Purposive sampling selected two Local Government Areas (LGA); Akko and Kaltungo based on mosquito breeding habitats, farming activities, LLINs use history, geographical location, zone, and epidemiological importance. Eight communities were randomly chosen, including four semi-urban; Sabon layi, Lapandintai in Kaltungo, Zagaina, Ajiya Quarters in Akko and four rural; Popandi, Lakolin in Kaltungo, Jauro Bakari, Kalshigi in Akko LGA respectively (Fig 1&2).Their coordinates are as follows: Ajiya quarters: 10.152312°N and 11.114179°E; Kalshingi: 10.103902°N and 11.248228°E; Jauro Bakari:10.144859°N and 11.135512°E; Zagaina: 10.191044°N and 11.105690°E in Akko (Figure 1) while Lakolin: 9.831042°N and 11.338485°E; Lapandintai: 9.822407°N and 11.331450°E; Popondi: 9.471161°N and 11.312323°E; SabonLayi: 9.816280°N and 11.311228°E communities in Kaltungo LGA (Figure 2). Immature *Anopheles* mosquitoes were collected from temporary and semi-permanent breeding habitats, and Pyrethrum Spray collection was conducted in two rooms per three houses in each community for adult collection.

2.4. Collection and Rearing of Immature Anopheles Mosquitoes

Larvae and pupae were collected from eight study communities across 200m radius in Akko and Kaltungo LGAs of Gombe, Nigeria, using standard dipping methods. Breeding sites coordinates were recorded using GPS software. Collected larvae were transported to Gombe State malaria control sentinel laboratory, pooled, and reared until adult emergence. Larvae were fed with yeast extract and Carbin biscuit, while emerged adults were maintained under controlled conditions.

2.5. Adult Indoor Mosquito Collection

Pyrethrum Spray Catch and Prokopack aspirator collections were carried out in three randomly selected houses per community from January to December, 2022. Eighteen (18) blood-fed female *Anopheles* mosquitoes were collected, and their DNA was extracted for *Plasmodium falciparum* infection rate determination using modified direct PCR techniques of Echeverry *et al.* (2016).

2.6. Morphological Identification of Anopheles Species

Morphological identification was performed on all reared and collected *Anopheles* using Coetzee's, (2020) morphological keys. Morphological characteristics were observed using an LCD digital microscope, and identified *Anopheles gambiae* complex specimens were stored for molecular study (Fig. 3a).

2.7. Molecular Characterization of Anopheles gambiae s.l.

Genomic DNA was extracted from 91 individual mosquitoes using the Livak method. The extracted DNA was used for PCR analysis to identify sibling species of the

An. gambiae complex. Molecular identification of sub-species was conducted using PCR techniques proposed by Santolamazza *et al.* (2008). Presence or absence of bands was visualized through gel electrophoresis.

2.8. Plasmodium falciparum sporozoite Infection of Indoor Blood-Fed Anopheles

DNA extraction was performed on 18 blood fed female *Anopheles* mosquitoes collected through Pyrethrum Spray and Prokopack. *Plasmodium falciparum* infection was determined through PCR analysis from blood fed *An. gambiae* s.l collected in Zagaina community using a modified direct PCR technique of Echeverry *et al.* (2016).

All molecular investigations were conducted at Bayero-Wellcome Trust Laboratory, Department of Biochemistry, Bayero University Kano, Nigeria.

3. Results

3.1. Diversity and composition of Anopheles mosquito species

The composition of *Anopheles* mosquito species based on the morphological identification revealed four (4) different species of Anopheline mosquitoes; *An. gambiae* s.l. (Fig. 3a)*, An. pretoriensis* (Fig. 3b)*, An. maculipalpis* (Fig. 3c) and *An. rufipes* (Fig. 3d). *An. gambiae* s.l accounted for 2,238 (58.33%) of the 3,837 adults raised from larvae collections (Table 1). *An. gambiae* s.l was the most abundant species followed by *An. pretoriensis* with 1,218 (31.74%), *An. maculipalpis* with 257 (6.70%) and

the least were *An. rufipes* 52 (1.36%). The distribution of *Anopheles* populations varied significantly (P<0.05) across the study communities. Out of the 2,238 (58.33%), *An. gambiae* s.l, 496 (22.16%) were found to be dominant in Zagaina with no other *Anopheles* species recorded, whereas Popondi had the least but with preponderance of *An. pretoriensis* 372 (30.54%). Sabon Layi had abundance of *An. maculipalpis* 108 (42.02%) compared with other communities. The finding from this work recorded zero *An. maculipalpis* and *An. rufipes* in Jauro Bakari, Kalshigi, Ajiya quarters and Zagaina communities of Akko LGA. In contrast, Lakolin, Lapandintai, Popandi and Sabon layi communities of Kaltungo LGA recorded the presence of *An. maculipalpis* and *An. rufipes* with Lapandintai having the most *An. rufipes*, 26 (50%) and Sabon layi having the least 5 (9.62%). Significant difference was observed between the reared *Anopheles* mosquitoes collected from all the communities (p<0.05, F=9.10), whereas no significant difference was observed among the total *Anopheles* reared to adulthood across the study communities (p>0.05, F=0.0129). The Shannon Weiner diversity index revealed that, *Anopheles gambiae* s.l was highly diverse when compared to other Anopheline species (1.896) and it dominated in all the eight communities (0.1649). The Evenness of *An. rufipes* was high (0.8516) compared to *An. pretoriensis* (0.7569), *An. maculipalpis* (0.8508) and *An. gambiae* s.l (0.8328) occurring in seven, four and three communities respectively (Table 2).
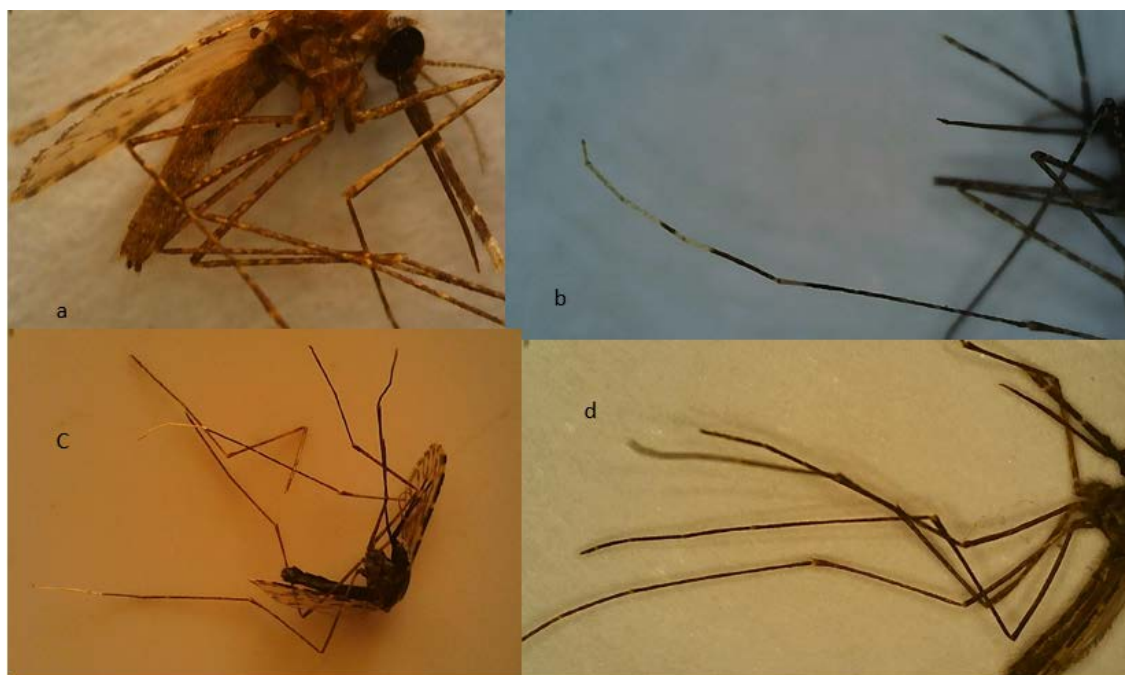
Figure 3: Morphological identification of *Anopheles* mosquitoes from eight study community in Gombe State. A = *Anopheles gambiae* s.l. b = *Anopheles pretoriensis* leg c = *Anopheles maculipalpis,* d = *Anopheles rufipes*

Table 1: Distribution and composition of members of *An. gambiae* s.l in the eight study communities

Communities	*An. gambiae*s.l. *n(%)*	*An. pretoriensis n(%)*	*An. Maculipalpis n(%)*	*An. Rufipes n(%)*	Unidentified n(%)	Overall n(%)
Ajiya quarters	440(19.66)	26(2.13)	0(0)	0(0)	0(0)	466(12.14)
JauroBakari	421(18.81)	59(4.84)	0(0)	0(0)	1(2.78)	481(12.54)
Kalshingi	340(15.19)	68(5.58)	0(0)	0(0)	2(5.56)	410(10.69)
Lakolin	220(9.83)	183(15.02)	90(35.02)	0(0)	5(13.89)	493(12.85)
Lapandintai	87(3.89)	341(28.00)	24(9.34)	26(50)	7(19.44)	485(12.64)
Popondi	46(2.06)	372(30.54)	35(13.62)	21(40.38)	18(50)	533(13.89)
Sabonlayi	188(8.40)	169(13.88)	108(42.02)	5(9.62)	3(8.33)	473(12.33)
Zagaina	496(22.16)	0(0)	0(0)	0(0)	0(0)	496(12.93)
Total	2238(58.33)	1218(31.74)	257(6.70)	52(1.36)	36(0.94)	3837(100)
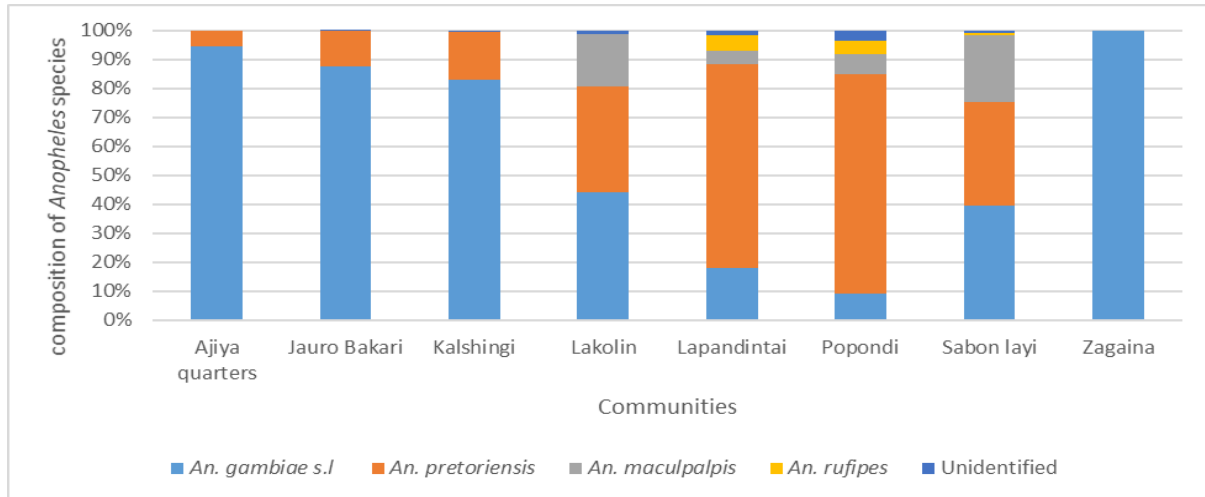
Figure 4. Species composition of *Anopheles* mosquitoes from the eight communities of the two LGAs of Gombe State, Nigeria

Table 2. Diversity indices of identified *Anopheles* mosquitoes across the sampling community

Species	Number of species	Dominance	Shannon (H)	Evenness (E)
An. gambiae s.l.	2238	0.1649	1.896	0.8328
An. pretoriensis	1218	0.2194	1.667	0.7569
An. maculipalpis	257	0.3265	1.225	0.8508
An. rufipes	52	0.4223	0.9379	0.8516

3.2. Molecular identification of the sibling species of Anopheles gambiae

Out of 2,238 *An. gambiae* complex, 91 were selected at random and molecularly identified. The molecular identification showed that *An. coluzzii* (Fig. 7) was abundant in Zagaina and *An. gambiae s.s* (Fig. 5) was predominant in Lakolin while *An. arabiensis* (Fig. 6) was found in Sabon Layi and Jauro Bakari (Table 3).
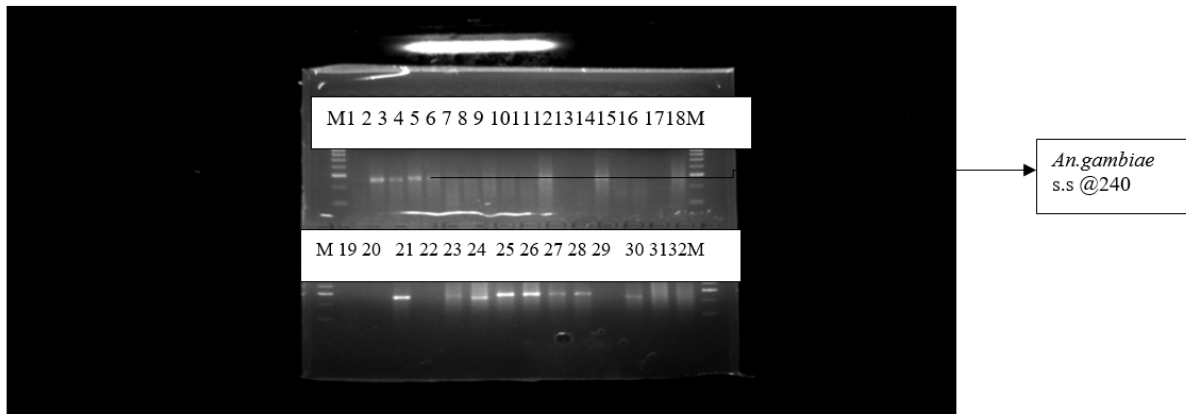
Figure 5: Agarose gel 3% for distinguishing *An. gambiae* s.l. after PCR with primers (SINE200F and SINE200R). Lane M= 100 bp hyper ladder visible at 300 bp. Positive samples show band size of 470bp to authenticate *An. coluzzii*, 240bp = *An. gambiae s.s* and 220bp = *An. arabiensis*. Lane 1= Negative control, 2-5, 7-9,11, 14, 18, 21, 23-28, 30-32 = *An. gambiae s.s.*, Lane 6 , 10, 12-13, 15-17, 19-20, 22, 29= not amplified.
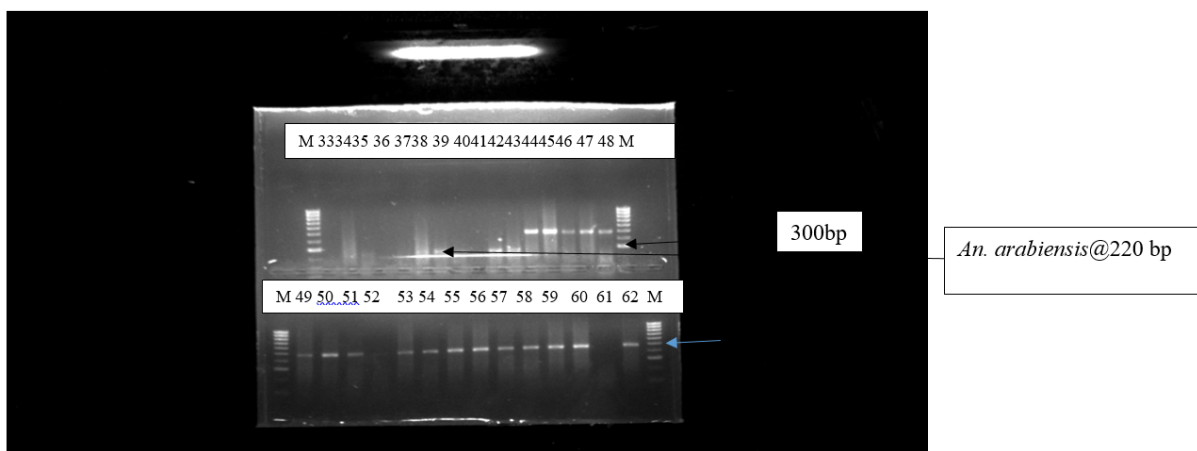
Figure 6: Agarose gel 3% for distinguishing *An. gambiae* s.l. after PCR with primers (SINE200F and SINE200R). Lane M= 100 bp hyper ladder visible at 300 bp. Positive samples show band size of 470bp to authenticate *An. coluzzii*, 240bp = *An. gambiae s.s* and 220bp = *An. arabiensis*. Lane 33 = negative control, Lane 34 = *An. arabiensis*, 38-39, 42-43 = *An. gambiae s.s.*, 44-60, 62 = *An. coluzzii,* 35-37, 40-41, 61, = not amplified.
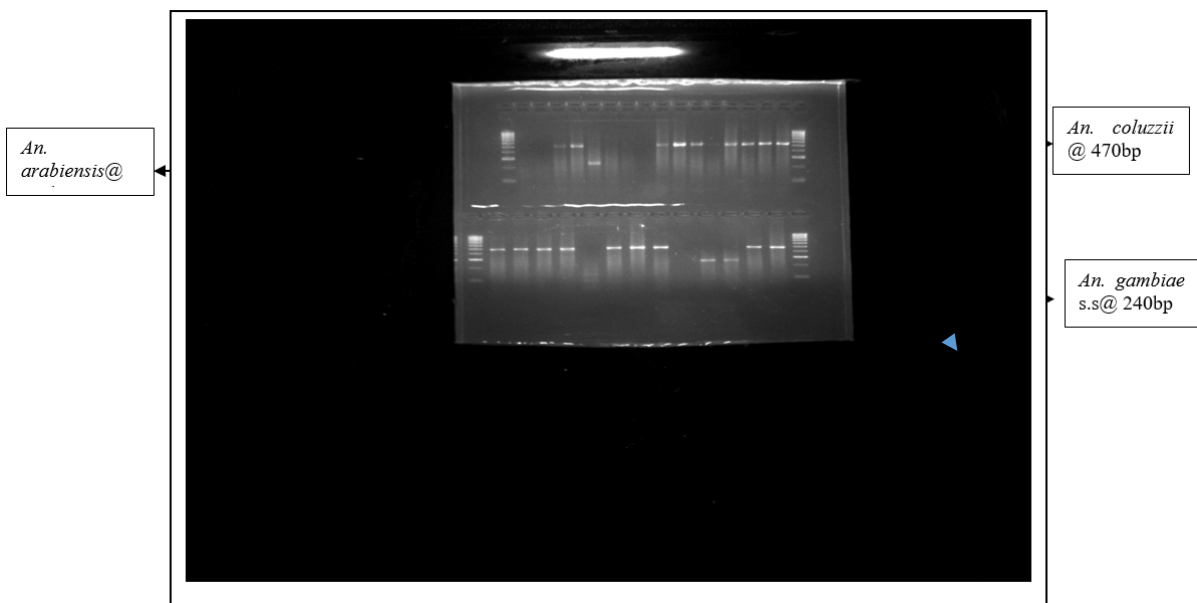
Figure 7: Three percent Agarose gel resolving *An. gambiae* s.l. after PCR with primers (SINE200F and SINE200R). Lane M= 100 bp hyper ladder visible at 300 bp. Postive samples show band size of 470bp to authenticate *An. coluzzii*, 240bp = *An. gambiae s.s* and 220bp = *An. arabiensis*. Lane 63 = Negative control; Lane 67 = *An. arabiensis,* Lane 88-89 = *An. gambiae* s.s. Lane 65-66, 71-82, 84-86, 90-91= *An. coluzzii*. Lane 64, 68-70, 83, 87 = not amplified.

Table 3. Distribution and Species composition of members of *An. gambiae* s.l in the eight study communities in 2 LGAs of Gombe State

				Species identified (%)			
LGA	Location	No examined (N)	No. PCR positive (%)	*An. Arabiensis* n(%)	*An. gambiae* s.s n(%)	*An. coluzzii* n(%)	Not amplified n(%)
Akko	Ajiya quarters	12	11(91.67)	0(0)	0(0)	11(91.67)	1(8.33)
	Jaurobakari	15	9(60)	1(6.6)	0(0)	5(53.33)	6(40)
	Kalshingi	12	12(100)	0(0)	0(0)	12(100)	0(0)
	Zagaina	09	7(77.78)	0(0)	2(22.22)	5(55.56)	2(22.22)
Kaltungo	Popondi	09	7(77.78)	0(0)	7(77.78)	0(0)	2(22.22)
	Sabonlayi	12	6(60)	2(16.67)	4(33.33)	0(0)	6(60)
	Lakolin	11	8(72.73)	0(0)	8(72.73)	0(0)	3(27.27)
	Lapandintai	11	3(27.27)	0(0)	3(27.27)	0(0)	8(72.73

3.3. Plasmodium falciparum Sporozoites Infectivity of Indoor Blood Fed Anopheles gambiae s.l.

A total of 18 blood fed *An. gambiae* s.l were collected from Zagaina and Ajiya quarters out of which 2 were positive for *P. falciparum* corresponding to 11% of all the samples collected (Fig. 8) from Zagaina. No blood fed *An. gambiae* s.l was found in all other study communities.
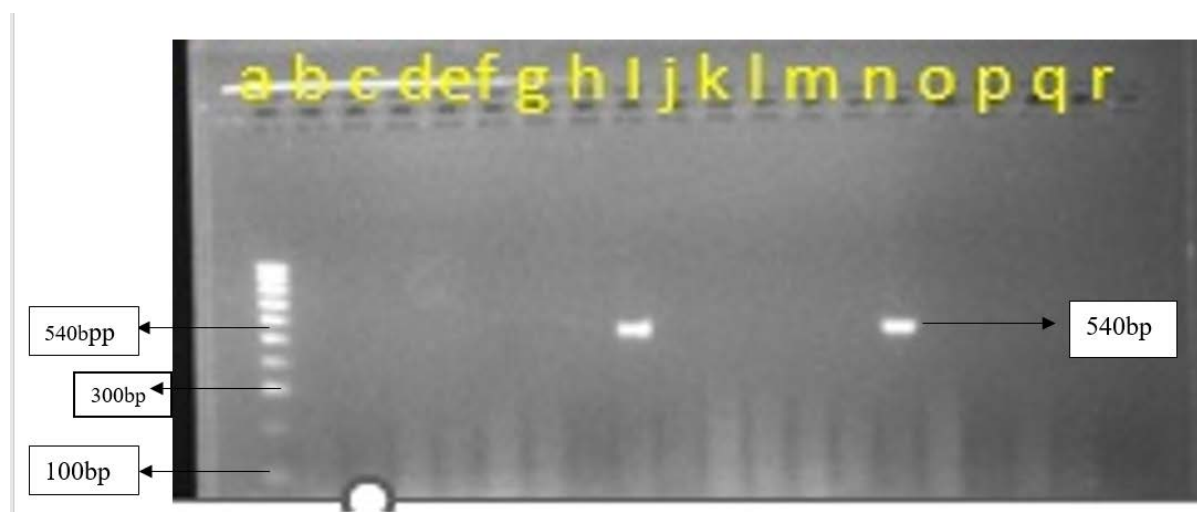
Figure 8: PCR bands of indoor collected blood fed mosquito from Zagaina tested for *P. falciparum* using COX1 gene. a = 100 bp hyper ladder, i and n = 540bp sporozoite for *P. falciparum*.

4. Discussion

The distribution of *Anopheline* mosquito from our findings revealed four (4) different species; *An. gambiae s.l., An. pretoriensis, An. maculipalpis* and *An. rufipes*. Similarly, Adeogun *et al.* (2023) reported seven *Anopheline species; An. salbaii, An. kingi, An. machardyi, An. pretoriensis, An. maculipalpis, An. stephensi* and *An. gambiae* s.l. from mosquito surveillance sites in 2020 though, in six LGAs of Gombe State among which one of the present study LGA (Akko) was inclusive. *An. gambiae* s.l dominated in six of the eight study communities with a percentage composition of 58.33% of the total collection. Similar results were obtained in Kontogora, Niger State (Garba, 2023), and from overall mosquito collection in Nigeria (60%) (Okorie *et al.*, 2011). Likewise, *Anopheles gambiae* complex constitute 98% of all the *Anopheles* collection for vector surveillance and insecticide resistance monitoring activities in Nigeria (NMCP, 2020; Adeogun *et al.,* 2023). The difference observed could be due to variation in the month of *Anopheles* larvae collection and year of the study. However, our study covered the whole year compared to their studies which was done during the rainy season when the vector population were in abundance though, the collection method was the same. The abundance and diversity of *An. gambiae* s.l. over *An. pretoriensis, An. maculipalpis* and *An. rufipes* is suggestive of anthropophilic behavior of *Anopheles gambiae* complex resulting into vectorial competence. It is also likely due to rainfall pattern coupled with relative humidity in the study sites. *An. gambiae* complex are the only *Anopheles* mosquitoes found in Zagaina (Evenness = 0) whereas two or more *Anophelines* were recorded in other communities. The preponderance of *Anopheles gambiae* s.l. is a result of its close proximity to residential houses and the suitability of the breeding water bodies. Findings from our work revealed the preponderance of secondary vectors; *An. pretoriensis, An. maculipalpis* and *An. rufipes* in Kaltungo study community. Similarly, Abba *et al.* (2024) reported the preponderance of secondary malaria vectors in Southern Gombe. However, our result is contrary to findings of Adeogun *et al.* (2023) who reported less than 2% in 12 out of 36 states of Nigeria. The abundance of *An. coluzzii* as the major malaria vector in the study area is not surprising as it was previously

reported to be approximately 98% of all the *Anopheles gambiae* complex collections in Yemaltu Deba LGA, Gombe State (Ahmed-yusuf *et al.,* 2020), Kano (Ibrahim *et al.,* 2019; Safiyanu *et al.,* 2019; Ononamadu *et al.*, 2020), South West (Omotoyo *et al.,* 2022) and two vegetation zones of North Eastern Adamawa State that share boundary with the study location (Wahedi *et al.,* 2020). Similarly, Ibrahim *et al.* (2023) observed *An. coluzzii* as the major malaria vector in the Sahelio-Sudanian region of Northern Nigeria, Niger, Cameroon and Chad. Our finding was also supported by the work of Adeogun *et al.* (2023) who reported the presence of all the sibling species of *An. gambiae* complex across Nigeria and *An. coluzzii* dominating most of Northern Nigeria. Efa *et al.* (2022) also reported *An. coluzzii* as a dominant species in Elobowa Southern Cameroon and Ellibou Southern Cote divore (N'Dri *et al.*, 2023). Our findings do not corroborate previous works reporting *An. gambiae s.s* as the major malaria vector in Nigeria and sub-Saharan Africa (Awolola *et al.*, 2009; Oduola *et al.*, 2012). *An. coluzzii* established mostly in Akko LGA that is neighboring Gombe metropolis. Similarly, *An. coluzzii* were known to dominate metropolitan area of Lagos (Omotayo *et al.,* 2022) which gives them the name Urban-mosquito and their establishment is likely due to high resistance to pyrethroids insecticides and other synthetic pesticide (Wahedi *et al.,* 2021). However, Oduola *et al.* (2019) previously reported preponderance of *An. gambiae* s.s. in Southern Gombe which is similar to present study. Previous studies have reported dominance of *An. gambiae* s.s. in Anambra and Katsina States (Irikannu *et al.*, 2019; Umar and Ndams, 2022) as opposed to zero record of *An. gambiae* s.s in Sudan Savannah of Northern Nigeria (Ibrahim *et al.*, 2014). The establishment of *An. gambiae* s.s is possible due to their preference for breeding in both permanent and temporary water bodies, Sunlit, found in both rainy and dry seasons likewise in areas within tense application of agrochemical pesticides (Defo-talom and Zeukeng, 2021). In this study, the *An. gambiae* s.s and *An. coluzzii* established in two separate ecological zone of Gombe with sympatric population of *An. arabiensis* agrees with a recent study conducted in twelve (12) States of Nigeria (Adeogun *et al.*, 2023). The rapid expansion of *An. coluzzii* among the sibling species in Nigeria specifically Gombe might be as a result of its adaptability to various ecological zones as well as climatic conditions. The co-habitation of *An gambiae* s.l. sibling species within a given habitat might threaten the recent achievement gained in malaria vector control programme in malaria endemic countries (Tokponnon *et al.*, 2023). This change in *An. gambiae* complex composition has implications on malaria vector management and control methods. It calls for the application of both indoor and outdoor vector control methods in order to minimize the expansion of *An. coluzzii* species population although no evidence of outdoor biting of *An. coluzzii* was documented.

This study is the first documented report of *P. falciparum* in *An. gambiae* complex from Gombe State with a prevalence rate of 11% compared to low sporozoites rate of 6.9% previously detected in *An. coluzzii* from neighbouring community of Adamawa State (Wahedi *et al.,* 2020). However, previous work by Rice *et al.* (2022) reported higher prevalence of *P. falciparum* (35%) in a University campus in Zaria. Conversely, low

sporozoites infection in *An. gambiae* s.s. was established in Southern Nigeria (Irikannu *et al.,* 2019; Obembe, 2023). Similarly, Altahir *et al.* (2022) reported 6.9% prevalence in *An. arabiensis* from Sudan while Mbewe *et al.* (2022) found low 0.16% sporozoite infection rate in two study areas in Malawi and Stephen *et al.* (2022) established 1.06% *Plasmodium* in *An. coustani* out of 376 blood fed *Anopheles* mosquito collected in coastal Kenya. Additionally, Moin-Vaziri *et al.* (2022) reported *Plasmodium* infection rate of 1.25 in *An. stephensi* from Afghanistan in contrast to study from South East, Nigeria where no *Plasmodium* was detected in all *Anopheles* mosquito species collected indoor and outdoor (Oduwole *et al.*, 2020). This is similar to finding in Chad where all 147 wild type blood fed *An. coluzzii* (Ibrahim *et al.,* 2019), and *An. stephensi* from Iran (Moin-Vaziri *et al.*, 2022) had no *P. falciparum* which could be due to active malaria vector control programme in Chad and Iran respectively. The low prevalence of *P. falciparum* observed could be as a result of mass distribution campaign of LLINs which kill, repels and prevent mosquito from taking blood when correctly used during sleeping hours. It was concluded from this study that *An. coluzzii* is the main malaria vector in Gombe contrary to earlier reports by Okorie *et al.* (2011) and Oduola *et al.* (2012).

5. Conclusion

The study established *An. gambiae* s.l. as the dominant malaria vector with sympatric populations of secondary vectors; *An. pretoriensis, An. maculipalpis* and *An. rufipes.* The presence of three sibling species; *An. gambiae* s.s, *An. arabiensis, An. coluzzii* co-habiting together and preponderance of *An. coluzzii* was also established. *An. coluzzii* is now becoming a major malaria vector in Gombe State due to speciation within the complex hence, vector surveillance is paramount. For the first time prevalence of *P. falciparum* sporozoite in *An. coluzzii* was established in Gombe State. Therefore, the State and National malaria elimination programme should focus more toward the control of both primary and secondary malaria vectors although; the latter is yet to be incriminated in malaria transmission in Gombe State.

6. Conflicts of Interest

The authors declare that they have no conflicts of interest.

7. Author's contribution

Authors A.B.S., I.S.N., S.G.J. and N.P.C. performed the field work, morphological identification, molecular analysis and developed the manuscript. Author E.A. and K.P.Y. analyzed the data. All authors proved read the manuscript and gave approval.

8. Funding

Acknowledgements

The authors sincerely thank the Gombe State Malaria vector surveillance laboratory, Gombe State University and Bayero Wellcome Research Unit, Department of Biochemistry, Bayero University Kano for working space to conduct molecular study.

References

Adeogun A, Babalola AS, Okoko OO, Oyeniyi T, Omotayo A, Izekor RT, Adetunji OA, Olakiigbe A, Olagundoye O, Adeleke M, Ojianwuna C, Adamu D, Daskum A, Musa J, Sambo O, Oduola A, Petrus UI, Samdi L, Obembe A, Dogara M, Yoriyo KP, Suleiman M, Samuel R, Amajoh C, Adesola M, Bala M, Esema M, Omo-Eboh M, Sinka M, Idowu OA, Ande A, Olayemi I, Yayo A, Uhomoibhi P, Awolola TS and Salako B. 2023. Spatial distribution and ecological niche modeling of geographical spread of *Anopheles gambiae* complex in Nigeria using real time data. *Nat Sci Rep.*, **13**:13679 https://doi.org/10.1038/s41598-023-40929-5

Ahmed-Yusuf M, Vatandoost H, Oshaghi MA, Ahmad AH, Enayati AA and Jalo RI. 2020. First report of target site insensitivity in pyrethroid resistant *Anopheles gambiae* from SouthernGuinea Savanna, Northern-Nigeria. *J Art-Bor Dis.*, **14(3)**, 228–238. https://doi.org/10.18502/jad.v14i3.4556

Altahir O, AbdElbagi H, Abubakr M, Siddig EE, Ahmed A and Mohamed NS. 2022. Blood meal profile and positivity rate with malaria parasites among different malaria vectors in Sudan. *Malar J.*, **21(1)**, 1–10. https://doi.org/10.1186/s12936-022-04157-y

Awolola TS, Oduola OA, Strode C, Koekemoer LL, Brooke B and Ranson H. 2009. Evidence of multiple pyrethroid resistance mechanisms in the malaria vector *Anopheles gambiae* sensu stricto from Nigeria. *Trans Roy Soc Trop Med and Hyg.*, **103(11)**, 1139–1145. https://doi.org/10.1016/j.trstmh.2008.08.021

Coetzee M. 2020. Key to the females of Afrotropical *Anopheles* mosquitoes (Diptera: Culicidae). *Malar J.*, **19(1)**, 1–20. https://doi.org/10.1186/s12936-020-3144-9

Defo-talom B and Zeukeng F. 2021. Divergence and Similarities on Insecticides Resistance Profiles Recorded with Populations of *Anopheles gambiae* sl Breeding in Vegetable Farms Within the Same City of Yaounde in Cameroon. *Socio Gen Sci.,* **4**:153-168

Echeverry DF, Deason NA, Davidson J, Makuru V, Xiao H, Niedbalski J, Kern M, Russell TL, Burkot TR, Collins FH and Lobo NF. 2016. Human malaria diagnosis using a single-step direct-PCR based on the *Plasmodium* cytochrome oxidase III gene. *Malar J.*, **15(1)**, 1–12. https://doi.org/10.1186/s12936-016-1185-x

Efa S, Elanga-Ndille E, Poumachu Y, Tene B, Mikande JZ, Zakariaou N, Wondji CS and Ndo C. 2022. Insecticide Resistance Profile and Mechanisms in *An. gambiae* s.l. from Ebolowa, South Cameroon. *Insects* **13(12)**. https://doi.org/10.3390/insects13121133

Ekedo CM and Ukpai OM. 2020. *Anopheles gambiae s.l.* insecticide susceptibility status in Umudike, Ikwuano LGA, Abia State, Nigeria. *Zoologist (The)*, **17**(February), 26–31. https://doi.org/10.4314/tzool.v17i1.5

Escobar D, Ascencio K, Ortiz A, Palma A and Fontecha G. 2020. Distribution and Phylogenetic Diversity of *Anopheles* Species in Malaria Endemic Areas of Honduras in an Elimination Setting. *Par Vect,* **13(1)**, 1-12.

Federal Ministry of Health. 2015. **National Malaria Strategic Plan 2021–2025**. *National Malaria Elimination Programme, May 2015*, 113. https://nmcp.gov.ng/

Garba Y. 2023. Species composition and distribution of *Anopheles* mosquito vectors in Kontogora, Niger State, Nigeria. *Inter Res J Nat Sci.,***11(1)**:43-50.

Ibrahim SS, Fadel AN, Tchouakui M, Terence E, Wondji MJ, Tchoupo M, Kérah-Hinzoumbé C, Wanji S and WondjiCS. 2019. High insecticide resistance in the major malaria vector *Anopheles coluzzii* in Chad Republic. *Infect Dis Pov*, **8(1)**. https://doi.org/10.1186/s40249-019-0605-x

Ibrahim SS, Manu YA, Tukur Z, Irving H and Wondji CS. 2014. High frequency of kdr L1014F is associated with pyrethroid resistance in *Anopheles coluzzii* in Sudan savannah of northern Nigeria. *BMC Infect Dis.*, **14(1)**, 1–8. https://doi.org/10.1186/1471-2334-14-441

Ibrahim SS, Muhammad A, Hearn J, Weedall GD, Nagi SC, Mukhtar MM, Fadel AN, Mugenzi LJ, Patterson EI, Irving H and Wondji CS. 2023. Molecular drivers of insecticide resistance in the Sahelo-Sudanian populations of a major malaria vector *Anopheles coluzzii*. *BMC Biol.*, **21(1),** 1–24. https://doi.org/10.1186/s12915-023-01610-5

Ibrahim SS, Mukhtar MM, Datti JA, Irving H, Kusimo MO, Tchapga W, Lawal N, Sambo FI and Wondji CS. 2019. Temporal escalation of Pyrethroid Resistance in the major malaria vector *Anopheles coluzzii* from Sahelo-Sudanian Region of Northern Nigeria. *Sci Rep.*, **9(1)**: 1–11. https://doi.org/10.1038/s41598-019-43634-4

Irikannu Kc, Pu U, Onwube, O and Jc O. 2019. Molecular characterization and malaria transmission potential of *Anopheles gambiae* complex in Awka, Anambra state, Nigeria. *Inter J Mosq Res.*, **6(6)**, 96–101.

Mbewe RB, Keven JB, Mzilahowa T, Mathanga D, Wilson M, Cohee L, Laufer MK and Walker ED. 2022. Blood-feeding patterns of *Anopheles* vectors of human malaria in Malawi: implications for malaria transmission and effectiveness of LLIN interventions. *Malar J.*, **21(1),** 1–12. https://doi.org/10.1186/s12936-022-04089-7

Medeiros-Sousa AR, Ceretti-Júnior W, de CG, Nardi MS, Araujo AB, Vendrami DP and Marrelli MT. 2015. Diversity and Abundance of Mosquitoes (Diptera:Culicidae) in an Urban Park: Larval Habitats and Temporal Variation. *Acta Trop.,* **150**, 200-209. doi:10.1016/j.actatropica.2015.08.002

Moin-Vaziri V, Djadid ND, Hoosh-Deghati H, Atta H, Raz AA, Seyyed-Tabaei SJ, Maleki-Ravasan N and Zakeri S. 2022. Molecular Detection of *Plasmodium* Infection among Anophelinae Mosquitoes and Differentiation of Biological Forms of *Anopheles stephensi* Collected from Malarious Areas of Afghanistan and Iran. *Ethiopian J Health Sci.,* **32(2)**, 269–278. https://doi.org/10.4314/ejhs.v32i2.7

N'Dri BP, Wipf NC, Saric J, Fodjo BK, Raso G, Utzinger J, Müller P and Mouhamadou CS. 2023. Species composition and insecticide resistance in malaria vectors in Ellibou, southern Côte d'Ivoire and first finding of *Anopheles arabiensis* in Côte d'Ivoire. *Malar J.*, **22(1)**, 1–13. https://doi.org/10.1186/s12936-023-04456-y

National Malaria Control Programme,(2020). **National Malaria Strategic Plan 2021-2025.** Federal Ministry of Health, Nigeria.

Obembe A. 2023. Molecular characterization and *Plasmodium falciparum* transmission risks of *Anopheles* mosquitoes in Malete, Nigeria. *UNED Res J.*, **15(2)**, e4689. https://doi.org/10.22458/urj.v15i2.4689

Oduola AO, Idowu ET, Oyebola MK, Adeogun AO, Olojede JB, Otubanjo OA and Awolola, TS. 2012. Evidence of carbamate resistance in urban populations of *Anopheles gambiae* s.s. mosquitoes resistant to DDT and deltamethrin insecticides in Lagos, South-Western Nigeria. *Par and Vect.*, **5(1):** 1. https://doi.org/10.1186/1756-3305-5-116

Oduwole OA, Oringanje CM, Oduola AO, Nwachuku NS, Meremikwu MM and Alaribe AAA. 2020. Species composition of *Anopheles* (Diptera: Culicidae) in selected forested tourist areas of Nigeria endemic for malaria. *J Med Entomol.*, **57(6),** 2007–2010. https://doi.org/10.1093/jme/tjaa110

Okorie PN, McKenzie FE, Ademowo OG, Bockarie M and Kelly-Hope L. 2011.   Nigeria Anopheles Vector Database: an Overview of 100 Years' Research. *Plos one*, **6(12)**, e28347.

Olatunbosun-Oduola A, Abba E, Adelaja O, Taiwo-Ande A, Poloma Y K and Samson-Awolola T. 2019. Widespread report of multiple insecticide resistance in *Anopheles gambiae* s.l. mosquitoes in eight communities in southern Gombe, north-eastern   Nigeria.   *J Arth-Bor Dis.*,   **13(1),**   50–61. https://doi.org/10.18502/jad.v13i1.932

Omotayo AI, Ande AT, Oduola AO, Adelaja OJ, Adesalu O, Jimoh TR, Ghazali   AI and Awolola ST. 2022. Multiple insecticide resistance mechanisms in urban   population   of *Anopheles coluzzii* (Diptera: culicidae) from Lagos, South-West Nigeria.   *Acta   Trop.*,   **227**(December   2021),   106291. https://doi.org/10.1016/j.actatropica.2021.106291

Ononamadu CJ, Datit JT and Imam AA. 2020. Insecticide Resistance Profile of *Anopheles gambiae* Mosquitoes: A Study of a Residential and Industrial Breeding Sites in Kano Metropolis, Nigeria.   *Environ   Health   Insights*,   **14**. https://doi.org/10.1177/1178630219897272

Owolabi DO and Ayankoya TA. 2023. Insecticides Susceptibility of Malaria Vectors in Okitipupa, Ondo State, Nigeria Using WHO Susceptibility Test. *J Drug Design Med Chem.,* **9(1)**:1-6 doi: 10.11648/j.jddmc.20230901.11

Rice AA, Mbah CE and George BDJ. 2022. Assessment of Mosquito Diversity and *Plasmodium falciparum* in Female *Anopheles* Mosquito in Students' Hostels, Ahmadu Bello University Zaria, Kaduna State Nigeria. *Dutse J of Pur and Appl Sci..*, **7(3b)**, 105–114. https://doi.org/10.4314/dujopas.v7i3b.12

Safiyanu M, Alhassan AJ, Yayo AM, Ibrahim SS, Imam AA and Abdullahi H. 2019. Detection of KDR 11014f mutation in pyrethroids susceptible *Anopheles gambiae* S.L from Ladanai, Kano state, northwest Nigeria. *Inter J Mosq Res.*, **6(3, Part A),** 10–15.

Santolamazza F, Mancini E, Simard F, Qi Y, Tu Z and Della Torre A. 2008. Insertion polymorphisms of SINE200 retrotransposons within speciation islands of *Anopheles gambiae* molecular forms. *Malar J.*, **7**: 1–10. https://doi.org/10.1186/1475-2875-7-163

Silva APB, Santos JMM and Martins AJ. 2014. Mutations in the voltage-gated sodium channel gene of anophelines and their association with resistance to pyrethroids - A review. *Par and Vect.*, **7(1)**: 1–14. https://doi.org/10.1186/1756-3305-7-450

Stephen A, Busula AO, Nicholas K, Mukabane K, Webale MK and OmukundaE. 2022. Detection of *Plasmodium* Sporozoites and Blood-Meal Source in a Population of *Anopheles Coustani* Senso Lato in Kakamega County, Western Kenya. *Inter J Inn Res Dev.*, **11(1)**. https://doi.org/10.24940/ijird/2022/v11/i1/jan22031

Tokponnon TF, Ossè R, Padonou GG, Affoukou CD, Sidick A, Sewade W, Fassinou A, Koukpo CZ, Akinro B, Messenger LA, Okê M, Tchévoédé A, Ogouyemi-Hounto A, Gazard DK and Akogbeto M. 2023. Entomological Characteristics of Malaria Transmission across Benin: An Essential Element for Improved Deployment of Vector Control Interventions. *Insects,* **14(1)**. https://doi.org/10.3390/insects14010052

Umar AM and Ndams IS. 2022. Species Composition, Distribution, Abundance and Vectorial Capacity of *An. gambiae* in parts of Katsina State, Nigeria. *Inter   J Zool Appl Biosci.,* **7(2)**:30-39. https://doi.org/10.55126/ijzab.2022.v07.i02.007

Wahedi JA, Ande AT, Oduola AO and Obembe A. 2021. Bendiocarb resistance andkdrassociated deltamethrin and DDT resistance in *Anopheles gambiae* s.l.populations from North Eastern Adamawa State, Nigeria. *Ceylon J Sci.*, **50(1)**, 63. https://doi.org/10.4038/cjs.v50i1.7848

Wahedi JA, Ande AT, Oduola, AO, Obembe A, Tola M, Oyeniyi TA and Awolola TS. 2020. Dynamics of malaria vector indices in two vegetation zones within North Eastern Adamawa State, Nigeria.   *Trop   Biomed.*,   **37(3)**,   637–649. https://doi.org/10.47665/tb.37.3.637

Weeraratne TC, Surendran SN, Reimer LJ, Wondji CS, Perera M DB, Walton C and Parakrama Karunaratne S. H. P. 2017. Molecular characterization of Anopheline (Diptera: Culicidae) mosquitoes from eight geographical locations of Sri Lanka. *Malar J.*, **16(1)**, 1–14. https://doi.org/10.1186/s12936-017-1876-y

WHO 2019. **World malaria report 2019.** In *WHO Regional Office   for   Africa.*   https://www.who.int/news-room/fact-sheets/detail/malaria

WHO 2020. **World Malaria Report. 2020.** Geneva: World Health Organization; 2020. Available from:

https://www.who.int/teams/global-malaria programme/reports/ world-malaria-report-2020

WHO 2022. **World Malaria Report, 2022**. WHO, Geneva, Switzerland

WHO. 2023. **World malaria report 2023** [Internet]. In *World Health Organization.* https://www.who.int/teams/global-malaria-programme/reports/world-malaria-report-2023

Genetic Diversity of South Libyan Elite Date Palm Using SSR Markers

Khaled Elmeer[1,*], Amna Ahmed[2] and Imene Mattat[3]

[1]Faculty of Agriculture, University of Tripoli, Libya;[2]University of Sabha, Libya; [3]Ministry of Municipality, Doha Qatar.

Abstract

Date palms (*Phoenix dactylifera*) reproduce through offshoots, a vegetative propagation method that results in offspring genetically similar to the parent plant. However, the genetic diversity of date palms, particularly in the Southern Libya Region (SLR), remains insufficiently understood at the molecular level. Previous studies relied heavily on phenotypic traits, fruit, leaf, and chemical analyses, which are susceptible to environmental influences and developmental variations. In this study, genetic diversity was assessed using microsatellite markers across 27 palm samples from three cultivars (Taghyat, Tafsert, and Thales) grown in three regions of SLR (Sabha, Ubari, and Murzuq). Twenty microsatellite primers were employed, producing polymorphic results across the samples. A total of 84 alleles were identified, with an average of 4.2 alleles per locus. Allelic distribution varied, with loci ranging from two alleles to seven. Genetic diversity analysis yielded an average diversity index of 0.61, with heterozygosity values ranging from 0% to 100%. The Polymorphism Information Content (PIC) values averaged 0.55, indicating moderate marker efficiency. Cluster analysis revealed two main genetic groups: one consisting of Taghyat and Thales and the other of Tafsert. The AMOVA results indicated that 24% of the genetic variance was attributed to differences between cultivars, while 76% was within cultivars. These findings provide valuable insights into the genetic structure and diversity of date palms in the SLR, highlighting potential for future breeding and conservation efforts.

1. Introduction

The date palm (*Phoenix dactylifera L.*) is a vital crop in arid and semi-arid regions, particularly in the Middle East, North Africa, and South Asia. It serves as a key source of food, income, and shelter for local communities. Beyond its fruit, every part of the date palm—from the leaves and trunk to the fibres has diverse uses, including construction, fuel, and handicrafts. Its economic and ecological value is significant, contributing to the sustainability of agriculture in fragile oasis ecosystems (Elmeer *et al.,* 2020).

Date palms are cultivated for high-quality fruit, classified into soft, semidry, and dry types, each meeting different market needs. Dry dates, prized for their low moisture and high sugar content, are ideal for long storage and have historically supported desert trade routes (Racchi *et al.,* 2014). By 2020, Libya's date palm cultivation covered 32,868 hectares, producing 177,629 metric tons, a crucial contribution to the country's agricultural output (FAOSTAT, 2020).

Globally, date palms contribute to food security and economic stability, while also supporting biodiversity and ecosystem services. Molecular tools like DNA fingerprinting and SSR (Simple Sequence Repeat) markers are essential in advancing date palm research, enhancing genetic diversity, fruit quality, and addressing challenges such as climate change, pests, and diseases (Jubrael *et al.,*

2005; Elmeer and Mattat, 2015). This study hypothesizes that SSR markers will provide insights into the genetic diversity of date palm cultivars in Southern Libya. By analyzing elite cultivars, the research aims to identify superior varieties for enhancing the quality and sustainability of date palm production in the region.

Despite the importance of date palms to local economies, there is a lack of comprehensive genetic studies on Southern Libyan cultivars. A clear understanding of genetic diversity is essential for improving fruit quality, yield, and resilience to environmental stressors. Without this knowledge, selecting and propagating high-performing cultivars remains challenging.

This study proposes using SSR markers to assess the genetic diversity of date palm cultivars in Southern Libya. By profiling elite cultivars (Taghyat, Tafsert, and Talis) from regions like Sabha, Ubari, and Murzuq, the research aims to generate genetic fingerprints that will help identify cultivars with the highest potential for cultivation and improvement.

Recent studies have demonstrated the effectiveness of SSR markers in assessing genetic relationships in date palms across various regions, including GCC countries (Elmeer *et al.,* 2020), Algeria (Abdelkrim *et al.,* 2023), Morocco (Khoulassa *et al.,* 2023), Tunisia (Abdallah *et al.,* 2020), Oman (Reddy *et al.,* 2022), and Pakistan (Faqir *et al.,* 2021). Additionally, microsatellite markers have been

---

successfully used for sex determination in *Phoenix dactylifera L.* (Salameh *et al.,* 2024)

In Libya, date palm cultivars are often categorized by texture and storage capacity, but genetic studies in the southern regions remain scarce. The Southern Libyan Region, with its diverse date varieties, holds significant potential for global date production if its genetic resources are fully understood and utilized.

This study focuses on the Southern Libyan Region, particularly the oases of Sabha, Ubari, and Murzuq, known for their unique date cultivars. By using SSR markers, the research aims to provide the first comprehensive genetic profile of elite cultivars from this area. The findings are expected to support conservation efforts, and strategies to improve date palm production and quality. Given the growing global demand for high-quality dates and challenges posed by climate change, this research is timely

and essential for the future of date palm cultivation in Libya and beyond.

2. Materials and Methods

2.1. Plant materials

Leaf samples were collected from 27 female date palm trees, representing three distinct cultivars: Tafsert (F), Talis (T), and Taghyat (G). The trees were sourced from three different farms, each located in a unique region: Ubari (26.5810° N, 12.7940° E), Sabah (27.0365° N, 14.4290° E), and Murziq (25.9182° N, 13.9260° E), as shown in Figure 1. These particular cultivars were selected for their status as elite date palm genotypes within the SLR plantation. Young leaves were carefully harvested from randomly selected mature trees, then dried and processed for DNA extraction.
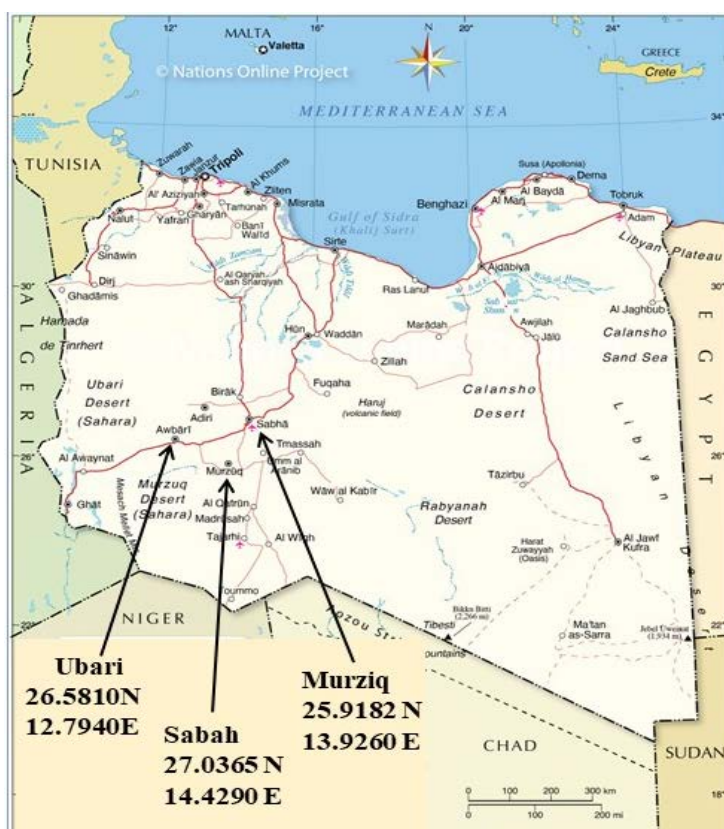
Figure 1 Map illustrating the three study locations within the Southern Libya region.

2.2. DNA extraction and genotyping

One gram leaf sample was finely ground using liquid nitrogen. DNA extraction was performed using the DNeasy Plant Maxi Kit (Qiagen, Venlo, Netherlands) according to the manufacturer's instructions. The extracted DNA was quantified using a Nanodrop spectrophotometer.

Twenty labeled primer pairs were synthesized by Applied Biosystems (Life Technologies BV, Kwartsweg, Bleiswijk, Netherlands). Eleven of these primers were previously described by Billotte *et al.,* (2004), and the remaining nine were outlined by Elmeer *et al.,* (2011). The list of primers can be found in Table 1. PCR amplification was conducted in a 25 μL reaction volume, consisting of 2 μL (5 ng) DNA, 12.5 μL of AmpliTaq Master Mix, 1 μL of each forward and reverse primer (at a concentration of 5 μM), and 8.5 μL of nuclease-free water.

DNA amplification was carried out using a Veriti 96 Thermal Cycler (Applied Biosystems) under the following conditions: an initial denaturation at 95°C for 10 minutes, followed by 35 cycles of denaturation at 95°C for 30 seconds, primer-specific annealing temperatures (as detailed in Table 1) for 30 seconds, and extension at 72°C for 1 minute. A final extension step was performed at 72°C for 7 minutes.

Microsatellite analysis was conducted using an ABI 3130 Genetic Analyzer (Applied Biosystems). For this, 1 μL of PCR product was mixed with 10 μL of Hi-Di formamide and 0.3 μL of GS500LIZ size standard, then denatured at 95°C for 3 minutes and cooled on ice. The samples were analyzed on the ABI 3130 Genetic Analyzer, and allele scoring was performed using the GeneMapper Software v4.0 (Applied Biosystems).

Table 1. Date palm-specific microsatellite primers (primer pairs 1-11 developed by Billotte et al., 2004, and primer pairs 12-20 developed by Elmeer et al., 2011).

No.	Primer code	Repeat motif	Primer sequences (5'–3')	Optimal Tm °C
1	mPdCIR010	$(GA)_{22}$	F: ACCCCGGACGTGAGGTG	55.9
			R: CGTCGATCTCCTCCTTTGTCTC	
2	mPdCIR015	(GA)15	F: AGCTGGCTCCTCCCTTCTTA	51.6
			R: GCTCGGTTGGACTTGTTCT	
3	mPdCIR016	(GA)14	F: AGCGGGAAATGAAAAGGTAT	51.7
			R: ATGAAAACGTGCCAAATGTC	
4	mPdCIR032	(GA)19	F: CAAATCTTTGCCGTGAG	51.5
			R: GGTGTGGAGTAATCATGTAGTAG	
5	mPdCIR035	(GA)15	F: ACAAACGGCGATGGGATTAC	53.9
			R: CCGCAGCTCACCTCTTCTAT	
6	mPdCIR057	(GA)20	F: AAGCAGCAGCCCTTCCGTAG	55.4
			R: GTTCTCACTCGCCCAAAAATAC	
7	mPdCIR070	(GA)17	F: CAAGACCCAAGGCTAAC	48.7
			R: GGAGGTGGCTTTGTAGTAT	
8	mPdCIR078	(GA)13	F: TGGATTTCCATTGTGAG	49.6
			R: CCCGAAGAGACGCTATT	
9	mPdCIR085	(GA)29	F: GAGAGAGGGTGGTGTTATT	50.4
			R: TTCATCCAGAACCACAGTA	
10	mPdCIR090	(GA)26	F: GCAGTCAGTCCCTCATA	48.6
			R: GCAGTCAGTCCCTCATA	
11	mPdCIR093	(GA)16	F: CCATTTATCATTCCCTCTCTTG	51.8
			R: CTTGGTAGCTGCGTTTCTTG	
12	DP151	(AC)37	F TTGCTGGTTGAAATGGTGTT	53.3
			R GCAACAGATGCTCTTGCTCA	
13	DP157	(TC)19	F TGGACAATGACACCCCTTTT	54.6
			R GCCCACACAACAACCTCTCT	
14	DP159	(TC)27	F AGCTCCAATTTGCTGCAGAG	54.3
			R GCTGACCTGGAGTCCAAAAC	
15	DP160	(GAAA)5	F AAGAGCGACAATCATGACCA	57.7
			R GGAAATTGAAGGGCATCTTG	
16	DP169	(AAT)12	F GCATGGACTTAATGCTGGGTA	57.1
			R GGTTTTCCTGCCAACAACAT	
17	DP170	(AGGG)5	F TCTTTGGGCTTACGACAACC	55.9
			R GTATGGCCCAAGATGCAGAT	
18	DP171	(TTC)10	F GTGGGAGTAGCGAGGTATGG	56
			R GTCCGGCACTTTAGGAAGTT	
19	DP172	(AGG)11	F GGTGTTTGGGCCTATTTCCT	54.2
			R GTCCTCCTCCTCCTCTGTCC	
20	DP175	(CA)19	F ACACACACACACACACACACC	57.6
			R GTGGCTTCTTTTTGGCTGTC	

2.3. Data analysis

The evaluation included the analysis of allele size (in base pairs), number of alleles per locus, major allele frequency, number of genotypes per locus, genetic diversity, and polymorphic information content, all performed using PowerMarker software v3.25 (Liu and Muse, 2005), with the Hamming similarity index and 100 bootstrap replications applied. Phylogenetic diagrams were constructed using Past software version 1.91 (Hammer, 2001). Molecular variance (AMOVA), genetic variation within and among populations, expected and observed heterozygosity, inbreeding coefficient, F-statistics, and genetic distances of southern Libyan date palm cultivars were analyzed using GenAlEx 6.5 software (Excoffier *et al.,* 2005).

3. Results

Date palms reproduce through offshoots, utilizing vegetative propagation to produce offspring that are genetically similar to the parent plant. However, the genetic diversity of date palms in the Southern Libyan Region (SLR) remains insufficiently explored at the molecular level. Previous studies on genetic diversity have primarily focused on phenotypic traits, such as fruit and leaf characteristics, and certain chemical properties. These approaches are influenced by environmental factors and variations across different growth and developmental stages of the plant.

Microsatellite marker analysis of various palm samples revealed polymorphism, attributed to variations in the number of alleles identified. In this study, 27 palm samples from three distinct cultivars and three regions were tested using 20 primers. Most primers successfully amplified specific regions of the palm samples, with the exception of two samples: the Taghyat cultivar from the second farm in the Sabha region (SG2) and the Tafsert sample from the third farm in the Sabha region (SF3).

3.1. Genetic Diversity

The analysis of genetic diversity encompassed the quantification of alleles and genotypes across twenty microsatellite loci within the three cultivars sourced from (SLR). The outcomes of this analysis are showcased in Table 2, revealing a cumulative count of eighty-four alleles, translating to an average of 4.2 alleles per locus. Allelic distribution per locus ranged from two alleles in mPdCIR010 and DP159 to seven alleles in DP157 (Table 2).

The study assessed the average genetic diversity of the Taghyat, Tafsert, and Thales cultivars grown across three regions of the Southern Libyan Region (SLR)—Sabha, Ubari, and Murzuq. Using twenty microsatellite markers, the analysis revealed an average genetic diversity value of 0.61, with a range from 0.17 (associated with the mPdCIR090 locus) to 0.80 (corresponding to the mPdCIR070 locus).

The heterozygosity index varied across the three cultivars, ranging from zero (indicating the absence of heterozygous alleles) at the mPdCIR035 locus to 100% at both the mPdCIR085 and DP160 loci. The average heterozygosity index for the cultivars was 0.62. Most of the loci analyzed exhibited heterozygosity greater than 50%, as expected for date palms, given their predominantly outcrossing nature.

Table 2. Genetic diversity analysis using 20 microsatellite polymorphism loci of southern Libyan date palm cultivars.

Marker	Az (bp)	Na	Maf	Ng	GD	PIC	He	Ho	Fis	Fst
mPdCIR010	124-134	2	0.68	2	0.44	0.34	0.42	0.64	-0.52	0.03
mPdCIR015	126-138	3	0.54	3	0.58	0.50	0.49	0.92	-0.87	0.16
mPdCIR016	126-132	4	0.38	6	0.72	0.67	0.50	0.83	-0.67	0.30
mPdCIR032	288-300	3	0.38	4	0.66	0.59	0.52	0.67	-0.29	0.22
mPdCIR035	181-187	3	0.56	3	0.57	0.49	0.18	0.00	1.00	0.68
mPdCIR057	250-258	3	0.54	4	0.59	0.52	0.44	0.33	0.25	0.25
mPdCIR070	186-206	6	0.28	5	0.80	0.77	0.43	0.74	-0.72	0.47
mPdCIR078	117-177	5	0.41	5	0.73	0.69	0.65	0.67	-0.03	0.12
mPdCIR085	168-182	6	0.33	6	0.75	0.71	0.55	1.00	-0.82	0.27
mPdCIR090	148-166	3	0.91	3	0.17	0.16	0.16	0.11	0.30	0.08
mPdCIR093	161-179	6	0.36	8	0.75	0.71	0.56	0.68	-0.21	0.25
DP151	170-174	3	0.54	3	0.54	0.45	0.47	0.79	-0.68	0.13
DP157	198-214	7	0.56	9	0.65	0.63	0.45	0.44	0.01	0.31
DP159	160-162	2	0.63	2	0.47	0.36	0.47	0.74	-0.59	0.00
DP160	116-122	4	0.39	4	0.67	0.60	0.55	1.00	-0.81	0.17
DP169	200-214	6	0.59	6	0.61	0.58	0.39	0.37	0.05	0.36
DP170	214-224	4	0.67	6	0.52	0.48	0.43	0.56	-0.30	0.17
DP171	198-214	5	0.39	4	0.73	0.68	0.65	0.96	-0.49	0.11
DP172	206-214	4	0.57	4	0.59	0.53	0.51	0.48	0.06	0.13
DP175	208-224	5	0.54	5	0.65	0.62	0.42	0.52	-0.24	0.36
Mean		4.2	0.51	4.6	0.61	0.55	0.46	0.62	-0.28	0.23

Az: allele size base pair, Na: number of alleles per locus, Maf: major allele frequency, Ng: number of genotypes per locus, GD: genetic diversity, Pic: polymorphic information content, He: expected heterozygosity, Ho: observed heterozygosity, Fis: inbreeding coefficient and Fst Wright's analysis of hierarchical F-statistics.

The Polymorphism Information Content (PIC) values, which assess the discriminatory power of markers and the quality of marker genotype data, were determined. The average PIC value for the primer sets was 0.55, with values ranging from 0.16 for the mPdCIR090 locus to 0.77 for the mPdCIR070 locus.

3.2. Cluster Analysis and Genetic Structure

The dendrogram (Fig. 2) illustrates the genetic divergence among the three date palm cultivars from the Southern Libyan Region (SLR) and reveals two main clusters. Cluster (A) includes the Taghyat and Talis cultivars, which, despite exhibiting varying degrees of dissimilarity, remain grouped together regardless of their geographical origins, indicating a closer genetic relationship. In contrast, Cluster (B) contains the Tafsert cultivar, which is distinctly separated from the other two cultivars.
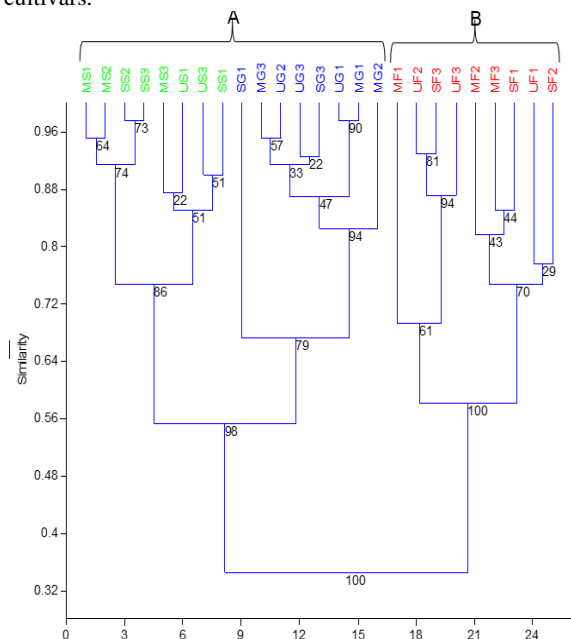

Figure 2. Dendrogram based on Hamming coefficient analysis depicting the genetic relationships among three date palm cultivars: Taghyat (G), Tafsert (T), and Talis (S), originating from Ubari (U), Sabha (S), and Murzuq (M) in southern Libya.

Genetic relationships among the three date palm cultivars from the Southern Libyan Region (SLR) were examined. The average number of alleles per locus ranged from 2.5 for Tafsert, 2.65 for Taghyat, and 2.8 for Talis, with an overall average of 2.65 alleles per locus. The expected heterozygosity was nearly identical across the cultivars, with an average of 0.46, while the observed heterozygosity had an average of 0.62. The percentage of polymorphic loci was 100% for Taghyat, and 95% for both Tafsert and Talis (Table 3). The similarity matrix computed for the three cultivars revealed an average similarity coefficient ranging from 20% to 97.5%

Table 3. Mean and standard error (SE) across loci for each population of the three date palm cultivars.

Population		N	Na	He	Ho	Fis	%P
Taghyat	Mean	8.70	2.65	0.43	0.60	-0.20	100
	SE	0.11	0.15	0.04	0.10	0.16	
Talis	Mean	8.65	2.80	0.50	0.69	-0.38	95
	SE	0.11	0.28	0.04	0.07	0.10	
Tafsert	Mean	9.00	2.50	0.46	0.58	-0.19	95
	SE	0.00	0.17	0.04	0.09	0.16	
Average		8.78	2.65	0.46	0.62	-0.26	96.67

N: number of accessions, **Na**: number of alleles per locus, **He**: expected heterozygosity, **Ho**: observed heterozygosity, **Fis**: fixation index values and **%P**: Percentage of Polymorphic Loci.

The dendrogram based on the Hamming genetic similarity coefficient among the date palm cultivars in the Southern Libyan Region (SLR) supports the findings of the principal coordinate analysis (PcoA), with the cultivars clearly divided into two distinct clusters. The first cluster includes the Taghyat and Thales cultivars, represented in blue and green in Fig. 3, while the second cluster, shown in red, distinctly separates the Tafsert cultivar from the other two. These relationships are further emphasized by the genetic distance analysis presented in Table 4.
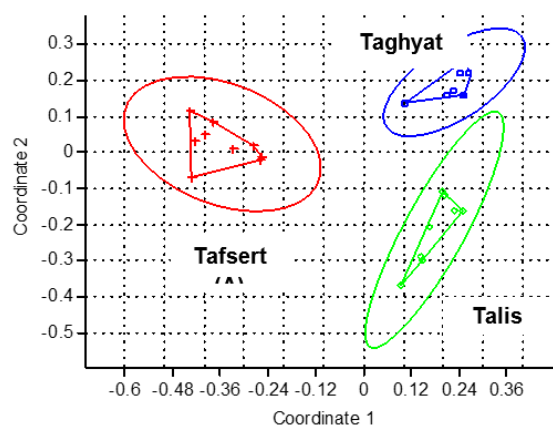
Figure 3. Scatter plot of Principal Coordinate Analysis (PCoA) based on 20 microsatellite loci among three date palm cultivars: Taghyat (G), Tafsert (T), and Talis (S), from Ubari (U), Sabha (S), and Murzuq (M) in southern Libya.

Table 4. Genetic distance of southern Libyan date palm cultivars.

Nei Genetic Distance			
	Taghyat	Tales	Tafsert
Taghyat	0	0.67	0.33
Tali s	0.67	0	0.63
Tafsert	0.33	0.63	0

The AMOVA results indicate that 24% of the total variance is attributable to differences between the cultivars, reflecting underlying structural genetic variation. The remaining 76% of the genetic variation is due to differences within each individual cultivar (Table 5).

Table 5. AMOVA table of southern Libyan date palm cultivars.

Source	df	Sum of Square	Estimated Variability	% of variation
Among Pops	2	76.944	1.912	24%
Among Indiv	24	97.222	0.000	0%
Within Indiv	27	163.500	6.056	76%
Total	53	337.667	7.968	100%

4. Discussion

A similar study involving Tunisian date palms reported successful amplification with sixteen primer pairs, although only fourteen primers produced positive results (Zehdi *et al.,* 2004). In Oman, 62.5% of primer pairs (10 out of 16) yielded successful amplification (Al-Ruqaishi *et al.,* 2008). The mean allele count in our study (2.65 alleles per locus) exceeded the 3.09 alleles per locus observed in a study of 72 wild date palms from Jordan (Al Asasfa *et al.,* 2015), likely due to the use of fewer primers in the latter. Our findings align with those from Qatar (4 alleles per locus), Saudi Arabia (4.1 alleles per locus), and Iran (4.8 alleles per locus) (Ahmed *et al.,* 2011; Al-Faifi *et al.,* 2016; Arabnezhad *et al.,* 2012). In contrast, higher allele counts have been reported in Libya, Iraq, Nigeria, Morocco, and Tunisia. For example, a Libyan study of 377 palms revealed 6.88 alleles per locus (Racchi *et al.,* 2014), while studies in Iraq, Nigeria, Morocco, and Tunisia reported averages ranging from 7 to 8.5 alleles per locus (Khierallah *et al.,* 2011; Yusuf *et al.,* 2015; Bodian *et al.,* 2012; Zehdi *et al.,* 2004).

The observed genetic diversity in this study suggests significant genetic variation in the Southern Libyan date palms (SLR), comparable to the 0.66 gene diversity in Qatari date palms (Elmeer and Mattat, 2015), though lower than the 0.75 reported in GCC date palms (Elmeer *et al.,* 2020). This diversity may stem from cross-pollination, where progeny retains the cultivar name despite potential genetic differences. This genetic variation is crucial for maintaining healthy populations and mitigating the risks of genetic bottlenecks. The observed heterozygosity (0.62) in this study was higher than in Moroccan palms (0.11-0.30) (Khoulassa *et al.,* 2023), but aligned with Saudi (0.68) and GCC palms (0.62) (Al-Faifi *et al.,* 2016; Elmeer *et al.,* 2020), though lower than the 0.72 found in Iraqi and Iranian date palms (Arabnezhad *et al.,* 2012).

The majority of primers in this study exhibited PIC values above 0.5, indicating their effectiveness in assessing genetic diversity, surpassing the 0.22 reported for Jordanian palms (Al Asasfa *et al.,* 2015) and matching the 0.68 for Saudi palms (Al-Faifi *et al.,* 2016), but falling short of the 0.72 observed in GCC palms (Elmeer *et al.,* 2020). Interestingly, the dendrogram analysis revealed that genetic structure is largely unaffected by geographical location, despite distances of 120-200 km between regions. This supports the genetic similarity observed between Taghyat samples from the Murzuq and Ubari regions, highlighting significant intra-cultivar variation despite geographical separation.

Inbreeding coefficients (Fis) ranged from 0.01 (DP157) to 1.0 (mPdCIR035), with genetic divergence noted in the highest similarity values (97.5%) between certain Taghyat and Talis cultivars across regions. The lowest similarity (20%) was found between Taghyat (Ubari) and Tafsert (Ubari). This divergence mirrors findings from studies in Oman and Morocco, where higher variance was observed within populations compared to among populations (Ibrahimi *et al.,* 2023; Reddy *et al.,* 2022), possibly due to the widespread practice of cultivating date palms via cross-pollinated offshoots. This approach increases genetic diversity and can contribute to disease resistance and improved genetic resilience. These results are consistent with findings by Bodian *et al.* (2012) on Moroccan germplasm.

5. Conclusion

This study is an initial exploration aimed at assessing the genetic diversity of date palms in southern Libya. The recorded genetic diversity rate of 0.61 is moderately high. Notably, 76% of the observed genetic variation originates from differences among cultivars. The current results could be attributed to the prevalence of cross-pollination among collected samples, resulting in the generation of novel and diverse genotypes. This process enriches the genetic traits of date palm cultivars in southern Libya, simultaneously diminishing the susceptibility to genetic issues like vulnerability, genetic drift, and disease susceptibility.

Ethics approval and consent to participate

This article does not contain any studies involving animals or human participants performed by any of the authors.

Consent for publication

Not applicable

Availability of data and materials

All data analysed during this study are included in this published article.

Competing interests

The authors declare that they have no competing interests.

References

Abdallah HB, Laajimi A, Guesmi F, Triki T, Ferchichi A, Hormaza JI and Larranaga N. 2020. Genetic diversity of endangered date palm (*Phoenix dactylifera L.*) in the oases of Nefzaoua Tunisia using SSR markers. Fruits, 75(2):84-91.

Abdelkrim R, Ziane L, Rima BH, Khaled C, Sarra C and Ali B. 2023. Molecular identification of genetic diversity in date palms (*Phoenix dactylifera L.*) from Algerian oases using Simple Sequence Repeats (SSR) markers. S. Afr. J. Bot. 157:438-446.

Ahmed MVOM, Bouna ZEO, Lemine FMM, Djeh TKO, Mokhtar T and Salem AOM. 2011. Use of multivariate analysis to assess phenotypic diversity of date palm (*Phoenix dactylifera L.*) cultivars. Sci. Hortic., 127(3):367-371.

Al Asasfa MA, Duwayri MA, Qasem JR and Al Abdallat AM. 2015. Characterization and assessment of genetic diversity of wild Date Palm (*Phoenix dactylifera L.*) in Jordan Jordan J. Agric. Sci., 23(11):75-94.

Al-Faifi SA, Migdadi HM, Algamdi SS, Khan MA, Ammar MH, Al-Obeed RS, Al-Thamra MI, El-Harty EH and Jakse J. 2016. Development, characterization, and use of genomic SSR markers for assessment of genetic diversity in some Saudi date palm (*Phoenix dactylifera L.*) cultivars. Electron. J. Biotechnol., 21:18-25.

Al-Ruqaishi IA, Davey M, Alderson P and Mayes S. 2008. Genetic relationships and genotype tracing in date palms (*Phoenix dactylifera L.*) in Oman, based on microsatellite markers. Plant Genet. Resour. 6(1):70-72.

Arabnezhad H, Bahar M, Mohammadi HR and Latifian M. 2012. Development, characterization and use of microsatellite markers for germplasm analysis in date palm (*Phoenix dactylifera L.*). Sci. Hortic.134:150-156.

Billotte N, Marseillac N, Brottier P, Noyer JL, Jacquemoud-Collet JP, Moreau C, Couvreur T, Chevallier MH, Pintaud JC and Risterucci AM. 2004. Nuclear microsatellite markers for the date palm (*Phoenix dactylifera L.*): characterization and utility across the genus *Phoenix* and in other palm genera. Mol. Ecol. Notes. 4(2):256-258.

Bodian A, El Houmaizi MA, Ndoye Ndir K, Hasnaoui A, Nachtigall M and Wehling P. 2012. Genetic diversity analysis of date palm (*Phoenix dactylifera L.*) cultivars from Figuig oasis (Morocco) using SSR markers. Int. J. Sci. Adv. Technol., 2(3):96-104.

Elmeer K and Mattat I. 2015. Genetic diversity of Qatari date palm using SSR markers. Genet. Mol. Res., 14(1):1624-1635.

Elmeer K, Mattat I, Al Malki A, Al-Mamari AG, Al-Jabri A, Buhendi A, Alkhabaz S, Abu-Idrees A, Abdulkaream A, Udupa SM and Baum M. 2020. Intra-cultivar variability at microsatellite loci in date palm cultivars across the GCC countries. QScience Connect, (1).3.

Elmeer K, Sarwath H, Malek J, Baum M and Hamwieh A. 2011. New microsatellite markers for assessment of genetic diversity in date palm (*Phoenix dactylifera L.*). 3 Biotech, 1:91-97.

Excoffier L, Laval G, Schneider S. 2005. Arlequin (version 3.0): an integrated software package for population genetics data analysis Evolutionary bioinformatics. Jan;1:117693430500100003.

FAOSTAT, 2020. FAO Statistical Yearbook World Food and Agriculture

Faqir N, Muhammad A. and Shehzad A. 2021. 16. Simple sequence repeat (SSR) markers show greater similarity among morphologically diverse Date palm (*Phoenix dactylifera L.*) cultivars grown in Pakistan. Pure Appl. Biol. (PAB), 5(3):483-498.

Hammer O. 2001. PAST: Paleontological statistics software package for education and data analysis. Palaeontol electron. 4, p.9.

Ibrahimi M, Brhadda N, Ziri R, Fokar M, Iraqi D, Gaboun F, Labhilili M, Habach A, Meziani R, Elfadile J. and Abdelwahd R. 2023. Analysis of genetic diversity and population structure of Moroccan date palm (*Phoenix dactylifera L.*) using SSR and DAMD molecular markers. J. Genet. Eng. Biotechnol. 21(1):66.

Jubrael JM, Udupa SM. and Baum M. 2005. Assessment of AFLP-based genetic relationships among date palm (*Phoenix dactylifera L.*) varieties of Iraq. J. Am. Soc. Hortic. Sci. 130(3):442-447.

Khierallah HS, Bader SM, Baum M. and Hamwieh A. 2011. Genetic diversity of Iraqi date palms revealed by microsatellite polymorphism. J. Am. Soc. Hortic. Sci. 136(4): 282-287.

Khoulassa S, Khurshid H, Fokar M, Eliddrissy H, Outeha Y, Elfadil J, Essarioui A, Benlyas M, Mentag R. and Elmoualij B. 2023. Genetic diversity of Moroccan date palm revealed by microsatellite markers. Genet. Mol. Biol. 46. p.e20220021.

Liu K. and Muse SV. 2005. PowerMarker: an integrated analysis environment for genetic marker analysis. Bioinformatics. 21(9):2128-2129.

Racchi ML, Bove A, Turchi A, Bashir G, Battaglia M. and Camussi A. 2014. Genetic characterization of Libyan date palm resources by microsatellite markers. 3 Biotech. 4:21-32.

Reddy H, AL-Rashdi FK, AL-Sulti HS, AL-Madhoshi MS, Hussain SA. and Gangireddygari VSR. 2022. Studies on Oman elite date palm varieties and preliminary establishment of identity through SSR marker. J. King Saud Univ. Sci. 34(8):102348.

Salameh A, Hamdan YA, Aslan K. 2024.Use of microsatellite markers for sex determination in date palm (*Phoenix dactylifera L.*) cv. Medjool. Genet. Resour. Crop Evol. 30:1-7.

Yusuf AO, Culham A, Aljuhani W, Ataga CD, Hamza AM, Odewale JO. and Enaberue LO. 2015. Genetic diversity of Nigerian date palm (*Phoenix dactylifera*) germplasm based on microsatellite markers. Int. J. Bio-Sci. Bio-Tech. 7(1):121-132.

Zehdi S, Trifi M, Billotte N, Marrakchi M. and Christophe Pintaud J. 2004. Genetic diversity of Tunisian date palms (*Phoenixdactylifera L.*) revealed by nuclear microsatellite polymorphism. Hereditas. 141(3):278-287.

COVID-19 Molecular Diagnosis Challenges Faced by Medical Laboratory Specialists in Hospitals of Jordan: A Qualitative Study

Arwa Qaqish[1,*], Ola Soudah[2], Mariam M. Al-Omari[2], Manal Mohammad Abbas[3,4], Mu'ath Al-Ajaleen[1], Feras Abu-Ali[5], Rana Said[4,6], Mahmoud Ghazo[7]

[1] *Department of Biology and Biotechnology, Faculty of Science, The Hashemite University, Zarqa, Jordan;* [2] *Department of Basic Medical Sciences, Faculty of Medicine, Yarmouk University, Irbid, Jordan;* [3] *Department of Medical Laboratory Sciences, Faculty of Allied Medical Sciences, Al-Ahliyya Amman University, Amman, Jordan;* [4] *Pharmacological and Diagnostic Research Lab, Al-Ahliyya Amman University, Amman, Jordan;* [5] *Newton Insurance Company, Amman, Jordan;* [6] *Department of Pharmacy, Faculty of Allied Medical Sciences, Al-Ahliyya Amman University, Amman, Jordan;* [7] *Jordan Ministry of Health, Laboratory Directorate, Amman, Jordan*

Abstract

Objectives: The primary goal of this study was to identify the main obstacles to COVID-19 diagnosis in Jordan's public and private hospitals.

Methods: A semi-constructive questionnaire was utilized to identify the main obstacles experienced by COVID-19 diagnosis in Jordanian public and private hospitals as narrated by laboratory specialists. Between June and December of 2021, when COVID-19 was still actively spreading, sixteen phone interviews were carried out. Using open coding, line by line, the transcribed narratives were subjected to thematic analysis in order to identify themes and related subthemes.

Results: A qualitative analysis of the interviews indicated that there are significant obstacles preventing molecular testing from being fully utilized. These obstacles include a lack of reagents and skilled personnel, as well as communication issues between the MOH and laboratories. Staff training and redistribution of previously trained personnel, as well as the digitalization of sample labeling and result release, were implemented as quick fixes for these issues.

Conclusion: The successful expansion of RT-PCR units to cover all country is considered an exceptional success of MOH and must be sustained after COVID-19. Nonetheless, in order to be ready for pandemics in the future, a stringent CPD system and the usage of RT-PCR outside of COVID-19 should be established.

KeyWords: COVID-19, RT-PCR, Molecular Diagnosis, Medical Laboratory Specialist, Jordan.

1. Introduction

Corona Virus Disease 2019 (COVID-19) was initially identified in Wuhan, China, leading to a nationwide outbreak. Since then, through international travels, the number of patients increased rapidly to spread all over the world (*Https://Www.Who.Int/Emergencies/Diseases/Novel-Coronavirus-2019*, n.d.). On March 2020, the World Health Organization (WHO) declared COVID-19 as a pandemic, a public health event that requires worldwide attention and collaboration.

As with most countries, Jordan was also severely affected by the contagion (*Https://Www.Who.Int/Countries/Jor/.*, n.d.). Because we are a middle-income nation with limited resources in an insecure Middle Eastern region, more obstacles were faced to effectively combat the pandemic (Al-Tammemi, 2020). Despite the fact that the Jordanian public health response was exemplary and promising in the early stages, by the end of December 2023, COVID-19 cases have increased to 1746997 infections and 14,122 deaths (*Https://Www.Who.Int/Countries/Jor/.*, n.d.).

Effective isolation and treatment of patients was essential to breaking the COVID-19 transmission chain (*Https://Www.Who.Int/Emergencies/Diseases/Novel-Coronavirus-2019*, n.d.). For this, among many protective measures, timely diagnosis using sensitive and specific laboratory screening was crucial (Al-Tammemi, 2020).

According to the World Health Organization (WHO) and the Center for Disease Control and Prevention (CDC), the gold standard for COVID-19 laboratory diagnosis remains the real-time polymerase chain reaction (RT-PCR) test (Hasell et al., 2020; Porte et al., 2020). Still, in addition to RT-PCR being expensive (Mathuria et al.,

---

* Corresponding author. e-mail: arwa@hu.edu.jo.

**Abbreviations:COVID-19: Corona Virus Disease 2019;MOH: Ministry of Health; WHO: World Health Organization; CDC: Center for Disease Control; RT-PCR: Real Time Polymerase Chain Reaction; CPD: Continuing Professional Development; SARS-CoV-2: Severe acute respiratory syndrome coronavirus 2; CPHL: Central Public Health Laboratory; USAID: United States Agency for International Development; LHSS: Local Health System Sustainability

2020), lack of reagents, test equipment, and kit assembly factories severely limited RT-PCR testing capabilities around the world (Natesan et al., 2020). With progressive viral spread, other challenges related to trained staff shortage and fear and anxiety among frontline healthcare workers were identified (Jafri et al., 2020). This has put the capacities of laboratories to detect COVID-19 infections in a timely manner to question (Mathuria et al., 2020).

Huge efforts were made by the Jordanian Ministry of Health (MOH) to make the detection of COVID-19 infection more accurate and time-efficient. As one of Jordan's responses to COVID-19, MOH partnered with commercial biotechnology and pharmaceutical firms to set up COVID-19 PCR testing facilities across the country. A total of 16 new PCR units for molecular diagnosis were operational by early 2021, ensuring that each governorate had its own laboratory (A. Qaqish et al., 2022)

Many studies have determined challenges facing Jordan's health sector in managing the COVID-19 pandemic. Most of them reported problems related to vaccination challenges and physician/nurse burnout, but never related to diagnosis (Abu Farha et al., 2021; Algunmeeyn et al., 2020; Hatmal et al., 2021; Sallam et al., 2020, 2021).

Given the rapid and huge expansion of RT-PCR based diagnosis driven by MOH during COVID-19 spread in the country, this study aimed to use a qualitative semi-constructive questionnaire to identify the main obstacles that medical laboratory specialists at public and private hospitals encountered when diagnosing COVID-19 patients, and to identify the approaches used to overcome these obstacles.

2. Methods:

2.1. Design, participants and study context

A qualitative study under phenomenological descriptive approach study design was used to describe in depth the challenges of COVID-19 pandemic on clinical laboratories sector. Purposive sampling was employed in the participant recruitment process. By using purposeful sampling, the researcher can find individuals who are more likely to offer a detailed understanding of the phenomenon under investigation (Campbell et al., 2020). Prospective participants had to have been involved in the molecular diagnosis of severe acute respiratory syndrome coronavirus 2 (SARS-CoV-2) infection for at least one month in order to be considered for inclusion in the study. Following a thorough explanation of the goals and methods of the study, participants were chosen and invited to participate. The sample size was estimated by achieving data saturation, which means no new data were identified in the analysis. The sample consisted of 16 medical laboratory specialists who worked in RT-PCR molecular diagnosis of COVID-19 from governmental and private hospitals located in various governorates of Jordan (table 1).

2.2. Ethical approval

The study was approved by the Institutional Review Board (IRB) at The Hashemite University of Jordan (No.4/14/2020/2021). Prior to participating in the trial, participants provided informed consent.

2.3. Patient and public Involvement

No patients or participants were involved.

2.4. Data collection and outcome measures

A semi-structured interview was employed to give a thorough understanding of the difficulties faced by clinical laboratory specialists involved in the molecular diagnosis of COVID-19 and their lived experiences in combating the pandemic in Jordan. Three authors reviewed and revised the interview questions, which focused on the work of the participants, obstacles and adaptations that participants went through during the early phases of the COVID-19 spread based on their lived experiences. A research assistant received training in qualitative interviewing. The semi-structured guide was then tested with two participants to assure its validity. To improve the interview's flow, a few minor changes were made to the questions and their arrangement. Table 2 details the questions of the semi-structured interview used in the study.

Phone interviews were done between June and December of 2021, while COVID-19 infections were still actively spreading. The researchers at the time believed that the most convenient and safest way to collect data was through phone interviews. The 30- to 45-minute interviews were recorded on audio with the participants' permission.

Privacy and confidentiality were assured by the investigators to all the participants. For privacy and confidentiality reasons, the names of the interviewees were not mentioned. Participants were referred to using a code, consisting of specifically designated hospital code.

2.5. Data analysis

This study employed a thematic analysis approach to identify key challenges, solutions, and insights related to the implementation of RT-PCR testing in Jordanian laboratories during the COVID-19 pandemic. Thematic analysis (Braun & Clarke, 2006) was chosen for its flexibility in identifying, analyzing, and reporting patterns within qualitative data. This approach allowed us to systematically capture the complex experiences of laboratory personnel across various sectors (governmental, private, and military hospitals). The analysis was conducted in the following phases: familiarization, coding, searching for themes, defining themes and naming, and produce report. For familiarization with the data, all interviews were transcribed verbatim, and the transcripts were read and re-read by the research team to gain a comprehensive understanding of the data. Then significant data were systematically coded across the entire dataset. Codes were grouped into broader themes. Through iterative discussions among the research team, themes were refined and organized based on their relevance to the research questions. The identified themes were reviewed in relation to the coded extracts and the entire dataset to ensure they accurately represented the data and reflected the key issues raised by the participants. The final themes and sub-themes were clearly defined and named to encapsulate the core findings of the study, including the challenges faced by the laboratories, the solutions implemented, and the potential future uses of RT-PCR technology. The themes were organized into a coherent narrative that reflected the experiences of the participants. Quotes pertinent to the themes that emerged were

translated from Arabic into English using forward and backward translations; to guarantee the analytical process's credibility. NVIVO were used to produce the map.

3. Results:

As depicted in Table 3 and Figure 1, upon interviewing the 16 laboratory diagnosis specialists enrolled in the study, 12 from governmental hospitals and 4 from private sector hospitals, 3 themes were identified: Challenges, Solutions, and Importance of RT-PCR beyond COVID-19. "Challenges" encompassed 3 sub-themes: shortage of resources, operational processes and staff well-being. On the other hand, "solutions" involved 5 sub-themes: RT-PCR laboratory capacity building, staff management, turnaround time, digitalization, and screening with RAPID antigen testing.

3.1. Theme 1: Challenges

3.1.1. Shortage of Resources

All laboratories identified high challenge in clinical laboratory capacity in terms of staff, equipment, and kits availability for COVID-19 PCR testing. All governmental hospitals, except the Central Public Health Laboratory (CPHL) in the capital Amman, did not have a RT-PCR service before COVID-19. Private hospitals already had RT-PCR services, but laboratories were not ready for the quick shift in service demand. Thus, finding well-trained medical technologists to conduct RT-PCR was very challenging. In addition, the quick spread of the pandemic made it difficult to train enough medical technologists in a short period of time. Many contamination events happened due to the lack of employee proper training and awareness in sample handling during RNA extraction step. During curfew, not all hospitals were able to perform COVID-19 tests due to lack of RT-PCR kits. Hence, testing was restricted to the CPHL.

3.1.2. Operational Processes

One big challenge was in the way of samples' data entry and result release that relied on a paper-based system. The error rate in sample collection, labelling, and storage was high due the huge number of tests. Moreover, lack of understanding of strict infection control policy in RT-PCR laboratories in some hospitals allowed patients to get into RT-PCR laboratories to ask for their test results.

Many labs pointed out the challenge of having clear policies and regulations from the government regarding coordinating COVID-19 testing between labs. The quick changing policies, especially at early stages of the pandemic, and the absence of effective communications sometimes hindered the work coordination between governmental hospital labs and the Ministry of Health Central lab. A medical technologist at Governorate Central Lab in the North of Jordan Stated,

"There was a problem in work coordination with the Ministry of Health Central Laboratory in Amman, when a large sample number that exceeded the lab storage capacity reached a central governmental laboratory in the Northern Jordan. This resulted in sample accumulation of several days before we were able to send them to Amman Central Lab. Moreover, there were quick changes in lab heads and managers. This led to having conflicts in workplace. New managers had different operational styles

and work organization. Hence, it was challenging to find a common language and reach a systematic work routine." Interview number 3

3.1.3. Staff Well-Being

Due to extended working hours to cover the screening demand, lab workers experienced harsh work burnouts and psychological stress. Some employees did not take a vacation for 2 years in arrow, and other did not see their families for months to prevent transmitting the disease to them.

3.2. Theme 2: Solutions

Many actions had been taken by the Ministry of Health and private sectors in order to address the pandemic stress on clinical laboratories. This emerged in 2 themes: RT-PCR laboratory capacity building and process improvement.

3.2.1. Capacity Building (RT-PCR Infrastructure)

The scarcity of RT-PCR kits during curfew was addressed by excluding these materials from import curfew restrictions and speeded up by collaboration with private vendors. In collaboration with private pharmaceutical and biotechnology companies, MOH established 16 new RT-PCR settings spread around the country to encompass every governorate and border crossing. Every laboratory was intended to contain two physically distinct rooms (the PCR and extraction rooms) and a separate workstation for preparing the master mix. The private firms constructed partition walls at multiple locations in order to comply with the construction standards for a PCR laboratory. This departmentation reduced sample contamination and employee infections rate. By the end of 2020/beginning of 2021, the MOH driven decentralization of COVID-19 molecular diagnosis allowed PCR testing at governmental labs outside the capital Amman to include every governorate in the country. Also, it allowed private labs to perform COVID-19 testing at borders and airports. Soon after, testing became available at the majority of well-equipped private labs in the country. As noted by a government hospital medical laboratory head in Central Jordan,

"We started doing RT-PCR in Oct. 2020 where medical technologists from the Ministry of Health Central Lab in Amman came and helped us to establish the molecular diagnosis department. Later, our lab technologists were trained by "Genetics", a private pharmaceutical/biotechnology company, which still supervises the work till now. Further extended training was accomplished by United States Agency for International Development (USAID)." Interview number 8

Most Private hospital laboratories had RT-PCR molecular diagnosis services before COVID-19 pandemic. However, these services had a low capacity in terms of equipment and staff. The pandemic pushed these hospitals to expand the service by doubling the RT-PCR machines and transforming the RNA extraction process into a fully automated one. New machines increased the lab testing capacity and the number of samples analyzed per day was doubled or tripled.

3.2.2. Staff Management

Shortage of well trained in RT-PCR medical technologists was overcame by staff reallocation, hiring

new employee, and having a temporarily supporter from other labs or supplying companies. The MOH along with the Local Health System Sustainability Project (LHSS)/USAID and RT-PCR supplying companies trained medical technologist how to conduct the test. LHSS, gave extensive explanation of the basic science behind the test, in addition to troubleshooting advice.

3.2.3. Process Improvement-Turnaround Time

COVID-19 testing at the early stage of the pandemic used to take from 3 to 7 days to reveal. Now it takes 24 hours, and the expedited test takes 3-5 hours. This was achieved by molecular diagnostics capacity building discussed previously. In addition, working hours changed to accommodate the needs from day shift into 24/7 around the clock service.

3.2.4. Process Improvement -Digitalization

Most of governmental clinical laboratories relied on the traditional paper-based method in ordering the test and reporting the results. This pushed MOH to purchase a digital platform that connects all labs and speeds up the result release to patients and healthcare providers. In addition, private labs COVID-19 test results were synched to the MOH COVID-19 patients tracing and tracking digital system.

"One of the biggest challenges we faced at the beginning of the pandemic is the manual and paper-based lab. order system. This was resolved by adopting SUNDUS information system for patients orders and results entry in the ministry of health governmental labs, which reduced a lot of effort and time." Interview number 2

3.2.5. Screening with Rapid Antigen Testing

COVID-19 rapid test was used as a quick screening method at emergency rooms, inpatient wards, and for the screening of healthcare workers. Only those with positive test or had COVID-19 symptoms and tested negative were then tested with RT-PCR for confirmation. This alleviated some of the pressure on RT-PCR service.

3.3. Theme 3: Future Perspectives

Every participant acknowledged the need for RT-PCR diagnostic testing to be expanded to detect other infections and cancer. Only one participant from a low volume private hospital expressed his doubts about the need of RT-PCR without COVID-19 pressure.

"We did not need such service at borderline before COVID-19; thus, I think we should expand such service in the Central Laboratory that could serve as a reference lab when such tests are needed." Interview number 6

4. Discussion:

After having only 1 central molecular diagnosis laboratory in the capital Amman, the establishment of 16 new RT-PCR units to cover every governorate in the country is considered an exceptional success of the MOH. Still, this was faced with many obstacles. Similar stories of rapid expansion in the number of sites conducting molecular testing for COVID-19 were reported in low-income countries such as Ethiopia and Indonesia (Abera et al., 2020; Aisyah et al., 2021; Hendarwan et al., 2020; Kebede et al., 2021). In fact, Ethiopia demonstrated the conversion from no molecular diagnosis laboratories at all to 65 RT PCR testing settings (Abera et al., 2020; Kebede et al., 2021). Despite these many reported expansion stories around the world, full utility of these settings was not reached. Even in high-income countries, such as the US, COVID-19 RT-PCR testing capacity did not meet the needs of the pandemic situation (Du et al., 2021).

In this qualitative investigation, we aimed at determining major challenges that faced COVID-19 diagnosis in governmental and private hospitals of Jordan as reported by medical laboratory specialists. Challenges reported here are very similar to those reported in similar settings in the literature. Major challenges limiting the full utility of molecular testing capacity were listed to include workforce shortage, problems in logistics distribution, complex administration, shortage of reagents, non-reliability of some tests and, particularly, shortage of skilled staff (Abera et al., 2020; Kebede et al., 2021; Kroft, 2020; B. Qaqish et al., 2022; Walker et al., 2020).

Challenges were tackled with prompt acting solutions. Like many parts of the world, increasing sample load was managed by increasing the number of RT-PCR settings, re-allocation of trained staff, adopting a 24-hour working model and the use of rapid antigen testing (Okeke et al., 2020). Biosafety issues and truthfulness of testing results were ensured by extensive training of working staff, applying strict quality control measures, and digitalization of sample labeling and result release (Braunstein et al., 2021; Hu, 2016; Mögling et al., 2020). Proper control of viral spread was achieved by collaboration between diagnostic, surveillance and infection control networks facilitated by a connecting digital network (Hu, 2016).

It could be very challenging to establish and run a quantitative molecular testing facility within high biosafety requirements, such as that of COVID-19 diagnosis, concurrently with an epidemic crisis, and even more, during peaks of transmission. In such a case, priorities are given to transmission control measures, accomplished by sample screening and testing rather than training. Still, proper training is essential for fulfilling such anticipated control. This brings an important question: Since the least educated of our participants holds a bachelor's degree in Biological Sciences, is RT-PCR and biosafety settings included in university curricular courses? If not in Biological Sciences, these must be listed in university curricula of Medical Laboratory Sciences. At least, graduates of such specialties must have the tools to self-educate themselves on every new technology in the world of diagnosis. This is an invitation for universities to update courses for the sake of coping with the accelerating developing technologies in such fields and to strengthen the basics that would help understanding emerging technologies after graduation. In addition, this is an invitation for MOH to give training courses on a yearly basis, to enable employees to catch up with all what is new in the world of diagnosis and to run annual examinations in order to encourage employees to keep up with the continuously evolving diagnostic technologies. Interestingly, in July 2021, LHSS/USAID signed a contract with MOH to strengthen the capacity of healthcare personnel to provide high-quality healthcare by instituting a system of ongoing professional development (CPD) that is required for the renewal of professional licenses (*Https://Jordankmportal.Com/Resources/as-Is-*

Process-for-Continuing-Professional-Development-and-Relicensing-Health-Care-Professionals-in-Jordan, n.d.).

Future pandemics are a possibility, thus being ready and able to act quickly is essential, including early identification and tracking of infected people (*Https://Www.Who.Int/Publications/i/Item/WHO-2019-NCoV-Lab-Testing-2021.1-Eng*, n.d.; Madhav et al., 2017). The use of molecular testing appears vital for rapid response to emerging infections (Okeke & Ihekweazu, 2021), which also reflects the ability to conduct molecular testing for other pathogens as well as other conditions, such as malignancies and genetic disorders.

One major limitation of this study lies in lack of information obtained from the Royal Medical Services and Private Diagnostic Laboratory Chains in the country. Both parties participated heavily in the molecular diagnosis of COVID-19 in Jordan but refused to take part in this study considering the unlikeliness of obtaining permissions from their managing heads.

5. Conclusions:

Challenges faced by medical technologists upon the establishment and expansion of molecular diagnosis facilities in Jordan to combat COVID-19 were successfully tackled with prompt acting solutions. However, this urgent experience highlighted the need for updating university curricula with newest diagnosis technologies and for offering relevant training to students in the medial field. In addition, a stringent CPD system and the usage of RT-PCR beyond COVID-19 should be implemented in order to be ready for pandemics in the future, for the expansion of RT-PCR diagnosis beyond infections and for maintaining high health care standards in the country.

Acknowledgments

Disclosure Statement

All authors declare no conflicts of interest. All authors declare no competing financial interests.

Funding

References

Abera, A., Belay, H., Zewude, A., Gidey, B., Nega, D., Dufera, B., Abebe, A., Endriyas, T., Getachew, B., Birhanu, H., Difabachew, H., Mekonnen, B., Legesse, H., Bekele, F., Mekete, K., Seifu, S., Sime, H., Yemanebrhan, N., Tefera, M., … Assefa, A. (2020). Establishment of COVID-19 testing laboratory in resource-limited settings: challenges and prospects reported from Ethiopia.Glob. Health Action, *13*(1). https://doi.org/10.1080/16549716.2020.1841963

Abu Farha, R. K., Alzoubi, K. H., Khabour, O. F., & Alfaqih, M. A. (2021). Exploring perception and hesitancy toward COVID-19 vaccine: A study from Jordan., Hum Vaccin Immunother *17*(8), 2415–2420. https://doi.org/10.1080/21645515.2021.1888633

Aisyah, D. N., Mayadewi, C. A., Igusti, G., Manikam, L., Adisasmito, W., & Kozlakidis, Z. (2021). Laboratory Readiness and Response for SARS-Cov-2 in Indonesia. Front. Public Health, *9*. https://doi.org/10.3389/fpubh.2021.705031

Algunmeeyn, A., El-Dahiyat, F., Altakhineh, M. M., Azab, M., & Babar, Z.-U.-D. (2020). Understanding the factors influencing healthcare providers' burnout during the outbreak of COVID-19 in Jordanian hospitals. J. Pharm. Policy Pract, *13*(1), 53. https://doi.org/10.1186/s40545-020-00262-y

Al-Tammemi, A. B. (2020). The Battle Against COVID-19 in Jordan: An Early Overview of the Jordanian Experience. Front. Public Health, *8*. https://doi.org/10.3389/fpubh.2020.00188

Braun, V., & Clarke, V. (2006). Using thematic analysis in psychology. Qual. Res. Psychol, *3*(2), 77–101. https://doi.org/10.1191/1478088706qp063oa

Braunstein, G. D., Schwartz, L., Hymel, P., & Fielding, J. (2021). False Positive Results With SARS-CoV-2 RT-PCR Tests and How to Evaluate a RT-PCR-Positive Test for the Possibility of a False Positive Result. J. Occup. Environ. Med., *63*(3), e159 e162.https://doi.org/10.1097/JOM.0000000000002138

Campbell, S., Greenwood, M., Prior, S., Shearer, T., Walkem, K., Young, S., Bywaters, D., & Walker, K. (2020). Purposive sampling: complex or simple? Research case examples. J Nurs Res, *25*(8), 652–661. https://doi.org/10.1177/1744987120927206

Du, Z., Pandey, A., Bai, Y., Fitzpatrick, M. C., Chinazzi, M., Pastore y Piontti, A., Lachmann, M., Vespignani, A., Cowling, B. J., Galvani, A. P., & Meyers, L. A. (2021). Comparative cost-effectiveness of SARS-CoV-2 testing strategies in the USA: a modelling study. Lancet Public Health, *6*(3), e184–e191. https://doi.org/10.1016/S2468-2667(21)00002-5

Hasell, J., Mathieu, E., Beltekian, D., Macdonald, B., Giattino, C., Ortiz-Ospina, E., Roser, M., & Ritchie, H. (2020). A cross-country database of COVID-19 testing. Sci. Data, *7*(1), 345. https://doi.org/10.1038/s41597-020-00688-8

Hatmal, M. M., Al-Hatamleh, M. A. I., Olaimat, A. N., Hatmal, M., Alhaj-Qasem, D. M., Olaimat, T. M., & Mohamud, R. (2021). Side Effects and Perceptions Following COVID-19 Vaccination in Jordan: A Randomized, Cross-Sectional Study Implementing Machine Learning for Predicting Severity of Side Effects. *Vaccines*, *9*(6), 556. https://doi.org/10.3390/vaccines9060556

Hendarwan, H., Syachroni, S., Aryastami, N., Su'udi, A., Susilawati, M., Despitasari, M., Mulyani, U., Sumiarsih, M., Puspandari, N., Indrati, A., Solikha, D., Riana, D., & Wahyuni, I. (2020). Assessing the COVID-19 diagnostic laboratory capacity in Indonesia in the early phase of the pandemic. WHO-SEAJPH, *9*(2), 134. https://doi.org/10.4103/2224-3151.294307

https://jordankmportal.com/resources/as-is-process-for-continuing-professional-development-and-relicensing-health-care-professionals-in-jordan. (n.d.).

https://www.who.int/countries/jor/. (n.d.).

https://www.who.int/emergencies/diseases/novel-coronavirus-2019. (n.d.).

https://www.who.int/publications/i/item/WHO-2019-nCoV-lab-testing-2021.1-eng. (n.d.).

Hu, Y. (2016). Regulatory Concern of Polymerase Chain Reaction (PCR) Carryover Contamination. In *Polymerase Chain Reaction for Biomedical Applications*. InTech. https://doi.org/10.5772/66294

Jafri, L., Ahmed, S., & Siddiqui, I. (2020). Impact of COVID-19 on laboratory professionals-A descriptive cross sectional survey at a clinical chemistry laboratory in a developing country. Ann. Med. Surg, *57*, 70–75. https://doi.org/10.1016/j.amsu.2020.07.022

Kebede, A., Lanyero, B., Beyene, B., Mandalia, M. L., Melese, D., Girmachew, F., Mekonnen, A., Ayana, G., Yemanebirhan, N.,

Hailu, G., Asrat, H., Nurahmed, N., Gashu, A., Eshetu, K., Assefa, Z., Abayneh, A., Musa, E., & Abate, E. (2021). Expanding molecular diagnostic capacity for COVID-19 in Ethiopia: operational implications, challenges and lessons learnt. Pan Afr. Med. J, 38, 68. https://doi.org/10.11604/pamj.2021.38.68.27501

Kroft, S. H. (2020). Well-Being, Burnout, and the Clinical Laboratory. Am. J. Pathol, 153(4), 422–424. https://doi.org/10.1093/ajcp/aqaa022

Madhav, N., Oppenheim, B., Gallivan, M., Mulembakani, P., Rubin, E., & Wolfe, N. (2017). Pandemics: Risks, Impacts, and Mitigation.

Mathuria, J. P., Yadav, R., & Rajkumar. (2020). Laboratory diagnosis of SARS-CoV-2 - A review of current methods. J INFECT PUBLIC HEAL, 13(7), 901–905. https://doi.org/10.1016/j.jiph.2020.06.005

Mögling, R., Meijer, A., Berginc, N., Bruisten, S., Charrel, R., Coutard, B., Eckerle, I., Enouf, V., Hungnes, O., Korukluoglu, G., Kossyvakis, T., Mentis, A., Molenkamp, R., Muradrasoli, S., Papa, A., Pigny, F., Thirion, L., van der Werf, S., & Reusken, C. (2020). Delayed Laboratory Response to COVID-19 Caused by Molecular Diagnostic Contamination. Emerging Infect. Dis., 26(8). https://doi.org/10.3201/eid2608.201843

Natesan, S., Bhatia, R., Sundararajan, A., Dhama, K., Malik, Y. S., & Vora, K. (2020). Ramping up of SARS CoV-2 testing for the diagnosis of COVID-19 to better manage the next phase of pandemic and reduce the mortality in India. VirusDisease, 31(4), 432–440. https://doi.org/10.1007/s13337-020-00622-x

Okeke, I. N., Feasey, N., Parkhill, J., Turner, P., Limmathurotsakul, D., Georgiou, P., Holmes, A., & Peacock, S. J. (2020). Leapfrogging laboratories: the promise and pitfalls of high-tech solutions for antimicrobial resistance surveillance in low-income settings BMJ Glob. Health., 5(12), e003622. https://doi.org/10.1136/bmjgh-2020-003622

Okeke, I. N., & Ihekweazu, C. (2021). The importance of molecular diagnostics for infectious diseases in low-resource settings. Nat. Rev. Microbiol, 19(9), 547–548. https://doi.org/10.1038/s41579-021-00598-5

Porte, L., Legarraga, P., Vollrath, V., Aguilera, X., Munita, J. M., Araos, R., Pizarro, G., Vial, P., Iruretagoyena, M., Dittrich, S., & Weitzel, T. (2020). Evaluation of a novel antigen-based rapid detection test for the diagnosis of SARS-CoV-2 in respiratory samples. Int. j. infect. dis : IJID: Official Publication of the International Society for Infectious Diseases, 99, 328–333. https://doi.org/10.1016/j.ijid.2020.05.098

Qaqish, A., Al-Omari, M., Abbas, M. M., Said, R., Al Tamimi, M., & Ghazo, M. (2022). Decentralization of COVID-19 molecular diagnosis, a success story from Jordan. J. Glob. Health, 12, 03045. https://doi.org/10.7189/jogh.12.03045

Qaqish, B., Sallam, M., Al-Khateeb, M., Reisdorf, E., & Mahafzah, A. (2022). Assessment of COVID-19 Molecular Testing Capacity in Jordan: A Cross-Sectional Study at the Country Level. Diagnostics, 12(4), 909. https://doi.org/10.3390/diagnostics12040909

Sallam, M., Dababseh, D., Eid, H., Al-Mahzoum, K., Al-Haidar, A., Taim, D., Yaseen, A., Ababneh, N. A., Bakri, F. G., & Mahafzah, A. (2021). High Rates of COVID-19 Vaccine Hesitancy and Its Association with Conspiracy Beliefs: A Study in Jordan and Kuwait among Other Arab Countries. Vaccines, 9(1), 42. https://doi.org/10.3390/vaccines9010042

Sallam, M., Dababseh, D., Yaseen, A., Al-Haidar, A., Ababneh, N. A., Bakri, F. G., & Mahafzah, A. (2020). Conspiracy Beliefs Are Associated with Lower Knowledge and Higher Anxiety Levels Regarding COVID-19 among Students at the University of JordanInt. J. Environ. Res. Public Health., 17(14), 4915. https://doi.org/10.3390/ijerph17144915

Walker, P. G. T., Whittaker, C., Watson, O. J., Baguelin, M., Winskill, P., Hamlet, A., Djafaara, B. A., Cucunubá, Z., Olivera Mesa, D., Green, W., Thompson, H., Nayagam, S., Ainslie, K. E. C., Bhatia, S., Bhatt, S., Boonyasiri, A., Boyd, O., Brazeau, N. F., Cattarino, L., … Ghani, A. C. (2020). The impact of COVID-19 and strategies for mitigation and suppression in low- and middle-income countries. Science (New York, N.Y.), 369(6502), 413–422. https://doi.org/10.1126/science.abc0035.

Supplementary Tables

Table 1: Demographic characteristics of the participants

Occupation	Gender	Hospital type	Age	Hospital's region	Educational level and specialty
LT	F	P	27	CR	BSc/Biotech
LS	M	P	29	CR	BSc/MLS
LM	M	P	36	CR	BSc/MLS
LM	M	P	44	CR	BSc/Biology
LM	M	G	49	SR	BSc/MLS
LS	F	G	45	SR	BSc/MLS
LM	M	G	39	CR	Pathologist
LS	F	G	39	NR	BSc/MLS
LT	M	G	33	NR	BSc/MLS
LS	M	G	33	NR	BSc/MLS
LM	F	G	53	CR	MSc/MLS
LM	F	G	47	CR	BSc/MLS
LM	F	G	37	NR	Not Available
LT	F	G	33	CR	MSc/biology
LS	F	G	41	CR	BSc/MLS
LT	F	G	44	SR	BSc/MLS
	F%: 56.2%		SD: 7.36		
	M%: 43.8%		Average :39.3		

LM, laboratory manager; LS, laboratory supervisor; LT, laboratory technologist.
MLS, medical laboratory science.
F, female; M, male.
P, private; G, governmental.
CR, central region; SR, southern region; NR, northern region.

Table 2. Interview Questions.

1. Did you have RT PCR based molecular diagnosis at your hospital before the emergence of COVID-19?

If the answer is yes:

- For the detection of what pathogen(s)/disease(s)?
- After the emergence of COVID-19, did you use the exact same RT PCR machines already present at your hospital/laboratory, or you had to order special machines and create special laboratory set ups for that purpose? Please, elaborate on the set ups.

If the answer for question 1 is no:

- did your hospital/laboratory collect nasopharyngeal swabs from suspected patients? Where did you use to send collected samples for diagnosis?
- do you perform RT-PCR diagnosis of COVID-19 at your hospital/laboratory now? Since when did you start? Were you trained by a specialist for molecular diagnosis? Whom provided your training? Were you supervised by a specialist at the start-up of your RT-PCR practice?

2. How do you compare the turnaround time of RT-PCR diagnosis of COVID-19 over time? Please, be specific. Elaborate on how many samples you were able to run per day and how many machines you had.

3. What are the major challenges you faced upon starting RT-PCR diagnosis of COVID-19 at your hospital/laboratory? Were you able to face and manage these challenges? How?

4. Did you use other COVID-19 diagnosis techniques, such as Rapid Antigen and/or Antibody detection? If yes, when did you start and under which conditions? Did that completely replace molecular diagnosis? What was the strategy you used for confirming test results?

5. After COVID-19 is over, do you see any benefits for establishing RT-PCR molecular diagnosis at your hospital/laboratory? Please, elaborate.

Table 3. Summary of the main themes and subthemes

| Codes	Sub-themes	Themes
• Sample number burst during the pandemic peak. • Manual data entry and result release. • Obstacles in communication and co-ordination between governmental labs. • Highly changing policies and regulations over short period of time. • Sample error: improper sample collection, labeling, and sample storage.	Operational Demands	Challenges
• Lack of testing kits during curfew. • Shortage of data entry staff. • Shortage of trained staff and slow training schedule.	Resource Shortages	
• Work burnouts • Psychological stress	Staff Well-being	
• Medical equipment and kits excluded from curfew. • Establish a new RT-PCR units in hospitals that doesn't have one. • Increase number of extraction and PCR machines. • Automation of the extraction procedure. • Departmentation: establish an extraction room and a PCR room. • Decentralization of COVID-19 testing labs to include all government hospitals and private sector. • Establish COVID-19 screening testing centers at borders.	RT-PCR infrastructure	Capacity Building
• Staff trained by the ministry of health, RT-PCR suppliers, and USAID. • Hire new trained staff. • Staff internal reallocation.	Staff management	
• Increase testing capacity (double number or tested samples). • Working hour became 24/7.	Turnaround time	Process Improvement
• Adopting an information system that digitalize test orders, and results release. • Synch all digital platform in all labs with the ministry of health COVID-19 test hub.	Digitalization	
• Used for screening in ER, inpatients and among healthcare workers.	Screening with Rapid test (Ag/Ab)	
• Expand the RT-PCR service to include other pathogens and cancer diagnostics.	Importance of RT-PCR service beyond COVID-19	Future perspectives
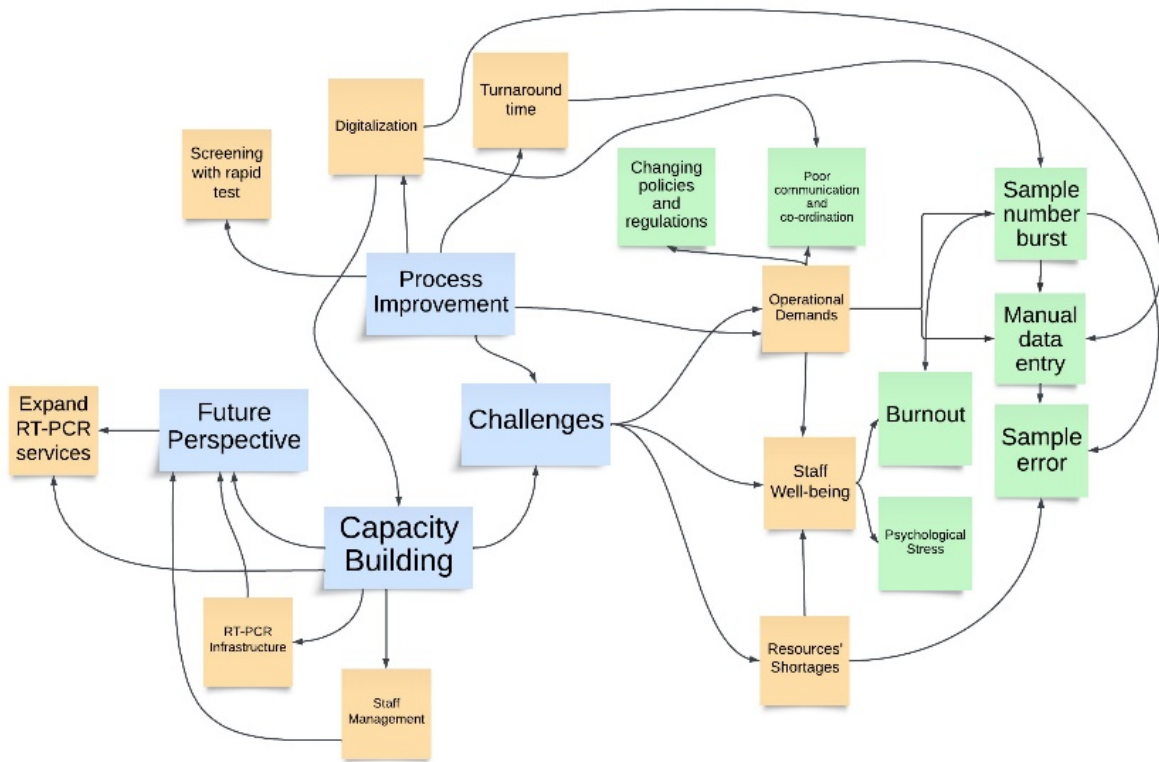
Figure 1. Thematic Analysis Map.

Role of Fluconazole Nanoemulsion in Inhibiting Liver Candidiasis in Female Mice and their Embryos

Sanaa H. Mohammed[1] , Ahmed H. Saleh[1] , Khaled H. Abu-Elteen[2] ,Batol I. Dheeb [3,*] and Safa M. Abdulateef[4]

[1]Biology Department, College of Science, University of Kirkuk, Kirkuk, Iraq; [2] Department of Biology and Biotechnology, Faculty of Science, The Hashemite University, Zarqa, Jordan; [3] Department of Pathological Analysis, College of Applied Science, Samaraa University, Iraq; [4]College of Science, Al Nahrain University, Jadriya, Iraq.

Abstract

The current study aims to reveal the role of fluconazole nanoemulsion (FLX-NE) in inhibiting the candidiasis infection in female mice and their embryos. In the current investigation, thirty-two normal female Mus musculus mice, eight pregnant mice per group, were utilized. The mice were between the ages of twelve and sixteen weeks and weighed an average of twenty to twenty-five grams. At random, the animals were divided into four groups as follows: Group control, *Candida albicans* infected group, FLX-NE treated group, and the treated (*C. albicans* was administrated with a suspension and treated with FLX-nanoemulsion) group. The findings demonstrated (according to the HPLC) that the NE system preparation used glycerin oil as the oil phase, ethanol as the co-surfactant, tween 80 as the surfactant to prepare the optimum FLX-NE. Infecting the tested animals with *C. albicans* led to some histological changes in the liver, including degeneration and necrosis of hepatocytes and infiltration of inflammatory cells. Furthermore, some morphological abnormalities were found in the embryos which included a decrease in their number, short front limbs, and red spots on the skin. Nevertheless, after FLX-NE treatment, the liver tissues and embryos became semi-normal compared with the control group, where the central veins and hepatocytes appeared normal and decreased the levels of degenerative changes. The levels of CD163 in infected mice displayed significantly ($P \leq 0.05$) higher levels than untreated group. On the other hand, there was an improvement in CD163 levels in the treated group; however, a significant ($P \leq 0.05$) change was still observed when compared to the untreated group. In conclusion, the study showed that fluconazole nanoemulsion has a very strong effect against *C. albicans* infection.

Keywords: *Candida albicans;* nanoemulsion; Fluconazole; UTI; CD163.

1. Introduction

High morbidity and mortality rates are a hallmark of mycoses (fungal infections), which annually impact a sizable portion of the global population (Matthaiou *et al.,* 2015; Schmiedel and Zimmerli 2016; Bongomin *et al.,* 2017; Atiencia-Carrera *et al.,* 2022; Mohammed *et al.,* 2024). Humans have consistently been at risk from fungus infections (Vallabhaneni *et al.,* 2016). Immunocompromised individuals who are hospitalized are particularly the main victims of the growing number of fungal illnesses (Garnacho-Montero *et al.,* 2024; Leelambigai *et al.,* 2024). A fungus called Candida can cause candidiasis which affects more than 4 billion individuals, annually (McDermott 2022). One of these species is common opportunistic *Candida albicans* which drew a lot of attention in both basic and clinical biology (McManus and Coleman 2014). Given that approximately 75% of women experience human papillomavirus (HPV) infection at least once during their lifetime, and around 70% of adults harbor it as a benign commensal in their genitourinary and digestive tracts (Sarvtin *et al.,* 2014), it

follows that these individuals are susceptible to one of the most prevalent reasons for gynecological consultations at basic healthcare facilities—vaginal candidiasis (Gonzalez *et al.,* 2011). Vulvovaginitis occurs when the infection affects the female genital areas and can result in intense itching and burning sensations, as well as potential white discharge (CDCP 2012). Materials utilizing nanoemulsion formulations hold great potential in this world. As practical dispersions of deformable nanoscale droplets with a range of flow characteristics and optical qualities, from opaque to almost transparent, nanoemulsions show considerable promise. These linkages and the formula's intriguing physical characteristics set them apart from common micro-emulsions (Lovelyn and Attama 2012). The nanoemulsion's droplet size ranges from 50 to 500 nm. The active components in citronella essential oil are anticipated to work more efficiently and effectively thanks to several benefits of this composition (Azmi *et al.,* 2019; Hussain *et al.,* 2024). Nanomaterials are typically described as environmentally friendly materials that have been used in a wide range of applications (Katva *et al.,* 2015). Previous research demonstrated the antibacterial properties of a nanomaterial in several ways. The

---

* Corresponding author. e-mail: batol.omran35@uosamarra.edu.iq ,batoolomran@yahoo.com .

formation of reactive oxygen species (ROS) and the interaction of proteins or DNA as intracellular inducing effects, for example, affect the bacterial division of cells (Makabenta *et al.,* 2021). Additionally, these substances may disrupt the bacterial film that is acting on intracellular components, leading to cellular dysfunction (Tacconelli *et al.,* 2018; Makabenta *et al.,* 2021). Fluconazole is a triazole antifungal drug that belongs to the triazole family (Zhou *et al.,* 2022). It is an FDA-approved medication for the treatment of different candidiasis infections. Additionally, it has been demonstrated that prophylaxis lowers the risk of candidiasis in bone marrow transplant recipients who are also undergoing radiation therapy or cytotoxic chemotherapy (Galgiani *et al*., 2016). Therefore, the current study aims to reveal the role of fluconazole nanoemulsion against the toxicity of *Candida albicans* on female mice and their embryos.

2. Materials and Methods

2.1. Collection of urine samples

Between February and May 2023, 50 urine samples were taken from women who visited Azadi Teaching Hospital (Iraq) and Maternity and Gynecological Hospital with signs and symptoms of infections of the urinary tract. The laboratory received the specimens and examined the microscopic E. coli bacteria.

2.2. Solubility studies

Solubility assessments were conducted for fluconazole in glycerin oil, olive oil, co-surfactants, and surfactants (Reddy *et al.,* 2012, Dheeb *et al.,*2022). In a glass tube with a screw cover, 2 ml of the excipient and fluconazole were combined. An isothermal shaker (Xiaoyang, China) was used to shake the mixture for 48 hours at 25º C in order to reach equilibrium. Before the HPLC analysis, each tube was spun at 5000 rpm for 15 minutes to determine the drug concentration. After that, the supernatant was diluted with methanol.

2.3. Construction of pseudo-ternary phase diagrams

To construct components for pseudo-ternary phase diagrams, a water titration technique was used to create oil, a mixture of surfactant and co-surfactant, and water (Schalbart *et al.,* 2010, Mohammed *et al.,* 2024, Hatem and Dheeb,2024). Co-surfactant and surfactant were combined in a variety of ratios (1:1, 1:2, 1:3, 1:4, and 2:1). Oil and surfactant: co-surfactant (Smix) were mixed in a variety of weight ratios up until the maximum ratio of Smix and oil was attained, following each phase diagram's instructions. The aqueous phase was then gradually added to each of these mixes, and each mixture was titrated using a moderate magnetic stirrer. By measuring the water concentration at which transparent-to-turbid transitions occurred, the titration's endpoint was identified (Ghareeb *et al.,* 2017).

2.4. Heating-cooling cycle (H/C cycle)

The stability of FLX-NE is dependent on temperature change, which was investigated by using a heating-cooling cycle. Six cycles, between 5 °C and 50 °C, were applied to the NE formulations, and they were kept at each temperature for at least 48 hours (Sadoon and Mowafaq, 2020).

2.5. Fourier transform infrared spectroscopy (FTIR)

The assessment of drug-formulation compatibility was conducted by employing FTIR with the acquisition of spectral data. It is utilized to pinpoint the functional groups' attachment methods as well as the molecule's unique fingerprint. The samples can be prepared using a reliable technique, such as Nujol mulls, and then scanned in FTIR at a slow scanning speed (4000 to 400 cm⁻¹) (Khalaf *et al*., 2018; Manyarara et al., 2018).

2.6. Field emission scanning electron microscope (FESEM)

Moreover, fluconazole nanoemulsions underwent a field emission scanning electron microscopy (FESEM) study. It was utilized to describe the size and shape of the droplets included within the generated fluconazole nanoemulsion. Furthermore, it is a device used to analyze the surface and dimensions of nanoemulsion (*Abu Bakar et al.,* 2011; Saleh and Abbood, 2020).

2.7. HPLC technique

The examination and determination of potential interactions between oil, drugs, and other excipients employed the HPLC method. A water-based HPLC system with an SPA-20A detector was used. Breeze software was used to control the system. The mobile phase had an acetonitrile:water ratio of 65:35 v/v, was flowing at a rate of 1 ml/min, and the injection volume was 10 l. The 239 nm detective wavelength was chosen. Before use, the mobile phase was filtered via a millipore solvent filtration device (0.45 m) (Channabasavaraj *et al*., 2010., Hashim *et al.,*2023, Hussain *et al.,* 2024).

2.8. Study animals

In the current study, 32 healthy female Mus musculus mice, aged 12 to 16 weeks, with average weights of 20 to 25 grams, and 8 pregnant mice per group, were employed. The animals were randomly divided into four groups as follows: Control group: administered with normal saline. infected mice: C. albicans (isolated from urinary tract infections) was administered (orally) at a concentration of 1.5 x 10^8 cfu/ml. FLX group: FLX-nanoemulsion, was administered with 0.1 ml. treated mice: C. albicans was administrated with a suspension and treated with FLX-nanoemulsion. The administration was made before pregnancy, after 10 days from fertilization, and continued until the 18th day of pregnancy, which represents the dissection day. Ethical approval was obtained from the Research Ethics Board at Kirkuk University (Ethical Approval number: KIEC\ 0544\0043 dated May 29, 2023).

2.9. Histological study

With a 4 mm ear-punch of 2% xylocaine as the anesthetic, liver samples were collected. The biopsies were routinely processed, fixed in 10% formalin, embedded in paraffin slices, stained with hematoxylin and eosin, and seen under a microscope (Abdul *et al*., 2023).

2.10. Investigation of the CD163 levels

Every study subject's serum contained CD163, which was identified. The standardized sandwich ELISA method was used to accomplish this. In summary, 50 μl of each specimen was added in each well that had previously been coated with sCD163 antibody. The wells were then incubated for 120 minutes at 37°C, washed with phosphate

buffer saline, and then 50 µl of streptavidin horseradish peroxidase was added. The wells were then again incubated for two hours at 37°C, and again were washed with phosphate buffer saline. Each well received 50 µL of substrate components A and B until color development. To terminate the reaction, 50 µL of a stop solution was added. Using an ELISA reader, the optical density at 450 nm was measured.

2.11. Statistical Analysis

Analysis of variance (ANOVA) was performed to examine experimental mean values; the one-way ANOVA test was employed to ascertain the degree of significance within a single experimental group, and the LSD (Fisher's least significant difference) test was used to determine the difference between different means, and $P < 0.05$ was considered statistically significant (Ahmed and Saleh 2021).

3. Results & Discussion

3.1. Diagnosis of Candida albicans isolates

After collecting urine samples from mice infected with *C. albicans* as well as from the control group, the urine samples were cultured on Sabouraud dextrose agar ((HiMedia, India) media. The group of infected mice showed positive growth of the fungus. *C. albicans* was identified based on cultural and microscopic characteristics and biochemical tests. *C. albicans* was also diagnosed on CHROM Agar Candida medium (CHROMagar Candida, France). To confirm infection with the fungus, the WBC count was examined among the infected mice before treatment, as well as in the control group.

The results showed that the mice injected with the fungal suspension had a significant ($P>0.01$) increase in the WBC count (16.28 ± 2.83 $X10^3$ cell/mm^2) compared to the control group (5.72 ± 1.64 $X10^3$ cell/mm^2). The significant increase in the number of WBC in mice injected with the fungal suspension than control mice indicates the extent of the intense immune response to the fungal infection, as white blood cells are considered the first line of defense for that response following various infections (Anderson 1980, Al Zaher *et al.,*2024, Abdulateef *et al.,*2024). In general, most parasitic and fungal infections are characterized by a noticeable increase in the number of white blood cells, which is one of the most prominent signs of the immune response to the infection. The rise is caused by histamine being released, particularly because it is a chemo-attractive agent, and a condition that leads to the destruction of mast cells, and thus the release of histamine from its granules helps to increase white blood cells, especially acidic ones (Archer 1980, Al-Sarraj *et al.,* 2024).

3.2. Fluconazole nanoemulsion properties

Some properties of Fluconazole nanoemulsion were studied, including Saturation solubility, FESEM, FTIR spectra and Validation of the HPLC method.

3.2.1. Saturation solubility of fluconazole

The NE system preparation used glycerin oil as the oil phase, tween 80 as the surfactant, and ethanol as a co-surfactant following the saturated solubility data obtained as shown in Table 1.

Table 1. Fluconazole solubility (mg/ml) in different oils, surfactants, and co-surfactants.

Compounds		Solubility mg/dl
Oil	Olive	8.5
	Glycerin	39.1
Surfactant	Tween 20	73.5
	Tween 80	96.2
Co-Surfactant	Ethanol	58.2
	Acetone	14.7

3.2.2. FESEM

Figure 1 demonstrates that the oil droplets produced by the improved formula are spherical in shape and accumulate smaller oil droplets (mentions the nano size of the droplets achieved), although the shape and size of the oil droplets did not significantly alter as they accumulated (Redzuan *et al.,* 2011; Bozdağ-Pehlivan *et al.,* 2011). This result appeared to be comparable with the findings of Yuan *et al. (*2008) on β-carotene nanoemulsion, where the oil droplet size remained unaltered after 1 month at 4°C storage.

3.2.3. FTIR Spectra

The typical peaks in the FTIR spectra of pure FLX powder are 3005.10 cm^{-1} due to vibrational (N-H) stretching, 2926.01-2854.65 cm^{-1} related to (=C-H) stretching, and 2673.34 cm^{-1} due to aliphatic (C-H) stretching. The stretching of ester (C=O) is responsible for 1710.86 cm^{-1}, aromatic C=C stretching is responsible for 1460.11 cm^{-1} and 1413.82 cm^{-1}, aliphatic CH bending is responsible for 1286.52 cm^{-1} and 1247.94 cm^{-1}, disubstituted orthobenzene stretching is responsible for 723.31 cm^{-1}, and CN stretching is responsible for 1089.78 cm1 and 937.40 cm^{-1}. Figure 2 shows the FTIR spectra of the FLX.
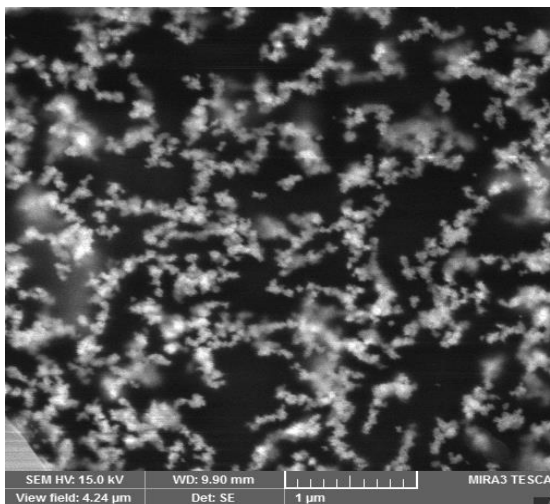

Figure 1. FESEM of optimized formula FLX-NE, the optimized formula produces spherical fluconazole oil droplets with a collection of smaller oil droplets.
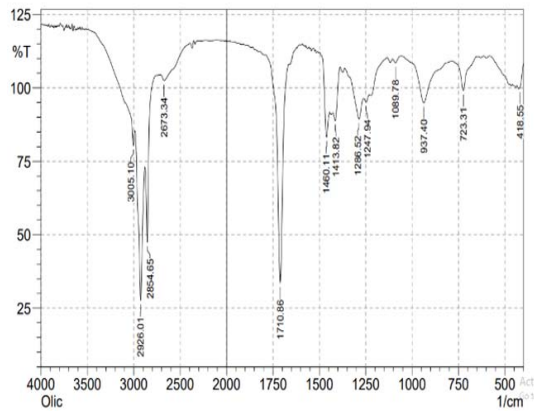
Figure 2. The FTIR spectra of FLX.3.2.4 Validation of the HPLC method

There was no difference in retention time between the chromatograms of Pure Drug FLX and FLX-NE, and no additional peaks were noted. Therefore, it was discovered that certain excipients were compatible with FLX. Chromatograms of FLX and FLX-NE were displayed in Figures 3 and 4, respectively.
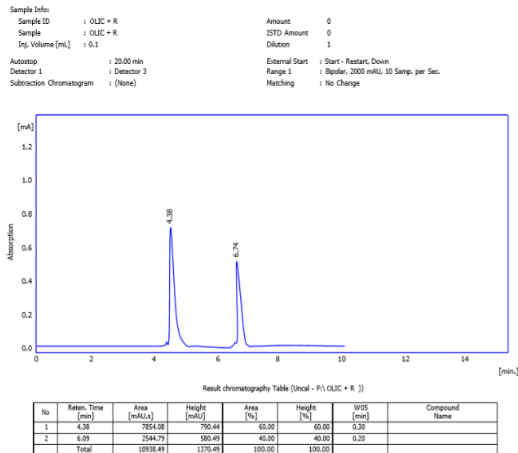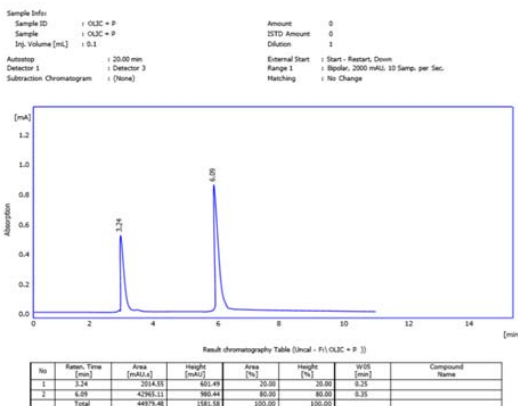

Figure 3. Chromatograms of FLX-NE

Figure 4. Chromatograms of Pure drug FLX.

3.3. In vivo study

The *in-vivo* study was conducted to reveal the role of FLX-NE against the toxicity of *C. albicans* which causes some histological changes in the liver. The section of liver

of control group showed normal structure (Figure 5); after infection with *C. albicans*, the liver of pregnant mice underwent several histological changes, including hepatocyte degeneration and necrosis, thickening of blood vessel walls, fibrocyte presence, and infiltration of mononuclear inflammatory cells (Figure 6); also the liver of FLX-NE group showed normal structure and cells (Figure 7) as shown in table 2. Moreover, various morphological anomalies were discovered in the embryos, such as short front limbs, red spots on the skin, thickening of the skin in some places, and a decrease in the number of embryos table 3. After treatment with FLX-NE, the liver of treated group (Figure 8) was closer to the control group, and the morphological changes of the embryos were limited and were closer to the control group.

Table 2. Histological changes in the pregnant mice livers.

Groups Lesions	Control Mice	Infected Mice	FLX-NE Group	Treated Group
Degeneration	Trace	++	Trace	Trace
Necrosis	Trace	++	Trace	Trace
Congestion	Nil	+	Nil	Nil
Fibrocytes	Nil	Trace	Nil	Nil
Infiltration of lymphocytes	Nil	++	Nil	Trace
Thickening walls	Nil	+	Trace	Trace

Table 3. Morphological changes in the pregnant mice embryos.

Groups Changes	Control Mice	Infected Mice	FLX-NE Group	Treated Group
No. of embryos	10±2	5±3	9±2	9±3
Red spots	Nil	+	Nil	Trace
Thickening of the skin	Nil	+	Nil	Trace
Short front limbs	Nil	+	Nil	Nil

Figure 5. The liver of control group showing the normal shape of central vein (CV) and hepatocytes (HC) with normal sinusoids (S) and kupffer cells (KC) H&E X400.

Figure 6. The liver of infected group showing thickening wall of central vein (TW) with congestion (CON), degeneration (D) of hepatocytes and lymphocytes infiltration (LI) H&E X400.

Figure 7. the liver of FLX-NE group showing the normal shape of central vein (CV) and hepatocytes (HC) with normal sinusoids (S) and kupffer cells (KC) H&E X400.
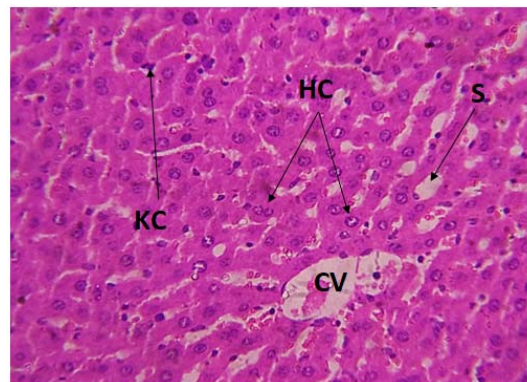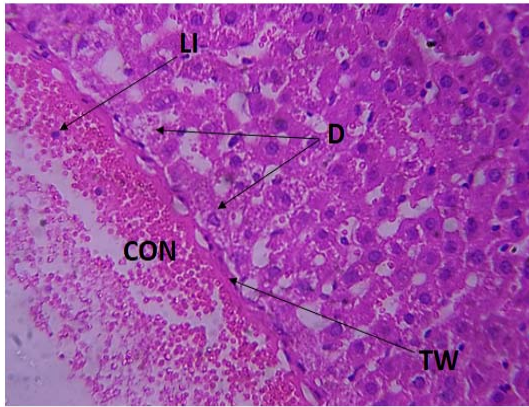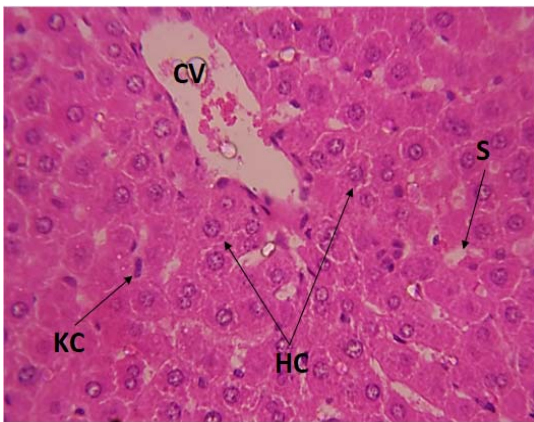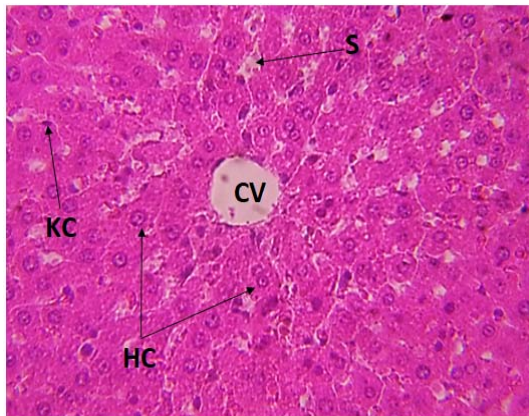

Figure 8. the liver of treated group showing the normal shape of central vein (CV) and hepatocytes (HC) with normal sinusoids (S) and kupffer cells (KC) H&E X400.

The results from the present study align with those from a previous investigation conducted by Mohamed *et al.* (2010). Their study similarly noted that the administration of *C. albicans* led to degenerative changes, irregular liver cell arrangement, and increased Kupffer cell presence, as well as the occurrence of congestion areas interspersed among the degenerative cells. Additional degenerative alterations encompassed the infiltration of mononucleated cells, the presence of necrotic foci surrounded by a high influx of inflammatory cells, and further degenerative changes. The results of our study align with those reported by AL-Naqeeb *et al.*, (2019), illustrating histological abnormalities in the livers of mice infected with *C. albicans*, such as hepatocyte necrosis and degeneration. Treatment with both fluconazole and fluconazole nanoemulsion in our current study notably improved the external appearance of the embryos and liver tissues in pregnant mice.

Fluconazole exerts its influence by blocking the conversion of lanosterol to ergosterol (Graybill 2001, Awad *et al.,* 2020), thus inhibiting fungal sterol synthesis (Kołaczkowska and Kołaczkowski 2016) and impeding cell membrane formation. These effects collectively account for the observed outcomes. Notably, fluconazole has been efficacious in treating Candida infections (Watt *et al.,* 2015). Nevertheless, it is important to acknowledge the existence of Candida species that display resistance to azole medications (D'asheesh *et al.,* 2020, Abdulateef *et al.,*2024).

In our study, nanoemulsions played a pivotal role due to their non-toxicity at biocidal dosages to mucosal and gastrointestinal tissues (Sonneville *et al.,* 2004.,Salih *et al.,* 2022), underscoring their significance in the administration of fluconazole. Consequently, our study's killing kinetics demonstrated the enduring fungicidal effects of fluconazole nanoemulsion.

Nanoemulsions at biocidal concentrations are nontoxic to mucosal membranes and gastrointestinal tract tissues (Krishnamoorthy *et al.*, 2021). This explains the absence of damage to liver tissue in the current study when using fluconazole nanoemulsion. On the other hand, the synergy between fluconazole and essential oil bioactive compounds, which produces strong antifungal activity against fungal infections, explains the current results (Al-Naqeeb *et al.*, 2018., Abed *et al.,* 2022).

The synergistic action between bioactive components of essential oils and nanodroplets is believed to contribute to the substantial antifungal activity against fungal infections, offering a plausible explanation for these findings (Ajaiyeoba 2000; Bala *et al.,* 2010; Abdullah *et al.,*2019; Hussein *et al.,* 2024).

3.4. Detection of CD16 in studied groups

Figure 9 showed significant ($P{\leq}0.05$) changes in the levels of CD163 between studied groups, where the concentrations of CD163 in infected mice ($29.51{\pm}6.03$) showed significant ($P{\leq}0.05$) elevated compared with control group ($12.74{\pm}3.84$); otherwise, there are non-significant ($P{\leq}0.05$) differences in level of CD163 in FLX-nanoemulsion group ($11.94{\pm}1.51$) compared with control group. On the other hand, there was an improvement in CD163 levels in the treated group ($20.42{\pm}2.36$), but there was still a significant ($P{\leq}0.05$) difference compared to the control group.
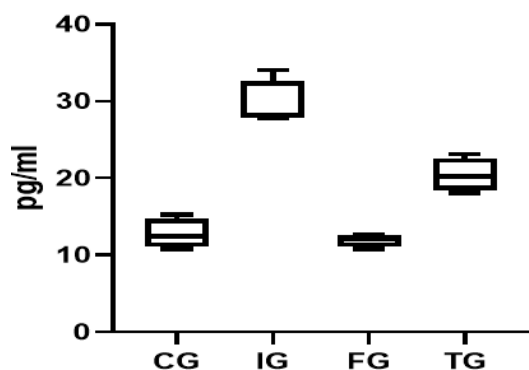
Figure 9. Levels of CD163 in studied groups.

CG: Control, IG: Infected mice, FG: FLX-nanoemulsion, TG: Treated group.

In the current investigation, it was discovered that pregnant female mice infected with candidiasis had elevated CD163 levels; following treatment, there was a minor improvement in comparison to the infection group. Melino *et al.* (2012) observed elevated circulating CD163 levels concurrent with elevated hepatic CD163 expression, which is consistent with our findings and suggests that changes in CD163 in inflammatory liver tissue can be observed in blood levels of CD163. These results provided credence to the idea that CD163 could serve as a non-invasive biomarker for the prognosis of hepatic inflammatory diseases. The findings of our investigation support the theory that some histological lesions in the liver are caused by candidiasis infection. The discovery was made by Kazankov *et al.* (2015), who found that patients with fatty liver disease had significantly higher levels of sCD163. This could be linked to early complications in the liver, activation of macrophages, and inflammatory changes that can happen before histological changes are noticed. Additionally, they asserted a correlation between progressive fibrosis and the amount of sCD163, indicating continuous activation of macrophages throughout the entire course of the disease. Additionally, sCD163 levels were higher in patients exhibiting acute liver failure. In the current study, FLX-nanoemulsion had a role in reducing CD163 levels after treatment. This may be because FLX-nanoemulsion treated the candidiasis infection that was the main cause of many histological changes in the liver, and thus CD163 levels improved in pregnant mice after treatment.

Since sCD163 levels are quite elevated in other acute inflammatory conditions such as liver disease including liver candidiasis (Coca *et al.*, 2009, Dheeb *et al.*,2023), and some studies have showed the effective role of Fluconazole in treating Liver Candidiasis resulting from infection with C. albicans (Pfaller *et al.*, 2004; Charlier-Woerther *et al.*, 2006., Mahmood *et al.*,2019), which enhances the effective role of Fluconazole Nanoemulsion in reducing the inflammatory condition as a result of the antifungal activity and thus reduces the need for pro-inflammatory parameters including CD163.

4. Conclusions

Based on the results of the current study, it is evident that fluconazole nanoemulsion exhibits a potent effect against *C. albicans* infection. Furthermore, it effectively treats histological abnormalities and fetal lesions induced by *C. albicans* in both pregnant mice and their fetuses.

5. Author contributions

SHM and AHS contributed equally to the study conception, material preparation, data collection, and analysis and design. Supervision was carried out by BID. The initial write-up of the draft manuscript was done by SHM and BID. The review and corrections for the previous version of the manuscript were carried out by KHA. All authors read and approved the final manuscript.

References

Abdul, MR, Rahim, SM and Saleh, AH. 2023. Cardioprotective activity of *Costus* root ethanol extract in experimentally-induced hypothyroidism in female albino rats. *HAYATI J of Biosci.*, **30(6)**: 1054–1060. https://doi.org/10.4308/hjb.30.6.1054-1060.

Abdulateef S M, Ibraheem S, Hussein H S, Dheeb BI, Khashman BM, Ahmed DM and Abu-Elteen KH . 2024. MMP-1 and MMP-7 expression is influenced by ginsenosides in mice exposed to aflatoxin B1: in vivo study. *Jordan J Pharm Sci.*,**17 (1)**: 135-1139.

Abdulateef SM., Hussein AS., Mohammed SH ., Dheeb BI and Jafar BJ., 2024. Effect of air pollution with *Aspergillus* spp.in occurrence of Aflatoxin M1 in milk and its products. *MCB*, **21**(4), 758.

AL-Naqeeb, SAR., Khalaf, M., and Abdullah, HN., 2019. Pathogenicity of mutant aspergillus fumigatus MAFU isolate in the lung of mice during infection period. *International J of Pharmaceutical Research*, 11(2): 54-59.

Abdullah HI, Hammadi SY, Hussein AS and Dheeb BI .2019. Investigation of genetic diversity and relationships among the clinical candida species using random amplified polymorphic DNA (RAPD) analysis., *Res J Biotechnol.*, **14(1)**:6–13.

Abed SM, Farhan MG, Madhloom NK and Dheeb BI. 2022. Magnetic field exposure to clinical isolates of *Acinitobacter* baumanii. *Biomed Pharmacol J.*, **15(4):** 2137–2143.

Abu Bakar A and Tommy J B. 2011. Development and stability evaluation of astaxanthin nanoemulsion. *Asian J Pharm Clin Res.*, **4(1)**:142-148. https://doi.org/10.13040/ 263011089

Ahmed, K.O. and Saleh, A.H.2021. Effects of estrogen in treating myocardial damages caused by ischemia in adult female rats. *Inter J of Drug Delivery Technol.*, **11(4)**: 1474–1477.

Ajaiyeoba E.O. 2000. Phytochemical and antimicrobial studies of *Gynandropsis gynandra* and *Buchholzia coriaceae*. *Afr J Biomed Res.*, **3**:161-165. https://www.ajol.info/index.php/ajbr/article/view/140995

Al Zaher RM., Abderrahman SM., Abdulateef SM., Dheeb BI., Massadeh MI, Hussein AS. and Farhan MS . 2024. Antimicrobial activity of Zn-nanoparticles synthesized by leaf extract of *Capparis spinosa*. Res J Biotechnol., **19**(11).639.

Al-Sarraj BM, Salman RD, Ahmed DM, Massadeh MI, and Dheeb BI. 2024. Bacteriological and molecular detection of fluoroquinolone resistance in Escherichia coli isolated from

women patients with urinary tract infections. farmacia.,72(4):840-847.

Anderson , JR.(Ed.) 1980. **Muirs Textbook of Pathology** . 11th . ed., Edward Arnold , London : 652PP. 2.

Al-Naqeeb SAR, Abdullah HN, and Khalaf MS.2018. Molecular identification of Echinococcosis granulosus using ISSR and RAPD markers. *J of Pharmaceutical Sciences and Research.,* 10(12): 3313-3316.

Atiencia-Carrera MB, Cabezas-Mera FS, Tejera E and Machado A. 2022. Prevalence of biofilms in *Candida* spp. bloodstream infections: a meta-analysis. *PLoS One*, **17**: e0263522. https://doi.org/10.1371/journal.pone.0263522.

Awad FM, Al-Samarrai AHM and Dheeb BI. 2020 .Study of the inhibitory effects of rheum ribes extracts on a pathogenic fungi and cancer cell line. *Plant Arch*, **20(1):** 3161–3168.

Azmi N. A. N., Amal A. M., Shiva R. M., Nurhusna S. and Salleh H M. S. 2019. Nanoemulsions: Factory for food, pharmaceutical and cosmetics. *Processes,* **7(9):** 617. https://doi.org/10.3390/pr7090617

Bala A, Kar B, Haldar P K, Mazumder U K and Bera S. 2010. Evaluation of anticancer activity of *Cleome gynandra* on Ehrlich's Ascites Carcinoma treated mice. *J Ethnopharmacol*., **129 (1):**131-134. https://doi.org/10.1016/j.jep.2010.03.010.

Bongomin F, Gago S, Oladele RO. and Denning DW. 2017. Global and multi-national prevalence of fungal diseases-estimate precision. *J Fungi*, **3**:57. https://doi.org/10.3390/jof3040057

Bozdağ-Pehlivan S, Subaşi B, Vural I, Ünlü N and Çapan Y. 2011. Evaluation of drug-excipient interaction in the formulation of celecoxib tablets. *Acta Pol Pharm -Drug Res*., **68(3):**423–433. https://pubmed.ncbi.nlm.nih.gov/21648198/.

Centers for Disease Control and Prevention. 2012. Invasive Candidiasis. Retrieved from http://www.cdc.gov/fungal/Candidiasis/invasive/

Channabasavaraj KP, Nagaraju PT, Kumar S, and Reddy PS. 2010. Reverse phase HPLC method for determination of lacidipine in pharmaceutical preparations. *Int J Pharm Sci Rev Res.*, **5(2):** 111-114.

Charlier-Woerther C., Hart E. and Lefort A. 2006. Fluconazole for the management of invasive candidiasis: Where do we stand after 15 years?. *J Antimicrob Chemother*., **57(3):**384-410

Coca A., Kemp W. B., Bethany M., Jennifer H. and John L. 2009. Macrophage activation syndrome: Serological markers and treatment with anti-thymocyte globulin. *Clin Immunol.,* **132**: 10–18

D'asheesh TAbid, Abbas AJ, and Neamah AM.2020.The succession of Bacteria on Rat carcass: A Forensic study. *J of Punjab Academy of Forensic Medicine & Toxicology*., 20(1): 76. DOI :10.5958/0974-083X.2020.00057.6.

Dheeb B I, Abdulla S N, AL-Qaysi SAS, Al-Sarraj BM and Farhan MS. 2023. Extraction of *Klebsiella pneumoniae* and *Candida albicans* biofilm and studying their cytotoxic effects on human lymphocytes. *Jordan J Biol Sci*., **16(4):** 717 – 726.

Dheeb BI, Hashim SS, Hussein HS. and Hamada TA.2022. Study of TGF- β Immune Marker Expression in Mice Exposed to Candida Spp. *AIP Conference Proceedings,* Vol (**2394):1**. https://doi. 10.1063/5.0121945.

Dheeb BI, Mohammad FI, Hadi YA, and Abdulhameed BA. 2013. Cytotoxic effect of aflatoxin B1, gliotoxin, fumonisin B1, and zearalenone mycotoxins on HepG2 cell line in vitro. *International Journal of Advance Research*.**1(8)**:355-363.

Galgiani JN, Ampel NM, Blair JE, Catanzaro A, Geertsma F, Hoover SE, Johnson RH, Kusne S, Lisse J, MacDonald JD, Meyerson SL, Raksin PB, Siever J, Stevens DA, Sunenshine R.

and Theodore N. 2016 Infectious Diseases Society of America (IDSA) Clinical Practice Guideline for the Treatment of Coccidioidomycosis. *Clin Infect Dis*. **63(6)**:e112-146.

Garnacho-Montero J., Irene B. and Cristina L.2024. Fungal infections in immunocompromised critically ill patients. *J Intensive Med*., **4(3)**: 299-306.

Ghareeb MM and Neamah AJ. 2017. Formulation and characterization of nimodipine nanoemulsion as ampoule for oral route. *Inter J Pharm Sci Res.,* **8(2):**591. https://doi.org/10.13040/IJPSR.0975-8232.8(2).591-02

Gonzalez ID, González FG, Cuesta TS, Fernández JM, Rodríguez JMD, Ferrairo RE, Alonso MCD, Arenas LB, Barrientos RR, Wiesmann EC, Romero CD, Díaz YG, Rodríguez-Moñino A, Teira BG, Pozo MS, Horcajuelo JF, Giraldo MJR, González PC, Cuadrad RV, Uriarte BL, Yepes JS, Sanz YH, Piñeiro MJI, Hernández ST, Alonso FG, González AIG, Fernández AS, Carballo, C, López, AR, Morales F, and López DM. 2011. Patient preferences and treatment safety for uncomplicated vulvovaginal candidiasis in primary health care. *BMC. Public Health.* **11**:63.

Hussein ZA, Majeed MJ, Al-Anbari LA, and Al-Naqeeb SAR. 2024. The Association Between the Levels of Phosphodiesterase 9, Insulin-Like Peptide 5 and Obesity in Women. *AL-Kindy College Medical J*., **20 (2)**: 117-21. https://doi.org/10.47723/6btq4431.

Hussain EM, Alkadhimy SM,Neamah AM, and Tousson E.2024. Beneficial role of amygdalin extracts against animal growth regulator Boldjan induced cardiac toxicity, injury and oxidative stress in male rats. *Toxicology Research*., 13:1–7. https://doi.org/10.1093/toxres/tfae042.

Hashim S S, Mahmood Z F, Abdulateef SM. and Dheeb BI. 2023. Evaluation Cytotoxicity Effects of *Centaurea Cineraria* Extracts Against some of Cancer Cell Lines. *Biomed Pharmacol J* .**16(1):** 243–249.

Hatem YQ and Dheeb BI ; 2024. Cytotoxic effects of Gliotoxin extracted from *Candida albicans* isolated from patients with urinary tract infection. *MCB* , **21**(2),1-12.

Hussain AF, Sulaiman GM, Dheeb BI, and Hashim AJ, Abd Alrahman ES, Seddiq SH and Khashman BM. **2020**. Histopathological changes and expression of transforming growth factor beta (TGF-β3) in mice exposed to gliotoxin, *J King Saud University – Science*, **32(1):** 716–725**.**

Katva S, Das S, Moti HS, Jyoti A and Kaushik S. 2018. Antibacterial synergy of silver nanoparticles with gentamicin and chloramphenicol against *Enterococcus faecalis*. *Pharmacogn Mag*., **13(4)**: S828-S833. https://doi.org/10.4103/pm.pm.120.17.

Kazankov K, Tordjman J, Møller HJ, Vilstrup H, Poitou C, Bedossa P, et al. 2015. Macrophage activation marker soluble CD163 and non-alcoholic fatty liver disease in morbidly obese patients undergoing bariatric surgery. *J Gastroenterol Hepatol*., **30(8)**:1293-1300. https://doi.org/10.1111/jgh.12943.

Kołaczkowska, A and Kołaczkowski, M. 2016. Drug resistance mechanisms and their regulation in non-*albicans Candida* species. *J Antimicrob Chemother*, **71(6):** 1438-1450. https://doi.org/10.1093/jac/dkv445.

Krishnamoorthy R., Mustafa A. G., Jegan A., Vaiyapuri Subbarayan P., Saradh P. and Ali A A. 2021. Antifungal activity of nanoemulsion from *Cleome viscosa* essential oil against food-borne pathogenic *Candida albicans*. *Saudi J Biol Sci*., **28(1):** 286-293.

Khalaf MS, Abdullah HN, and Rashid SA.2018. Sequencing of Zona Pellucida 4 (ZP4) Gene in Patients with Polycystic Ovary Syndrome Infected with Toxoplasmosis. *J Global Pharma Technol*.; **10(7)**:115-119.

Leelambigai D., Shanthi T M. and Bernaitis L. 2024. Fungal infections in immunocompromised hosts. *Global J Res Medical Sci.,* **4(6):** 5–8.

Lovelyn C and Attama A A. 2011 Current state of nanoemulsions in drug delivery. *J Biomater Nanobiotechnol.,* **2:** 626–639. https://doi.org/ 10.4236/jbnb.2011.225075.

Mahmood MN,Mahal MH,Mohammed HE, Tariq TA. , Mohammed AJ and Dheeb BI. 2019. Evaluation of enzymes liver and kidney function in serum people the exposures at risk of chemicals volatile in the lab pharmaceutical samarra. J Global Pharma Technol.;**11**(7), pp. 331–336.

Makabenta JMV, Nabawy A, Li CH, Schmidt-Malan S, Patel R. and Rotello VM. 2021. Nanomaterial-based therapeutics for antibiotic-resistant bacterial infections. *Nat Rev Microbiol.* , **19**: 23-36. https://doi.org/10.1038/s41579- 020-0420-1

Manyarara TE, Khoza S, Dube A and Maponga CC.2018. Formulation and characterization of a paediatric nanoemulsion dosage form with modified oral drug delivery system for improved dissolution rate of nevirapine. *MRS Advances.* **3(37)**: 2203-2219. https://doi.org/ 10.1557/adv.2018.320

Matthaiou DK, Christodoulopoulou T. and Dimopoulos G. 2015. How to treat fungal infections in ICU patients. *BMC Infect Dis.,* **15**:1–8. https://doi.org/10.1186/s12879-015-0934-8.

McDermott A.2022. Drug-resistant fungi on the rise. *PNAS.* **119 (48):** e2217948119. https://doi.org/10.1073/pnas.2217948119.

McManus BA and Coleman DC. 2014. Molecular epidemiology, phylogeny and evolution of *Candida albicans. Infect Genet Evol.,* **21**:166–178. https://doi.org/10.1016/ j.meegid.2013.11.008.

Melino M, Gadd VL, Walker GV, Skoien R, Barrie HD, Jothimani D, et al. 2012. Macrophage secretory products induce an inflammatory phenotype in hepatocytes. *World J Gastroenterol.,* **18(15):**1732-1744. https://doi.org/10.3748/wjg. v18.i15.1732.

Mohamed, B J, AL- Hussain, R A and AL Thwani, AN.2010. Study the INH inhibitory effect of *Lactobacillus acidophilus* isolated from yoghurt as probiotics on *Candida albicans* growth *in vitro* and *in vivo*. *Iraqi J Biotech*., **9(2):** 167-179.

Mohammed, S H, Hawazin A A, Anmar S H, Batool I D and Nehan B J. 2024. Detection of anti-mannan antibodies and TLR9 as alternative methods for diagnosis of candidiasis in immunocompromised patients with vulvovaginitis. *J Appl Natural Sci.,* **16(3)**: 1183 - 1188. https://doi.org/10.31018/jans.v16i3.5460.

Pfaller MA, Messer SA, Boyken L et al. 2004. Geographic variation in the susceptibilities of invasive isolates of *Candida glabrata* to seven systemically active antifungal agents: a global assessment from the ARTEMIS Antifungal Surveillance Program conducted in 2001 and 2002. *J Clin Microbiol.,* **42**: 3142–6.

Reddy R B, Kumari C T, Sowjanya G N, Sindhuri S L and Bandhavi P. 2012. Nanoemulsions an emerging trend. *IJPRD*, **4(6)**: 137-152.

Redzuan M, Julianto T and Majeed A. 2011. Development and stability evaluation of astaxanthin nanoemulsion. *Asian J Pharm Clin Res*., **4(1)**:142-148.

Sadoon N A and Mowafaq MG. 2020. Formulation and characterization of isradipine as oral nanoemulsion. *Iraqi J Pharm Sci*., **29(1)**: 43-53.

Saleh, A.H. and Abbood, H.A.R. 2020. The role of silver (Ag) nanoparticles synthesis by *Penicillium* spp against the toxicity of *Echinococcus granulosus* in adult albino male rats. *Medico-Legal Update*, **20(1):** 532–537. https://doi.org/10.37506/v20/ i1/2020/mlu/194377.

Salih, II, Seddiq SH, Hashim SS. and Dheeb BI. 2022. Application of Omics and Proteomics in Fungi. *AIP Conference Proceedings,* Vol. **(2394):1.**

Sarvtin MT, Shokohi T, Hajheydari Z, Yazdani J, and Hedayati MT. 2014. Evaluation of candidal colonization and specific humoral responses against *Candida albicans* in patients with psoriasis. *Int J Dermatol*. **53**:e555–560. https://doi.org/10.1111/ijd.12562.

Schalbart P, Kawaji M and Fumoto K. 2010. Formation of tetradecane nanoemulsion by low-energy emulsification methods. *Inter J Refrig*., **33:** 1612-1624. https://doi.org/10.1016/j.ijrefrig.2010.09.002.

Schmiedel Y and Zimmerli S. 2016. Common invasive fungal diseases: an overview of invasive candidiasis, aspergillosis, cryptococcosis, and *Pneumocystis pneumonia*. *Swiss Med Wkly* **146**:1–12. https://doi.org/10.4414/smw.2016.14281.

Sonneville A O, Simonnet J and L'Alloret F. 2004. Nanoemulsions: a new vehicle for skin care products. *Adv. Colloid Interface Sci.*, **108–109**:145-149. https://doi.org/10.1016/ j.cis. 2003.

Tacconelli E, Carrara E, Savoldi A, Harbarth S, Mendelson M and Monnet DL. 2018. Discovery, research, and development of new antibiotics: the WHO priority list of antibiotic-resistant bacteria and tuberculosis. *Lancet Infect Dis*., **18 (3)**:318-327. https://doi.org/10.1016/S1473-3099(17)30753-3.

Vallabhaneni S, Mody RK, Walker T and Chiller T. 2016. The global burden of fungal diseases. *Infect Dis Clin*., **30:**1–11. https://doi.org/10.1016/j.idc.2015.10.004

Watt K M, Gonzalez D, Benjamin DKJ, Brouwer KL, Wade KC, Capparelli E, Barrett J and Cohen-Wolkowiez M. 2015. Fluconazole population pharmacokinetics and dosing for prevention and treatment of invasive Candidiasis in children supported with extracorporeal membrane oxygenation. *Antimicrob Agents Chemother*., **59(7)**:3935-3943. https://doi.org/10.1128/ AAC. 00102- 15.

Yuan Y, Gao Y, Zhao J and Mao L. 2008. Characterization and stability evaluation of β-carotene nanoemulsions prepared by high pressure homogenization under various emulsifying conditions. *Food Res Int.,* **41**: 61-68.

Zhou J., Zipeng W., Baohua X., Maobai L., Ruichao X. and Xuemei W. 2022. Pharmacovigilance of triazole antifungal agents: Analysis of the FDA adverse event reporting system (FAERS) database. *Front Pharmacol*. **13**:1039867. https://doi.org/10.3389/fphar.2022.1039867.

JJBS

Jordan Journal of Biological Sciences

Methane Emissions from Seedlings of the Cyprus Variety of Faba Bean (*Vicia faba* L.) Under Drought and Heat Stress Factors at Elevated Carbon Dioxide

Mohammad Abo Gamar*, Riyadh Muhaidat, and Khaled Al-Ahmad

[1]Department of Biological Sciences, Faculty of Science, Yarmouk University, Irbid 21163, Jordan

Abstract

Global warming is caused by a group of greenhouse gaseous pollutants emitted by human activities into the atmosphere, mainly carbon dioxide (CO_2) and Methane (CH_4). However, CH_4 is the most potent contributor to the warming of Earth and a changing climate, despite its lower concentration than CO_2. There are many natural sources of methane emission in nature including plants, which have been shown to produce more CH_4 under stressful environmental conditions, particularly heat and drought. However, the combined effects of these two factors on methane emissions from plants have little been investigated. This study was designed to examine the combined effects of heat and drought on CH_4 emissions from Cyprus faba bean (*Vicia faba* L.) seedlings at elevated CO_2. Plants were grown in controlled-glass cabinets under two temperature regimes (20º/17ºC day/night for control and 30º/26ºC day/night for heat-stressed plants), two CO_2 concentrations of 400 ppm (ambient) and 800 ppm (elevated), and two watering regimes (well-watered and drought-stressed) for 14 days following cultivation of plants for 12 days. The effects of temperature, CO_2 concentration and watering regime on CH_4 emissions, growth, physiological, and biochemical parameters of fava bean seedlings were examined. Our results showed that heat and drought-stressed seedlings emitted significantly more CH_4 under single stress factor or their combination compared to control seedlings. Moreover, stress factors inhibited growth and development of faba bean seedlings. Elevated CO_2, in turn, decreased CH_4 emissions from stressed plants and enhanced their growth under control and stress conditions. Moreover, our results showed that elevated CO_2 enhanced the antioxidant capacity of all seedlings by increasing their flavonoids, chlorophyll and moisture contents. In conclusion, findings of this study corroborated the hypothesis that atmospheric CO_2 enrichment decreased plants' abilities to emit CH_4 in stressful environments and accordingly improve their growth under the predicted trends of climate change.

Keywords: Abiotic stress, Climate change, Faba bean (*Vicia faba* L.), Drought, Elevated CO_2, Heat, Methane emissions, Plant growth.

1. Introduction

Climate change and global warming are major issues of international concerns. Increasing emissions of gaseous wastes due to human actions, particularly CO_2 and CH_4, continuously add to those naturally occurring in the atmosphere, leading to an altered climate and a steady increase in temperature of the globe (Lomborg, 2020). An increase of 0.65-1.06°C in the Earth's temperature was recorded from 1880-2012 with additional increases over the next years (IPCC, 2013). Much of the warming and elevated global temperature has occurred in more recent years, and a temperature rise reaching as high as 4.1°C is highly expected by the end of the century (Lomborg, 2020). The consequences of climate change and global warming are likely catastrophic to the natural environments and human lives if human-induced emissions of gaseous waste products are not diminished. Global warming is linked with severe shifts in other climatic factors including wind and precipitation patterns, enhanced drought, flooding, heat waves, and air pollution (AghaKouchak *et al.,* 2020). These drastic climatic changes have thus become issues of major concern to scientists and international communities around the world. Of all greenhouse gases, CO_2 is the greatest contributor to increasing Earth's temperature; however, CH_4 is more potent, although it is emitted in less quantities and has a shorter atmospheric lifespan than CO_2. It has been reported that CH_4 contributes to about 25% of the change in climate over the last quarter-millennia, with a heat trapping capacity that is up to 23 times greater than that of CO_2 (Chai *et al.,* 2020). Although the largest proportion of CH_4 emissions come from human activities, other organisms (methanogenic archaea, cyanobacteria, fungi, algae, and plants) contribute to CH_4 release as well (Ernst *et al.,* 2022). As major producers of the biosphere and the most diverse, plants have gained special attention in studying their contribution to the atmospheric budget of CH_4, under the environmental challenges imposed by climate change and global warming (Turner *et al.,* 2020).

* Corresponding author. e-mail: mohammad.abogamar@yu.edu.jo.
*Note: This manuscript is based on the master thesis of the third author who was supervised by the first and second authors.

A series of studies over the past decade have made it clear that plants produce CH_4 aerobically, and these emissions are influenced by a variety of abiotic stress factors, particularly heat and drought (two key ecological components of climate change) (Wang *et al.,* 2021; Ernst *et al.,* 2022; Gautam *et al.,* 2024). It's well established that abiotic stresses exert deleterious effects on plants and induce CH_4 emissions (Wang *et al.,* 2021; Yao *et al.,* 2023). However, it is evident that environmental factors, temperature and drought stresses in particular, increase aerobic CH_4 emissions, but the interactive effects of stress factors on CH_4 emissions remain poorly understood, though evidence suggests that tailored responses occur in response in plants to the combination of environmental stresses. Moreover, these responses occurring only from the combination of stress factors, cannot be inferred from results of individual stress factor experiments, and therefore multiple-factor studies are essential (Zandalinas *et al.,* 2021). Elevated CO_2 (the third key component of climate change) has experimentally been shown to compensate for stressful conditions by alleviating the negative consequences of abiotic environmental stresses on plants (Abo Gamar *et al.,* 2023; Rakhmankulova *et al.,* 2024; Vijayalakshmi *et al.,* 2024).

It has been reported that the main components of climate change (heat, elevated CO_2 and drought) cause plants to experience changes in their physiology, anatomy, morphology and biochemistry in their natural habitats (Abo Gamar *et al.,* 2023).

Faba bean belongs to the family Fabaceae or Leguminosae, and it is among the oldest crops grown worldwide (Hobdari *et al.,* 2023). Faba bean is also known as broad bean, horse bean and field bean, and it is the fourth most main crop in the world (Davies *et al.,* 2022). The crop has been consumed in different ways, such as dry seeds, green vegetable, or as processed food. Its products, especially seeds, are very rich with high-quality protein for human diet. Also, its dry seeds, green haulm and dry straw have been used as resources for animal feeds (Davies *et al.,* 2022). The seeds of faba bean contain high protein content of 24-33% (Warsame *et al.,* 2022). In Jordan, the crop is cultivated either under irrigation or rainfed for the purposes of fresh pod utilization and dry seed production (Thalji, 2015). Four most common faba bean cultivars have been grown by Jordanian farmers. These include Cyprus (large seed), Equina-Syria-1 (medium seed), Balady and MinorBeck- Giza (small seed) (Thalji, 2015).

The potential of plants to release CH_4 into the atmosphere under normal or stress conditions were investigated in this study using Cyprus faba bean (*Vicia faba* L.), which is commonly grown in Jordan. We hypothesize that heat and drought stresses would reduce growth of Cyprus faba bean seedlings and induce them to emit CH_4, and that elevated CO_2 could enhance their growth and decrease CH_4 emissions under our experimental stress treatments. The specific objectives of this study are to: (1) investigate the individual and combined effects of temperature, CO_2, and watering regimes on CH_4 emission from Cyprus faba bean seedlings; (2) investigate if elevated CO_2 alleviated the negative impacts of heat and drought stresses on Cyprus faba bean seedlings, and thus, CH_4 emissions; and (3) address the possible mechanism (s) by which elevated CO_2 alleviate the negative impacts of heat and drought stresses

on Cyprus faba bean seedlings. To the best of our knowledge, this study is the first to be conducted related to CH_4 emission on crops grown in Jordan.

2. Materials and methods

2.1. Plant materials and growth conditions

The experiment was conducted inside the greenhouse of Yarmouk University from March to June 2021 on Cyprus faba bean seedlings to investigate the effects of temperature, CO_2, and watering regimes and their interactions on the growth and CH_4 emission from Cyprus faba bean seedlings. In this study, faba bean seeds (obtained from the National Agricultural Research Center [NARC] in Baqaa, Jordan) were sown in pots containing a mixture of soil, perlite and peat moss (1:1:1, by volume). In each pot, a seed of fava bean was sown to start germination under greenhouse conditions; 20°C day/17°C night, 14 hr light/10 hr dark, photosynthetic photon flux density (PPFD) of 530 photons m^{-2} s^{-1} and relative humidity at 55 % ± 2 %. The germination process, in total, took about 7 days and pots were watered with tap water to help seeds to germinate. Following germination, seedlings were kept in these conditions for a period of 5 days until all had produced at least four true leaves. NPK fertiliser was added (18-18-18, Navarsol IV, Timac Agro Italia). Afterward, seedlings were transferred to four controlled-glass cabinets (90 cm depth × 95 cm width × 70 cm height each) maintained in a naturally-illuminated greenhouse. The temperature, humidity and light were monitored by a cabinet control and logging computer to establish experimental conditions. The first two cabinets represent the non-heat stress treatment (normal temperature treatment; 20°C day/17°C night), and the other two represent the heat stress treatment (30°C day/26°C night). Temperatures were selected to match the current average temperatures in Jordan from March to June. For the two cabinets, which were under the non-heat stress treatment, the first one was provided with the atmospheric CO_2 concentration, which was around 400 ppm (ambient CO_2) and the second one with 800 ppm CO_2 concentration (elevated CO_2). Moreover, half of the seedlings were supplied with water to the field capacity (well-watered) and the other half were drought-stressed. Same treatments were applied for the two cabinets, which were under the heat stress condition. A split-split-plot design with three factors (temperature, CO_2, and watering regime) was used, and in total, eight different experimental treatments were conducted as follows: (1) normal temperature, ambient CO_2 and well-watered (control); (2) normal temperature, ambient CO_2 and drought-stressed; (3) normal temperature, elevated CO_2 and well-watered; (4) normal temperature, elevated CO_2 and drought-stressed; (5) heat stress, ambient CO_2 and well-watered; (6) heat stress, ambient CO_2 and drought-stressed; (7) heat stress, elevated CO_2 and well-watered; and (8) heat stress, elevated CO_2 and drought-stressed. CO_2 circulation in each cabinet was kept constant by using a small electrical fan and the relative humidity was also maintained at 55 % ± 2 %. Flow of gas from the CO_2 cylinder to the cabinets was regulated by a pSense portable CO_2 meter (K30 CO_2 Sensor). Seedlings were grown under their respective treatment for 14 days in cabinets.

2.2. Measurement of methane emissions

After 14 days of growth under experimental conditions and from each condition, three samples of fresh leaves were detached and incubated inside 4ml plastic syringes for 3 hr under the temperature of 20°C and PPFD of 530 photons m^{-2} s^{-1}. Two ml of gas was pulled from each syringe, and was injected manually into Hewlett-Packard 5880 Series II gas chromatograph equipped with a flame-ionization detector (Palo Alto, CA) operated at 200°C, a 2-m stainless steel column packed with 13 XMS (60/60 mesh). The injector temperature was 56°C, and the carrier gas was N$_2$ flowing at 31 ml min^{-1}. The retention time (~2.9 mins) of external standard was used to identify CH$_4$, and the standard curve of certified CH$_4$ gas was used to quantify its emissions rate on basis of dry biomass by drying leaves at 60°C for 48 hr.

2.3. Determination of growth parameters

After 14 days of growth, stem length was measured from the soil surface to apical meristem of each surviving plant using a ruler. Stem diameter was also measured on each plant using a Digimatic caliper (Digimatic CD15DCX; Mitutoyo) placed at the midway point between soil and the apical meristem. Three plants from each trial were harvested and dried at 60°C for 72 hr in a forced air oven in order to determine leaf mass, stem mass, root mass, and leaf area. The leaves, stems, and roots of each plant were weighed separately on analytical balance (Mettler Toledo, Columbus, XP205) in order to determine dry and fresh masses accumulation of each plant. An average-sized leaf from each plant was removed and weighed on an analytical balance (Mettler Toledo, Columbus, XP205) before and after drying in order to determine leaf moisture content. Leaf area of each plant was determined using an image J software (http://rsb.info.nih.gov/ij/). Growth indices were measured using the dry matter data; measurements included leaf area ratio (LAR) (cm^2 g^{-1}), leaf mass area (LMA) (g m^{-2}), leaf mass ratio (LMR), and shoot:root dry mass ratio.

2.4. Stress indicators

2.4.1. Measurement of proline

Proline content was estimated according to Bates et al. (1973). Three fresh leaf samples (60 mg) from three separate plants were collected from each treatment and quickly homogenized in 5 ml of 3% aqueous sulfosalicylic acid by using a mortar and pestle. After centrifuging the homogenate for 10 mins at 4000g, 2 ml of the filtrate were combined with 2 ml glacial acetic acid and 2 ml acid-ninhydrin. The mixture was boiled at 100°C for 30 mins., then cooled in the ice bath, and extracted with 5 ml of toluene. A UV/visible spectrophotometer (UV-550; Jasco, Japan) was used to measure the absorbance of the aqueous upper layer at 520 nm, and toluene was used as a blank. A standard curve was used to determine the proline content on a fresh mass basis (µmol g^{-1} FM).

2.4.2. Measurement of lipid peroxidation

Lipid peroxidation was determined by measuring the malondialdehyde (MDA) using 2-thiobarbituric acid assay procedure according to Abo Gamar et al. (2023) with some modifications. Three fresh leaf samples (50 mg) from three separate plants were collected from each treatment and fast frozen in liquid nitrogen and homogenized, by using a mortar and a pestle in a solution composed of 1.5 ml 0.5% 2-thiobarbituric acid and 1.5 ml 0.1% trichloroacetic acid. After centrifuging the homogenate at 4000g for 15 mins at 4°C, the supernatant was boiled for 10 mins and cooled on ice. A UV/visible spectrophotometer (UV-550; Jasco, Japan) was used to measure the absorbance at 532 nm and 600 nm using 1 ml of the supernatant. The 0.5% 2-thiobarbituric acid and 0.1% trichloroacetic acid were used as a blank. MDA content (nmol g^{-1} FM) was calculated by using the following formula: $[((A532 - A600) \times v) \times 1000]/ (\varepsilon \times M)$. In the formula, 'ε' stands for specific extinction coefficient (= 155 mM^{-1} cm^{-1}), 'v' for the volume of extracting medium, 'M' for the leaf fresh mass, and 'A600' and 'A532' for absorbance at 600 and 532 nm wavelengths, respectively.

2.4.3. Measurement of membrane permeability

Membrane permeability was estimated by measuring the electrical conductivity using the method of Abo Gamar et al. (2023). Three leaf samples (100 mg) from three different plants were obtained from each treatment and washed with distilled water before being put in test tubes containing 15 ml of double distilled water and incubated at room temperature for 24 hr. The initial conductivity (C1) of the fresh tissue was measured with a Mettler Toledo MPC 227 equipped with Mettler Toledo Inlab 730 conductivity electrode. Samples then were boiled for 1 hr at 100°C before being allowed to cool to room temperature. The dead tissue's maximal conductivity (C2) was measured, and electrolyte leakage was computed as the percentage ratio of C1–C2.

2.4.4. Measurement of nitrogen balanced index (NBI), flavonoids and anthocyanins by dualex machine

Nitrogen balance index (NBI), chlorophyll, flavonoids, and anthocyanins measurements were taken from at least three leaves from separate plants in each treatment. Each measurement of optical absorbance was recorded for the values of the four components, which were taken using the Dualex Scientific® machine (Dualex Scientific, Force-A, Orsay Cedex, France).

2.5. Analysis of photosynthetic pigments

Chlorophyll (Chl) *a*, Chl *b*, carotenoids, total Chl and Chl *a:b* ratio were measured according to Hiscox and Israelstam (1979). From each treatment, three leaf samples (~ 50 mg) were harvested from three different plants and were incubated at room temperature in 5 ml of dimethylsulfoxide for 24 hr in the dark until the pigments were completely bleached. After that 1 ml of each solution was placed into a cuvette and measured for absorbance at 664 nm, 648 nm, 470 nm using a UV-visible spectrophotometer (UV-550; Jasco, Japan). Concentrations of Chl *a*, Chl *b*, carotenoids, total Chl and Chl *a:b* were calculated from the absorbencies measured (Chappelle *et al.,* 1992).

2.6. Data analysis

The effects of temperature, CO$_2$, watering regime, and their interactions on the CH$_4$ emission and growth from Cyprus faba bean plants were determined using a general linear model procedure. A three-way analysis of variance from this output was used to determine the differences between normal (20/17°C) or heat stress (30/26°C) at a well-watered (watered to field capacity) or drought-

stressed (watered at leaf wilting point) state without supplying CO_2 or with supplying CO_2 (SAS Institute, 2011). A one-way ANOVA procedure was used to establish significant differences among each of the eight experimental treatments as well as among the three factors being manipulated, using Scheffé's multiple-comparison procedure at the 5% confidence level. For most of the parameters, three trials were used.

3. Results

3.1. Methane emissions

Methane emissions were greater in heat-stressed seedlings of faba bean than seedlings grown under normal temperatures (Table 1; Figure 1). However, less CH_4 emissions were detected when seedlings were grown under elevated CO_2 compared to those grown under ambient CO_2 (Table 1; Figure 1). Drought-stressed seedlings emitted more CH_4 than well-watered seedlings (Table 1; Figure 1). Temperature, CO_2, watering regime, the two–way interaction between temperature (T) × CO_2, CO_2 × watering regime (W), and the three–way interaction among T × CO_2 × W significantly affected CH_4 emissions (Table 2). The T × CO_2 interaction revealed that CH_4 emissions were significantly highest for seedlings grown under heat stress at ambient CO_2, but significantly lowest for seedlings grown under normal temperatures at elevated CO_2 (Figure 1). The CO_2 × W interaction showed that CH_4 emissions were significantly highest for drought-stressed seedlings at ambient CO_2, but significantly lowest for well-watered seedlings at elevated CO_2 (Figure 1). Based on the T × CO_2 × W interaction, CH_4 emissions were significantly highest for seedlings grown under heat, ambient CO_2 and drought-stressed, but significantly lowest for seedlings grown under normal temperatures, elevated CO_2 and well–watered (Figure 1).

Table 1. Individual effects of temperature, carbon dioxide and watering regime on methane emissions, growth, stress indicators, biochemical parameters and photosynthetic pigments of Cyprus faba beans (*Vicia faba* L.) seedlings.

Parameter	Temperature		Carbon dioxide		Watering regime	
	Normal	Heat	Ambient	Elevated	Well-watered	Drought-stressed
Methane (ng g^{-1} DM h^{-1})	33.06 ± 2.85B	48.34 ± 5.27A	48.59 ± 5.29A	32.81 ± 2.68B	31.46 ± 2.38B	49.93 ± 5.03A
Stem length (cm)	37.93 ± 3.11A	25.09 ± 1.53B	28.32 ± 2.93B	34.7 ± 3.02A	37.96 ± 3.03A	25.06 ± 1.67B
Stem diameter (mm)	0.47 ± 0.06A	0.30 ± 0.03B	0.33 ± 0.04B	0.44 ± 0.06A	0.49 ± 0.06A	0.28 ± 0.02B
Leaf area (cm^2 plant^{-1})	159.6 ± 15.83A	122.01 ±15.1B	130.04 ± 16.1B	151.57 ± 6.21A	189.71 ± 7.56A	91.89 ± 7.12B
Leaf number (plant^{-1})	10.7 ± 0.79A	7.54 ± 0.57B	8.36 ± 0.68B	9.89 ± 0.9A	10.87 ± 0.79A	7.38 ± 0.46B
Leaf moisture (%)	87.86 ± 2.14A	81.09 ± 2.93B	80.68 ± 2.57B	88.09 ± 2.47A	90.86 ± 1.56A	77.9 ± 2.26B
Root length (cm)	30 ± 3.64A	24.2 ± 1.59B	23.69 ± 2.83B	30.52 ± 2.69A	32.27 ± 2.96A	21.94 ± 1.93B
Stem fresh mass (g)	4.4 ± 0.52A	2.73 ± 0.3B	3.03 ± 0.47B	4.09 ± 0.47A	4.7 ± 0.46A	2.42 ± 0.22B
Leaf fresh mass (g)	3.54 ± 0.36A	2.36 ± 0.22B	2.67 ± 0.27B	3.23 ± 0.39A	3.77 ± 0.31A	2.13 ± 0.14B
Root fresh mass (g)	3.91 ± 0.43A	3.42 ± 0.42A	3.19 ± 0.44B	4.08 ± 0.38A	4.75 ± 0.29A	2.65 ± 0.21B
Total fresh biomass (g)	12.05 ± 1.28A	8.97 ± 0.74B	9.46 ± 1.05B	11.57 ± 1.14A	13.35 ± 1.0A	7.68 ± 0.39B
Stem dry mass (g)	3.6 ± 0.42A	2.15 ± 0.13B	2.56 ± 0.37B	3.19 ± 0.37A	3.59 ± 0.42A	2.17 ± 0.16B
Leaf dry mass (g)	3.02 ± 0.26A	1.73 ± 0.18B	2.16 ± 0.27A	2.59 ± 0.3A	2.86 ± 0.3A	1.88 ± 0.2B
Root dry mass (g)	3.34 ± 0.35A	3.39 ± 0.14A	3.17 ± 0.27A	4.08 ± 0.38A	3.92 ± 0.2A	2.8 ± 0.21B
Total dry biomass (g)	9.77 ± 0.97A	7.26 ± 0.36B	7.89 ± 0.82B	9.14 ± 0.78A	10.37 ± 0.79A	6.66 ± 0.32B
Leaf area ratio (LAR) (cm^2 g^{-1})	16.45 ± 0.62A	16.31 ± 1.21A	16.4 ± 0.52A	16.33 ±1.24A	18.19 ± 0.79A	14.52 ± 1.0B
Leaf mass area (LMA) (g m^{-2})	0.081 ± 0.008A	0.016 ±0.001B	0.018 ± 0.0017A	0.016 ± .0012A	0.014 ±0.0013A	0.019 ± 0.0015A
Leaf mass ratio (LMR)	0.29 ± 0.011A	0.23 ± 0.014B	0.27 ± 0.016A	0.26 ± 0.015A	0.27 ± 0.015A	0.25 ± 0.017A
Shoot:root dry wt. ratio	1.97 ± 0.1A	1.15 ± 0.08B	1.53 ± 0.16A	1.59 ± 0.15A	1.64 ± 0.15A	1.48 ± 0.15A
Proline (µmole g $^{-1}$ FM)	35.2 ± 3.75B	72.38 ±5.52A	59.53 ± 8.99A	48.05 ± 4.53B	44.59 ± 5.97B	62.99 ± 7.61A
MDA (µmole g $^{-1}$ FM)	0.31 ± 0.07A	0.18 ± 0.02A	0.29 ± 0.07A	0.2 ± 0.04A	0.16 ± 0.01B	0.33 ± 0.07A
Electrical conductivity (%)	16.9 ± 1.4B	31.4 ± 1.8A	27.5 ± 2.6A	20.9 ± 2.4B	20.8 ± 2.2B	27.7 ± 2.8A
Nitrogen balance index	89.92 ± 5.98A	80.67 ± 4.09B	86.73 ± 3.89A	83.22 ± 6.33A	98 ± 4.1A	71.95 ± 2.82B
Chlorophyll (µg cm^{-2} FM)	27.83 ± 1.37B	32.65 ±1.2A	28.37 ± 0.65B	32.11 ± 1.82A	27.73 ± 1.28A	23.75 ± 1.26B
Flavonoids (µg cm^{-2} FM)	0.36 ± 0.04B	0.44 ± 0.4A	0.34 ± 0.02B	0.46 ± 0.05A	0.3 ± 0.02B	0.5 ± 0.04A
Chl *a* (µg mg^{-1} FM)	2.1 ± 0.29A	2.45 ± 0.38A	2.04 ± 0.39A	2.51 ± 0.27A	2.83 ± 0.23A	1.72 ± 0.35B
Chl *b* (µg mg^{-1})	1.58 ± 0.22B	3.37 ± 0.26A	2.6 ± 0.38A	2.35 ± 0.34A	2.58 ± 0.34A	2.37 ± 0.38A
Carotenoids (µg mg^{-1} FM)	0.54 ± 0.08A	0.49 ± 0.05A	0.47 ± 0.06A	0.57 ± 0.07A	0.57 ± 0.07A	0.56 ± 0.08A
Total Chl (µg mg^{-1} FM)	3.68 ± 0.5B	5.82 ± 0.31A	4.46 ± 0.46A	4.86 ± 0.58A	4.86 ± 0.58A	4.09 ± 0.43B
Chl *a/b*	1.37 ± 0.09A	0.89 ± 0.16B	1.06 ± 0.18A	1.19 ± 0.1A	1.19 ± 0.1A	0.98 ± 0.17B

Cyprus faba bean seedlings were grown under normal temperatures (20/17°C) or heat stress (30/26°C), ambient CO_2 (400 ppm) or elevated CO_2 (800 ppm) and well-watered or drought-stressed conditions. Plants were grown under experimental conditions in controlled-environment glass cabinets for 14 days, following an initial germination period of 7 days and growth period of 5 days under greenhouse conditions. Data are means ± SE of at least 9 samples from three different experiments. Means ± SE followed by different upper-case letters within rows and factors are significantly different ($P < 0.05$) according to Scheffé's test.
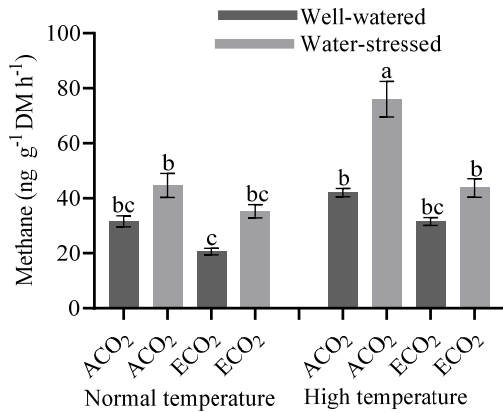
Figure 1. Methane emissions for 26-day-old Cyprus faba bean (*Vicia faba* L.) seedlings grown in controlled-environment glass cabinets for 14 days under eight experimental conditions including two temperature regimes, two CO_2 concentrations and two watering regimes after 12 days of initial germination and growth under greenhouse conditions. *ACO_2* ambient CO_2, *ECO_2* elevated CO_2

Table 2. Analysis of variance for the individual effects of temperature, carbon dioxide and watering regime and their interactions on methane emissions from Cyprus faba bean (*Vicia faba* L.) seedlings.

		Methane (ng g^{-1} DM h^{-1})
Source	df	
Temperature (T)	1	48.99*
Main plot error	2	-
Carbon dioxide (CO$_2$)	1	61.49**
T x CO$_2$	1	7.73*
Subplot error	4	-
Watering regime (W)	1	71.91****
T x W	1	4.5
CO$_2$ x W	1	5.34*
T x CO$_2$ x W	1	7.15*
Split-subplot error	8	-

Note: *$P < 0.05$; **$P < 0.01$; ***$P < 0.001$; ****$P < 0.0001$. Cyprus faba bean seedlings were grown under normal temperatures (20/17ºC) or heat stress (30/26ºC), ambient CO_2 (400 ppm) or elevated CO_2 (800 ppm) and well-watered or drought-stressed conditions. Plants were grown under experimental conditions in controlled-environment glass cabinets for 14 days, following an initial germination period of 7 days and growth period of 5 days under greenhouse conditions.

3.2. Plant growth

Elevated CO_2 increased stem length and diameter, leaf area and number, leaf moisture content and root length of seedlings, while heat and drought stresses decreased them in seedlings (Table 1; Figure 2A-F). Temperature, watering regime and the two–way interactions between T × W significantly affected stem height (Table 3). The T × W interaction revealed that seedlings grown under normal temperatures and well–watered were significantly the tallest, while those grown under heat and drought–stressed were significantly the shortest (Figure 2A). Temperature and watering regimes significantly affected stem diameter of the test plants (Table 3). Temperature, CO_2 and watering regimes significantly affected leaf area and number (Table 3). Moreover, leaf moisture content and root length were significantly affected by CO_2 and watering regimes (Table 3). Furthermore, root length was significantly affected by the two–way interaction between T × W (Table 3). The T × W interaction showed that roots of seedlings grown under normal temperatures and well–watered were significantly the tallest, while roots of seedlings grown under normal temperatures and drought–stressed were significantly the shortest (Figure 2F).
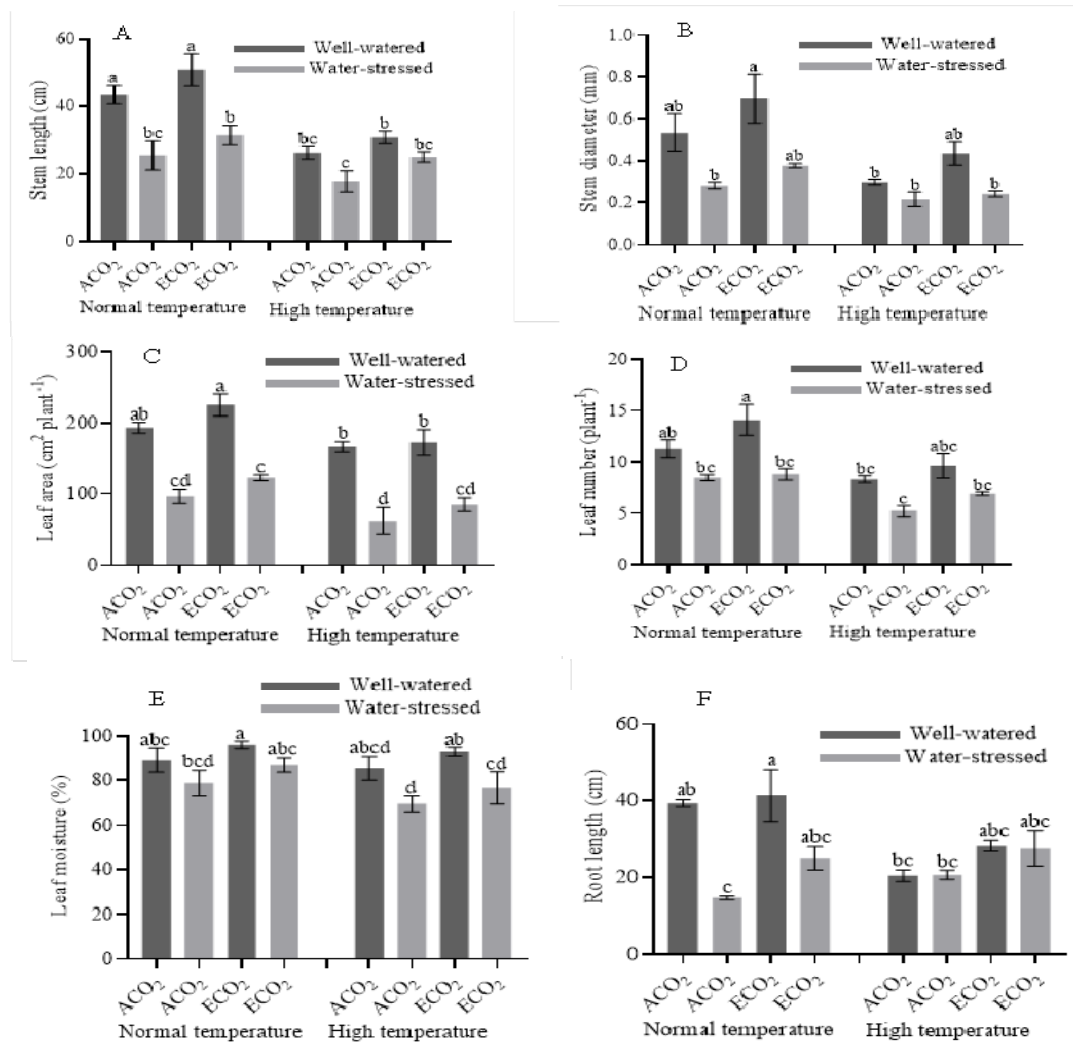
Figure 2. Stem length (A), stem diameter (B), leaf area (C), leaf number (D), leaf moisture content (E) and root length (F) for 26-day-old Cyprus faba bean (*Vicia faba* L.) seedlings grown in controlled-environment glass cabinets for 14 days under eight experimental conditions including two temperature regimes, two CO_2 concentrations and two watering regimes after 12 days of initial germination and growth under greenhouse conditions. *ACO_2* ambient CO_2, *ECO_2* elevated CO_2

Table 3. Analysis of variance for the individual effects of temperature, carbon dioxide and watering regime and their interactions on stem length, stem diameter, leaf area, leaf number, moisture content and root length of Cyprus faba bean (*Vicia faba* L.) seedlings.

		Stem height (cm)	Stem diameter (mm)	Leaf area (cm² plant⁻¹)	Leaf number (plant⁻¹)	Moisture content (%)	Root length (cm)
Source	df						
Temperature (T)	1	1480.4***	57.92*	97.34*	25.07*	5.10	4.27
Main plot error	2	-	-	-	-	-	-
Carbon dioxide (CO₂)	1	7.31	6.30	53.75**	11.47*	15.44*	12.24*
T x CO₂	1	0.03	0.31	6.53	0.00	0.00	0.10
Subplot error	4	-	-	-	-	-	-
Watering regime (W)	1	388.21****	23.87**	234.66****	62.27****	51.29****	16.46**
T x W	1	73.85****	2.89	0.08	1.71	3.14	15.68**
CO₂ x W	1	0.22	1.08	0.19	1.46	0.01	0.52
T x CO₂ x W	1	2.23	0.07	0.67	2.48	0.06	0.81
Split-subplot error	8	-	-	-	-	-	-

Note: *$P < 0.05$; **$P < 0.01$; ***$P < 0.001$; ****$P < 0.0001$. Cyprus faba bean seedlings were grown under normal temperatures (20/17°C) or heat stress (30/26°C), ambient CO_2 (400 ppm) or elevated CO_2 (800 ppm) and well-watered or drought-stressed conditions. Plants were grown under experimental conditions in controlled-environment glass cabinets for 14 days, following an initial germination period of 7 days and growth period of 5 days under greenhouse conditions.

3.3. Biomass accumulation

3.3.1. Fresh mass accumulation

Heat and drought stresses reduced stem (Table 1; Figure 3A), leaf (Table 1; Figure 3B), root (Table 1; Figure 3C) and total fresh biomass (Table 1; Figure 3D), but elevated CO_2 increased them (Table 1; Figure 3A-D). Stem, leaf, and total fresh biomasses were significantly affected by temperature, carbon dioxide, watering regime

and by the two–way interaction between T × W (Table 4). Root fresh mass was only significantly affected by watering regime (Table 4). For the T × W interaction, well-watered seedlings grown under normal temperatures had significantly the highest stem, leaf and total fresh biomass, whereas drought-stressed seedlings grown under heat stress had significantly the lowest stem, leaf and total fresh biomass (Figure 3A,B,D).
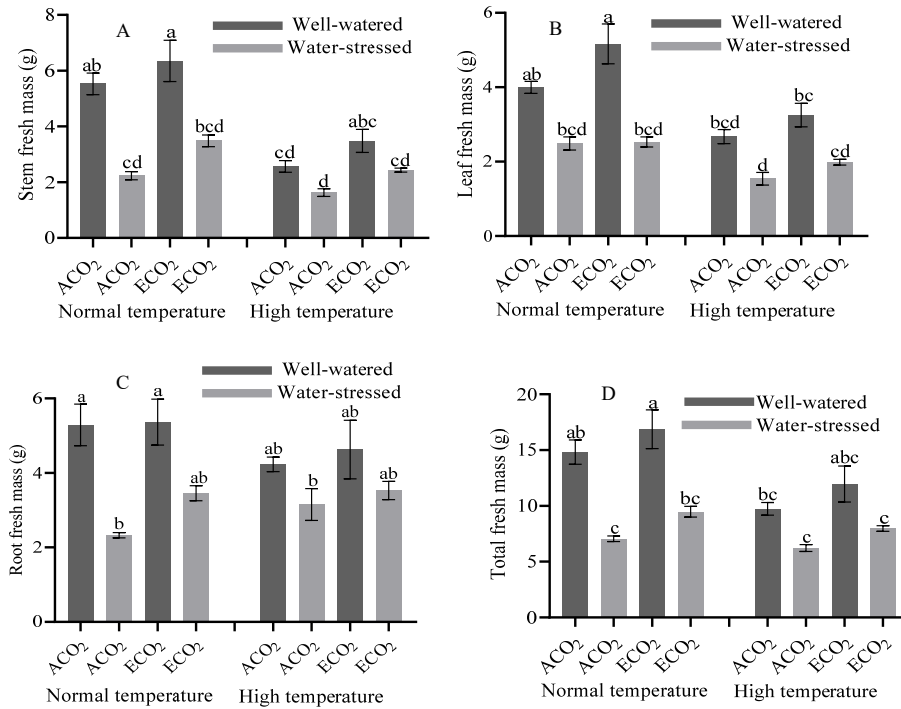

Figure 3. Stem fresh mass (A), leaf fresh mass (B), root fresh mass (C) and total fresh mass (D) for 26-day-old Cyprus faba bean (*Vicia faba* L.) seedlings grown in controlled-environment glass cabinets for 14 days under eight experimental conditions including two temperature regimes, two CO_2 concentrations and two watering regimes after 12 days of initial germination and growth under greenhouse conditions. *ACO_2* ambient CO_2, *ECO_2* elevated CO_2.

Table 4. Analysis of variance for the individual effects of temperature, carbon dioxide and watering regime and their interactions on stem fresh mass, leaf fresh mass, root fresh mass and total fresh biomass of Cyprus faba bean (*Vicia faba* L.) seedlings.

Note: *$P < 0.05$; **$P < 0.01$; ***$P < 0.001$; ****$P < 0.0001$. Cyprus faba bean seedlings were grown under normal temperatures (20/17°C)

	df	Stem fresh mass (g)	Leaf fresh mass (g)	Root fresh mass (g)	Total fresh biomass (g)
Source					
Temperature (T)	1	71.77*	66.63*	6.29	107.65**
Main plot error	2	-	-	-	-
Carbon dioxide (CO_2)	1	25.13**	14.94*	7.11	26.36**
T x CO_2	1	0.02	0.09	0.12	0.1
Subplot error	4	-	-	-	-
Watering regime (W)	1	91.29****	114.72****	39.21***	93.43****
T x W	1	11.54**	8.12*	1.03	10.67*
CO_2 x W	1	0.02	4.2	0.00	0.00
T x CO_2 x W	1	0.6	2.64	0.00	0.12
Split-subplot error	8	-	-	-	-

or heat stress (30/26°C), ambient CO_2 (400 ppm) or elevated CO_2 (800 ppm) and well-watered or drought-stressed conditions. Plants were grown under experimental conditions in controlled-environment glass cabinets for 14 days, following an initial germination period of 7 and growth period of 5 days under greenhouse conditions.

3.3.2. Dry mass accumulation

Seedlings grown under heat stress had lower stem, leaf and total dry biomass than seedlings grown under normal temperatures (Table 1; Figure 4A,B,D). Seedlings grown under elevated CO_2 had higher stem and total dry biomass than those grown under ambient CO_2 (Table 1; Figure 4A,D).

Drought-stressed seedlings had lower stem, leaf, root and total dry biomass than well-watered seedlings (Table 1; Figure 4A,B,C,D). Stem dry mass was significantly affected by temperature, carbon dioxide, watering regime and the two–way interactions between T × W (Table 5). Leaf dry mass was significantly affected by temperature and watering regime (Table 5). Root dry mass was significantly affected by watering regime and the two–way interactions between T × W (Table 5). Total dry biomass was significantly affected by temperature, carbon dioxide, watering regime and the two–way interaction between T × W (Table 5). The T × W interaction revealed that seedlings grown under normal temperatures and well–watered had significantly the highest stem and total dry biomass, whereas seedlings grown under heat and drought–stressed had significantly the lowest stem and total dry biomass (Figure 4A,D). The T × W interaction showed that seedlings grown under normal temperatures and well–watered had significantly the highest root dry mass, while those grown under normal temperatures and drought–stressed had significantly the lowest root dry mass (Figure 4C).
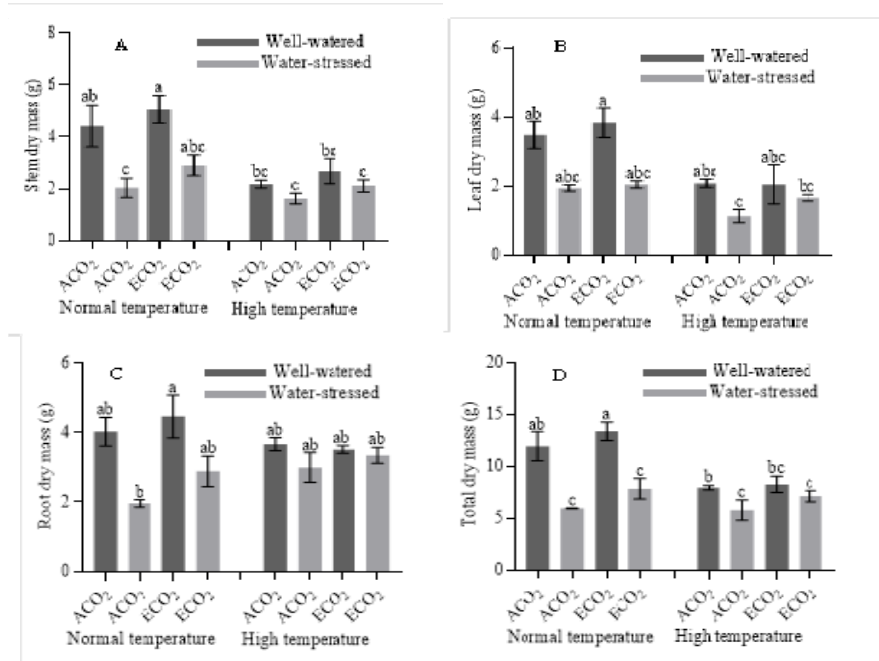

Figure 4. Stem dry mass (A), leaf dry mass (B), root dry mass (C) and total dry mass (D) for 26-day-old Cyprus faba bean (*Vicia faba* L.) seedlings grown in controlled-environment glass cabinets for 14 days under eight experimental conditions including two temperature regimes, two CO_2 concentrations and two watering regimes after 12 days of initial germination and growth under greenhouse conditions. *ACO₂* ambient CO_2, *ECO₂* elevated CO_2.

Table 5. Analysis of variance for the individual effects of temperature, carbon dioxide and watering regime and their interactions on stem dry mass, leaf dry mass, root dry mass and total dry biomass of Cyprus faba bean (*Vicia faba* L.) seedlings.

		Stem dry mass (g)	Leaf dry mass (g)	Root dry mass(g)	Total dry biomass (g)
Source	df				
Temperature (T)	1	19.07*	18.79*	0.03	27.23*
Main plot error	2	-	-	-	-
Carbon dioxide (CO_2)	1	28.36**	2.28	3.30	11.09*
T x CO_2	1	1.25	0.42	1.82	1.2
Subplot error	4	-	-	-	-
Watering regime (W)	1	37.07***	22.39**	21.12**	72.5****
T x W	1	13.54**	2.21	8.2*	22.27**
CO_2 x W	1	0.05	1.69	1.63	0.74
T x CO_2 x W	1	0.06	0.00	0.00	0.12
Split-subplot error	8	-	-	-	-

Note: *$P < 0.05$; **$P < 0.01$; ***$P < 0.001$; ****$P < 0.0001$. Cyprus faba bean seedlings were grown under normal (20/17°C) or heat stress (30/26°C), ambient CO_2 (400 ppm) or elevated CO_2 (800 ppm) and well-watered or drought-stressed conditions. Plants were grown under experimental conditions in controlled-environment glass cabinets for 14 days, following an initial germination period of 7 days and growth period of 5 days under greenhouse conditions.

3.4. Growth indices

Seedlings grown under heat stress had lower leaf mass area (LMA), leaf mass ratio (LMR) and shoot:root dry wt. ratio than seedlings grown under normal temperatures (Table 1; Figure 5B,C,D). Drought-stressed seedlings had lower leaf area ratio (LAR) than well-watered seedlings

(Table 1; Figure 5A). LAR was only significantly affected by watering regime (Table 6). Shoot:root dry wt. ratio was only significantly affected by temperature (Table 6). None of the interactions among the three main factors significantly affected any of the measured growth indices (Table 6).
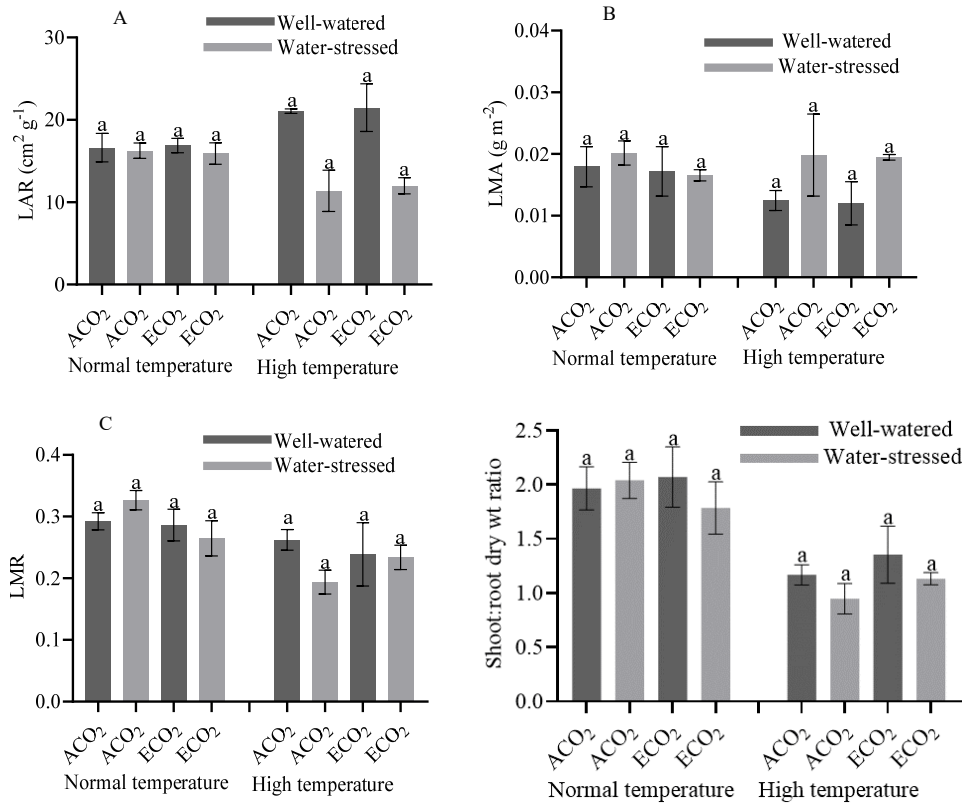

Figure 5. Growth indices for 26-day-old Cyprus faba bean (*Vicia faba* L.) seedlings grown in controlled-environment glass cabinets for 14 days under eight experimental conditions including two temperature regimes, two CO_2 concentrations and two watering regimes after 12 days of initial germination and growth under greenhouse conditions. LAR (A), LMA (B), LMR (C) and shoot:root dry wt ratio (D). *LAR* leaf area ratio, *LMA* leaf mass area, *LMR* leaf mass ratio, *ACO₂* ambient CO_2, *ECO₂* elevated CO_2.

Table 6. Analysis of variance for the individual effects of temperature, carbon dioxide and watering regime and their interactions on leaf area ratio, leaf mass area, leaf mass ratio and shoot:root dry wt. ratio of Cyprus faba bean (*Vicia faba* L.) seedlings.

		Leaf area ratio($cm^2 g^{-1}$)	Leaf mass area ($g m^{-2}$)	Leaf mass ratio	Shoot:root dry wt. ratio
Source	df				
Temperature (T)	1	0.00	0.61	7.92	202.78**
Main plot error	2	-	-	-	-
Carbon dioxide (CO_2)	1	0.08	0.76	0.98	0.15
T x C	1	0.11	0.35	2.66	0.84
Subplot error	4	-	-	-	-
Watering regime (W)	1	15.6**	3.24	0.58	1.38
T x W	1	11.81	2.11	1.15	0.17
C x W	1	0.01	0.09	0.01	0.42
T x C x W	1	0.02	0.11	2.2	0.41
Split-subplot error	8	-	-	-	-

Note: *$P < 0.05$; **$P < 0.01$; ***$P < 0.001$; ****$P < 0.0001$. Cyprus faba bean seedlings were grown under normal (20/17ºC) or heat stress (30/26ºC), ambient CO_2 (400 ppm) or elevated CO_2 (800 ppm) and well-watered or drought-stressed conditions. Plants were grown under experimental conditions in controlled-environment glass cabinets for 14 days, following an initial germination period of 7 days and growth period of 5 days under greenhouse conditions.

3.5. Proline, lipid peroxidation and electrical conductivity

Proline content was increased by heat and drought stresses, but decreased by elevated CO_2 in faba bean

seedlings (Table 1; Figure 6A). Significant effects of temperature, carbon dioxide, watering regime and the two–way interactions between T × CO_2 and CO_2 × W were observed on proline content (Table 4). For the T × CO_2 interaction, seedlings grown under heat stress and ambient

CO_2 had significantly the highest proline content, while those grown under normal temperatures and ambient CO_2 had significantly the lowest proline content (Figure 6A). The $CO_2 \times W$ interaction showed that seedlings grown under ambient CO_2 and drought-stressed had significantly the highest proline content, whereas seedlings grown under ambient CO_2 and well-watered had significantly the lowest proline content (Figure 6A).

Malondialdehyde (MDA) generation increased under drought-stressed condition in faba bean seedlings (Table 1; Figure 6B). MDA generation was significantly affected by carbon dioxide and watering regime (Table 7). None of the interactions among the three main factors had significant effect on the MDA content (Table 7).

Electrical conductivity was increased by heat and drought stresses, but decreased by elevated CO_2 in faba bean seedlings (Table 1; Figure 6C). Effects of temperature, carbon dioxide, watering regime, the two–way interactions between $T \times CO_2$, $T \times W$ and the three–

way interaction among $T \times CO_2 \times W$ were significant on the electrical conductivity (Table 7). The $T \times CO_2$ interaction revealed that seedlings grown under heat stress at ambient CO_2 resulted in significantly the highest electrical conductivity, but normal temperatures at ambient CO_2 resulted in significantly the least electrical conductivity in seedlings (Figure 6C). The $T \times W$ interaction showed that heat and drought–stressed seedlings had significantly the highest electrical conductivity, whereas those grown under normal temperatures and well-watered conditions had significantly the lowest electrical conductivity (Figure 6C). On the basis of the $T \times CO_2 \times W$ interactions, seedlings grown under heat stress, ambient CO_2, and drought–stressed conditions had significantly the highest electrical conductivity, whereas those grown under normal temperatures, ambient CO_2 and well-watered conditions had significantly the lowest electrical conductivity (Figure 6C).
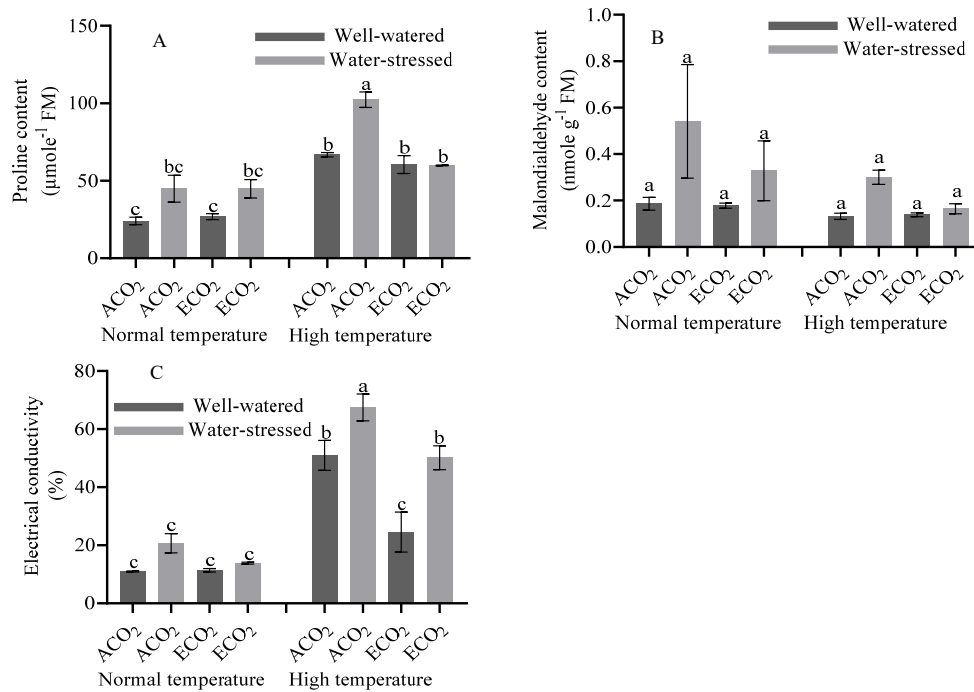

Figure 6. Proline content (A), Malondialdehyde content (B) and electrical conductivity (C) for 26-day-old Cyprus faba bean (*Vicia faba* L.) seedlings grown in controlled-environment glass cabinets for 14 days under eight experimental conditions including two temperature regimes, two CO_2 concentrations and two watering regimes after 12 days of initial germination and growth under greenhouse conditions. *ACO$_2$* ambient CO_2, *ECO$_2$* elevated CO_2.

3.6. Nitrogen balance index (NBI), chlorophyll and flavonoids

NBI decreased under heat and drought stress conditions in faba bean seedlings (Table 1; Figure 7A). NBI was significantly affected by temperature and watering regime, but not significantly affected by the interactions among the three main factors (Table 7).

Chlorophyll content was significantly increased by heat stress and elevated CO_2, but drought stress increased it (Table 1; Figure 7B). Chlorophyll content was significantly affected by all the main factors and the two–way interactions between $T \times CO_2$, $T \times W$ and $CO_2 \times W$ (Table 7). The $T \times CO_2$ interaction showed that elevated

CO_2 caused highest chlorophyll content for seedlings grown under heat stress, but elevated CO_2 caused lowest chlorophyll content for seedlings grown under normal temperatures (Figure 7B). The $T \times W$ interaction revealed that seedlings grown under heat stress and drought-stressed had the highest chlorophyll content, while those grown under normal temperatures and well-watered had the lowest chlorophyll content (Figure 7B). The $CO_2 \times W$ interaction showed that drought-stressed seedlings grown under elevated CO_2 had the highest chlorophyll content, whereas well-watered seedlings grown under elevated CO_2 had the lowest chlorophyll content (Figure 7B).
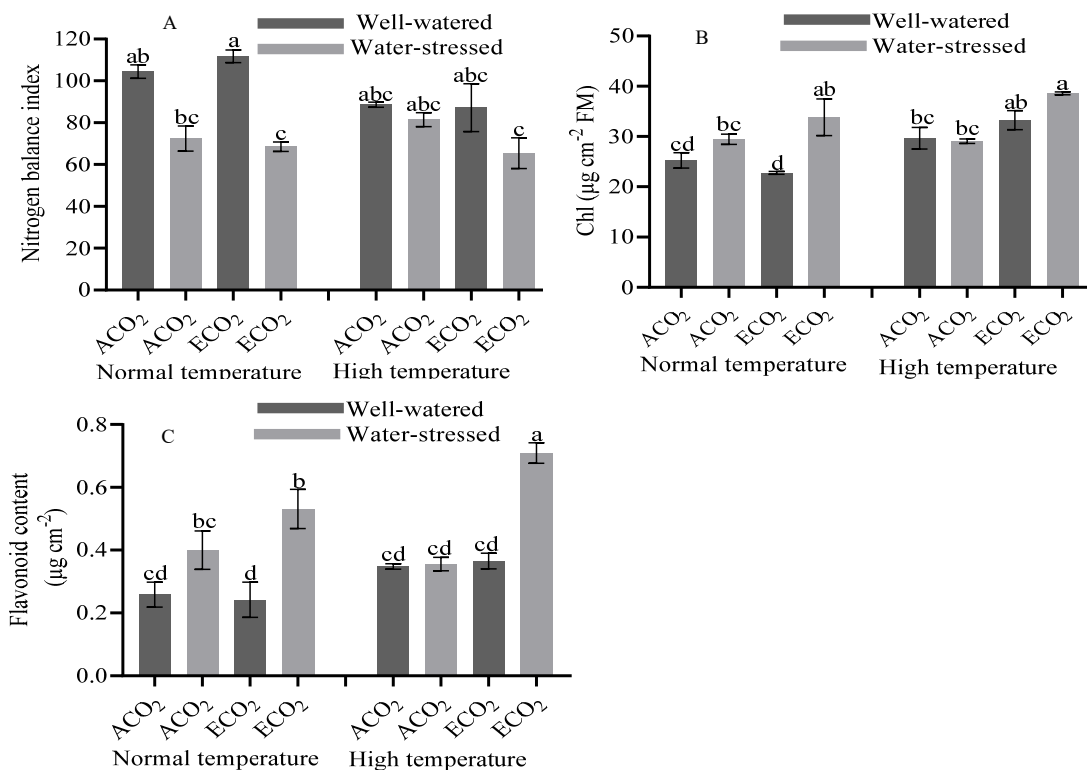
Figure 7. NBI (A), chlorophyll content (B) and flavonoid content (C) measured by Dualex machine for 26-day-old Cyprus faba bean (*Vicia faba* L.) seedlings grown in controlled-environment glass cabinets for 14 days under eight experimental conditions including two temperature regimes, two CO_2 concentrations and two watering regimes after 12 days of initial germination and growth under greenhouse conditions. *ACO2* ambient CO_2, *ECO2* elevated CO_2.

Table 7. Analysis of variance for the individual effects of temperature, carbon dioxide and watering regime and their interactions on proline content, MDA content, electrical conductivity, NBI, chlorophyll and flavonoids of Cyprus faba bean (*Vicia faba* L.) seedlings.

		Proline content ($\mu mole\ g^{-1}\ FM$)	MDA content ($\mu mole\ g^{-1}\ FM$)	Electrical conductivity (%)	NBI	Chlorophyll ($\mu g\ cm^{-2}\ FM$)	Flavonoids ($\mu g\ cm^{-2}\ FM$)
Source	df						
Temperature (T)	1	192.82**	1.91	272.05**	35.84*	21.84*	18.23
Main plot error	2	-	-	-	-	-	-
Carbon dioxide (CO_2)	1	14.59*	10.70*	62.01**	1.52	55.55**	79.15***
T x CO_2	1	18.25*	0.73	34.18**	3.37	31.2**	22.07**
Subplot error	4	-	-	-	-	-	-
Watering regime (W)	1	24.33**	5.41*	75.92****	25.82**	45.26***	101.69****
T x W	1	0.07	1.06	23.13**	5.11	12.33**	1.05
CO_2 x W	1	6.77*	1.33	0.09	1.59	18.41**	39.08***
T x CO_2 x W	1	5.01	0.04	6.91*	0.03	0.11	5.92*
Split-subplot error	8	-	-	-	-	-	-

Note: *$P < 0.05$; **$P < 0.01$; ***$P < 0.001$; ****$P < 0.0001$. Cyprus faba bean seedlings were grown under normal (20/17ºC) or heat stress (30/26ºC), ambient CO_2 (400 ppm) or elevated CO_2 (800 ppm) and well-watered or drought-stressed conditions. Plants were grown under experimental conditions in controlled-environment glass cabinets for 14 days, following an initial germination period of 7 days and growth period of 5 days under greenhouse conditions. NBI, chlorophyll content and flavonoid content were measured by Dualex machine.

3.7 Photosynthetic pigments

Overall, heat stress increased Chl *b* and total Chl, but decreased Chl *a:b* ratio (Table 1; Figure 8). Drought stress decreased Chl *a*, total Chl and Chl *a:b* ratio (Table 2; Figure 8).

Chl *a* content was significantly affected by carbon dioxide, watering regime, the two–way interactions of T × CO_2, T × W, CO_2 × W and the three–way interaction of T × CO_2 × W (Table 8). For the T × CO_2 interaction,

seedlings grown under heat stress and ambient CO_2 had significantly the highest and lowest Chl *a* content (Figure 8A). The T × W interaction revealed that seedlings grown under heat stress and well–watered had significantly the highest Chl *a* content, while those grown under heat stress and drought-stressed had significantly the lowest Chl *a* content (Figure 8A). The CO_2 × W interaction showed that seedlings grown under ambient CO_2 and well-watered had significantly the highest Chl *a* content, whereas seedlings

grown under ambient CO_2 and drought-stressed had significantly the lowest Chl *a* content (Figure 8A). Based on the T × CO_2 × W interaction, seedlings grown under heat stress, ambient CO_2 and well-watered conditions had significantly the highest Chl *a* content, whereas seedlings grown under heat stress, ambient CO_2 and drought-stressed conditions had significantly the lowest Chl *a* content (Figure 8A).

Chl *b* content was significantly affected by the two–way interaction of CO_2 × W and the three–way interaction of T × CO_2 × W (Table 8). For the CO_2 × W interaction, seedlings grown under ambient CO_2 and drought-stressed had significantly the highest Chl *b* content, whereas seedlings grown under elevated CO_2 and drought-stressed had significantly the lowest Chl *b* content (Figure 8B). On the basis of the T × CO_2 × W interaction, seedlings grown under heat stress, ambient CO_2 and drought-stressed conditions had significantly the highest Chl *b* content, whereas seedlings grown under normal temperatures, elevated CO_2 and drought-stressed conditions had significantly the lowest Chl *b* content (Figure 8B).

Carotenoid content was significantly affected by the carbon dioxide and the two–way interaction of CO_2 × W (Table 8). The CO_2 × W interaction showed that seedlings grown under elevated CO_2 and drought-stressed had

seedlings grown under ambient CO_2 and drought-stressed had significantly the lowest carotenoid content (Figure 8C).

Total Chl was significantly affected by watering regime, but not significantly affected by the interactions among the three main factors (Table 8).

Chl *a:b* ratio was significantly affected by the three main factors, the two–way interactions of T × CO_2, CO_2 × W and the three–way interaction of T × CO_2 × W (Table 8). The T × CO_2 interaction indicated that seedlings grown under normal temperatures and elevated CO_2 had significantly the highest Chl *a:b* ratio, while those grown under heat stress and ambient CO_2 had significantly the lowest Chl *a:b* ratio (Figure 8E). The CO_2 × W interaction revealed that seedlings grown under elevated CO_2 and well-watered had significantly the highest Chl *a:b* ratio, while those grown ambient CO_2 and drought-stressed had significantly the lowest Chl *a:b* ratio (Figure 8E). Based on the interactions among T × CO_2 × W, seedlings grown under normal temperatures, elevated CO_2 and well-watered conditions had significantly the highest Chl *a:b* ratio, whereas seedlings grown under heat stress, ambient CO_2 and drought-stressed conditions had significantly the lowest Chl *a:b* ratio (Figure 8E).
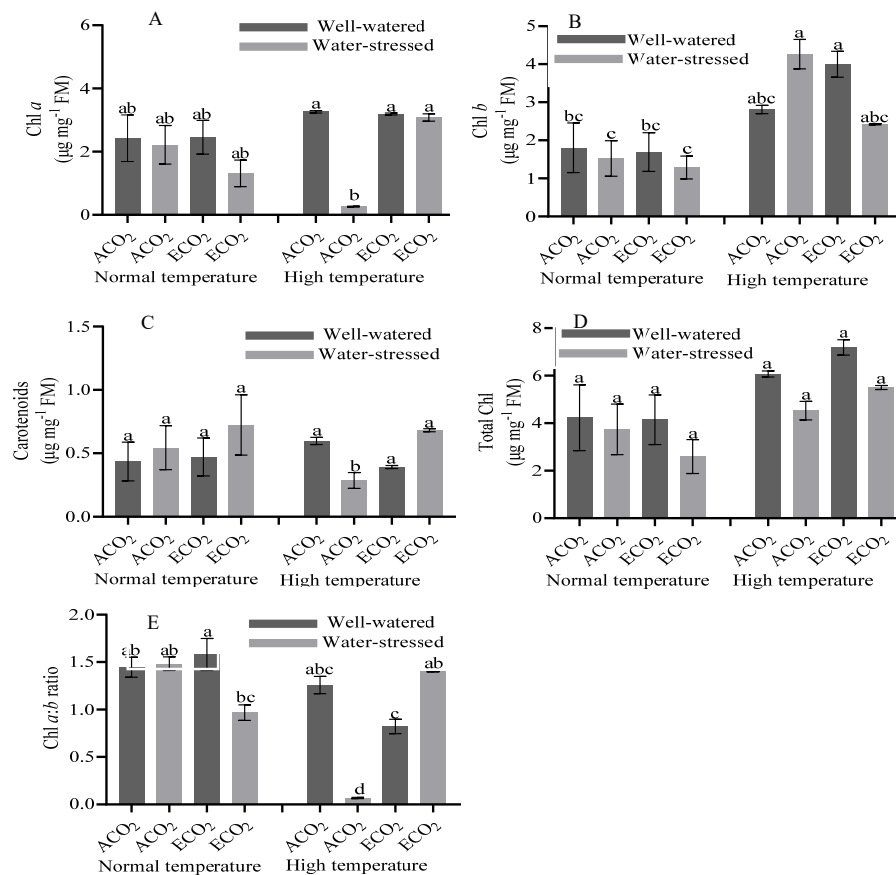
significantly the highest carotenoid content, while

Figure 8. Chl *a* (A), Chl *b* (B), carotenoids (C), total Chl (D) and Chl *a:b* ratio (E) for 26-day-old Cyprus faba bean (*Vicia faba* L.) seedlings grown in controlled-environment glass cabinets for 14 days under eight experimental conditions including two temperature regimes, two CO_2 concentrations and two watering regimes after 12 days of initial germination and growth under greenhouse conditions. *ACO₂* ambient CO_2, *ECO₂* elevated CO_2.

Table 8. Analysis of variance for the individual effects of temperature, carbon dioxide and watering regime and their interactions on Chl *a*, Chl *b*, carotenoids, total Chl and Chl *a/b* ratio of Cyprus faba bean (*Vicia faba* L.) seedlings.

Source	df	Chl *a* (μg mg^{-1} FM)	Chl *b* (μg mg^{-1} FM)	Carotenoids (μg mg^{-1} FM)	Total Chl (μg mg^{-1} FM)	Chl *a:b* ratio
Temperature (T)	1	0.36	14.92	0.10	4.25	29.18*
Main plot error	2	-	-	-	-	-
Carbon dioxide (CO_2)	1	18.55*	2.25	8.34*	0.98	45.14**
T x CO_2	1	69.61**	0.20	0.03	14.45	277.79****
Subplot error	4	-	-	-	-	-
Watering regime (W)	1	444.23****	1.14	2.69	32.89***	17.64**
T x W	1	69.43****	0.56	3.39	1.71	0.02
CO_2 x W	1	85.03****	17.38**	12.91**	1.70	15.62**
T x CO_2 x W	1	325.7****	14.72**	4.87	1.00	73.01****
Split-subplot error	8	-	-	-	-	-

Note: *P < 0.05; **P < 0.01; ***P < 0.001; ****P < 0.0001. Cyprus faba bean seedlings were grown under normal (20/17ºC) or heat stress (30/26ºC), ambient CO_2 (400 ppm) or elevated CO_2 (800 ppm) and well-watered or drought-stressed conditions. Plants were grown under experimental conditions in controlled-environment glass cabinets for 14 days, following an initial germination period of 7 days and growth period of 5 days under greenhouse conditions.

4. Discussion

Results from this study show that heat stress significantly increased CH$_4$ emissions, proline content, electrolyte leakage, Chl content measured by Dualex Scientific, flavonoids, Chl *b* and total Chl, but decreased plant growth parameters, leaf moisture content, fresh and dry mass accumulation except for root fresh and dry mass, LMA, LMR, shoot:root dry wt ratio, NBI and Chl *a:b* ratio in seedlings (Table 1).

In line with our results, heat stress enhanced CH$_4$ emissions (Table 1) from faba bean seedlings (Gautam *et al.,* 2024). The increase of proline content in seedlings grown under heat stress (Table 1) is inconsistent with previous study on Giza faba bean (Abo Gamar *et al.,* 2023) and other plant species (Jiang *et al.,* 2023). The increase in the electrolyte leakage under heat stress indicates the inability of plants to prevent oxidative damage of their cell membranes (Alamri *et al.,* 2014). Chlorophyll measured by Dualex Scientific, Chl *b*, and total Chl was significantly increased under heat stress (Table 1), which was contrary to expectations. However, Chl *a* has been suggested as precursor of CH4 in phytoplanktons (Ordóñez *et al.,* 2023). Since heat stress increases the level of reactive oxygen species (ROS) within the leaves, increased flavonoids (Table 1) is likely both a method of protection against oxidative damage as well as a mechanism to induce abiotic stress tolerance in faba bean seedlings (Ernst *et al.,* 2022). The reduction in growth parameters and leaf moisture content (Table 1) because of heat stress led to biomass decrease of different plant parts and is consistent with earlier studies on cucumber (*Cucumis sativus* L.) (Hongal *et al.,* 2023). Furthermore, heat stress might have also decreased growth in faba bean seedlings through reducing photosynthesis via the inactivation of the Rubisco (ribulose-1,5-bisphosphate carboxylase/ oxygenase) enzyme (Way and Oren, 2010). Reduced LMA and LMR caused by heat stress (Table 1) could result from the production of smaller and thicker leaves, which might be an adaptation to decrease loss of water from leaves of stressed seedlings. Moreover, reduction in shoot:root dry wt ratio (Table 1) could be another mechanism of adaptation to help stressed seedlings to manage their water

balance and survive under heat stress condition. NBI is a patented calculation that estimates the levels of nitrogen nutrition by establishing a ratio of chlorophyll to flavonoids. A lower NBI under heat stress (Table 1) indicates alterations to the allocation of carbon/nitrogen in leaves to produce more flavonoids, which is consistent with the increase in flavonoid content in our plants. Heat stress was shown to increase the chlorophyll a/b contents (Zahra *et al.,* 2023), which is in agreement with our results.

Elevated CO_2 significantly increased plant growth parameters and leaf moisture content, fresh and dry mass accumulation, chlorophyll measured by Dualex Scientific, flavonoids, but decreased CH$_4$ emissions, proline content and electrolyte leakage in seedlings (Table 1). It has been well acknowledged that elevated CO_2 enhances growth and biomass of plants by increasing the photosynthesis rate of leaves and water use efficiency, and decreasing the transpiration rate (Wei *et al.,* 2022). Increase of chlorophyll content (Table 1) in seedlings grown under elevated CO_2 is inconsistent with previous studies on basil (*Ocimum basilicum* L.) (Barickman *et al.,* 2022). The increase in flavonoid content (Table1) under elevated CO_2 indicated the increase of seedling abilities to reallocate the extra nitrogen, carbon and other crucial materials away from the photosynthetic machinery to synthesize antioxidant-defense materials, such as flavonoids. Moreover, it has been shown that elevated CO_2 concentration mitigates stress-induced emissions of CH$_4$ from plants by preventing photorespiration (Mattoo and B M, 2023), which has been suggested as one of the main causes for CH$_4$ emissions from plants under stress conditions. In our study, elevated CO_2 reduced proline content (Table 1), which is in agreement with previous studies on faba bean (*Vicia faba* L.) (Abo Gamar *et al.,* 2023) and maize (*Zea mays* L.) (Vanaja *et al.,* 2024). Seedlings grown under elevated CO_2 had lower electrolyte leakage (Table 1), which indicates that CO_2 protect cell membranes by alleviating oxidative stress enhanced by stress factors (Shabbaj *et al.,* 2021).

Drought stress increased CH$_4$ emissions, proline, MDA content, electrolyte leakage, and flavonoids, but decreased plant growth parameters and leaf moisture content, fresh and dry mass accumulation, LAR, NBI, chlorophyll

measured by Dualex Scientific, Chl *a*, total Chl and Chl *a/b* ratio in seedlings (Table 1). Our results showed that drought stress enhanced plant CH_4 emissions (Table 1), which supports previous results that drought-stressed plants emit more CH_4 than well-watered plants (Zhou et al., 2021). CH_4 has been shown to reduce osmotic stress induced on mung bean (*Vigna radiata* L.) plants by polyethyleneglycol (PEG), through regulating the status of reactive oxygen species (ROS), which enhance homeostasis of sugar, ascorbic acid, and glutathione (Zhang *et al.,* 2018). Drought stress enhanced proline content in faba bean seedlings (Table 1). Proline has been found to have a role in protecting and stabilizing different antioxidant enzymes, such as superoxide dismutase (Khatun *et al.,* 2020). Reactive oxygen species has been found to enhance the MDA content in drought-stressed plants, which might be led to membrane injury (Hassan *et al.,* 2020) and increasing electrical conductivity in tested plants. An increase of flavonoids in drought-stressed seedlings (Table 1) shows an increase in antioxidant contents. Because drought stress increases the level of ROS within the leaves, increased flavonoids is likely both a method of protection against oxidative damage as well as a mechanism to induce abiotic stress tolerance by reducing photorespiration (Bita and Gerats, 2013) and, in turn, reducing CH_4 emissions. Reduction in the growth and biomass of drought-stressed seedlings (Table 1) is expected and in agreement with findings on faba bean (*Vicia faba* L.) (Kibbou *et al.,* 2022; Abo Gamar *et al.,* 2023). Decreased LAR in drought-stressed seedlings (Table 1) may have contributed to the reduced biomass. A significant reduction in nitrogen balance index (NBI) supports the significant changes in flavonoids, chlorophyll measured by Dualex Scientific, Chl *a* and Total Chl (Table 1), as a decreased NBI suggests that nitrogen fertility is low, and the plant is allocating resources to regenerating flavonoids as opposed to making chlorophyll (Tremblay *et al.,* 2012). This could contribute to the decrease in net photosynthesis of drought-stressed faba bean seedlings and, in turn, reduction in their growth and biomass. The reduction in the Chl *a/b* ratio (Table 1) in drought-stressed seedlings could be explained by the decrease of Chl *a* and the increase of Chl *b*.

Climate change is inevitable within our lifetime, even if the production of greenhouse gases is stopped today (IPCC 2013). In this study, from 33 cases of interactions, 26 of two-way (see Tables 2, 3, 4, 5, 7, and 8) and 7 of three-way interactions (see Tables 2, 7, and 8) were significant. Plant parameters were significantly affected by T × CO_2 in 7 cases (see Tables 2, 7 and 8), by T × W in 11 cases (see Tables 3, 4, 5, 7, and 8), by CO_2 × W in 8 cases (see Tables 2, 7 and 8), and by T × CO_2 × W in 7 cases (see Tables 2, 7 and 8).

In agricultural systems, heat and drought stresses, which result in more methane emissions and smaller plants, can have large impacts on crop performance and yield. Elevated CO_2 mitigated many of the negative effects of increased temperature and drought stress on plants. Thus, it is important to study the individual effects of the main climate change factors (temperature, CO_2 and watering regime) along with their combined effects on methane emissions and growth of plants.

The interaction of all three factors (T × CO_2 × W) mainly had significant effects on CH_4 emissions (Table 2),

electrolyte leakage (Table 7), flavonoids (Table 7), Chl *a*, Chl *b* and Chl *a/b* ratio (Table8.). CH_4 emissions were significantly highest for seedlings grown under heat stress, ambient CO_2 and drought-stressed, but significantly lowest for seedlings grown under normal temperatures, elevated CO_2 and well–watered (Table 2; Figure 1). It has been suggested that CH_4 could enhance the resistance of plants to different types of abiotic stress by supporting their antioxidant defense system (Gautam *et al.,* 2024). Moreover, it was shown that CH_4 emissions from plants have a major role in protecting them from ROS, functioning as an important signaling molecule, and controlling multiple stress associated genes in plants that influence their growth and development (Gautam *et al.,* 2024).

Seedlings grown under heat stress, ambient CO_2, and water–stressed conditions had significantly the highest electrical conductivity, whereas those grown under normal temperatures, ambient CO_2 and well-watered conditions had significantly the lowest electrical conductivity (Table 7; Figure 6C), which agrees with earlier study on faba bean (*Vicia faba* L.) (Abo Gamar *et al.,* 2023). Flavonoid content was significantly highest for seedlings grown under heat stress, elevated CO_2 and drought-stressed, but significantly lowest for seedlings grown under normal temperature, elevated CO_2 and well–watered (Table 7; Figure 7C). Total antioxidant capacity was shown to significantly enhanced by the combination of heat and drought stresses, and to a higher extent at elevated CO_2 (Zinta *et al.,* 2018). More flavonoid content in seedlings grown under heat and drought stresses, individually and together, indicated increased antioxidant capacity. Because the combination of heat and drought stresses increases the concentration of ROS in plant leaves, increased flavonoids may be protecting plants against being damaged by oxidation (Tourky *et al.,* 2023). Our study revealed that the combination between heat and drought stresses decreased Chl *a* and Chl *a:b* ratio, but increased Chl *b* (Table 8; Figure 8). On the other hand, elevated CO_2 didn't affect Chl *a* under the combination of stress factors and negatively affected Chl *b* under drought stress (Table 8; Figure 8). It is clear, from these results, that the combination of heat and drought stresses had antagonistic effects with elevated CO_2 on photosynthetic pigments, and that elevated CO_2 had negative effects on photosynthetic pigments. It is possible that the variations in photosynthetic pigments, particularly in Chl *a*, could have affected gas exchange and, consequently, affected faba bean seedlings growth and biomass.

5. Conclusions

Studies focusing on addressing the effects of an individual environmental factor on methane emissions from plants and their growth and development may not give a correct or truthful scenario of the response of plants to future climates. It is important to study the combination of as many environmental components as possible, with superior focus being employed on those environmental factors (heat, elevated CO_2 and drought stress) that have the potential to change under the future climate change scenario. Our results showed that these three factors may modify CH_4 emissions from plant bodies and imposed some consequences for future climate. Heat and drought

stresses caused seedlings to emit more CH_4 at present atmospheric CO_2. Elevated CO_2 decreased aerobic CH_4 emissions, but cannot completely inverse the enhancement effects of heat and drought stresses on CH_4 emissions from plants. Moreover, elevated CO_2 antagonize stress effects of heat and drought stresses on seedlings mainly by enhancing their antioxidant activities through increasing flavonoid and improving plant chlorophyll and water contents.

Regardless of the small input of CH_4 emissions to the global CH_4 budget from plants, environmental stressors will proliferate in the upcoming days, resulting in an increased influence of this source of CH_4 to the worldwide budget.

Acknowledgement

Conflicts of Interest

Authors declare no conflict of interest.

References

Abo Gamar M, Muhaidat R, Fhely T, Abusahyoun F and Al-Deeb T. 2023. The impact of selected ecological factors on the growth and biochemical responses of Giza faba bean (*Vicia faba* L.) seedlings. *Jordan J. Biol. Sci.*, **16:** 307-321.

AghaKouchak A, Chiang F, Huning LS, Love CA, Mallakpour I, Mazdiyasni O, Moftakhari H, Papalexiou SM, Ragno E and Sadegh M. 2020. Climate extremes and compound hazards in a warming world. *Annu. Rev. Earth Planet. Sci.*, **48:** 519-48.

Alamri SA, Siddiqui MH, Al-Khaishany MY, Khan MN, Ali HM and Alakeel KA. 2019. Nitric oxide-mediated cross-talk of proline and heat shock proteins induce thermotolerance in *Vicia faba* L. *Environ. Exp. Bot.*, **161:** 290-302.

Barickman TC, Brazel SR, Sehgal A, Walne CH and Reddy KR. 2022. Daily UV-B treatments and elevated CO_2 increases pigment concentrations and net photosynthesis of basil (*Ocimum basilicum* L.). *Technol. Hortic.*, **2:** 1-7.

Bates LS, Waldren RP and Teare I. 1973. Rapid determination of free proline for water-stress studies. *Plant Soil*, **39:** 205-207.

Bita CE and Gerats T. 2013. Plant tolerance to high temperature in a changing environment: scientific fundamentals and production of heat stress-tolerant crops. *Front. Plant Sci.*, **4:** 273.

Chai F, Li L, Xue S and Liu J. 2020. Auxiliary voltage enhanced microbial methane oxidation co-driven by nitrite and sulfate reduction. *Chemosphere*, **250:** 126259.

Chappelle EW, Kim MS and McMurtrey III JE. 1992. Ratio analysis of reflectance spectra (RARS): an algorithm for the remote estimation of the concentrations of chlorophyll a, chlorophyll b, and carotenoids in soybean leaves. *Remote Sens. Environ.*, **39:** 239-247.

Davies RW, Kozior M, Lynch AE, Bass JJ, Atherton PJ, Smith K and Jakeman PM. 2022. The effect of fava bean (*Vicia faba* L.) protein ingestion on Myofibrillar protein synthesis at rest and after resistance exercise in healthy, young men and women: a randomised control trial. *Nutrients*, **14:** 3688.

Ernst L, Steinfeld B, Barayeu U, Klintzsch T, Kurth M, Grimm D, Dick TP, Rebelein JG, Bischofs IB and Keppler F. 2022. Methane formation driven by reactive oxygen species across all living organisms. *Nature*, **603:** 482-487.

Gautam H, Khan S, Nidhi, Sofo A and Khan NA. 2024. Appraisal of the role of gaseous signaling molecules in thermo-tolerance mechanisms in plants. *Plants*, **13:** 791.

Hassan N, Ebeed H and Aljaarany A. 2020. Exogenous application of spermine and putrescine mitigate adversities of drought stress in wheat by protecting membranes and chloroplast ultra-structure. *Physiol. Mol. Biol. Pla.*, **26:** 233-45.

Hiscox J and Israelstam G. 1979. A method for the extraction of chlorophyll from leaf tissue without maceration. *Canad. J. Bot.*, **57:** 1332-1334.

Hobdari V, Jani S, Hoxha E, Elezi F and Robert D. 2023. Phenotypic characterization of the accessions of faba bean (*Vicia Faba* L.) stored in the genetic bank of Albania. *Agric. For.*, **69:** 117-130.

Hongal DA, Raju D, Kumar S, Talukdar A, Das A, Kumari K, Dash PK, Chinnusamy V, Munshi AD, Behera TK and Dey SS. 2023. Elucidating the role of key physio-biochemical traits and molecular network conferring heat stress tolerance in cucumber. *Front. Plant Sci.*, **14:** 1128928.

IPCC. 2013. Climate change 2013: Summary for policymakers. Contribution of working groups I, II, and III to the fifth assessment report of the Intergovernmental Panel on Climate Change. IPCC, Geneva, Switzerland.

Jiang J, Guo Z, Sun X, Jiang Y, Xie F and Chen Y. 2023. Role of proline in regulating turfgrass tolerance to abiotic stress. *Grass Res.*, **3:** 1-7.

Khatun M, Matsushima D, Rhaman MS, Okuma E, Nakamura T, Nakamura Y, Munemasa S and Murata Y. 2020. Exogenous proline enhances antioxidant enzyme activities but does not mitigate growth inhibition by selenate stress in tobacco BY-2 cells. *Biosci. Biotechnol. Biochem.*, **84:** 2281-2292.

Kibbou F, El Bouhmadi K, Marrou H, Sinclair TR and Ghanem ME. 2022. Impact of drought and temperature constraints on development and growth of faba bean (*Vicia faba* L.). *J. Crop Improv.*, **36:** 57-72.

Lomborg B. 2020. **False alarm: How climate change panic costs us trillions, hurts the poor, and fails to fix the planet**, Hachette, UK.

Mattoo R and B M, S. 2023. Millet's Rhizosphere metagenomics for the understanding of rhizobiome multifunctionalities. In: Pudake, R.N., Kumari, M., Sapkal, D.R., Sharma, A.K. (eds) Millet Rhizosphere. **Rhizosphere Biology.** Springer, Singapore, pp. 239-257.

Ordóñez C, DelSontro T, Langenegger T, Donis D, Suarez EL and McGinnis DF. 2023. Evaluation of the methane paradox in four adjacent pre-alpine lakes across a trophic gradient. *Nat. Commun.*, **14:** 2165.

Rakhmankulova Z, Shuyskaya E, Prokofieva M, Toderich K, Saidova L, Lunkova N and Voronin P. 2024. Drought has a greater negative effect on the growth of the C_3 *Chenopodium quinoa* crop halophyte than elevated CO_2 and/or high temperature. *Plants*, **13:** 1666.

SAS Institute. 2011. SAS/STAT User''s Guide. Version 9.3. SAS Institute, Cary, North Carolina.

Shabbaj II, AbdElgawad H, Tammar A, Alsiary WA and Madany MM. 2021. Future climate CO_2 can harness ROS homeostasis and improve cell wall fortification to alleviate the hazardous effect of Phelipanche infection in pea seedlings. *Plant Physiol. Biochem.*, **166:** 1131-41.

Thalji T. 2015. agronomical assessment of faba bean (*Vicia faba* L.) cultivars on seed yield and production components under

different ecological conditions in Jordan. *Aust. J. Basic & Appl. Sci.*, **9:** 315-318.

Tourky SM, Shukry WM, Hossain MA, Siddiqui MH, Pessarakli M and Elghareeb EM. 2023. Cobalt enhanced the drought-stress tolerance of rice (*Oryza sativa* L.) by mitigating the oxidative damage and enhancing yield attributes. *S. Afr. J. Bot.*, **159:** 191-207.

Tremblay N, Wang Z and Cerovic ZG. 2012. Sensing crop nitrogen status with fluorescence indicators. A review. *Agron. Sustain. Dev.*, **32:** 451-64.

Turner JC, Moorberg CJ, Wong A, Shea K, Waldrop MP, Turetsky MR and Neumann RB. 2020. Getting to the root of plant-mediated methane emissions and oxidation in a thermokarst bog. *J. Geophys. Res. G: Biogeosciences.*, **125:** e2020JG005825.

Vanaja M, Sarkar B, Sathish P, Jyothi Lakshmi N, Yadav SK, Mohan Ch, Sushma A, Yashavanth BS, Srinivasa Rao M, Prabhakar M and Singh VK. 2024. Elevated CO_2 ameliorates the high temperature stress effects on physio-biochemical, growth, yield traits of maize hybrids. *Sci. Rep.*, **14:** 2928.

Vijayalakshmi D, Priya JR, Vinitha A and Ramya G. 2024. Interactive effects of elevated CO_2 with combined heat and drought stresses on the physiology and yield of C_3 and C_4 plants. *J. Crop Sci. Biotechnol.*, **27:** 1-6.

Wang G, Xia X, Liu S, Zhang L, Zhang S, Wang J, Xi N and Zhang Q. 2021. Intense methane ebullition from urban inland waters and its significant contribution to greenhouse gas emissions. *Water Res.*, **189:** 116654.

Warsame AO, Michael N, O'Sullivan DM and Tosi P. 2022. Seed development and protein accumulation patterns in faba bean (*Vicia faba* L.). *J. Agric. Food Chem.*, **70:** 9295-304.

Way DA and Oren R. 2010. Differential responses to increased growth temperatures between trees from different functional groups and biomes: a review and synthesis of data. *Tree Physiol.*, **30:** 669-688.

Wei Z, Abdelhakim LO, Fang L, Peng X, Liu J and Liu F. 2022. Elevated CO_2 effect on the response of stomatal control and water use efficiency in amaranth and maize plants to progressive drought stress. *Agric. Water Manag.*, **266:** 107609.

Yao Y, Song Y, Su P, Wang J, Miao C, Luo Y, Sun Q, Wang J, Zhang G, Bu N and Li Z. 2023. Asymmetric responses of functional microbes in methane and nitrous oxide emissions to plant invasion: A meta-analysis. *Soil Biol. Biochem.*, **178:** 108931.

Zahra N, Hafeez MB, Ghaffar A, Kausar A, Al Zeidi M, Siddique KH and Farooq M. 2023. Plant photosynthesis under heat stress: effects and management. *Environ. Exp. Bot.*, **206:** 105178.

Zandalinas SI, Fritschi FB and Mittler R. 2021. Global warming, climate change, and environmental pollution: recipe for a multifactorial stress combination disaster. *Trends Plant Sci.*, **26:** 588-99.

Zhang Y, Su J, Cheng D, Wang R, Mei Y, Hu H, Shen W and Zhang Y. 2018. Nitric oxide contributes to methane-induced osmotic stress tolerance in mung bean. *BMC Plant Biol.*, **18:** 1-2.

Zhou X, Smaill SJ, Gu X and Clinton PW. 2021. Manipulation of soil methane oxidation under drought stress. *Sci. Total Environ.*, **757:** 144089.

Zinta G, AbdElgawad H, Peshev D, Weedon JT, Van den Ende W, Nijs I, Janssens IA, Beemster GT and Asard H. 2018. Dynamics of metabolic responses to periods of combined heat and drought in *Arabidopsis thaliana* under ambient and elevated atmospheric CO_2. *J. Exp. Bot.*, **69:** 2159-70.

Name: …………………………………………………………………..………………….: الاسم

Specialty: ……………………………………………………………..………………….: التخصص

Address: ……………………………………………………………………………….. : العنوان

P.O. Box: ……………………………………………………………….: صندوق البريد

City &Postal Code:………………………………………………..…………: المدينة: الرمز البريدي

Country: ……………………………………………………………………….. : الدولة

Phone: …………………………………………………..…………………………….: رقم الهاتف

Fax No.: …………………………………………………………………………. : رقم الفاكس

E-mail: ………………………………..………………………………………….: البريد الإلكتروني

Method of payment: …………………………………………………..………….. : طريقة الدفع

Amount Enclosed: ………………………………………………………………….. : المبلغ المرفق

Signature: …………………………………………………………..……….. : التوقيع

Cheque should be paid to Deanship of Research and Graduate Studies – The Hashemite University.

I would like to subscribe to the Journal

For

- ☐ One year
- ☐ Two years
- ☐ Three years

One Year Subscription Rates		
	Inside Jordan	Outside Jordan
Individuals	JD10	$70
Students	JD5	$35
Institutions	JD 20	$90

Correspondence

Subscriptions and sales:

The Hashemite University
P.O. Box 330127-Zarqa 13115 – Jordan
Telephone: 00 962 5 3903333
Fax no. : 0096253903349
E. mail: jjbs@hu.edu.jo

المجلة الأردنية

للعلوم الحياتية

This title is indexed in Scopus

refine your research
SCOPUS